CREEP PROPERTIES OF EVAPORITE ROCKS

WITH PARTICULAR REFERENCE TO GYPSUM

by

Subhi Aziz Ali

(B.Sc., M.Sc.)

November 1979

A thesis submitted to the University
of Sheffield for the Degree of
Doctor of Philosophy.

To my parents ....

... for their love and encouragement.

Acknowledgments

The author wishes to thank his supervisor, Dr. F.T. Williams, Senior Lecturer, for his guidance, assistance, helpful advice and encouragement throughout the research and for his help during the presentation of this thesis.

He also wishes to thank the Government of Iraq and University of Mosul for their financial supports.

Professor D. Bond, the Head of the Department of Civil and Structural Engineering and Professor T.H. Hanna of the Department of Civil and Structural Engineering are also to be thanked for their assistance in many ways.

Thanks are also due to the Department technical staff, in particular Mrs. D. Hutson and Mr. E.R. Barwell for their help.

Grateful thanks to the British Gypsum Ltd. for supplies of the rock used during the tests.

Finally, the author thanks Mrs. Czerny for her neat typing of the manuscript of this thesis.

SUMMARY

The bulk of the rock material in the neighbourhood of an excavation, beneath a foundation or inside mine pillars is in fact triaxially loaded over long periods. Strata exposed in mines and excavations is subjected to bending over long periods also. In many mines and underground workings the rock is nearly saturated, also information on the three dimensional creep behaviour of any rock is very limited.

It was felt that studying the three dimensional creep behaviour under confinement in both dry and saturated conditions could add valuable information to the knowledge available on rock behaviour in such conditions. Gypsum was chosen as a suitable evaporite rock for carrying out this work.

To assess the significance and the nature of the time-dependent behaviour of gypsum in engineering applications, triaxial compression creep tests were carried out at 10, 20 and 30 N/mm^2 confining pressure. Bending and uniaxial compression creep tests were also performed on the rock. Axial and lateral creep strains were measured from which volumetric creep strain was calculated. All the creep tests were carried out in dry and water saturated conditions at room temperature. Instantaneous strengths of gypsum under bending, uniaxial tensile, uniaxial and triaxial compression were found. The effects of specimen size and water saturation on these strengths were determined at room temperature. Empirical equations describing the individual creep curves in bending, uniaxial compression and triaxial compression were determined for both dry and saturated conditions, in the latter two cases equations for both axial and lateral strains were obtained.

CONTENTS

LIST OF FIGURES

LIST OF TABLES

NOTATIONS

Note: Notations used in the literature review have been explained as they appear in the thesis.

L/D	Length to diameter ratio.
σ_t	Tensile stress.
σ	Compressive stress.
M	Bending moment.
b	Width of the beam.
d	Height of the beam.
L	Length of the beam.
L	Length of the cylindrical specimen.
ε_t	Tensile bending strain of the outer lower fibre.
ε_c	Compressive bending strain of the outer upper fibre.
P	Total applied load.
A_s	Cross-sectional area of specimen.
A_r	Cross-sectional area of ram.
F_m	The axial load applied on the ram of the triaxial cell.
F_d	Upward force due to the effect of confining pressure acting on the difference between the cross-sectional area of the ram and the specimen.
F_f	Friction force between the ram and the oil seal at specified value of confining pressure.
γ	Surface free energy.
C_o	Half length of the Griffith's Crack.
V	Volume of specimen.
ε	Strain.
ε	Long-term creep strain.
D	Specimen diameter.
σ_1	Major principal stress.
σ_3	Minor principal stress.

σ_n	Normal stress on a plane.
τ_s	Shear stress on a plane.
Z	Axial stress immediately after fracture.
θ	Measured angle of fracture, angle between the plane of failure and the major principal stress.
θ_M	Angle of fracture predicted from the Mohr's envelope.
θ_G	Angle of fracture calculated from Griffith's equation.
μ	Coefficient of friction.
ϕ	Angle of friction.
σ_m	Maximum normal stress.
τ_m	Maximum shear stress.
P_m	Mean pressure.
$\sigma_{unst.}$	Stress required to develop unstable fracture.
t	Loading time.
σ_u	Ultimate stress.
E_{dry}	Young's Modulus of dry rock.
$E_{sat.}$	Young's Modulus of saturated rock.
$\dot{\varepsilon}$	Creep rate.
$(\sigma_1 - \sigma_3)$	Differential stress.
ρ	Poisson's Ratio.
A,B,C and n	Individual creep equation constants.
D, E and F	Constants of empirical equations of bending creep.
R and K	Constants of creep rate-axial stress relationship.
a, b and c	Constants of empirical equations in axial creep.
d, e and f	Constants of empirical equations in lateral creep.

Chapter 1.

INTRODUCTION

1.1 General Introduction.

In mining and Civil Engineering, one of the major considerations in the rock excavation design process is the fracture of the rock material. In the design of the underground structures in rock, the level of stress and displacement that is likely to occur in the rock mass surrounding an excavation is of practical interest in the field of rock mechanics. The influence of high temperature, confining pressure, presence of solution, etc. have well known effects of the failure properties of rock. Only some of these factors will be effectively applicable to any given rock structure situation, but such a structure can hardly be unaffected by the influence of time. A study of performance of underground openings in rock indicates that in many cases the effect of time can be very significant. Continuing deformation, changes in shape, crushing of tunnel supports and linings are some of the evidence to indicate that the effect of time on rock deflection can be important. The consideration of time-dependent behaviour of rocks indicates that the rock failure may occur in a mine or under a foundation even when the rocks are subjected to loads well below their normally determined short term rate strengths.

McClain[81] studied the behaviour of long pillars with respect to time in potash mines of Alsace districts, France, and reported that the pillars exhibited a time-dependent strain (creep) and the edge of the pillars had deformed so much that they were no longer supporting their portions of the redistributed of the cover load. Bradshaw et al.[82] studied the vertical and horizontal deformation of the Hutchinson and

and Lyons salt mines pillars, in U.S.A., and reported that both deformations depend on time. Hebblewhite et al.[103] have made a radial creep measurements of a shaft excavation for a potash mine in Britain. They reported that the deformation rate decreases as the age of the excavation increases.

Hence, from the foregoing investigations and other field observations it is evident that crushing of pillars in room and pillar workings, closure of salt workings if left undisturbed for a long time, convergence of roof and floor in coal mine gate roads, widening of junction on roadways, sagging and settling of the strata behind long-wall faces in coal mines, settlement of foundations, etc. suggest that they are time-dependent or "creep" processes.

Where the time-dependent effects are significantly large introducing large scale flow at sub-failure stresses over a given time period, it is necessary to adopt a design for the structure such that flow is reduced to acceptable level or to design a satisfactory support framework for the structure (Farmer[85]). Thus, knowledge of the time-dependent behaviour (creep) of rocks can be of considerable help in understanding many aspects of rock engineering and is clearly important to civil and mining engineers. It is not only important from the question of the time factor, it is also important for question of stress, for difference of stress distribution must occur if we compare slow or fast advance rates in tunnels and workings. Knowledge of the rock creep properties gives a better picture of excavation behaviour and the movement of the rock masses surrounding an excavation prior to fracture. Particularly in rock subject to large creep strains, a knowledge of its creep properties is essential in determining the time during which a temporary excavation may be safely used. To maintain the stability of the excavation and any construction such as

a lining or foundation. Within it, it is essential to have a knowledge of the deformational characteristics of the rock and to be able to predict the future time-dependent deformation and hence the stability of the entire system. The understanding of creep properties of rock could also be used in mine design, i.e. mine layout, sizes of galleries and supporting pillars in an estimation of the useful life of mine structures.

The field of the rock creep is still in the early stages, and much work remains to be done in this problems area. However, the results of investigators who have been engaged on the study of creep rocks suggest that creep is a very sensitive property and appreciably affected by a number of factors, e.g.

a) Applied stress, value and method of application.

b) Temperature of specimen.

c) Structure of rock specimen, material, orientation, porosity and permeability, composition, etc.

d) Confining pressure.

e) Presence of solutions.

Stress, confining pressure, and presence of solutions are the main factors which may affect the creep behaviour of rocks at depth. However, a review of published work on the creep of rocks (see chapter 2) indicates that in practice very few investigations have been done on the three dimensional creep behaviour of rocks. Also, apart from one experiment by Griggs[70,71] (1939,1940) who did some tests on creep of alabaster in water and hydrochloric acid, very few investigations of the effect of water on the creep of rocks have been performed.

In the research work described here, the effect of applied stress, confining pressure and water saturation on the axial, lateral, and volumetric creep characteristics of gypsum at room temperature was studied.

1.2 Stress Conditions.

The rock tensile stresses are exploited in many mining operations, i.e. failure of strata in mines and excavations often takes place under bending (tension). On the other hand, the bulk of the rock material in the neighbourhood of an excavation or beneath foundation which is of concern to the design engineer is in atriaxially and compressively loaded state. However, stresses applied naturally to the rock in the earth crust or in any rock structure may have a wide variety of forces, and in many cases it is extremely difficult to assess at the design stage the exact nature of a stress field in a rock structure, especially when the rock mass is in a fractured state. It is possible to recognise that in a large number of rock structure problems the following states of loading are of importance:

a) Bending (tension).

b) Uniaxial Compression.

c) Triaxial Compression.

It was therefore decided to study the creep properties of gypsum under the influence of various percentages of their instantaneous strength in the above systems of loading.

1.3 Environmental Conditions.

Knowledge of the strength and physical properties of engineering materials aids in the design of safer and more economic structures. Water is always present and stored in the rock masses of the earth crust. In the majority of mines and underground workings the rock is nearly saturated. It is well known that the presence of the water modifies the behaviour of various rocks because ofits mechanical, physical and chemical effects. These effects influence!

1) Deformation of rocks.

2) Resistance of rocks to fracture.

3) Stability of rock masses.

Rock masses are exposed to the influence of water in varying degrees during most of the active life of mines, dams and underground excavations. The influence of water is thus an important consideration for the inherent safety of underground supports, mining or construction works, deep foundation stability, large dams or surface excavations, etc.

It was therefore decided to study some of the mechanical properties and axial, lateral and volumetric creep properties of gypsum in dry and saturated conditions. Appendix (A) gives the petrological description of the gypsum

1.4 The aims of this Research.

The main aim of this work is to carry out bending, uniaxial and triaxial creep tests on dry and water saturated gypsum for determination of the three dimensional creep properties under the two environmental conditions. The aim of this work is also to determine the bending, uniaxial tensile, uniaxial compressive and triaxial compressive strengths of the rock and to evaluate the effect of the specimen size and water saturation on the strength of the gypsum under these systems of loading.

1.5 Practical Significance of the Work.

Since the research studied three dimensional deformational creep behaviour of the rock, and the experiments carried out under dry and water saturated conditions with the evaluation of the confinement on the creep, these conditions are hopefully very close to the in situ natural conditions of this rock. It is hoped that the information obtained on the creep behaviour, may be of use in mines etc. in which the material forms the strata of the workings.

Knowledge of the three dimensional creep behaviour of any rocks in dry and water saturated conditions under confinement is very limited. The results obtained are thus an addition to knowledge in this field of

study. The primary contribution of this study has been to lay additional groundwork for future research in this area.

Movements of evaporite rocks in the earth's crust and the geological structures so produced may perhaps be better understood with additional knowledge of the creep properties of these materials. In this respect the extension of the work to oil reservoir Cap rocks and repository for terminal storage of nuclear waste materials in the evaporite rocks should result in information of use in other engineering fields.

1.6 Summary of the Research Programme.

Short term loading tests were carried out on the gypsum to find its instantaneous strength in bending, uniaxial tensile, uniaxial and triaxial compression. Four different specimen sizes were used to evaluate the size effect on these strengths. An exception was that the triaxial tests were performed on two sizes due to the limitation of the available triaxial cell size. Seven levels of confining pressure were used, namely; 5, 10, 15, 20, 25, 30 and 35 N/mm^2. All these tests were carried out in dry and water saturated conditions to evaluate the water saturation effects on the mentioned strengths.

The creep tests were then carried out under bending, uniaxial and triaxial compression conditions in both dry and water saturated states at various percentages of the instantaneous strength using the same systems of loading as used in the corresponding short term tests. In the tri-axial compression tests 10, 20 and 30 N/mm^2 confining pressures were used. All the short term and creep tests were carried out on the rock specimens cut from rock mass in such a manner that the major stress was applied perpendicular to the rock bedding. All the tests were performed at room temperature.

Chapter 2.

LITERATURE REVIEW.

Although the main aim of this study was to investigate details of the creep properties of the gypsum, the tensile and compressive strength of the gypsum will also be discussed briefly. This chapter will thus contain a review of some of the published works on tensile and compressive strength of rocks, followed by a summary of the studies published on the creep properties of rocks and some of the factors influencing them.

2.1 Direct and indirect tensile strength of rocks.

Early works, investigating the bending of the rock, such as that of fayols, as mentioned by Phillips[1], employed the bending test by loading cantilever beams of sandstone and shale with their bedding phases horizontal in order to study the fracture characteristics, fractures after bending were inclined upward and outward from the fixed end.

Phillips[1] (1948) carried out investigations of rock properties with respect to the application of various external forces. He produced test results on bending of rock beams which indicate that within certain limits the stress-deflection and load-deflection relationships are quite comparable to the predictions of the theory of elasticity. He correctly established that the position of the neutral axis in a beam under bending is solely dependent on the relative values of the elastic moduli in tension and compression and not on the relative strength in tension and compression. If the moduli in tension and compression are equal the neutral axis will be in the middle of the beam, otherwise the neutral axis will be out of the middle.

Pomeroy and Morgans[2] (1956), performed the bending tests on various coals, using the four point loading system to get pure bending in different sizes of tested beams. Tensile strength was calculated

from the simple beam theory, it is concluded that the strength depends on the direction of the loading relative to the bedding planes, and as the specimen size increased the tensile strength decreased. They noted that for a particular specimen size the tensile strength is of the order of one-tenth the compressive strength. Three alternative methods for measuring the tensile strength of brittle materials were investigated by Berenbaum and Brodie[3] (1959), namely, bending, indentation, and diametral compression tests. The results from the artificial brittle materials, plaster of paris, coal, and cement were compared with the conventional direct pull method. They found that the indentation and the disk test results were in good agreement with the conventional test results, while the bending test results differed from the others by a factor of two or more and they attributed this discrepancy to the formation of strong surface skin on the side of the beam during casting and/or machining. The results also showed that the tensile strength decreased by increasing the disk thickness and by increasing the beam thickness in case of flexural test.

Evans[4] (1961) studied the tensile strength of the coal by means of a bending test using the apparatus designed and described by Pomeroy and Morgans[2], diametrical compression, and indentation methods. The strengths obtained showed that the disk and indentation methods were not, in general, in agreement with those obtained by the bending method. Investigating the effect of specimen size by tensile stress applied to a disk by diametrial loading in which specimens of thicknesses varied between 0.31 to 1.9 inch, showed that the tensile strength decreased with increasing specimen size according to the power law:

$$\text{tensile strength} \quad \alpha \ (\text{thickness})^{-0.23 \pm 0.03}$$

Hobbs[5] (1964) used the diametrical compression of disks with a central hole for determining the tensile strength of sandstone, siltstone, mudstone, and limestone; he found that the tensile strength is greatest when the applied tensile stress is at 0^{o} to the lamination and smallest at 90^{o} to the lamination, and he noted that a relationship between the tensile strength and uniaxial compressive strength may exist. Hobbs in 1965 extended the study of the tensile strength[6], by using the bending test, indentation, diametrical compression of solid disks, and diametrical compression of disks with central hole tests. All the specimens were moulded of plaster. The diametrical compression of disks with hole gave the highest tensile strength and the results of bending, indentation, and solid disk differ from that of disk with hole by ratios of 0.6, 0.3 and 0.3 respectively. He reported that this difference in strength was not because of a toughened surface skin, and the strength variation was not present in the disk with hole. The effect of specimen size in perforated disks has been investigated with Darly Dale sandstone specimens the tensile strength was found to increase with increasing the external diameter and decrease with increasing the internal diameter (6).

Experimental results for similar tests on sandstone, marble, and trachyte are given by Jaeger and Hoskin[7] (1966). The values of the tensile strengths so obtained are compared with those from direct tension, Brazilian, and bending tests. The tensile strength for bending (three point loading) was considerably higher than those for direct tension or the indirect brazilian test by a factor of two or more.

Lundborge[8] (1967) investigated the specimen size effect on the tensile strength of granite by using the brazilian methods to test cylindrical specimens of L/D = 1 at diameters 2, 3, 4 and 6 cm. He found that the tensile strength decreased with increasing the specimen size and that the relation is well described by Weibull theory.

Hobbs[9] (1967) suggested a method of estimating the compressive strength by using the measuring tensile strength; he produced the formula, C = 2.84 T - 484, where C and T are the compressive and the tensile strength respectively.

Direct pull tests under well controlled conditions have been carried out among three indirect methods, namely, diametric compression of solid disks, diametric compression of perforated disks, and hoop stress loading by Hardy and Jayaraman[10] (1970). They found that the uniaxial tensile method provided meaningful tensile strength of the three tested rocks and it is considered as a base for the relative comparisons.

The indirect tensile tests have an important place in rock testing, but their interpretation must be in terms of the uniaxial value obtained by direct tests (Hawkes & Mellor, 1969)[11] Datta[12] (1964) concluded that the modulus of rupture is an exaggeration of the true tensile strength of the rock, and it is much higher than the strength obtained by brazilian test, and that the true tensile strength can only be determined by a uniaxial tensile test on a prismatic test-piece.

Hardy, Hudson and Fairhurst, carried out a theoretical[13] and experimental[14] (1973) investigation concerning the failure of intact rock, and the beam test in particular. Theoretical analysis indicated that the tensile strength is not a material property, it varies with specimen geometry and that no unique trend is evident for the size-strength relationship. Laboratory study of plexiglas beams showed excellent agreement with the theoretical approach while the granite beam results were not in good agreement with the theoretical.

Williams and Elizzi[15,16] (1976) used the bending test by means of four point loading to determine the tensile strength of gypsum and anhydrite. Tests were performed at room temperature and at atmospheric

pressure. The specimens had the dimensions; 240 mm long by 40 mm wide by 12 mm thick and 240 mm long by 40 mm wide by 20 mm thick. They found that the tensile strength of the later is more than that of the former.

2.2 Compressive strength of rocks.

The compressive strengths of rock materials have been measured for many years and a wide range of the researches have been performed relating to factors influencing the compressive strength of rocks since the beginning of this century. Brief review of some of the published studies within the recent decades will be given here.

In 1901 Adams and Nicholson[17] (1901) carried out a compression investigation of a marble. They applied axial load to some specimens and to get confinement the core was surrounded by a tight fitting steel cylinder. Further studies[18], were carried out using steel jacket cylinders at later dates by Adams, 1910, 1912; Adams and Coker, 1910; Adams and Bancroft, 1917; and King, 1912, 1917. Their conclusions were that the ultimate strength and ductility of rock increases with the amount of confinement.

Von Kármán[19] (1911) recognized the inadequacies inherent with steel jacketed testing and he conducted the first tests of Carrara marble and red sandstone, by applying confining pressure to the specimens through surrounding liquid in 1911, he also discovered the necessity of placing an impermeable membrane around the rock core to separate the pore space in the rock from the confining liquid. Von Karman described the relationship between the confining pressure and the strength for the first time, and presented the results in terms of Mohr's stress circles with curvilinear envelope. The conclusion was that Mohr's theory affords a suitable method of representing triaxial test data for the rock specimens, and that the lateral confinement had great effects on the rock strength.

A series of high pressure tests were conducted by Griggs[20] (1936) on Solenhofen limestone, marble and quartz. Two types of failure were observed by Griggs, shear and tension. The shear surfaces he observed gave evidence of fracturing and powdering of the constituent crystals. The slip planes developed by shear failure were always at an angle with the direction of the axial load. The tension fracture on the other hand, occurred by splitting parallel to the direction of compression. He observed the splitting failure could be prevented as the confining pressure increased, and shear fracture would predominate.

Robertson[21] (1955) used three triaxial procedures; compression of solid cylinders, crushing of hollow cylinders and punching of disks,on various rocks namely; Solenhofen limestone, granite, marble, quartzite, diahase, slate, soapstone, verde antique and sandstone. Confining pressures applied were as high as 60000 psi on rubber jacketed specimens. Plastic flow was observed in the case of limestone and marble specimens, which was absent in the silicate rocks. He concluded that the maximum shear stress criterion was reliable in predicting the yield point for the limestone, but only found a rough empirical criterion for the silicate rocks.

Handin and Hager[22] (1957) carried out a triaxial test on 23 dry rocks at room temperature at various confining pressures varying from 0 to 2000 atm. For each rock the stress-strain curves and the curve for ultimate strength and ductility (percent strain before rupture) as a function of confining pressure were presented. Relationship showing maximum shear stress and ductility as a function of the mean pressure (one third of the sum of three principal stresses) were given for each rock type; anhydrite, dolomite, limestone, sandstone, slate and siltstone. They reported that all the investigated rocks exhibited increase in

elasticity and yield stress and large increase in ultimate strength under confining pressure. Most of the rocks showed increase of ductility with confining pressure. The specimens fractured by shearing with the angle of the failure plane about 60^{o} to 70^{o} with the minor principal stress axis. The maximum shear stress was found about 0.7 - 0.8 of the mean pressure for anhydrite, dolomite and limestone. Whereas for sandstone about 0.6 and for shale about 0.6 or less. They also reported that the stress-strain curves for all the ductile rocks under confining pressure are essentially similar, with a straight elastic part, and a more or less defined yield stress (at the knee of the curve). It was found that the dry sedimentary rocks at room temperature fractured when the ratio of the extreme principal stresses in triaxial compression reached 3 to 4.

Price[23] (1958) studied the influence of triaxial pressure on the elastic behaviour of a number of typical coal measure rocks, with confining pressures up to 5000 psi and specimen length/diameter ratio (L/D) = 2. The strength data are expressed in terms of Mohr's envelopes for each type of rock. Price found that; (1) the ultimate strength of the rock increased with the confining pressure, (2) the greater strength of the rock in uniaxial compression the greater the increase in strength due to confining pressure, (3) the rocks brittle in uniaxial compression, fail by shear under confining pressure, (4) strength perpendicular to the bedding is greater than that parallel to the bedding, (5) Young's Modulus Perpendicular to the bedding is slightly less than that parallel to the bedding and (6) Poisson's ratio is increased by increasing the greatest principal stress at constant confining pressure.

Murrell[24] (1958) and Hobbs[25] (1964) found that the failure of coal specimens under triaxial condition at various confining pressures can be represented by a generalization of Mohr's theory.

Shih[26] (1963) carried out an investigation of uniaxial compression on a Gaspe Skarn. Among his results he found that, Poisson's ratio increased with uniaxial compressive strength, Young modulus increased with the compressive loads, strength decreased with increasing length to diameter ratio (between 0.2-3) and the deformation in lateral direction was less than that in the longitudinal direction.

A study of the behaviour of Indiana limestone, stone mountain granite, Pottsville sandstone and Georgian marble under uniaxial and triaxial compression has been performed by Schwartz[18] (1964) dry,wet and saturated specimens were used. He observed failure as splitting, shear, or a combination of these. Conclusions indicated that the failure of rock was ductile or brittle depending upon the amount of confinement, and that the angle of shear failure is closely predicted by the Mohr's criterion.

Höfer and Thoma[27] (1968) reported a triaxial study on rock salt, anhydritic hard salt, and fragment carnalite, under a confining pressure as high as 200 Kp/cm^2. The stress-deformation characteristics of different salt rocks were found to vary considerably. Carnalite behaved elastically and showed brittle fracture under confining pressure up to at least 100 Kp/cm^2, while the other salt rocks displayed brittle fracture only under low confining pressure. Bieniawski et al.[28] (1969) carried out uniaxial and triaxial experiments on soft rock (sandstone) and hard rock (quartz with norite). It was concluded that failure is essentially the same in all cases be it uniaxial or triaxial compression, and when free of machinery influence, fracturing in the direction of the major applied load is the true failure mode of rock in compression.

Bodonyi[29] (1970) determined a linear relationship between the principle stresses at failure, and a linear relationship between the confining pressure and the axial strain, using sandstone and limestone

specimen of 3 cm in diameter by 6 cm in length under confining pressure between 50-250 Kp/cm^2. Wawersik and Fairhurst[30] (1970) conducted a uniaxial and triaxial compression study of five different rocks. The results together with direct tensile strength data gave poor agreement with the failure theories (Griffith, Mohr Coulomb, and McClintock-Walsh), the uniaxial failure showed local fracture (splitting) and combination of splitting with shear failures.

Peng[31] (1971) carried out theoretical and experimental investigations to define the form of the stress and strain within cylindrical elastic specimens, subjected to end boundary conditions encountered in the laboratory testing, namely: perfect confinement, direct contact, uniform loading and Teflon inserts. Strains were measured using five strain gauges along the 2½" in length by 1¼" in dia. specimens at equal intervals. gauges mounted horizontally and vertically and two for each strain reading (total of 20 strain gauges for each specimen). Among results obtained Peng found that in the direct contact condition in which the specimen was supported at one end by the platen and the other end by a spherical seat, the vertical and circumferential strain profiles indicated uniform strain at the middle one third of the specimen, and this observation was in good agreement with the theoretical analysis.

Brady[32] (1971) reported a three dimensional axisymmetric finite element investigation which showed that rock specimens of L/D = 2 or more give the true Young Modulus and Poisson's ratio, in this case the end-effects are negligible provided that the measurements are made in the central portion of the specimen.

A study of the deformation behaviour of the concrete and rocks has been performed by Dhir and Sangha [33,34] (1974,1975). The effect of the strain rate within the range of confining pressure 17.2 - 137.9 N/mm^2

on the strength of rocks and concrete was found to be negligible, and has greatest effect on strength of unconfined loading; the transition of the failure mode from brittle to ductile took place at a confining pressure approximately equal to the unconfined compressive strength; the effect of lateral pressure on the lateral deformation was found to be more than that of the axial deformation which indicated decreasing Poisson's ratio, and as the confining pressure was increased the onset of dilation became closer to the failure stress.

Janach[35] (1977) found the triaxial data of westerly granite at confining pressures up to 800 MN/m^2 are not in agreement with the common failure criteria. Coulomb or Mohr's criterion are of an empirical nature and do not take into account the microscopic phenomena of cracking, and, the Griffith's Criterion and its modifications are based on the behaviour of the small pre-existing cracks. Aquadratic relation between σ_1 and σ_3 was obtained, $\sigma_1^2 = K\,\sigma_3$ as

$$\sigma_1^2 = 1.05 \times 10^4\ (\sigma_3 + 5) \text{ in } MN/m^2.$$

Most of the studies and the experimental information available on the influence of specimen size on the compressive strength is for coal and is concerned specially with unconfined compression on cubes of various side lengths.

Gaddy[36] (1946) tested small cubes of coal, the specimen sizes were varied from 5 to 23 cm, he reported decrease of the strength by increasing the specimen size and gave the following relationship:

$$\sigma = C\,d^{-0.5}$$

where d is the cube side and C is the coefficient representing the physical characteristics of the coal bed.

Evans and Pomeroy[37] (1958) and Evans et al.[38] (1961) showed that cubes of a particular size show a very wide range of strength, also both mean and modal crushing strengths σ_c decrease with the side length a of cube according to a power law:

$$\sigma_c = K \; a^{-\alpha}$$

where α is a constant with values between 0.17 and 0.32 for various coals.

Skinner[39] (1959) tested model pillars of anhydrite with sizes varying from 0.38 cm x 0.38 cm x 0.11 cm up to 25.4 x 25.4 x 15.21 cm and observed a decrease in compressive strength with increase in size. Mogi[40] (1962) carried out unconfined compression tests on marble prisms with height to width ratio of 2 and heights of 4, 6, 12 and 20 cm. A decrease in strength of 10 percent was determined for the given specimens.

Jaeger[41] (1967) presented a relation which is described as well obeyed in practice, namely the strength σ_a at a failure of cube of side a and the probability P_o of the cube surviving this stress is:

$$(\sigma_a)^{\beta/\alpha} \quad \ln P_o = \text{constant.}$$

The β constant indicates the form of distribution of flaws, its value would be one for linear and three for volume distribution.

Lundborg[8] (1967) carried out uniaxial compression tests on granite cylinders of L/D = 1 at diameters 2, 3, 4 and 6 cm. He concluded that the strength decreases with increasing specimen size with a range from 2190 to 1750 Kg/cm^2 (20% reduction). His results were in reasonable agreement with the Weibull theory. Bieniawski[42] (1960) also reported the effect of specimen size on the compressive strength of coal. Cubical specimens of sizes ranging from 7.5 cm to 200 cm were used. Decrease of the strength with increasing the specimen size was observed within specimens of less than

5 ft in side. The Weibull relationship was applicable only within certain limits (neigher the very small sizes nor the large ones). Bieniawski established two empirical relationships:

$$\text{i)} \quad \sigma = \frac{W^{0.16}}{h^{0.55}} \text{ - - - - - - - } W/h > 1$$

Specimen size < 5 ft.

$$\text{ii)} \quad \sigma = 400 + 200\,\frac{W}{h} \text{ - - - - } W/h < 1$$

Specimen size < 5 ft.

Where σ is the specimen strength in psi, W is the width in feet and h is the height in feet.

Pratt et al.[43] (1972) conducted uniaxial compression investigations of quartz diorite and grano diorite on an in situ specimen of a right triangular prism ranging in length from 1 to 9 ft., laboratory cylindrical specimens of 3.18 and 4.25 inch in length and triangular prisms ranging from 4.5 to 12 inch in length, the length to edge or length to diameter was 1.5 to 1 or more. He observed a decrease of maximum stress by a factor of 10 as specimen size increased, asymptotically approaching a constant value at 3 ft. length and greater. All the specimens failed by a shearing mechanism and most of them exhibited dilatancy prior to failure. Young Modulus was found to decrease only slightly or remain constant with respect to the specimen size.

Mead[44], in (1925) stated that the dilatancy is the property of granular masses of expanding in bulk with change in shape, and that it is due to increase of space between the individually rigid particles as they change their relative positions. He summarized that the granular masses in a condition of maximum-density packing (in case of rock, presence of sufficient pore and soft material around the particles, to give maximum

density) the deformation of these masses requires an increase in volume, and when the conditions are those of minimum density, the masses can deform to a larger extent without increase in volume. Bridgman[45] (1949) used the dilatometer to measure the volume change of a number of metals and three rocks, namely, soapstone, marble and diabase under simple compression. Specimen sizes were 2.5" in length by 1 to 1.5" in diameter. Bridgman observed that the volume decreased with the applied load to a certain amount, due to volume compressibility of the specimen, then the volume started increasing with load and this ther dominated the situation. This increase can be ascribed to an opening of interstices in the structure as a premonition of the fracture that would occur at a load only slightly beyond the maximum reached.

Two soft and high porosity rocks, calcarenites and tuffs were subjected to hydrostatic and triaxial stress by Pellegrino[46] (1970). It was shown that the rocks undergo large volume strain, the pattern of the strain with stress was; at relatively low stress small volumetric strain was observed accompanied by nearly constant modulus, this strain results mainly from deformation of grains and of cementing bonds. At increasing stress, the volumetric strain gradient increased rapidly due to progressive breakdown of the bonds which was followed by interparticle slips. At this point most of the bonds are broken and the material became practically cohesionless and quite similar to granular soil. A further increase in stress causes a decrease in volume strains because of the decreasing porosity. This investigator reported that the behaviour of these rocks was changed by increasing hydrostatic or triaxial stresses from rockllike behaviour (small strain, nearly linear stress-strain relation and brittle failure) to soil-like behaviour.

The dilatancy of hollow cylinders of Witwatersrand quartz has been measured by Cook[47] (1970). Specimens of 11.4 cm in length with inside and outside diameters of 1.3 and 3.7 cm were subjected to 138, 276, 276 and 414 bar confining pressure. The dilatancy of the internal and external surfaces of the specimen was measured by means of two separate screw-driven piston intensifiers for the control of oil confining pressure, the intensifiers were fitted with sensitive electrical pressure and displacement transducers. It was found that both internal and external dilatancy were almost identical which proved the dilatancy is a pervasive volumetric phenomenon.

Crouch[48,49] (1970,1972) measured the volumetric, radial and tangential strains in triaxial compression tests on Wombeyan marble, sandstone, norite and quartzite, by means of immersing the sample in a fluid-filled vessel and observing fluid level changes in a stand pipe during the test. The lateral component of the volumetric strain is a direct measure of the amount by which the volume must be adjusted. Volumetric strain was calculated as the sum of axial, radial, and tangential strains. The rate of lateral expansion was measured by monitoring the confining pressure behaviour. Among the concluded results, Crouch reported; (1) The volume of the specimen increases near the maximum load and accelerated as the failure progressed. (2) The lateral strain decreases with the confining pressure. (3) The lateral expansion rate of marble is greater during failure than during plastic deformation, and (4) The volumetric expansion of all specimens began at about one-half the maximum axial stress.

Price and Farmer[50] (1979) carried out triaxial tests on Portland stone specimens of 150 mm long by 75 mm dia. at a constant strain rate of 2×10^{-5} sec.$^{-1}$, and under 7, 14, 21 and 28 N/mm^2 confining pressure.

They found that the axial stress-strain relationships are linear up to about 90% of the maximum stress followed by a non-linear stage to the maximum stress then converted to a steep negative slope (characteristic of unstable deformation) down to a nearly constant residual stress level, this dominate a range up to 13% axial strain. Maximum stress and axial strain at maximum stress were found to increase with increasing confining pressure. They also found that the volumetric strain, measured using an extension of Crouch's method, increases linearly with the axial strain at constant confining pressure.

2.3 The influence of water on some rock properties.

In a series of investigation reports issued since 1928, it has been established that the resistance of solids to rupture and strain is reduced by adsorption of fluid from the surrounding medium[51] (1957). The reason has been described as being due to the decrease in surface energy of the interfaces newly formed in the defect (ultra-microcracks) arising in the strained solids, these phenomena depend on the rate of new surface and of penetration of the adsorption layer in ultra microcracks.

Extensive experimental works have been carried out to study the effect of saturation on rock properties especially in more recent years. Price[52] (1960) performed uniaxial compression tests on air dried and saturated specimens of a number of British Coal measure rocks (certain sandstones). The results showed that the compressive strength of saturated specimens is about 45% of the completely dried rock specimens. The effect of the saturation on the elastic properties of three sandstones has been studied by Mann and Fatt[53], (1960). The saturation increased the compressibility by 10 to 30 percent, decreased the Young Modulus by 8 to 20 percent and increased the Poisson's ratio by 100% for Bandera Sandstone.

Boozer et al.[54] (1962) carried out a triaxial compression test on rock specimens of Indiana limestone and Navajo Sandstone saturated with oleic acid, oleylamine, distilled water, and n-hexadencon. Confining pressure up to 20000 psi at a temperature from 78 to 300° F were used. The effects of the fluids were observed to be a decrease in the ultimate strength of the sandstone and of the yield stress in the case of limestone, which deformed in a ductile manner, however the type of failure of limestone in certain cases changed from ductile yielding to a more brittle type when the saturation fluid was changed. Boozer explained these effects as indirect results of the decrease in the free surface energy caused by the strong adsorption of the liquids. Effects of solubility of rocks, lubrication at grain contacts and others resulting from the physical properties of the fluid such as viscosity and compressibility have been shown as unremarkable effects. The brittle failure of sandstone was confirmed as a result of the growth of pre-existing and newly-developed cracks which eventually weaken the rock and lead to macroscopic failure.

Clocback and Wiid[55] (1965) carried out uniaxial and triaxial compression tests on two quartzitic rock types. Specimens had a length to diameter ratio of 2. The uniaxial compression tests performed for eight different moisture contents ranging from zero (dried over $Ca\ Cl_2$ or $P_2\ O_5$) to saturated (submerged in water) and triaxial tests for three moisture contents dry, 98% and submerged in water, four confining pressures were used.

The uniaxial compressive strength was found to decrease with increasing the moisture content of the rocks. They reported that the compressive strength of rocks under saturated conditions (submerged in water) is of the order of 50% of that under dry conditions (dried over $Ca\ Cl_2$ or $P_2\ O_5$). It was shown that the Mohr's envelope of the dry condition is parallel to

that of saturated condition, indicating no change in the coefficient of the internal friction took place due to the wetting. They explained the reduction of the compressive strength of the saturated rocks relative to dry condition as a lowering of the surface free energy of the rocks by immersing in water.

Wiid[56] (1970) studied the influence of saturation on the prerupture fracture of dolomite and sandstone, by means of the volumetric strain techniques. The volumetric strain-axial stress relationship shows the pattern; fracture initiation, beginning of the unstable fracture (beginning of dilation) and unstable fracture propagation. It was observed that the uniaxial compressive stress of the saturated sandstone at fracture initiation is 63% of that of the corresponding dry stress, 62% in case of unstable fracture propagation and 65% in the case of failure compressive strength. Wiid found 20% reduction in the tensile strength measured by Brazilian method. He suggested the explanation that the moisture increases lowering of the surface free energy and hence the intrinsic strength of the rock.

Mogilevskaya[57] (1970) found that water saturation decreases the Modulus of Elasticity of four rocks by 5 to 20%. Rutter[58], reported 30% reduction in uniaxial compressive strength of the Solenhofen limestone due to water saturation and he concluded that the strength decreases as the strain rate decreased with an increase of ductility and dilatancy took place at high strain rate.

A brief description of the observed strength reduction from oven dry to fully saturated specimens of three different rocks is given by Broch and Franklin[59] (1972), granite with zero porosity, a weak sandstone with 12.5% porosity and a strong sandstone with 1.6% porosity. The point load strength reductions were found to be 13.3%, 33% and 22% respectively.

Farmer[60] (1973) reported that the compressive strength of the saturated dolomite, limestone and sandstone is 95%, 90% and 66% of the dry compressive strength respectively. He also studied the effect of the particle strength on the compression of crushed aggregate from the three mentioned rocks. The aggregate specimens of a certain particle size range were put in 150 mm diameter by 100 mm deep steel cylinder and subjected to axial stress. Tests were carried out on an oven dried (24 hrs at 110° C) and water saturated (24 hrs vacuum) samples. Among the results obtained, it is noted that at 20 N/mm^2 axial stress, the saturation increased the compressive strain of the limestone from 23.5% to 27.5% and of the sandstone from 32% to 34.5%. Farmer stated that the effect of saturation reduced the rock strength of the weaker sandstone, and, the increase in compressibility of the stronger rocks exceeded that attributed solely to a reduction in strength. It is explained that the water weakens the surface irregularities of the aggregate particles rather more than the body of each aggregate, in addition, as these irregularities created by the crushing would contain several microfractures allowing a high water penetration facility, this was in agreement with Rehbinder's (1948) conclusion that the surface hardness of rocks is influenced more by wetting than their compressive strength.

Parate[61] (1973) carried out tensile and compression tests on dry and saturated limestone. The tensile strength determined by uniaxial, biaxial, simple Brazilian and confined Brazilian, compression tests performed under uniaxial, biaxial, and triaxial stresses. He reported that a good parallelity of the Mohr's envelope of the dry and saturated conditions was found, indicating no change of the angle of friction or coefficient of internal friction with water saturation. Reduction of the strength was found in all cases after saturation and this was explained as

a result of the lowering of the free surface energy of the rock by absorption of water.

Broch[62] (1974) conducted a study to determine the influence of water on point load, uniaxial and triaxial compression strengths of rocks having very high strength with low porosity varying between 0.3 and 1.2%. The point load strength showed a reduction varying between 20 and 45% with 34 as an average value and in the case of uniaxial compressive strength the reduction was between 33% and 53%. The strength of rocks under triaxial stress with confining pressures 0, 10, 20, 30 and 50 N/mm^2 gave a remarkable reduction due to water saturation. Broch also explained the reduction of the strength as being due to the lowering of the surface free energy for some rocks and due to reducing of the internal friction for others.

Vutukuri[63] (1974) saturated limestone with water, glycerine, ethylene, glycol, nitrobenzene ethylalcohol, benzaldehyde and n-butyl alcohol. The tensile strength was measured by means of ring test, and it was found that all liquids decreased the tensile strength and that this is due to the reduction of the free surface energy of the rock which is proportional σ^2 (where σ is the strength). The greater the surface tension of the saturated liquid the lower the cohesion (and hence the strength) between the particles making up the solid. Vutukuri gave the tensile strength (σ_t) of saturated rocks in terms of the surface tension (x) of the saturation liquid:

$$\sigma_t = e^{mx+c}$$

where m and c are the regression line constants.

Van Eeckhout[64] (1976) reported very many explanations of the mechanism of reducing strength due to moisture; fracture energy reduction

capillary tension decrease, pore pressure increase, frictional reduction and chemical and corrosive deterioration. Uniaxial compression, Brazilian and three point (beam) loading tests were performed on a coal mine shale at various humidities up to 100%. The reduction of the strength was explained as, expansion of the material by water adsorption, (moisture content variation causes expansion - contraction characteristics which lengthen internal cracks), and, lowering of the surface energy (fracture work) with increasing moisture.

In an ASTM publication (1976), Ballivy et al.[65], carried out indirect tensile tests and triaxial compression tests on a gneiss, cemented sandstone and fine grained limestone. The specimens were saturated by either immersing in water under vacuum or by injecting the saturation fluid through the specimen under pressure. The strength of the saturated specimen at any confining pressure was found to be about 70-80% of the dry ones. The type of saturation fluid was observed to have a considerable effect on the strength, that being due to combination of changing the free surface energy in rock and the role of the fluid viscosity.

2.4 Creep of Rocks.

The subject of creep in rocks has been studied for over fifty years. The time-dependent behaviour in several rocks has been studied in the laboratory under compression, bending and torsion, but still there is a general lack of data on the subject. Some of the creep measurements and behaviours recorded in the literature related to some factors influencing such behaviour will be briefly reviewed in this section.

Michelson[66] (1917, 1920) measured creep in some rocks (limestone, marble, calcite, etc.) subjected to torsion. He suggested an empirical formula for the torsional strain at room temperature of the form:

$$\phi_t = \theta_o + F_1 [1 - \exp(-\alpha t^{\frac{1}{2}})] + F_2 t^n$$

where the coefficients F_1 and F_2 are of the form:

$$F(T) \cdot C \exp(\beta C)$$

and θ_t is twist at any time t, t is the time in minutes, C is applied torque, F(T) is a function of temperature, n is found to be about 1/3, θ_o being the elastic deformation and α and β are arbitrary constants. The part of the strain represented by the second term; $F_1 [1-\exp(-\alpha t^{\frac{1}{2}})]$ has been called"elastic-viscous displacement" and was found to be recoverable with time. The third term; $F_2 t^n$ has been called "viscous displacement" by Michelson which he found to be irrecoverable. He did not find steady-state or secondary creep.

Phillips[1,67] (1932,1948) conducted tests on creep in bending of shale and uniaxial compression of siltstone. He determined the lateral and longitudinal creep strains in the compression tests. He also found that the creep of the wet specimen is comparatively greater than the dry specimens, and the lateral creep strain found to be more than that of the longitudinal creep strain. Phillips did not make a detailed study of creep behaviour of rocks and did not attempt to derive a creep equation.

Evans[68] (1936) carried out creep tests on granite, marble, slate, sandstone and concrete. He observed two components of creep strains, one of which was recoverable, and according to him creep and recovery could be described by the equation:

$$\varepsilon = A [1-\exp(B-Ct^n)]$$

where ε is the creep strain, t is the time, A,B,C and n are constants. n is found to be approximately 0.4.

Evans and Wood[69] (1937) conducted compression creep tests on marble, granite and slate. They observed the longitudinal and the transverse creep strains, and found that the rate of the transverse creep increased more rapidly with the stress than the longitudinal creep rate particularly in the case of laminated rocks stressed parallel to the planes of lamination. The transverse creep rate showed a particularly marked increase at stress about 50 to 66 percent of the compressive strength. Creep was also observed in sandstone and concrete subjected to tension.

Griggs[20,70,71] (1936,1939,1940) carried out time-dependent measurements under compression on limestone, talc, shale, glass, alabaster and single crystals of calcite and halitite. His works are considered as the first systematic study of the creep in geologic material and, in fact, he has laid the foundation of the ideas of the time-dependent deformation behaviour of rocks. He found that the creep of rocks is affected by stresses, temperature, confining pressure, structure of the material and the presence of various solutions. He expressed his results in terms of the equations:

i) for creep $\varepsilon = \varepsilon_o + B\log t + ct$

ii) for recovery $\varepsilon = A - B\log t$

Where ε is total deformation, ε_o is elastic deformation, t is time, A, B and C are constants depending on stress and the material under test. The second term "Blogt" represents the primary creep. He called it "elastic flow" and it was recoverable. The term "ct" represents the secondary creep and it was found to be irrecoverable. Griggs called this "Pseudo-viscous flow", and calculated an equivalent coefficient of viscosity of solid for this flow using the method given by Jeffreys and suggested the equations $\eta = \frac{\sigma}{3\dot{\varepsilon}}$ where η is the equivalent coefficient

of viscosity, σ is the applied stress and $\dot{\epsilon}$ is the constant rate of the strain with respect to time. He mentioned that the foregoing creep equation do not describe the relation adequately for the short time intervals, since the logarithmic term approaches minus infinity ($-\infty$) as the time approaches zero. Similarly, the logarithmic term approaches infinity as the time approaches infinity.

Griggs[70] observed steady-state creep in boric anhydride glass at 243° C. Earlier he found[20] that when the limestone was subjected to a high confining pressure a level of differential stress could be reached at which steady state creep occurred. This is clearly related to the fact that confining pressure increases the differential stress at which fracture occurs, so that considerable plastic deformation occurs when a high enough confining pressure is applied.

Griggs[71] conducted creep experiments on alabaster immersed in solution. It was supposed that according to the principle originally put forward by Rieck on thermodynamic grounds, solution would occur at the most highly stressed regions of alabaster and re-deposition would occur at free faces, resulting in a creep by process of recrystalization. He found that immersion in water markedly increased the creep rate and enabled steady-state creep to occur at stresses which were insufficient for dry alabaster. The effect is not simply a function of solubility of the alabaster, however, since it was found that the creep rate in a solution of calcium chloride (in which the solubility of gypsum was lowered approximately 45 percent) was greater than in the pure water; there is no satisfactory explanation of these results as yet. It might be that diffusion of the solution into the alabaster could be a key process, but Griggs found no difference between specimens tested immediately after being immersed and others which had been soaked for 68 days

before testing. The explanation will have to be sought in terms of ideas of plastic deformation of ionic crystals. Finally Griggs' observations of delayed fracture should be mentioned; he observed the third stage of creep, tertiary, in the case of Solenhofen limestone subjected to confining pressure[20] and of alabaster immersed in water[71]. Not surprisingly he found that the time to fracture decreased as the differential stress was increased, this was accompanied, of course, by an increase in the steady-state creep rate.

Pomeroy[72] (1956) performed creep measurements on coals (Barnsley Hards), subjected to bending. Specimens of the dimension 8.5 x 1.62 x 0.24 cm (leng x width x thickness) were loaded in cantilever. He found that creep and recovery could be represented by the equations given by Griggs. No creep was observed in the case of anthracite at equivalent stress.

Lomnitz[73] (1956) tested slender cylindrical specimens of grano-diorite and gabbro of 45.75 cm long by 2.22 cm central diameter in torsion at room temperature and at atmospheric pressure. He mainly observed transient creep and recovery, and found the creep for constant torque up to one week can be represented by the equation:

$$\varepsilon_t = \frac{\tau}{G} [1 + q \ln (1+\alpha t)]$$

where ε_t is the total shear strain in radians, τ is the constant shear stress, G is the modulus of rigidity, t is the time in second, α is the coefficient such that $\alpha t \gg 1$ and q is constant. The above equation is applicable only in the range of small strains and for stresses not more than 0.05 percent of the rigidity modulus.

Terry and Morgans[74] (1958) conducted some observations of short duration creep in compression on a number of 38.1 mm cubes of Barnsley Hards. They found instantaneous elastic strain as soon as the load was

applied, primary creep, they called it "retarded elastic strain", and a secondary creep or steady-state flow.

Kendall[75] (1958) reported a study of creep on Solenhofen limestone, rocksalt and cement mortar under uniaxial and triaxial compression. The maximum confining pressures were 15000 psi (103.4 N/mm^2) for limestone, 1000 psi (6.9 N/mm^2) for cement and 2000 psi (13.8 N/mm^2) for rock salt. He found that the creep strain obtained could be represented by the relationship;

$$\varepsilon = A + B \log t + Ct^n$$

where ε is the creep strain at any time t, A, B, C and n are constants. He also indicated that the modulus of elasticity for the limestone and cement remain essentially constant and independent of both the confining pressure and the history of the stress-strain application. Transient creep was observed in specimens loaded below their fundamental strength, whereas for specimens loaded at stresses greater than that, the transient creep again was observed followed by rapidly increasing deformation until complete failure occurred.

Matsushima[76] (1960) studied the creep behaviour of some of the igneous rocks at atmospheric pressure and room temperature. He reported that the longitudinal creep of granite could be expressed by the equation:

$$\varepsilon = A_o + A_1 e^{-\alpha_1 t} + A_2 e^{-\alpha_2 t} + A_3 e^{-\alpha_3 t} + B \log t + ct$$

where ε is the creep deformation, t is the time, A, B and C are constants and α_1, α_2 and α_3 are reciprocals which represent the retardation time of Kelvin's model and are of the order 10, 10^2 and 10^4 seconds respectively.

Robertson[78] (1960) has made some observations of short duration (17 min. to 167 min.) creep of Solenhofen limestone, Danby marble, Rutland White marble and calcite. He applied confining pressures between

290 bars to 4150 bars at a differential stress of 1400 to 8400 bars, all experiments were at room temperature. Robertson observed only transient creep and found that the rate of this creep per unit of the differential stress decreased by an order of 100-fold when the confining pressure increased from 1000 to 2000 bars in the case of Solenhofen limestone. The following equations have been suggested to represent his results:

$$\dot{\varepsilon} = \frac{K}{t}$$

and

$$\dot{\varepsilon} = K_1 S - K_2$$

where $\dot{\varepsilon}$ is the creep rate, t is the time in seconds, S is the differential stress in bars and K, K_1 and K_2 are constants.

Misra[79] (1962) carried out creep tests on ten rocks namely; Anhydrite, Beerstone (olictic limestone), calcareous sandstone, Darly-Dale sandstone, dolomite, granodiorite, limestone, marble, olivine and pennant sandstone. The creep tests performed under uniaxial, torsion and four point bending loading. Most of these rocks were tested at room temperature, at elevated temperature (300-700° C which is far away from the melting point of the rocks) and while surrounded by different solutions (six solutions including the distilled water). Misra found that creep strain increased by increasing the applied stress, and the effect of higher temperature is to increase the creep strain of the rock. His results were fitted by logarithmic and power relationships in the following forms:

i) At a low temperature:

$$\varepsilon = A + B \log t$$

ii) At elevated temperature:

$$\varepsilon = ct^n$$

where ε is the total creep strain, A, B, C and n are constants with $n \approx 0.3$ in the case of temperatures above about half the melting temperature. The creep rate $\dot{\varepsilon}$ was found to be a function of the applied stress of the form:

$$\dot{\varepsilon} = K \sigma^n$$

where σ is the applied stress and K and n are constants. He reported that immersion in solutions increased the creep strain and the creep rate, and solutions which lower the strength of rock most cause it to creep more in their presence. Misra explained that neither the lowering of free surface energy nor the build up of pore pressure by the presence of the solution in the pore space account for increased creep in rock observed. It appears that a phenomenon of partial adsorption and partial solution may be the cause of this increase in creep. Price[80] (1964) conducted bending creep tests on beams of Pennant and Wolstanton sandstones and uniaxial compressive creep tests on cylindrical specimens of L/D = 2 of sandstone, siltstone and muddy limestone at a temperature 23 ± 1.5^{o} C. He found that beams of Pennant sandstone exhibited primary and secondary creep at 24-72% of the instantaneous strength and Wolstanton sandstone when subjected to loads ranging from 65-85% of the instantaneous failure load. It is reported that a linear relationship between the creep rate of the secondary stage and the applied stress was found for both sandstones. The long term strength of Pennant and Wolstanton sandstone were determined as 20 and 60 percent of their instantaneous strength using graphical method. (By plotting constant rate of the creep versus the applied stress, intercept of the straight line with the stress axis at zero rate indicating the long term strength.) The creep strain of the bending can be expressed directly in terms of the theoretical behaviour of a B-V model;

a rheological model comprising a Bingham body with a voigt unit attached in series.

In the case of the compression creep results, it was observed that the primary and secondary creep stages and the creep rate data were not in agreement with the behaviour of the B-V rheological model.

McClain[81] (1964) measured the time-dependent deformation of the pillars in a potash mine in France, using the borehole extensometer to measure the axial deformation of the borehole, which was located horizontally in the pillars. Deformation was measured at horizontal depths of 2.5, 5, 10 and 20 meters. Laboratory creep tests were carried out on specimens of 7.5 cms square by 5 cm high taken from the same mine. It is reported that the curves of the horizontal creep obtained from the underground measurements exhibited primary followed by secondary creep. The rate of the secondary creep decreased with the horizontal depth in the pillars, and the deformation was found to be very large at the edge of the pillars and decreased very rapidly with the distance in the pillars. The vertical creep data obtained from the laboratory specimens showed that the creep rate in the steady-state was increased with the applied stress.

Bradshaw et al.[82] (1964) carried out creep measurements on pillar models of the salt. The models had a diameter to height ratio of 4 and subjected to stress of 4000, 5000, 6000, 7000, 8000, 10000 and 12000 psi. It was found that the creep rate decreases with the time at constant stress level. Empirical equations have been developed for the prediction of the vertical creep rate ($\dot{\varepsilon}$) in the salt mine openings up to 70 years. The equation is in the form

$$\dot{\varepsilon} = B\,\sigma^{m}\,t^{n}$$

and a reasonable fit was obtained with

$$\dot{\varepsilon} = 9 \times 10^{-8} \times \sigma^{3.1} \times t^{-0.6}$$

where $\dot{\varepsilon}$ is a strain rate in microstrains per day, B is a constant dependent on unit of $\dot{\varepsilon}$, σ is the average pillar stress in psi, t is the time in hours and n is the slope of $\dot{\varepsilon}$ Vs t on log-log plot (negative).

Comte[83] (1965) carried out triaxial creep tests on artificial rock salt specimens of 41.9 mm long by 12.7 mm diameter. The specimens were tested at various temperatures ranging from room temperature to 300° C, various confining pressures ranging from 1 to 1000 bars, stress differences up to 138 bars and grain size in the range of 0.1 to 0.15 mm for all specimens (except for two specimens where the sizes were 0.55 and 0.63 mm). Comte observed three stages of the creep and he found that as the temperature increases the creep rate increases, i.e. at 1000 bars confining pressure and 69 bars axial stress, creep rate was increased by a factor of 4-5 when the temperature increased from 29 to 104.5° C and by a factor of 22 when the temperature was raised from 29 to 198.2° C. Creep rate was decreased by increasing confining pressure, i.e. at 104° C and 69 bars axial stress, an increase of 1000 bars in confining pressure decreased the creep rate by a factor of 4 and finally the increase of grain size caused a decrease of the creep rate, i.e. when the grain size increased from 0.1 to 0.63 mm the creep rate decreased by a factor of 2. He reported that the creep for the various conditions of temperature, confining pressure and differential stresses could be represented by the relationship of the form:

$$\varepsilon = A + Bt^{n}$$

where ε is deformation at a given time t, A is the instantaneous deformation and B and n are constants depending on the conditions of the experiments, with $0 < n < 1$.

Hendron[84] (1968) conducted triaxial extension and uniaxial compression creep tests on rock salt. Tests were performed at various confining pressures ranging from 100-1000 psi at 23° C and under stress differences ($\sigma_1-\sigma_3$) ranging from 1000 to 3750 psi. He observed the instantaneous elastic strain, primary creep, secondary creep and the tertiary creep (the latter found only at ($\sigma_1-\sigma_3$) of 3750 and 2125 psi). The rate of the steady-state creep was found to be higher for specimens loaded to larger stress differences. Uniaxial compression creep tests were performed at 23° C and 65.5° C and at axial stresses varying from 525 to 3000 psi. He reported that increasing temperature increased the creep strain, i.e. at a constant axial stress of 1750 psi, the creep strain increased by a factor of 2 when the temperature rose from 23° C to 65.5° C. Increased temperature was also found to increase the creep rate in the secondary stage. Creep data in triaxial extension was expressed in terms of the equation:

$$\varepsilon = K \sigma^{n} t^{m}$$

where ε is the axial creep strain, σ is the stress difference in psi, t is the time in hours and K, n and m are constants. Hendron mentioned that the secondary creep rate in triaxial extension was less than that of the uniaxial compression at the same constant stress difference.

Farmer[85] (1968) reported that the form which represents most of the creep results of rock to a reasonable extent and its applicability has been confirmed by various workers is:

$$\varepsilon = \varepsilon_o + A \, \text{ℓn} \, t$$

where ε is the total creep strain at any time (t), ε_o is the instantaneous elastic strain and A is known as the creep constant and depends on the applied stresses and could be given by the formula:

$$A = \left(\frac{\sigma}{E}\right)^n \qquad \text{in the case of uniaxial stress}$$

and

$$A = \left(\frac{\sigma_1 - \sigma_3}{2G}\right)^n \qquad \text{in the case of triaxial stresses.}$$

where σ is the uniaxial applied stress, E is the modulus of elasticity, σ_1 is the axial stress, σ_3 is the confining pressure, G is the modulus of rigidity and n is a constant equal to between 1 and 2 at low stresses and between 2 and 3 for high stresses. Farmer also mentioned that secondary creep was ignored in the above equation which is normally represented by a term Bt. In fact only secondary creep exists at a temperature of between 20 and 50 percent of the absolute melting temperature of rocks and cannot exist below a temperature of about 100^{o} C.

Myrvange[86] (1970) performed uniaxial compressive creep tests on five rocks, dimensions of the specimens were 80 mm long by 32 mm diameter tested at room temperature. The duration of each of the tests was 10 days and under a constant stress of 650 Kp/cm^2, which is more than the expected stress in the mine from which the specimens are collected. He reported that most of the rocks exhibited primary and secondary creep stages, and have shown small creep tendencies except in a porous amphibolite which showed rather distinct creep properties.

Hobbs[87] (1970) conducted incremental creep tests on different coal measure rocks, namely Siltstone,shales, mudstone, and sandstone with strengths varying from 61 to 206 MPa. Specimens were subjected to compressive stresses from 26.4 to 41.4 MPa with tests extending to 4000 minutes. He found that the longitudinal strain-time behaviour can be approximated by an equation of the following form:

$$\epsilon = \frac{\sigma}{E_c} + g\sigma^n t + K\sigma \log (t+1)$$

where; E_c is mean incremental modulus, σ is stress level, t is time in minutes and g, K and n are constants. The strain rate predicted by this relationship is less than those observed when t is small. Hobbs also found that after unloading the instantaneous recovery was followed by time-dependent recovery which ceased after about 15000 minutes.

Kanagawen and Nakaari[88] (1970) carried out creep tests on specimens of slate and porphyrite under dry and wet conditions. They reported that the creep of the saturated specimens was more than that of the dry specimens. The creep rate of the wet specimens during the initial periods was 2-5 times the dry specimens and after about 20 to 100 days the steady state creep rates tended to be more or less the same. The stabilization period depended on the type of rock, applied stresses and possibly on the moisture content of the rock specimen.

Cruden[89] (1971) conducted a study involving the forms of the creep law of the rock under uniaxial compression by using data of works published previously and he processed these data statistically. He reported that the power law of the transient creep in the form,

$$\dot{\varepsilon} = b_1 t^{b_2}$$

where $\dot{\varepsilon}$ is the strain rate, b_1 is the strain rate at unit time and b_2 is the strain hardening parameter usually with a value about -1, appears to fit all the data satisfactorily without the addition of any component of steady-state creep, and he stated that this is the most satisfactory basis for the explanation of creep experiments over longer times.

Hofer and Knoll[90] (1971) studied the creep behaviour of carnallite subjected to uniaxial compression; they correlated the laboratory test results of small specimens with observations in a salt mine in East Germany in an area liable to sudden failure of pillars. They tried to derive a creep equation from the latest findings of solid-state physics

on deformation behaviour of polycrystalline materials. From the experimental investigation it was concluded that at low stress and temperature the creep data is represented by the logarithmic law:

$$\varepsilon = C_1 + C_2 \ln t$$

and at high stress and temperature the creep data fits the power law

$$\varepsilon = Kt^n$$

and at very high stress, which approaches the ultimate stress the creep deformation according to the power law quickly increases. Hofer and Knoll determined the stresses at which the transition from the logarithmic creep equation to a power law creep form has taken place for specimens of different L/D (length to diameter) ratio. If these stresses are plotted as abscissae versus L/D as ordinate a limiting curve is obtained. Logarithmic creep without fracture occurs below this curve and above power law creep with fracture takes place after a more or less longer period of time. This curve is considered as the true boundary curve of the limiting creep stresses. They noted that if the creep behaviour of the pillars corresponded to the logarithmic law of the type mentioned above, the pillar could be supposed stable, and if the creep law of the pillars corresponded to the power law of the type stated above, the pillars were unstable.

Winkel et al.[91] (1972) studied the time-dependent deformation of the Carlsbad potash subjected to uniaxial compression in the laboratory on a specimen of 203.3 mm long by 69.9 mm dia. and using data obtained by other investigators from multiaxial testing of a similar material. They tried to derive a three dimensional constitutive equation and compared this with a numerical solution using finite element analysis. They tried also to record field observations from a cylindrical opening in two mine pillars to define the time-dependent behaviour of the opening,

but they failed to get accurate observations in the mine from which the laboratory specimens were collected. A large difference was found between the predicted results and the field measurements of the other mine, due, it was felt, to the difference in the material between the two mines. Prediction of the behaviour from the multiaxial results of other investigators on rock salt was found to be represented fairly by the general shape of the time-dependent deformation curve.

Peng[92] (1973) studied the creep behaviour of specimens of Tennessee marble and Arkose sandstone of size 2.5 inches long by 1.25 inch diameter, using a servocontrolled hydraulic testing machine. The creep measurements were performed after fracture had occurred under stresses ranging from 10 to 95 percent of the ultimate load, i.e. the stress applied in order to cause fracturing. He reported that the fractured specimens sustained creep load, and the time to creep fracture was inversely proportion to the creep load. The fracture time was found to be from 2-8 minutes for the marble and 2-10 minutes for the sandstone. It was noted that the creep curves of the fractured specimen in which the cracks had not fully propagated to separate the specimen into two or more pieces consists of two stages, the steady state creep and the rupture creep, whereas those that were separated into pieces but held by friction exhibited three creep stages; transient, steady-state and creep rupture.

King[93] (1973) studied the creep behaviour of models of Saskatchewan potash pillars. The models had the length to diameter ratio 4 and 8. The tests were performed at a constant temperature varying from $27^{o}C$ to 60^{o} C and the load was applied uniaxially using a compressed Nitrogen/hydraulic pressure system. King found that the creep strain of the two sizes of models could be represented by the power law of the form:

$$\varepsilon = At^{B}$$

where ε is the axial creep strain, t is the time in hours, A and B are constants with $0 < B < 0.25$. The creep predicted from these models is compared with the creep measurements in situ done by other investigators for several years and it was found that the model's creep behaviour was in very close agreement with that in situ. King stated that creep tests on model pillars can yield information of practical application to the design of pillars underground. In particular the influence on creep behaviour due to the increase in temperature associated with mining at greater depths can be studied by this means with some confidence.

Matveyev and Kartashov[94] (1974) carried out creep tests on a coal, halite, combustible shale, limestone, sandstone, clay and marble. The specimens were subjected to uniaxial compression by means of a compressed nitrogen/hydraulic pressure system capable of accommodating 6 specimens a time. The specimen size was 70 mm long by 30 mm diameter and the stress level was from 10 to 90 percent of the rock strength. They suggested an equation of the following form to represent the creep data:

$$\varepsilon = \varepsilon_o \left(1 + \frac{A}{1-B} \; t^{(1-B)} \right)$$

where ε is the creep strain at a given time t, ε_o is the instantaneous strain, A and B are constants. Values of these constants was found for different stress levels using a computer program. The value of the constants A and B obtained from the laboratory measurements and those obtained in underground tests (long-term compression of rock prisms in mines) appears to be essentially the same for many types of rocks, e.g., sandstone, coal, halite, etc.)

Afrouz and Harvey[95] (1974) conducted creep tests on several rocks within the soft to medium strength range in the laboratory and in situ. The laboratory tests were performed under uniaxial compression on dry and

saturated specimens of cylindrical shape at room temperature ($20 \pm 4^{o}C$) and at atmospheric pressure. Whereas the in situ measurements of creep deformation were carried out on the underclay along the floor of a mine roadway (Britannia Colliery, S. Wales). They chose 15 empirical equations and analysed them in the light of their laboratory experimental results and in situ time-dependent behaviour. Close similarity was found to exist between the laboratory and in situ time dependent behaviour, enhancing the possibility of predicting, within reason, the in situ creep of these rocks.

The laboratory and in situ results indicated the following conclusions:

1. The instantaneous strain (ε_o) is directly proportional to the applied stress (σ) and can be expressed by the form:

$$\varepsilon_o = m\,\sigma^n$$

where m and n are constants with $0 < m < 1$ and $0 < n < 1$ depending on the rock type, porosity, temperature and the state of moisture.

2. The average secondary creep rate ($\dot{\varepsilon}$) with respect to applied stress could be represented by the formula:

$$\dot{\varepsilon} = m\,\sigma^n$$

3. In the saturated coal and underclay, the overall creep rate increased three and eight times their creep rate in the dry condition.

4. Air dried soft to medium strength rocks behaved in an elasto-plastic manner and very close to a Maxwell-Kelvin model. This can be given by the following equation:

$$\varepsilon_{dry} = A + Bt^c + D\,[1-\exp(Et)]$$

Due to the water effect, water saturation indicating more plasticity in the rocks, and the saturated rocks generally exhibited plastic behaviour and the creep data fits the equation

$$\varepsilon_{sat.} = A + Bt^c + Dt^f$$

where ε is the creep strain at time t, A, B, D, E, c and f are constants.

Wawersik[96] (1974) carried out a study of the creep behaviour of westerly granite and Navajo sandstone in dry and saturated conditions. Dry specimens were subjected to uniaxial compression while the saturated specimens were subjected to triaxial compression with confining pressure up to 68.95 MN/m^2. All tests were performed at room temperature (21° C). The axial strains were measured by means of DCDT transducers which were mounted to the loading pistons. Lateral (tangential) strains were measured by means of strain gauges on air dried specimens, and the saturated specimens in triaxial tests by means of the measurements of the integrated sample deformation. (This technique based on the fact that the volume adjustments of the confining pressure medium, which are needed to maintain a constant confining pressure during radial sample deformation, are directly proportional to the average radial specimen strain).

It was reported that the strength of the saturated rocks was found about 10-15 percent less than the dry rocks regardless of the magnitude of the confining pressure. In all cases, the stress-strain curves obtained in the saturated condition coincided with, or were closely similar to those in the dry conditions. The creep rate in the steady-state condition was found to be greater in the saturated specimens than in the dry specimens. The plot of the creep rate versus the applied stress indicated a linear relation for both dry and saturated conditions with good parallelity. Both the axial and lateral creep of the saturated condition under triaxial stresses exhibited the three general creep stages. The creep in both directions follows the same pattern. The primary creep was described by the power law of the form

$$\varepsilon = 10^{c} t^{n}$$

where ε is creep strain at time t, n and c are constants, their values found by plotting log t versus log ε.

In saturated conditions the secondary creep rate in the axial direction showed a slightly non-linear relation with shear stress $(\frac{\sigma_1 - \sigma_3}{2})$ and the volumetric secondary creep rate showed a linear relation with the shear stress $(\frac{\sigma_1 - \sigma_3}{2})$.

Wawersik mentioned that in general the rate of the lateral and volumetric strains in Westerly granite exhibited the same trend with respect to $(\frac{\sigma_1 - \sigma_3}{2})$ and $\sigma_m(\sigma_1+\sigma_2+\sigma_3/3)$ as the secondary axial creep rates. The differences in water content changed the rate of creep and thus the time-dependent deformation in general by at least two orders of magnitude. The time-dependent deformation was found to decrease strongly with increasing confining pressure.

Singh[97] (1975) performed creep tests on Sicilian marble subjected to uniaxial compression at room temperature (24.5 ± 0.5^{o} C) load again being applied by a nitrogen/hydraulic system and loading frame. Both axial and lateral creep behaviours have been determined. The curves of the creep in both directions exhibited the three general creep curve stages; primary, secondary and tertiary and the two curves follow the same pattern as far as the different stages of creep are concerned. Singh also measured the creep of two other rocks at various stress levels and concluded that the creep rate in steady state increased with the applied stress.

The creep data of the marble was represented by a power relationship of the form

$$\varepsilon = a\, t^{b}$$

where ε is creep strain at any time (t), and a and b are constants.

It was found that the lateral creep rate increased far more than the axial creep rate when the specimens were subjected to sustained stresses greater than their yield strength.

Wu and Thomsen[98] (1975) studied the behaviour of the micro-fracturing activities with axial, lateral and volumetric creep of Westerly granite under uniaxial compression, and tried to determine the effects of the water and temperature on the total time to failure. They reported that at a constant uniaxial stress, three stages of micro-fracturing and deformation have been distinguished. The first stage is of transient creep and microfracturing, the second is the steady-state with axial, lateral and volumetric creep increasing linearly but with micro-fracturing activity (which is represented by the sum of square root of energy; $\Sigma\sqrt{E}$) increasing exponentially and the third stage where the axial, lateral and volumetric creep increase at an accelerated rate while the microfracturing activity increases at a superexponential rate. They mentioned also that under constant stress, initially the volumetric strain increased sharply indicating a volume decrease, then after a short time the trend reversed indicating volume increase until this became more than the original volume of the specimen (dilatancy) with linear relationships governing the trend of the lateral and axial strain until the tertiary stage when the volumetric creep increases again slightly. It is also reported that the water saturation decreases the creep time to failure by one to two orders of magnitude, and the heating of the specimen to 150^{o} C increases the creep time to failure and the strength.

Cogan[99] (1976) carried out triaxial creep tests on saturated samples of Opohonga limestone and Ophir shale at different constant stress levels and various confining pressures to study the effects of volume behaviour upon the creep properties of these rocks. The volume change was measured by monitoring the amount of water which either left or entered the sample during testing. Axial load and confining pressures were applied by means of nitrogen/hydraulic system. Some of the tests

were performed in the sequence of consolidation, creep and quick stress-strain tests. Cogan observed the primary and secondary stages of volumetric creep, the consolidation or decrease of the volume accompanied primary creep and dominate a very short time indicating the occurrence of only elastic volume contraction. The consolidation continued to develop the secondary creep stage accompanied by volume expansion, and the time to develop this stage appears to increase with the axial load, the rate of the expansion gradually increased until a steady rate is reached. It is also mentioned that the process of consolidation affects the ability of the rock to deform, the increase in consolidation appears to retard the ability to creep under a given state of external stresses. It is noted for both rocks that the pre-consolidation of the sample retarded secondary creep rates.

Williams and Elizzi[16,100] (1976,1977) carried out creep tests on the Sherburn gypsum in an air dried condition and at room temperature.

Bending creep tests were performed[16] on beams of dimension 240 mm long by 40 mm wide by 12 mm thick. The beams were subjected to pure bending using the four point loading method, and the applied stresses have been chosen as 20, 40, 60 and 80 percent of the ultimate stress. They found that the creep data at low stress level followed the logarithmic relationship of the form:

$$\varepsilon = A + B \log t$$

at high stress level the data followed the power law of the form

$$\varepsilon = C\, t^{n}$$

and at the medium stress level, the early stage of the creep followed the logarithmic equation and the later stages of creep followed the power law relationship mentioned above. Where ε is the creep deformation, t

is the time in hr, A is the creep value at unit time and B is the slope of the line obtained by plotting (ε Vs log t), C is the creep value at unit time and n is the slope of the line obtained by plotting (log ε Vs log t).

Triaxial creep tests have been studied on the same rock by Williams and Elizzi[100] at different constant stress levels ranging from 30 - 80 percent of maximum stress and at various confining pressure ranging from 0 to 30 MPa. They used a triaxial apparatus suitable for the long term tests which is designed by the same investigators[101,15], the load and the confining pressure was applied by means of a compressed nitrogen/hydraulic loading system (details of the apparatus given by Williams and Elizzi[101]). They reported the following results and conclusions:

At a given time the creep strain increases with the confinement, the rate of the creep decreases with respect to confining pressure and this effect is larger at low confining pressure than higher and also at the earlier stage of the creep, creep rate increases as the confining pressure increases at a constant differential stress up to 45 MPa and for values of the deviator stress more than 45 MPa the creep rate starts to decrease with confining pressure to certain value and increase thereafter.

The creep data for the uniaxial loading at low stresses and for the triaxial loading at low stress with 10 MPa confining pressure and within time less than 24 hrs. was represented by logarithmic equation

$$\varepsilon = A + B \log t$$

and for all other stresses and confining pressures the creep data was represented by the power law of the form:

$$\varepsilon = C\, t^{n}$$

where ε is the creep strain at a given time t, A, B, C and n are constants.

Elizzi[15] (1976) reported the creep properties of gypsum and anhydrite under bending, uniaxial and triaxial compression at room temperature. The beams had the dimensions 240 mm long by 40 mm width by 20 mm thick and subjected to stresses varying from 30 to 80 percent of maximum stress. The triaxial specimens were 75 mm long by 25 mm diameter and subjected to axial stresses from 30-80 percent of the maximum stresses and at confining pressures of 0, 10, 20 and 30 MPa. Some of his conclusions on the creep behaviour of the tested rock are summarized here:

a. The creep data of both rocks at low stresses and confining pressure expressed by the logarithmic relationship of the form:

$$\varepsilon = A + B \log t$$

and at higher stresses and confining pressure expressed by the power law of the form:

$$\varepsilon = C\, t^{n}$$

The constants A, B, C and n are increased with axial stress at constant confining pressure and decreased with confining pressure at constant axial stress, in addition C and n increased linearly with confining pressure at constant differential stresses.

b. The creep rate increases with the axial stress at constant confining pressure and decreased with confining pressure at constant axial stress.

c. The creep rate ($\dot{\varepsilon}$) represented as a function of axial stress (σ_1) in the form of the power relation:

$$\dot{\varepsilon} = K\, \sigma_1^{g}$$

where K and g are constants with $g > 1.0$.

Varo and Passaris[102] (1977) carried out creep tests on halite under various humidity levels from 13 to 87%. Tests were also performed on

water saturated and brine saturated specimens at room temperature. Specimen size of 100 mm long by 50 mm diameter were used for the various humidity tests and of 65 mm long by 50 mm diameter for the saturated specimens. They reported that the creep rate increased as the humidity increased, the initial increase in rate was found to be at least 500% and when the humidity reaches high value, i.e. 87%, the creep rate accelerated very rapidly. Small differences in humidity level (13% to 42%) did not change the slope of the "straight line", as they called it, portion of the creep curve. The effect of the humidity upon the total strain has been shown to be non-linear and has little effect at low humidity relative to that at higher humidity levels. It is also reported that the saturated specimens subjected to 120 bars showed the three stages of the general creep curves with very rapid increase in creep rate. The effects were explained as recrystallisation which occurred during the creep in saturated brine, and in water the halite dissolved and because of the solution the creep rate increased very rapidly to cause a rapid failure.

Habblewhite et al.[103] (1977) studied the time-dependent deformation of the evaporites in situ by installing four radial boreholes each 4.6 meter deep around a 7.6 meter diameter shaft excavation through the evaporite deposits at a depth of 1065 metres in a deep level potash mine in Britain. In each hole four anchors were located at 0.6, 1.5, 3 and 4.5 metres with rods attached for reacing movements with dial gauges at the outer station. The data were regressed using least square curve fitting with consideration of seven curve types (log, ln, power functions, ... etc.). It was found that the power law function gave the best representation of the data in every case, the equation was in the form:

$$\dot{\varepsilon} = At^{B}$$

$$\varepsilon = Ct^{(B+1)}$$

where $\dot{\varepsilon}$ is the creep rate, ε is the deformation in mm, t is the time in days, A, B and C are constants with (B+1) ≃ 0.4–0.5 and C decreases with the radius of the anchor. They also concluded a formula for prediction of the creep at any radial depth into the rock mass as a function of depth and time.

Kranz[104] (1979) carried out creep tests on Barre granite specimens of 1.27 cm in diameter subjected to 87% of the ultimate fracture strength. Axial and radial strains were measured using strain gauges mounted parallel and perpendicular to the applied load. Kranz observed the three stages of the general creep curve in both axial and radial directions before the specimens failed. The radial creep was always found higher than the axial creep rate, it was explained, may mean that crack widths are increasing very rapidly or that crack coalescence, at a small angle to the axial direction, is contributing more to radial creep strain. It was also mentioned that under constant load the crack grew or propogated toward the maximum stress direction.

CHAPTER 3.

SHORT TERM TESTS.

In these tests the behaviour of the gypsum in tension and compression was studied, under dry and saturated conditions. Tensile strength tests were carried out in two different ways, direct pull and flexural methods, while the compression experiments were performed under uniaxial and tri-axial loading. The effect of size on the tensile strength was studied by using four different beam thicknesses and four core sizes in the direct pull method of tensile testing, while in compression four core sizes in uniaxial and two core sizes in triaxial tests were used.

On the basis of these, which were considered as instantaneous strengths, the loading stresses were chosen in the long term tests under the same stress application method.

In this chapter, some of the experimental techniques, apparatus and equipments and test procedures will be discussed briefly.

3.1 Experimental Techniques.

The techniques of preparing the specimens, saturating the specimens, drying them, controlling the saturation and the connection of the strain gauges in various configurations between themselves and the strain gauge indicator will be given briefly in this section.

3.1.1 Specimen Sizes and Preparation.

The sizes of the specimen used in each of the short term tests and the methods of the preparations of these specimens will be discussed in this section.

3.1.1.1 Bending Test Specimens.

In examination of the few works published on the flexural behaviour of rocks, shows that there is no standard or recommended size of the beam which should be used. Hardy et al.[13] found that the theoretical

correct ratio for a Plexiglas beam which gives maximum load-carrying capacity of the beam is 9.06 : 4.14 : 1 (length : depth : width), then from his experimental study[14], he concluded that this result is not in good agreement with beams made of rock. Elizzi[15] tested gypsum beams of dimension 240 mm long by 40 mm width by 6 mm thickness. He found that the thickness was not suitable because of the extension of some crystals through thickness of the specimen, which produce weak section at these points. In consequence he used 240 mm by 40 mm by 20 mm for his study.

In order to evaluate the effect of the specimen size, the following sizes were chosen; 240 mm by 40 mm by 15 mm, 240 mm by 40 mm by 20 mm, 240 mm by 40 mm by 25 mm and 240 mm by 40 mm by 28 mm (length by width by thickness). The beams were cut from blocks by a diamond cut-off saw, Fig.(3.1),to the required size approximately, grinding of the beam faces was carried out using the surface grinder, Fig.(3.2), which grinds to an accuracy of 0.001 mm. The actual dimensions of each beam were measured by micrometer to the nearest 0.01 mm. During the cutting and grinding, water was used as a coolant, the specimens were then ovendried at a temperature not more than 70^{o} C for 24 hrs. in order to retain the chemically held water in the gypsum and not to change the phase of Ca SO_4-H_2O system from the Ca $SO_4.2H_2O$ condition, (this will be explained in the next sections).

All beam sizes were cut parallel to the bedding and tested so that the load was applied perpendicular to the bedding.

3.1.1.2 Uniaxial Compression Specimens.

In order to study the specimen size effect on the uniaxial compressive strength, four core sizes were used, all the sizes having the same length to diameter ratio (L/D).

Hawkes and Mellor[11] reported that taking into account all the available earlier works and all the information concluded therefrom, the

minimum acceptable length to diameter ratio (L/D) was 2. They mentioned that practical experience seemed to show that values up to L/D = 4 are usually safe even with an imperfect loading system. An A.S.T.M. publication[105] strongly concluded that the L/D ratio should be more than 2.5. Elizzi[15] used gypsum cores of 75 mm long by 25 mm diameter (L/D = 3). In this research the length to diameter ratio used is also 3, and the following dimensions of the specimens were chosen:

76.2 mm long by 25.4 mm dia. 95.25 mm long by 31.75 mm dia. 114.3 mm long by 38.1 mm dia. 152.4 mm long by 50.8 mm dia.	L/D = 3

Specimens were obtained by core drilling from blocks, using a bench coring drill machine with water as a coolant, Fig.(3.3). The drilling direction was perpendicular to the bedding of the rock. A diamond cut-off saw was used to bring the cores to the approximate required specimen length, after which the specimen end surfaces were polished to attain the required final measurements using the grinder and lapping machines, see Figs. (3.2) and (3.4). Two grades of carborundum abrasive were used on the lapping wheel (400 and 800 mesh). In this operation the specimen was placed in a close fitting steel tube with flat flange to produce smooth parallel end faces which are accurately at right angles to the longitudinal specimen axis. It is vitally important that the end surfaces of the specimen be accurately perpendicular to the longitudinal axis of the same, and that the end surfaces are flat so as to prevent eccentric compressive loading of the specimen when tested. A micrometer was used to measure the actual dimensions of the specimens to the nearest 0.01 mm, and finally the specimens ovendried at 70° C for 24 hrs. as in the case of the beams.

3.1.1.3 Uniaxial Tensile Specimens.

Hawkes and Mellor[11] recommended that the test specimen or the neck portion of the dumbell specimens, should have L/D between 2.5 and 3 and if the butt-jointing method is used, it might be desirable to adopt L/D = 2.5. Obert and Duvall[106], stated that it is satisfactory to use core diameter $1\frac{1}{8}$ inch and length 4 inch (L/D ≃ 3.6) to core diameter $2\frac{1}{8}$ inch and length 4 inch (L/D ≃ 1.9). In this study it was decided to use L/D = 3 in order to maintain geometric similarity between both uniaxial compressive and uniaxial tensile tests.

To evaluate the effect of specimen size on the tensile strength four different core sizes were used with L/D = 3. Dimensions of these specimens were chosen the same as uniaxial compressive cores, and the rock specimens were prepared using the same procedure described in Section (3.1.2). To test the specimen by using Hounsfield Tensometer, two steel plates were bonded with epoxy resin to the rock specimen end surfaces, to transmit forces to the sample in the tensometer. The diameter of the platens were the same as the rock specimens, Fig.(3.5a). It is very important to choose a suitable cement for bonding the steel platens as it should give a bond strength between steel and rock in tension greater than the tensile strength of the rock.

Dhir[107] tested several cements for this purpose and found that the cement obtained by mixing Araldite AV121 resin with HY151 hardener, suitable for setting stressmeters in laboratory conditions, and it gave a bond between steel and Darley Dale sandstone greater than the tensile strength of that rock. Datta[12] found that Araldite AV121/hardener HY951 Cement and FR 1131A/FR 1131B Cement were suitable for sandstone.

In this study the cement obtained by mixing equal quantities of AV121 (resin) and HY951 (hardener) was used and it consistently gave bond strength

more than the tensile strength of the gypsum rock. (Fig.3.5a shows a sketch of a prepared specimen). Fairhurst[108] employed a similar method for the uniaxial tensile test and for preparing the test specimens.

3.1.1.4 Triaxial Test Specimens.

Two specimen sizes were used in this test with L/D = 3. These sizes were limited to the clear space inside the triaxial cell which is available in the laboratory. The dimensions of both sizes were chosen as the same dimensions of the uniaxial tests (76.2 mm long by 25.4 mm diameter and 95.25 mm long by 31.75 mm diameter). The specimens were prepared using the same procedure described in Sec. (3.1.1.2). The penetration of the hydraulic fluid into the pore space in the specimen when being loaded is prevented by the use of P.V.C. jackets 0.9 mm thick. To insert the specimen into the jacket, powdered talc was used as a lubricant, and to provide the necessary oil seal the jacket was extended beyond the specimen ends on to the platens.

3.1.2 Saturation of the Specimens.

To saturate the specimens, a procedure recommended by Hawkes and Mellor[11] and used by many investigators[53,54,99] was followed. The specimens were first ovendried for 24 hrs at a temperature of 70° C, a temperature at which the chemical composition of the gypsum does not change (this will be described in the next section). They were then placed in a vacuum desicator and evacuuated to 0.001 mm mercury for at least 3 hours in the dry condition. Distilled water was introduced into the desicator so that all specimens were completely submerged, then the water and the specimens were evacuuated until no air bubbles were observed which takes about 4 hrs, finally soaking was continued under vacuum for 24 hrs. Samples were removed for test after the vacuum had been released for at least 2½ hrs. By this procedure the specimens were made essentially

100% saturated[11,53]. To ensure that no water was gained by the samples after 24 hrs, samples were stored for 48, 72, and 96 hrs in the water, and it was shown by weighing that no moisture increase occurred after the first 24 hrs. A sketch of the apparatus used is shown in Fig.(3.6).

3.1.3 Drying Temperature.

When gypsum is heated to a moderate temperature (about 175° C) it loses about 75% of its chemically held water[109]. Some investigators[110,111,112] have found that gypsum ($Ca\ SO_4.2H_2O$) converts to a different phase of the $Ca\ SO_4/H_2O$ system at this temperature. Macdonald[111] had accepted that Kelly's dehydration reaction plot showed that gypsum and anhydrite are the two most stable phases in the system.

Gypsum heated in air is slowly converted to the hemihydrate at about 70° C or less depending on the moisture content of the air, and rapidly at about 90° C or over. Soluble-anhydrite (γ - $Ca\ SO_4$ may be produced by a rapid heating at 90° C or more[112]. Posnjak[110] concluded that the assumption of Van't Hoff and his associates which is that gypsum forming the hemihydrate, anhydrite (β - $Ca\ SO_4$) or a soluble-hemihydrite (γ -$Ca\ SO_4$) is erroneous, he found that the gypsum can only form hemihydrate at a temperature of 97.5 ± 1° C.

To determine the temperature at which the given gypsum converts to hemihydrate in the laboratory, a method which is basically similar to that discussed by Posnjak[110] was followed. Samples were heated at a temperature of 25, 50, 60, 75, 90 and 135° C (five samples at least were used for each temperature) and the weights of the samples were determined at 4, 8, 12, 24, 36, and 48 hrs. Fig.(3.7) shows the relationships between the weight loss and time for the various temperatures, and it is clear that the samples heated at 25, 50, 60 and 75° C lost only a very small percentage of their weight (maximum 0.4%) after 24 hrs. and remain constant

up to 48 hrs. While the samples heated at 90 and 135° C lost 9.3% and 28% respectively after 24 hrs. The temperature Vs weight loss after 24 hrs of heating was plotted in Fig.(3.8). A sudden increase in weight loss occurs at 75° C, and, it is concluded that the weight lost up to this temperature is due to the evaporation of the uncombined moisture content of the rock, while the considerable change in weight at temperatures more than 75° C indicates that the gypsum starts to lose its chemically held water which changes the Ca SO_4-H_2O phase system of the gypsum (Ca SO_4-$2H_2O$) to the hemihydrate. In consequence a temperature of 70° C over a period of 24 hrs was used for the drying of the specimens in this study.

3.1.4 Saturation Controlling Procedure.

The saturation of the specimens should be kept under close control over the whole experimental loading period, at the same time the wet specimen must not be allowed to effect the strain gauges circuit. Specimens were therefore coated with a very thin layer of a waterproof selfsticking material. This material consisted of a mixture of FEBWELD No. 1 basic component, and FEBWELD No. 1 reactor component (FEB "Great Britain" Ltd.). Broch[62] used selfsticking Polyethylene to cover his saturated samples (this material being claimed to have superior electrical properties).

The effect of the sealing process was examined by coating six specimens each time, the weight of the specimens being recorded at different coating ages. This procedure was repeated four times, the results showed that no measurable weight losses occurred within the first 33 days after coating.

Stress-strain relationships of coated and uncoated specimens were determined at different coating ages (up to 33 days) under the same loading

conditions. All the results showed no noticable effect of the coating on the stress-strain behaviour of the gypsum.

3.1.5 The Connection of Strain Gauges Between Themselves and the Strain Gauge Indicator.

The number of strain gauges used for each specimen in short or long term tests is more than 2 in most of the cases as mentioned (or will be mentioned). To measure the strain using 2 strain gauges, the average strain required, a full bridge connection was used (two active strain gauges and two dummy). In the case of using a single strain gauge, the half bridge connection was used (one strain gauge was active and one dummy). The bridge circuits are shown in Fig.(3.9). Dummy strain gauges of the same type as the active were bonded to a similar piece of rock (not loaded) to give temperature compensation. Peekel strain gauge indicator type T-200 (Automation-Peekel,N.V., Rotterdam, Holland) was used to measure the variation of the strain over the period of the test. The direct connection to one side of the Peekel (2 sides provided) should be either half or full bridge. So in case of two full, two single or one single and one full bridges direct connection to the Peekel was used (i.e. the case of short and long term tests of the bending). Fig.(3.9) shows the connecting method between strain gauges and the Peekel. In case of using more gauges than this, an Extension Box, Type 23U (Laboratorium Voor electronica N.V. Peekel, Rotterdam, Holland) which is specified for use with the Peekel meter has been used in combination with the Peekel strain indicator. In this way the capacity is increased by 23 new measuring points. These can be selected by means of a rotary switch in the extension box. The system has a constant series resistance making it possible to switch over automatically by means of the box selector using one control dummy gauge (all the active strain gauges of one type). In

case of different active gauges, the 23 points can be used by supplying each point with its own dummy gauge. Normally the switch of the extension box has no noticeable influence on the accuracy of the measurements. Fig. (3.10) shows the circuit of the extension box.

3.2 Apparatus, Equipment and Test Procedures.

Experiments performed were aimed at finding out the flexural behaviour, uniaxial compressive strength, uniaxial tensile strength and triaxial compressive strengths of the dried and water saturated gypsum.

3.2.1 Bending Tests.

Knowledge of the behaviour of the rock in bending is of great importance from the practical pcint of view, because failure of strata in mines, tunnels and excavations often takes place under conditions of bending. The bending test is also one of the indirect methods of measuring the tensile strength. In the case of rocks, the tensile strength determined from bending tests are usually significantly greater than the uniaxial tensile strength. The bending test has been frequently used to obtain the tensile strength of rocks due to a number of practical difficulties in performing the conventional tensile tests. These include gripping the test-piece, preparing a suitable test-piece and avoiding the generation of eccentricity in loading. The use of epoxy-based cements has more recently overcome much of the difficulty in gripping the sample and obviated the necessity of dumbell shaped rock samples in tensile testing.

3.2.1.1 Bending Test Apparatus.

The beam specimens were loaded under four point loading in order to achieve pure bending conditions. The apparatus used in this study was designed by Williams and Elizzi[15,16], and used by the designers for the same type of rock. In this experimental set up the beam was supported at two outer points 200 mm apart and loaded at two inner points 100 mm

apart. The outer and inner points are symmetrically interposed about the centre of the beam. This is done by placing the beam between four knife-edges, two under the beam and two above it, held by two horizontal steel bars. See Fig.(3.11). The lower bar rests on the lower platen of a testing machine and the load is applied through a steel ball in a hemi-spherical recess at the centre of the upper bar. The 100 mm length of the beam between the inner knife edges will thus be subjected to a bending moment of constant magnitude and hence will be in pure bending. It has been reported[16] that the advantages of the system are; (a) It gives maximum bending moment between the two inner knife edges, so that the fracture point will be away from the points of application of load; (b) The positioning of the knife edges gives complete stability within the apparatus during test.

The load was applied by using a 10 ton Wykenham Farrance compression testing machine. The machine is motor operated geardriven, the rate of platen displacement can be varied by changing the 8 different wheels in 6 gear positions (42 different speeds can be used). The range is between 0.00008 mm/min to 4.0 mm/min. A proving ring with a 0.002 mm dial gauge, the sensitivity of which 2.882 N (0.648 lb) per division was used for the measurement of the applied load.

3.2.1.2 Test Procedure and Stress Measurements.

Strains were measured on the upper (compression) and lower (tension) surfaces of the beams, and these measurements were made by bonding two electrical strain gauges at the centre of the upper outer fibres and two at the centre of the lower outer fibres, the strain gauges used having a gauge length of 10 mm, nominal resistance of 120 Ohms, and a gauge factor of 2.07. The beam was placed in the experimental rig and the load applied gradually by the compression machine. The strain at the two outer fibres

was recorded at different loads before failure took place (in order to find the stress-strain relationships). Finally the strains within the ultimate load were recorded at a stress as near failure as possible. A description of the circuit and the measuring meter were given in Section (3.1.5).

Many investigators have concluded that, in the case of rocks the neutral axis of bending beams of rectangular cross-section is not located at the middle. Jaeger and Cook[113], mentioned that during the bending the neutral axis moves towards the concave sides of the beam, and this is due to a decreasing value of the Young's Modulus in tension. Datta[12] also concluded that the neutral axis shifts towards the compression surfaces (concave) of the beam, and when the beam fails the neutral plane is near the surface in compression. He also found that total shift of the neutral axis varies with different rocks. Williams and Elizzi[15,16] stated that the stress-strain behaviour of the gypsum in tension and compression are dissimilar, and thus the neutral axis of the gypsum rock is not located at the middle.

In this case, using the formula $\sigma_t = \frac{MC}{I}$ gives incorrect values of the tensile strength of the rocks.

Datta[12] found that

$$\sigma_t = K \frac{M}{bd^2}$$

where K is a constant and much less than 6 as it varies with various rocks. The modified formula suggested by Duckworth[114] and used by Williams and Elizzi[15,16] in finding the tensile strength of the gypsum rock, was also used in this research.

The Duckworth formula is:

$$\sigma_t = \frac{3M(\varepsilon_t + \varepsilon_c)}{bd^2 \varepsilon_t}$$

where

σ_t = Tensile strength at the lower surface of the beam, N/mm^2

M = Applied bending moment, N-mm.

ε_t = Tensile bending strain of the outer lower fibre.

ε_c = Compressive bending strain of the outer upper fibre.

b = Width of the beam, mm.

d = Height of the beam, mm.

3.2.2 Uniaxial Compression Tests.

The uniaxial compression test is the oldest and the simplest rock strength test, and continues to be the most convenient and useful way for determining an index of the properties of the rock. The results of such tests are directly applicable to studies of mining, tunnelling, drilling, cutting, crushing and blasting, and indirectly applicable to consideration of the behaviour of large jointed rock masses. The uniaxial compression test is a special case of the triaxial compression test in which the confining pressure is zero. In the next section a brief description of the testing apparatus and testing procedure with the stress measurement methods used will be given.

3.2.2.1 Uniaxial Compression Apparatus.

A 100 ton Avery Universal testing machine was used for this purpose. This compression machine capable ot applying loads on five different ranges, namely; 50, 100, 200, 500 and 1000 KN. Any constant load rate can be chosen at any particular load range, and this is done by using the marked rotating pacing disc provided with a calibration chart. A spherical seat was used beneath the specimen during the test. Electrical resistance strain gauges of 10 mm gauge length were used for the determination of axial strain and of 5 mm gauge length for the lateral strain measurements.

3.2.2.2 Test Procedure and Stress Measurements.

To test the specimen uniaxially in compression, it is placed on a spherical seat in the compression zone of the universal compression machine. The purpose of this seat is to ensure the intimate contact over the whole specimen end surface between the testing machine platens and the end of the test specimen as the crossheads move together. The load range selected was greater than the expected ultimate strength of the rock to obviate unloading and range changing during the test. In choosing the loading rate, published works on rock testing have been reviewed. It was found that Obert and Duvall[106] stated that the compressive strength increases with loading rate, but that the loading rates between 100-400 psi/sec. gave negligible differences in compressive strength. The U.S. Bur. of Mines[115] specified the rate of loading should be 100 psi/sec. Hawkes and Mellor[11] mentioned that the A.S.T.M.-C170-150 recommendation for rate of loading is that it should not be more than 100 psi/sec and A.S.T.M.-E111-61 reporting "The speed of testing shall be low enough to make negligible the thermal effects of adiabatic expansion or contraction, and high enough to make creep negligible".

On the basis of the above discussion, a rate of loading of 25 $N/mm^2/min$ ($\simeq$ 60 psi/sec.) was used in this study. The same rate of loading used by Elizzi[15] in his tests on evaporite rocks.

Three electrical strain gauges were bonded longitudinally at the middle of the length at 120^o apart around the circumference to measure the axial strain. Six strain gauges were bonded transversely to measure the tangential strain. These were arranged in three pairs,one in the middle and two at the end of the middle third of the specimen. The strain gauges of each pair were bonded at 180^o apart. See Fig. (3.5b). Thus all the gauges were within the middle third of the specimen. It has been reported[11]

that the length of a strain gauge should be at least five times the maximum grain diameter of the rock, longitudinal gauges should not encroach beyond the limit of D/2 of the specimen ends, and in the case of tangential strain, this should be measured within the midportion of the specimen and not closer than D/2 from the specimen ends. These recommendations are met in the tests described and in fact no measurements were made closer than D from the specimen ends.

A Peekel strain gauge indicator type T-200 and Extension Box type 23U (Automation-Peekel N.V. Rotterdam) were used in measuring specimen strains, using the method described in Section (3.1.5) for the connections.

The compressive strength was calculated by using the direct formula:

$$\sigma = \frac{P}{A_s}$$

where σ = Uniaxial compressive strength, N/mm^2.

P = Total applied load, N.

A_s = Cross-section area of specimen, mm^2.

The number of tested specimens, results and discussion will be given in later articles.

3.2.3 Uniaxial Tensile Tests.

Rocks and indeed all brittle materials are inherently weak in tension, and tensile stresses will probably be the cause of rock failure in many cases. It is well known that the tensile stresses play an important role in design of underground openings, particularly in the design of optimum roof span in room and pillars mining, and in the design of bolting and other roof support systems. Knowledge of the tensile strength which is one of the fundamental properties of rock is particularly important from a practical point of view for mining and civil engincers.

It should be possible to determine the tensile strength of rocks either directly or by some indirect method by which failure in tension is induced. In the following sections apparatus and test procedure for the uniaxial tensile strength (direct pull) will be given.

3.2.3.1 Uniaxial Tensile Apparatus.

In these tests 2 ton Hounsfield Tensometer testing machine (Tensometer Ltd., Surrey) was used, see Fig.(3.12). It can be motor driven or manually operated. The specimen chuck attachments are spherically mounted to ensure axial alignment. The pull in the test specimen (tensile load) is transmitted through a tension head to a calibrated spring beam, the deflection of which is proportional to the load. The deflection of the beam is transmitted to a mercury column in a glass tube, the end of the column gives direct reading of the tensile load on a graduated scale lying along the mercury tube. The magnifying cursor slides along the mercury tube and the scale to enable accurate viewing of the mercury movement and the failure load to be performed. This magnification range is from 4:1 to 16:1. Seven different spring beams with seven interchangeable scales graduated to suit the strength of the beam, can be used. These beams correspond to the loads 2 ton, 1 ton, 500 lb, 250 lb, 125 lb and 62.5 lb.

3.2.3.2 Test Procedure and Stress Measurement.

The direct pull tensile test is generally considered as an uncommon test, because of the difficulties of preparing the test specimen, generation of eccentricity in loading and the difficulties in gripping. To avoid these difficulties in this study, regular cylindrical specimens were used and ball joints were used in applying the load to minimize the bending stress transmitted to the specimen and finally to overcome the difficulty in gripping, a method used by Fairhurst[108] in 1961 was used, that is

the cementing of the specimen ends to the steel end pieces having the same cross-section of the specimen. Epoxy-based cement used in recent years has made the bonding of the metal to rock practicable, thus overcoming the difficulty of specimen gripping.

Specimens bonded to the steel platens prepared by the method described in section (3.1.3) were placed in the Housfield Tensometer by inserting the ball jointed nose piece into the platen sockets and ensuring the dowel pins are fully inserted (using ball joint to ensure accurate alignment in loading). The zero loading was adjusted by bringing the mercury to zero load mark. Then the specimen was loaded at a rate of 3.3 $N/mm^2/min$ (480 psi/min). Obert and Duvall[106] reported that the rate of loading of 500 psi/min would be consistent with general practice. The cursor was moved with the head of mercury column during the application of the load, and observing the movement of the mercury was done by using the magnifying glass to ensure the fracture load reading being accurately obtained. Three electrical strain gauges were bonded within the middle third of the specimen length at 120^{o} apart, see Fig. (3.5a). A Peekel strain gauge indicator was used to measure the strain variation (method of connecting the strain gauge with the meter described in Section (3.1.5)). Tensile load-strain measurements were thus done during the test to provide the uniaxial tensile stress-strain behaviour of dry and saturated gypsum. Finally, the fracture load and maximum strain were recorded at the specimen failure.

Uniaxial tensile stress was determined by using the general direct equation

$$\sigma_t = \frac{P}{A_s}$$

where: σ_t = Uniaxial tensile stress, N/mm^2.

P = Applied load, N.

A_s = Cross-sectional area of the specimen, mm^2.

The number of specimens tested, results and discussion of these will be given in the next chapter.

3.2.4 Triaxial Compression Tests.

Knowledge of the strength and physical properties of rocks aid in the design of more economical structures. Knowing the strength behaviour of rocks in triaxial stress conditions is important in problems of roof control and other aspect of rock working underground. The first attempt to determine the strength of rock under condition similar to its natural confinement began more than 75 years ago when Adam and Nicholson[17] in 1901 applied axial load to core sample of marble which was surrounded by a tight fitting steel cylinder. Many serieses of work have been done in this field[18] since that time. Von Karman used liquid to surround the specimen and apply confining pressure through it in 1911, U.S. Bureau of Reclamation in 1950 jacketed the specimen of rock by a rubber membrane and found this a suitable way to protect it from the surrounding oil effects, and since then many variable parameters have been studied in various cases of the triaxial stress condition. In this section triaxial stresses were applied by the author to core specimens of two different sizes with gypsum under both dry and saturated conditions.

3.2.4.1 Triaxial Apparatus.

The Apparatus used by Murrell[116] and Elizzi[15] for testing many types of rock was used in this study, a brief description of the apparatus follows:

The apparatus consists of a triaxial cell and hydraulic pressure system. The cell was designed and built to test the rock samples under confining pressure up to 400 N/mm^2 (60000 psi), the base of the cell and the load piston were designed for a maximum specimen diameter of 31.75 mm (1.25 inch). The specimen was placed between two loading blocks of

stainless steel, flat in the sides in contact with the specimen and spherical in the opposite side of the upper block which was matched to a spherical depression in the piston, to ensure full contact between the specimen ends and the platens. A valve located at the top of the cylinder allowed air to escape as the cell was being filled with hydraulic fluid through the entry port through the base. View of the cell shown in Fig. (3.13). The pressure control system consists of electrically driven pump which was used to provide the hydraulic pressure and system of pressure valves. These valves are stop valves, needle valves, and pressure control valves. Pressure was adjusted and controlled at a constant level during each test at pre-determined values. The maximum confining pressure can be obtained directly in this system is 60 N/mm^2. (≈ 9000 psi). Fig.(3.14) shows the hydraulic circuit of the apparatus. High pressures require the use of hydraulic intensifier.

3.2.4.1.1 Calibration of the Apparatus.

The apparatus was calibrated to find the friction force which was created when pushing the ram by vertical load while the confining pressure has been applied. The following procedure was used. The cell was placed in the testing machine, then filled with oil, a chosen confining pressure was applied and kept constant, followed by applying the vertical load to push the ram slowly into the pressure cell against the confining pressure. Then the friction force calculated as:

(Vertical force to push the ram) - (Upward force acting on the ram due to confining pressure).

The same procedure was repeated for a set of confining pressures, from which friction force with the confining pressure relation was found, see Fig.(3.15).

3.2.4.2 Test Procedure.

Specimens prepared using the method described in Section 3.1.1.4 with an enclosing rubber membrane was placed inside the triaxial cell between

the platens. The cell was then closed and placed in the compression zone of the Universal Avery Compression machine. After filling the cylinder with hydraulic fluid by means of the pump, the confining pressure was raised to the required value (at which it was then maintained constant by the needle valve). Then vertical load was applied by the compression machine at a rate of 25 $N/mm^2/min.$ up to specimen fracture or plastic deformation. The vertical load was then decreased gradually followed by the confining pressure. The specimen was removed from the cell and photographed showing the fracture and/or plastic deformation.

In the case of testing a specimen of 25.4 mm dia x 76.2 mm long, the applied axial load calculated using the equation:

$$P = F_m - (F_d + F_f)$$

where:

P = The actual axial load applied on the specimen, N.

F_m = The axial load applied on the ram of the cell which can be read directly on the testing machine dial, N.

F_d = Upward force due to the effect of confining pressure acting on the difference between the cross-sectional area of the ram and the specimen, N.

F_f = The friction force between the ram and the oil seal at that value of confining pressure which can be determined from Fig. (3.15), N.

And in the case of specimen of 31.75 mm dia by 95.25 mm long when the diameter of the specimen is similar to the ram diameter, the axial load is calculated from the equation:

$$P = F_m - F_f$$

FIG. (3-1) DIAMOND CUT-OFF SAW

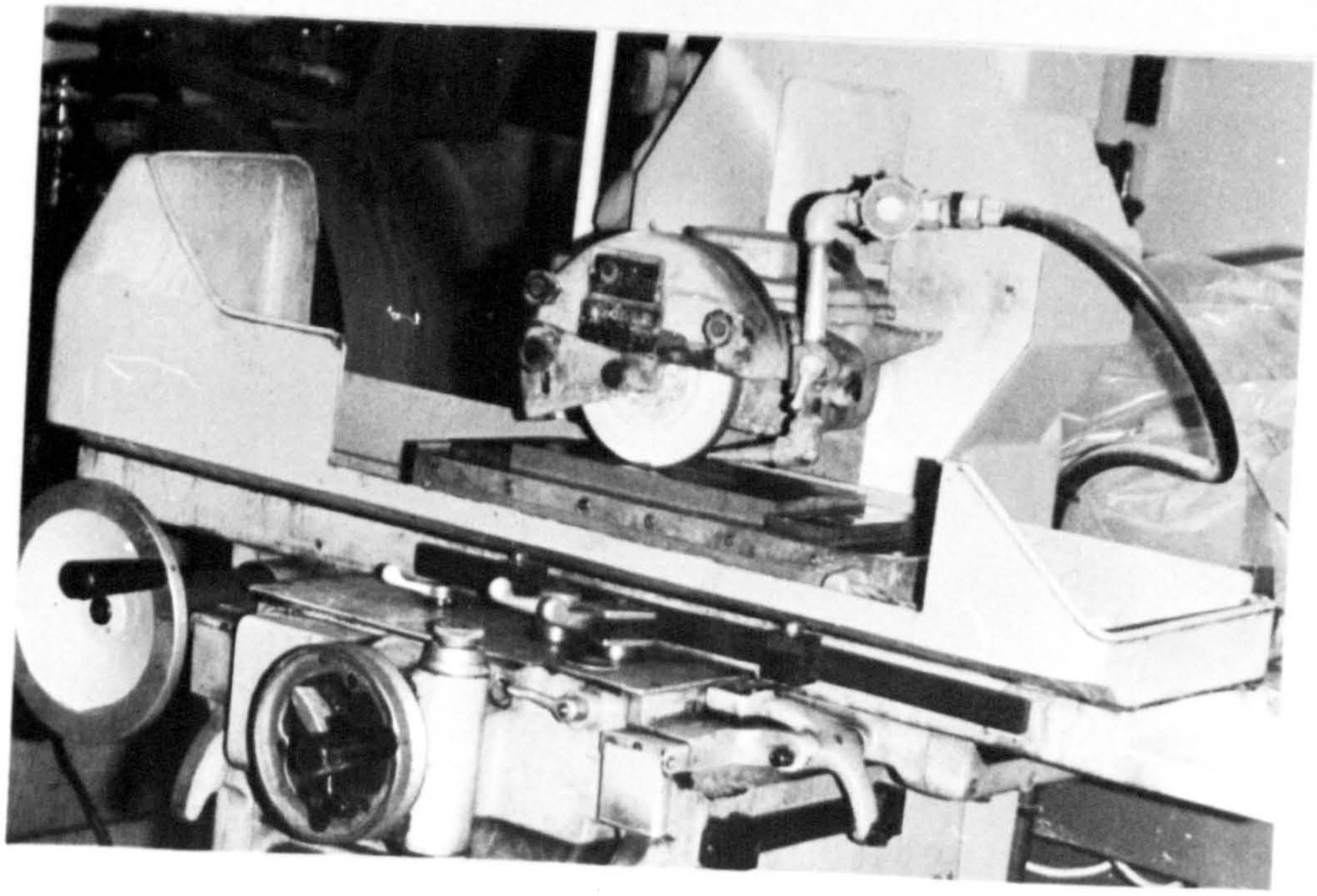

FIG. (3-2) SURFACE GRINDER

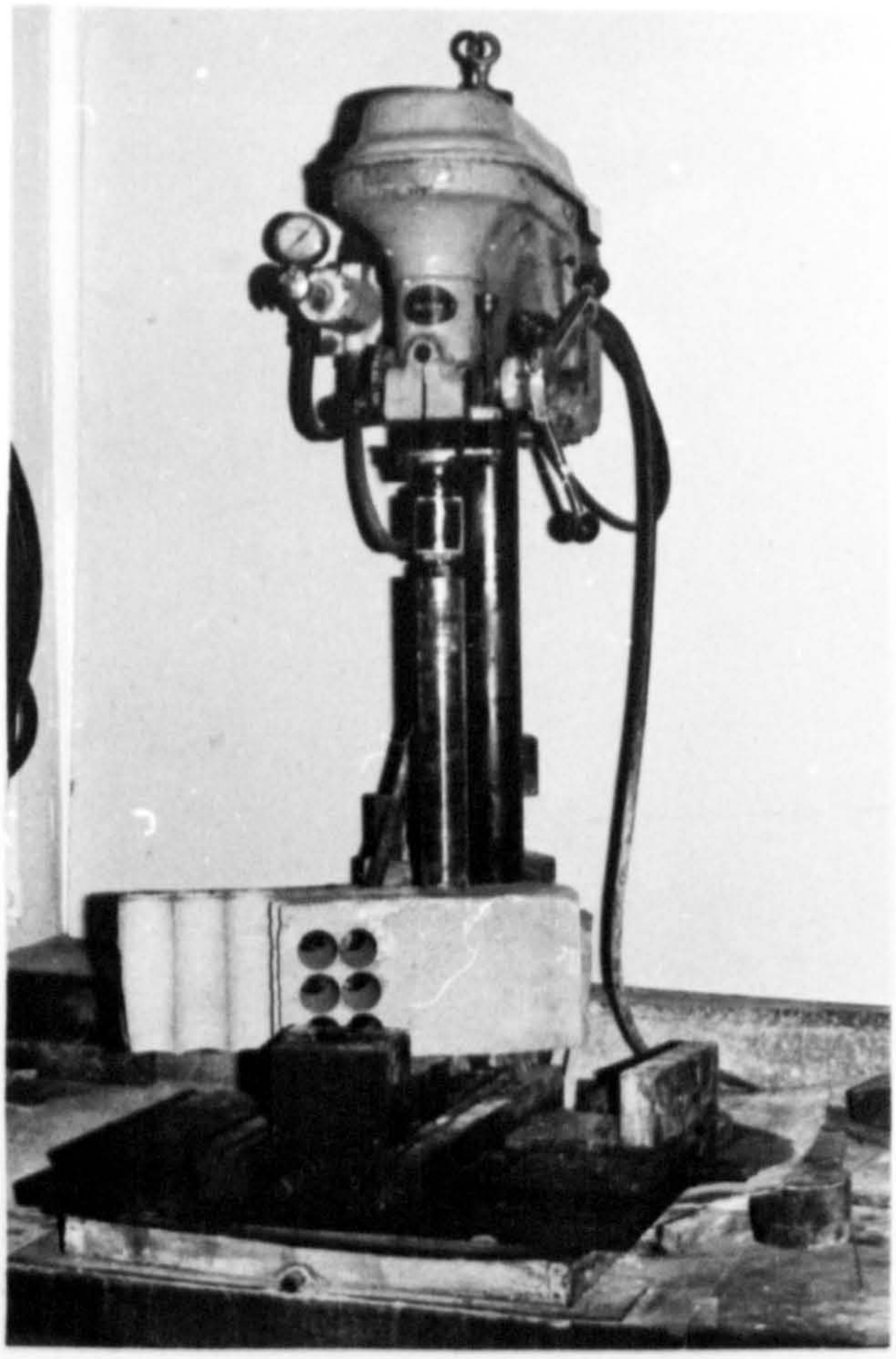

FIG. (3-3) BLOCK OF ROCK ON THE DRILLING MACHINE BENCH

FIG. (3-4) TREATMENT OF SPECIMEN ON THE LAPPING MACHINE

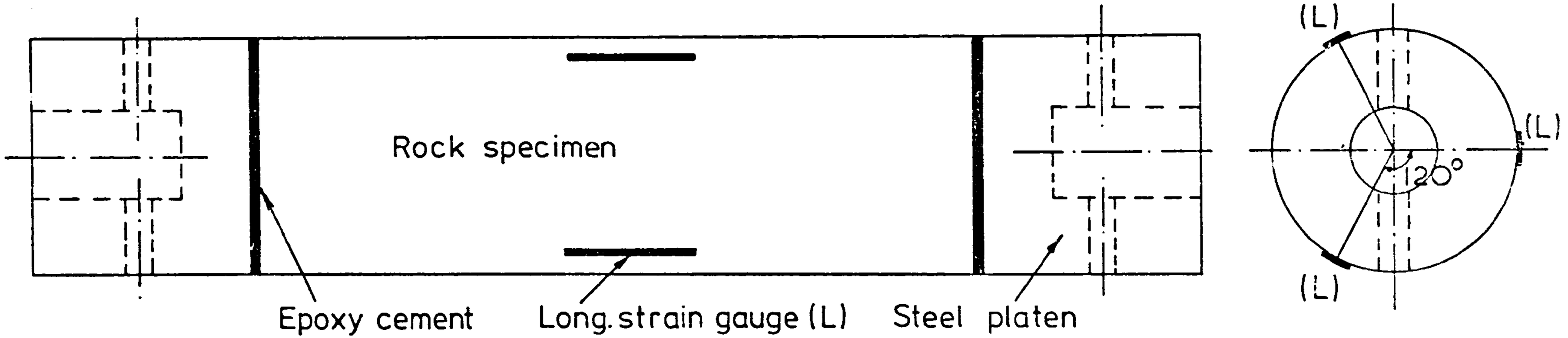

a. Tensile test specimen

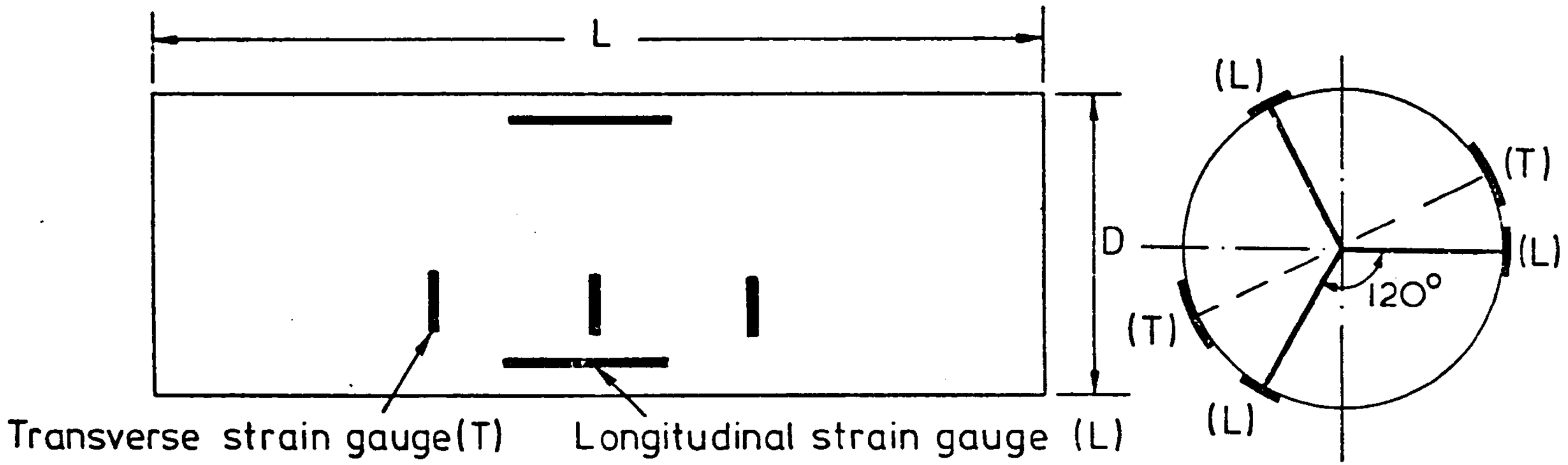

b. Compression test specimen

FIG. (3-5) UNIAXIAL TENSILE AND COMPRESSION SPECIMENS

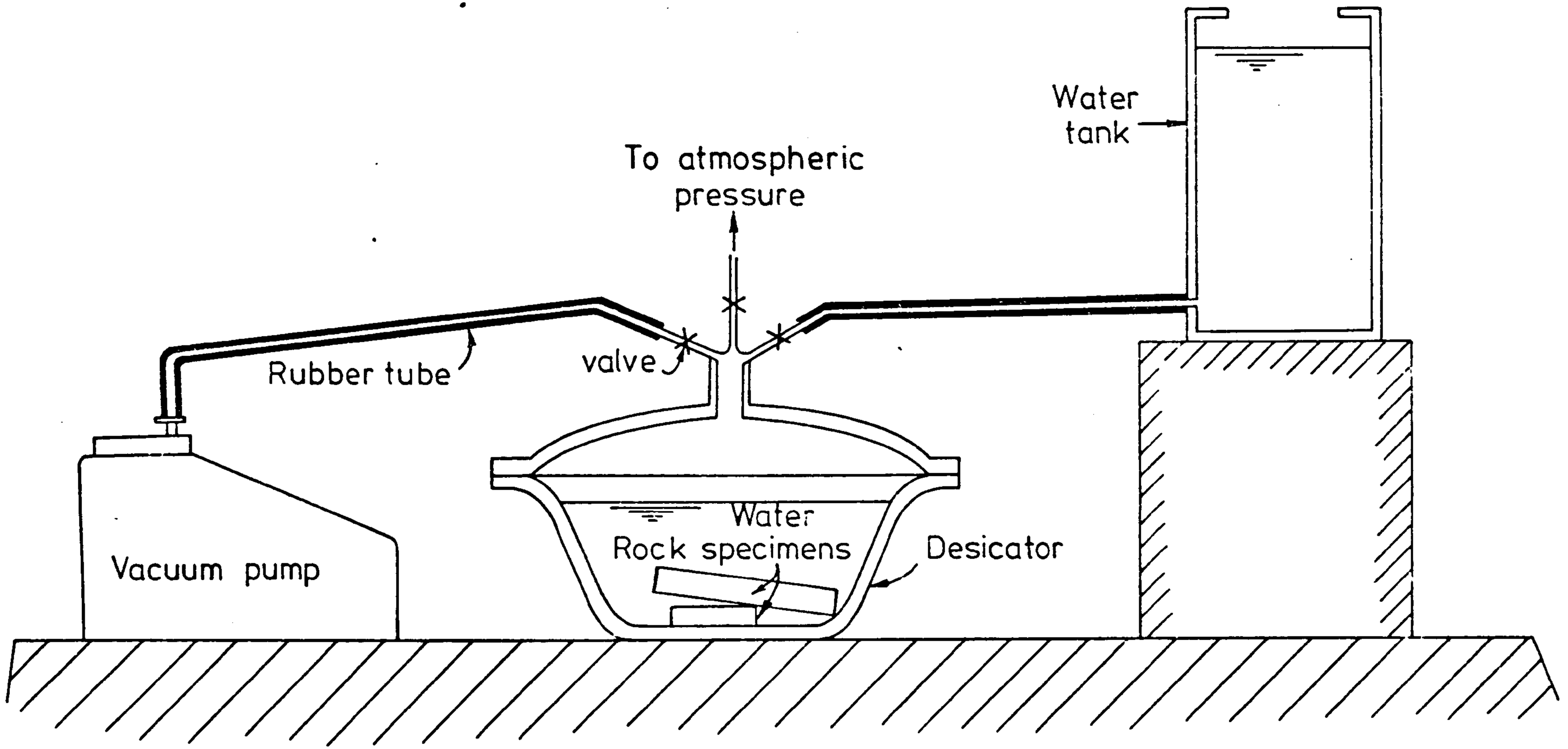

FIG. (3 – 6) ELEVATION OF SATURATION APPARATUS

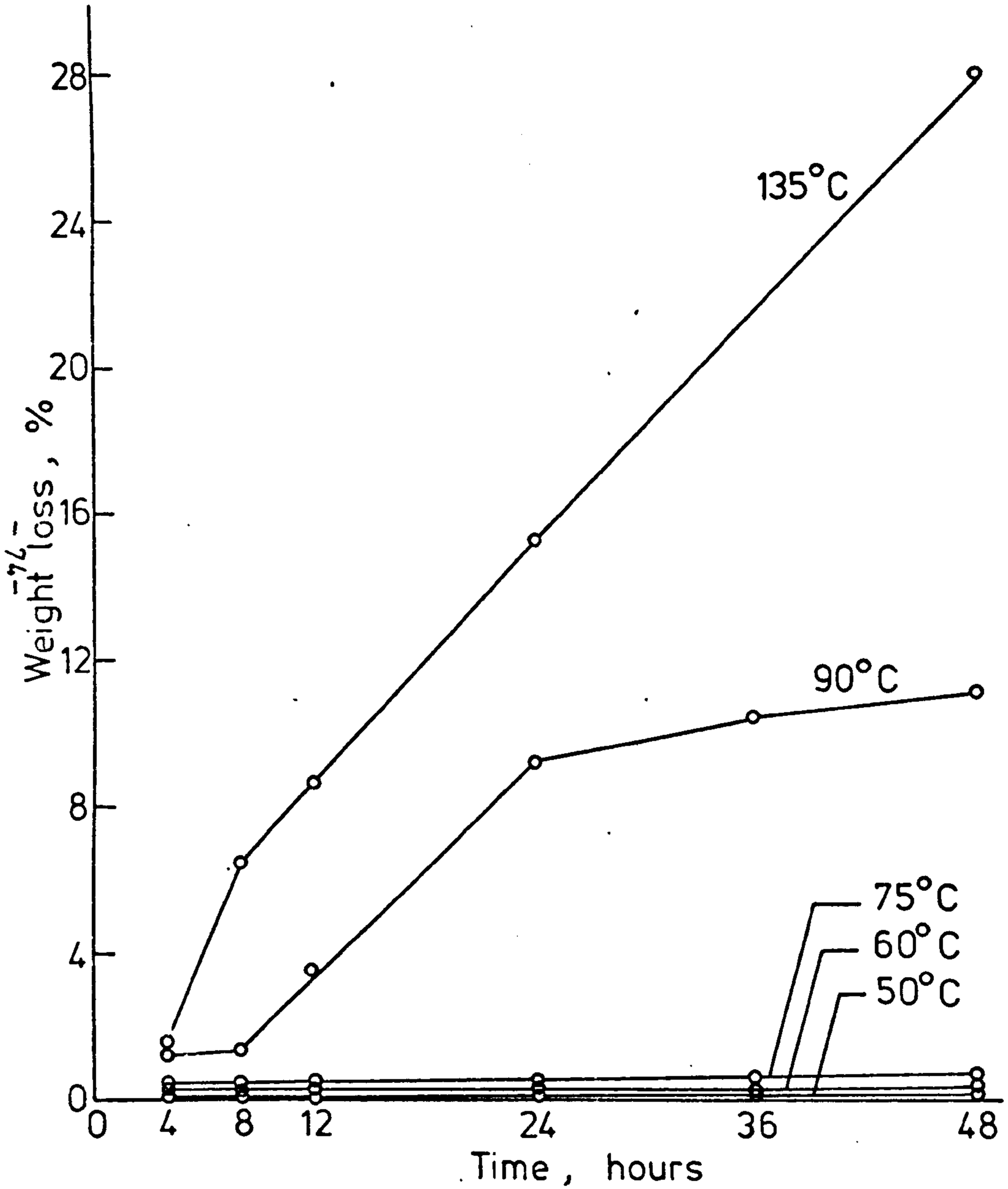

FIG. (3-7) WEIGHT LOSS Vs TIME AT VARIOUS TEMPERATURES

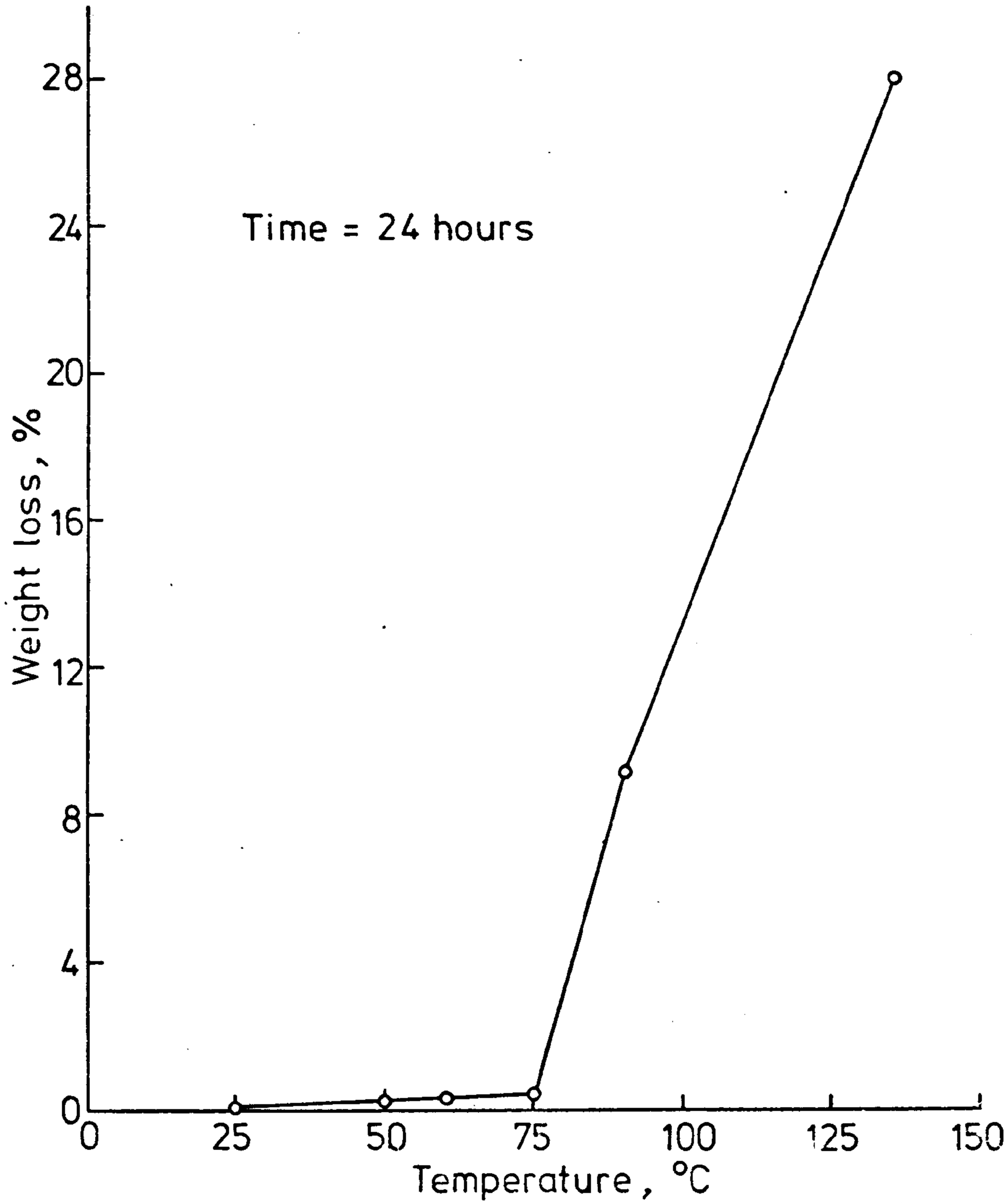

FIG. (3-8) WEIGHT LOSS Vs TEMPERATURE

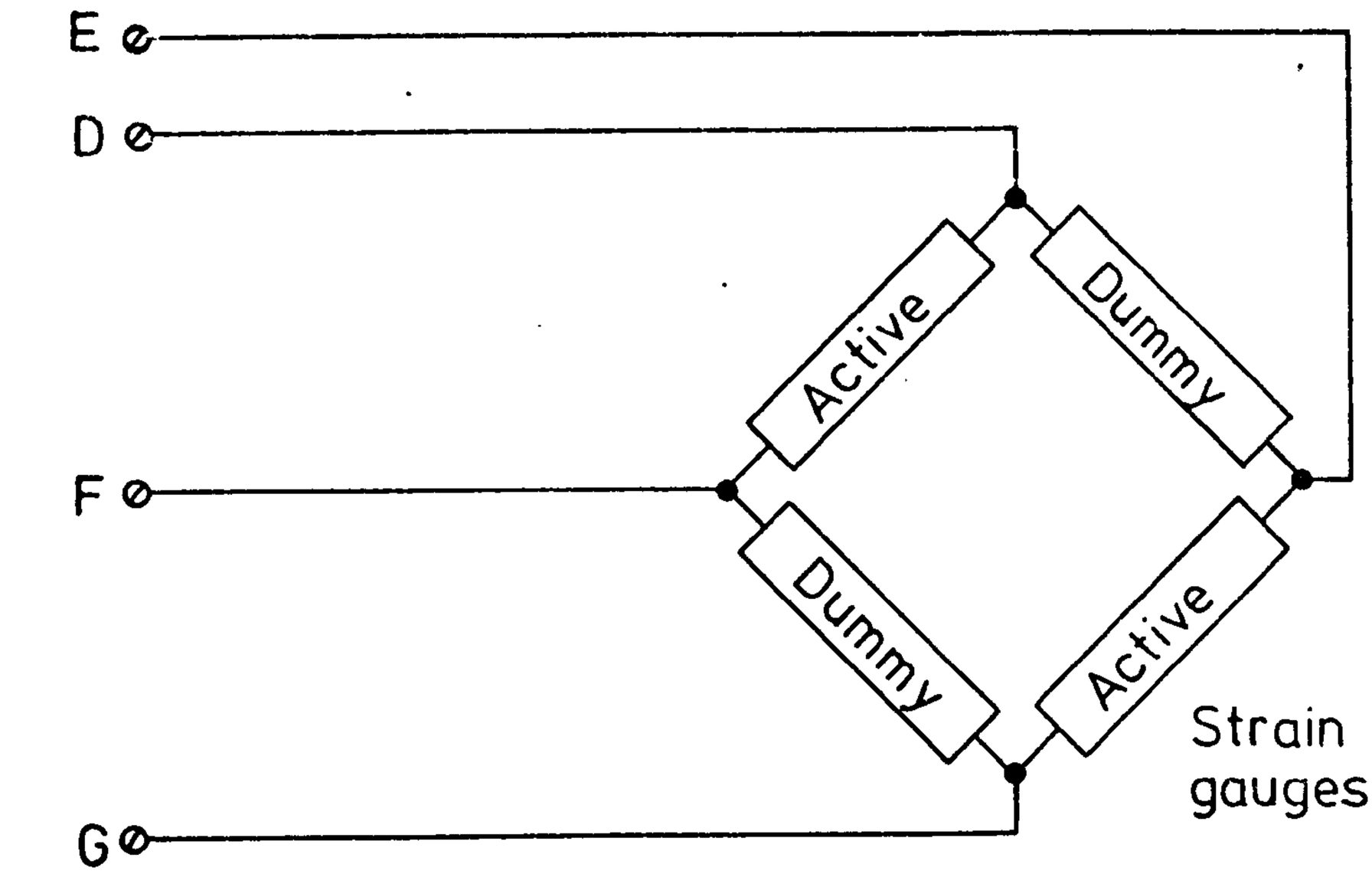

a. Full bridge circuit

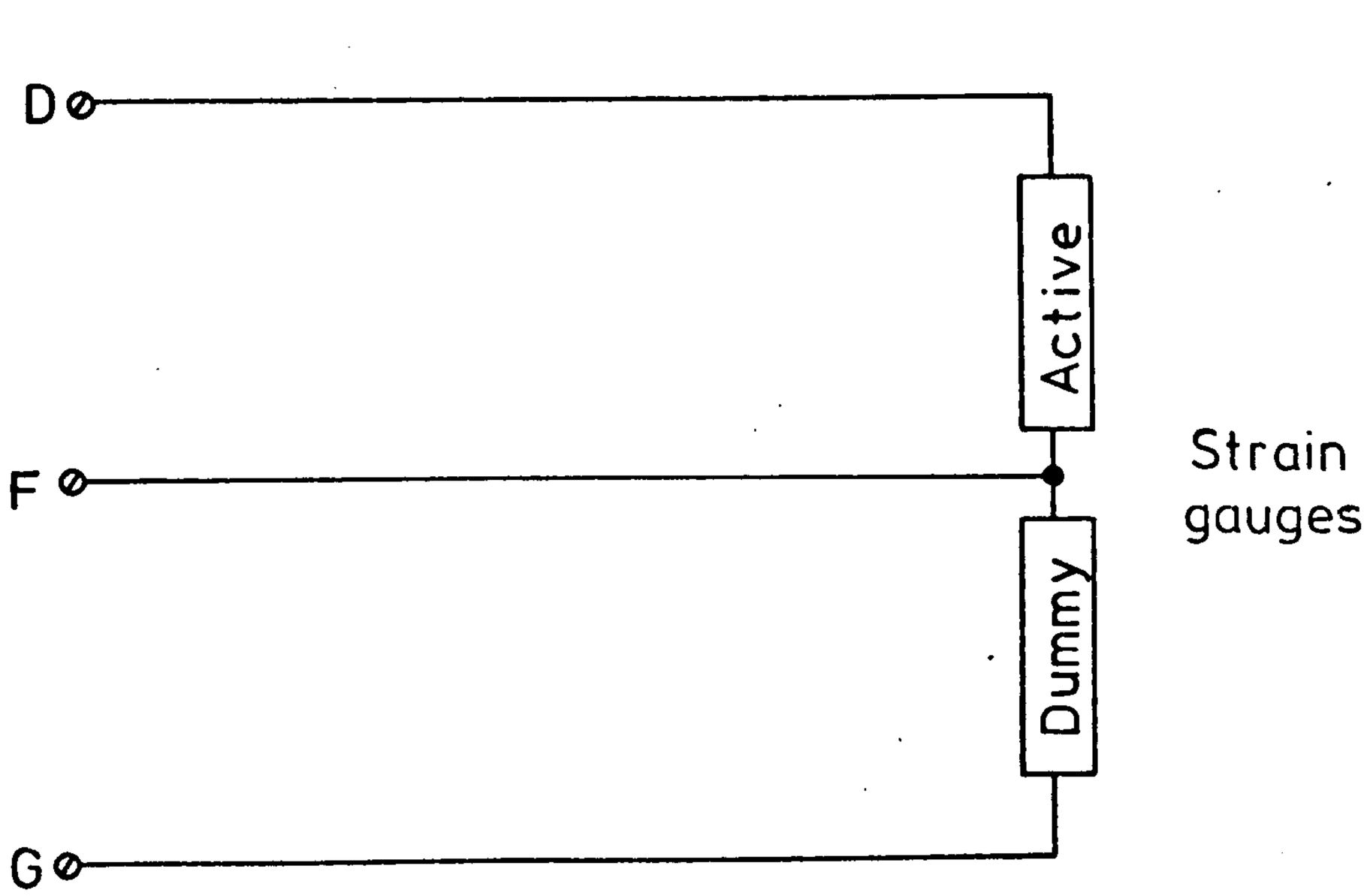

b. Half bridge circuit

FIG. (3-9) CONNECTION OF STRAIN GAUGES

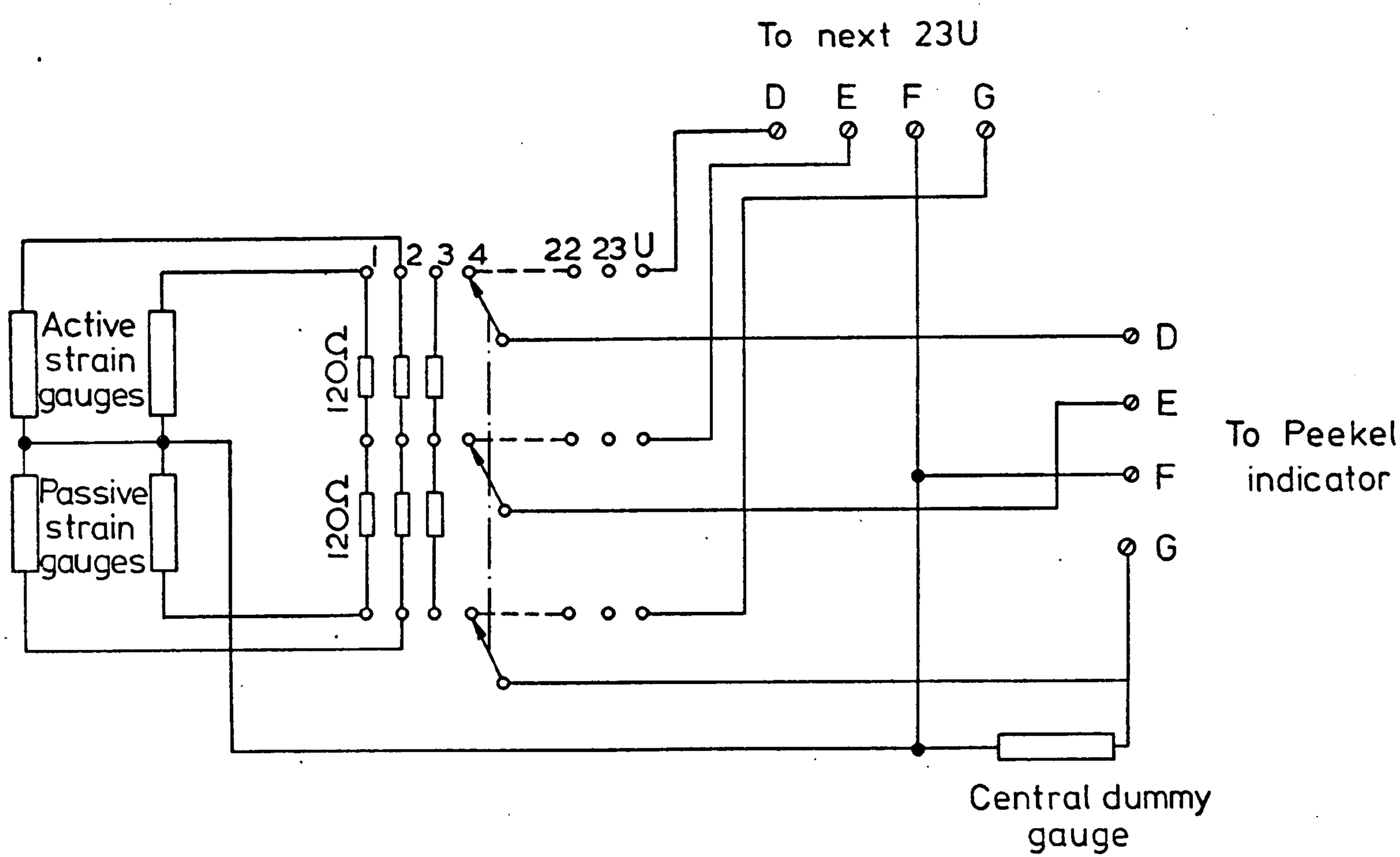

FIG. (3–10) CIRCUIT OF THE EXTENSION BOX

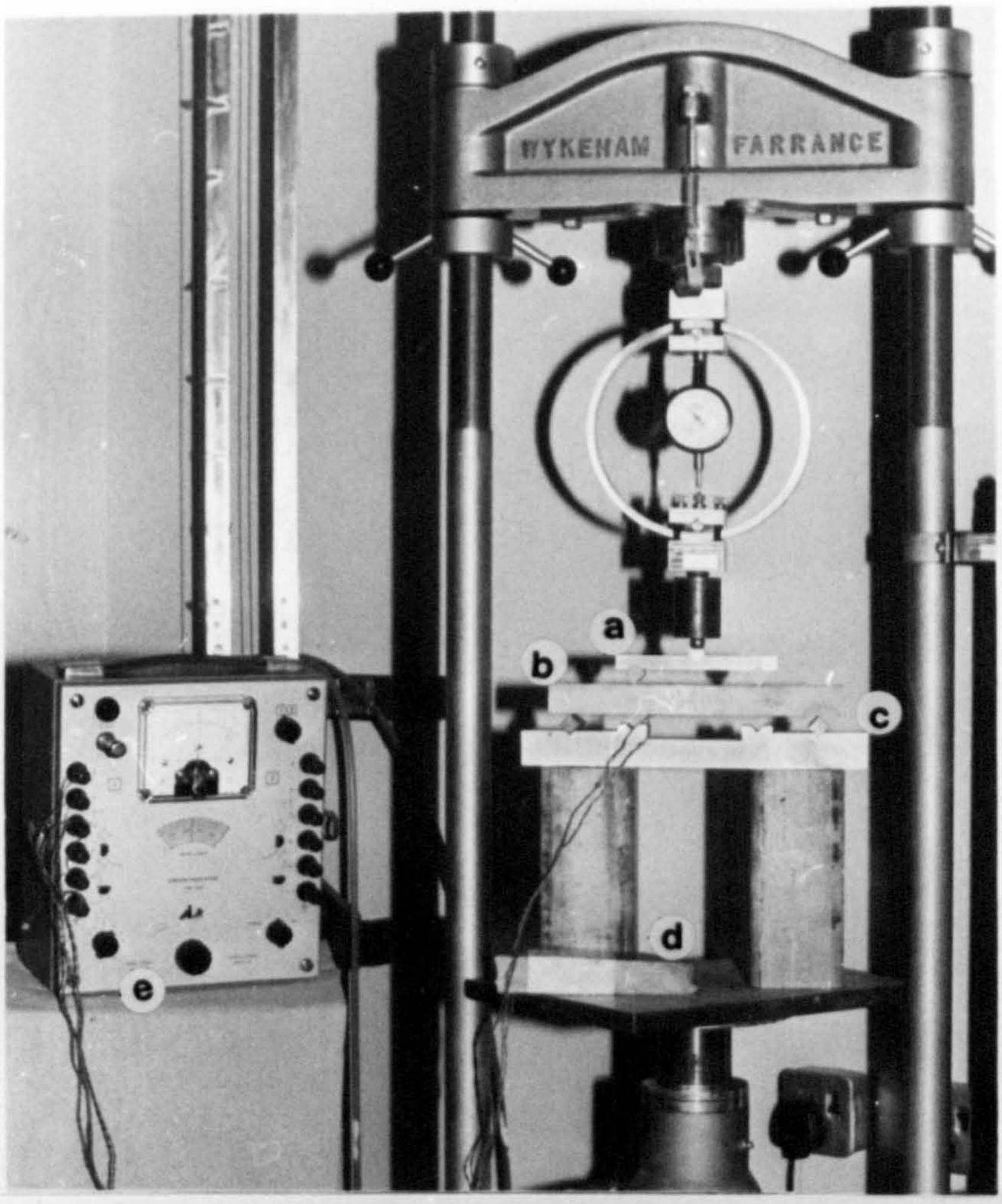

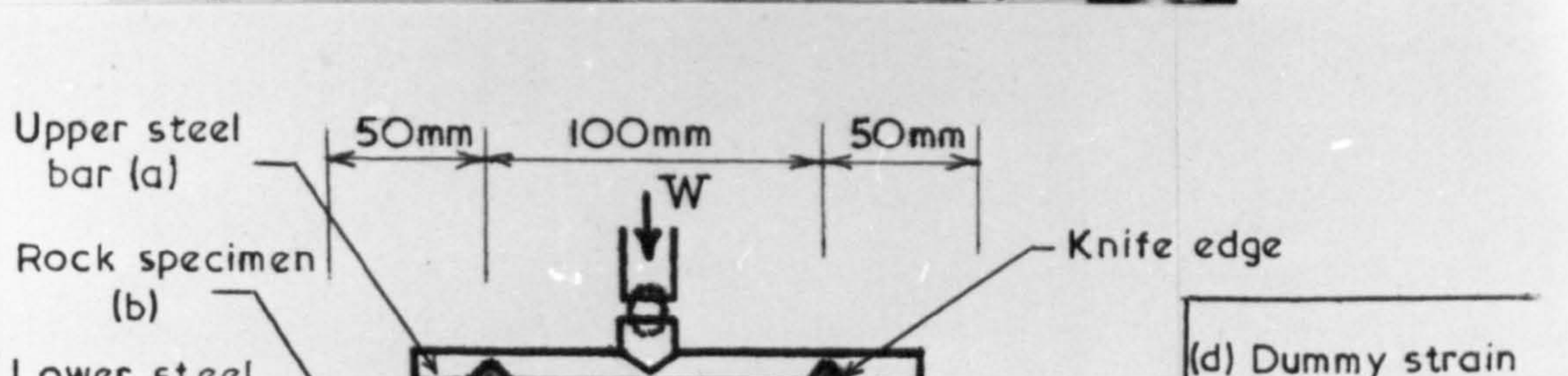

FIG. (3-11) BENDING TEST IN PROGRESS

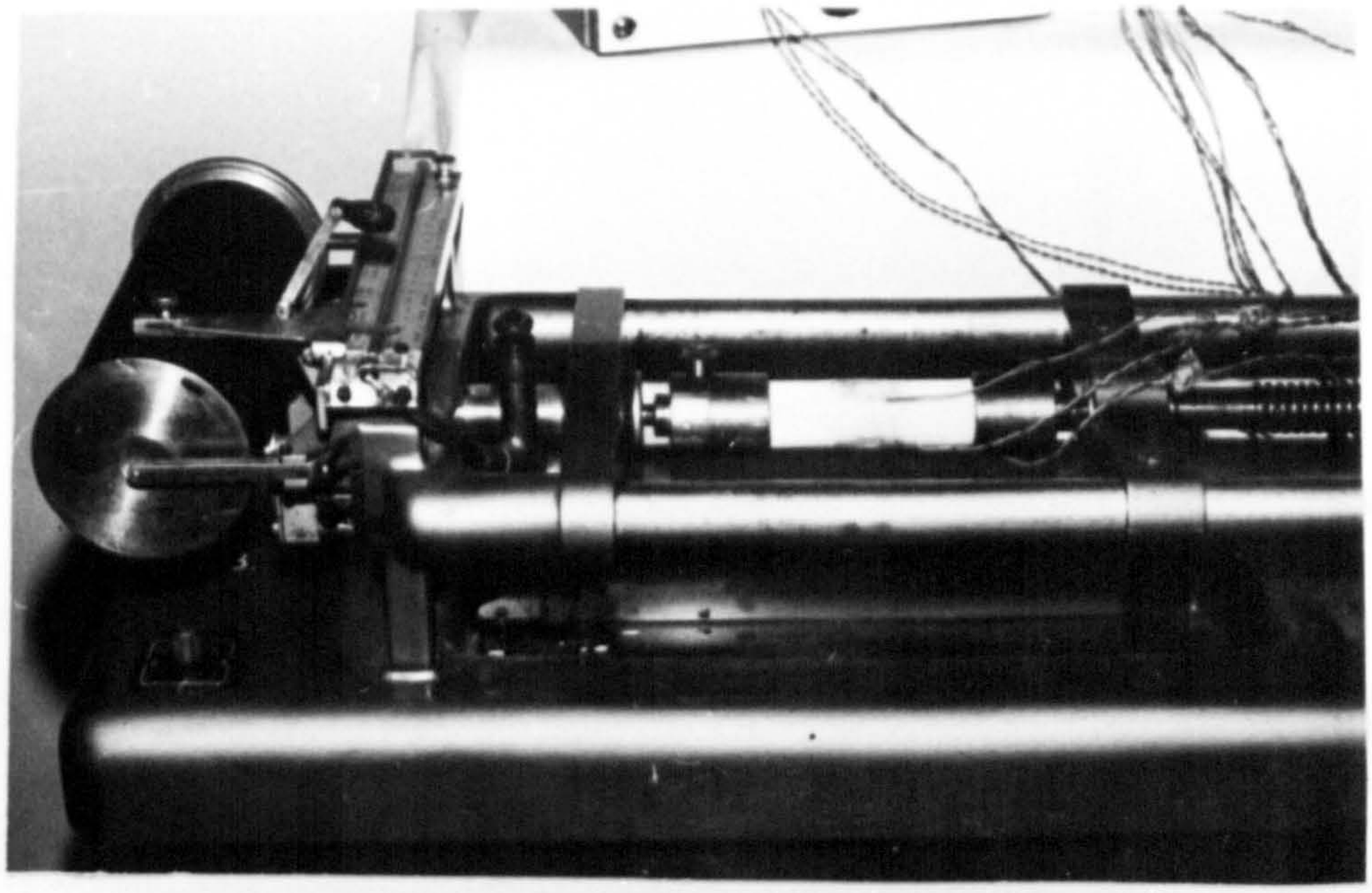

(A) Specimen in position

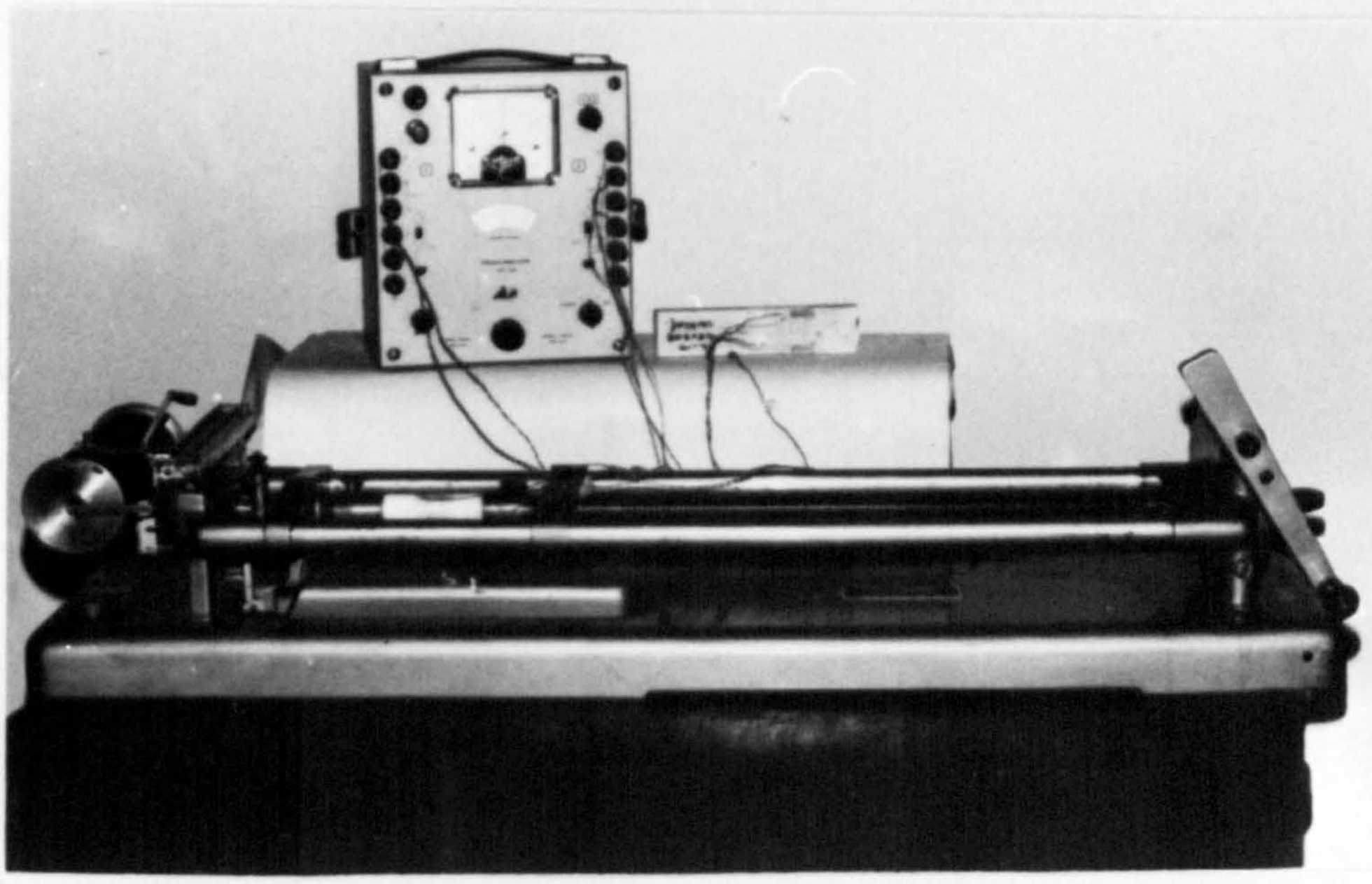

(B) Tensometer and Peekel indicator

FIG. (3-12) UNIAXIAL TENSILE TEST IN PROGRESS

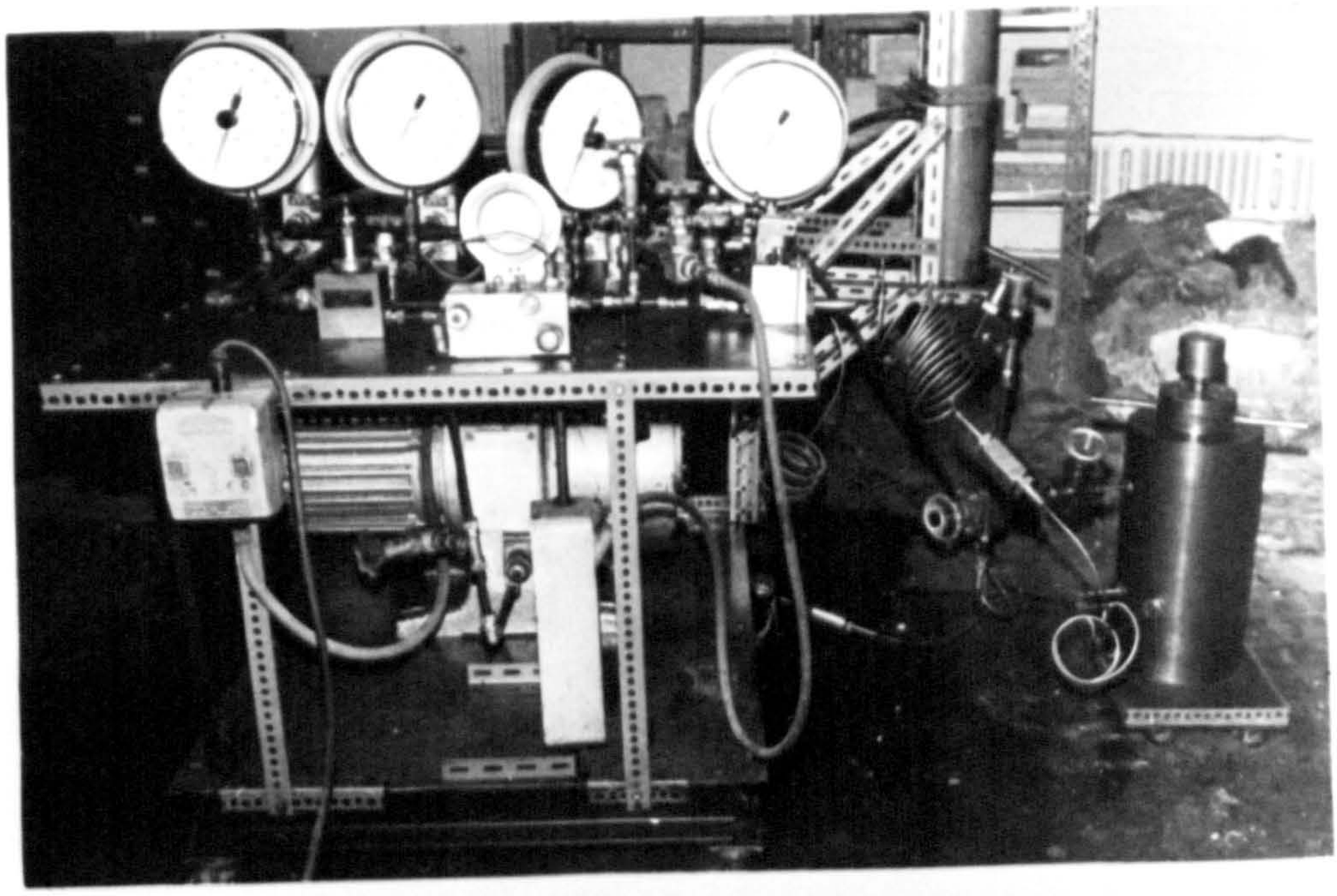

(A) General view

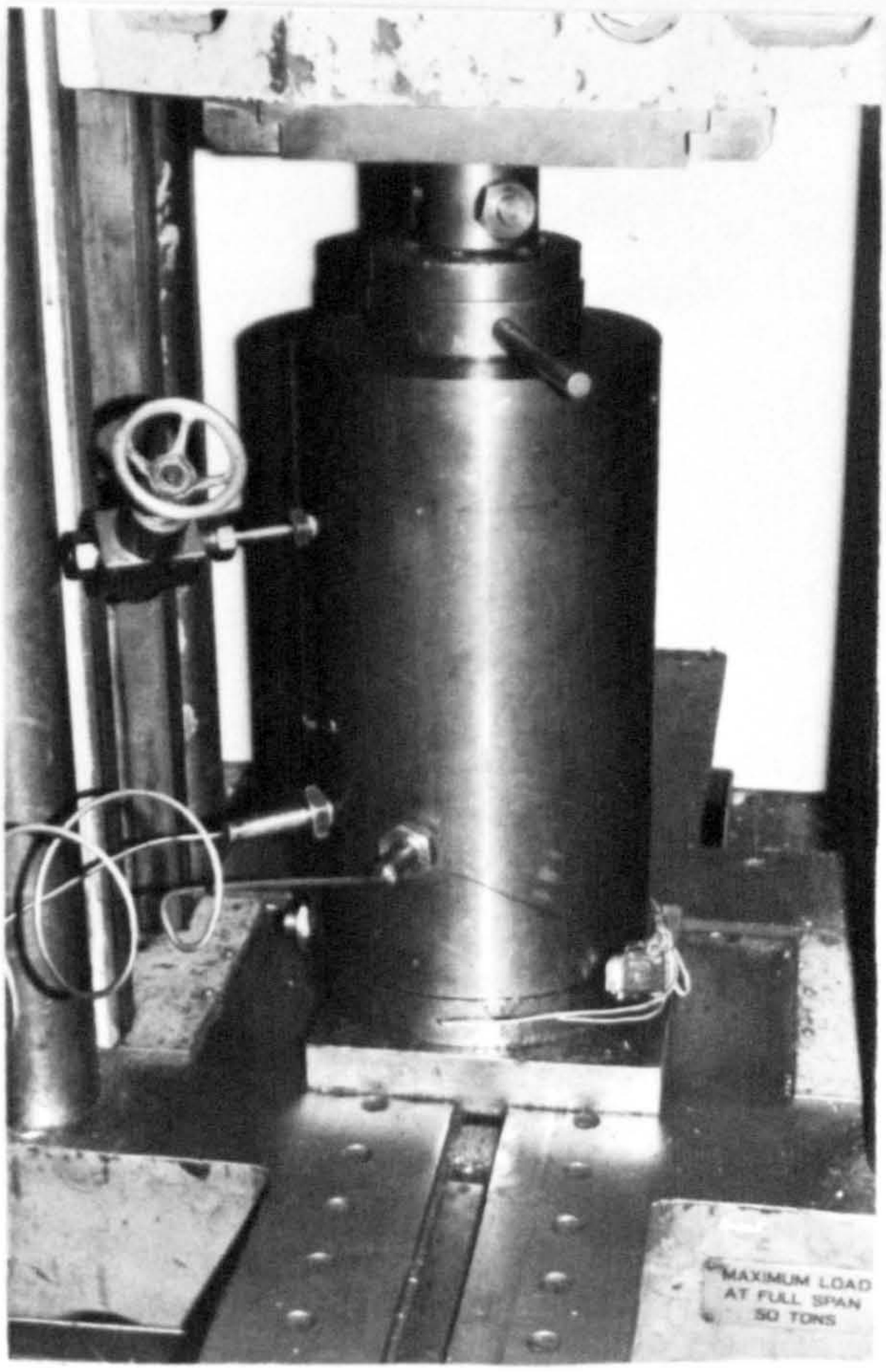

(B) Triaxial cell

FIG. (3-13) TRIAXIAL TESTING APPARATUS

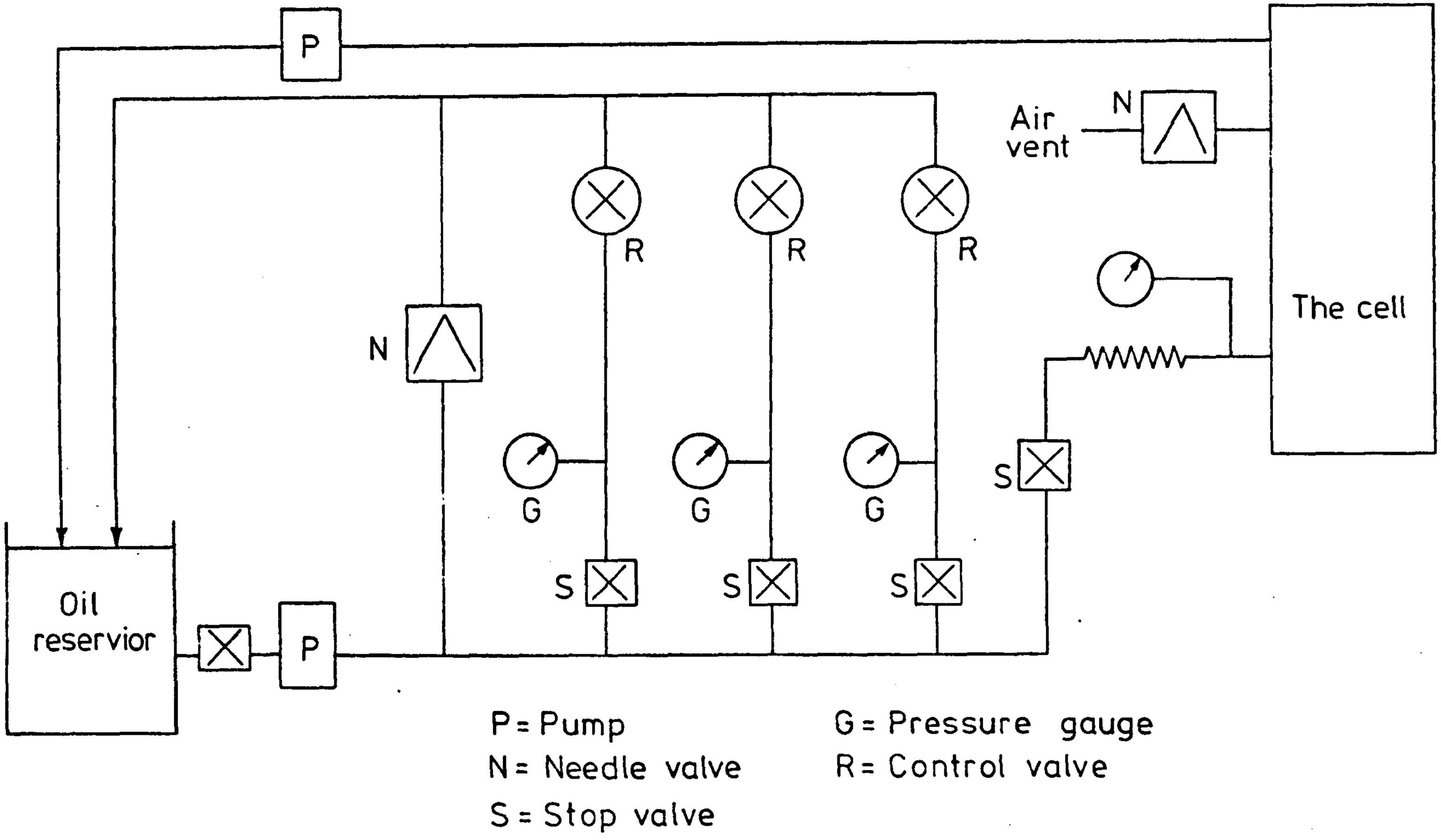

FIG. (3-14) HYDRAULIC CIRCUIT OF TRIAXIAL APPARATUS

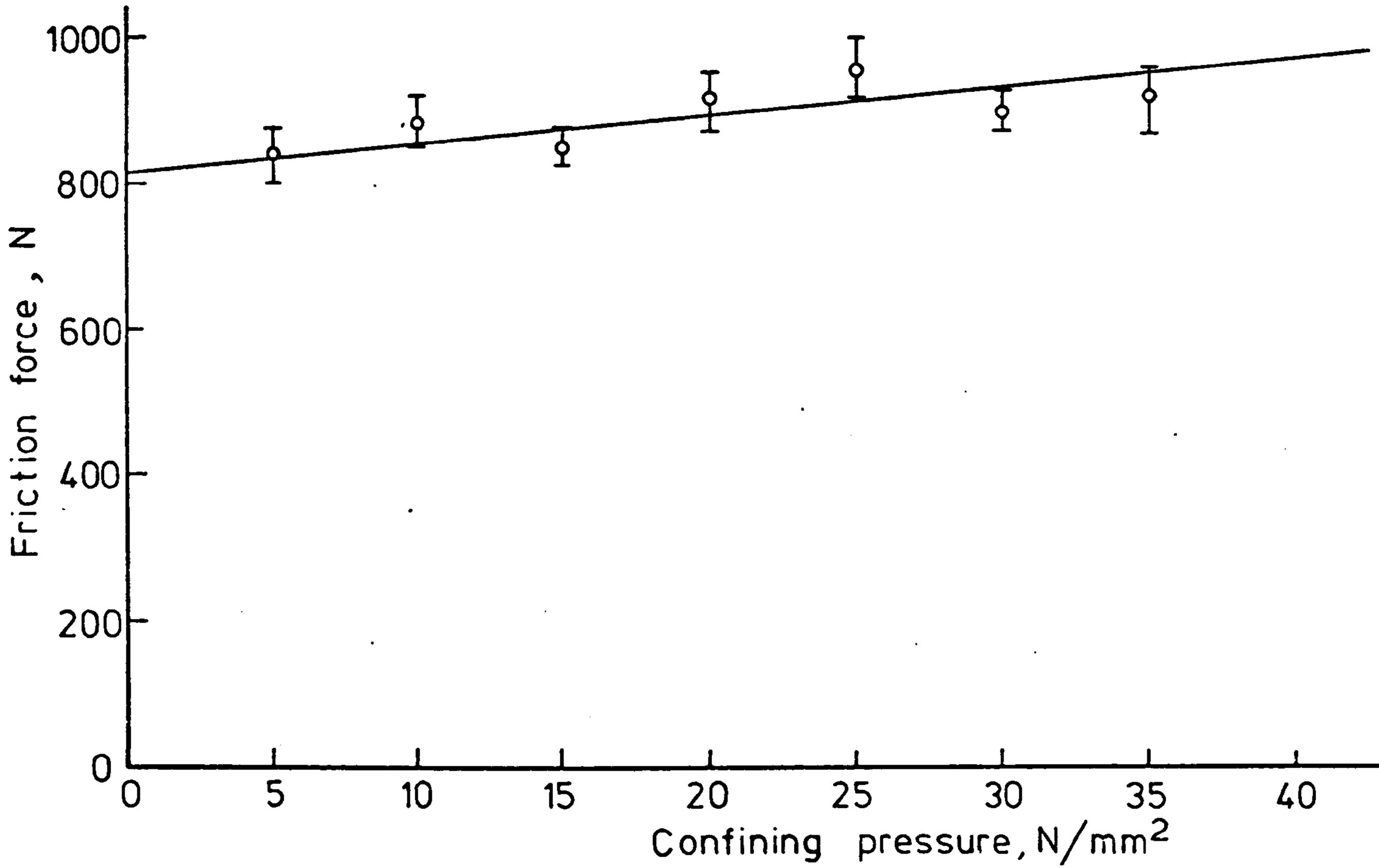

FIG. (3-15) FRICTION FORCE FOR TRIAXIAL CELL AT VARIOUS CONFINING PRESSURES

Chapter 4.

RESULTS AND DISCUSSION OF SHORT TERM TESTS.

Although the main aim of this research is to study the creep behaviour of the dry and saturated gypsum, it is essential to introduce the compressive and tensile strength results of gypsum related to factors influencing these strengths (specimen size and saturation) in order to make clear the relationships between the short term properties and the long term behaviour of this rock.

4.1 Bending.

Many specimens were tested using four point loading in dry and saturated conditions, at various rock beam thicknesses. Beam dimensions were 240 mm long by 40 mm wide with four different thicknesses varying from 15 mm to 28 mm (15, 20, 25 and 28 mm). All tests carried out at room temperature (21 ± 2^{o} C).

The measured tensile and compressive strains of all beam specimens showed that the tensile strain (at lower surface) is greater than the compressive strain (at upper surface), see Figs. (4.1) and (4.2). This indicated that the position of the neutral axis is nearer the compression side, not at the centre of the beam, and as load increases it keeps on moving towards the upper surface. This is in agreement with Datta's[12] results on beams of sandstone, granite and marble, he reported that the neutral axis is not in the centre and it moves up from the tension side to compression side as the load increases. Whereas Williams and Elizzi[15,16] found in some of the gypsum and anhydrite beam specimen that the neutral axis is nearer the tension side.

In each of the Figs. (4.3) and (4.4) the stress-tensile strain of four gypsum beams tested under the same conditions of dimensions, direction

of loading, rate of loading and humidity are given for dry and saturated conditions respectively. It can be seen that there is a noticeable variation in their behaviours. This is presumably due to petrological differences in these beams, i.e. grain sizes, cementing material, inhomogeneity, etc.[15].

4.1.1 Specimen Size Effects.

Tables (4.1) and (4.2) give the tensile strength calculated from the bending observations in dry and saturated conditions respectively. The mean values and standard deviations of the strength of each specimen size are given. Table (4.3) gives the summary results related to the specimen size effect. It can be seen that the tensile strength decreases with increasing specimen size (increasing the thickness).

This reduction is of the order of 8 percent in the case of dry specimens and 9 percent in the case of saturated specimens within the tested specimen size (thickness varies between 15 mm to 28 mm). Fig. (4.5) shows the relation between the tensile strength and beam thickness. A considerable drop in strength is shown with increasing size in the case of smaller specimens but little reduction is shown with larger specimen sizes in both dry and saturated conditions. The investigators; Berenbaum and Brodie[3], Pomeroy and Morgans[2] and Evans[4] have also reported a decrease of tensile strength from bending with increasing the specimen size. Hardy et al.[13,14] found that flexural strength is not a material property in rocks, it varies with the specimen geometry and there is no unique trend for the size-strength relationship.

The reduction of the strength with specimen size obtained by the author seems to agree with Pomeroy and Morgans[2] explanation of this which states; that the failure is a function of gross weaknesses in the specimen, that the rock (coal) is ramified with weaknesses of various

Table (4.1) Results of bending tests (Dry)

Beams of 240 x 40 x d (L x bxd), mm.

Beam Thick. (d), mm	Specimen No.	Tensile Stress at bottom surface N/mm^2	Mean N/mm^2	S.D.*	Beam Thick. (d), mm	Specimen No.	Tensile Stress at bottom surface N/mm^2	Mean N/mm^2	S.D.*
15	15D-1 15D-2 15D-3 15D-4 15D-5 15D-6	8.97 8.32 8.45 8.13 8.22 9.00	8.52	0.38	25	25D-1 25D-2 25D-3 25D-4 25D-5 25D-6	7.69 8.42 8.53 8.12 7.00 7.62	7.90	0.57
20	20D-1 20D-2 20D-3 20D-4 20D-5 20D-6	7.70 7.40 8.30 8.50 8.10 8.10	8.02	0.40	28	28D-1 28D-2 28D-3 28D-4 28D-5 28D-6	8.52 8.31 6.80 7.62 7.12 8.54	7.82	0.75

*S.D. - Standard deviation.

Table (4.2) Results of Bending tests (Saturated)

Beams of 240 x 40 x d (L x b x d), mm.

Beam Thick. (d)mm	Specimen No.	Tensile Stress at bottom surface N/mm^2	Mean N/mm^2	S.D.	Beam Thick. (d)mm	Specimen No.	Tensile Stress at bottom surface N/mm^2	Mean N/mm^2	S.D.*
15	15S-1 15S-2 15S-3 15S-4 15S-5 15S-6	6.31 5.78 5.29 5.93 7.11 4.62	5.84	0.85	25	25S-1 25S-2 25S-3 25S-4 25S-5 25S-6	5.13 6.25 5.58 5.68 4.89 4.98	5.42	0.52
20	20S-1 20S-2 20S-3 20S-4 20S-5 20S-6	6.00 5.62 5.35 5.30 5.69 5.54	5.58	0.26	28	28S-1 28S-2 28S-3 28S-4 28S-5 28S-6	5.40 4.96 5.10 6.64 4.45 5.47	5.34	0.74

*S.D. - Standard deviation.

Table (4.3) Effects of Specimen Size and Saturation on Bending Results.

Specimen Size (L x b x d) mm	Tensile Strength N/mm^2		Reduction due to Saturation %
	Dry	Saturated	
240 x 40 x 15	8.52	5.84	31.46
240 x 40 x 20	8.02	5.58	30.42
240 x 40 x 25	7.90	5.42	31.39
24 x 40 x 28	7.82	5.34	31.71

magnitudes so that once the largest has been eliminated the next largest confers only slightly greater strength and so on. Further a large specimen is more likely to contain a gross weakness than a small one and so is likely to have a lower strength. Figs. (4.1) and (4.2) show that there is some effect of the specimen size (thickness) on the stress-strain behaviour at both tension and compression sides of the specimen for dry and saturated gypsum respectively. The effect is of decreasing the strains with increasing the beam thickness at any particular stress. It is in agreement with Hardy et al.'s[13,14] theoretical and experimental conclusions, which stated that if the size of the beam is changed the complete force-displacement curve will not be proportionately scaled for two reasons; the microstructures always have the same absolute dimensions, and thus the length of any pre-existing cracks is not proportionately scaled, and, the work of fracture associated with a given relative increment in crack length is not constant, thus the correspondence of the required energy (as a function of area) with the available energy (as a function of volume) is no longer the same.

4.1.2 Saturation Effects.

In order to give a clear idea about the effect of the saturation on the tensile strength of the gypsum in bending, six specimens at least for each of the four mentioned sizes were saturated with water, and the tensile strength as well as stress-strain relationship in tension and compression were determined. Table (4.2) gives the details of strength results for all specimen sizes with means and standard deviations. Table (4.3) gives the summary results compared with dry specimen results. Fig.(4.5) gives the relationship between tensile strength and specimen size, and a comparison between dry and saturated conditions. It can be seen that the saturation by water decreases the tensile strength of gypsum by

about 30 to 32 percent for all given specimen sizes. It seems that the reduction of the tensile strength due tc saturation is not influenced by changing the specimen size. The saturated specimens showed a greater strain at both tension and compression surfaces than that of the corresponding dry specimens at any particular stress, see Fig. (4.2).

Reducing of the resistance to rupture and the increasing strain due to saturation could be explained as a lowering of the surface free energy [51,54]. The tensile strength (σ_t) of the material is directly related to the molecular cohesive strength which is proportional to $\sqrt{\gamma}$, where γ is the surface free energy of the rocks (Griffith's equation: $\sigma_t = (\frac{2E\gamma}{\pi C_o})^{\frac{1}{2}}$, E - Young's Modulus and C_o the half length of the so called Griffith's crack assumed to be exist). The surface free energy is lowered with adsorption of water, thus lowering the cohesion between the particles making up the solid rock and hence the strength [63,64]. Tested specimens dry and saturated conditions are shown in Fig. (4.7).

4.2 Uniaxial Tensile Strength.

All the investigations [10,64] which have been published on this test method have recommended that the uniaxial tensile test (direct pull) is carried out under well controlled conditions. This is to ensure that meaningful tensile strengths are obtained. It is probable that the values of strength obtained are then the minimum tensile strength of the bonding between the grains in the rock.

Several cylindrical specimens were tested using the Hounsfield Tensometer following the method described in Sec. (3.2.3.2). During the study four specimen sizes were used and in dry and saturated conditions in order to show the specimen size and the saturation effects on the tensile strength of the gypsum. All the specimens had L/D = 3 (length/diameter) with diameters 25.4, 31.75, 38.1 and 50.8 mm. Six specimens

at least were tested in every case. Fig.(4.8) shows photographs of some of the tested specimens at various sizes under the two environmental conditions.

4.2.1 Specimen Size Effects.

The tensile strength of all the tested specimens with various sizes and the mean values with the standard deviations are given in table (4.4) for dry and table (4.5) for saturated gypsum. Table (4.8) gives the summary of results related to the specimen size effects. It is clear that the tensile strength decreases with increasing specimen size. A reduction of about 43 percent in dry specimens and about 28 percent in saturated specimens were found within the specimen size ranges tested. Specimen volume-tensile strength relationships were plotted in Fig.(4.6) which shows clearly the decrease in the strength with the specimen volume. These size effects attributed to the presence of flaws in the rock and as a statistical effect that a larger sample is more likely to contain larger cracks within its microstructure.

Wijk et al.[117] found that the direct value of the uniaxial tensile strength does not vary with the size, while the tensile strength of the rocks from the indirect tests decreases with the specimen volume. Hardy et al.[13,14], reported that there is no unique trend for the size-tensile strength relationship in the rock, whereas Evans[4], Hobbs[6] and Lundborg[8] found that the tensile strength of the rocks is specimen size dependent. Lundborge[3] found a reduction of 38 percent in L:D = 1:1 granite cylinders of diameters ranging from 1.9 to 5.8 cm.

A comparison between the theoretical predictions and the present experimental results can be made by considering the statistical theory of Weibull's relationship, which states:

$$m \log \frac{\sigma t_1}{\sigma t_2} = \log \frac{V_2}{V_1}$$

Table (4.4) Uniaxial tensile strength - (Dry)

L = length , D = diameter.

Specimen Dims. mm	Specimen No.	Tensile strength N/mm^2	Mean N/mm^2	S.D.*	Specimen Dims. mm	Specimen No.	Tensile strength N/mm^2	Mean N/mm^2	S.D.*
L=76.2 D=25.4	1D-1	5.59	5.30	0.32	L=114.3 D=38.1	3D-1	3.53	3.52	0.11
	1D-2	5.41				3D-2	3.61		
	1D-3	5.55				3D-3	3.43		
	1D-4	5.05				3D-4	3.41		
	1D-5	4.87				3D-5	3.67		
	1D-6	5.51				3D-6	3.46		
L=95.25 D=31.75	2D-1	4.17	4.49	0.36	L=152.4 D=50.8	4D-1	2.76	3.01	0.22
	2D-2	4.42				4D-2	2.87		
	2D-3	4.14				4D-3	2.96		
	2D-4	4.42				4D-4	2.96		
	2D-5	5.11				4D-5	3.16		
	2D-6	4.67				4D-6	3.37		

S.D. - Standard deviation.

Table (4.5) Uniaxial tensile strength - (Saturated)

L = Length , D = diameter.

Specimen Dims. mm	Specimen No.	Tensile strength N/mm^2	Mean N/mm^2	S.D.*	Specimen Dims. mm	Specimen No.	Tensile strength N/mm^2	Mean N/mm^2	S.D.*
L=76.2 D=25.4	1S-1	2.47	2.75	0.23	L=114.3 D=38.1	3S-1	2.26	2.12	0.18
	1S-2	2.84				3S-2	1.92		
	1S-3	3.00				3S-3	2.15		
	1S-4	2.66				3S-4	2.19		
	1S-5	2.53				3S-5	1.89		
	1S-6	3.00				3S-6	2.21		
L=95.25 D=31.75	2S-1	2.78	2.64	0.29	L=152.4 D=50.8	4S-1	1.72	2.00	0.18
	2S-2	2.59				4S-2	1.89		
	2S-3	3.12				4S-3	2.19		
	2S-4	2.59				4S-4	2.10		
	2S-5	2.49				4S-5	1.95		
	2S-6	2.26				4S-6	2.15		

*S.D. - Standard deviation.

where σt_1 and σt_2 are the tensile strengths of the specimens with volume of V_1 and V_2 respectively, and m is the constant for the rock. The experimental data are plotted as log σ_t Vs log V for the dry and saturated specimens in Fig.(4.10). It will be seen from this figure that the above expression gives a straight line, the slope of which is the constant m. This gives m = 3.58 for the dry tensile strength and m = 6.84 for the saturated tensile strength. This indicates that the tensile strength of the saturated specimen varies more with the volume than that of the dry specimens. These results are in good agreement with Jahn[118] and Lundborg[8] whose results of tensile strength also fitted the Weibull theory.

Fig. (4.11) shows the tensile stess-strain characteristics of the dry and saturated gypsum for three specimen sizes, it can be seen there is a small change in behaviour by changing the specimen size. Although no unique pattern is clearly evident, there is some tendency towards a lower modulus in the case of larger specimens particularly in the case of the saturated materials.

4.2.2 Saturation Effects.

To show the effects of the water on the uniaxial tensile strength of the gypsum, several specimens of four sizes (the same sizes used for the dry specimens) were saturated with water and the tensile strengths by direct pull were determined. Details of the results are given in Table (4.5), and comparisons of the results for all sizes with the dry specimens is given in Table (4.8). It can be observed that the reduction of the strength due to saturation varies from 33% to 48% for all the specimen sizes, this reduction decreases with the specimen size, as shown in Fig.(4.6).

Fig.(4.11) gives the tensile stress-strain relationship for the wet specimens as well as the dry specimens. Little change in behaviour is shown due to specimen size in saturated conditions. The decrease of strength and increase of strain at given stress in the case of the saturated samples due to lowering of the surface free energy of the rock specimen by adsorption of the water[4,51,54,63], has been explained in the previous section, sec. (4.1.2).

4.2.3 Comparison between the Uniaxial and Bending tensile Strengths.

In order to compare the tensile strength determined by the direct and indirect methods, the following ratios should be tabulated:

For dry condition:

(1) Highest bending tensile strength to highest uniaxial tensile strength = 1.6.

(2) Lowest bending tensile strength to lowest uniaxial tensile strength = 2.6.

For saturated condition:

(3) Highest bending tensile strength to highest uniaxial tensile strength = 2.12.

(4) Lowest bending tensile strength to lowest uniaxial tensile strength = 2.67.

It can be seen from the above ratios (because of the strength changes with the specimen size, two ratios were considered to give a clear idea about the comparison) that the tensile strength determined by different methods is not the same. These results are in agreement with the investigators; Berenbaum and Brodie[3] who found that the ratio of tensile strength obtained by bending to the uniaxial is 2.3, Jaeger and Hoskins[7] obtained the ratio values of 2.2, 1.7 and 1.8 for sandstone, marble and trachytle respectively. Datta[12] found the ratios 1.9 and 1.86 for sandstone and

marble respectively, Tso-Min-Shi[26] tested specimens of Gasp Skarn and reported the ratio of the bending tensile strength to the uniaxial tensile strength is 2.8 and Wyang Yu[119] found that the bending tensile strength of some rocks was about 3.18 times the uniaxial tensile strength.

The variation in the tensile strength indicated by the two methods might possibly be due in part to the specimen preparation technique of the beams,which conceivably could produce a toughened surface skin or other surface effect due to the high speed grinding that is a part of the preparation technique and it is possible that the temperature of the rock in contact with the grinding wheel is high enough to chemically change or plasticise a very thin layer at the surface[3,4]. Jaeger and Hoskin[7] suggested that this discrepancy was due to the fact that in the direct test the stresses are uniform (or nearly so) over the section in which failure takes place while in the bending test they vary almost linearly across it.

In comparing the stress-strain relations in tension from bending and uniaxial tests, these relations are constructed in Fig.(4.12). These show that at any particular stress, the strain in the uniaxial test is greater than that in bending, approaching double that in bending in the case of the saturated condition. The higher indicated strain in the direct tests gives rise to flatter stress-strain curve than that demonstrated in the bending tests. The curves are virtually straight lines up to 2.0 N/mm^2 and 3.0 N/mm^2 for the direct tensile and bending tests respectively in dry condition. The initial tangent modulus is 4.286 $x10^4$ N/mm^2 compared with $4.834x10^4$ N/mm^2 in the curves from bending. In saturated conditions the curves are virtually straight lines up to 1 N/mm^2 and 1.5 N/mm^2 for direct tensile and bending rests respectively, the initial tangent modulus is $2.22x10^4$ N/mm^2 compared with $3.76x10^4$ N/mm^2

in the curves from bending. These results are in agreement with Datta's[12] results on specimens of dry sandstone.

4.3 Uniaxial Compressive Strength.

The uniaxial compressive test is frequently used as a criterion whereby the breakdown of rocks under pressure may be compared. In the mining industry data on the compressive strength of rocks are of greatest interest to engineers and scientists working on problems related to cutting and crushing of rocks, and strata control.

It is realised that the strength of rocks is fundamentally related to its petrology. It is essential to take into account also the of the porewater, temperature, specimen size, etc. during the determination of the compressive strength of rocks.

In this study the effect of specimen size and water saturation on the uniaxial compressive strength of gypsum were investigated by using four different specimen sizes with L/D = 3 at room temperature (21 ± 2^{o} C). Tested specimens of various sizes under dry and saturated conditions are shown in Fig. (4.13).

4.3.1 Specimen Size Effects.

In order to show the effect of specimen size on the uniaxial compressive strength, the constant specimen shape of L/D = 3 was used with diameters: 25.4 mm, 31.75 mm, 38.1 mm and 50.8 mm. These were tested under two environments (dry and saturated conditions), not less than six specimens being used in each case. Tables (4.6) and (4.7) give the results of all tests with means and standard deviations of strength for dry and saturated conditions respectively. Table (4.9) gives the summary of the results related to the specimen size effect. It is clear that the uniaxial compressive strength decreases with specimen size. This ranges from 41.59 N/mm^2 to 32.25 N/mm^2 (22.5% reduction)

Table (4.6) Uniaxial Compressive Strength - (Dry)

L = length , D = diameter.

Specimen Dims., mm	Specimen No.	Compressive strength N/mm^2	Mean N/mm^2	S.D.	Specimen Dims., mm	Specimen No.	Compressive strength N/mm^2	Mean N/mm^2	S.D.*
L=76.2 D=25.4	1D-1	42.78	41.59	1.29	L=114.3 D=38.1	3D-1	35.35	32.46	3.47
	1D-2	41.76				3D-2	30.08		
	1D-3	40.13				3D-3	31.75		
	1D-4	43.40				3D-4	37.54		
	1D-5	40.54				3D-5	32.01		
	1D-6	40.94				3D-6	28.00		
L=95.25 D=31.75	2D-1	32.21	32.82	4.86	L=152.4 D=50.8	4D-1	29.30	32.25	2.49
	2D-2	36.68				4D-2	34.20		
	2D-3	40.36				4D-3	29.90		
	2D-4	27.16				4D-4	32.60		
	2D-5	29.68				4D-5	31.70		
	2D-6	30.82				4D-6	35.80		

*S.D. - Standard deviation.

Table (4.7) Uniaxial Compressive Strength - (Saturated)

L = length , D = diameter.

Specimen Dims., mm	Specimen No.	Compressive Strength N/mm^2	Mean N/mm^2	S.D.	Specimen Dims., mm	Specimen No.	Compressive Strength N/mm^2	Mean N/mm^2	S.D.*
L=76.2 D=25.4	1S-1 1S-2 1S-3 1S-4 1S-5 1S-6	20.92 21.79 20.67 21.79 20.92 20.67	21.13	0.53	L=114.3 D=38.1	3S-1 3S-2 3S-3 3S-4 3S-5 3S-6	15.56 17.98 17.63 19.06 15.28 16.42	17.00	1.48
L=95.25 D=31.75	2S-1 2S-2 2S-3 2S-4 2S-5 2S-6	16.67 15.79 17.05 14.78 22.10 17.33	17.29	2.53	L=152.4 D=50.8	4S-1 4S-2 4S-3 4S-4 4S-5 4S-6	17.50 15.20 16.50 19.30 15.80 16.80	16.85	1.44

*S.D. - Standard deviation.

Table (4.8) Effects of specimen size and saturation on the Uniaxial tensile strength.

Specimen size (L x D), mm	Uniaxial tensile strength N/mm^2		Reduction due to saturation %
	Dry	Saturated	
76.2 x 25.4	5.30	2.75	48.11
95.25 x 31.75	4.49	2.64	41.20
114.3 x 38.1	3.52	2.12	39.77
152.4 x 50.8	3.01	2.00	33.56

Table (4.9) Effects of specimen size and saturation on the Uniaxial compressive strength.

Specimen size (L x D), mm	Uniaxial compressive strength N/mm^2		Reduction due to saturation %
	Dry	Saturated	
76.2 x 25.4	41.59	21.13	49.19
95.25 x 31.75	32.82	17.29	47.32
114.3 x 38.1	32.46	17.00	47.63
152.4 x 50.8	32.25	16.85	47.75

under dry condition and from 21.13 N/mm^2 to 16.85 N/mm^2 (20.3% reduction) under saturated condition. The relationship between the strength and the specimen volume as determined experimentally from the present tests is graphically depicted in Fig. (4.9) for both dry and saturated conditions. It can be seen from this figure that although the strength decreases as the specimen size (volume) increases, the curve nearly flattens out to a constant strength at the specimen size of about 114.3 x 38.1 mm (LengthxDiameter).

For the comparison of the present experimental results with Weibull theory, Fig.(4.10) is constructed as log V vs log σ relationship (where V and σ are the volume and strength of the specimen respectively). It can be seen from this figure that a straight line of m = 12 for dry specimens and m = 12.65 for saturated specimens (where m is the slope of the straight line) can be fitted to the Weibull's relationship

$$m \log \frac{\sigma_1}{\sigma_2} = \log \frac{V_2}{V_1}$$

in which σ_1 σ_2 is the strength of the specimens with volumes V_1 and V_2 respectively.

The following investigators have reported the effect of specimen size on the compressive strength, and most of them are in agreement with the results obtained in this study;

Gaddy[36], Evans and Pomeroy[37] and Evans et al.[38] tested cubical specimens of more than one type of coal and they found that the compressive strength decreases as the specimen size increases. Skinner[39] tested prismatic model pillars of anhydrite and Mogi[40] tested a marble prism ; their results also indicated decreasing of the compressive strength with specimen size. Ludborg[8] tested granite cylinders of the same height and diameter (2,3,4 and 6 cm) and observed

a range of 2190 to 1750 kg/cm^2 (20% reduction in crushing strength), and he found a reasonable agreement with Weibull theory, his results fitted straight line with m = 12 for dry condition. Bieniawski[42] tested a cubical specimen of Norite with side length from 1.3 to 17.8 cm, he found a reduction in the strength from 1.3 to 12.2 cm sizes and concluded that there would be no strength reduction thereafter, and Pratt et al.[43] tested in situ specimens of quartz dionite and granodiorite ranging from 1 to 9 ft in length and laboratory specimens ranging from 3.2 inch to 12 inch in length. He found the reduction of the strength by a factor of about 10 as specimen size increased up to 3 ft and no strength reduction was observed therafter.

Two factors might cause the decrease in the strength due to size effects: (1) As the specimen size increases the probability of the flaws of a particular size present in the specimen increases. Depending on the density of the flaws, a decrease in strength with increase in size of the specimen would be thus expected, and it is expected that with a sufficiently large specimen, flaw distribution would not be affected by size, when strength would not be affected with further increase in size. (2) The surface imperfections created either during the cutting of the specimen from the parent material, the machining of the specimen surface or by the natural reaction of the rock mineral to the free surface may also affect strength. For a certain specimen shape, the surface area per unit volume decreases with increase in size, when the strength would be expected to decrease with increasing the specimen size[120].

4.3.2 Saturation Effects.

To show the effects of the water on the uniaxial compressive strength of the gypsum, several specimens were saturated with water,

specimen sizes were the same sizes used in uniaxial tensile tests and in the dry uniaxial compressive strength tests in order to get a geometrical similarity and to make the comparison under closely controlled conditions. Table (4.7) gives the details of results obtained with the mean and standard deviations of the strengths for the wet specimens of all sizes,and table (4.9) gives the effect of saturation on the uniaxial compressive strength related to the various sizes. Fig.(4.9) shows the comparison between the dry and saturated uniaxial compressive strengths for the different specimen sizes. It can be seen from the results of the present study that the saturation of the water decreases the compressive strength. A range of 47.3% to 49.2% reduction of the compressive strength was observed due to saturation, only small differences in the percentages of strength reduction were observed due to different specimen sizes. It seems that the lowering of the strength under the influence of the saturation does not affected by changing the specimen size.

The following investigators reported the values of the compressive strength reduction due to water saturation as a percentage of dry strength; Price[52] found a reduction of 55% with sandstone, Cloback and Wiid[55] reported a reduction of 50% with quartizic shale and quartizic sandstone, Wiid[56] indicated 35% reduction with sandstone, Rutter[58] observed a reduction of 30% with Solenhofen limestone, Broch[62] found a reduction from 33 to 55% with the very high strength and low porosity rocks respectively, Eeckhout[64] reported a reduction from 5 to 74% from 43 sources with fifteen rocks.

The effect of the water on the strength of the gypsum may be explained as follows:

Since the formation of new surface during the process of the fracturing is dependent upon the surface energy of the rock, its strength will

be dependent upon the decrease or increase of that surface energy. As the water decreases that surface energy of the rock then the strength will decrease[51,54,55]. This could be explained using the Griffith's Criterion. Although this criterion was originally defined for the tensile strength situation, it is reported[64] that experimental observations suggest that strength in uniaxial compression is affected by tensile brittle cracking and energy exchange, so that the Griffith's criterion also applies to the compressive stress situation. Assuming an equation of the form:

$\sigma = K (E\gamma/C_o)^{\frac{1}{2}}$ holds, where γ is the energy required per unit advance of the crack (the work of fracture), and C_o is some measure of the critical flaw length, then if γ is lowered with absorption of water, the fracture strength will be lowered and hence the strength.

It is also possible that certain minerals may decompose and/or be dissolved when they come in contact with water. If the water attacks the crack tips, dissolving and/or decomposing the minerals, this will increase the stress at the apex which helps in their propagation, again causing a decrease in the strength of the rock[120].

4.3.3 Axial, Lateral and Volumetric Strains.

The stress-axial strain relationships for dry and saturated gypsum under uniaxial loading are shown in Fig.(4.14). There is a good agreement between the results from various specimen sizes in both conditions.

The low stress part of the two plots is non-linear with a very small curvature, this gradually ceasing with the stress, this is generally attributed to progressive closure of cracks and pores under stress. At somewhat higher stress a linear relation followed which describes the elastic straining of the constituent grains after pore closure ceased. As the stress approaches the uniaxial strength the slope of stress-strain

curve decreases due to formation and extension of microcracks which progressively destroy the load-bearing capacity of the rock and cause irreversible strains to occur.

Higher strains are indicated at given stresses in the saturated specimens giving rise to a flatter stress-strain curve than that demonstrated in dry conditions. This is again due to decrease in the surface free energy of the interfaces newly formed in the defects (ultra-microcracks) arising in the strained solids[51].

Lateral strain was measured by attaching five strain gauges along the specimen surface at six equal intervals, two gauges were mounted on the opposite sides of the specimen for each strain reading. It was found that the lateral strain (which is equal to the tangential strain as a result of axially summetrical loading[31,48,121]) is nearly uniform within the middle third of the specimen length, and that is in agreement with the Peng's[31] results for the same given end conditions. The average lateral strain at the middle third was considered as the characteristic strain measurement in the present study.

Fig.(4.15) shows the stress-lateral strain relationship for both dry and saturated conditions. The three stages in the curve can be seen, in the initial phase of loading when cracks or pores are closing there is very little lateral strain (no curves are seen) and thus the curve rises steeply. At the onset of "linear" compression the slope of the curve decreases, as the internal cracking starts elastic compression of the rock grains is countered by crack formation and the lateral strain increases rapidly as the volume of the specimen of the rock starts to increase.

As an average value the saturation decreased the Modulus of Elasticity of the gypsum from 3.28×10^4 N/mm^2 to 1.76×10^4 N/mm^2 (46%

reduction and increased the Poisson's ratio from 0.396 to 0.488 (23% increase). Mann and Fatt[53] found that the presence of water decreased the Modulus of Elasticity of the sandstone by about 10-30% and increased the Poisson's ratio by about 100% for one type and a small amount only for another type of the sandstone. Mogilevskaya[57] reported 5-20% reduction of Young's modulus of four rocks due to saturation.

Volumetric strains were calculated from the axial strain (ε_A) and lateral strain (ε_L). Considering the axial strain (shortening) as a positive and lateral strain (expansion) as a negative, so the volumetric strain (ε_V);

$$\varepsilon_V = \varepsilon_A - 2\varepsilon_L$$

Axial stress-volumetric strain relationships for both dry and saturated conditions are constructed in Fig.(4.16). The curves show the first region (lower stresses) which represent the closure of the pre-existing cracks, followed by the linear elastic deformation. A further increase in stress causes microcracking initiation which is indicated by a deviation from linearity of the stress-volumetric strain curve at about 15 N/mm^2 in dry condition and 6.0 N/mm^2 in saturated condition (points A and B respectively). The fracture initiation apparently takes place at 39% and 33% of the maximum stress for dry and saturated conditions respectively. The stage of fracture propagation continues up to the points where the curve changes direction and gives a negative slope, (referred to as the onset of the unstable fracture[56]), this point is at about 29 N/mm^2 ($\simeq$ 74% of maximum stress) in case of dry and at about 13 N/mm^2 ($\simeq$ 72% of maximum stress) in saturated condition. This change in the direction of the curve indicated an increase in specimen

volume related to the state of the specimen immediately before the onset of the unstable fracture. The specimensfailed before their volume became more than the original volumes.

Brodia[122] tested sandstone cylinders with L/D = 1 and he found the onset of the unstable fracture at about 50% maximum stress and dilation took place at about 98% maximum stress. Wiid[56] studied the volumetric strain behaviours of the dry and saturated dolerite, and he reported that the stress at fracture initiation was 60% and 58% maximum stress for dry and saturated conditions respectively. The onset of the unstable fracture took place at a stress of 89% and 86% maximum stress for dry and saturated rock respectively.

4.4 Triaxial Compressive Strength.

Knowledge of the compressive strength behaviours of rocks under triaxial loading is of fundamental importance in rock mechanics. This behaviour is influenced by a number of factors, one of which is the moisture content of the rock. The present work deals with the effect of saturation on the compressive strength of the gypsum under triaxial loading. It also deals with the effect of the specimen size, but due to the limited size of the triaxial cell available in the laboratory, only two sizes were used in which case it is only possible to partly investigate the effect of the specimen size on the compressive strength.

The confining pressure levels used were; 5, 10, 15, 20, 25, 30 and 35 N/mm^2. The specimen sizes were; 76.2 mm long by 25.4 mm dia. and 95.25 mm long by 31.75 mm dia. both sizes had L/D = 3. Axial load was applied perpendicular to the rock bedding, and the experiments performed at room temperature (21 ± 2^{o} C). Tested specimens in dry and saturated conditions are shown in Figs. (4.17) and (4.18) for the two mentioned sizes.

4.4.1 Influence of Saturation.

Triaxial tests were performed on four specimens at every chosen confining pressure under both dry and saturated conditions. The same experiments under the same conditions were carried out on the two mentioned specimen sizes. A summary of the results obtained for the various specimen sizes and under dry and saturated conditions is given in tables (4.10), (4.11), (4.12) and (4.13). The details of all the tested specimen results are presented in Appendix "B" table (B4.1), (B4.2), (B4.3) and (B4.4).

Mohr's circles for dry and saturated specimens were constructed in Fig. (4.19) for the specimen size of 76.2 mm x 25.4 mm and in Fig.(4.20) for specimen size 95.25 x 31.75 mm, and an envelope was fitted to the stress circles in each case. It can be seen that some of the circles do not touch the envelope, indicating lower strength values than those predicted from the Mohr's envelope drawn. These small differences can be attributed to possible error arising from random variation in the rock specimens. It is clear that the envelopes illustrated in all cases are non-linear, and similar to the shape of the envelope of rocks obtained by many previous investigators; Robertson[21], Price[23], Murrell[24,116], Hobbs[25] and others. To better define the shape of the envelope, especially at the low stresses region, the uniaxial tensile tests which were performed give a "negative" stress circle. It was assumed that the tensile strength developed in the material under a condition of pure shear would be the same as that in simple tension, a circle representing a condition of pure shear is shown, drawn about the origin of σ,τ axis, Figs. (4.19) and (4.20). It is noted that the shear circle represents the only possibility for both shear and tension circles to be a tangent to the envelope. The tensile strength and the shear intercept for each case are given in table (4.14).

Table (4.10) Triaxial Test results of dry specimens

76.2 x 25.4 mm (L x D)

No. of Specimen Tested	$\sigma_2 = \sigma_3$ (N/mm^2)	Mean σ_1 (N/mm^2)	Mean Z (N/mm^2)	Mean angle of fracture (deg.)			σ_n (N/mm^2)	τ_s (N/mm^2)	$\sigma_m = \frac{\sigma_1 + \sigma_3}{2}$ (N/mm^2)	$\tau_m = \frac{\sigma_1 - \sigma_3}{2}$ (N/mm^2)	$P_m = \frac{\sigma_1+\sigma_2+\sigma_3}{3}$ (N/mm^2)	Max Strain %
				θ	θ_M	θ_G						
6	0	41.59	0	63.8	64.5	60	-	-	20.80	20.80	13.86	0.11
4	5	50.21	30.13	62.1	62.7	57.5	10.50	10.39	27.61	22.61	20.07	0.20
4	10	62.41	38.03	60.8	58.5	55.7	16.61	11.91	36.21	26.21	27.47	0.25
4	15	67.30	59.70	59.1	56.0	54.2	26.80	19.71	41.15	26.15	32.43	0.36
4	20	78.15	73.96	58.3	55.0	53.7	34.95	24.16	49.08	29.08	39.38	0.38
4	25	86.84	80.12	56.5	53.5	52.6	41.84	25.39	55.92	30.92	45.61	0.44
4	30	102.87	99.71	51.0	52.5	52.8	57.72	34.24	66.44	36.44	54.29	0.49
4	35	109.23	103.17	53.3	51.8	52.3	59.37	32.67	72.12	37.12	59.74	0.54

Table (4.11) Triaxial test results of Saturated specimen

76.2 x 25.4 mm (L x D)

No. of specimen tested	$\sigma_2 = \sigma_3$ (N/mm^2)	Mean σ_1 (N/mm^2)	Mean Z (N/mm^2)	Mean angle of fracture (deg)			σ_n (N/mm^2)	τ_s (N/mm^2)	$\sigma_m = \frac{\sigma_1 + \sigma_3}{2}$ (N/mm^2)	$\tau_m = \frac{\sigma_1 - \sigma_3}{2}$ (N/mm^2)	$P_m = \frac{\sigma_1+\sigma_2+\sigma_3}{3}$ (N/mm^2)	Max Strain %
				θ	θ_M	θ_G						
6	0	21.13	0	62.8	64.5	60	-	-	10.57	10.57	7.04	0.13
4	5	35.24	18.01	62.0	60.5	56	2.42	4.66	20.12	15.12	15.08	0.22
4	10	45.39	33.90	60.2	58	54.5	14.18	9.10	27.70	17.70	21.80	0.26
4	15	58.12	53.19	58	57	53.5	21.09	17.24	36.56	21.56	29.37	0.38
4	20	71.69	66.97	56.8	56	53.2	29.77	19.04	45.85	25.85	37.23	0.46
4	25	80.61	77.26	55.8	55.5	52.6	41.13	24.3	52.81	27.81	43.53	0.48
4	30	92.02	86.1	55	54	52.3	45.7	25.2	61.01	31.01	50.67	0.52

Table (4.12) Triaxial test results of dry specimens
95.25 x 31.75 mm (L x D).

No. of Specimen tested	$\sigma_2 = \sigma_3$ (N/mm^2)	Mean σ_1 (N/mm^2)	Mean Z (N/mm^2)	Mean angle of fracture (deg)			σ_n (N/mm^2)	τ_s (N/mm^2)	$\sigma_m = \frac{\sigma_1 - \sigma_3}{2}$ (N/mm^2)	$\sigma_m = \frac{\sigma_1 - \sigma_3}{2}$ (N/mm^2)	$P_m = \frac{\sigma_1 + \sigma_2 + \sigma_3}{3}$ (N/mm^2)	Max Strain %
				θ	θ_M	θ_G						
6	0	32.82	0	65.5	67	60	-	-	16.41	16.41	10.94	0.1
4	5	53.80	31.15	64.3	61	57.3	102.21	9.9	29.40	24.40	21.27	0.18
4	10	64.1	44.19	58.7	55	55.7	15.18	19.23	37.05	27.05	28.03	0.24
4	15	72.31	61.32	54.5	53.5	54.5	21.92	30.62	43.66	28.66	34.10	0.37
4	20	76.62	72.93	53.5	53	53.5	25.31	38.71	48.31	28.31	38.87	0.39
4	25	85.83	81.14	52	52	53	27.23	46.27	55.42	30.42	45.27	0.43
4	30	96.45	93.34	51	51	52.6	30.78	55.09	63.23	33.23	52.15	0.48
4	35	103.12	99.58	50.5	50.5	52.1	31.70	60.79	69.06	34.06	57.71	0.53

Table (4.13) Triaxial test results of saturated specimens.
95.25 x 31.75 mm (L x D).

No. of specimen tested	$\sigma_2 = \sigma_3$ (N/mm^2)	Mean σ_1 (N/mm^2)	Mean Z (N/mm^2)	Mean angle of fracture (deg)			σ_n (N/mm^2)	τ_s (N/mm^2)	$\sigma_m = \frac{\sigma_1 + \sigma_3}{2}$ (N/mm^2)	$\tau_m = \frac{\sigma_1 - \sigma_3}{2}$ (N/mm^2)	$P_m = \frac{\sigma_1+\sigma_2+\sigma_3}{3}$ (N/mm^2)	Max. Strain %
				θ	θ_M	θ_G						
6	0	17.29	0	67	65	60	-	-	8.65	8.65	5.76	0.14
4	5	35.77	20.13	60	59	56	8.77	6.55	20.39	15.39	15.26	0.22
4	10	47.83	32.32	57	54	54.5	16.62	10.20	28.92	18.92	22.61	0.28
4	15	53.0	45.45	53.5	51.5	53	25.78	14.56	34	19.0	27.67	0.39
4	20	61.17	57.68	50.5	49.5	52.3	35.25	18.49	40.59	20.59	33.72	0.45
4	25	67.0	63.27	49	48.5	51.6	40.78	18.95	46	21	39	0.49
4	30	74.71	72.81	48	48	51.2	49.16	21.28	52.36	22.36	44.90	0.55
4	35	78.83	77.06	48	48	50.6	52.94	19.93	56.92	21.92	49.61	0.57

Table (4.14) Tensile strength and sheer intercept for various conditions.

Condition	Specimen size (L x D) mm	Tensile strength N/mm^2	Shear axis intercept N/mm^2
Dry	76.2 x 25.4	5.30	8
	95.25 x 31.75	4.49	7.5
Saturated	76.25 x 25.4	2.75	3.7
	95.25 x 31.75	2.64	3.9

From the experimental results, the values of the normal stress (σ_n) and shear stress (τ_s) immediately after fracture have been calculated at various confining pressures using the following equations:

$$\sigma_n = \frac{z + \sigma_3}{2} + \frac{z - \sigma_3}{2} \cos 2\theta$$

$$\tau_s = \frac{z - \theta_3}{2} \quad 2\theta$$

where

z = Axial stress immediately after fracture, N/mm^2.

σ_3 = Confining pressure, N/mm^2.

θ = Measured angle of fracture which is the angle between the plane of failure and the minor principal stress.

These values are given in tables (4.10) and (4.11) for specimens 76.2 x 25.4 mm under dry and saturated conditions respectively and in tables (4.12) and (4.13) for specimen 95.25 x 31.75 mm under dry and saturated conditions respectively, then the values (σ_n and τ_s) are plotted in Figs. (4.19) and (4.20), and fitted straight lines in all cases shown as broken lines. The slope of these lines gives the coefficient of friction within the fractured specimen of the rock. It is clear then that if the above straight line meets the Mohr's envelope, there will

be a stress at which no reduction of load will occur after fracture since the applied shear stress does not exceed the frictional force on the surface.

The Mohr's envelope of failure stress circles at various confining pressures gives the relationships between the normal and shear stresses on the failure surface. It can be seen from each of the Figs. (4.19) and (4.20) that these envelopes under dry and wet conditions are approximately parallel. This implies that there is no change in internal friction when gypsum is saturated with water. To study the influence of water saturation on the internal friction, for every circle the angle of friction ϕ was measured and the coefficient of friction (μ) calculated as:

$$\mu = \tan \phi$$

where $$\phi = 2\theta - 90^{o}$$

(θ is the measured angle between the minor principal stress and the plane of failure).

The coefficient of friction (μ) for both dry and saturated specimens at various confining pressures is plotted in Fig. (4.21) as μ-σ_3 relations. It will be seen that the differences of the coefficient of friction between the dry and the saturated conditions are very small, indicating that μ remains constant and does not change with the water saturation. The small differences observed can be attributed to experimental errors.

It can therefore be concluded that the reduction in compressive strength with water, is due to something other than change of internal friction. It follows that the explanation given earlier that the presence of water reduces the tensile strength (or uniaxial compressive strength) by reducing the surface free energy of the rock still holds. Similar explanations of the strength reduction due to water have been

given by investigators; Price[23], Cloback and Wiid[55], Boozer et al.[54], Broch[62] and others.

Tests on different specimen sizes under the dry and saturated environments have indicated a total reduction of the compressive strength of the saturated specimens of between 10% to 33%, with 25% as an average value.

The relationship between the major principal stress (σ_1) and the total confining pressure (σ_3) under both conditions are shown in Figs. (4.22) and (4.23) for the small and larger specimen sizes respectively. The plots show a non-linear increase in the rock strength as the confining pressure increases in the two different environments. The curves obtained were close to being completely parallel. This is in agreement with the results obtained by Price[23], Cloback and Wiid[55], Broch[62] and others. It can be seen that the major principal stress at failure (σ_1) of the wet specimen at any constant confining pressure (σ_3) is less than that of the dry specimens, due to the effect of water on the surface free energy of the specimen as explained above in this section. The value of the angle of fracture calculated from the various envelopes (θ_M), the actual angle determined by experimental measurements of the angle between the plane of failure and the minor principal stress (θ) and the angle of fracture calculated frith Griffith's equation (θ_G) as:

$$\cos 2\theta = -\frac{1}{2}\left(\frac{\sigma_1-\sigma_3}{\sigma_1+\sigma_3}\right)$$

where σ_1 σ_3 are the major and minor principal stresses. which are given in tables (4.10, 4.12) and (4.11, 4.13) for the dry and saturated specimens respectively. In all cases the measured angle of fracture (θ) is in close agreement with the angle predicted from the Mohr's envelope (θ_M), the small differences between them more presumably

due to sample variations and/or the difficulty of determining with accuracy the average inclination of small rough surfaces. On the other hand in most cases and under dry and wet environments there are larger differences between the measured angle of fracture (θ) and the angle calculated from Grifith's equation (θ_G); this is possibly due to the fact that the Griffith's theory predicts only the orientation of the most dangerous crack which propagates and initiates fracture, Murrell[116], and that the Griffith's Crack under shear may not propagate in the direction of its major axis and that the observed fracture surface thus develops by linking of a number of propagating cracks[15].

The relationships between the maximum normal stress $\sigma_m = \frac{\sigma_1+\sigma_3}{2}$ and the maximum shear stress $\tau_m = \frac{\sigma_1-\sigma_3}{2}$ under both conditions are shown in figs. (4.24) and (4.25) for the specimens 76.2 x 25.4 mm and 95.25 x 31.75 mm (LxD) respectively. The curves of both dry and saturated conditions are slightly concave downwards but nearly linear, the slope of each curve decreases with increasing the maximum normal stress (σ_m). Elizzi[15] found the same behaviour on a similar type of rock in dry conditions. The relationship between the mean pressure P_m ($P_m = \frac{\sigma_1+\sigma_2+\sigma_3}{3}$) and the maximum shear stress τ_m for the two environments are shown in Figs. (4.26) and (4.27) for the smaller and larger specimens respectively. It can be seen that this curve (sometimes called the strength/pressure curves[22]) are linear for both environments, with a small range of scatter. The parallel nature of these lines in dry and saturated conditions is very marked in the smaller specimens and only slightly less so in the case of larger specimens. The slope of the lines is 0.8 in 3 cases except the saturated specimen of the larger specimens which is 0.7. It is clear that this slope can never exceed 1.5 which is the slope of the curve at the uniaxial compression. Handin

and Hager[22] tested a dolomite and anhydrite and they found that the strength curves are nearly straight lines. Elizzi[115] reported that the strength relationships he obtained for anhydrite and gypsum are slightly concave downward but nearly linear.

Figs. (4.28) and (4.29) show the total strain before fracture (maximum strain) versus confining pressure and mean pressure (P_m) respectively. Each figure shows the relationship in dry as well as saturated conditions. The relationship is non-linear in all cases and the curves are concave downward. These curves are sometimes known as ductility curves. It can be seen that the maximum strain (ductility) increases with the confining pressure and with the mean pressure. The ductility under the saturated condition is greater than that of the dry at any particular confining pressure or mean pressure, indicating that the saturated gypsum starts to deform plastically at lower stresses than the dry one.

4.4.2 Axial, Lateral and Volumetric Strains.

The stress-axial strain relationship at various confining pressures, under dry and saturated conditions are constructed in Figs. (4.30) and (4.31) respectively. Each curve represents the average value obtained from several specimens tested at the given confining pressure. Figs. (4.32) and (4.33) show the stress-axial strain curves of four specimens tested at 10 N/mm^2 confining pressure for dry and saturated gypsum respectively. The nearest curve to the average value considered as an average curve at that pressure level as shown on the graph. The small differences between the results of the same pressure which give a scatter in the results, presumably due to sample variations and experimental errors.

It can be seen from the stress-axial strain curves in both conditions that the relationship indicates a linear portion during the early stages of deformation and at low stress level which means that the specimen deformed elastically at this stage, then as the stress increases the relation becomes non-linear and the strain starts to increase rapidly until the curve becomes parallel to the strain axis especially at high confining pressure, see Figs. (4.30) and (4.31), which reflect the plastic behaviour of the gypsum at this stage.

The strain of the saturated gypsum at any constant axial stress and confining pressure is more than that of the dry gypsum, and the plastic zone of the saturated samples starts at a lower stress level than that for dry gypsum. In both environments, at any particular axial stress the strain decreases as the confining pressure increases, the stress-strain curve slope increases as the confining pressure increases.

Boozer et al.[54] found that the water saturation decreases the yield stress of the limestone tested under triaxial loading system at various confining pressures, and he stated that the effect of water on the deformation behaviour of the limestone can only be discussed in terms of a mechanism first suggested by Rebinder[51]. It is assumed that these effects are the direct results of a decrease in the free surface energy caused by the strong absorption of water.

Lateral strain of the specimens under triaxial loading was measured as an average value of the lateral strain of the middle third of the specimen, (Peng[31]). The stress-lateral strain relationship at various confining pressures for dry and saturated conditions are shown in Figs. (4.34) and (4.35) respectively. The linear stage of the axial strain/stress relationship is accompanied by a very little lateral strain after which the strain increased rapidly with the stress in a non-linear manner.

The shape of the stress-lateral strain curves at various confining pressure and under the two environments compared with the shape of the stress-axial strain curves at the same conditions are found to be similar to the curves obtained by Dhir and Sangha[33,34] using the specimens of sandstone and concrete. It can be seen from the figs. (4.34) and (4.35). that at any given axial stress and confining pressure the lateral strain of wet specimens is much more than that in the dry condition, occasionally reaching double that of the dry specimens. Under the two conditions the lateral strain decreases with the confining pressure at constant axial stress, and it can be noted that the effect of the confinement on the lateral strain is greater than on the axial strains. In order to show this effect clearly; Poisson's ratio versus axial stress (expressed as percentage of strength) level for various confining pressures are plotted in Figs. (4.36) and (4.37) for dry and saturated conditions respectively. Results are given in table (4.15). It can be seen from the graphs and tabulated results that the Poisson's ratio decreases as the confining pressure increases at any particular axial stress level, indicating that the resistance to the lateral deformation with increasing confinement is greater than the corresponding resistance to the axial deformation. These results are in agreement with the results obtained by other investigators[33,34]. These results show that the water saturation increases the Poisson's ratio if the specimens are tested under the same stress level and confining pressure.

Volumetric strains ε_V, were calculated from the axial strain ε_A and lateral strain ε_L as: $\varepsilon_V = \varepsilon_A - 2\varepsilon_L$ at various confining pressures. Axial stress-volumetric strain relationships for various confining pressures are shown in Fig. (4.38) and (4.39) for dry and saturated conditions respectively. It can be seen that at all pressure levels the three

stages of the relationship explained under the uniaxial loading can be observed, these are; (a) the stage of the closure of pre-existing cracks the so-called "compaction region" (Bordia[122]), which gives a small non-linear region, (b) the linear relationship which represents the elastic deformation, and (c) the fracture initiation which is manifested by a deviation from the linearity of the curve and then changes the direction of the curve indicating the onset of the unstable fracture propagation at axial stress $\sigma_{unst.}$. This indicates the commencement of specimen volume increase relative to its volume immediately before the attainment $\sigma_{unst.}$, increase of specimen volume continues up to failure.

It is clear from the illustrated figures that at a constant axial stress the volumetric strain increases as the confining pressure increases which indicates that the rate of increase of the axial strain (shortening) is more than the rate of increasing of the lateral strain (expansion). Volume of the specimen decreases with the confining pressure and can be explained as the confining pressure having the effect of resisting the lateral deformation more than the axial deformation.

Dilation takes place when the lateral expansion of the specimen becomes more than the shortening, i.e. $|2\varepsilon_L| > |\varepsilon_A|$ or the Poisson's ratio equals 0.5 or more.

It can be seen from Figs. (4.38) and (4.39) that the axial stress (as a percentage of the maximum stress) required to develop the onset of the unstable fracture $\sigma_{unst.}$ increases as the confining pressure increases, in both dry and saturated conditions, i.e. as the confining pressure increased from 0 to 30 N/mm^2 in dry conditions $\sigma_{unst.}$ increased approximately from 75 to 91 percent maximum stress, and from 73 to 80 percent maximum stress in the case of saturated specimens, see Table

(4.16). Dhir and Sangha[33,34] reported that as the confining pressure was increased from zero to 139.7 N/mm^2 dilation stress of the sandstone increased from approximately 80 to 95% maximum stress.

Water saturation decreases the volumetric strain of a specimen when compared with a dry one at the same axial stress and confinement (decrease of the specimen volume in the case of saturation is less than that in a dry condition). The onset of unstable fracture stress (expressed as a percentage of strength) at any confining pressure is decreased with water saturation, see Table (4.16).

Wiid[56] tested a dolomite specimen under axial loading; he found that the stress required to develop the onset of the unstable fracture of the dry specimen is 89% and the saturated specimens is 86% of the maximum stress. Wiid reported that the reduction of the stress due to saturation is due to the lowering surface free energy of the rock and hence the intrinsic strength of the rock.

Table (4.15) Effect of confinement on the Poisson's Ratio.

Condition / σ_3, N/mm^2 / $\frac{\sigma}{\sigma_1} \times 100$ %	Dry				Saturated			
	0	10	20	30	0	10	20	30
20	0.25	0.15	0.10	0.08	0.35	0.29	0.24	0.17
40	0.3	0.2	0.15	0.11	0.42	0.35	0.31	0.29
60	0.31	0.22	0.20	0.18	0.45	0.4	0.38	0.36
80	0.36	0.24	0.23	0.22	0.47	0.43	0.41	0.40
90	0.42	0.33	0.31	0.29	0.48	0.45	0.43	0.42

Table (4.16) Effect of confining pressure and saturation on $\sigma^*_{unst.}$

σ_3, N/mm^2	$\sigma^*_{unst.}$, expressed as a percentage of Maximum Stress, %	
	Dry	Saturated
0	75	73
10	81	76
20	85	78
30	91	80

$^*\sigma_{unst.}$ - Stress required to develop the onset of the unstable fracture.

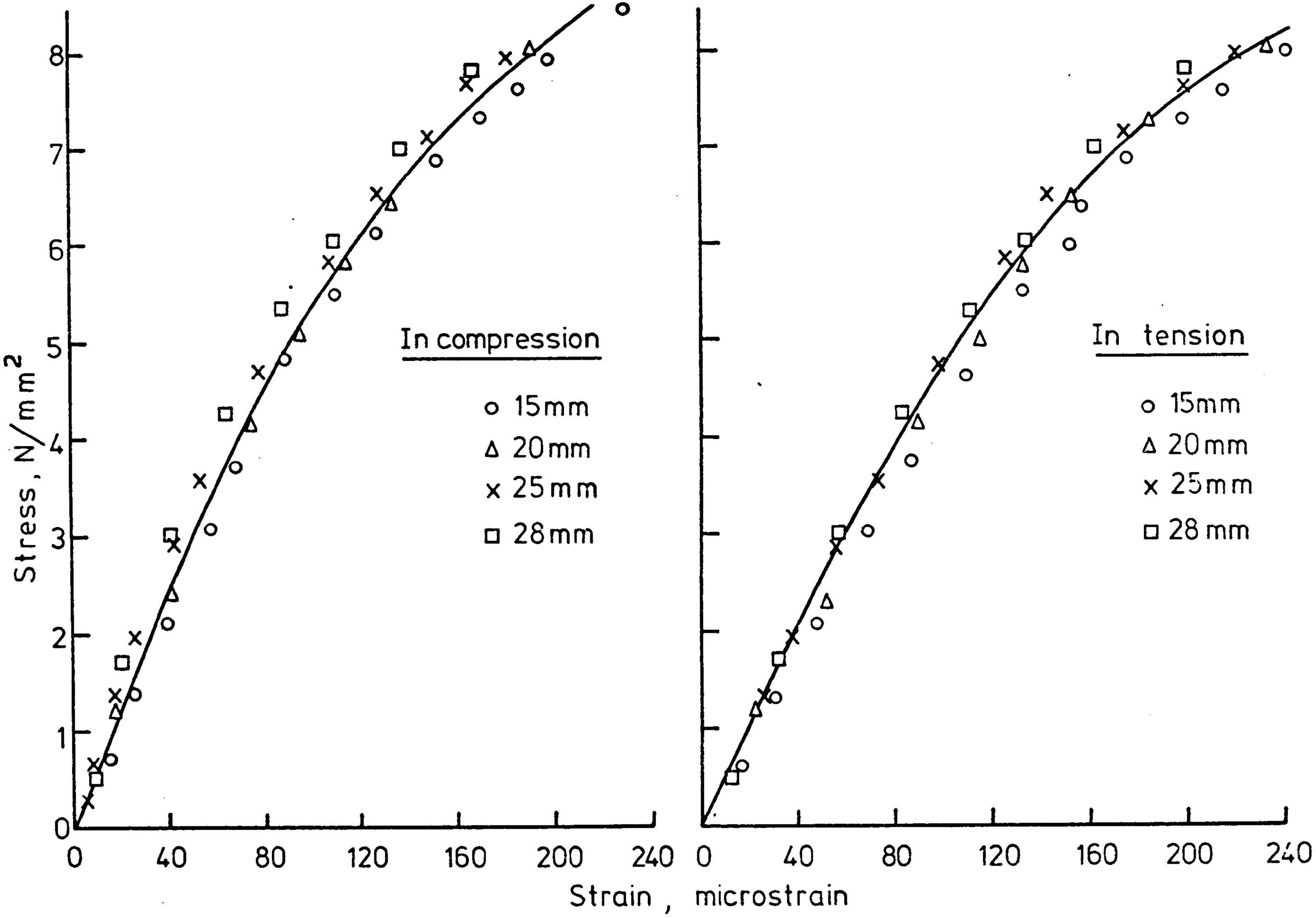

FIG.(4-1) STRESS – STRAIN RELATIONSHIP IN TENSION AND COMPRESSION FROM BENDING TESTS FOR VARIOUS BEAM THICKNESSES IN DRY CONDITIONS

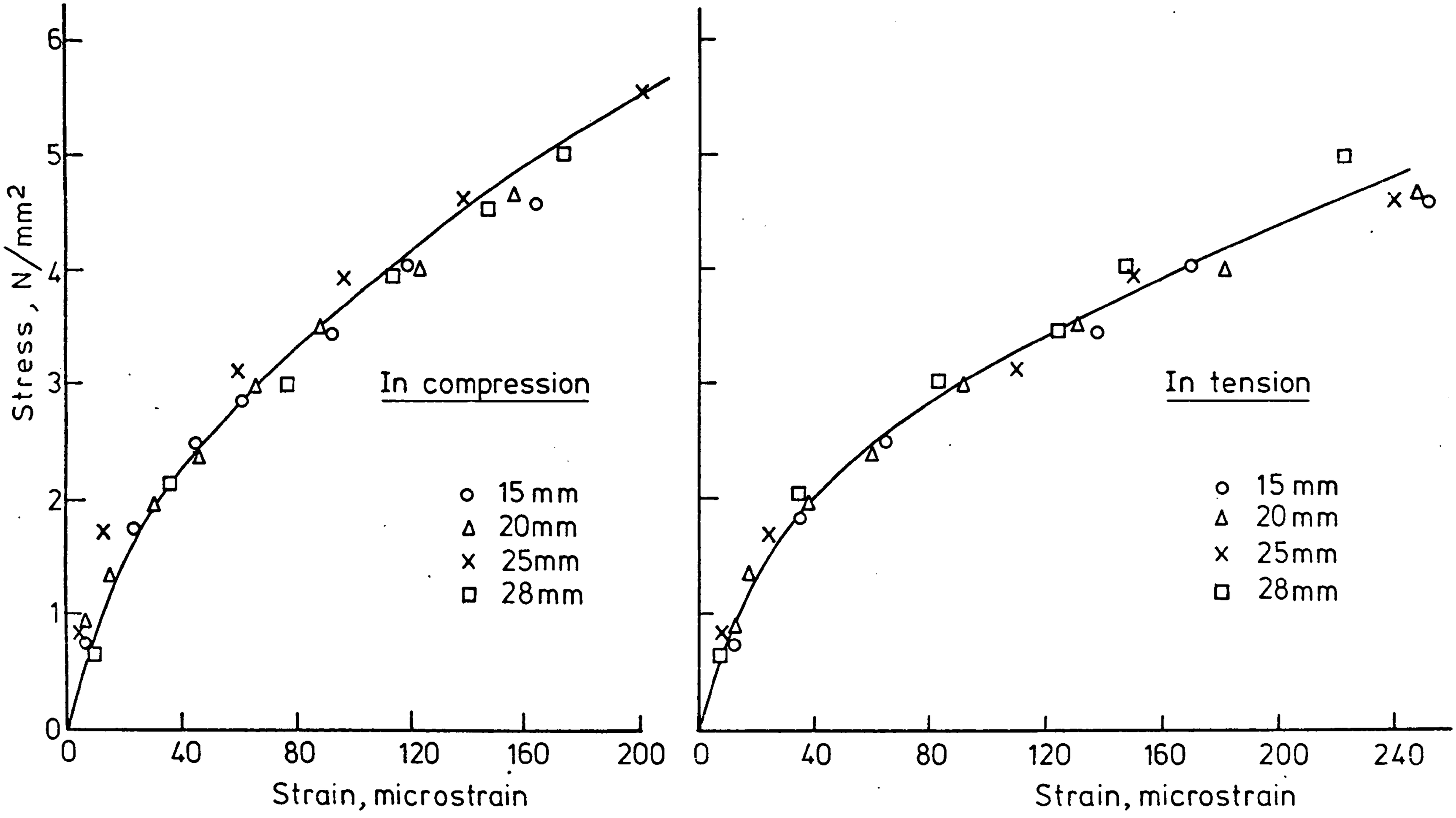

FIG. (4-2) STRESS–STRAIN RELATIONSHIP IN TENSION AND COMPRESSION FROM BENDING TESTS AT VARIOUS BEAM THICKNESSES IN SATURATED CONDITIONS

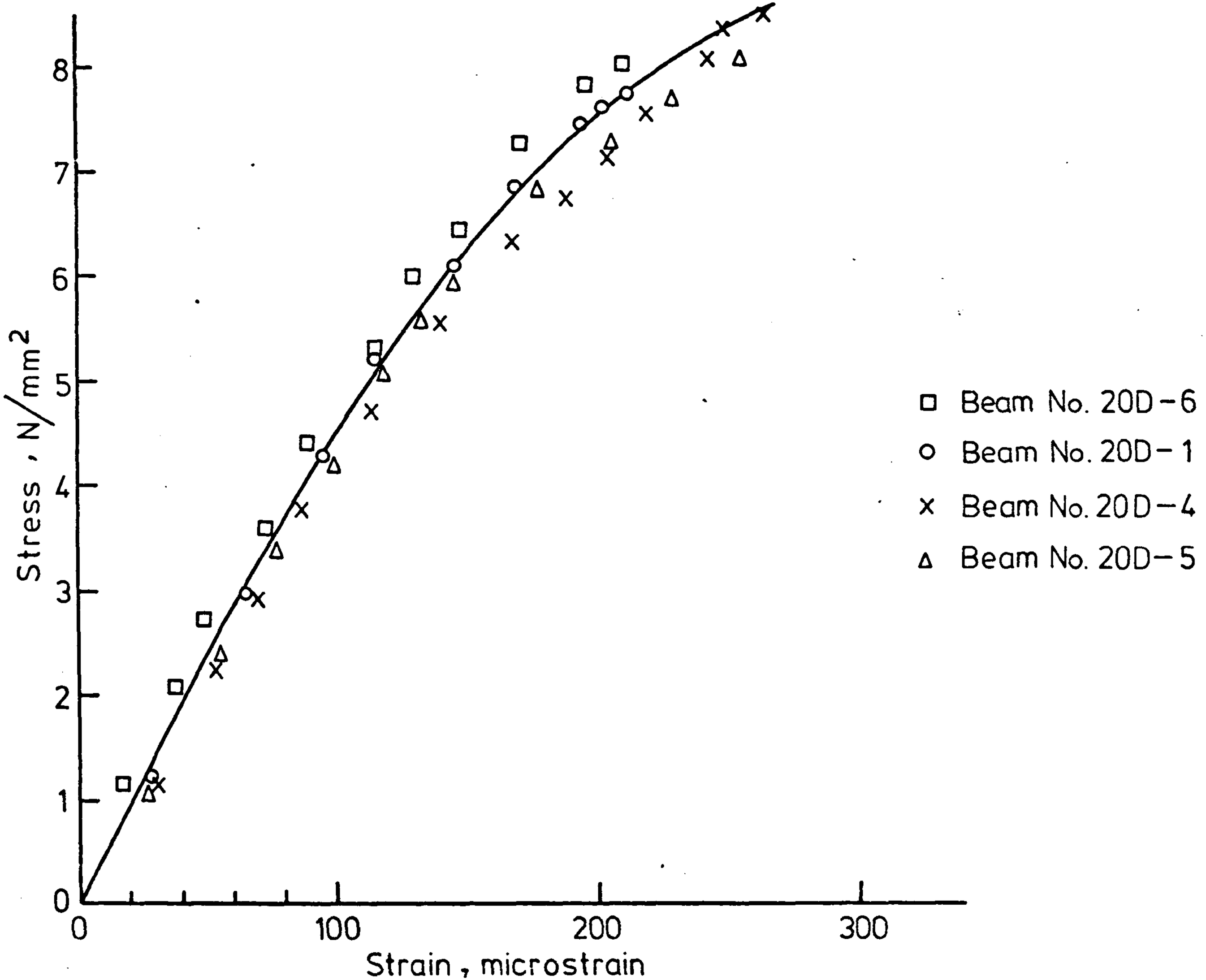

FIG.(4-3) STRESS - STRAIN RELATIONSHIP OF DRY GYPSUM IN TENSION FROM BENDING TESTS

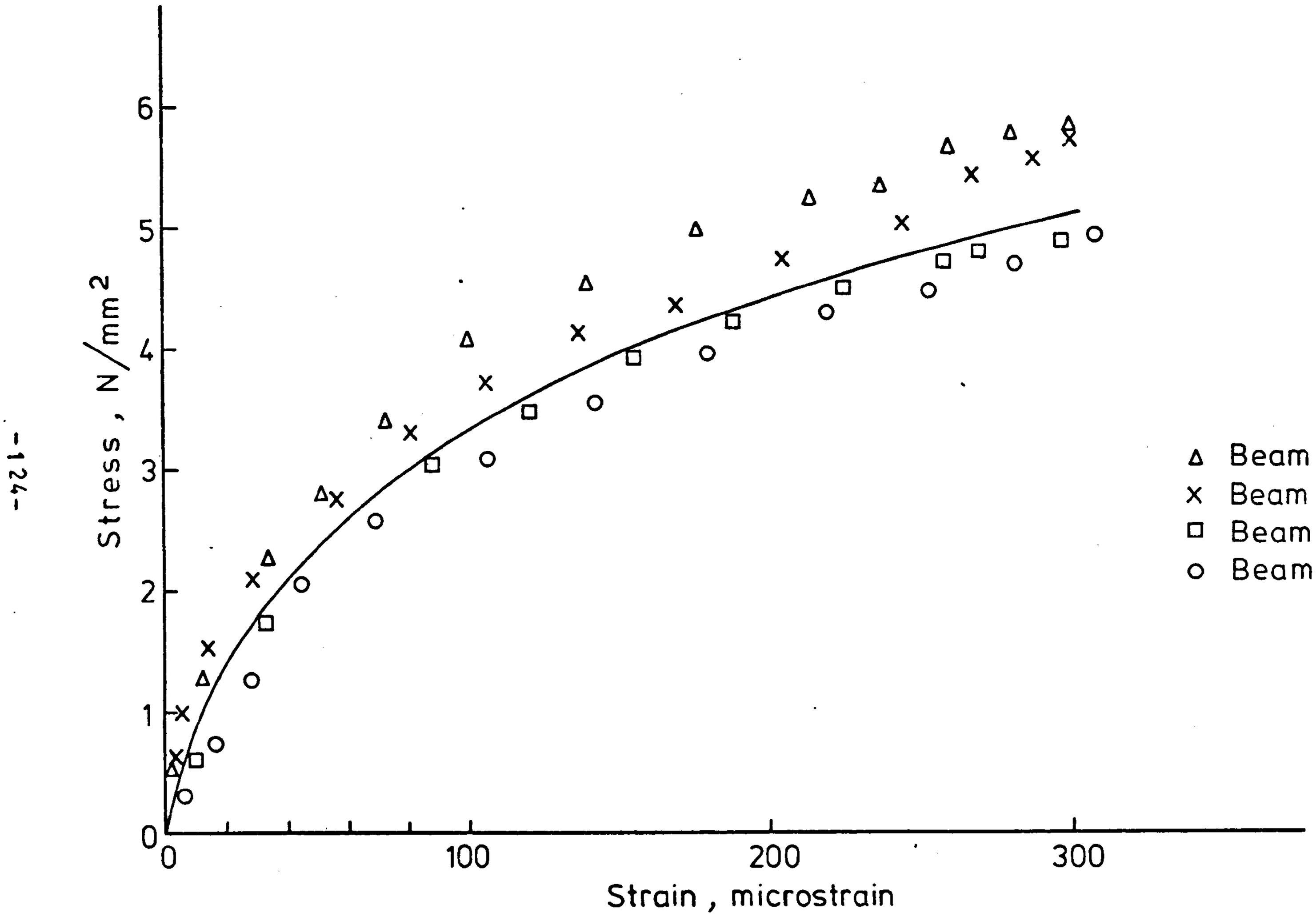

FIG. (4-4) STRESS—STRAIN RELATIONSHIP OF SATURATED GYPSUM IN TENSION FROM BENDING

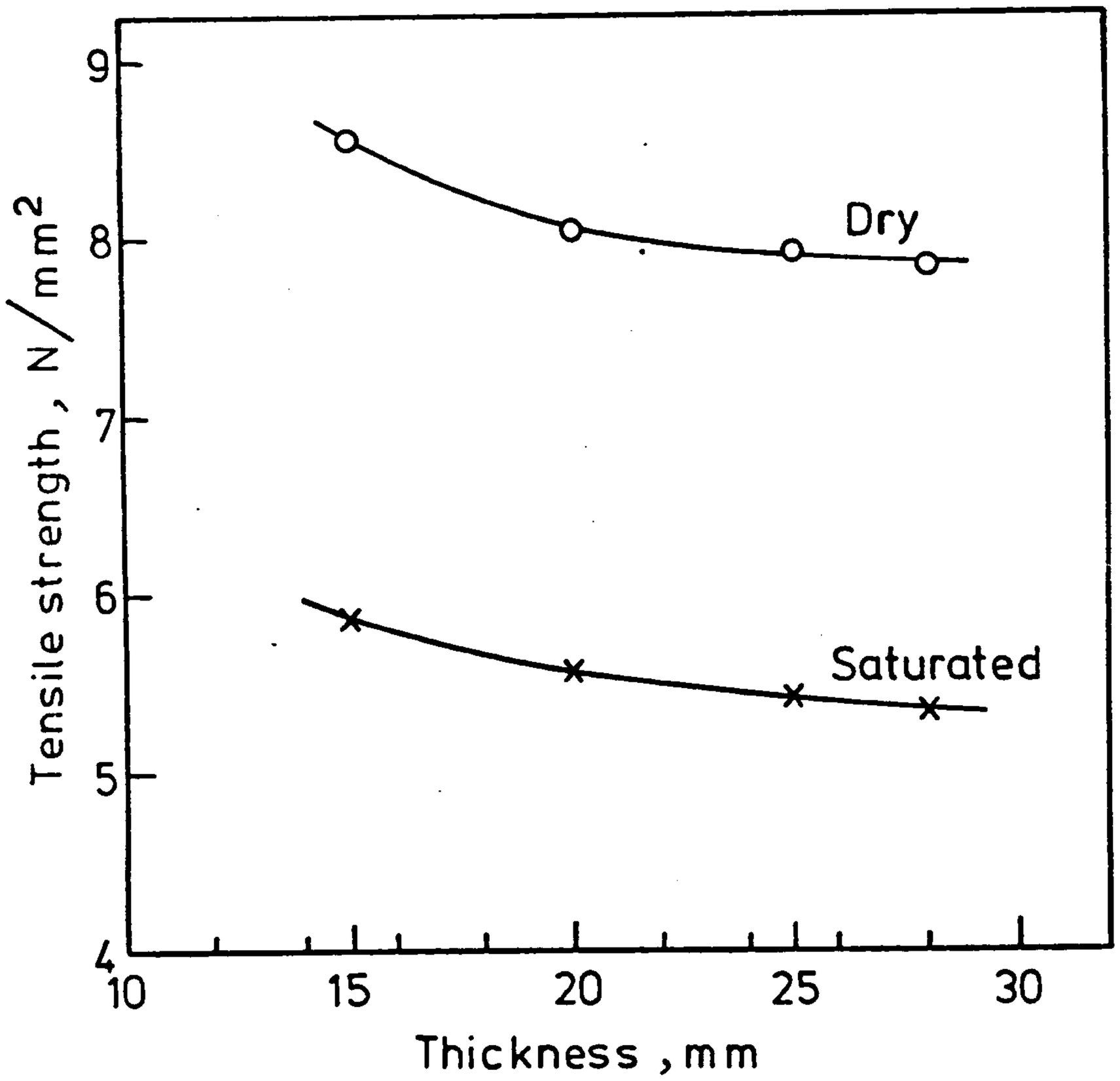

FIG. (4-5) TENSILE STRENGTH Vs BEAM THICKNESS

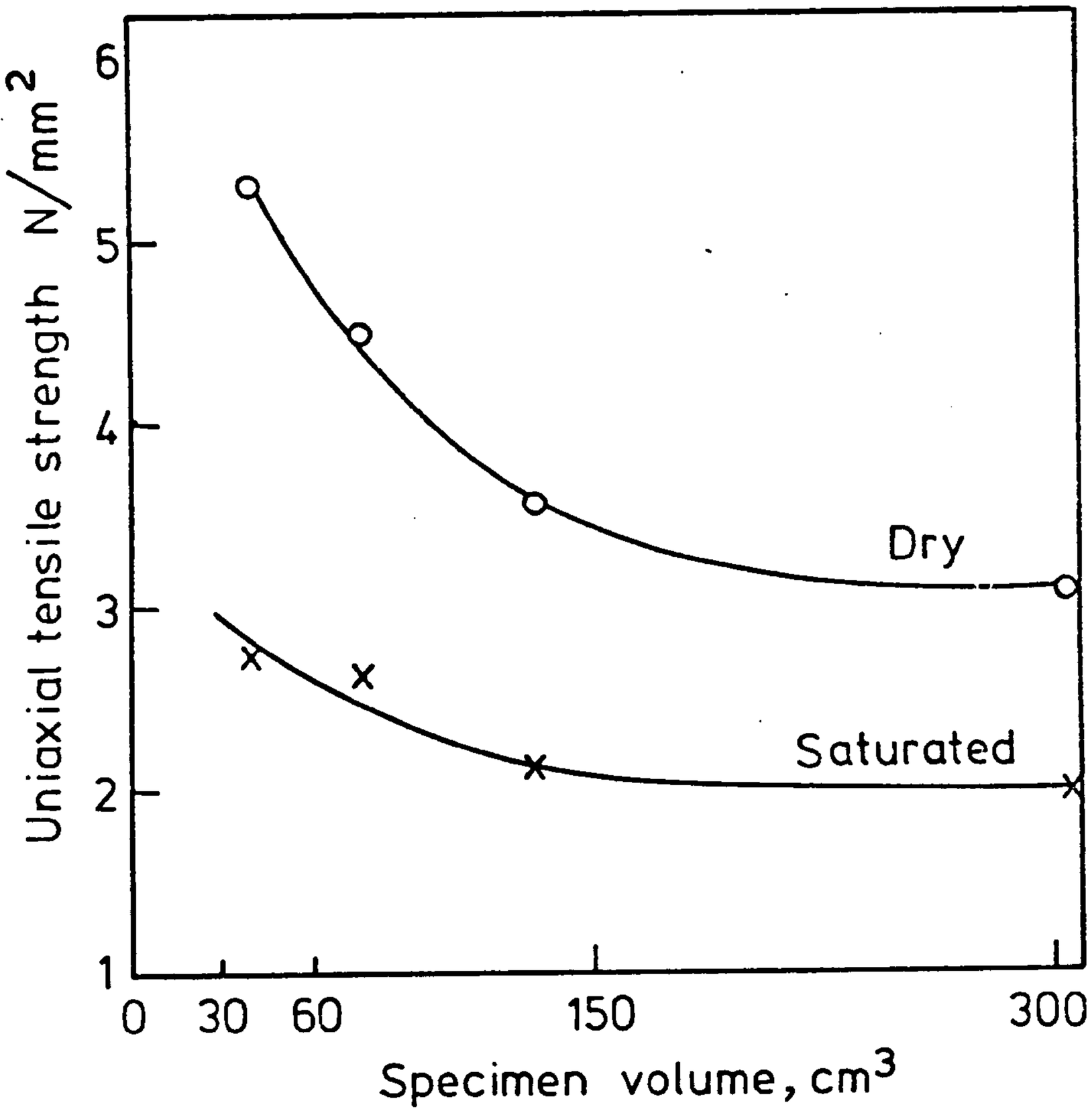

FIG. (4-6) EFFECT OF SPECIMEN SIZE ON THE UNIAXIAL TENSILE STRENGTH

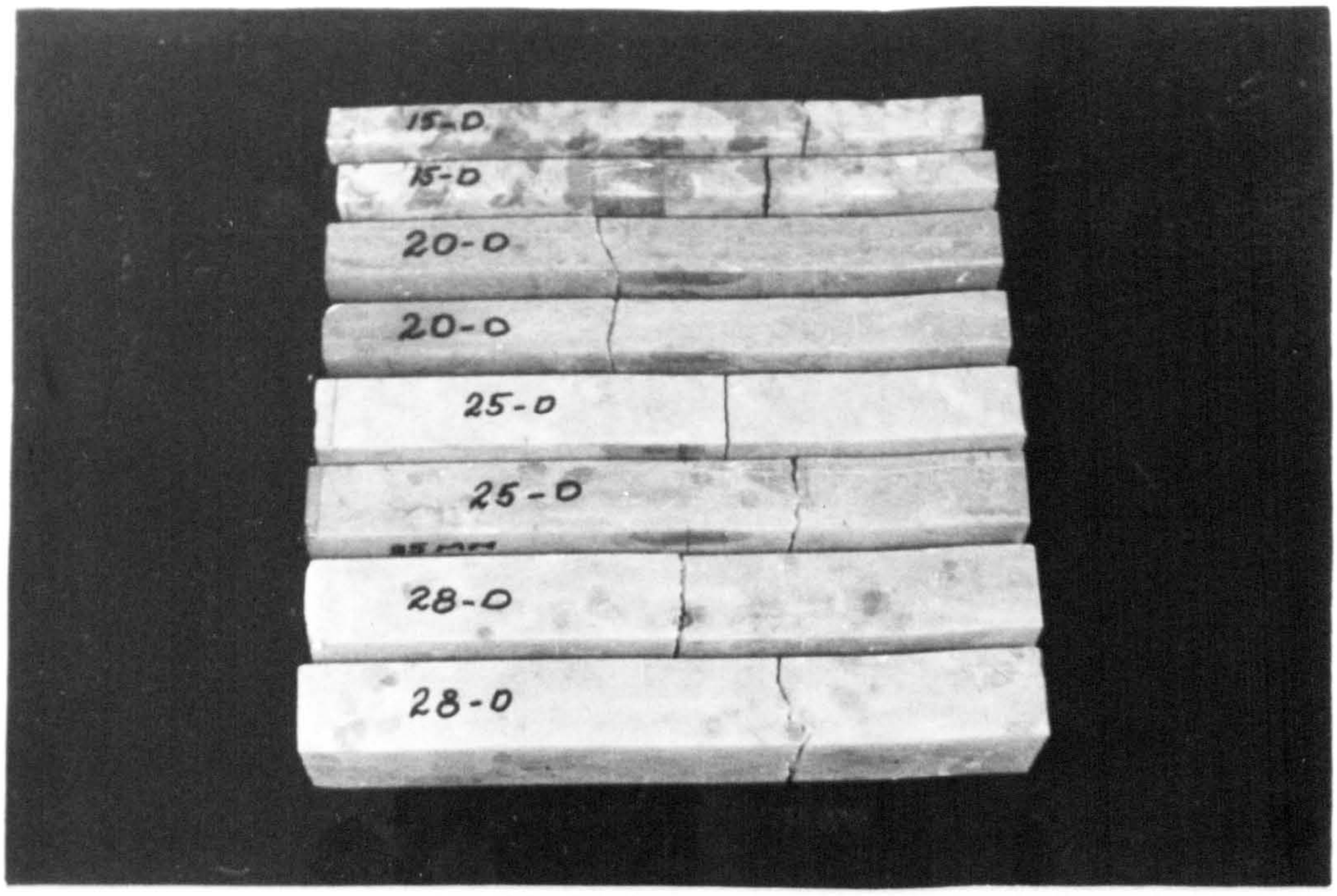

(A) Dry

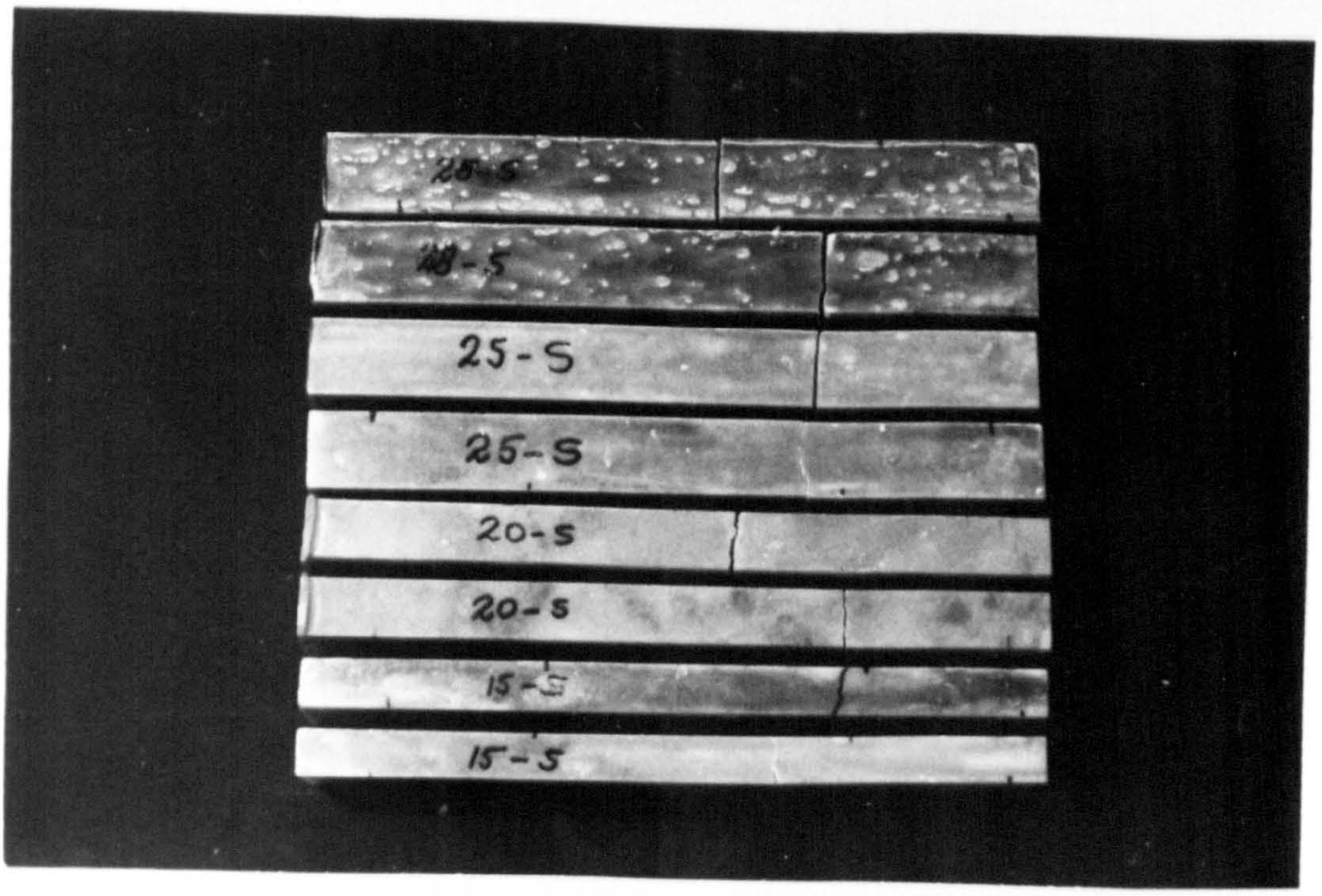

(B) Saturated

FIG. (4-7) FRACTURED SPECIMEN OF VARIOUS SIZES IN BENDING TESTS

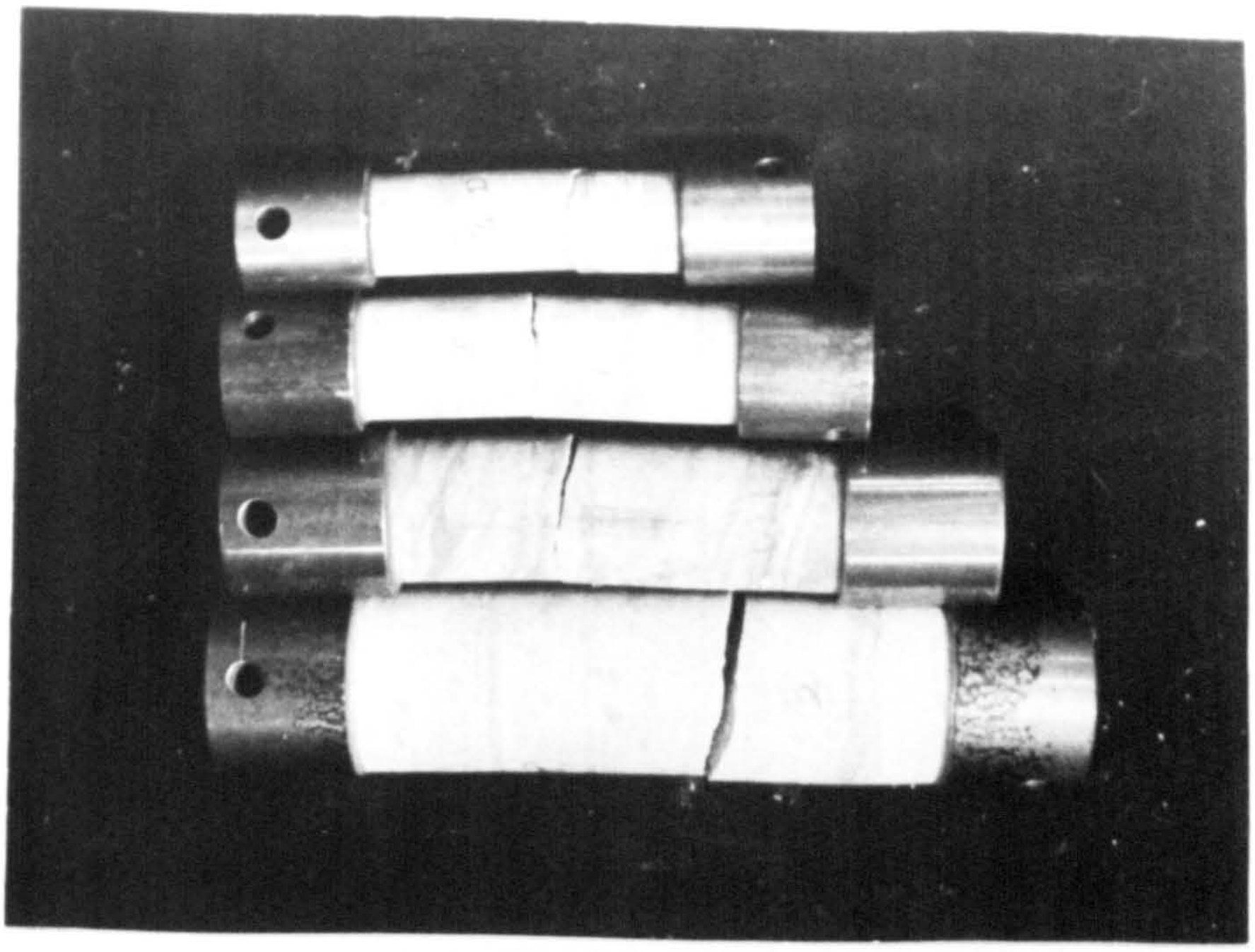

(A) Dry

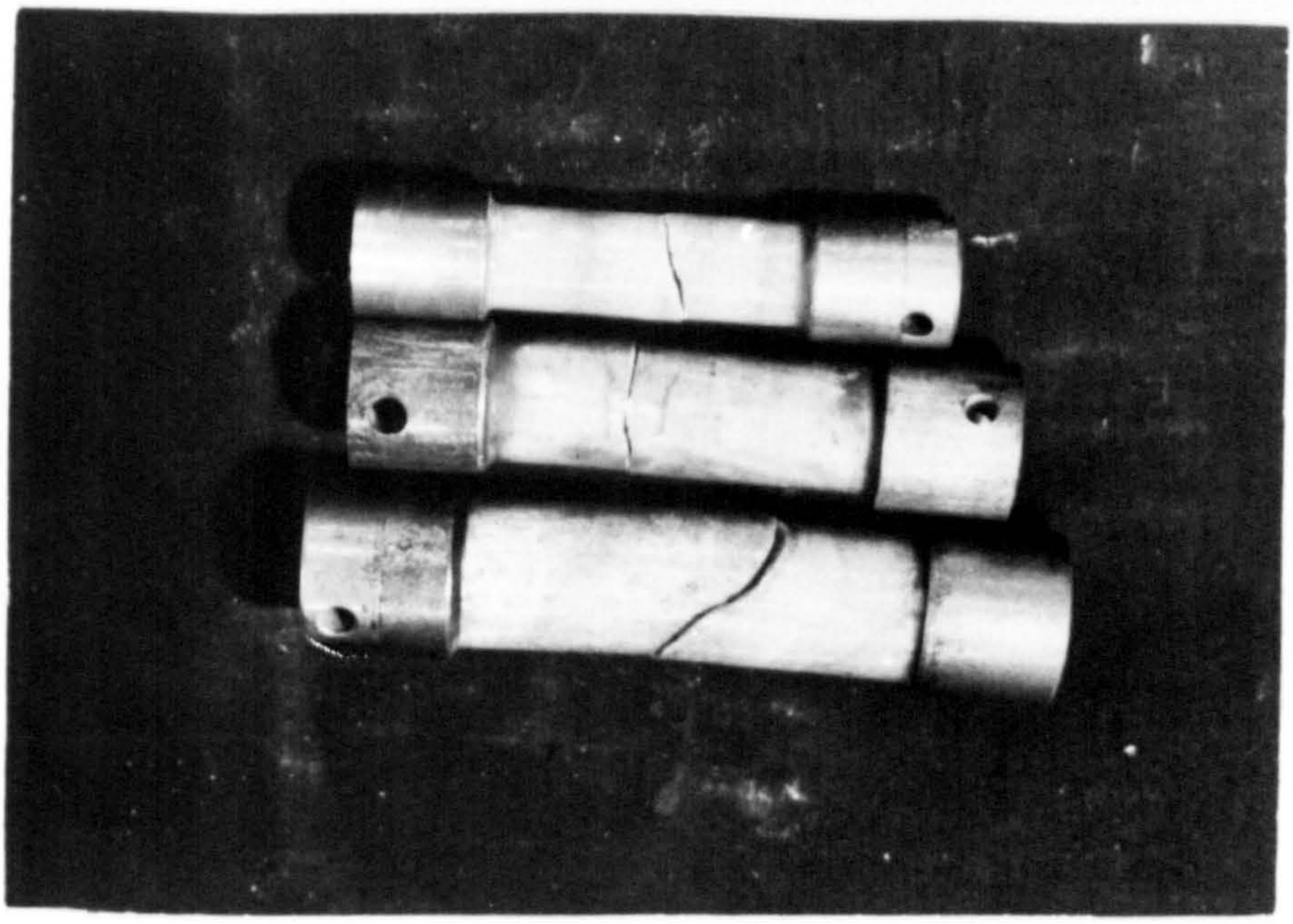

(B) Saturated

FIG. (4-8) FRACTURED SPECIMENS OF VARIOUS SIZES IN UNIAXIAL TENSILE TESTS

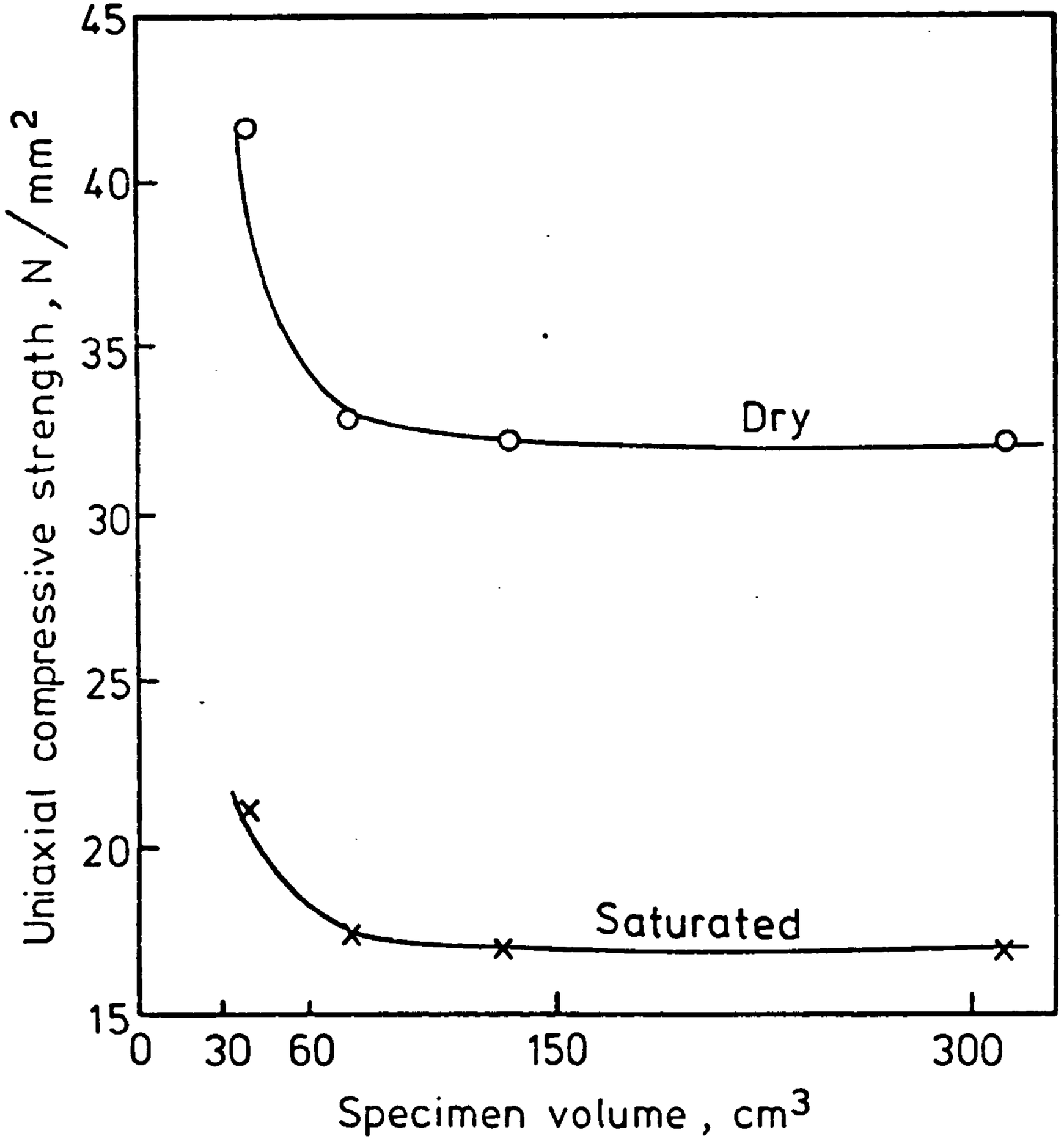

FIG.(4-9) EFFECT OF SPECIMEN SIZE ON THE UNIAXIAL COMPRESSIVE STRENGTH

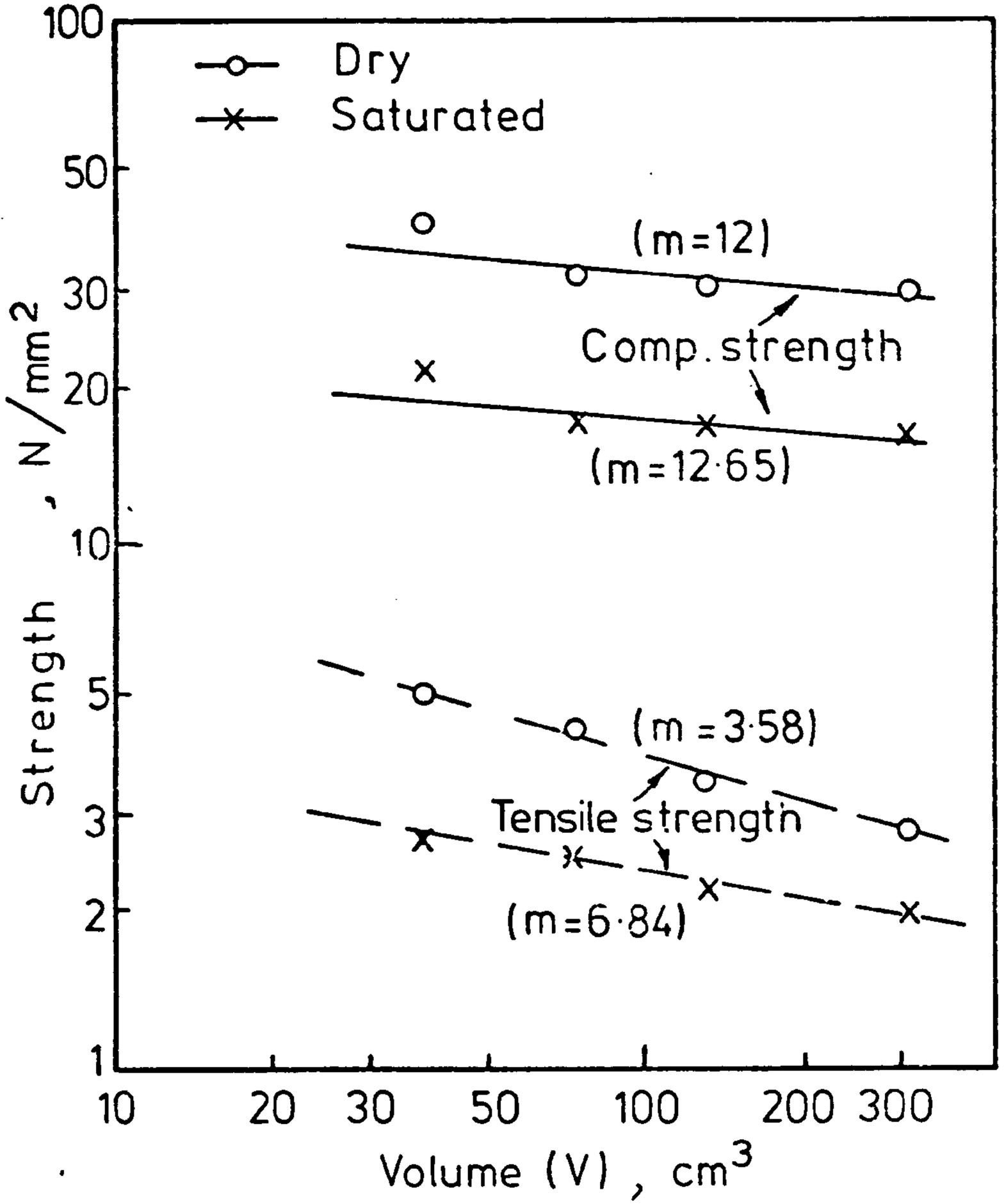

FIG. (4–10) STRENGTH Vs. SPECIMEN VOLUME (Log — Log graph)

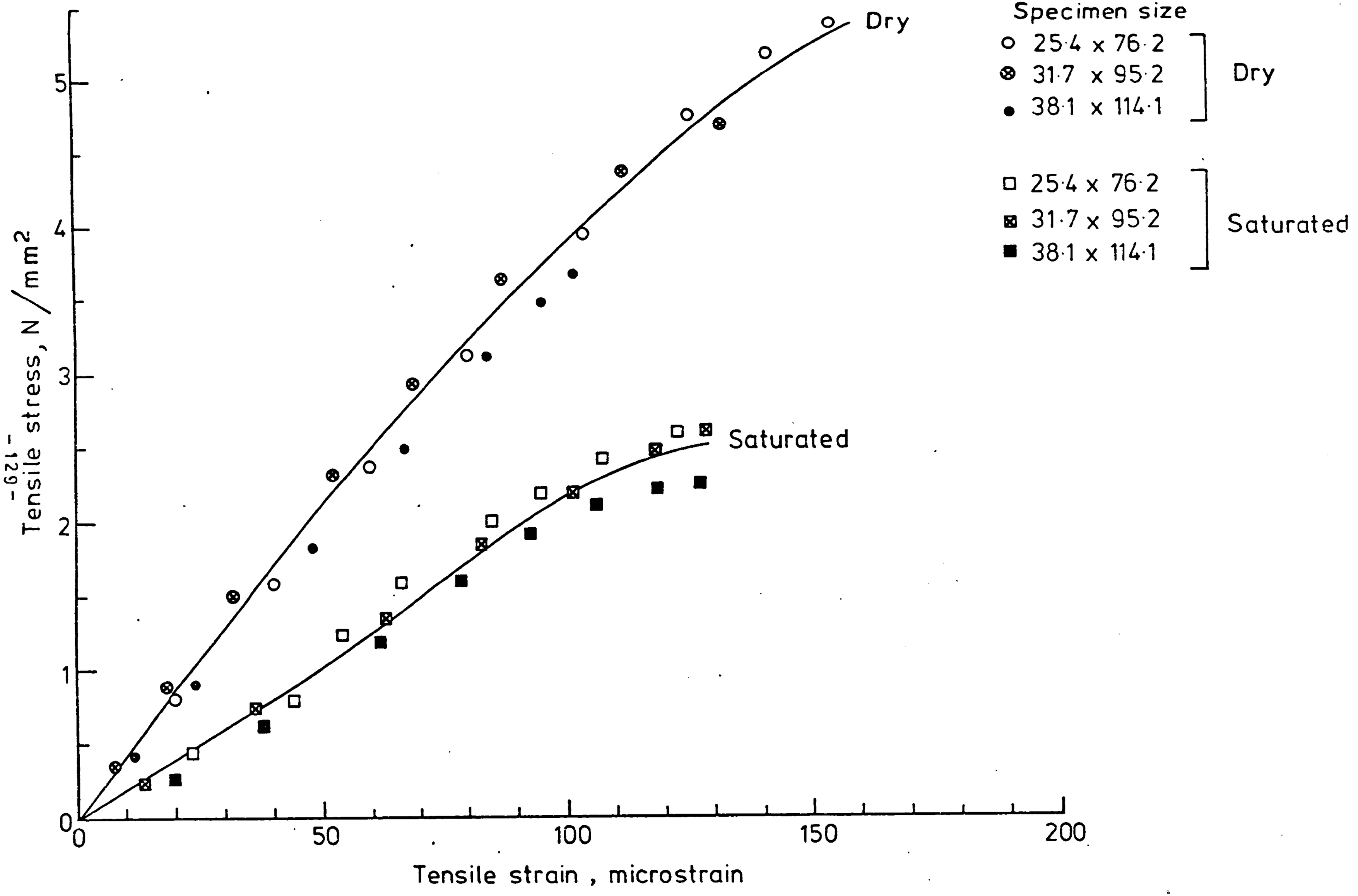

FIG. (4–11) UNIAXIAL TENSILE STRESS–STRAIN RELATIONSHIPS OF DRY AND SATURATED GYPSUM

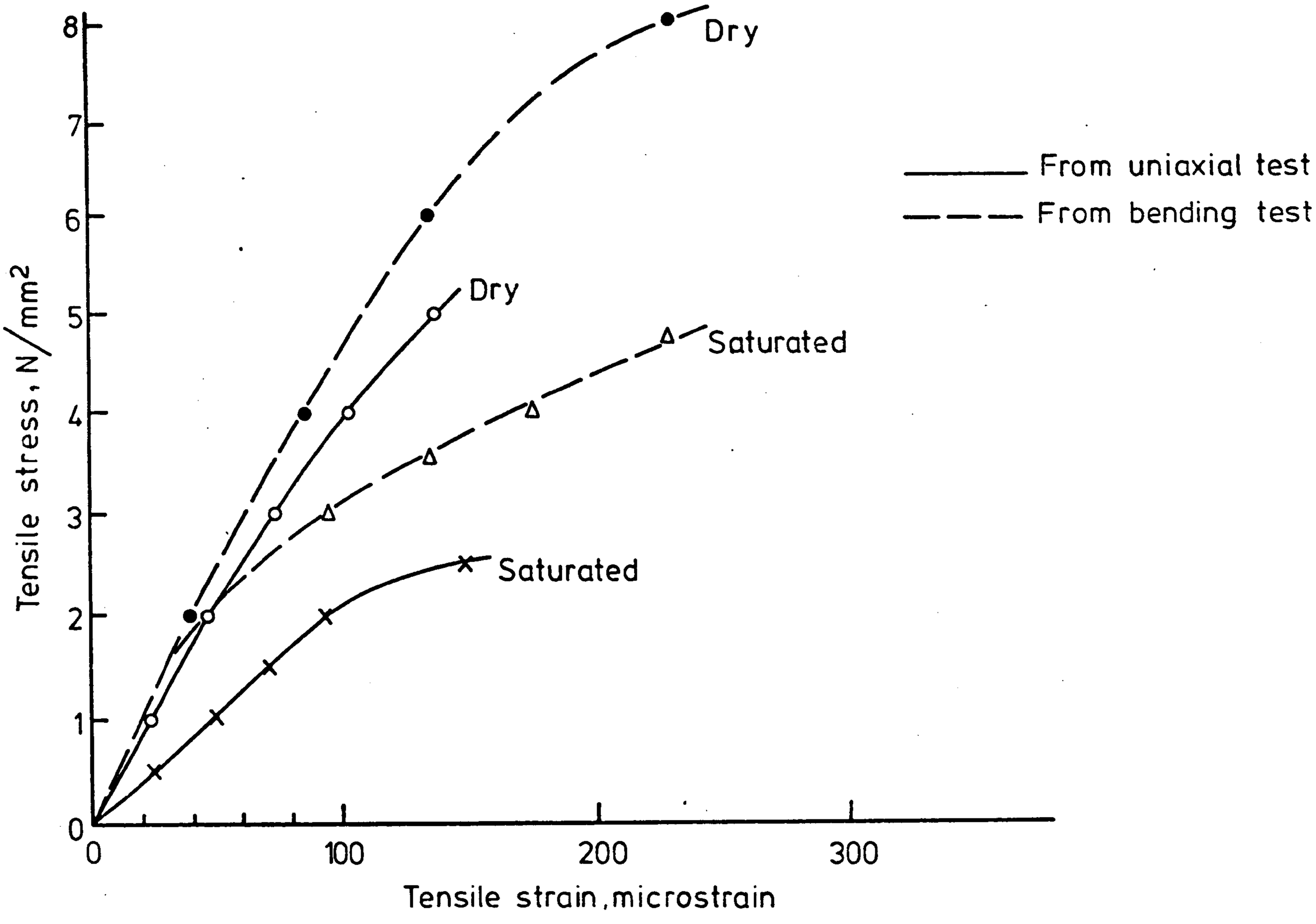

FIG.(4-12) COMPARISON OF STRESS- STRAIN IN TENSION FROM BENDING AND UNIAXIAL TESTS

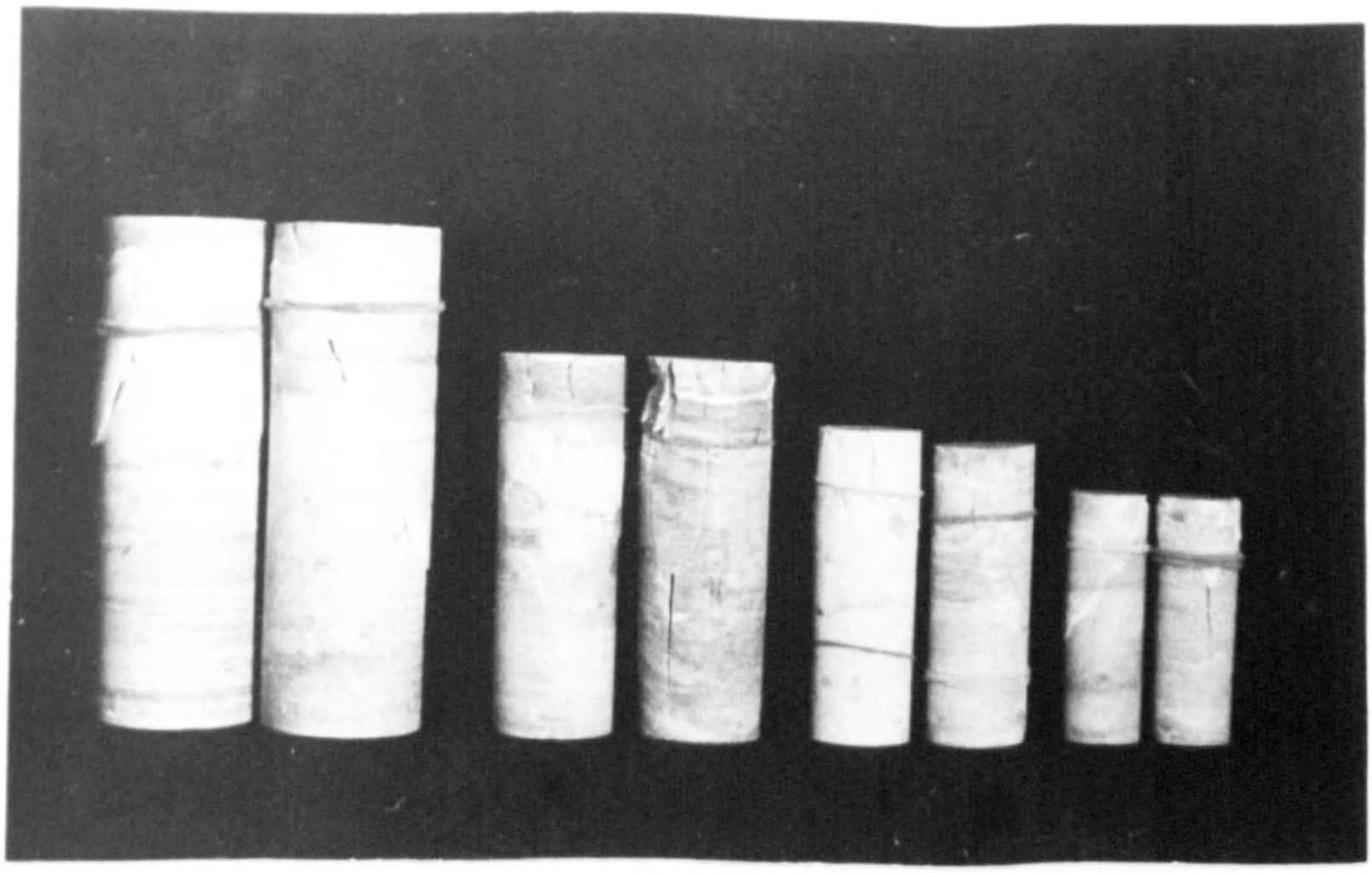

(A) Dry

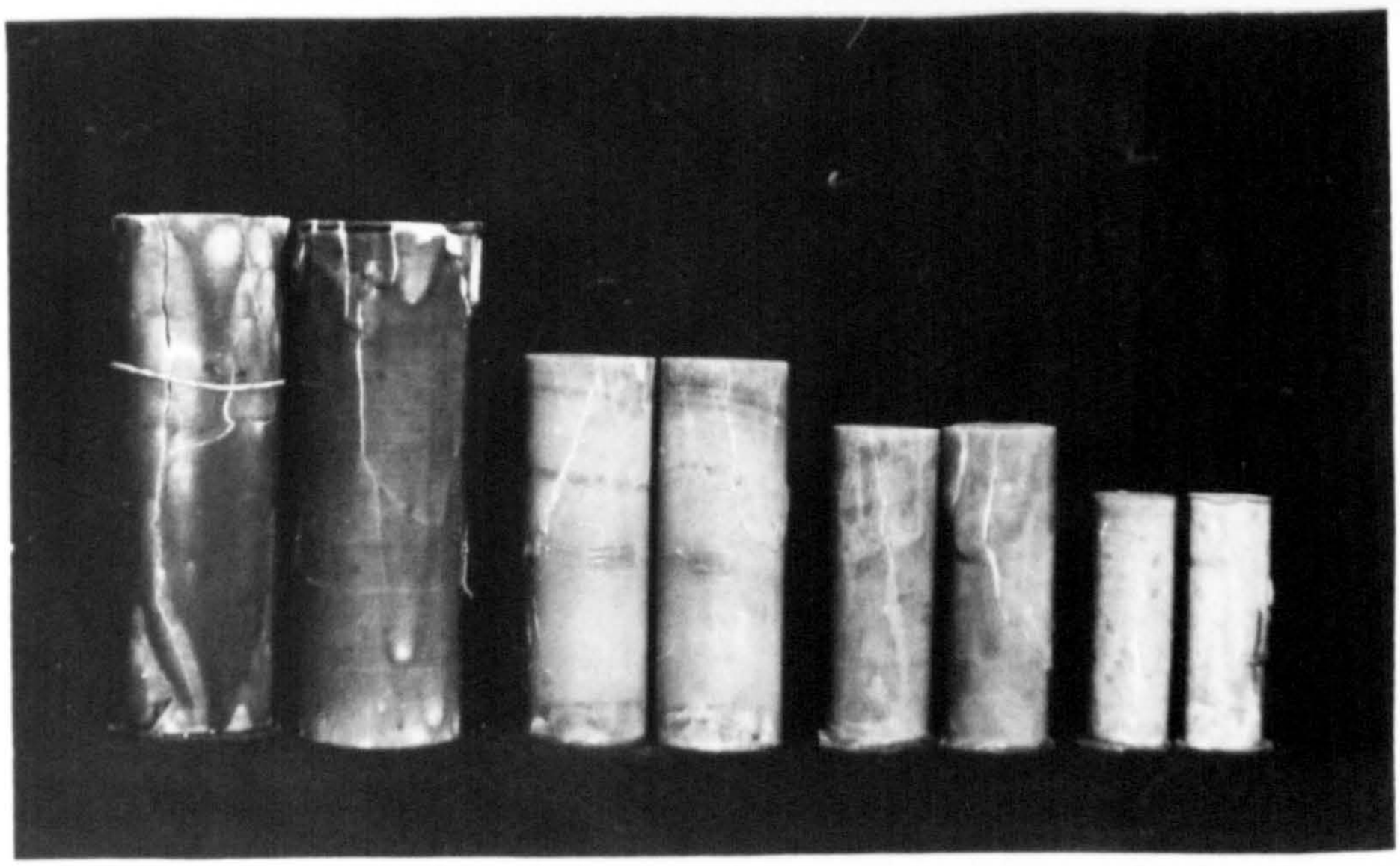

(B) Saturated

FIG. (4-13) FRACTURED SPECIMENS OF VARIOUS SIZES IN UNIAXIAL COMPRESSION TESTS

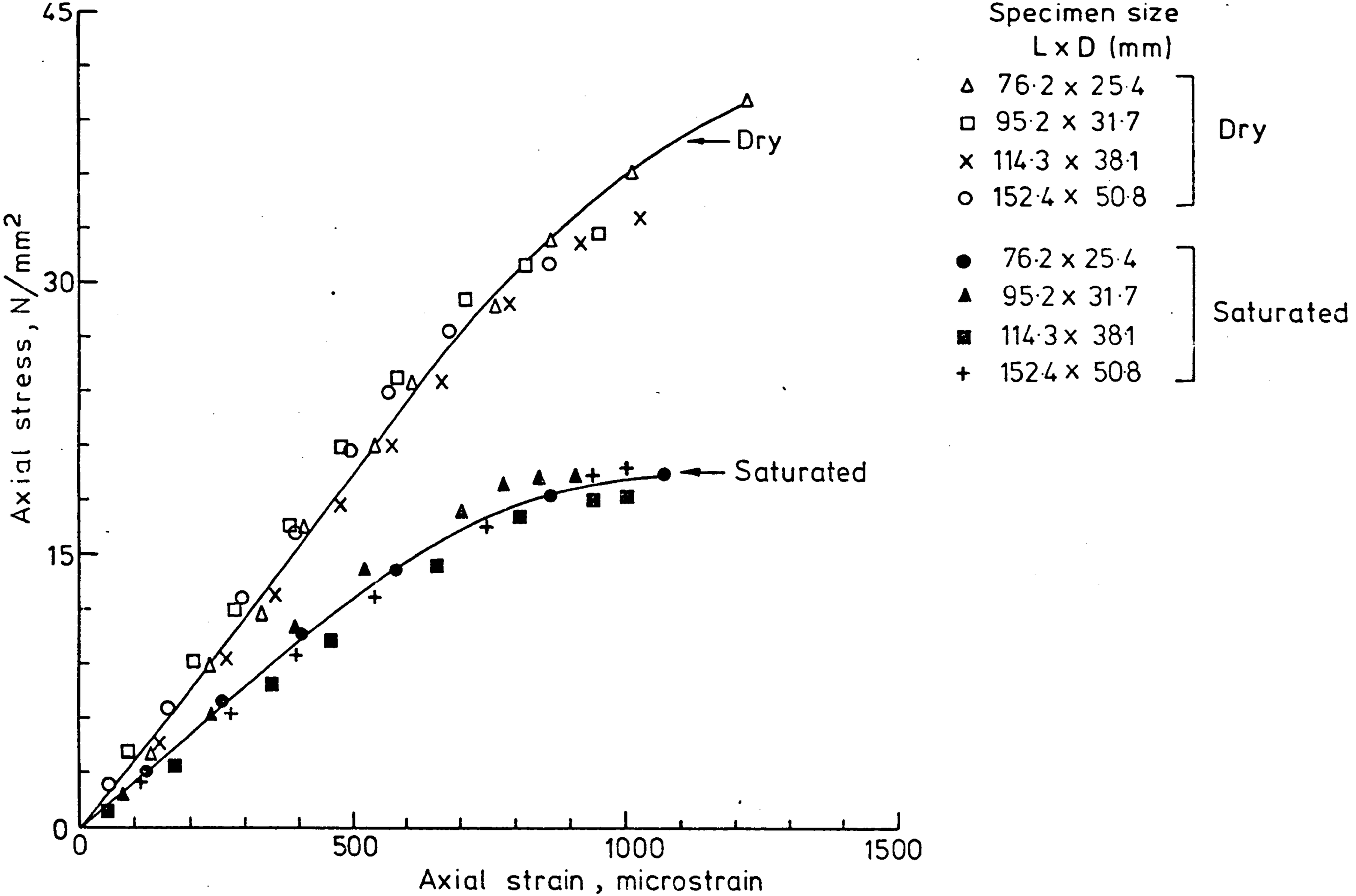

FIG. (4-14) STRESS – STRAIN RELATIONSHIP OF DRY AND SATURATED GYPSUM IN UNIAXIAL COMPRESSION TEST

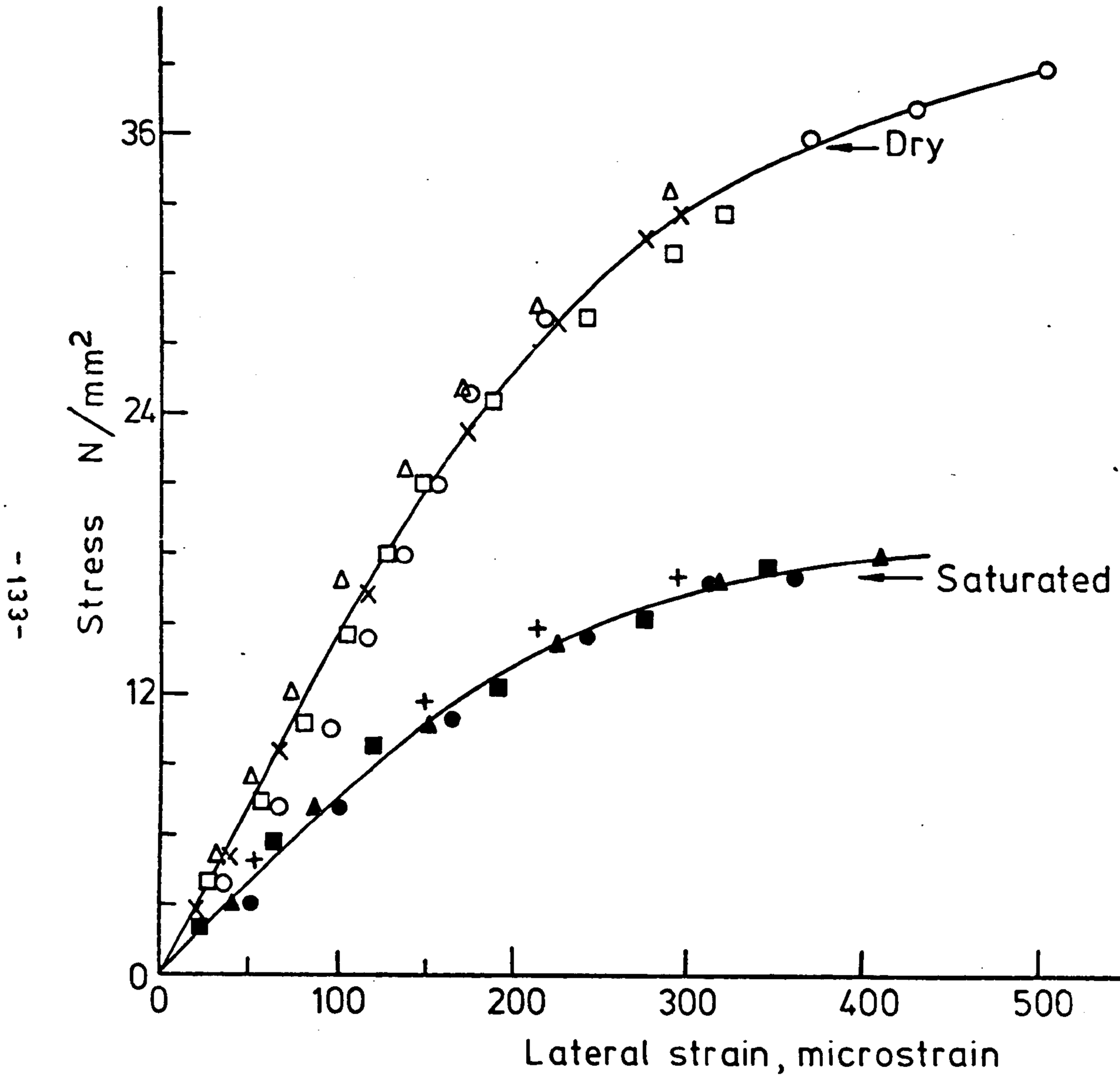

FIG. (4-15) STRESS–LATERAL STRAIN RELATIONSHIP OF DRY AND SATURATED GYPSUM IN UNIAXIAL COMPRESSION TEST

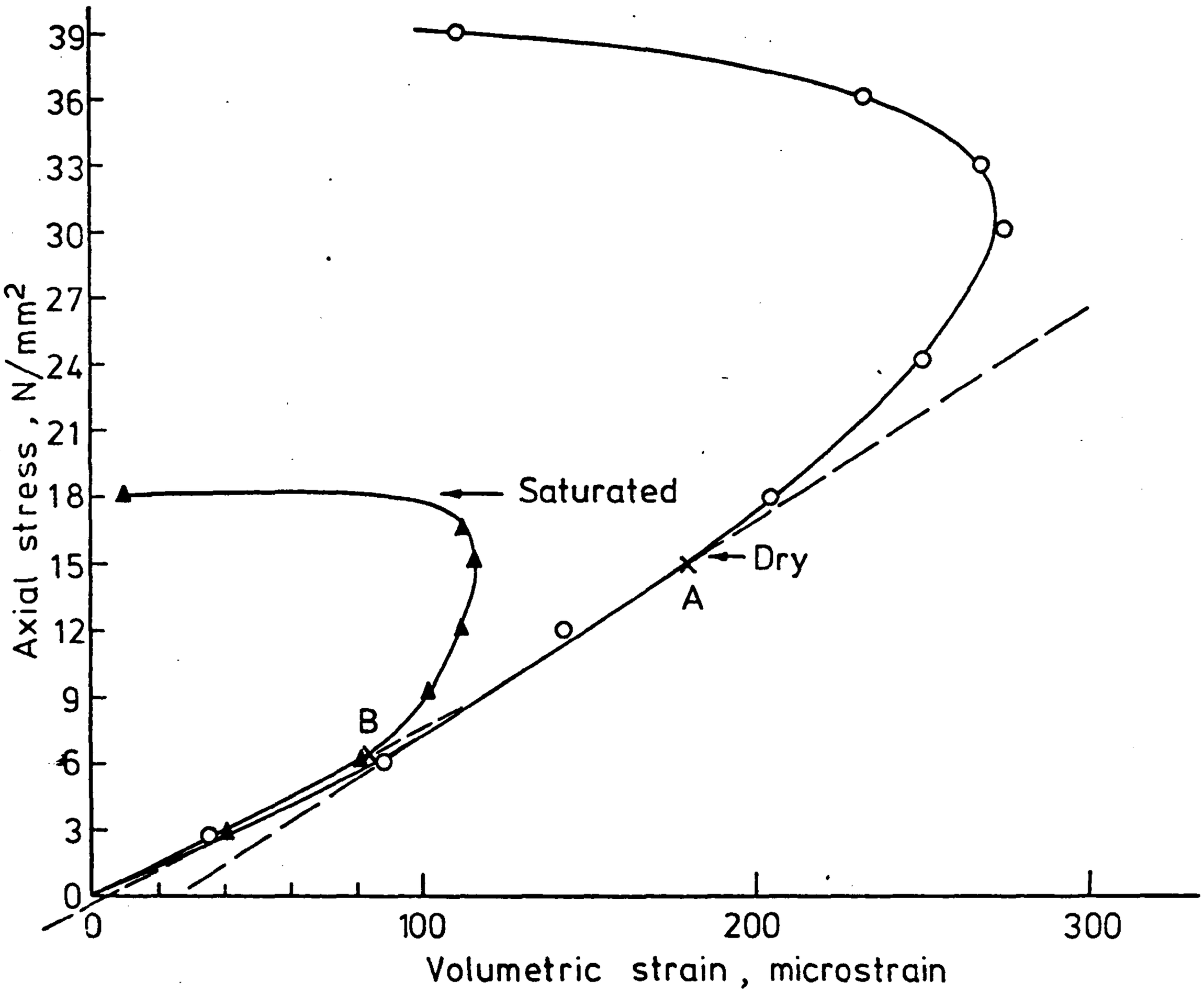

FIG. (4–16) AXIAL STRESS Vs. VOLUMETRIC STRAIN IN UNIAXIAL COMPRESSION TEST

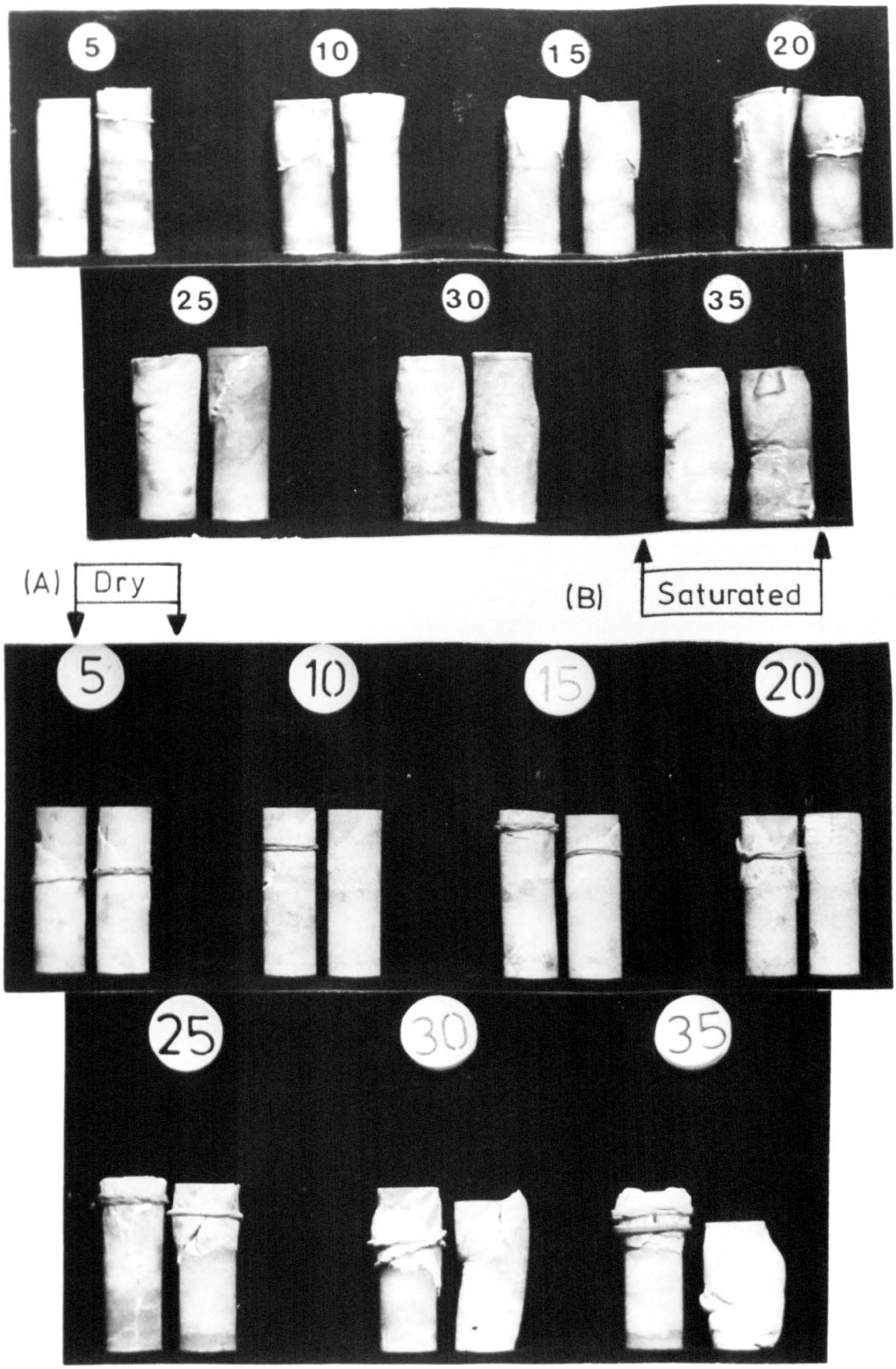

Number above the specimens represents confining pressure, N/mm^2

FIG (4-17) TESTED SPECIMENS AT VARIOUS CONFINING PRESSURES, SIZE −76·2 x 25·4 mm (L x D)

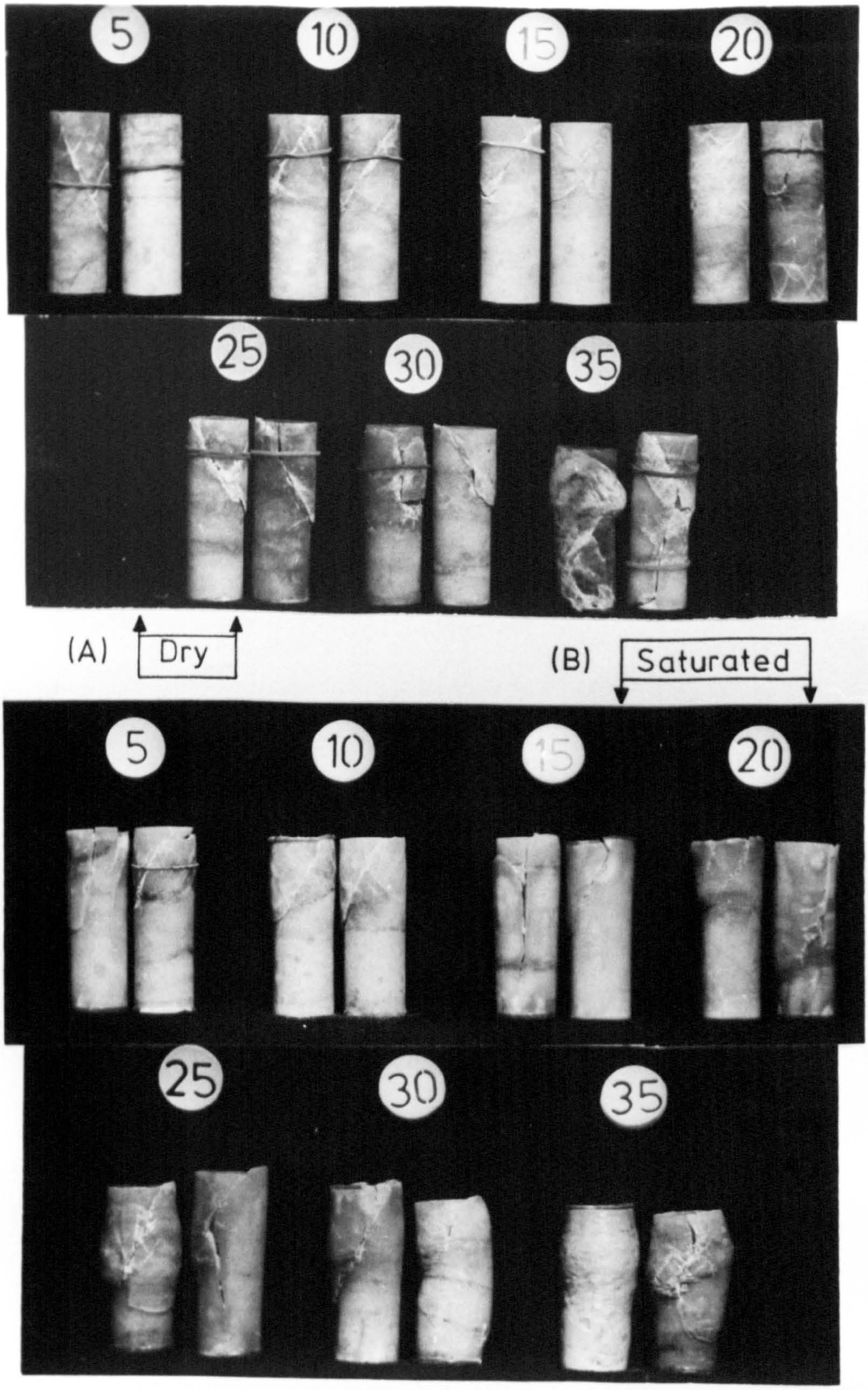

Number above the specimen represents confining pressure, N/mm^2

FIG (4-18) TESTED SPECIMENS AT VARIOUS CONFINING PRESSURES, SIZE - 95·25x 31·75 mm (L x D)

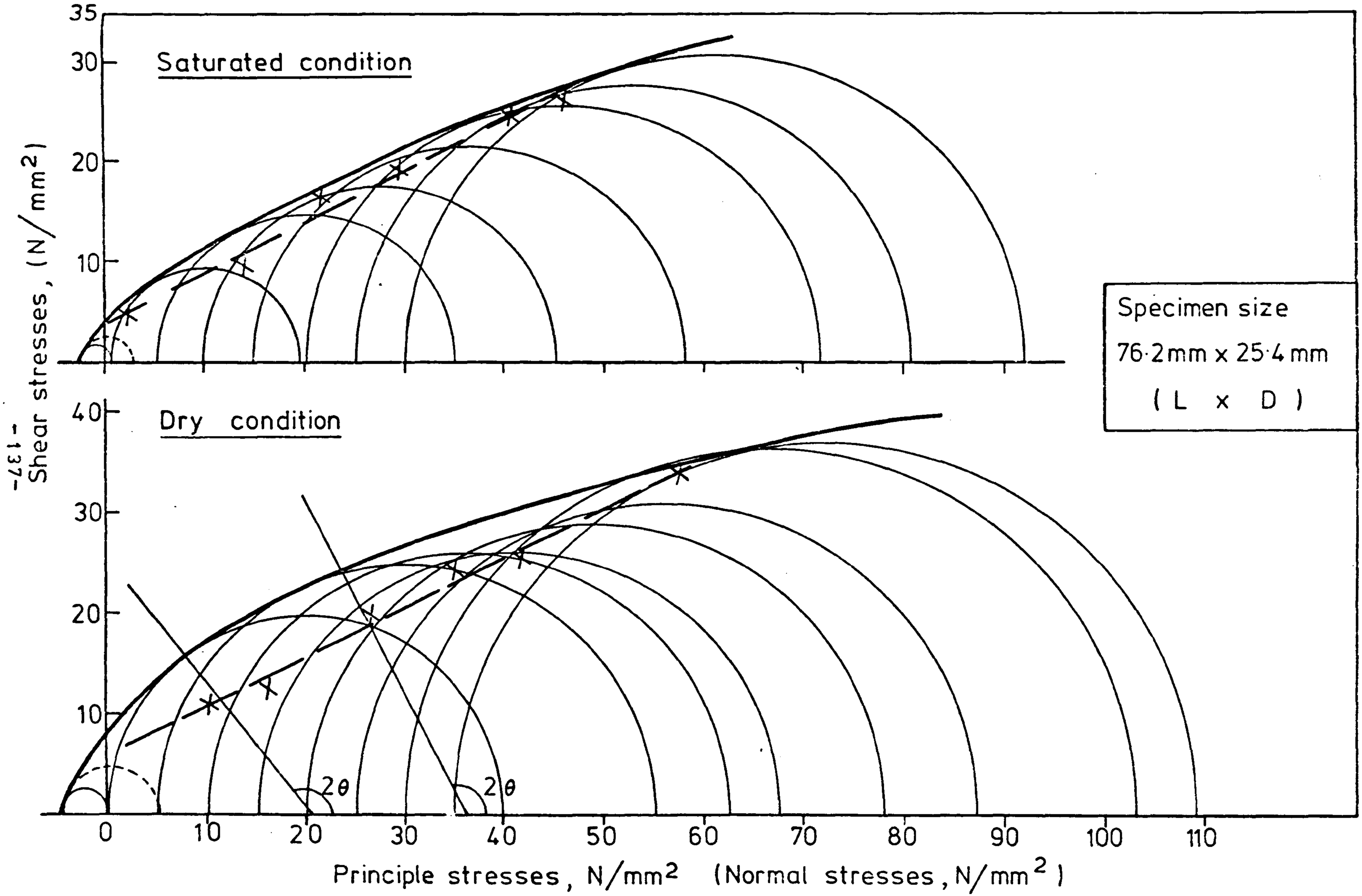

FIG. (4-19) MOHR'S ENVELOPE FOR DRY AND SATURATED GYPSUM AT THE SPECIFIED SPECIMEN SIZE

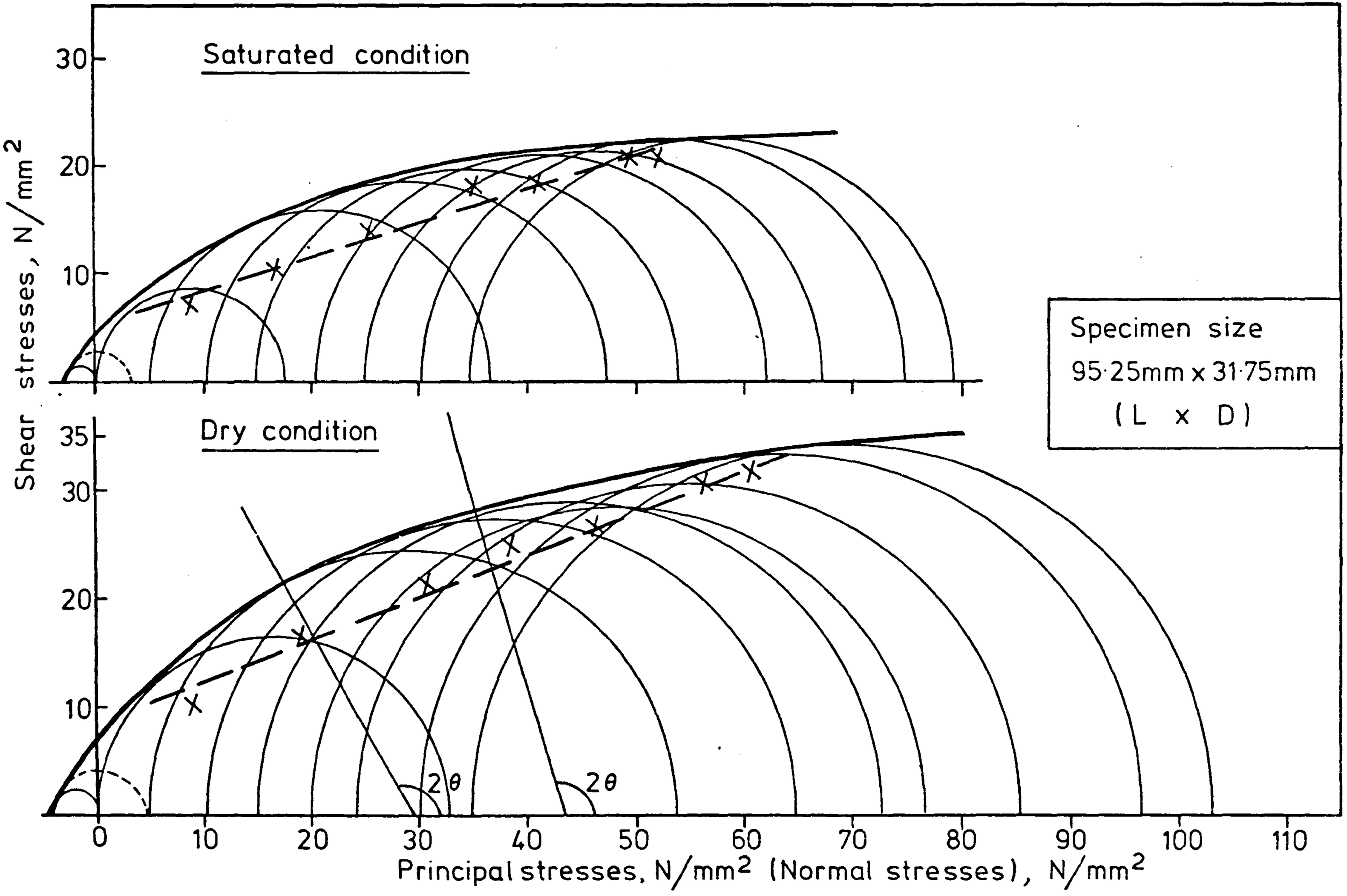

FIG. (4-20) MOHR'S ENVELOPE FOR DRY AND SATURATED GYPSUM AT THE SPECIFIED SPECIMEN SIZE

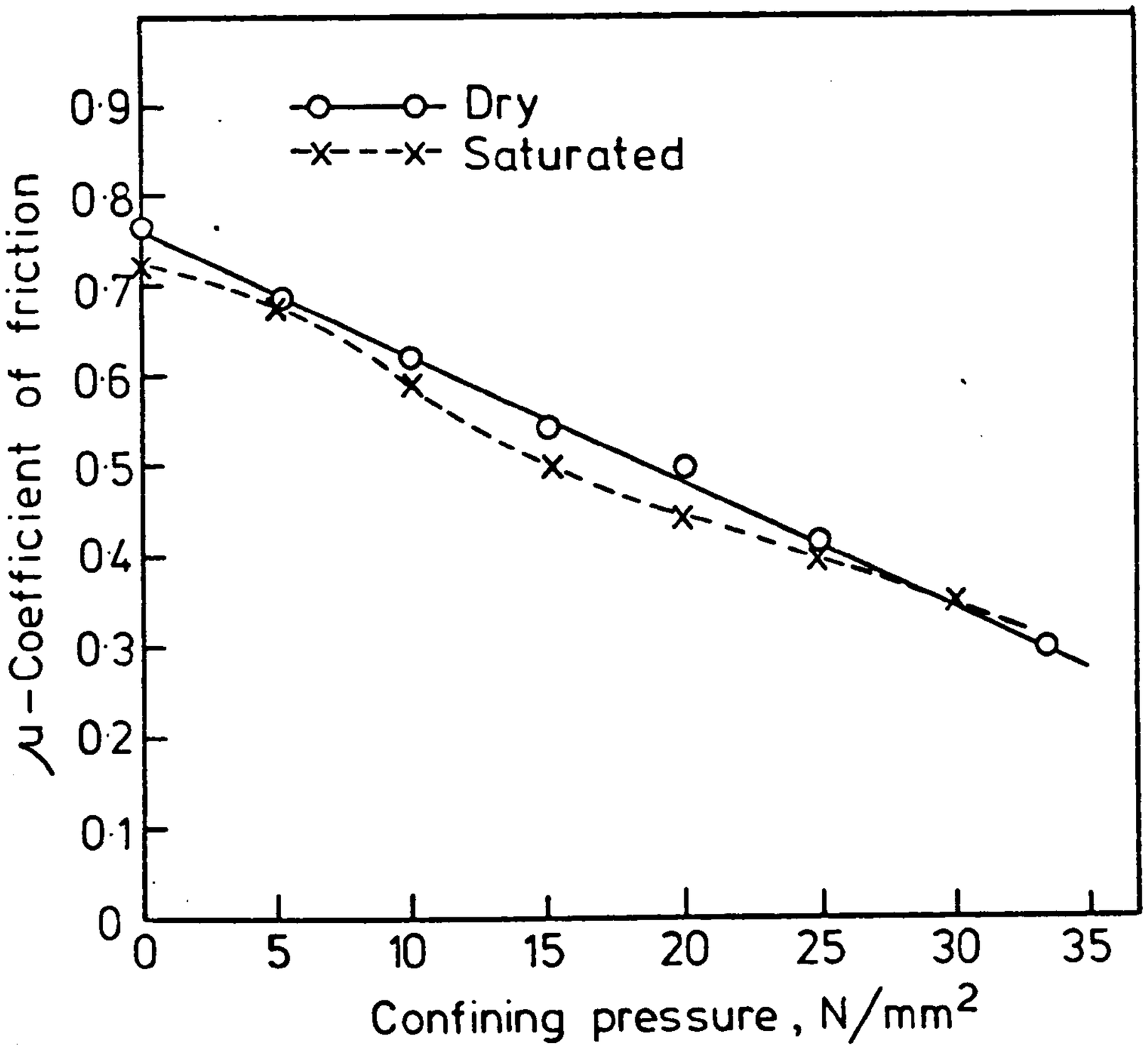

FIG. (4-21) SATURATION EFFECT ON THE COEFFICIENT OF FRICTION AT VARIOUS CONFINING PRESSURES

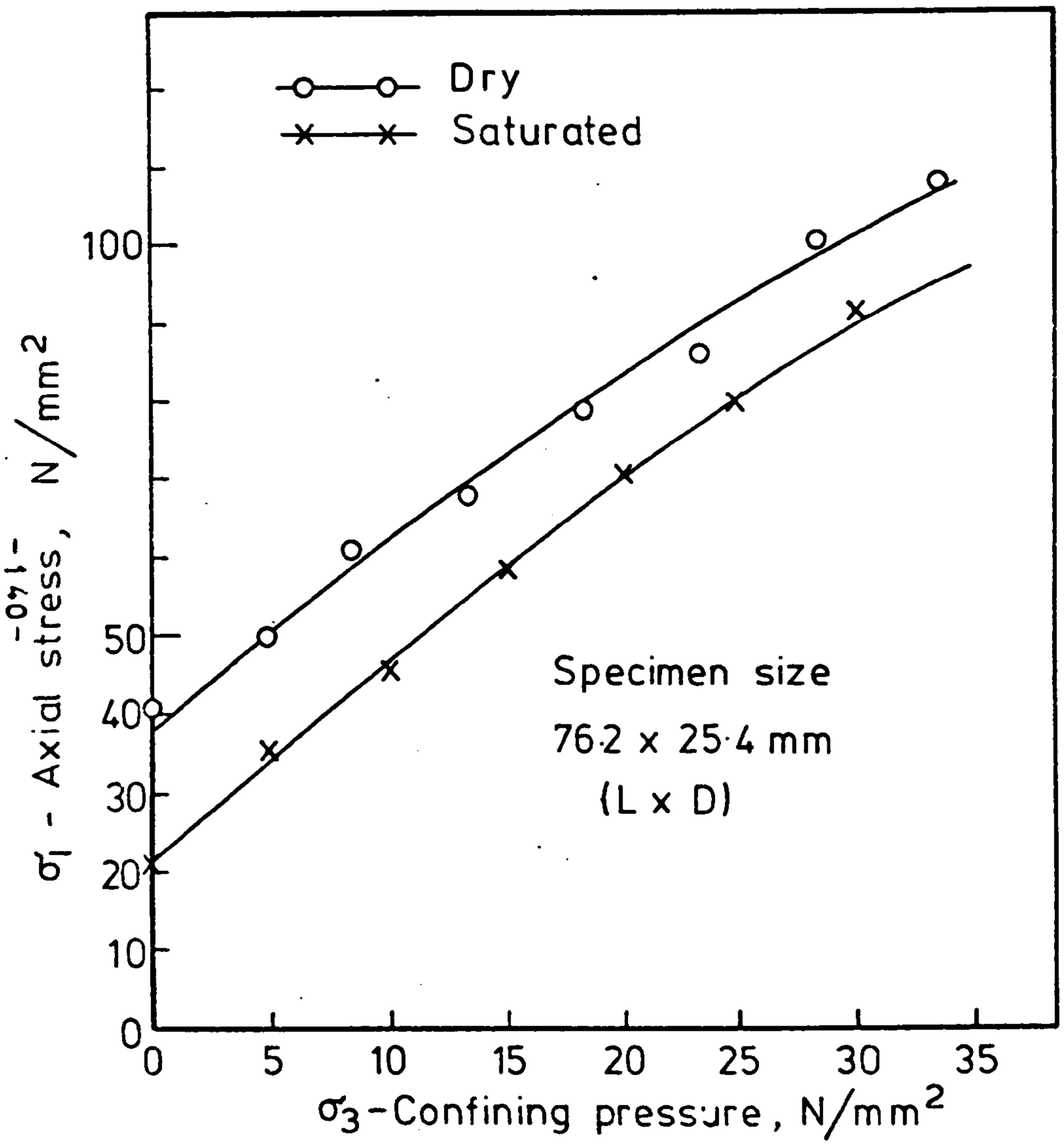

FIG.(4-22) RELATIONSHIP BETWEEN σ_1 & σ_3

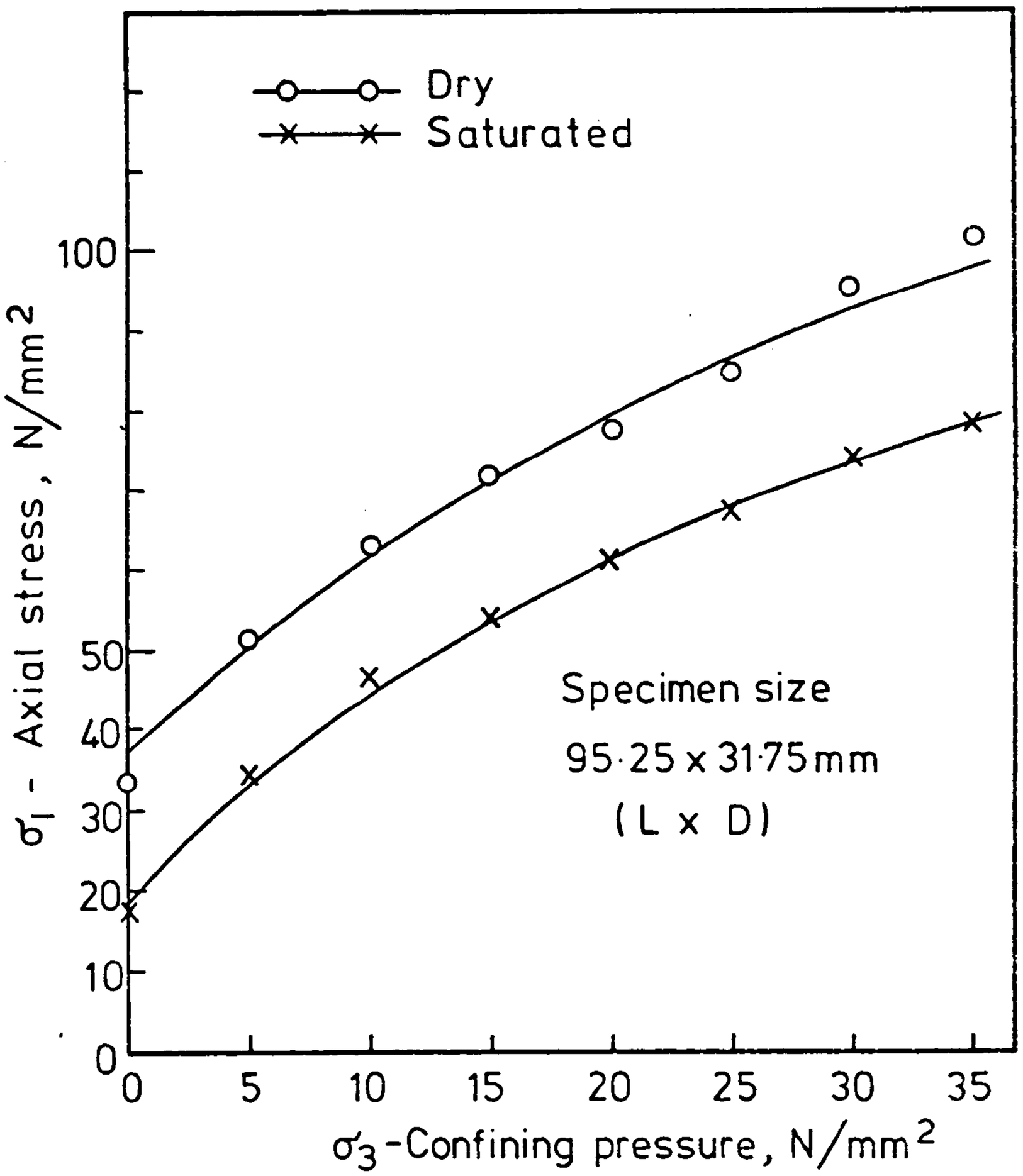

FIG. (4-23) RELATIONSHIP BETWEEN σ_1 & σ_3

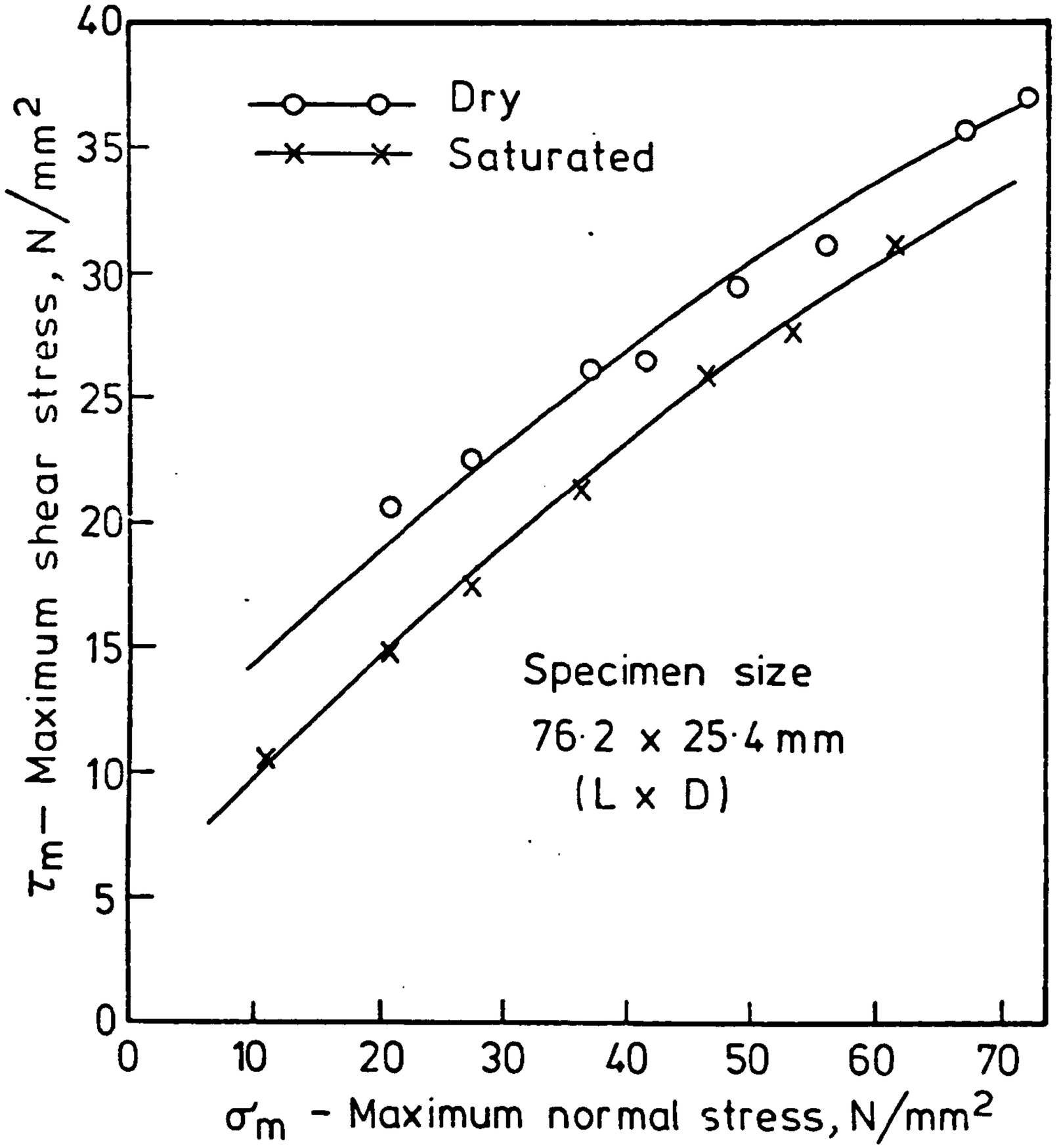

FIG. (4-24) RELATIONSHIP BETWEEN σ_m & τ_m

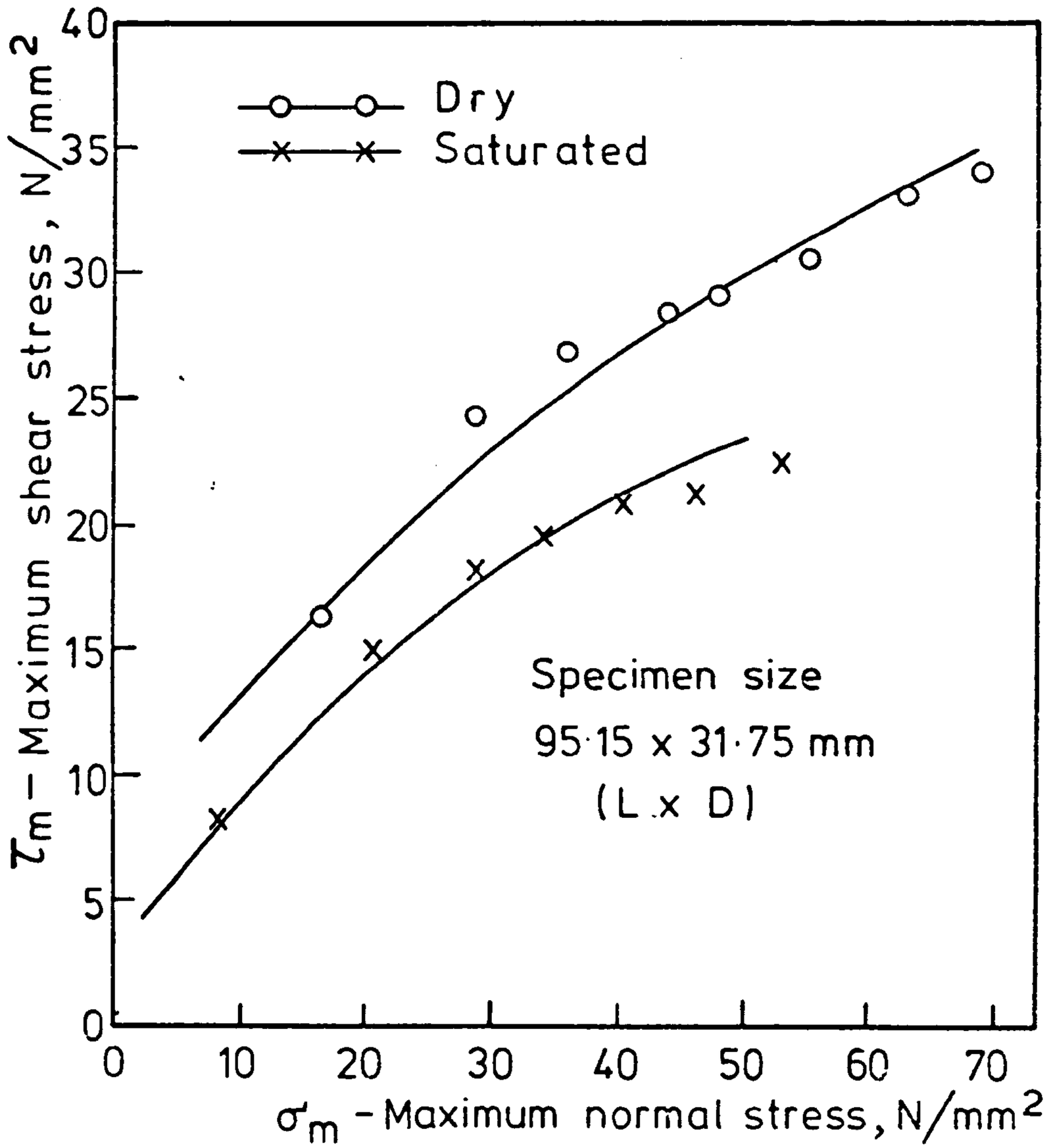

FIG. (4-25) RELATIONSHIP BETWEEN σ_m & τ_m

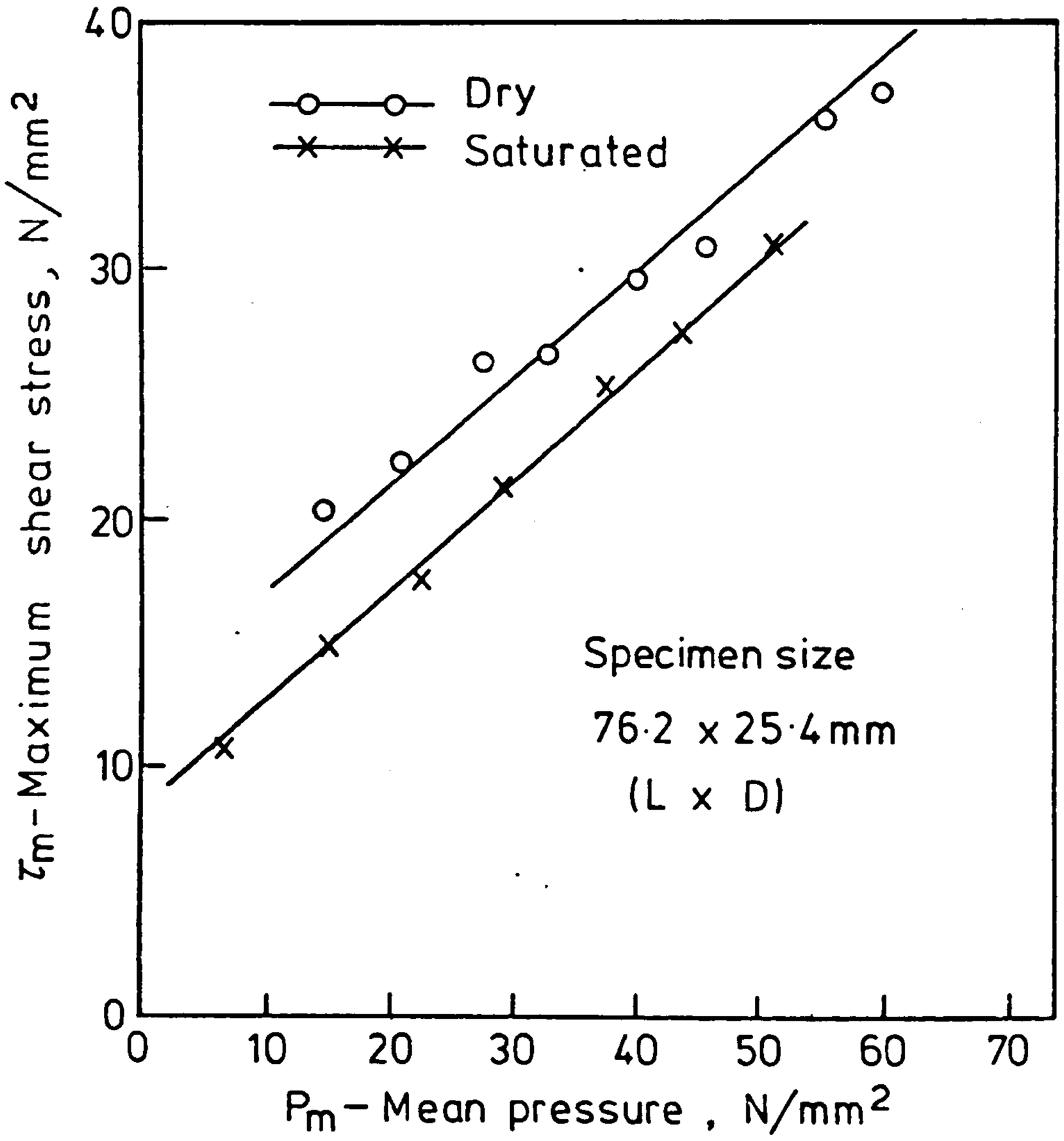

FIG. (4-26) MAX. SHEAR STRESS Vs. MEAN PRESSURE

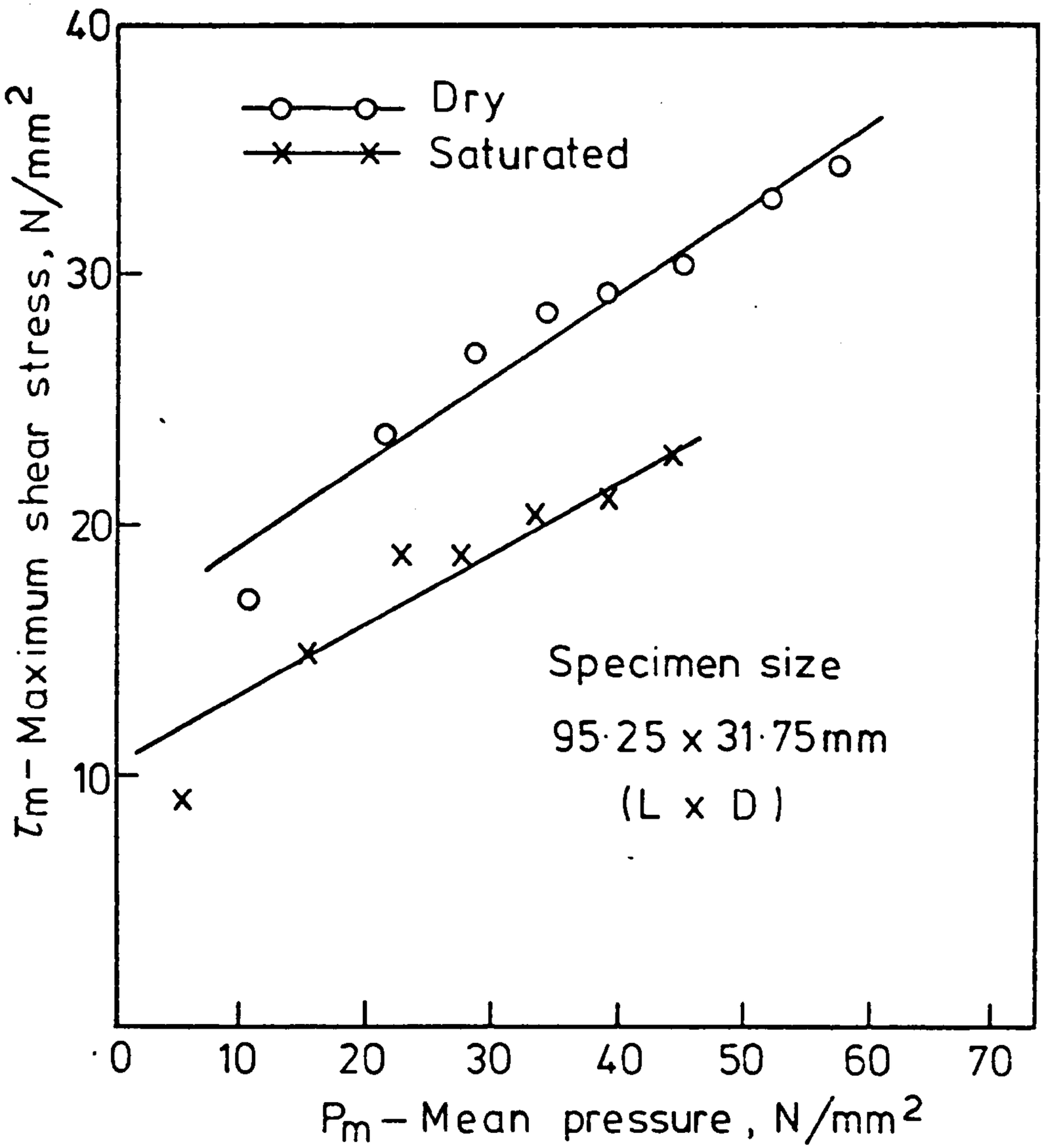

FIG.(4-27) MAX. SHEAR STRESS Vs. MEAN PRESSURE

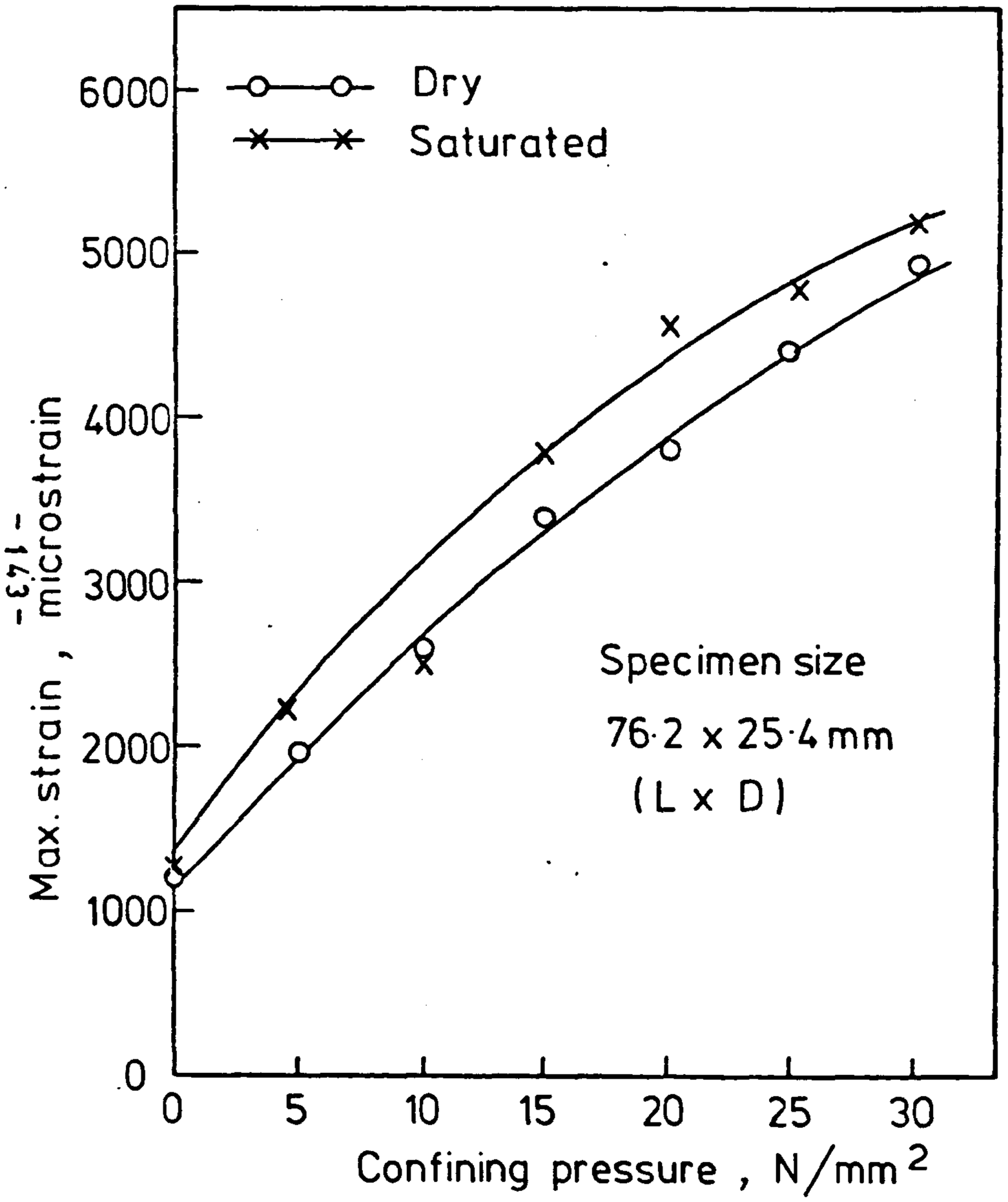

FIG. (4-28) CONFINING PRESSURE Vs. MAX. STRAIN

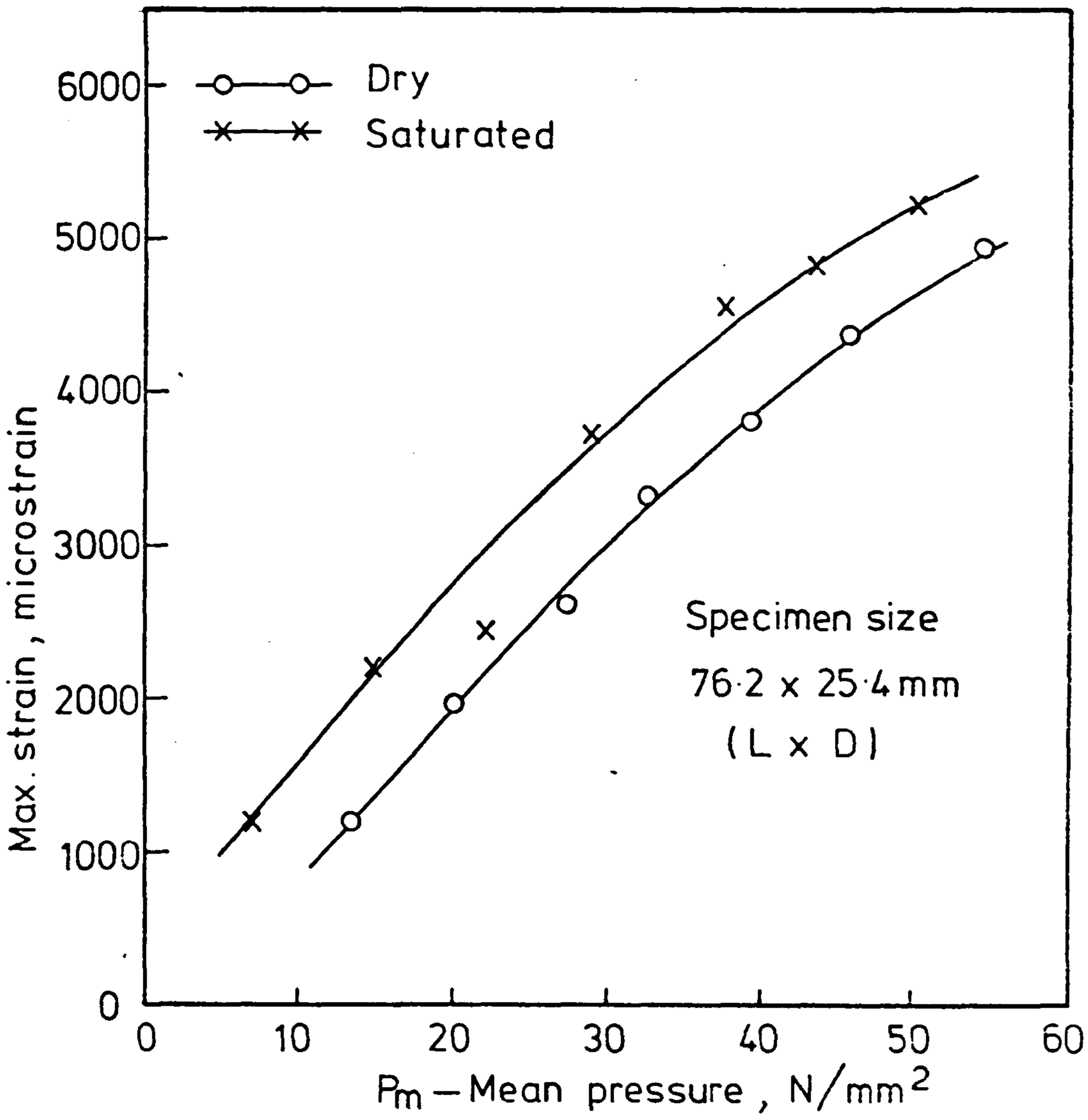

FIG. (4-29) MEAN PRESSURE Vs. MAX. STRAIN

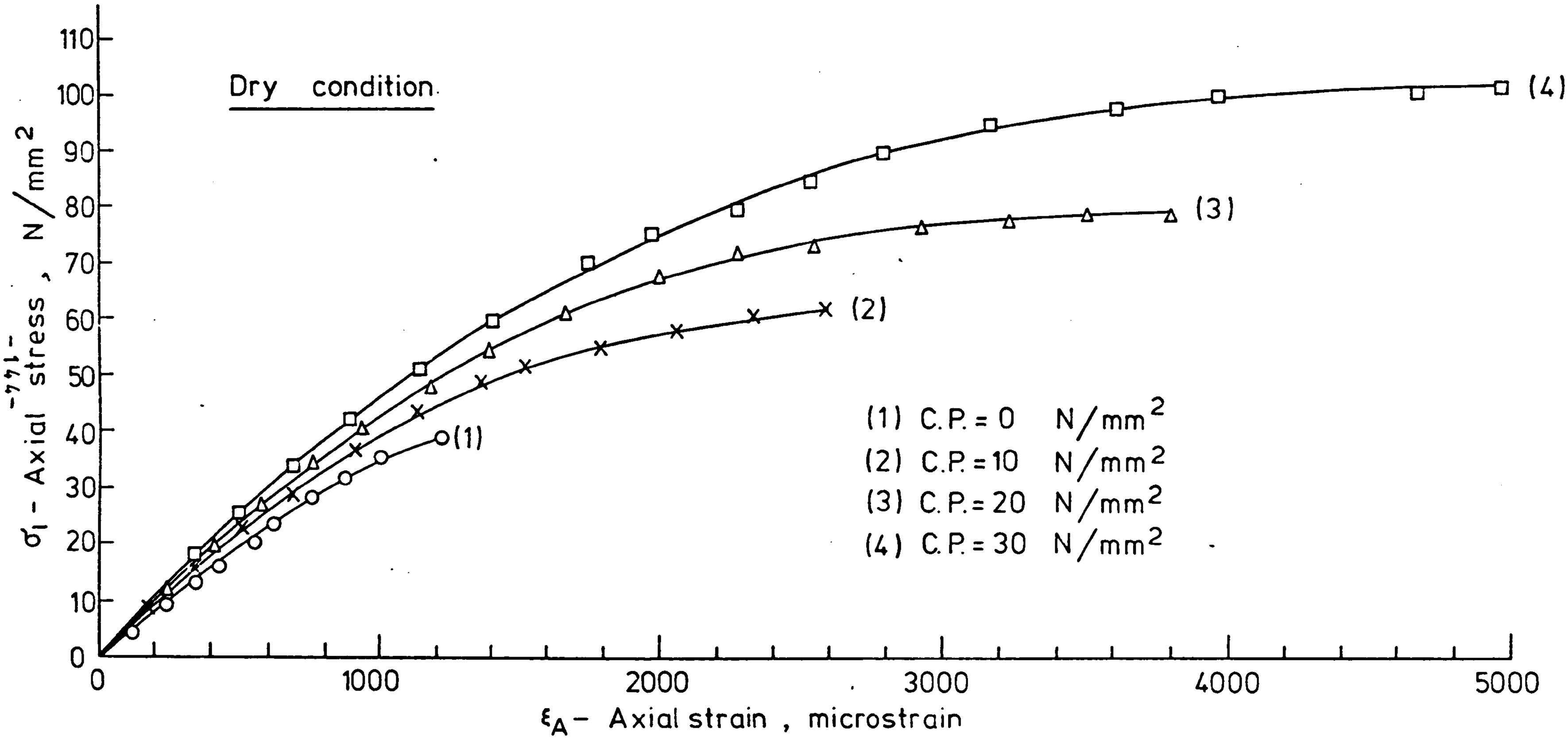

FIG. (4-30) STRESS – AXIAL STRAIN RELATIONSHIP AT VARIOUS CONFINING PRESSURES

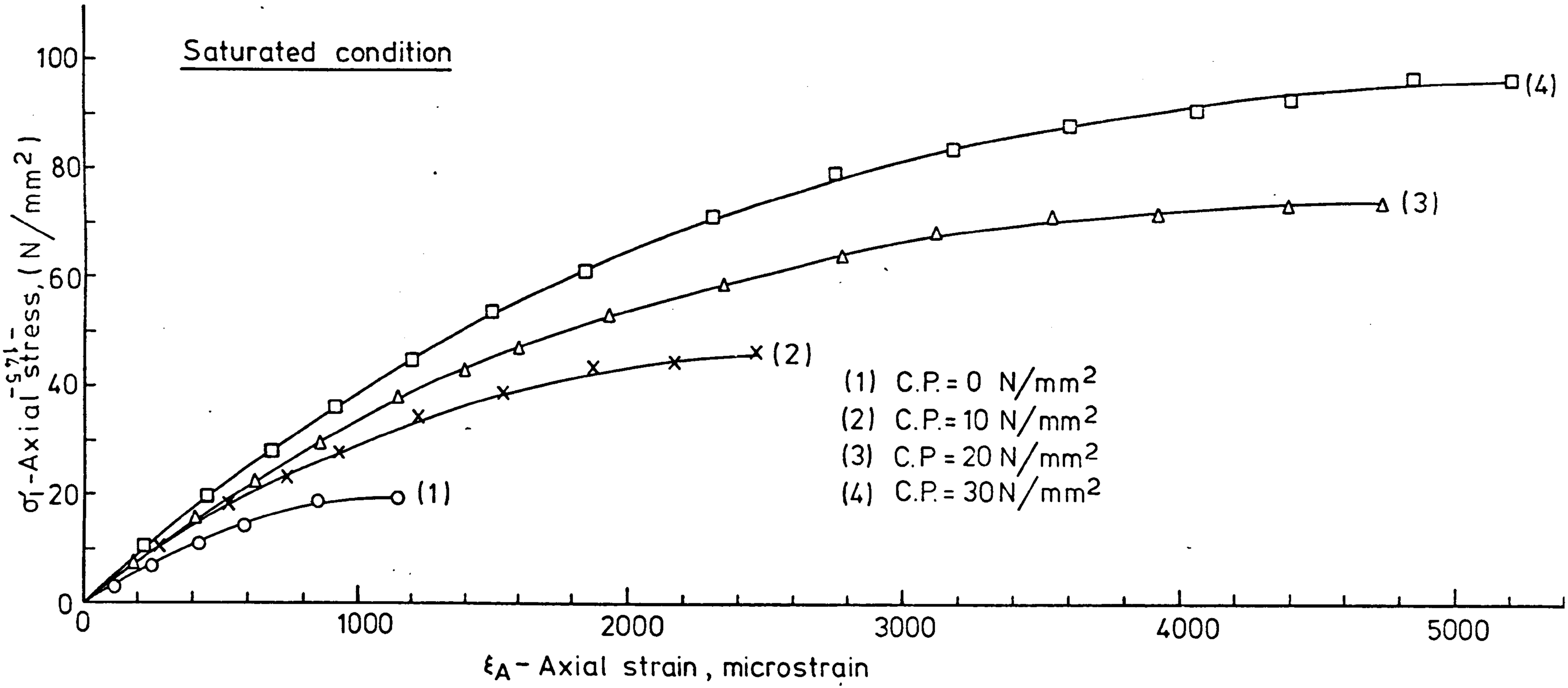

FIG. (4-31) STRESS - AXIAL STRAIN RELATIONSHIP AT VARIOUS CONFINING PRESSURES

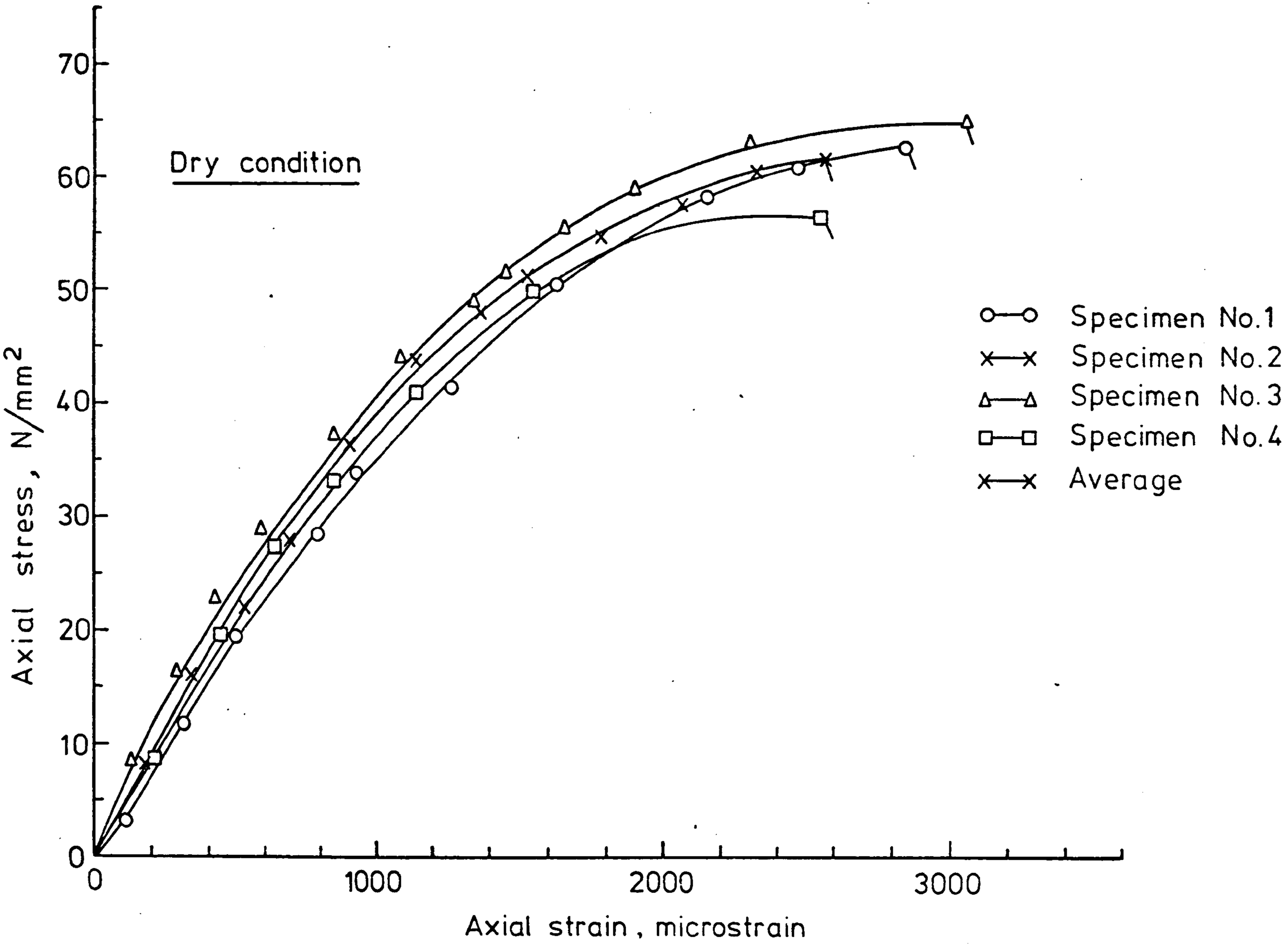

FIG. (4-32) STRESS-AXIAL STRAIN CURVES AT CONFINING PRESSURE = 10 N/mm²

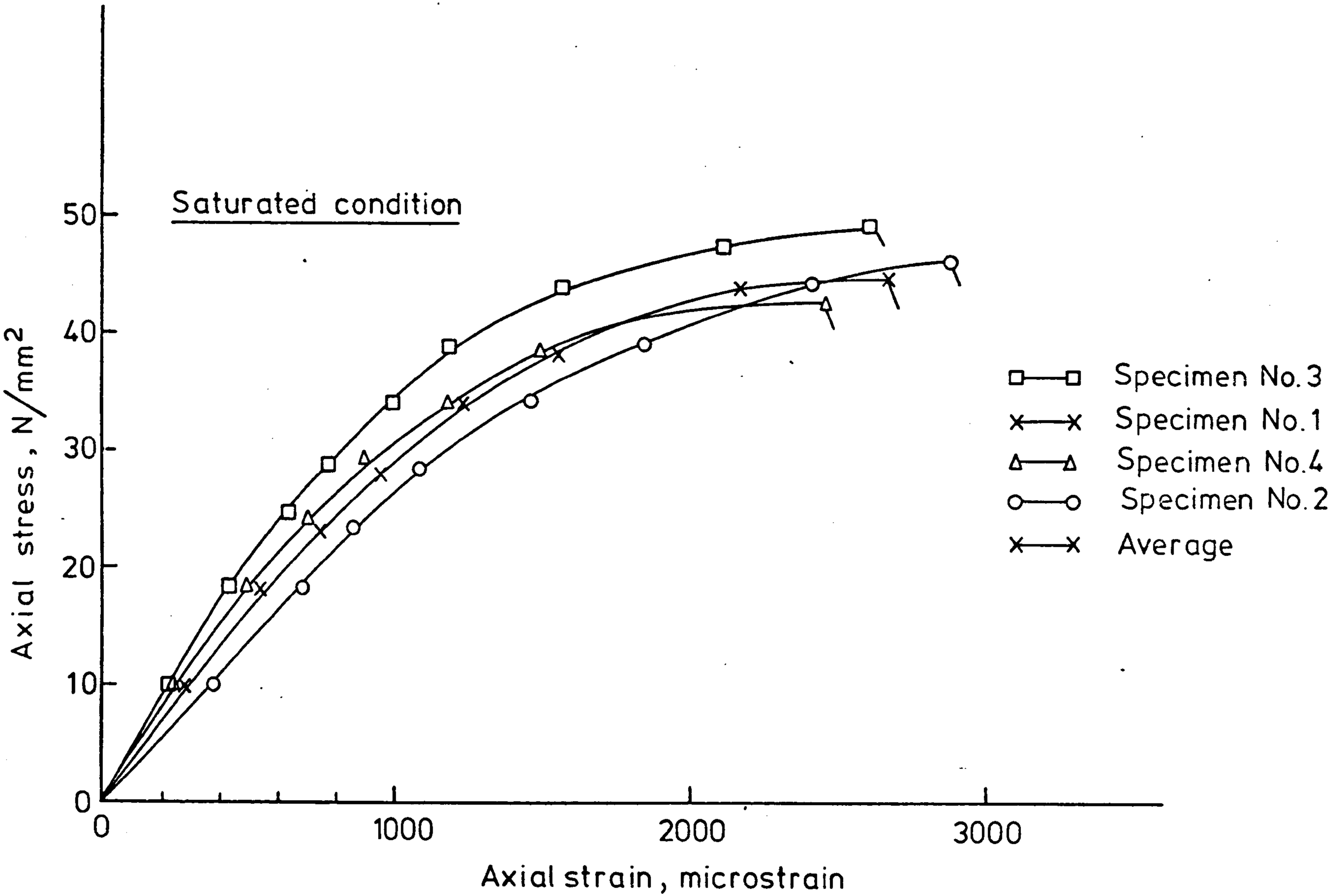

FIG. (4-33) STRESS-AXIAL STRAIN CURVES AT CONFINING PRESSURE = 10 N/mm^2

Dry condition

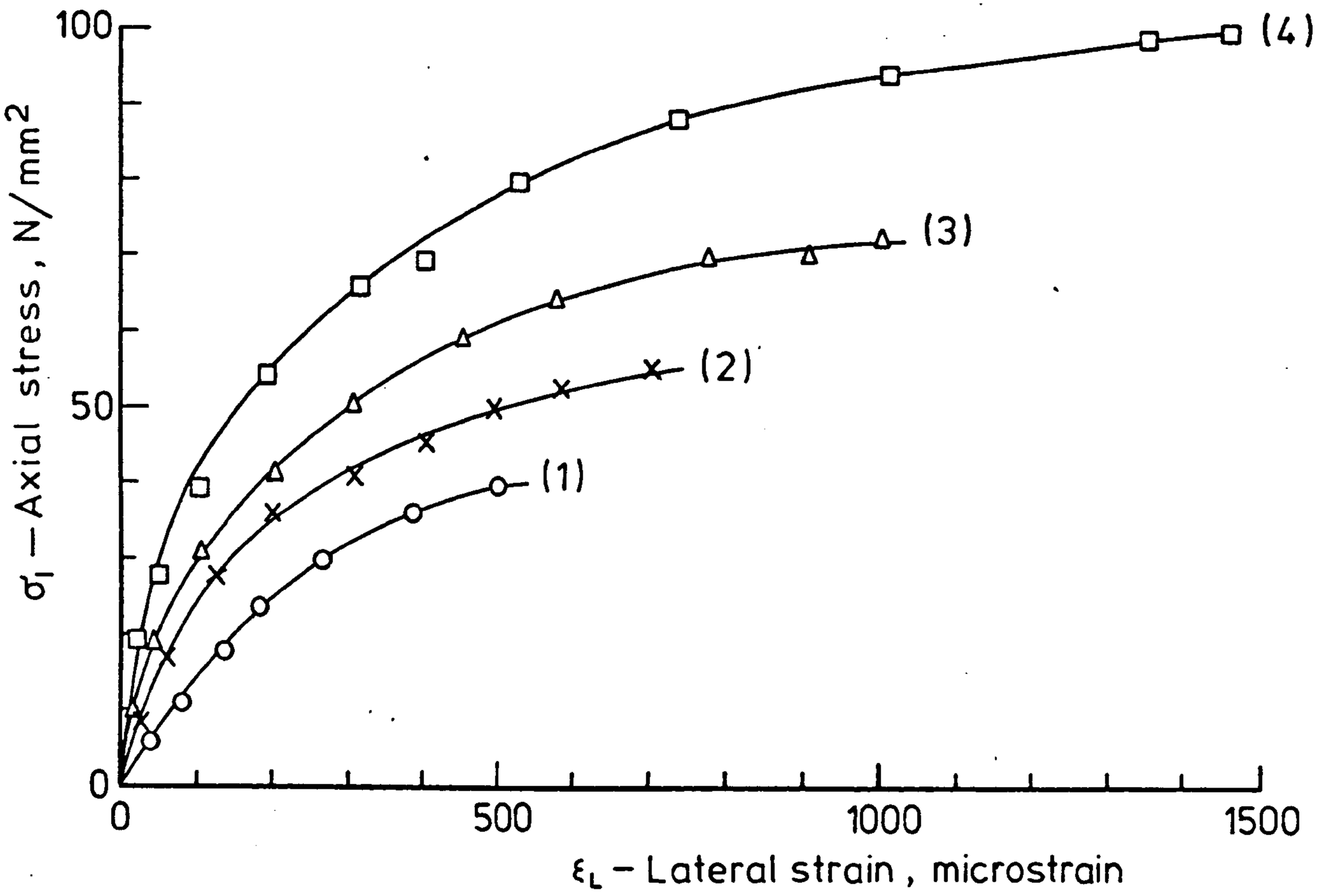

(1) C.P. = 0 N/mm^2
(2) C.P. = 10 N/mm^2
(3) C.P. = 20 N/mm^2
(4) C.P. = 30 N/mm^2

FIG. (4–34) STRESS – LATERAL STRAIN RELATIONSHIP AT VARIOUS CONFINING PRESSURE

Saturated condition

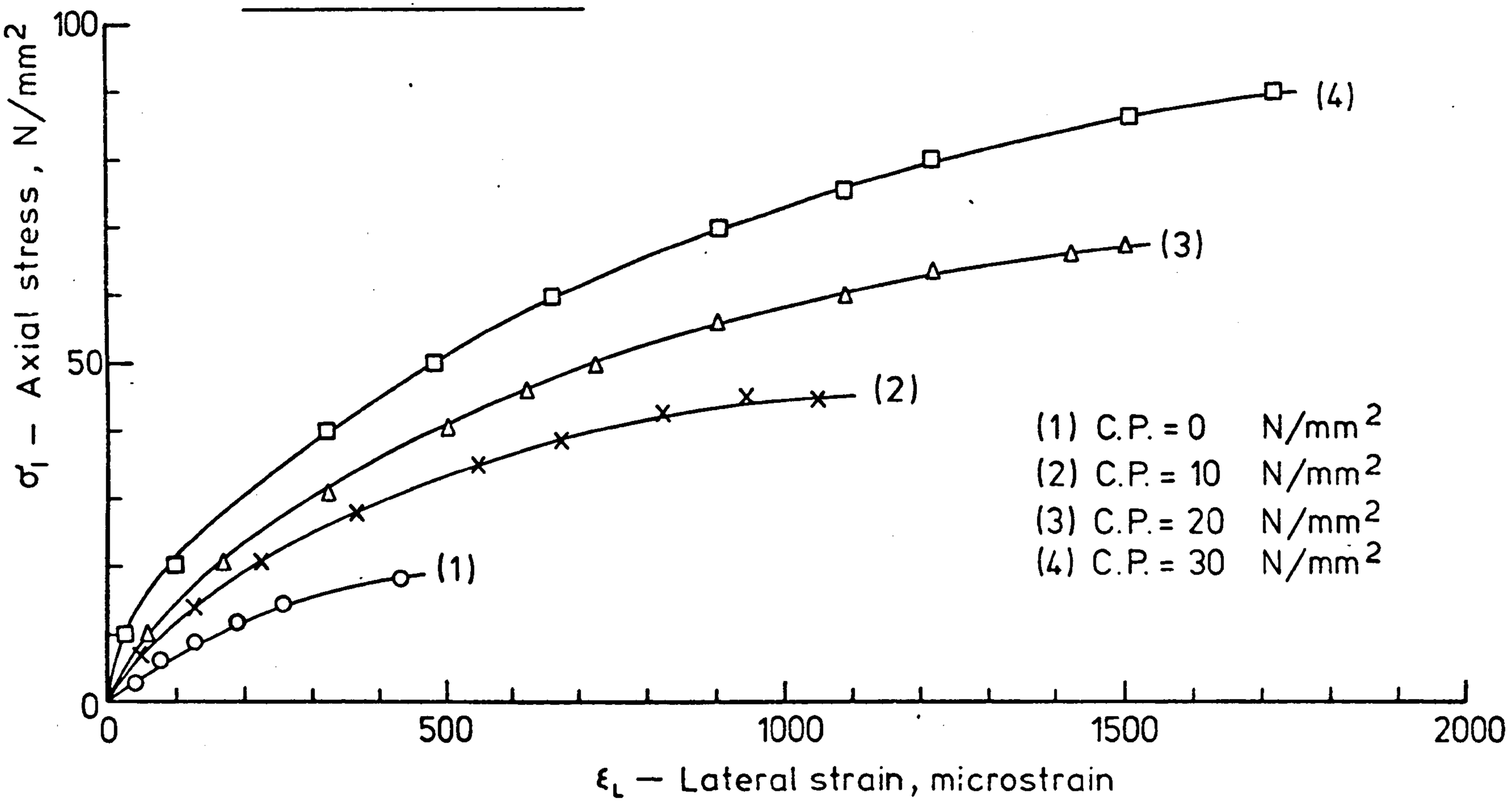

FIG. (4-35) STRESS – LATERAL STRAIN RELATIONSHIP AT VARIOUS CONFINING PRESSURES

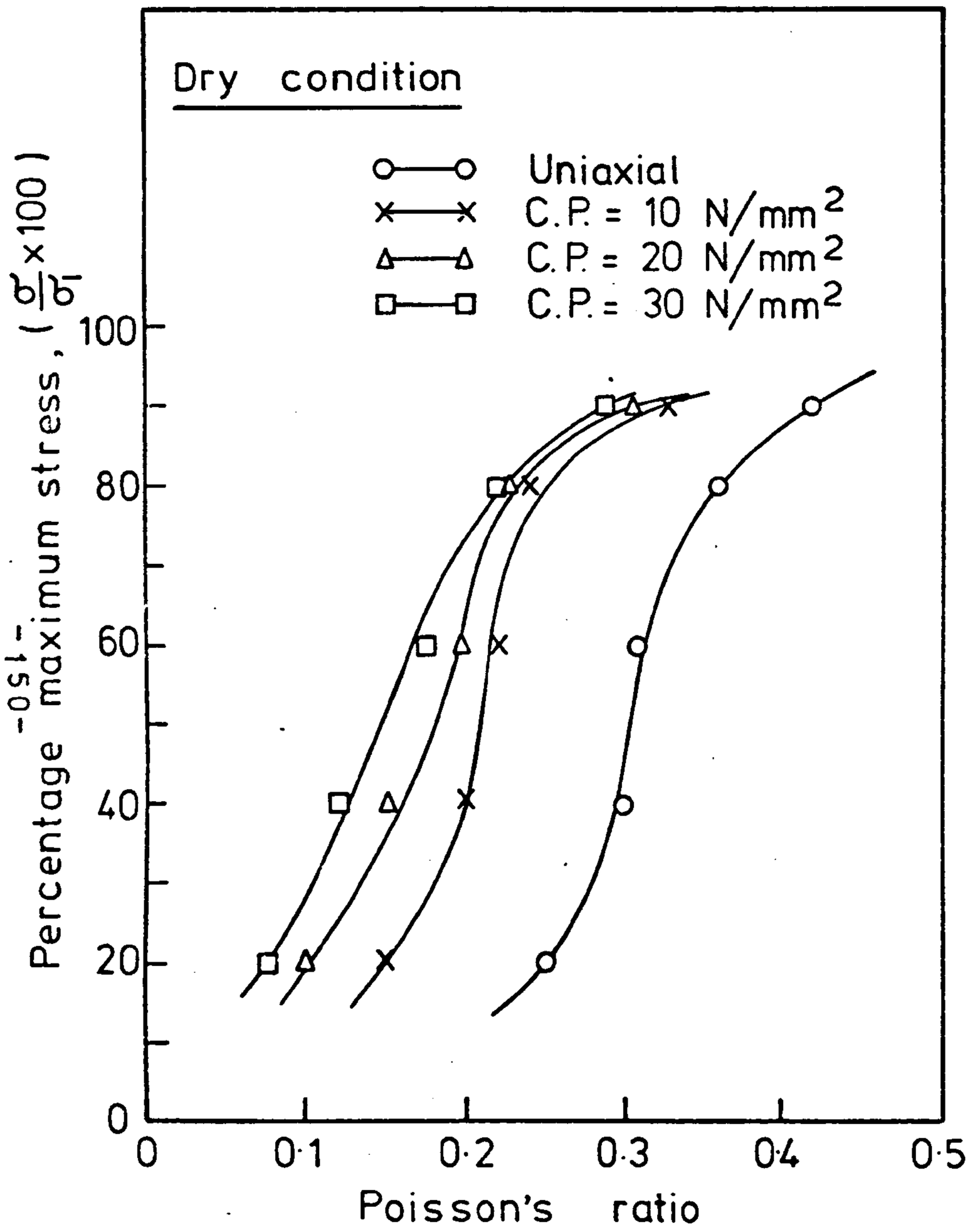

FIG. (4-36) EFFECT OF CONFINING PRESSURE ON POISSONS RATIO

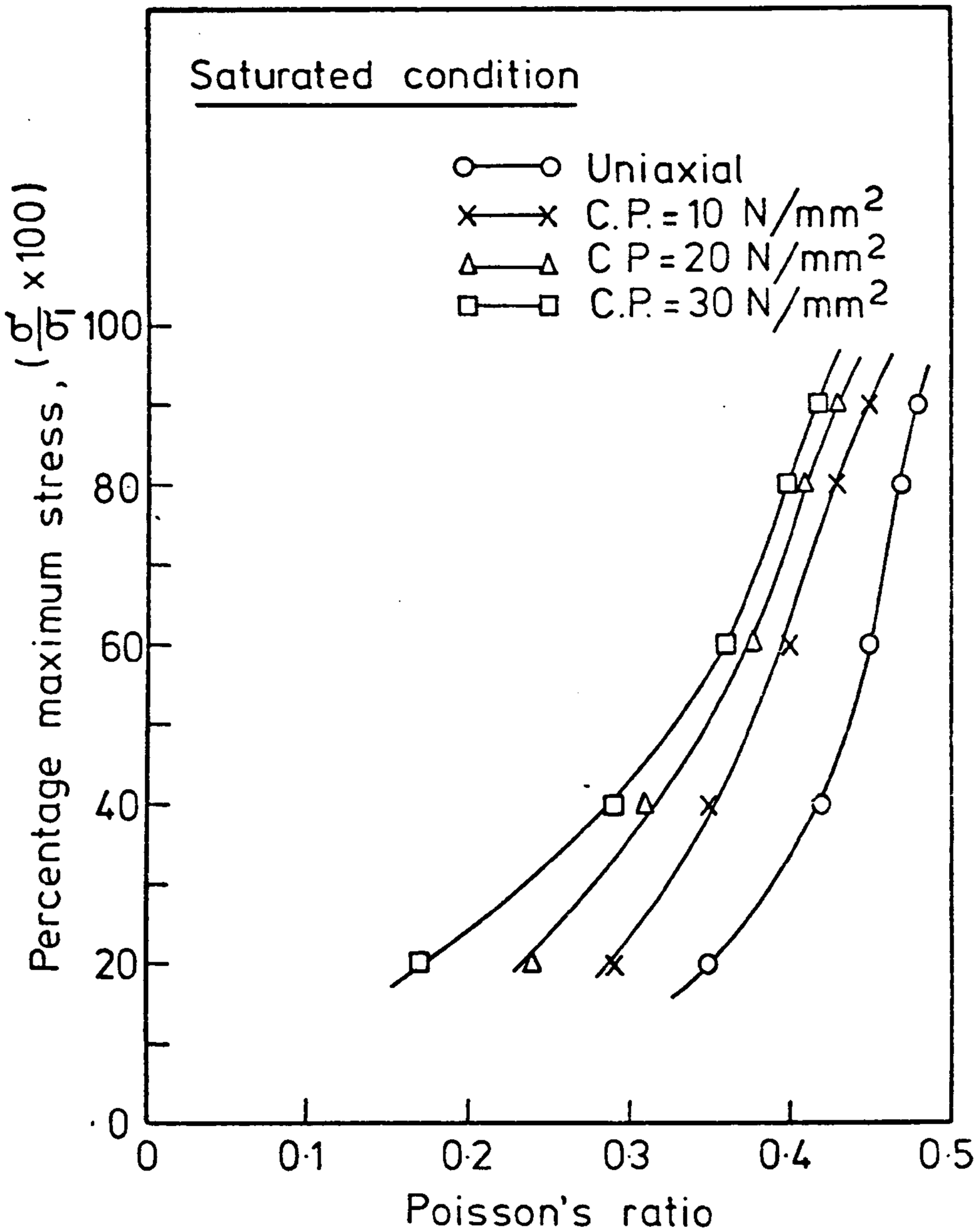

FIG. (4-37) EFFECT OF CONFINING PRESSURE ON POISSONS RATIO

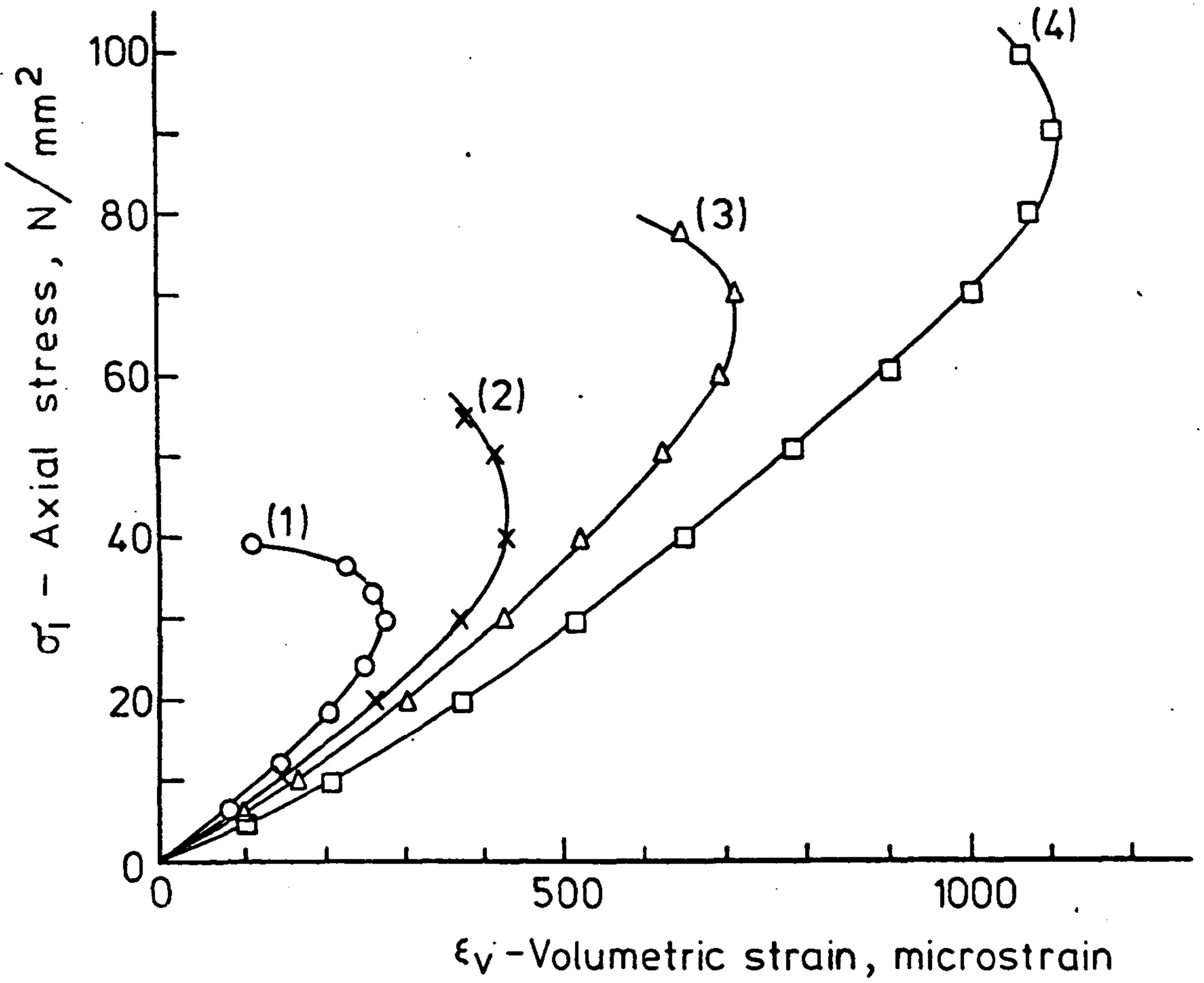

FIG. (4—38) VOLUMETRIC STRAIN Vs. AXIAL STRESS AT VARIOUS CONFINING PRESSURES

Saturated condition

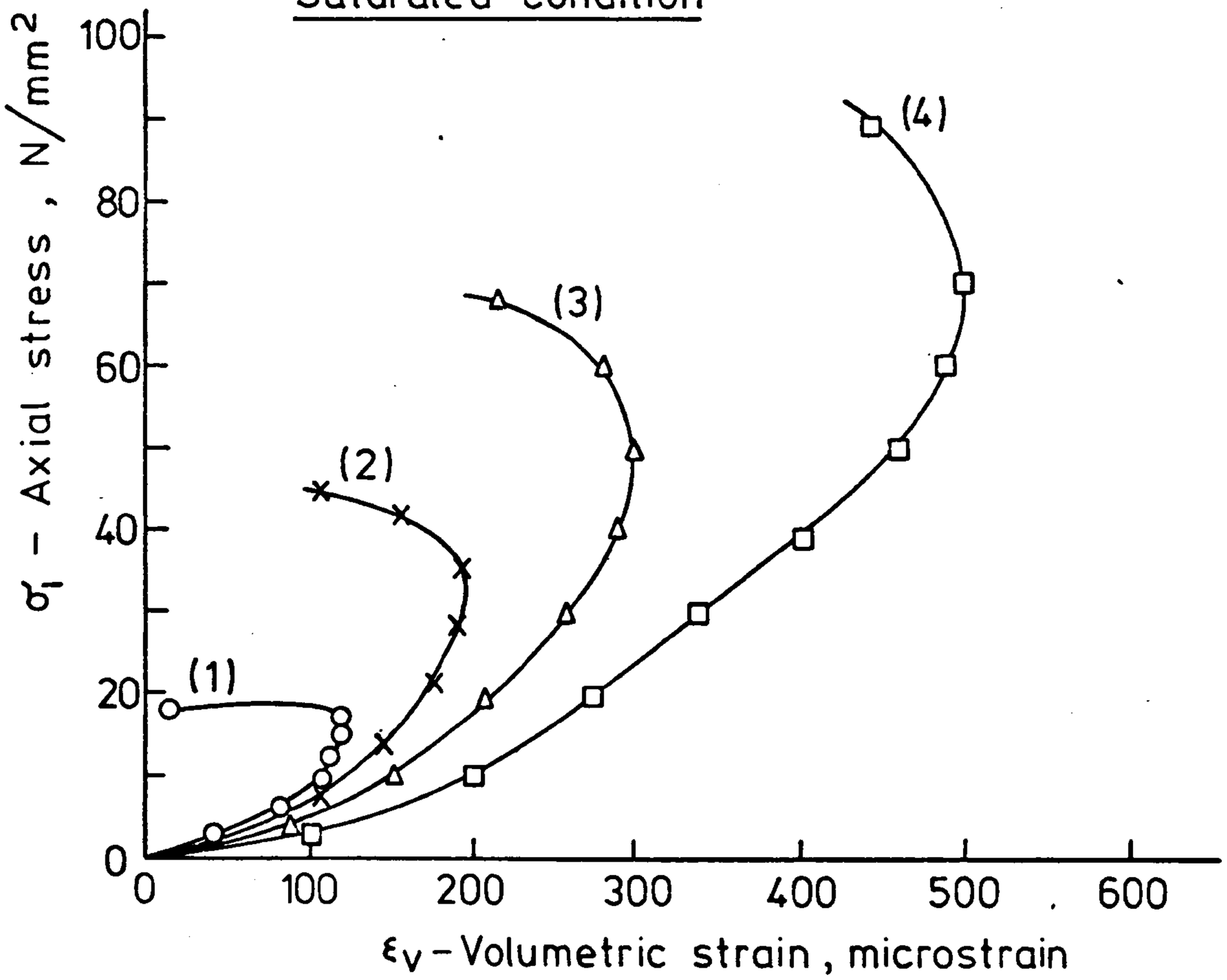

(1) C.P. = 0 N/mm^2
(2) C.P. =10 N/mm^2
(3) C.P. =20 N/mm^2
(4) C.P. =30 N/mm^2

FIG. (4–39) VOLUMETRIC STRAIN Vs. AXIAL STRESS OF VARIOUS CONFINING PRESSURES

Chapter 5.

LONG TERM TESTS.

In these tests the time-dependent effects or the creep behaviour in bending, uniaxial and triaxial compression were studied. Tests were carried out under dry and water saturated conditions. The equipment and apparatus used in the present study satisfied the following essential requirements:

(1) The equipment must be of sufficient capacity and be capable of maintaining constant load on the specimen over the whole period of the test.

(2) The strain measuring instruments should be stable and unaffected by the surrounding environment changes of humidity and temperature.

The first point was achieved by using dead-weight and weight through levers in both uniaxial and bending creep apparatus, while in triaxial creep apparatus a compressed nitrogen/hydraulic system was used with automatic control valves for both axial and confining pressure, in addition an automatic blow-off valve (relief valve) was used to maintain the exact required confining pressure in the event of rapid displacement.

The second point was achieved by using stable methods of compensation and measuring devices of proven stability.

In this chapter the experimental techniques, apparatus, equipment, and the test procedure used in creep tests will be described briefly.

5.1 Experimental Techniques.

5.1.1 Specimen Sizes and Preparation.

The various sizes of the specimens used in the bending creep tests and the sizes used in uniaxial and triaxial compression creep tests will be discussed in this section. The preparation of these specimens will be given here as well.

5.1.1.1 Bending Creep Specimens.

In bending creep tests, it is found that there is no standard or recommended dimensions for the laboratory testing rock beams, as was the case in the short term tests (described in Section 3.1.1.1).

Pomeroy[72] used beams of Barnsley Hards of a 85 mm long x 16.2 mm wide x 2.4 mm thick. Misra[79] used beams of a size 140 mm long x 32 mm wide x 6.4 mm thick of several rocks. Price[80] tested sandstone beams of a size 102 mm long by 12.7 mm wide by 2.5 mm thick and Williams and Elizzi[15,100] tested gypsum beams of sizes 240 mm long x 40 mm wide x 12 mm thick and 240 x 40 x 20 mm and anhydrite beams of size 240 x 40 x 20 mm.

In this study four beam sizes were chosen with the same dimensions used in short term tests, and subjected to a stress of 4 N/mm^2 in dry conditions to find the proper size for the creep tests (this will be discussed later). These sizes were:

240 mm long x 40 mm wide x 15 mm thick

240 mm long x 40 mm wide x 20 mm thick

240 mm long x 40 mm wide x 25 mm thick

240 mm long by 40 mm wide x 28 mm thick

Then the tests were carried out to study the creep behaviour in bending under dry and saturated conditions on beams of size 240 mm long x 40 mm wide x 20 mm thick.

The beams were prepared in the same method as described in Section (3.1.1.1). The centre zone of the lower surface of the beam then manually ground by rubbing it with fine emergy cloth and cleaned by acetone to make sure that it was free from any grease or dust. Two electrical strain gauges were bonded to this zone 30 mm apart. Finally leads were soldered to active and dummy gauges and connected to the Peekel strain gauge indicator by means of a full bridge circuit.

5.1.1.2 Uniaxial and Triaxial Compression Creep Specimens.

The specimen sizes used in compression creep tests in both dry and saturated conditions was 76.2 mm long by 25.4 mm diameter (length to diameter ratio, L/D = 3) one of the sizes used to find the instantaneous rock strength in both uniaxial and triaxial compression tests in the two environmental conditions. Misra[79] carried out uniaxial compression creep tests on specimens of 76.2 mm long by 25.4 mm diameter of several rocks in dry and saturated conditions. Williams and Elizzi[15,100] used the same specimen size for creep testing of dry gypsum and anhydrite subjected to uniaxial and triaxial stresses.

The drilling, sawing, polishing and measuring of the specimen sizes were performed as described in section (3.1.1.2). The specimens were then manually ground by rubbing with fine emery cloth and cleaned with acetone to make sure that they were free from grease or dust. Three axial electrical strain gauges were bonded within the middle third of the specimen, these strain gauges bonded at 120° apart. Ten lateral electrical strain gauges of smaller gauge length were bonded transversely along the specimen length. These were arranged in five pairs, the strain gauges of each pair were bonded at 180° apart. The five pairs of gauges were at equal intervals along the specimen length (12.7 mm spaced). Finally the leads were soldered to the gauges and connected to the strain measuring instruments, Extension box type 23U and Peekel strain gauge indicator. In the case of the specimens tested using Williams and Elizzi triaxial apparatus, two strain gauges were bonded at the middle of the specimen at 180° from each other around the circumference of the specimen. These gauges were for the determination of the lateral strain in the specimen. Only two gauges were used because of the limited space inside the pressure cell to accommodate the wires of the strain gauges and the transducers. In

this apparatus the axial strains were measured by using three transducers spaced at 120° around the specimen and within the middle third. (This will be discussed in detail later in this chapter).

5.1.2 Drying, Saturation and Saturation Controlling Procedures.

As mentioned before water was used as coolant in drilling and grinding of the specimens. In the case of tests in the dry condition, the specimens were ovendried at 70° C for 24 hrs to retain in the gypsum the chemically held water (as discussed in Sec.3.1.3), then the specimens were left for at least 2 days at the laboratory temperature before the tests. In the case of tests under saturated conditions, the specimens were ovendried at 70° C for 24 hrs, then saturated using the same method described in Sec. (3.1.2). The saturation was kept under close control during the whole test period by coating the specimens as discussed in Sec. (3.1.4). The effectiveness of the coating was examined up to 33 days, and it was found that no measurable loss of water occurred (see Sec.3.1.4). None of the creep tests under saturated conditions was extended more than 33 days to ensure that the specimen was still in a fully saturated condition.

5.2 Apparatus, Equipment and test procedures.

In this section, a description of the important features of the testing equipment is given. Apparatus and equipment used for bending, uniaxial and triaxial creep tests are given with a brief discussion of testing procedure including the strain measurements in each case.

5.2.1 Bending Creep Tests.

5.2.1.1 Apparatus.

To apply true bending to the rock specimen, the four point loading apparatus described in section (3.2.1.1) was used. Dead-weights were used to keep the applied stress constant over the whole test period. Two systems were used to apply the load using dead-weights:

(1) When the applied stress is low, needing only a few kilogram weights, the weights were placed directly on the pan provided as shown in Fig.(5.1).
(2) When the applied stress is greater than in case (1), the dead weights were applied through a lever. The system gives a mechanical magnification advantage of 10 : 1, i.e. one kilogram on the weight pan produces 10 kilograms on the specimen. Fig. (5.2) shows tests in progress under this system.

This system of loading consists of a 600 mm steel lever hinged at one end to a steel frame fixed to the wall, and hinged with a vertical adjustable steel rod through which the load applied to the specimen. This hinge was located at 540 mm from the end remote from the wall frame where the weight pan is hung A weight was used at the end of the lever remote from the pan to balance the weight of the pan, weight of the lever itself and the weight of the adjustable vertical rod. Friction effects of the hinge were investigated and found to be too small to consider. The advantages of the lever system are; (1) it reduces the weight required on the pan by 10 times, (2) it reduces the loading time, and (3) it enables the load to be applied without shocks being imputed to the sample.

5.2.1.2 Test Procedure and Strain Measurements.

Specimens prepared by the method described in Sec.(5.1.1.1) were marked accurately at one side by two marks 10 mm apart and at the other side 20 mm apart in the middle zone of the beam symmetrically about the centre. The beam was placed between the four knife edges, two of them under it 20 mm apart held by the lower horizontal steel bar, and the other two knife edges above it 10 mm apart held by the upper steel bar. The pre-determined load was applied either using the dead-weights directly on the pan or the lever loading system depending on the magnitude of the load. The load was applied to the beam by the vertical adjustable rod

through a steel ball in a hemispherical recess at the centre of the upper part to the upper steel bar.

The strain at the lower outer face of the specimen beam was measured by bonding two strain gauges at the centre of this face, these being connected with two dummy strain gauges of the same type mounted on an unloaded piece of similar rock by means of a full bridge circuit (as described in Sec. 3.1.5). Each strain gauge has a gauge length of 10 mm, 120 ohm $\pm$ 0.1 resistance and a gauge factor of 2.07. The Peekel strain gauge indicator type T-200 was used to measure the strain for the whole period of the test. This indicator has excellent long term stability which satisfies one of the requirements for the long term measuring instruments.

5.2.2 Uniaxial Compression Creep Tests.

5.2.2.1 Apparatus.

Two machines were used for this purpose, one of them based on the dead-weight loading by levers and in the other the load applied by means of nitrogen gas-hydraulic system with loading frame.

5.2.2.1.1 Deadlweights and levers machine.

This machine is similar to the one used by Misra[79] in 1962 and Elizzi[15] in 1976. Figs. (5.3) and (5.4) show a view and a schematic diagram of the machine respectively. It consists of two levers, lever No. 1 provided with three steel knife edge pivots P_1, P_2, and P_3 and lever No. 2 provided with another three knife pivots P_5, P_5 and P_6. Lever No. 1 fulcrum at the knife edge P_2 and lever No. 2 at the knife edge P_6. The two knife edges P_3 on lever No. 1 and P_5 on lever No. 2 are connected together by means of two tie rods and a turn-buckle. The purpose of this is to adjust the distance between the two knife edges P_3 and P_5 according to the load required. Lever No. 2 carried a weight pan at the knife edge P4.

A reversing jig attached to the knife edge P_1 and connected at the bottom to a spring and hydraulic jack underneath the platform of the angle iron framework. The lever system by reversing the load direction twice gave a mechanical advantage of ratio approximately 118:1 in a relatively small space. By loading the weight pan by means of dead weights a tensile pull is created at the vertical axis of the knife edge P_4. This pull is converted into a compressive load at the axis of the rock specimen by means of the attached reversing jig. Fig.(5.5) shows the reversing jig with a specimen in position. The loading platens in the reversing jig were designed to carry a spherical seating for maintaining a uniaxial load on the specimen during the test period. The purpose of the spring and jack assembly incorporated beneath the framework platform is to take up the elastic deformation of the framework and other tension members and also to initially apply the load smoothly and gradually at any required rate to the specimen. A spirit level on lever No. 2 indicating a horizontal lever when the bubble in its centre, which means the applied load and the weight on the pan are balanced. Dead weights at the end of the lever No. 1 and projecting arm of lever No. 2 act as balancing weights. A thrust ball bearing and clamping nut is provided on the connecting rod of the hydraulic jack underneath the platform as a means of locking the system for taking up the distortion of the framework. To prevent the effect of any shocks in the floor due to external mechanical disturbance, sponge seatings underneath the framework were placed to absorb any probable shocks.

5.2.2.1.2 Calibration of the Machine.

To find the actual ratio between the weights on the pan and the load applied on the specimen, it is necessary to calibrate the machine. A 20,000 lb (89 kN) proving ring was first calibrated using a clockhouse

compression machine and a curve was plotted of load applied on a proving ring versus its deformation (dial gauge reading), Fig. (5.6a). Afterwards the proving ring was placed in the creep machine and the deformation recorded with the weights on the pan, another curve was plotted of load on pan versus dial gauge reading, Fig. (5.6b). These two curves give separate linear relationships on the graph, with a common term which is proving ring deformation (dial gauge reading). This gives a basis of comparison betwen the load on the pan and the compressive load applied to the specimen. A third curve was constructed to show the linear relationship between the applied load on specimen (kN) and the weight on the pan (Kg), Fig. (5.6c). This curve is the machine calibration and it was found that the mechanical advantages ratio of the machine is 117.2:1, i.e. one kilogram on the weight pan produces 117.2 Kg on the specimen. The calibration procedure was repeated four times in order to minimize any experimental errors.

5.2.2.1.3 Test Procedure.

The specimen was placed between the loading platens of the creep machine in its exact central position. The initial reading of the strain at this zero loading was recorded from the Peekel-T-200 indicator. The weights corresponding to a pre-determined applied stress were calculated from the calibration curve of the machine and put on the weight pan. The hydraulic jack was then operated until the lever No. 2 became horizontal. This is indicated by the spirit level mentioned above. The clamping nut provided underneath the platform on the connecting rod of the load reversing jig is turned until it became firmly seated against the framework platform. At this moment, a second reading of the strain was recorded from the strain gauge indicator. The difference between the first and second reading gives the "instantaneous" strain in the

specimen at that stress. Subsequent strain readings taken at known times after this provide the necessary information on the time-dependent behaviour of the specimen.

5.2.2.1.4 Gas/Hydraulic System Machine.

The long-term loading machine consists of a gas-hydraulic loading system and a loading frame. These units were installed in an approximately constant temperature room (21 $\pm$ 2^{o} C). This machine was used for the uniaxial and triaxial compression creep. The view of the complete machine will be described here, except for the Hoek triaxial cell which was used for the triaxial tests which will be described later in this chapter.

(a) Pressure Source and Control System.

The general layout of the gas-hydraulic loading system of the machine is shown in Fig.(5.7). High pressure nitrogen is fed from the cylinder into the pressure control system. The nominal pressure of the nitrogen in a full bottle is 13.8 N/mm^2(2000 psi). The existing pressure can be checked at any time by the pressure gauge (C1). High pressure 12.7 mm (0.5 inch)outside diameter steel pipes are used for connecting the pressure units. The system then divides into two subsystems. The first which is used for the lateral confining pressure comprises a shut-off valve (b3) for controlling the gas flow through the pipes, a fine filter (d1) to ensure foreign matter does not affect the operation, automatic pressure control valve (e1) for applying pressure and maintaining it constant on the output side also used for releasing the pressure, pressure gauge (C2) for reading the pressure at this location, intensifier (f) gives 4.7:1 ratio in pressure increase which is observed by the pressure gauge (g). The pressure applied to the specimen read directly by the gauge (g).

The second subsystem used for the axial loading consists of shut-off valve (b5), fine filter (d2), automatic pressure control valve (e2) for applying and releasing axial pressure, and the oil storage (h) connecting to the hydraulic jack (i) by high pressure rubber tube. Fig.(5.8) shows the view of the machine.

(b) Loading Frame.

The loading frame consists of an adjustable rig, hydraulic jack and proving ring. Figs. (5.9) and (5.10) shcw the frame with specimen in position.

The rig consists of a base plate 100 mm thick by 380 mm diameter and upper adjustable plate 4 cm thick by 38 cm diameter. These two plates are connected by three rod stands of 38 mm Ø with nuts. The clear vertical distance between the two plates can be adjusted by moving the upper plate up and down by means of nuts. A hydraulic jack of 100 mm in diameter by 150 mm high with 50 mm Ø ram located at the centre of the base plate and connected by a high pressure rubber pipe to the loading control system. An 89 kN (20000 lb) calibrated proving ring with 0.002 mm per division dial gauge was connected to the centre of the upper plate. The function of the proving ring is to measure the axial load applied on the specimen.

5.2.2.1.5 Test Procedure.

A specimen prepared by the method described in section (5.1.1.2) was placed between the two platens on the hydraulic jack ram and in full contact with the specimen lower end surface. The upper platen with a hempspherical seat was placed in full contact with the specimen upper end surface. The spherical seat mounted on the proving ring from the other end of the set up. See Fig. (9.10). Active and dummy strain gauges were connected to the strain measuring extension box by means of

either half or full bridge circuits, the extension box being connected to the Peekel strain gauge indicator, Type T-200, to measure the strain variation over the whole of the test period. The initial readings of the strain were recorded at zero load. To apply the required stress to the specimen, a corresponding proving ring reading was calculated from the calibration curve of the ring. The shut-off valve (b5) was completely opened and the pressure applied very carefully using the automatic control valve (e2) (Fig.(5.7) and (5.8)) up to required load. This indicated by the deformation of the proving ring (dial gauge reading). At this moment a second reading of the strains was recorded, the difference between the initial and the second readings gave the"instantaneous"strain in the specimen at the given stress. After that many readings were recorded over the whole of the test period according to a pre-arranged time-table for this purpose.

5.2.2.1.6 Strain Measurements.

The measurements of the strain in uniaxial compression creep for the two testing methods which are described in the previous sections are similar. Three electrical resistance strain gauges were bonded in the central zone of the specimen within the middle third at 120^{o} apart to measure the axial strain. Each one of these gauges had 10 mm long, 120 ohm $\pm$ 0.1 resistance and gauge factor of 2.07. Ten strain gauges were bonded transversely in five pairs along the specimen length at equal intervals. Each two gauges of the pair were at 180^{o} to each other. These strain gauges were used to measure the tangential strain at different points along the specimen surface. Each gauge was 5 mm long, of 120 $\pm$ 0.1 ohm resistance and gauge factor of 1.98. Dummy strain gauges of the same type as the active were bonded on unloaded piece of rock similar to the specimen, these gauges were used for temperature compensation. All

active and dummy gauges were connected between themselves by means of either half or full bridge circuits as described in Section (3.1.5) and shown in Fig. (3.9). Then they were connected to the extension box type - 23U which is in turn connected to the Peekel strain gauge indicator type T-200. This indicator having a high stability in the long term test measured the axial and lateral strains for the test period.

5.2.3 Triaxial Creep Tests.

Since in practical circumstances the bulk of the rock material in the neighbourhood of an excavation or beneath a foundation is in fact triaxially loaded over long time periods, the creep characteristics under combined loading are more meaningful for design than uniaxial creep or simple bending in such cases, and the results of the triaxial creep testing are of high importance.

It is one of the major aims of this research to study the creep behaviour of the gypsum subjected to triaxial stresses, and under two environmental conditions, dry and water saturated. In this section the instruments used in the research for determining the creep under triaxial stresses, test procedure, and the strain measurements will be described briefly.

5.2.3.1 Apparatus.

Two sets of apparatus were used in this research to study the creep behaviour of the dry and saturated gypsum under triaxial stresses. The first was developed by Williams and Elizzi[101] and the second using the cell developed by Hoek and Franklin[123] in combination with either the loading system using the dead weight and levers or the gas-hydraulic system with the loading frame.

5.2.3.1.1 Williams and Elizzi's Apparatus.

This apparatus developed by Williams and Elizzi[15,101] in 1976 in the Department of Civil and Structural Engineering in Sheffield, and used[15,100]

to study the creep behaviour of air dried gypsum and anhydrite rocks.

This apparatus has the following specifications:

(1) Accommodating rock specimens of 3 inch (76.2 mm) long by 1 inch (25.4 mm) diameter and measuring the axial load within the pressure cell.

(2) Providing confining pressure up to 50 N/mm^2 and axial pressure up to 135 N/mm^2 which can be increased to 400 N/mm^2 by adding an extra axial intensifier.

(3) It has satisfied all the long-term test apparatus requirements; maintaining the applied pressure constant over the whole test period, the sensitivity of the strain measuring instruments and the independence of the apparatus from difficulties due to switching off in electrical system or power cuts etc.

(4) Provides means of measuring displacements by instrumentation within the cell.

The apparatus consists of three main parts, (a) pressure source and control system, (b) pressure cell and (c) load and displacement measurement system.

(a) Pressure Source and Control System.

Figs. (5.11) and (5.12) show the schematic diagram and general view of the pressure control system respectively. The commercially available nitrogen gas cylinder is used as a suitable power source, it is connected to the control system via a high pressure hose. The existing pressure in the cylinder can be checked at any time by the pressure gauge (b1). The gas passes through the shut-off valves (a1) and (a2) which are used for the relief of excess pressure when required, then through a fine filter (r1) for the removal of the scale or other foreign matter. The system then divides into two subsystems. The first is the axial loading system which includes; the automatic control valve (c1) which maintains gas

pressure constant on the output side provided that the input pressure is in excess of the required output. Any excess pressure can be relieved using shut-off valve (a3), and observing the adjustment of the pressure reading on the monitoring gauge (d1). The gas then passes through the two filters (r2) and (r3) to the intensifier and triaxial cell. The second subsystem is the confining pressure system which consists of a largely similar arrangement; automatic control valve (c2), shut-off valve (a4), monitoring gauge (d2) and two filters (r4) and (r5), with the addition of an automatic relief valve (f) which is a variable pressure setting device adjusted to operate at a pressure slightly above the required gas pressure and serves to prevent the development of excess confining pressure in the event of the loading ram entering the pressure cell rapidly at a possible rapid deformation or failure of the rock specimen. Two intensifiers are provided in the axial loading system to produce higher pressure than that supplied from the gas cylinder. The first one (e2) gives a magnification ratio of 2.25:1 and the second which is within the cell head gives a magnification ratio of 4:1, so with both of them in use they give a ratio of 9:1. Fig.(5.13) shows these intensifiers in full detail. The accurate total magnification was found by calibrating the apparatus (this will be discussed in this chapter later).

In case of confining pressure, another intensifier (e1) is provided to increase the pressure to the required high pressure for the tests. The magnification ratio of this intensifier is 4.7:1. Dimensions and details of this are given in Fig.(5.13). A pressure gauge (b2) reads the confining pressure and valve (K) is used for filling and emptying the pressure cell with oil. The pressure gauge, (d2) on the gas side of the intensifier and (b2) on the oil side of it also serve as a check on the behaviour of the intensifier (e1).

(b) The Pressure Cell.

The overall dimensions of the cell are 341 mm height by 100 mm diameter, Fig. (5.13), it is suitable to accommodate a rock specimen of 76.2 mm (3 inch) long by 25.4 mm (1 inch) diameter. The cell consists of three main parts; cell body, cell base and the cell head.

The cell base is provided with twenty three insulated sockets and leads which are carried through the base via an epoxy resin sealed hole. The function of these to facilitate the connection of strain gauges mounted on the internal load cell and the LVDT's around the specimen with the external measuring meters. (See Fig. (5.14). The cell body is a hollow steel cylinder of internal diameter 64 mm and of length 228 mm, this gives sufficient space for the specimen and the internal strain and load measuring units; transducers, load cell (specimen seat) and the spherical seating.

The cell head consists of a piston and plunger system having a ratio of area 4 to 1, so that the stress applied to the specimen is approximately 4 times the oil pressure applied to the piston, this means that the head acts as an axial intensifier.

(c) Load and Displacement Measurement Systems.

The triaxial cell is provided with an internal load cell which forms a base upon which the rock specimen stands, Fig. (5.14). This load cell is used for the internal measurement of the axial load applied to the specimen free from the effects of the O-ring piston seals and other friction factors. It is of top-hat shape in cross-section, the measuring zone being tubular, and fitted with 8 foil strain gauges 4 vertical and 4 horizontal connected in series pairs to form a full bridge circuit giving temperature compensation.

Axial strain measured over the middle third of the rock specimen inside the cell, using the provided measuring system, this system consists of three linear variable differential transformers (LVDTs) spaced at 120^{o} intervals. These are used to measure the displacement of two annular steel rings clamped to the specimen at a gauge length of 25.4 mm and attached to the LVDT cores, see Figs. (5.14) and (5.15). The LVDT's are connected together via a balancing circuit mounted within the pressure cell. This circuit combines the individual LVDT outputs and balances their performance and is connected to the sockets in the cell base. The displacement readings are obtained by the use of a Sangamo Weston C52/5 transducer multimeter which is a combined 5 KHz oscillator and output meter containing further balancing, amplification and attenuation circuits (Fig.5.12).

The lateral strains were measured in this study by bonding two strain gauges transversely at the middle of the specimen and at 180^{o} to each other, see Fig. (5.15). The strain gauge leads were brought out of the specimen jacket through very small holes which are sealed thereafter by the mixture of CN and P2 adhesives to ensure no leakage takes place at any time in the test period. The strain gauge leads were also connected to the sockets in the pressure cell base. A full or half bridge circuit was made up by using two dummy strain gauges mounted on an unloaded piece of rock similar to the specimen for temperature compensation. The strain variation was measured by using the strain gauge indicator Peekel type T-200.

5.2.3.1.2 Calibration of the Apparatus.

In order to determine the effect of the friction between the moving parts at the oil seals, and because most of the O-rings were renewed, re-calibration of the apparatus was considered essential.

(a) Calibration of the Load Cell.

The load cell (specimen seat) was calibrated by using an Avery 100 ton Universal testing machine. The load cell was located in the compression zone of the machine. The strain gauge circuit was connected to the strain gauge indicator. The load cell was loaded by 10 KN increments up to 100 KN and the output of the strain gauges was recorded at each load; the same procedure was performed under various confinement pressures to find the effect of this on the gauge output. Relationship between the strain gauge output and the applied load was plotted in Fig. (5.16). In order to check if there was any drift in the strain gauge output and/or creep in the cell material, the load cell was subjected to various constant loads for periods up to 35 days. It was found that the behaviour of the load cell was very stable.

(b) Calibration of the Transducers.

New wiring of the transducers was made following the manufacturer's instructions (Sangamo Weston Controls Ltd.). It was considered necessary to recalibrate the system with the new components and wiring.

The two annular rings were assembled at a gauge length of 25.4 mm with the three transducers and their corresponding cores. This assembly was placed between Wykeham Farrance compression testing machine platens, and the balancing circuit of the transducers was connected to the C52/5 transducer multimeter. A dial gauge of 0.002 mm/division was used to measure the displacement between the two rings. The relationship between the transducer meter reading and the displacement obtained by the dial gauge was plotted in Fig. (5.17). Deformation in microstrain versus the meter reading was determined and plotted on the same graph for the given 25.4 mm gauge length.

(c) Calibration of the Axial Intensifiers.

New oil seals were used in the two axial intensifiers. The theoretical magnification ratio of the two intensifiers is 9:1 between the end of the anvil near the specimen and the gas pressure. It was necessary to calibrate the apparatus to find the actual ratio between the axial load gauge gas pressure reading (Bar) and the applied load on the specimen (KN). This is necessary because of the effect of the friction losses in the oil seals (O-rings) of the ram entering the pressure cell and the oil seals of the two intensifiers, also, because of the difference in the cross-sectional area of the ram and the rock specimen. The apparatus was calibrated using the following method:

A duralumin specimen of 76.2 mm long by 25.4 mm diameter was placed on the load cell of the creep apparatus and both were put in the compression zone of the Avery testing machine. The strain gauge circuit was connected to the indicator and the load was applied by the compression machine. The applied load and the strain gauges output were determined and plotted in Fig. (5.18a). Then the load cell and the duralumin specimen were placed in the creep apparatus. Load was applied to the specimen and the output of the strain gauges was measured using the same meter. The relationship between the applied load observed from the axial load gauge gas pressure Fig.(5.11 d1) and the strain gauges output was plotted in Fig.(5.18b). These two relationships were found to be linear with a common factor which is the load cell strain gauge output. A new relationship between the axial load gauge pressure reading in bars and the axial load applied to the specimen in KN's was plotted in Fig. (5.18c). The obtained linear relationship is the calibration curve; it is indicated that for each one KN load on the specimen, the reading on the axial gas pressure gauge should be 1.518 bars.

The required axial load gauge gas pressure reading (R) at any particular confining pressure and axial stress is calculated in the following method:

The load on specimen = $A_s \cdot \sigma$ in N

The upward force due to the effect of confining pressure on the difference between the ram and specimen area will be equal to

$$= (A_r - A_s) \cdot \sigma_3 \text{ in N}$$

where:

A_s = specimen cross-sectional area, mm^2.

σ = required axial stress in the specimen, N/mm^2

σ_3 = confining oil pressure, N/mm^2.

A_r = ram cross-sectional area, mm^2 (which enters the pressure cell).

Then the total applied load = $A_s \cdot \sigma + (A_r - A_s) \cdot \sigma_3$

From the calibration curve, the axial gauge pressure reading (R) equals:

$$R = 1.518 \text{ (Applied load in KN)}$$

$$= 1.518 \left[A_s \cdot \sigma + (A_r - A_s) \cdot \sigma_3\right] \times 10^{-3}$$

$$= (A_s \cdot \sigma + A_r \cdot \sigma_3 - A_s \cdot \sigma_3) \times 1.518 \times 10^{-3}$$

$$= \left[A_s (\sigma - \sigma_3) + A_r \cdot \sigma_3\right] \times 1.518 \times 10^{-3}$$

By substituting the value of $A_r = 789.24\ mm^2$

$$\therefore R = \left[1.518\ A_s (\sigma - \sigma_3) + 1198.07\right] \times 10^{-3}$$

The above equation was used for applying the axial stress (σ) under the confining pressure (σ_3)

5.2.3.1.3 Test Procedure.

The specimen prepared by the method described in section (5.1.1.2) was jacketed in a P.V.C. tube, the ends of which extended over two steel

platens where O-rings are used to prevent the access of the hydraulic oil to the specimen, see Fig. (5.15). Two feeler strips 0.05 mm thick were used between the jacket and the specimen to prevent the penetration of the oil to specimen at points where annular ring screws are tightened on the specimen. The transducers were assembled and clamped to the specimen with gauge length between the annular rings 25.4 mm, the leads were plugged into the base sockets and the sample located on its seat (load cell). The pressure cell then filled with hydraulic oil by using a manual pump connected to the valve K, Figs. (5.11) and (5.12). The transducer meter is then switched on to be warmed for ten minutes in order to ensure stable operation. Then the initial readings (at zero load) were taken from the instruments indicating load and displacements. By operation of the gas pressure control valve (c2), Figs. (5.11) and (5.12) confining pressure was applied and the actual magnitude was obtained on the pressure gauge (b2). For applying axial stress for the given confining pressure, the reading on the axial pressure gauge (d1), Figs. (5.11) and (5.12), was calculated using the equation stated in the previous section, see (5.2.3.1.2-c). The gas pressure control valve (c1) was used to apply the axial load until it reached the pre-calculated reading valve on the pressure gauge (d1), then this was adjusted using the output of the load cell strain gauges which is pre-determined from the calibration curve, Fig. (5.16). At this moment the second reading of the strains were recorded, the difference between the two readings gives the "instantaneous" strain. Then the strains were recorded according to the pre-arranged time-table to obtain time-dependent strain or creep behaviour of the rock specimen. Checks were made from time to time on the behaviour of the confining pressure and axial load systems.

5.2.3.1.4 Triaxial Apparatus with Hoek's Cell.

Triaxial cell developed by Hoek and Franklin[123] in 1968 for rock testing was used in these tests. This cell, Figs. (5.19) and (5.20), is capable of confining pressure up to 70 N/mm^2 and can be used for short and long term tests. It consists of a steel cylinder and two screw end caps. The internal diameter of the cylinder is 27 mm with overall length of 100 mm. The cell is provided with two oil inlets, one for supplying the oil pressure and the other for air bleeding. Special one-piece synthetic rubber sleeves are provided with the cell, for the protection of the test specimen from the penetration of the surrounding hydraulic oil.

This cell was used for some low confining pressure triaxial creep tests. Specimens were prepared by the method described in Section (5.1.1.2) with three axial and five tangential strain gauges attached they were jacketed with the special rubber sleeve and the strain gauge leads were taken from under the sleeve. Fig. (5.20) shows section in the cell with the specimen in position. The cell was then assembled and filled with the pressuring oil. Two apparatus were used for applying the axial stress.

(a) The cell was placed in the load reverser jig of the lever operated uniaxial creep machine, Fig. (5.21). The axial load was applied in a similar method to that described in sections (5.2.2.1.3) for the uniaxial creep test. The confining pressure was applied and controlled by using the hydraulic-gas confining pressure system with the intensifier which is described with the uniaxial hydraulic-gas system in section (5.2.2.1.4-a). The automatic control valve (e1), Fig. (5.7) was used to apply the confining pressure. This pressure was adjusted according to the pressure gauge (c2), Fig. (5.7).

(b) The cell was placed in the loading frame rig of the gas-hydraulic operated uniaxial creep machine, Fig. (5.22), on the hydraulic jack with steel platens. The axial load was applied in similar method described in section (5.2.2.1.5) for the uniaxial creep test. The confining pressure was applied and controlled using the same system described in point (a).

The axial and lateral strain gauges were connected together with the dummy strain gauges bonded to an unloaded piece of rock similar to the specimen by half or full bridge circuits. A Peekel strain gauge indicator type T-200 in combination with the Extension box - type 23U. The method of the connection and measuring are described in Section (3.1.5).

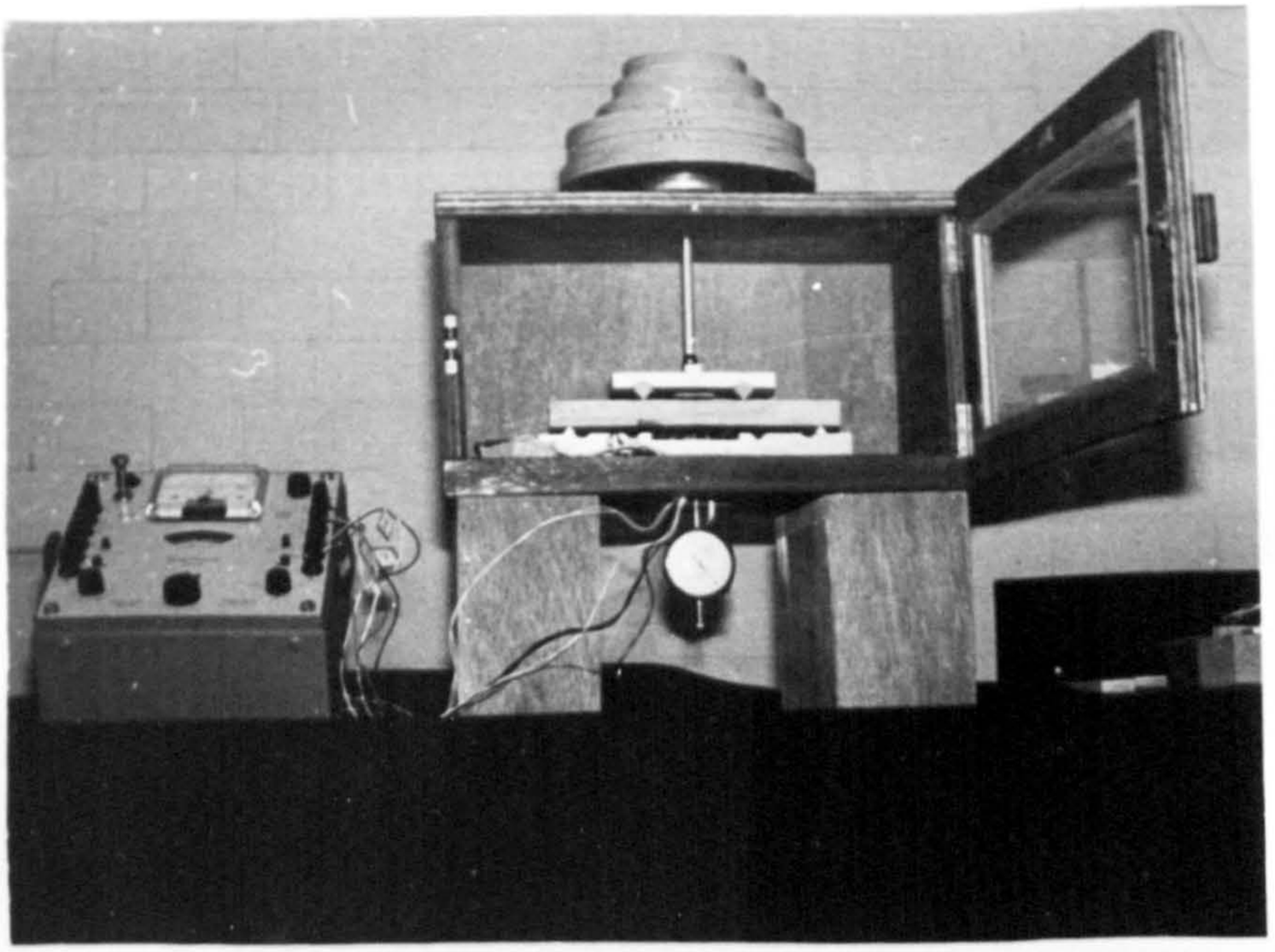

FIG. (5–1) BENDING CREEP APPARATUS WITHOUT LEVER

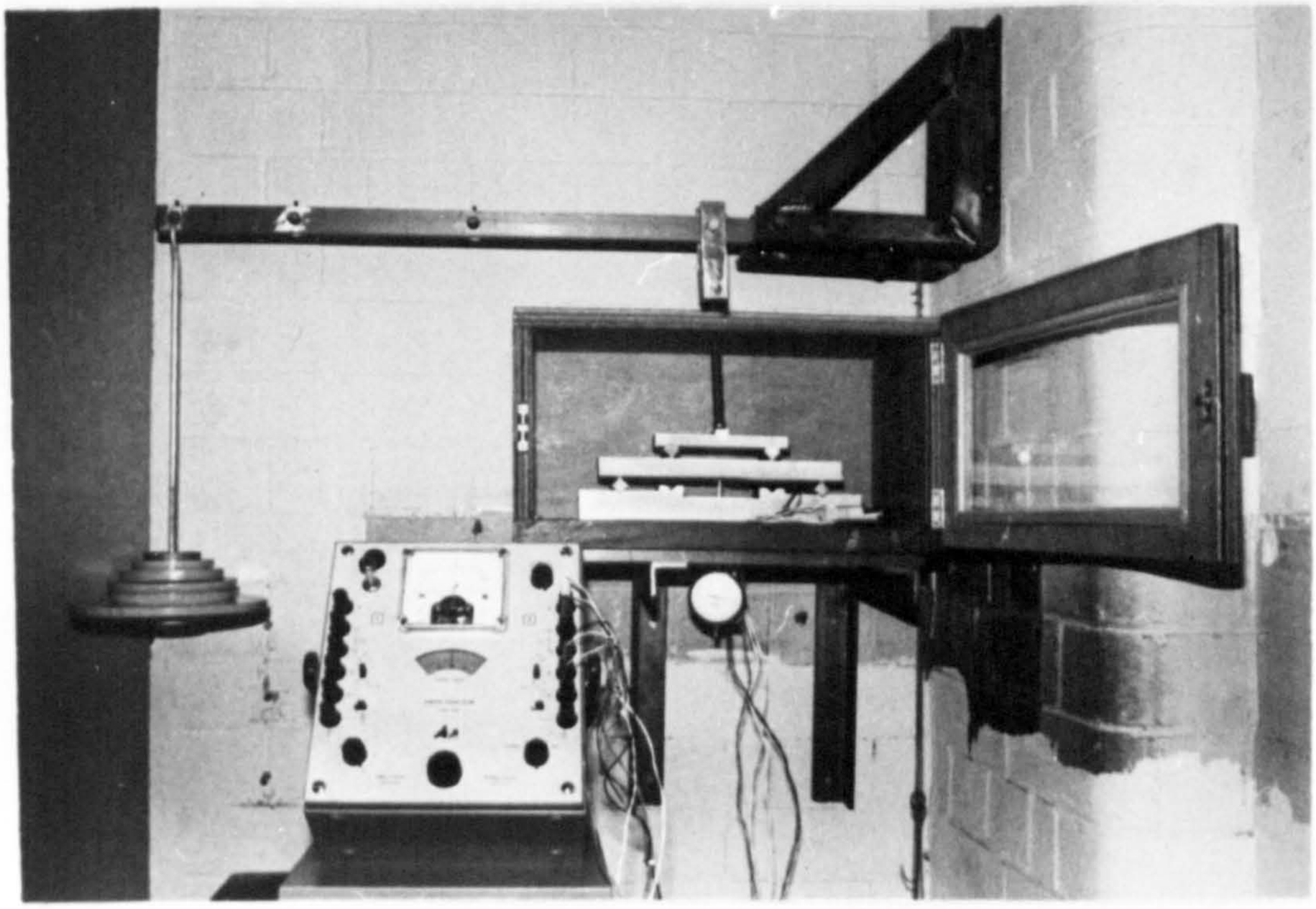

FIG. (5-2) BENDING CREEP APPARATUS WITH LEVER SYSTEM OF LOADING

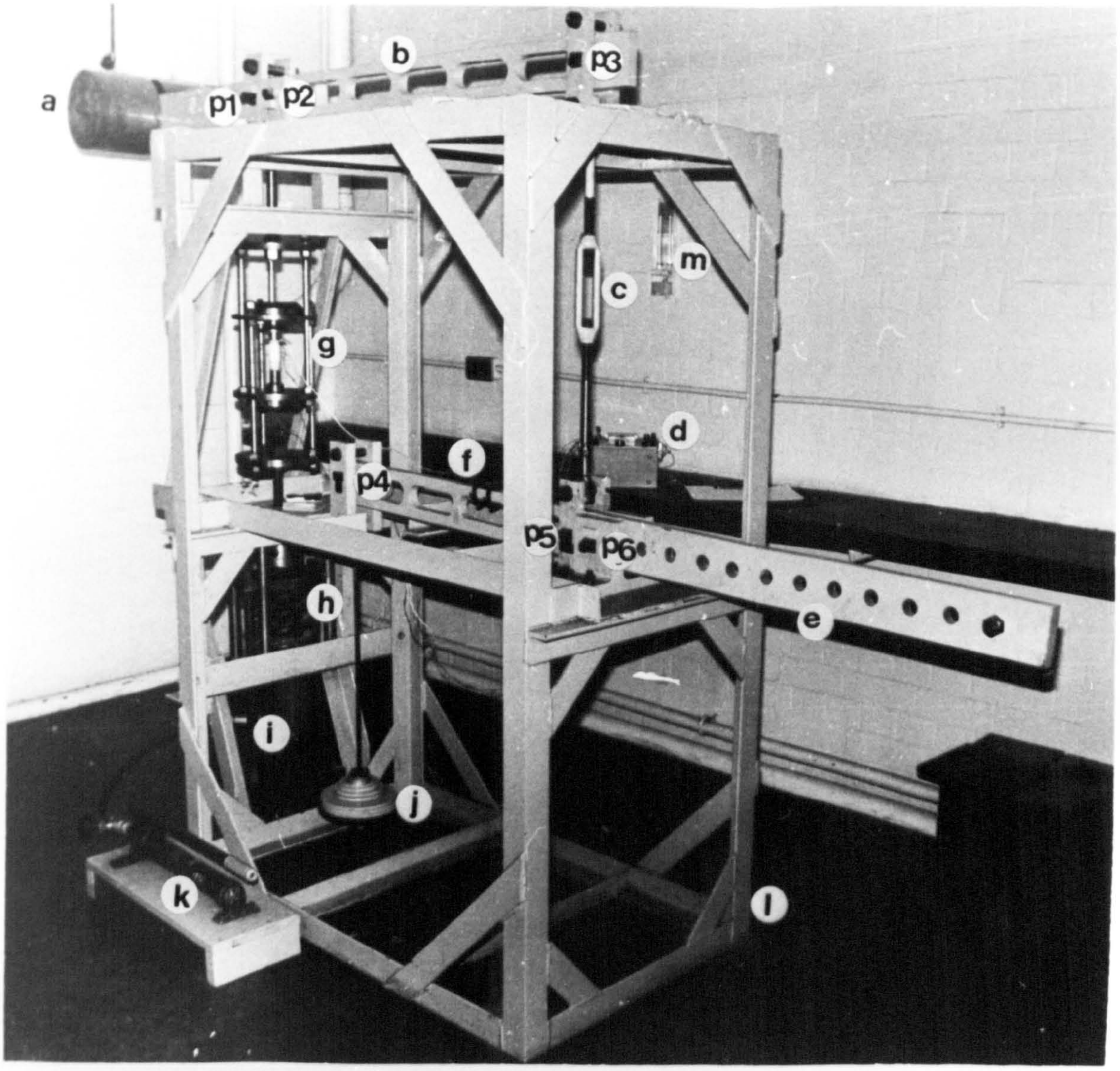

FIG. (5-3) UNIAXIAL CREEP TEST IN PROGRESS

(a) Balance weight
(b) Lever No.1
(c) Turn buckle
(d) Peekel strain gauge indicator
(e) Lever No.2
(f) Spirit level
(g) Load reversal jig and specimen
(h) Spring
(i) Hydraulic jack
(j) Weight pan and weights
(k) Pump
(l) Angle iron frame and sponge seating
(m) Thermometer

P1), P2), P3), P4), P5) & P6)

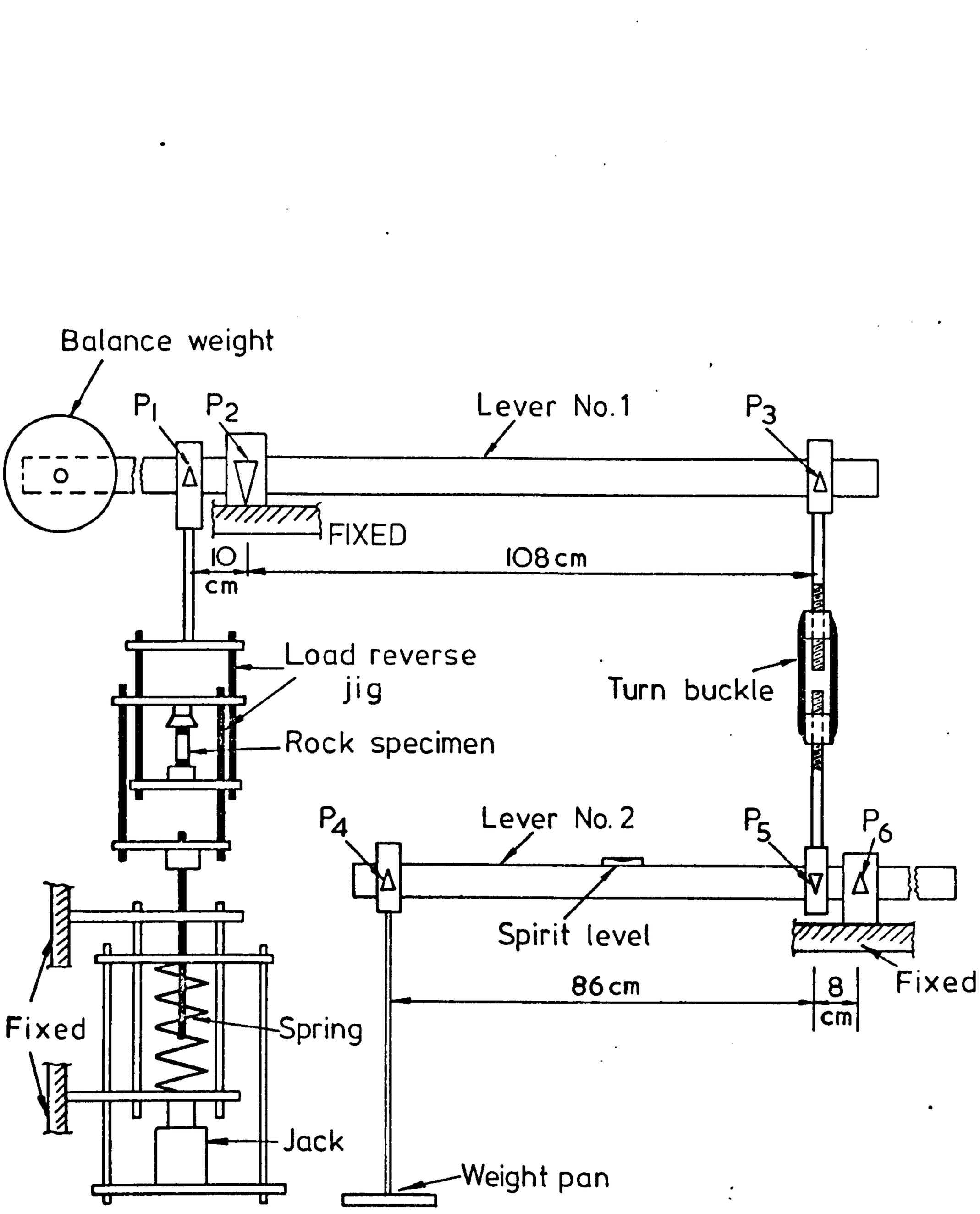

FIG. (5-4) SCHEMATIC DIAGRAM OF COMPRESSION CREEP MACHINE

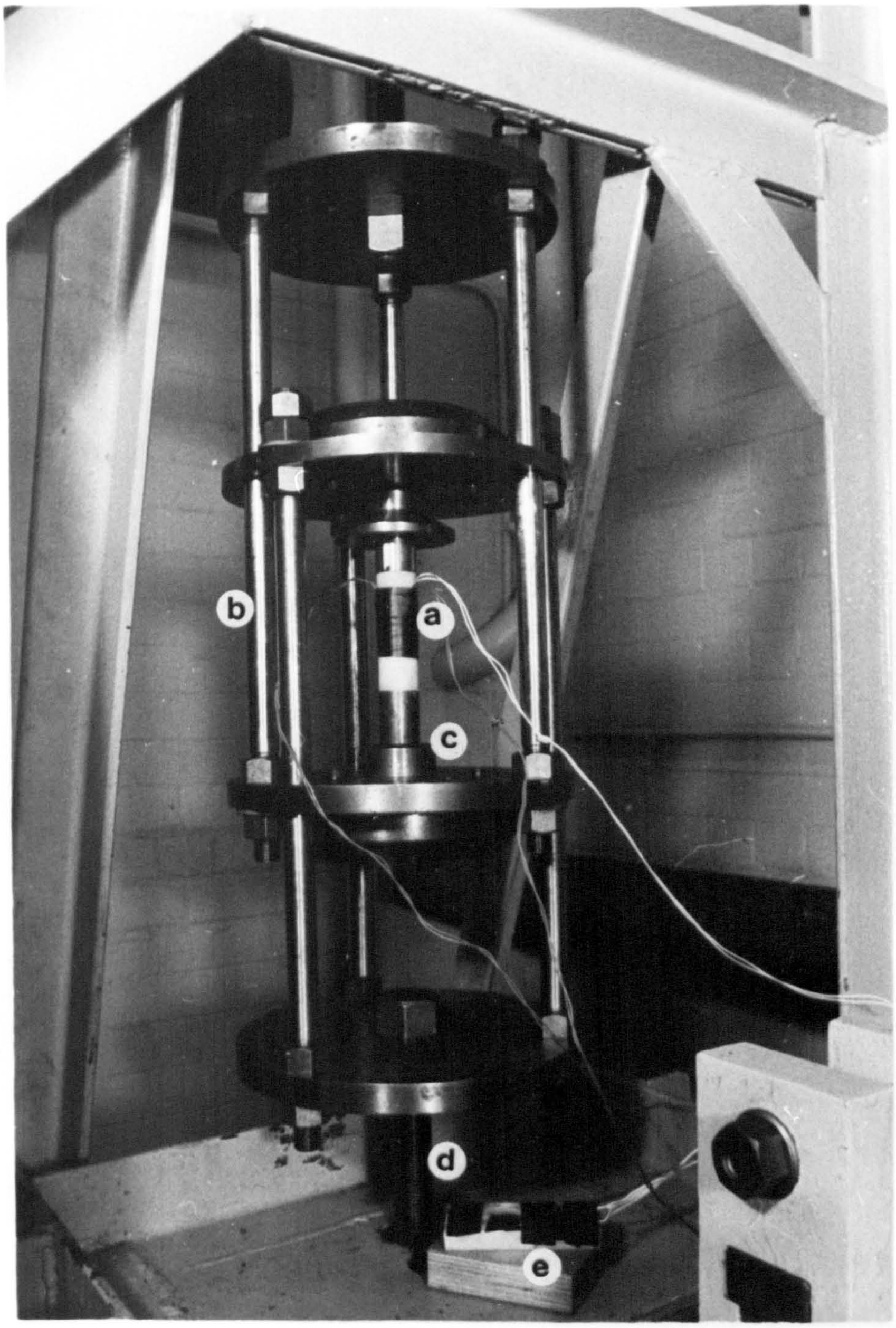

FIG. (5-5) LOAD REVERSAL JIG WITH SPECIMEN IN POSITION

(a) Specimen with strain gauges
(b) Load reverse jig
(c) Spherical seat
(d) Steel rod to the spring and hydraulic jack
(e) Dummy strain gauge on a piece of rock

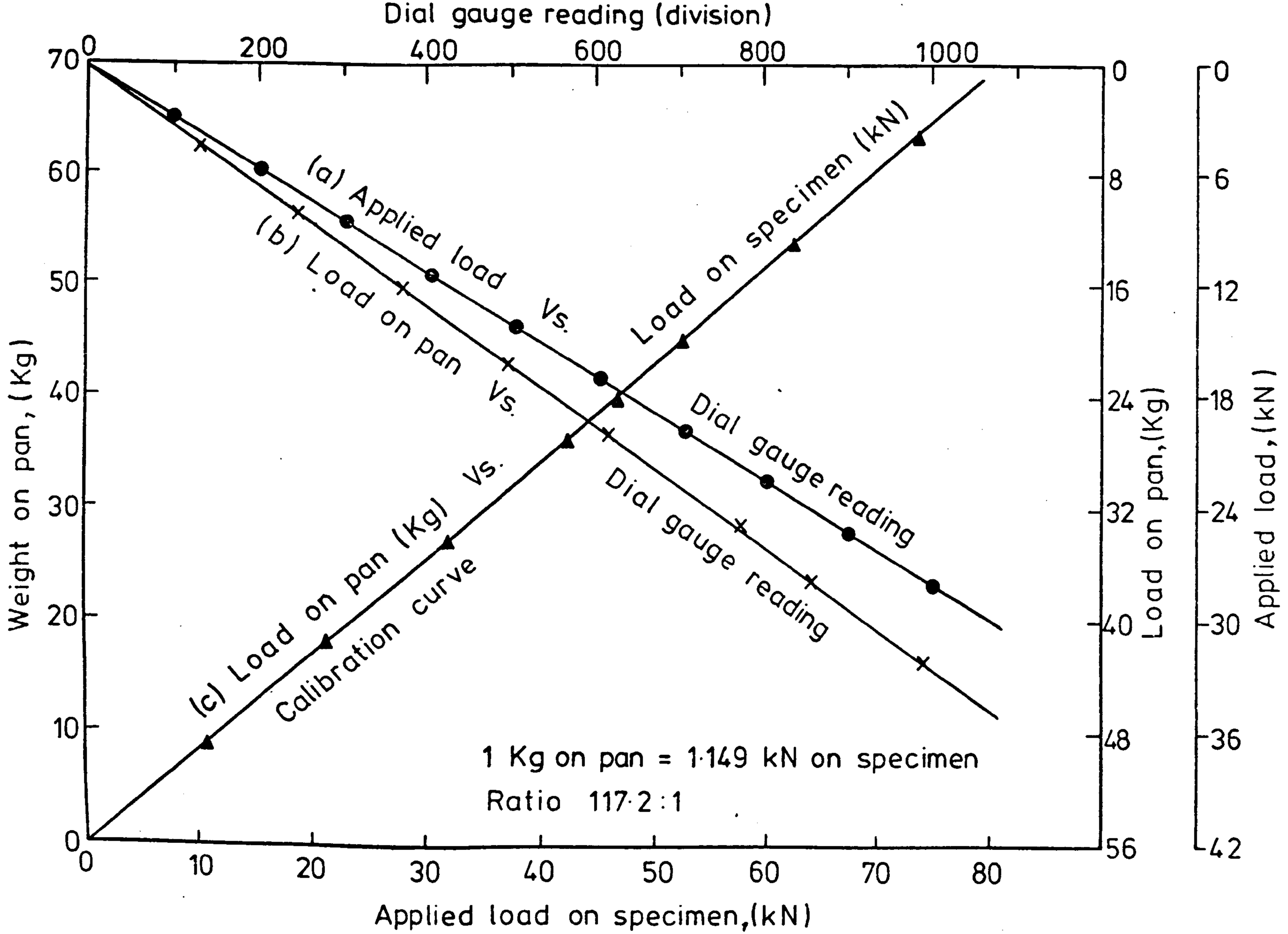

FIG. (5-6) CALIBRATION CURVE OF COMPRESSION CREEP MACHINE

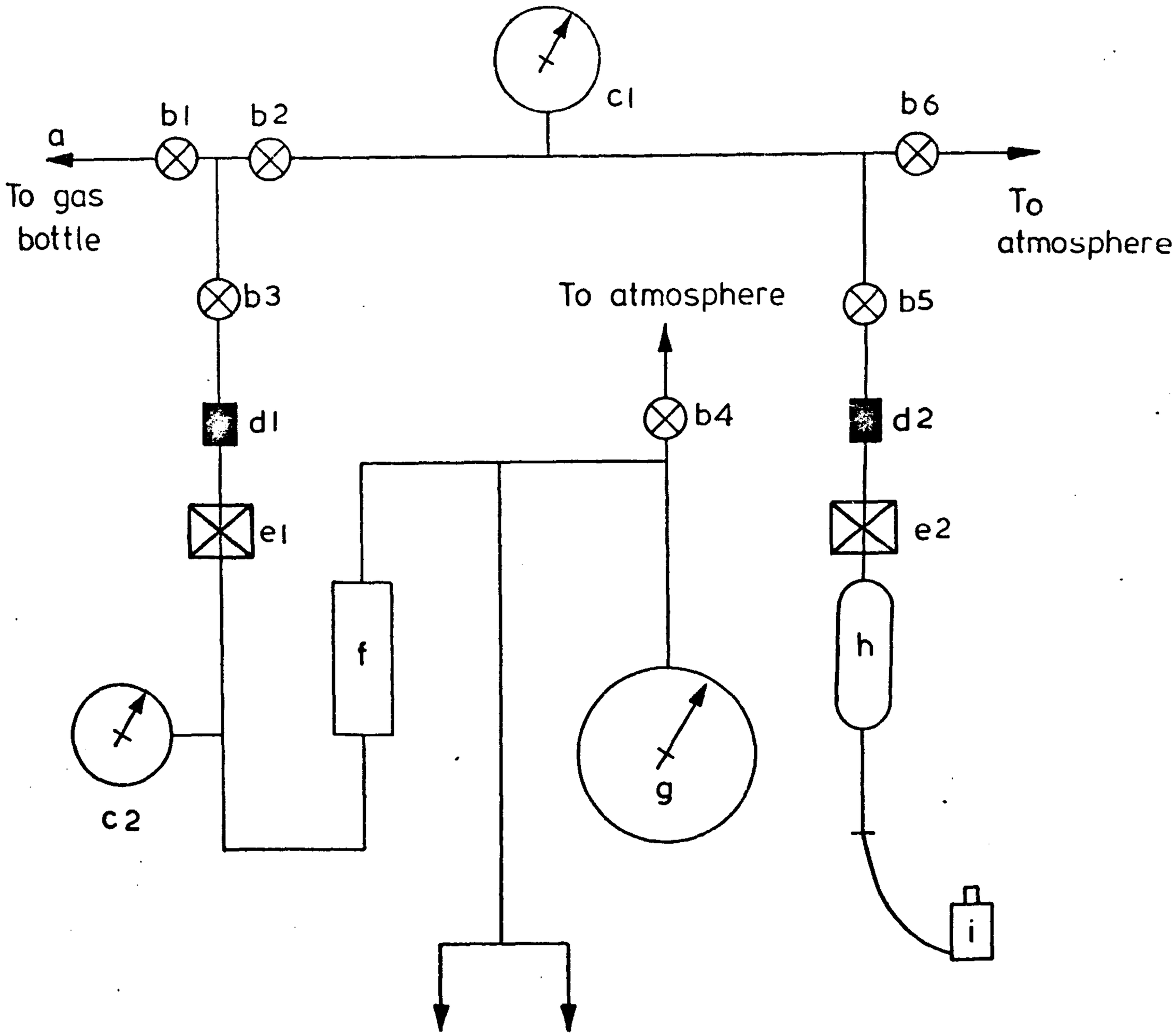

a — To gas bottle

b1 , b2, -----, b6 — Shut-off valve

c1 & c2 — Pressure gauge

d1 & d2 — Filter

e1 & e2 — Automatic pressure control valve

f — Intensifier

g — Large scale pressure gauge

h — Oil storage

i — Hydraulic jack

FIG.(5-7) SCHEMATIC DIAGRAM OF COMPRESSION CREEP LOADING CONTROL SYSTEM

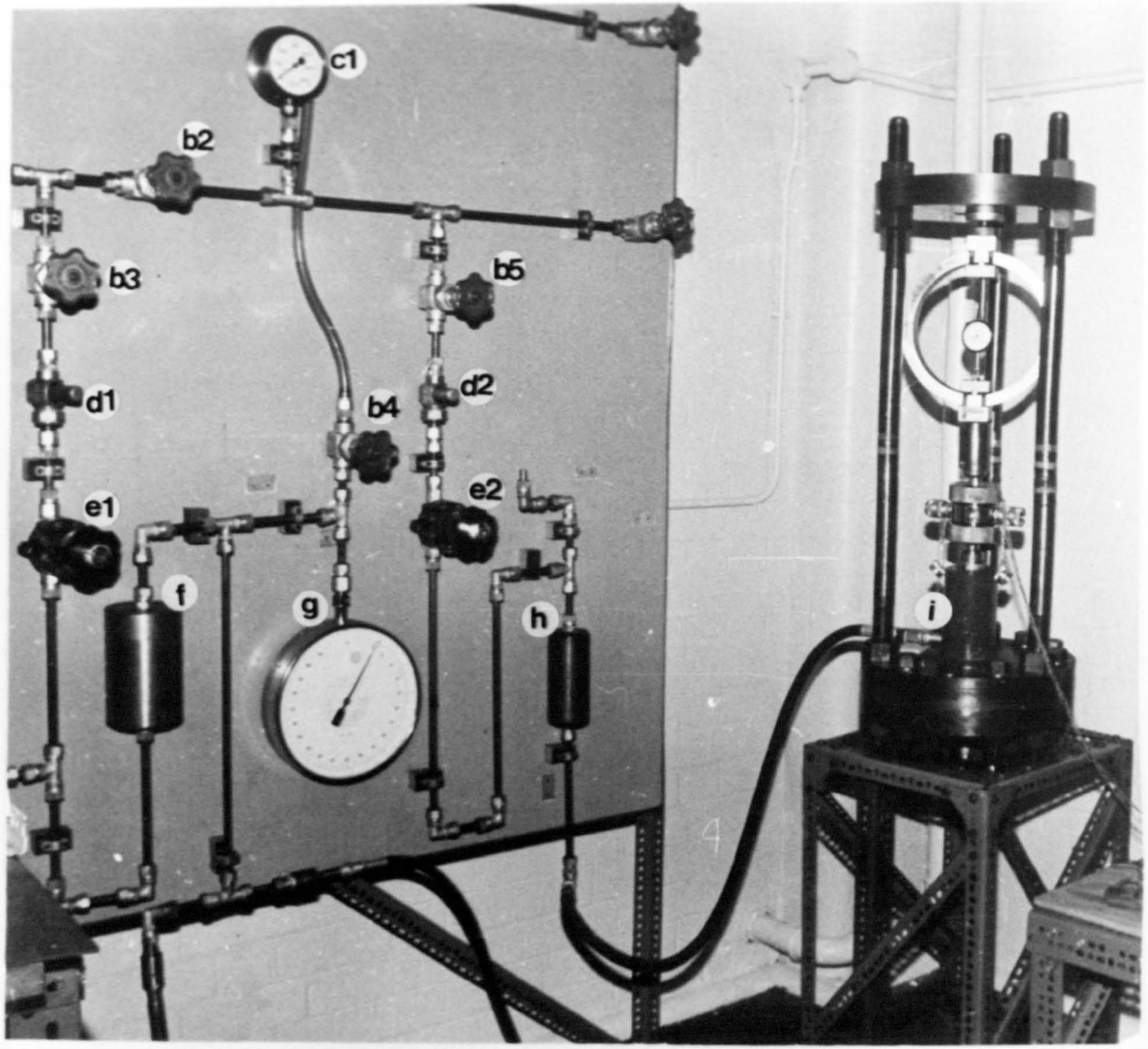

FIG.(5-8) GAS/HYDRAULIC SYSTEM AND LOADING FRAME
FOR SYMBOLS SEE FIG.(5-7)

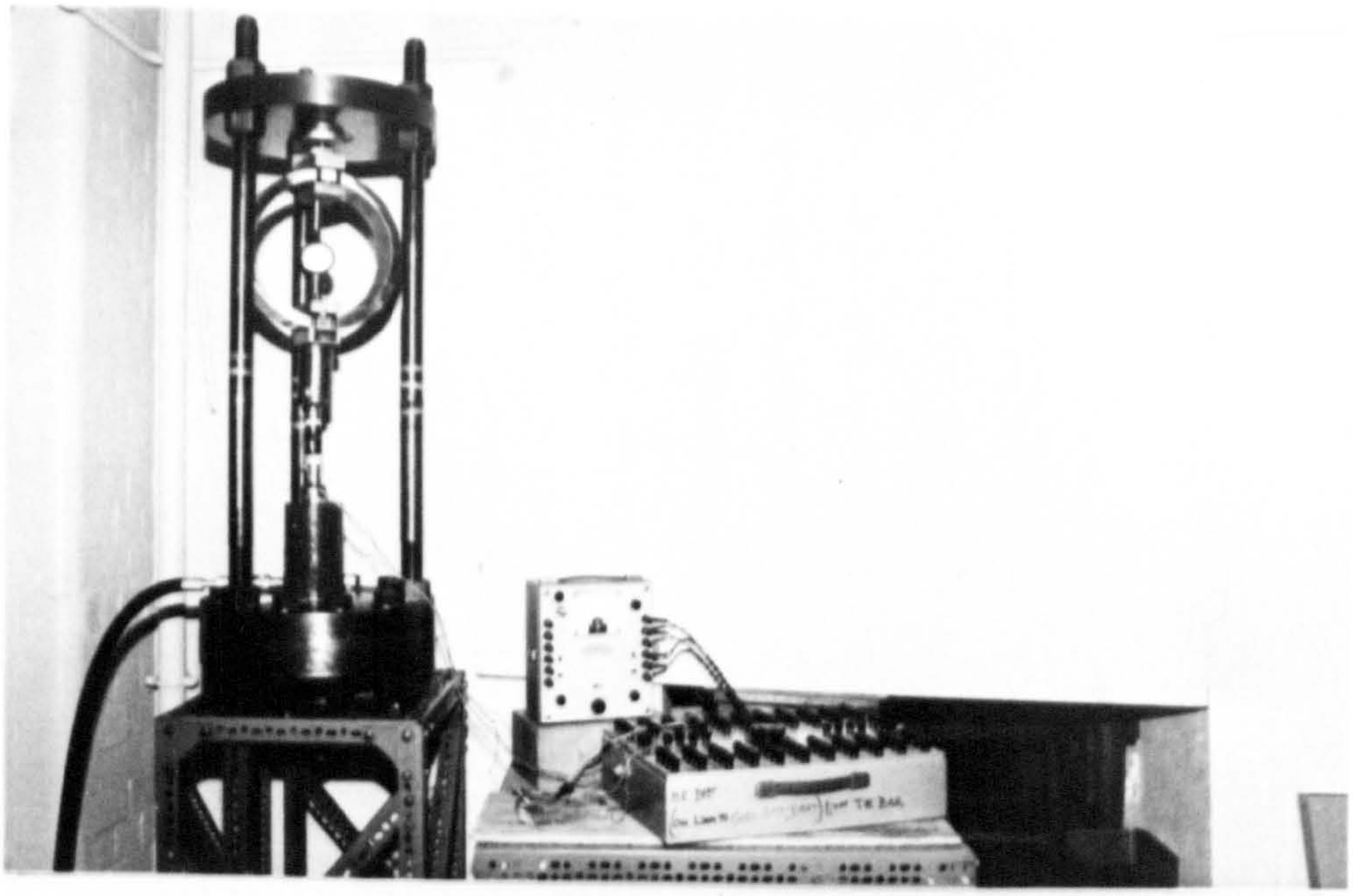

FIG. (5-9) UNIAXIAL COMPRESSION CREEP TEST IN LOADING FRAME

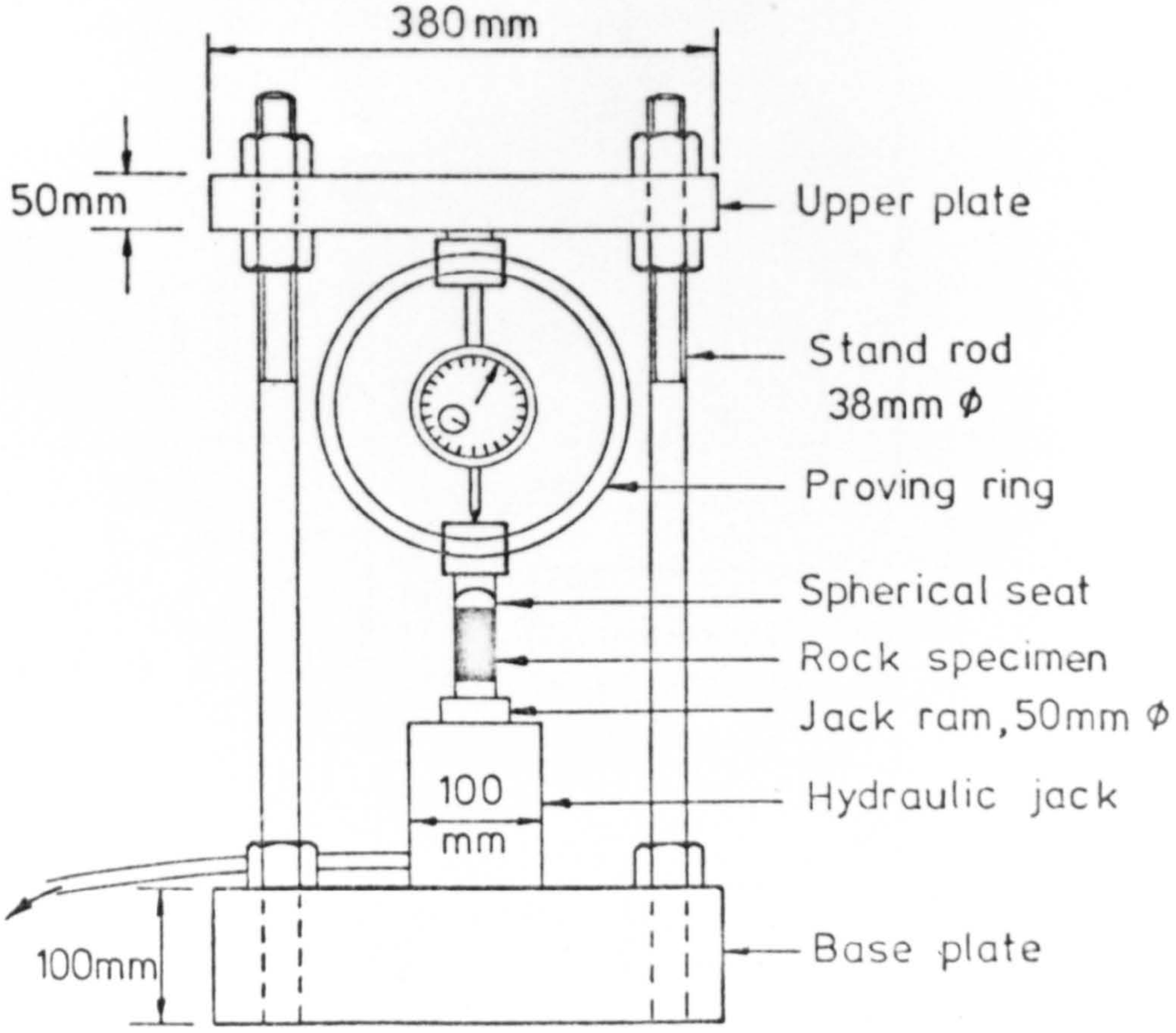

FIG. (5-10) COMPRESSION CREEP LOADING FRAME

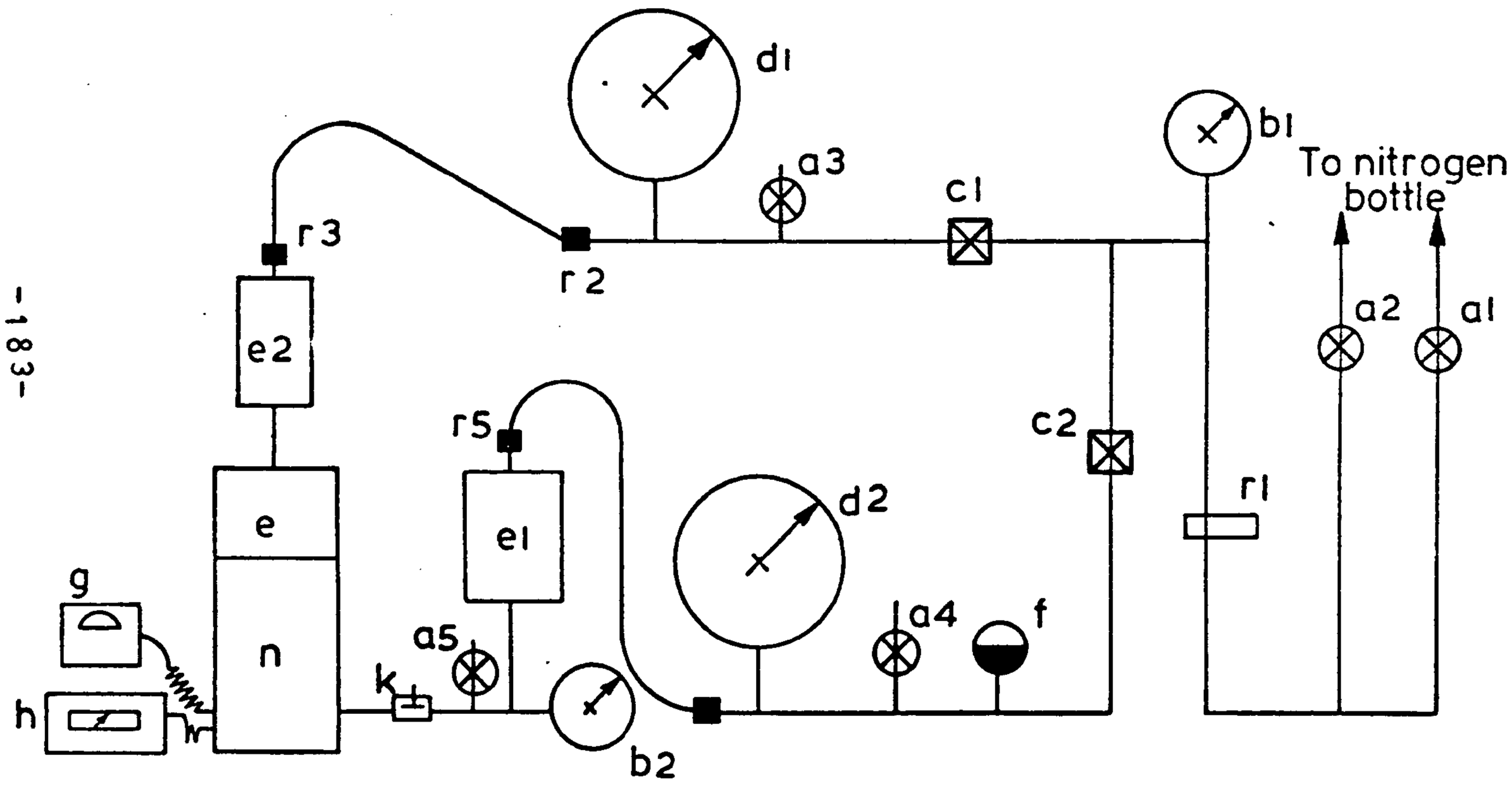

a1 , a2,----,a5—Shut-off valve
b1 — Nitrogen bottle pressure gauge
b2—Confining pressure gauge
c1 —Axial pressure control valve
c2—Confining pressure control valve
d1— Axial pressure gauge
d2— Confining pressure gauge
e1 — Confining pressure intensifier
e2—Axial load intensifier
e3— Pressure cell head
f — Automatic relief valve
g — Strain gauge indicator
h — Transducer multimeter
k — Oil inlet valve
n — Pressure cell
r1 , r2----,r5 —Filter

FIG. (5-11) SCHEMATIC DIAGRAM OF TRIAXIAL CREEP APPARATUS

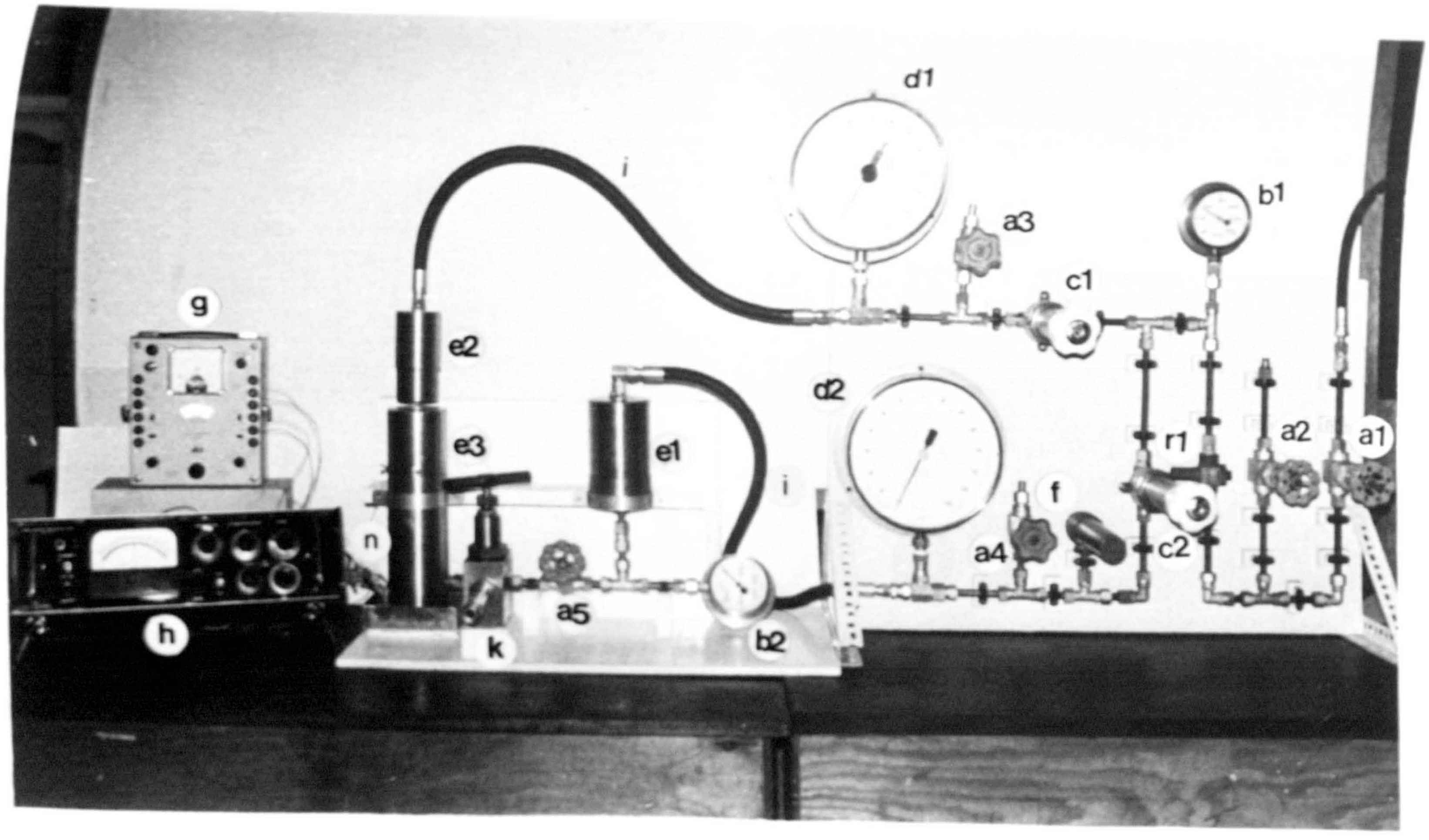

FIG (5-12) TRIAXIAL CREEP APPARATUS , FOR SYMBOLS SEE FIG (5-11)

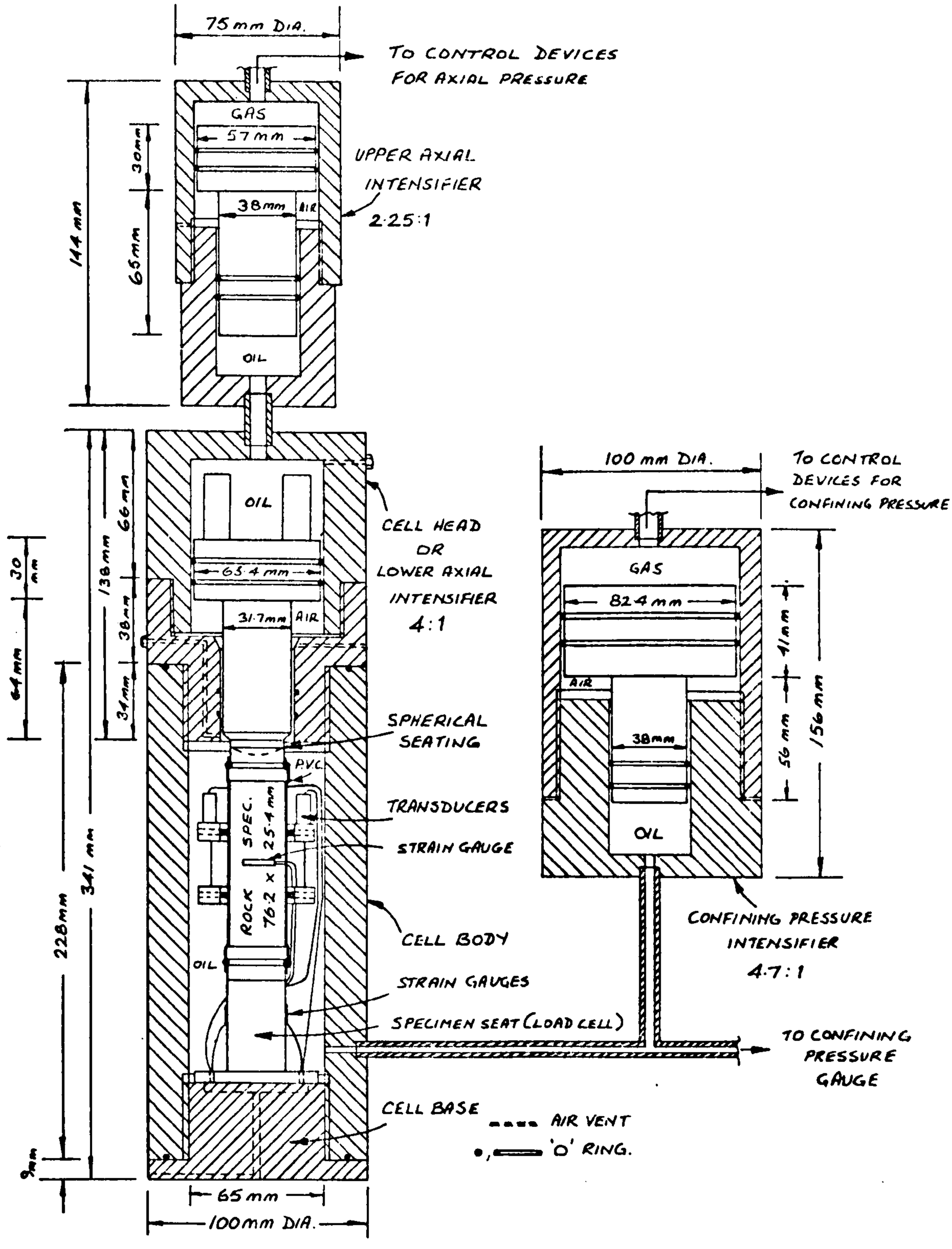

FIG. (5-13) TRIAXIAL CREEP CELL AND INTENSIFIERS

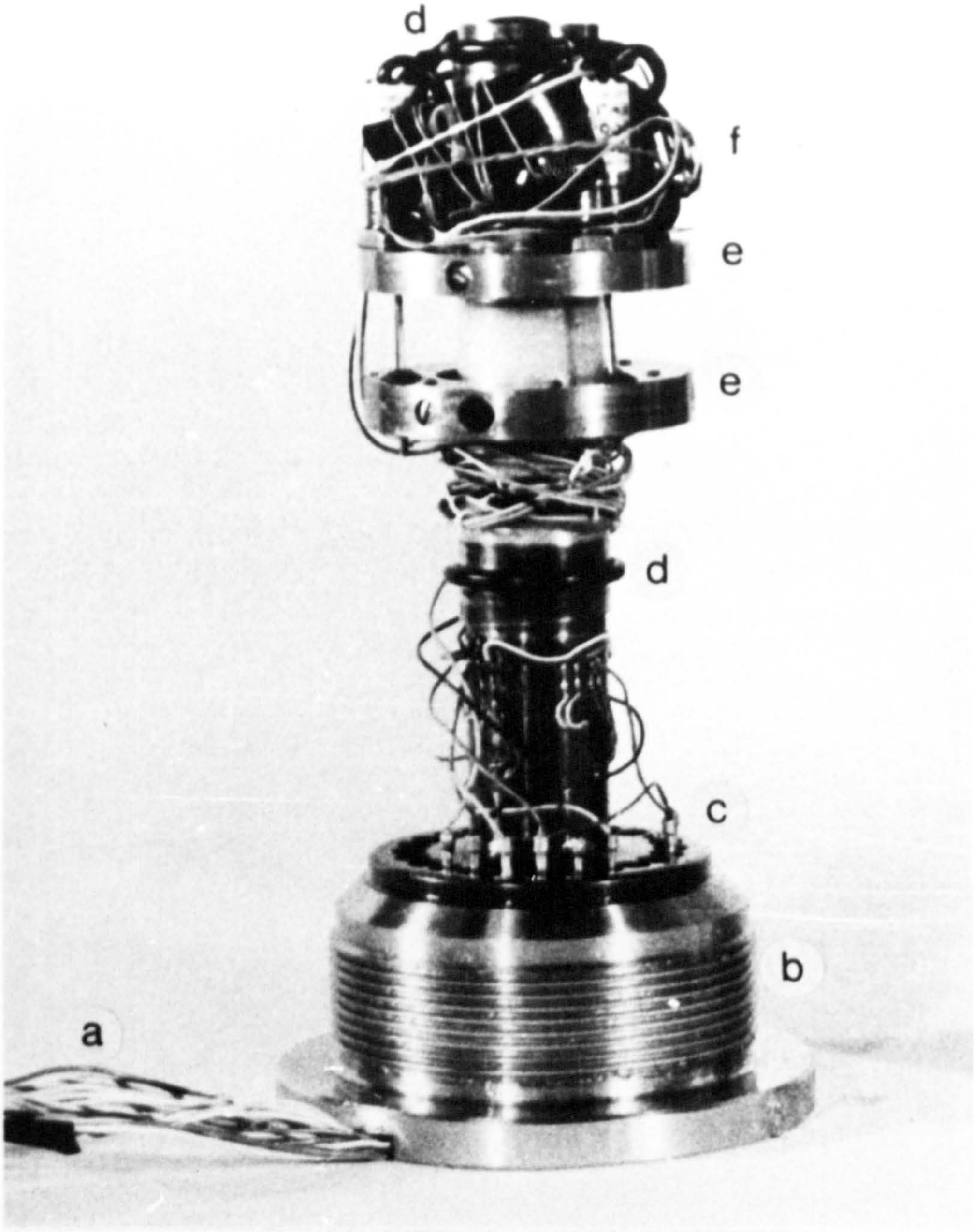

Fig. (5-14) Rock Specimen, Tranducers and Load Cell

a. External leads

b. Cell base

c. Load cell

d. Specimen oil seal

e. Annular transducer rings

f. Transducers and balancing circuit

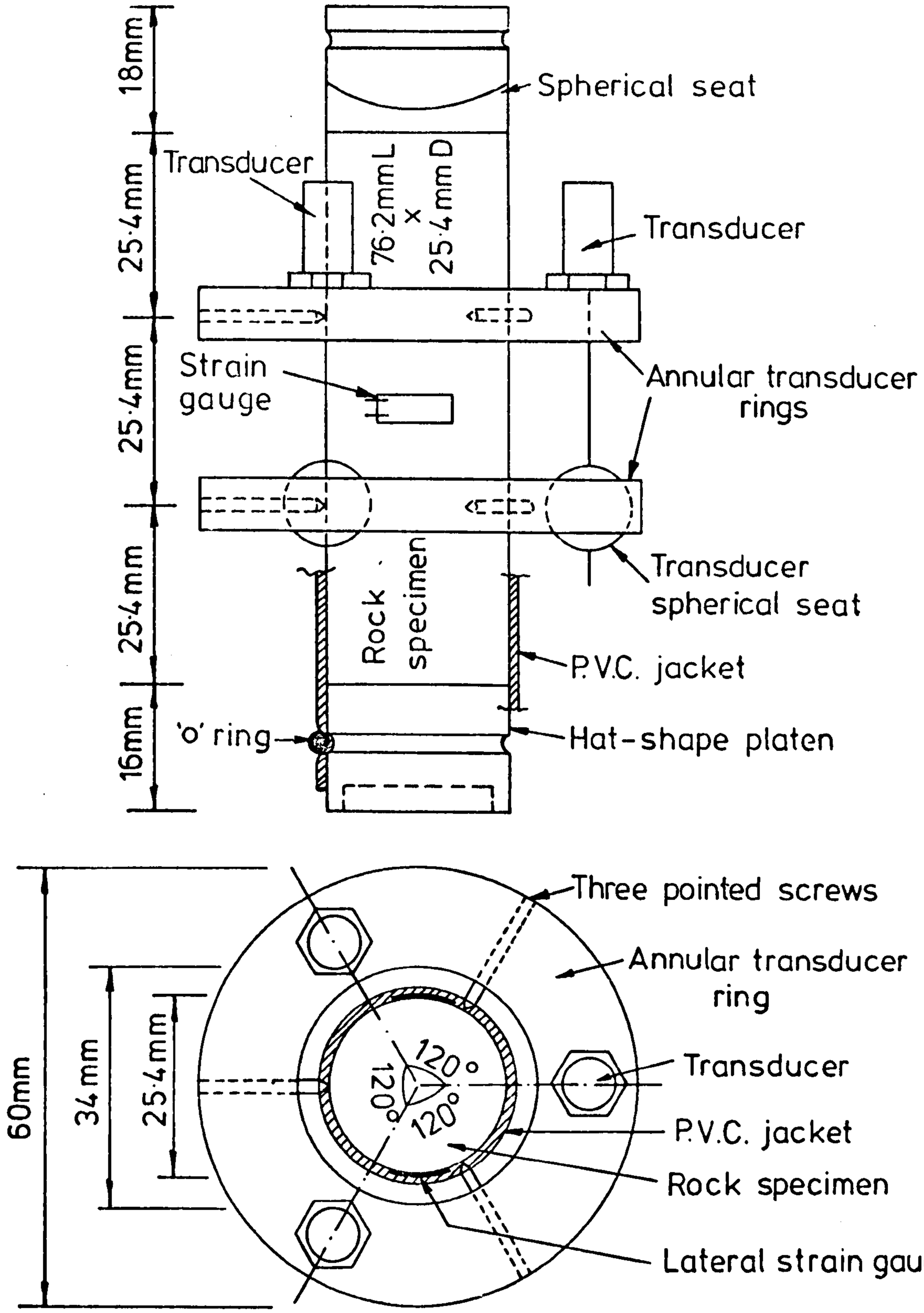

FIG (5-15) METHOD OF ATTACHING TRANSDUCERS TO THE SPECIMEN

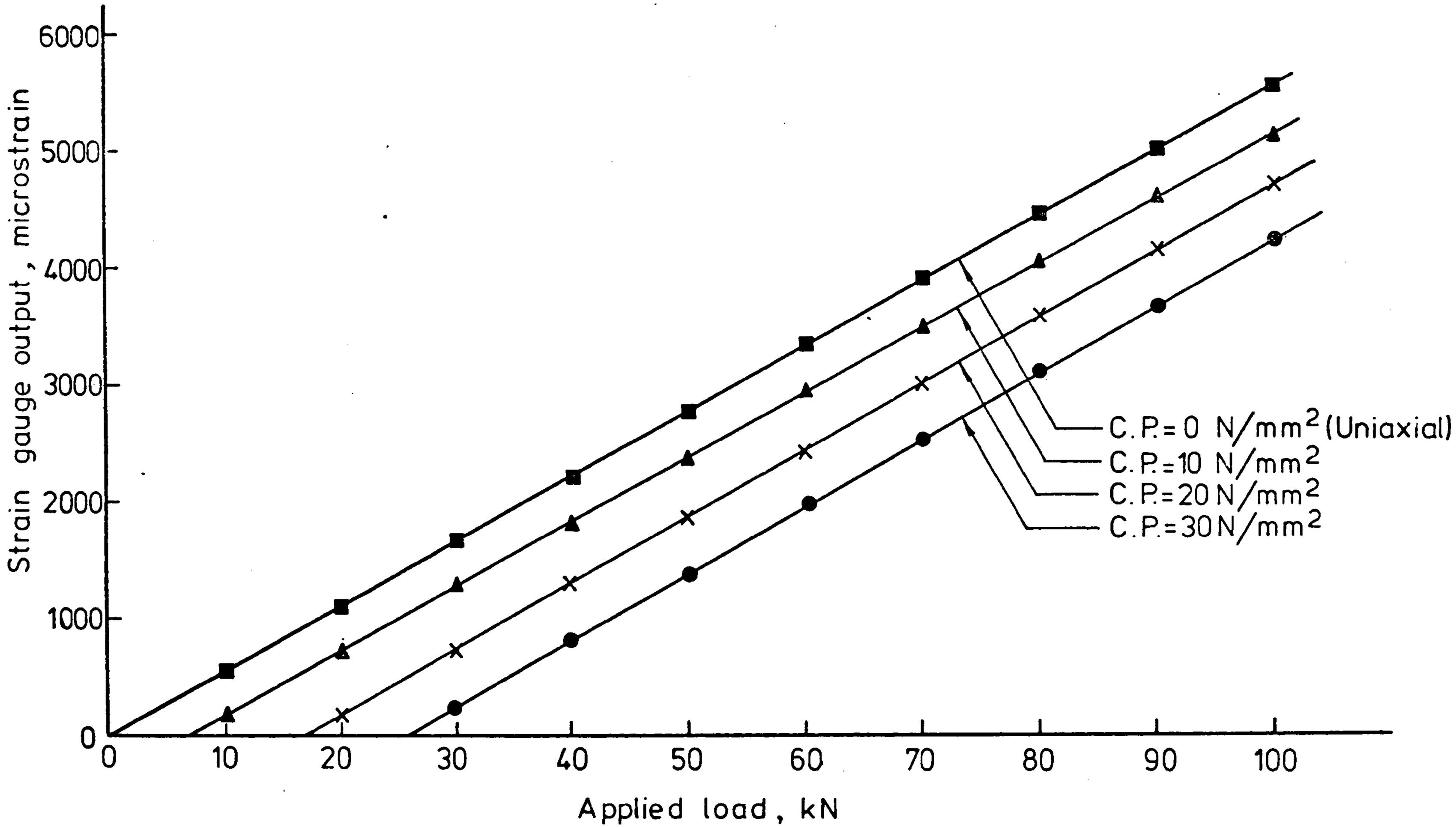

FIG. (5-16) CALIBRATION CURVES OF THE LOAD CELL (SPECIMEN SEAT)

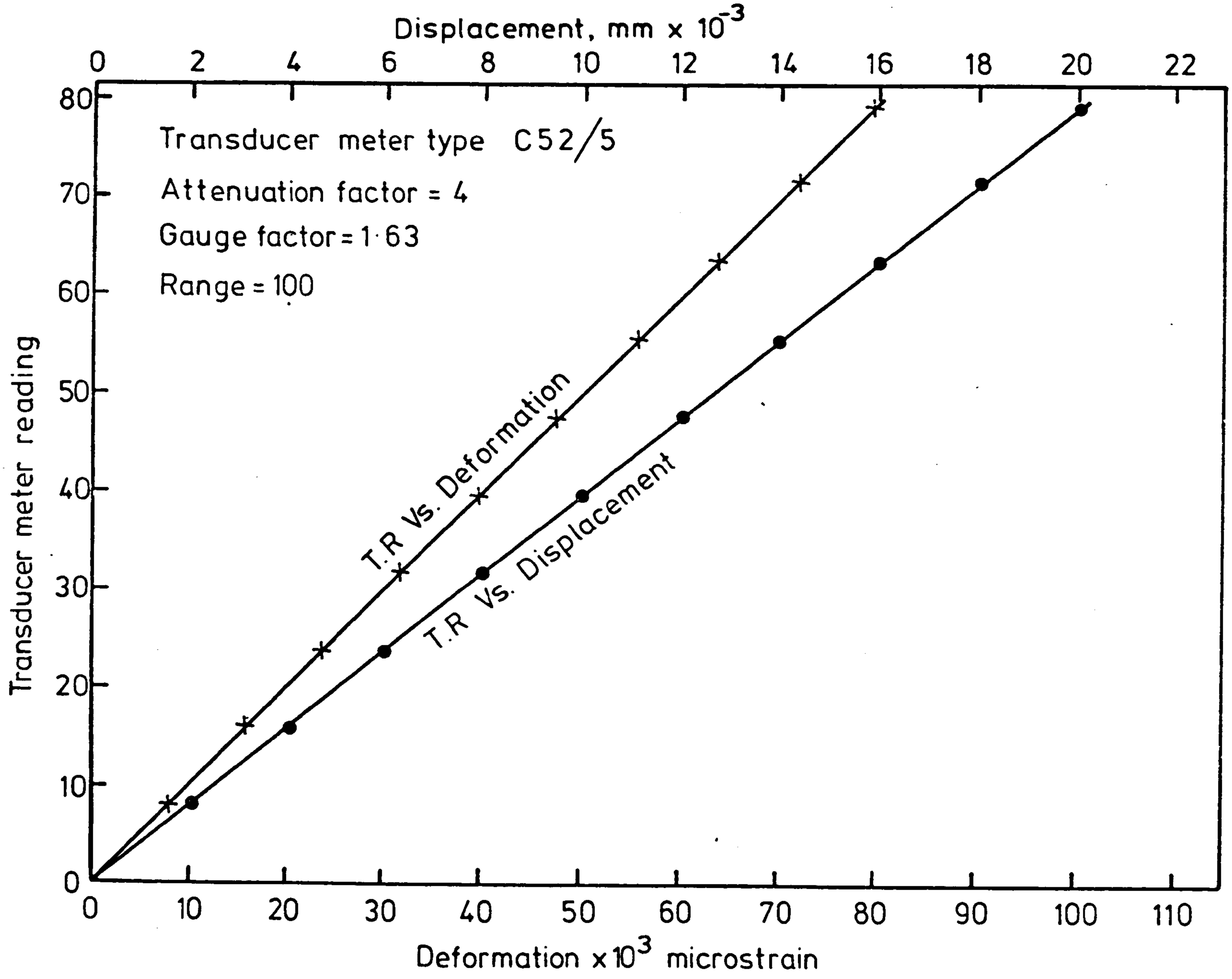

FIG.(5-17) TRANSDUCERS CALIBRATION CURVES

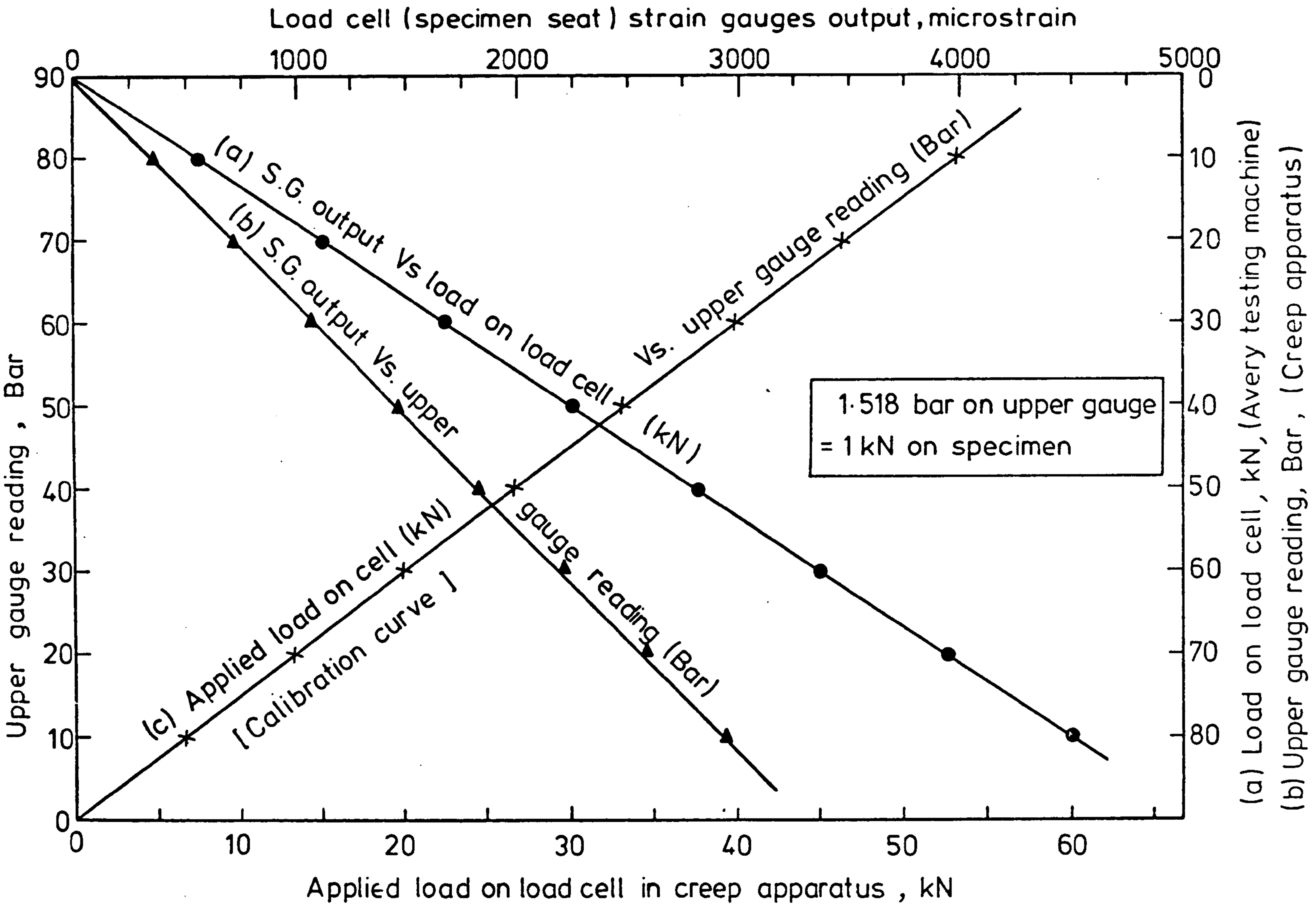

FIG (5-18) CALIBRATION CURVE OF THE TRIAXIAL CREEP APPARATUS

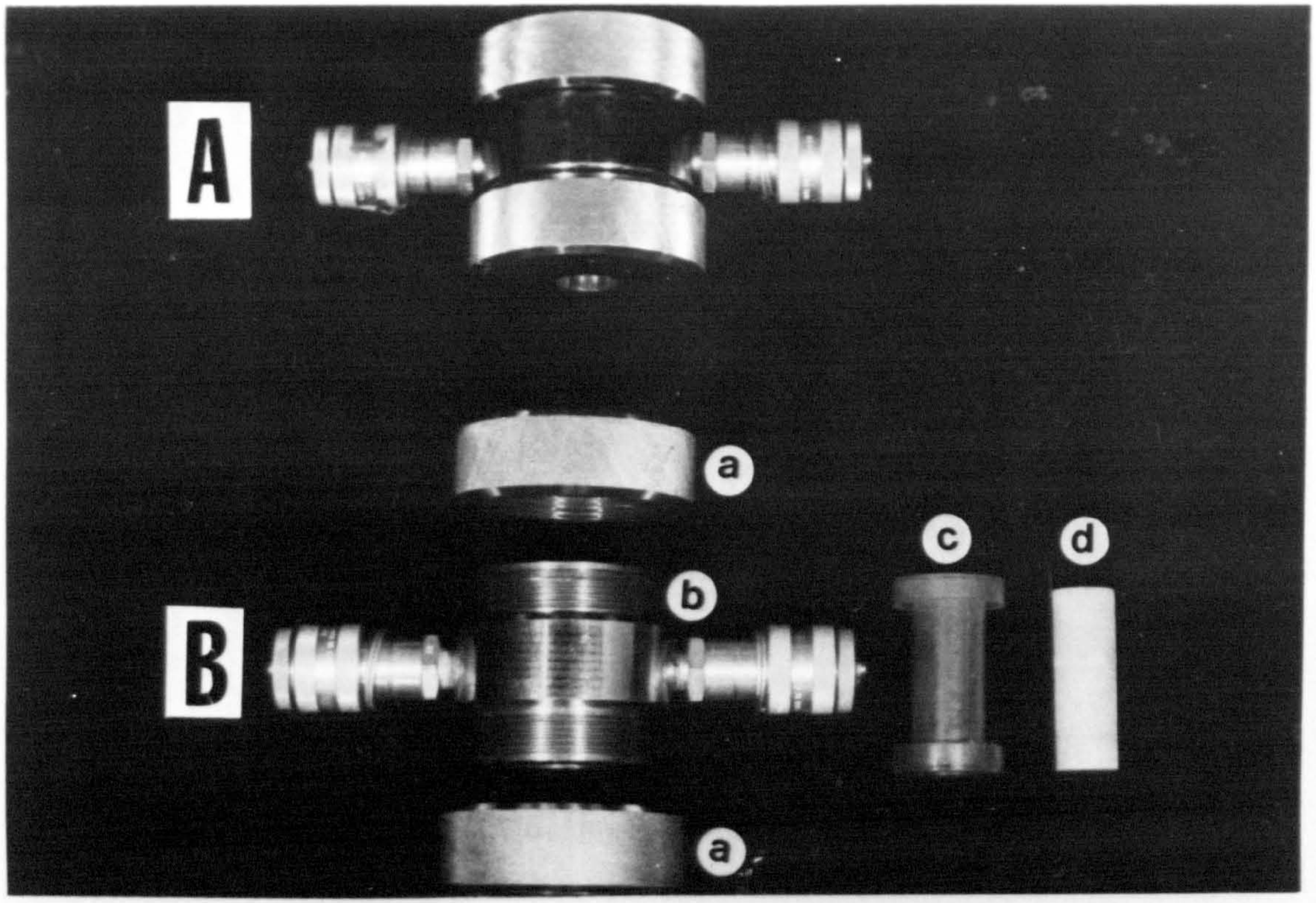

FIG. (5-19) HOEK AND FRANKLIN TRIAXIAL CELL

A. Assembled

B. Exploded
a) End cap
b) Cell body
c) Rubber celling sleeve
d) Rock specimen

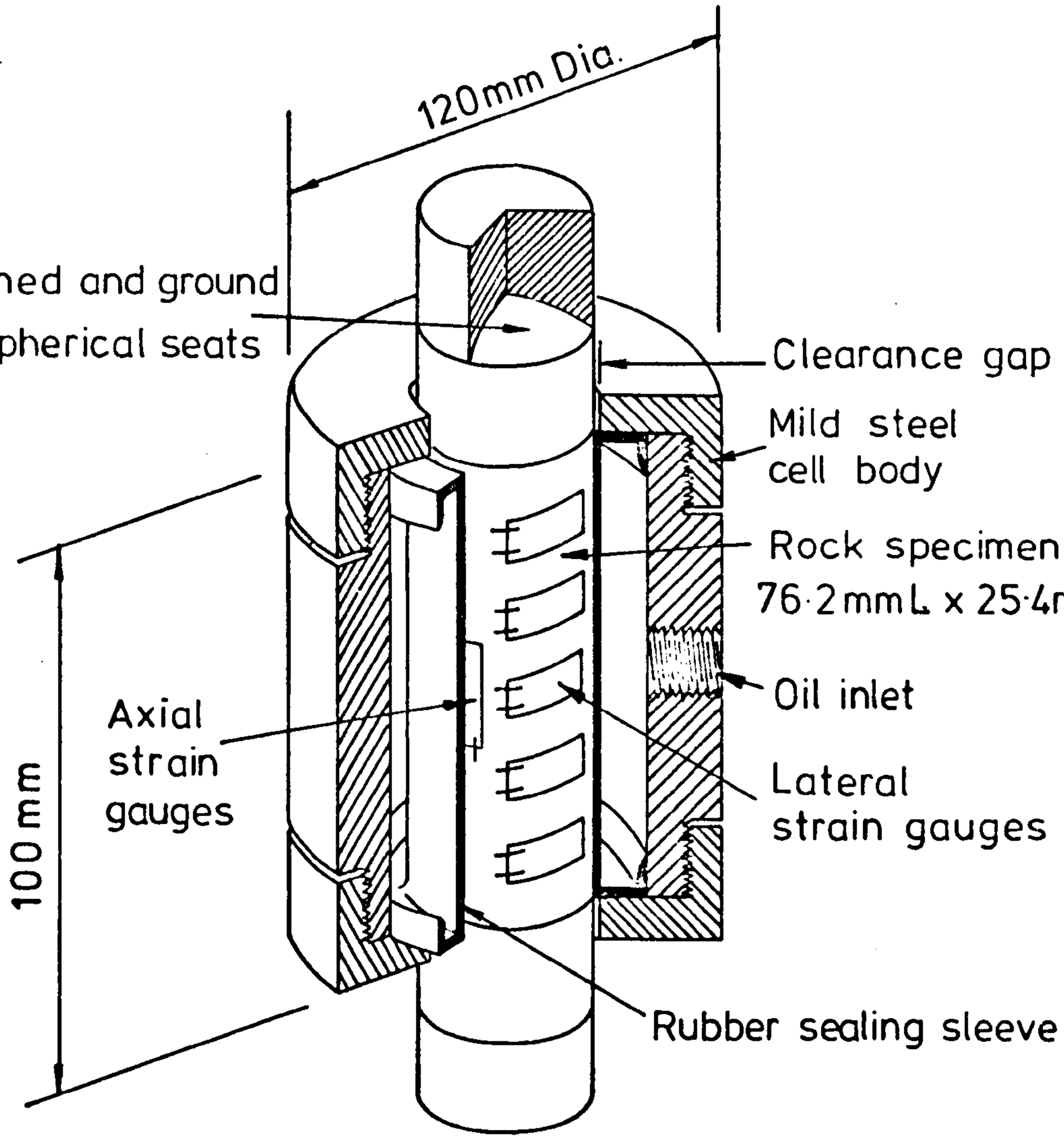

FIG. (5-20) CUTAWAY VIEW OF HOEK'S TRIAXIAL CELL

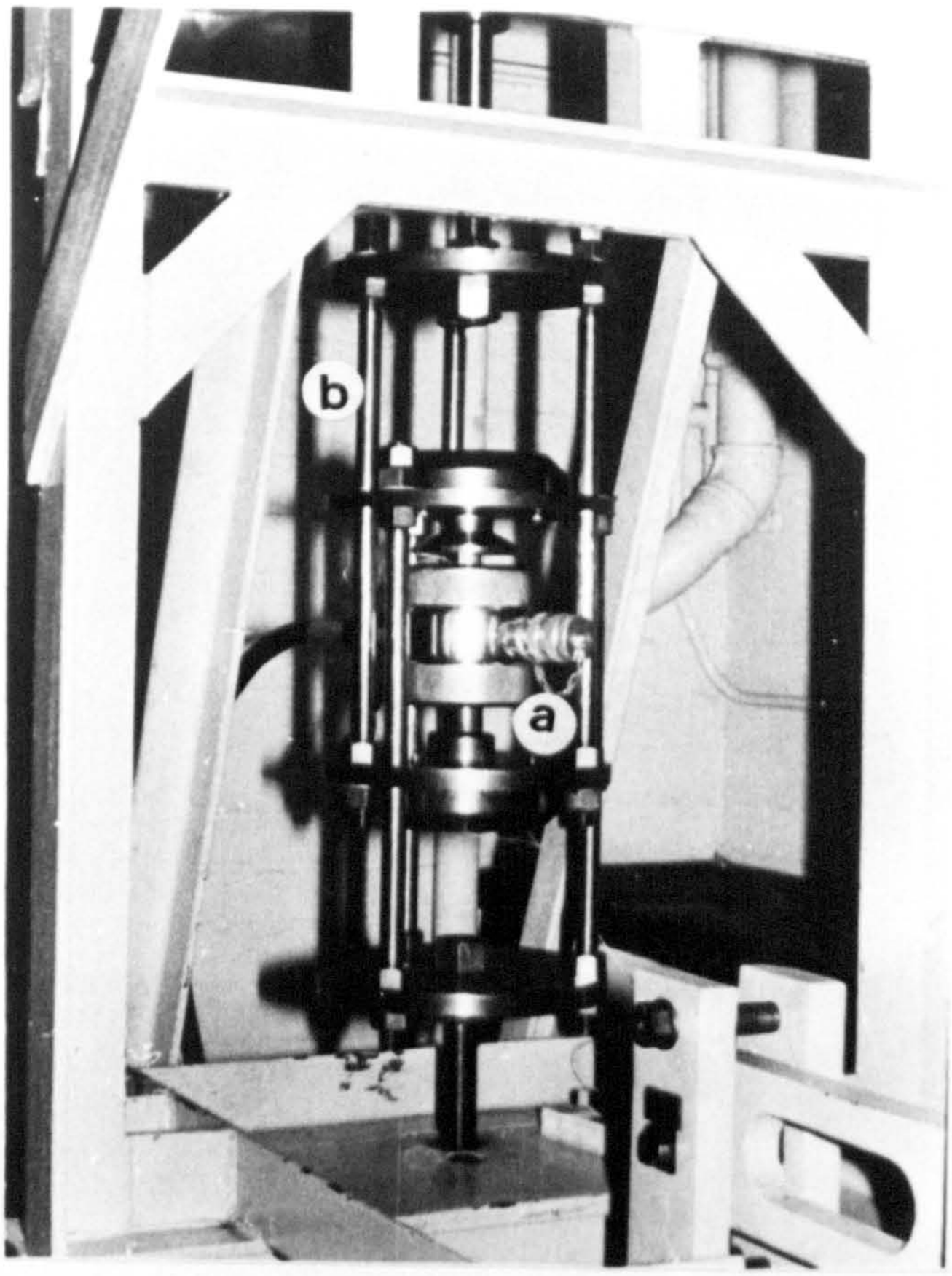

FIG. (5-21) HOEK'S CELL IN THE CREEP MACHINE
(a) The cell
(b) Load reverser of the creep machine

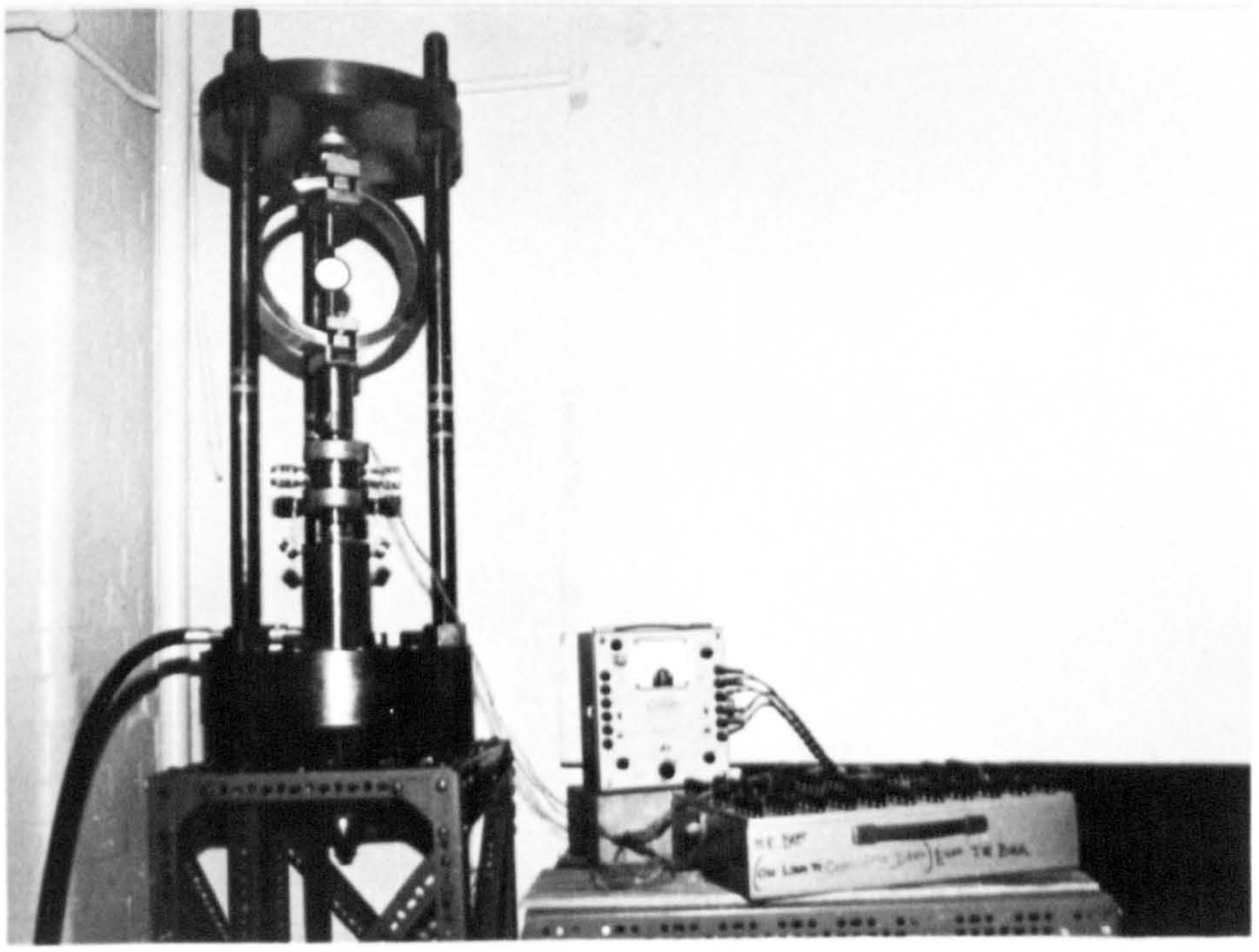

FIG. (5-22) HOEK'S CELL IN THE LOADING FRAME AND STRAIN MEASURING METERS

Chapter 6.

BENDING AND AXIAL CREEP.

6.1 Bending creep.

All bending creep tests were carried out at room temperature (21 ± 2^{o} C). As mentioned previously the creep strain at the centre of the bottom face of each rock beam was determined by using two strain gauges. The average strain was used in drawing the conclusions of this investigation.

6.1.1 Effect of the Specimen Thickness.

In order to find the proper beam thickness to study the creep behaviour under bending, four beam sizes were first used. At least three beams from each size were tested in the dry condition and the average value was considered. These sizes were:

(1) 240 mm long by 40 mm wide by 15 mm thick.

(2) 240 mm long by 40 mm wide by 20 mm thick.

(3) 240 mm long by 40 mm wide by 25 mm thick.

(4) 240 mm long by 40 mm wide by 28 mm thick.

All the specimens were subjected to the same nominal tensile stress which was 4 N/mm^2 to determine the creep behaviour of the material at various thicknesses. The results obtained were plotted as a creep strain (in microstrain) versus time (in hours). Fig. (6.1) shows the effect of the beam thickness on the bending creep. Table (6.1) gives full details of creep strain for all the tested specimens.

It can be seen from the figure and the table that the creep strain and the instantaneous strain increase with decreasing specimen thickness, in a way which shows a very small increase when the thickness decreases from 28 mm to 25 mm where no change in creep curve behaviour can be noticed. Whereas a great difference in creep strain takes place when the specimen

Table (6.1) Creep of dry gypsum in Bending at various beam thicknesses, under 4 N/mm^2.

Beams of 240 mm long x 40 mm wide x d thick.

Time hours	Beam thickness (d), mm			
	15	20	25	28
	Instantaneous strain - Microstrain			
	105	86	80	78
	Creep strain, Microstrain			
0.1	2.6	2.6	1.2	1.3
0.3	4.5	5.2	1.6	2.2
0.5	6.1	7.3	2.2	3.1
1.0	9.4	8.1	3.2	4.0
2.0	11.3 ± 4%	11.1 ± 3%	4.6 ± 4%	4.5 ± 5%
3.0	13.0	13.0	5.3	5.3
4.0	14.8	15.1	6.1	5.9
5.0	16.1	16.7	6.9	6.2
6.0	17.3	17.3	7.5	6.9
12.0	20.8	19.8	10.1	8.2
24.0	24.6 ± 5%	21.9 ± 3%	13.0 ± 6%	13.0 ± 4%
42.0	29.9	23.3	15.7	15.7
72.0	34.3	25.1	18.2	17.7
96.0	38.9	26.1	20.3	19.2
120.0	43.3	27.0	22.2	20.5
144.0	48.5	28.1	23.8	21.9
168.0	52.7	29.0	25.6	23.4
192.0	55.8	29.7	26.8	24.8
216.0	59.1	30.8	28.0	25.9
240.0	62.7 ± 5%	31.7 ± 5%	28.8	27.0 ± 4%
264.0	65.5	32.4	29.7	28.2
288.0	69.0	32.9	30.6	29.1
312.0	71.9	33.4	31.2	30.1
336.0	74.3	33.9	31.5	30.4
360.0	77.1	34.3	32.1	30.9
384.0	79.4	34.7	32.5	31.2
408.0	81.4	35.1	33.1	31.6
432.0	83.5	35.2 ± 5%	33.6	31.9
456.0	85.8		33.8	32.1
480.0	87.5		34.1 ± 6%	32.1 ± 3%
504.0	89.5			
528.0	90.9			
552.0	92.5			
576.0	94.5			
600.0	96.0			
624.0	97.5			
648.0	98.4			
672.0	99.3			
696.0	100.2			
720.0	101.0 ± 6%			

thickness decreases from 20 to 15 mm. The creep strain of the 15 mm thick specimens increases rapidly and gave a strain 3 times that of the 20 mm thick specimens. The creep strain and the behaviour of the three thicknesses 20, 25 and 28 mm was in reasonable agreement with each other relative to the specimens of 15 mm thickness.

It was found that the bending creep of the four beam sizes followed a logarithmic relationship under 4 N/mm^2 stress;

$$\varepsilon = A + B \log t$$

where ε is the creep strain, t is the time of loading in hours and A and B are constants dependent on the tested material and stress conditions. This behaviour indicates that the creep diminishes with time. The creep strain was plotted versus the time on a semi-log paper, straight lines were obtained, Fig. (6.2), for all specimen sizes. The constant A in the above equation is the creep strain at time t = 1 hour and B is the slope of the straight line on the semi-log graph.

The following equations were found for the creep of the various beam sizes subjected to 4 N/mm^2 stress;

(a) For a specimen of a size 240 mm long by 40 mm wide by 28 mm thick and 240 mm long by 40 mm wide by 25 mm thick

$$\varepsilon = 5.2 + 5.3 \log t \quad \ldots\ldots \quad (6.1)$$

(b) For a specimen of size 240 mm long by 40 mm wide by 20 mm thick

$$\varepsilon = 10.5 + 8.3 \log t \quad \ldots\ldots \quad (6.2)$$

(c) For a specimen of size 240 mm long by 40 mm wide by 15 mm thick.

$$\varepsilon = 10.5 + 10.5 \log t \quad \ldots \quad t < 92 \text{ hours} \ldots (6.3)$$

$$\varepsilon = 114 + 75 \log t \quad t \geq 92 \text{ hours} \ldots (6.4)$$

It can be seen that the constant B in the above relationships decreases as the beam thickness increases from 15 mm to 25 mm then both 25 and 28 mm thickness give the same relationship with the same constants. The creep rate at any time increases as the specimen thickness decreases, and rapidly increased in specimen thickness 15 mm at t > 92 hrs. Wheras both 25 mm and 28 mm thicknesses gave the same creep rate.

Williams and Elizzi[15,16] tested two specimen sizes of gypsum, namely; 240 mm long by 40 mm wide by 15 mm thick and 240 mm long by 40 mm wide by 20 mm thick. They found that the constant B and the creep rate of the 15 mm thick specimens are more than that of the 20 mm thick specimens.

Due to the limited number of specimen sizes used (4 - sizes) and the use of only one stress level in the experiments, (4 N/mm^2) a clear and detailed view of the effect of beam thickness on creep behaviour was not obtained and a further study of this factor is needed.

Following this study, however, beam specimens of dimensions; 240 mm long by 40 mm wide by 20 mm thick were chosen to study the creep behaviour of gypsum in bending under dry and saturated conditions subjected to various stresses.

6.1.2 Effect of Stress in the dry condition.

Three or four specimens were tested under each pre-determined stress. The stresses were chosen on the basis of percentages of the rock instantaneous strength (σ_u) at approximately 40%, 50%, 60% and 80% σ but aiming to provide similar stresses in both dry and saturated conditions for direct comparison and determination of saturation effect. The stresses were chosen as follows;

3 N/mm^2 (37.5% σ_u), 4 N/mm^2 (50% σ_u), 5 N/mm^2 (62.5% σ_u) and 6.5 N/mm^2 (81.3% σ_u).

The creep results are given in Table (6.2), and Fig.(6.3) shows the effect of the stress on the bending creep in dry conditions. It can be seen that both instantaneous strain and creep strain are increased with the applied stress. The creep behaviour was found to follow the logarithmic relationship, $\varepsilon = A + B \log t$ at low stresses ($\sigma_t \lesssim 50\% \sigma_u$) whereas it follows a power law relationship, $\varepsilon = Ct^n$ at high applied stress ($\sigma_t > 50\% \sigma_u$). Where ε is the creep strain (in microstrain) at time t (in hours). In the first relationship A is a constant representing the creep strain at t = 1 hr. and B is constant representing the slope of a creep curve on a semi-log graph, Fig.(6.4) in which; $B = \frac{\varepsilon_2 - \varepsilon_1}{\log t_2 - \log t_1}$; where ε_2 and ε_1 are creep strain at times t_2 and t_1 respectively. In the second relationship, C is a constant representing the creep value at a time t = 1 hr and the power n represents the slope of the creep curve on log-log graph, Fig. (6.5) in which:

$$n = \frac{\log\varepsilon_2 - \log\varepsilon_1}{\log t_2 - \log t_1} .$$

The following relationships were obtained according to the applied stress;

(a) At stress $\sigma_t = 3\ N/mm^2\ (37.5\%\ \sigma_u)$

$$\varepsilon = 7.3 + 5.4 \log t \quad \ldots\ldots \quad (6.5)$$

(b) At stress $\sigma_t = 4\ N/mm^2\ (50\%\ \sigma_u)$

$$\varepsilon = 10.5 + 8.3 \log t \quad \ldots\ldots \quad (6.6)$$

(c) At stress $\sigma_t = t\ N/mm^2\ (62.5\%\ \sigma_u)$

$$\varepsilon = 9.8\ t^{0.357} \qquad t \lesssim 7\ hrs \ \ldots\ldots \quad (6.7)$$

$$\varepsilon = 12.3\ t^{0.244} \qquad 5 > 7\ hrs \ \ldots\ldots \quad (6.8)$$

(d) At stress $\sigma_t = 6.5\ N/mm^2\ (81.3\%\ \sigma_u)$

$$\varepsilon = 13.4\ t^{0.362} \quad \ldots\ldots \quad (6.9)$$

Table (6.2) Creep of dry gypsum in Bending.

Time hours	Applied stress, N/mm^2			
	3.0 37.5% σ_u	4.0 50% σ_u	5.0 62.5% σ_u	6.5 81.3% σ_u
	Instantaneous strain, Microstrain			
	64	86	112	150
	Creep strain, Microstrain			
0.1	1.5	2.6	3.4	2.1
0.3	3.0	5.2	5.5	5.8
0.5	4.4	7.3	7.9	10.2
1.0	6.2	8.1	10.3	14.6
2.0	10.0 ± 7%	11.1 ± 5%	12.7 ± 6%	18.7 ± 5%
3.0	12.4	13.0	15.2	21.1
4.0	12.8	15.1	17.3	23.6
5.0	14.6	16.7	19.2	26.5
6.0	15.0	17.3	21.1	28.1
12.0	15.7	19.8	23.5	33.8
24.0	16.1 ± 7%	21.9 ± 5%	25.6 ± 6%	41.9 ± 5%
48.0	16.3	23.3	29.1	52.9
72.0	16.6	25.1	32.5	58.4
96.0	17.3	26.1	35.1	63.5
120.0	18.2	27.0	37.4	69.3
144.0	18.9	28.1	39.7	72.2
168.0	19.5	29.0	42.1	79.7
192.0	19.5	29.7	44.2	82.2
216.0	19.5	30.8	45.7	91.0
240.0	19.6 ± 8%	31.7 ± 4%	47.1 ± 5%	95.0 ± 4%
264.0		32.4	48.5	98.5
288.0		32.9	49.6	103.2
312.0		33.4	51.1	108.1
336.0		33.9	52.8	113.1
360.0		34.3	54.4	116.0
384.0		34.7	56.0	118.6
408.0		35.1	58.3	121.2
432.0		35.2 ± 4%	59.9	124.0
456.0			60.8	127.0
480.0			61.9	131.3
504.0			62.9	134.6
528.0			63.6	137.2
552.0			64.2	138.8
576.0			65.0	140.6
600.0			65.3	142.9
624.0			65.3	143.8
648.0			66.0 ± 3%	144.8
672.0			66.5	145.5
696.0				146.2
720.0				146.7 ± 4%

It can be observed from the above relationships and the data given in Table (6.3), that the creep equation constants A, B, C and n increase with increasing the applied stress.

Griggs[70], Misra[79], Williams and Elizzi[15,16] and others, reported the increase of the constants A and B with the applied stress.

Misra[79] reported that both C and n increase by increasing the stress. Whereas Elizzi[15] reported that as the stress increases the value of C increases and the value of n remains nearly constant and $\simeq \frac{1}{3}$.

Table (6.5) gives the creep rate of the dry specimens at various times under constant applied stress. The results indicate that the creep rate increases with increasing the applied stress at a given time, see Fig.(6.13), on the other hand, the creep rate decreases with the time at constant stress. This indicates that the creep strain diminishes with time. These results are in agreement with the results obtained by the investigators;

Griggs[70], Misra[79], Price[80], Wawersik[96], Singh[79], Williams and Elizzi[16] and others with different rocks.

The creep strains given in Table (6.2) were plotted against the applied stress at constant time on semi-log graph. Straight lines were obtained, Fig.(6.6), indicating that the relationship between the creep strain (ε) and the applied stress (σ_t) at a constant time (t) follows a logarithmic relationship of the form:

$$\log\varepsilon = \alpha + \beta\sigma_t$$

or

$$\varepsilon = 10^{\alpha+\beta\sigma_t} \quad \ldots\ldots \quad (6.10)$$

where α and β are constants.

6.1.2.1 Empirical Equations:

The creep strain of dry gypsum in bending can be determined by using formulae $\varepsilon = A + B\log t$ or $\varepsilon = Ct^n$ depending on the stress level, while the

Table (6.3) Constants of Bending Creep equations in dry condition

$$\varepsilon = A + B \log t$$

$$\varepsilon = Ct^n$$

σ_t N/mm^2	$\frac{\sigma_t}{\sigma_u}$ x 100	Constants				
		A	B	C	n	
3	37.5	7.5	5.4	-	-	
4	50	10.5	8.3	-	-	
5	62.5	-	-	9.3	0.357	t<7 hrs.
		-	-	12.3	0.244	t>7 hrs.
6.5	81.3	-	-	13.4	0.362	

Table (6.4) Constants of Bending Creep equations in saturated condition.

$$\varepsilon = C\, t^n$$

σ_t N/mm^2	$\frac{\sigma_t}{\sigma_u}$ x 100	Constants		
		C	n	
2	35.5	48	0.418	t < 6 hrs.
		61	0.298	t > 6 hrs.
3	53.6	62	0.435	t < 4 hrs.
		75	0.310	t > 4 hrs.
4	71.4	75	0.450	t < 4 hrs.
		92	0.319	t > 4 hrs.
4.5	80.4	85	0.518	t < 4 hrs.
		111	0.326	t > 4 hrs.

Table (6.5) Creep rate of dry gypsum at Bending Creep tests.

σ_t N/mm^2	$\frac{\sigma_t}{\sigma_u}$ x 100		Creep rate, microstrain, at t =									
			1 hr.	12 hr.	24 hr.	48 hr.	96 hr.	120 hr.	240 hr.	360 hr.	480 hr.	720 hr.
3	37.5	*	5.4	0.45	0.23	0.12	0.06	0.05	0.03	-	-	-
4	50	*	8.3	0.7	0.35	0.18	0.09	0.07	0.04	0.02		
5	62.5	*	3.5	-	-	-	-	-	-	-	-	-
		**	-	0.46	0.27	0.17	0.10	0.08	0.05	0.04	0.03	-
6.5	81.3	**	4.9	1	0.64	0.41	0.26	0.23	0.15	0.11	0.09	0.07

*Creep follows logarithmic law

**Creep follows power law

creep strain at any constant time can be calculated as a function of stress by using the formula given in Eq. (6.10).

In order to predict the creep strain in bending with respect to applied stress and loading time, the results obtained were regressed, using the multiple regression curve fitting computer program with creep (ε) as the dependent variable and the loading time (t) and applied stress (σ_t) as independent variables. This program considered the creation of five new variables including exponential functions, logarithmic functions, power law functions, etc. The data were analysed several times with different numbers of readings of the variables t and σ_t, so that an equation could be obtained at a number of time (t) periods and stress (σ_t) levels. After each period a function of logε, logt and σ_t gave the best fit for the given loading time, and applied stresses. This function is in the following form:

$$\varepsilon = D \cdot 10^{E\sigma_t} \cdot t^F$$

where D, E and F are constants

and $\varepsilon = 1.162 \times 10^{0.18559\sigma_t} \times t^{0.29844}$ ..... (6.11)

For t > 24 hours.

The predicted creep using this formula compared with the actual values, the variation was between 0% to 13% as opposed to 29% for the second best correlation. The correlation coefficient was found to be 0.989 which indicates good significant correctness.

6.1.3 Creep of Water Saturated Specimens.

Three or four water saturated beams were tested under each of the pre-determined nominal stress levels. The stresses were chosen as percentages of the instantaneous saturated rock strength (σ_u). Approximate values of their percentages were chosen in order that results could

be obtained such that similar stresses were used in both saturated and dry gypsum in some cases. These stresses were:
2 N/mm^2 (35.5% σ_u), 3 N/mm^2 (53.6% σ_u), 4 N/mm^2 (71.4% σ_u) and 4.5 N/mm^2 (80.4% σ_u).

The results obtained are given in Table (6.7), and Fig. (6.7) shows the effect of the stress on the creep behaviour of the saturated gypsum in bending. It can be seen from these results that the instantaneous and the creep strains are increased with increasing the applied stress. The creep behaviour was found to follow the power law relationship of the form; $\varepsilon = Ct^n$ in all cases, where ε is the creep strain (in microstrain) at a loading time (t) in (hours). C and n are constants with C representing the creep strain at time t = 1 hr and n the slope of the creep curve on a log-log graph, see Fig. (6.9). The following relationships were obtained in the case of the saturated gypsum:

(a) At stress σ_t = 2 N/mm^2 (35.5% σ_u)

$$\varepsilon = 48\ t^{0.418} \quad \ldots\ldots \quad t < 6 \text{ hrs.} \quad \ldots\ldots \quad (6.12)$$

$$\varepsilon = 61\ t^{0.298} \quad \ldots\ldots \quad t \geq 6 \text{ hrs.} \quad \ldots\ldots \quad (6.13)$$

(b) At stress σ_t = 3 N/mm^2 (53.6% σ_u)

$$\varepsilon = 62\ t^{0.435} \quad \ldots\ldots \quad t < 4 \text{ hrs.} \quad \ldots\ldots \quad (6.14)$$

$$\varepsilon = 75\ t^{0.310} \quad \ldots\ldots \quad t \geq 4 \text{ hrs.} \quad \ldots\ldots \quad (6.15)$$

(c) At stress σ_t = 4 N/mm^2 (71.4% σ_u)

$$\varepsilon = 75\ t^{0.450} \quad \ldots\ldots \quad t < 4 \text{ hrs.} \quad \ldots\ldots \quad (6.16)$$

$$\varepsilon = 92\ t^{0.319} \quad \ldots\ldots \quad t \geq 4 \text{ hrs.} \quad \ldots\ldots \quad (6.17)$$

(d) At stress σ_t = 4.5 N/mm^2 (80.4% σ_u)

$$\varepsilon = 85\ t^{0.518} \quad \ldots\ldots \quad t < 4 \text{ hrs.} \quad \ldots\ldots \quad (6.18)$$

$$\varepsilon = 111\ t^{0.326} \quad \ldots\ldots \quad t \geq 4 \text{ hrs.} \quad \ldots\ldots \quad (6.19)$$

Table (6.6) Creep rate of saturated gypsum at Bending Creep tests.

σ_t N/mm^2	$\frac{\sigma_t}{\sigma_u}$ x 100		Creep rate, microstrain, at t =									
			1 hr.	12 hr.	24 hr.	48 hr.	96 hr.	120 hr.	240 hr.	360 hr.	480 hr.	720 hr.
2	35.5	*	20.1	-	-	-	-	-	-	-	-	-
		**	-	3.2	2.0	1.2	0.74	0.63	0.39	0.29	0.24	0.18
3	53.6	*	27	-	-	-	-	-	-	-	-	-
		**	-	4.2	2.6	1.6	1.0	0.86	0.53	0.4	0.33	0.25
4.0	71.4	*	33.8	-	-	-	-	-	-	-	-	-
		**	-	5.4	3.4	2.1	1.3	1.1	0.7	0.53	0.43	0.33
4.5	80.4	*	44.0	-	-	-	-	-	-	-	-	-
		**	-	6.8	4.3	2.7	1.7	1.4	0.9	0.68	0.56	0.43

*Creep follows logarithmic law

**Creep follows power law

Table (6.7) Creep of Saturated gypsum in Bending.

Time hours	Applied stress, N/mm^2			
	2.0 35.5% σ_u	3.0 53.6% σ_u	4.0 71.4% σ_u	4.5 80.4% σ_u
	Instantaneous Strain, Microstrain			
	43	94	154	186
	Creep strain, Microstrain			
0.1	16.3	20.8	20.9	23.2
0.3	27.3	33.4	39.7	45.3
0.5	36.6	48.7	55.5	60.7
1.0	47.0	65.5	77.3	83.1
2.0	62.2 ± 5%	85.1 ± 6%	105.9 ± 4%	111.5 ± 5%
3.0	75.9	102.7	133.8	140.0
4.0	85.9	120.3	155.9	165.4
5.0	94.1	135.1	182.9	190.4
6.0	102.1	147.3	198.4	204.1
12.0	127.6	170.9	241.5	262.0
24.0	170.4 ± 5%	182.9	302.4 ± 5%	340.5 ± 4%
48.0	199.6	240.3 ± 6%	340.0	380.1
72.0	225.2	264.7	355.7	405.3
96.0	244.0	280.8	369.6	430.4
120.0	262.8	298.7	383.9	451.7
144.0	278.1	314.3	410.0	475.9
168.0	291.5	340.1	435.4	496.3
192.0	300.1	352.6	458.9	516.2
216.0	324.5	368.5	474.2	534.0
240.0	338.6 ± 4%	384.8 ± 5%	500.1 ± 5%	556.1 ± 4%
264.0	353.2	795.5	516.2	573.1
288.0	366.2	408.1	435.1	591.4
312.0	380.3	425.1	550.0	609.2
336.0	387.8	443.3	560.3	625.2
360.0	393.7	457.7	575.3	637.1
384.0	397.7	459.5	593.3	652.7
408.0	401.8	482.8	610.4	668.8
432.0	407.3	487.7	625.7	679.2
456.0	412.3	510.6	635.4	690.0
480.0	416.9	522.6 ± 4%	643.6 ± 6%	705.1
504.0	420.1	535.9	652.5	728.3
528.0	423.9	544.4	664.9	745.4
552.0	427.3	557.2	681.9	762.8
576.0	428.3	567.6	695.5	770.6
600.0	431.6	573.4	702.1	779.5
624.0	433.0	579.4	706.0	789.0
648.0	434.5	584.3	708.8	795.5
672.0	435.0	589.4	711.5	799.3
696.0	435.5	593.6	712.8	803.2
720.0	436.0 ± 4%	595.2 ± 3%	714.0 ± 6%	806.1 ± 3%

It can be seen from these relationships and the data given in Table (6.4) that both the constants C and n of the creep equation increase with increasing the applied stress.

Griggs[71] suggested that the creep of alabaster at low stress in the presence of solution followed the power function, $\varepsilon = Ct^n$. Afronz and Harvey[95] reported that the creep of saturated soft rocks followed a power law of the following form:

$$\varepsilon = A + (B \cdot t^C) + (D \cdot t^E)$$

where A, B, C, D, E are constants.

The creep rate was calculated and given in Table (6.6) for various applied stresses at different loading times. It was found that the creep rate increases with the applied stress at a given time, and decreases with the time at a constant applied stress, see Fig. (6.13). This indicates that the creep strain diminishes with the time. Griggs[71] reported that the creep rate of alabaster in water increased with the applied stress and that rupture occurs in a period less than that of the smaller stress. Wawersik[96], Afronz and Harvey[95], Cogan[99], and others observed the same behaviour in the creep of different rocks in wet conditions.

Fig. (6.10) shows the relationships between the applied stress (σ_t) and the creep strain (ε) at various loading times (t). These relationships are linear and nearly parallel to each other on a semi-log graph. The relationships can be represented by the equation:

$$\log\varepsilon = \alpha + \beta\sigma_t$$

or

$$\varepsilon = 10^{\alpha+\beta\sigma_t} \quad \ldots\ldots \quad (6.20)$$

where α and β are constants.

6.1.3.1 Empirical equations.

As discussed in the previous section, the bending creep of gypsum in saturated conditions can be determined under constant stress by using the power law, $\varepsilon = Ct^n$, and at constant time for any stress by using the equation of the form Eq. (6.20). In order to predict the creep strain in saturated conditions with respect to applied stress and loading time, the data were regressed using the multiple regression curve fitting computer program following the same method used with the results of the dry specimens. A combination of the functions $\log\varepsilon$, $\log t$ and σ_t gave the best fit of the data in the following form:

$$\varepsilon = D \cdot 10^{E\sigma_t} \cdot t^F$$

where D, E and F are constants.

$$\therefore \quad \varepsilon = 38.11 \times 10^{0.09652\sigma_t} \times t^{0.31179} \quad \ldots\ldots \quad (6.21)$$

For $t > 24$ hours.

Where: ε is the creep strain, in microstrain

t is the loading time, in hours, and

σ_t is the applied stress, in N/mm^2.

When the predicted creep from this formula was compared with the actual creep strain, it was found that errors ranging from 0% to 8% were obtained. Correlation coefficient was found to be 0.991 which indicates good significant correctness.

6.1.4 The Role of Water in bending creep.

As mentioned previously the dry and saturated specimens were subjected to the similar stresses in some cases to ensure the best comparisons and to determine the effect of water on the creep behaviour under closely controlled conditions. Stresses of 3 N/mm^2 and 4 N/mm^2 were chosen for this purpose. Tables (6.2) and (6.3) give the creep results of the dry

and saturated conditions respectively. It can be noted that the instantaneous strain increased due to saturation, from 64 to 94 microstrain (47% increase) under 3 N/mm^2 and from 86 to 154 microstrain (79% increase) under 4 N/mm^2 stress.

The instantaneous strains obtained were used to calculate the Modulus of Elasticity by plotting the applied stress as a percentage of maximum stress (σ_u) against the corresponding instantaneous strain, see Fig. (6.11). From these curves the Modulus of Elasticity (E) for the two environmental conditions are calculated;

a) For dry condition:

$$E_{dry} = \frac{100}{100} \times \frac{8}{178} \times 10^6 = 4.49 \times 10^4 \ N/mm^2$$

b) For saturated condition:

$$E_{sat.} = \frac{100}{100} \times \frac{5583}{223} \times 10^6 = 2.5 \times 10^4 \ N/mm^2$$

i.e., the water decreases the Modulus of Elasticity of the gypsum in bending by about 44%.

Mann and Fatt[53] reported a decrease in Young's Modulus of Elasticity of three sandstones due to water saturation of 8-20%. Mogilevskaya[57] reported a decrease in Modulus of Elasticity of limestone of 5 - 20% when the rock was saturated with water. In an A.S.T.M. publication 1976, Chamberlain et al.[124], reported that three shales exhibited a decrease in Modulus of Elasticity under 100% humidity of 10%, 59% and 61%.

The effect of saturation was found to increase both the creep strain and the creep rate by appreciable amounts. Fig. (6.12) shows the influence of water on the bending creep subjected to two stresses. It can be seen from this figure and Tables (6.2) and (6.7) that the creep

strain is increased by the saturation up to 30 fold under 3 N/mm^2 stress and up to 20 fold under 4 N/mm^2 applied stress.

The creep behaviour in dry condition follows the logarithmic law at stresses up to 50% σ_u, and follows the power law at stresses more then 50% σ_u. Whereas in saturated conditions the creep behaviour follows the power law relationships at all stress levels. This indicates that the water increases the plasticity of the gypsum in bending even at low applied stresses.

The prediction of the creep strain with respect to loading time and applied stress follows a similar function of the form

$$\varepsilon = D \times 10^{E \sigma_t} \times t^F$$

where D, E and F are constants,

in both cases, but these constants are increased by the water saturation.

Fig. (6.13) shows the effect of stress and saturation on the creep rate. It can be seen that the creep rate increases in both dry and saturated conditions with the applied stress in a linear relationship on the semi-log graphs ($\log \dot{\varepsilon} - \sigma_t$). The straight lines are parallel or nearly parallel to each other. From the data given in Tables (6.5) and (6.6) and shown in Fig. (6.13) it is clear that the water saturation increases the creep rate by appreciable amounts. This increase ranging from 4 to 26 fold with 10 as an average. The effect of the water on the creep rate increases with time.

Griggs[70] (1939) reported that the creep and creep rate of the gypsum (alabaster) immersed in water increased markedly. It has been suggested that the creep takes place by a process of recrystallization (solution occurs at the most highly stressed region and deposition at the free regions). Griggs[71] also suggested (1940) that the rate of

the creep of the immersed alabaster is not due to simple recrystallization but may be a function of ionic mobility of gypsum in solvent (Ca^{++} and SO_4^{--}).

Misra[79] found that the bending creep of saturated anhydrite and beerstone increased by 12 and 5 times respectively and the creep rate increased by remarkable amounts. He also reported that both these rocks are partially soluble in water, and the effect of the water on their creep is mainly due to solution. Afronz and Harvey[95] found that in saturated soft rocks, the creep rate increased by 3 fold in coal and 8 fold in shales. Varo and Passaris[102] reported that the creep rate of the halite in water was accelerated rapidly, and the main effect of water on the creep of halite is one of solution and that failure was caused by its solution.

The creep behaviour of gypsum in this study was in all cases changed by water saturation from a logarithmic law in dry condition to a power law in saturated conditions under the similar stress. Griggs[70] (1939) explained this kind of change in the creep behaviour of the gypsum (alabaster) as being due to recrystallization.

It is suggested that the effect of the water on the creep of the gypsum in this research is caused by either recrystallization as described by Griggs[70] or solution or partly by both. The consideration of the water effects will be given in detail in the next section.

6.2 Axial Creep in Compression.

Uniaxial and triaxial creep tests were carried out on 76.2 mm long by 25.4 mm dia. gypsum core samples. These tests were performed under dry and saturated conditions at room temperature (21 ± 2^{o} C). From the results published by previous investigators in the field of creep in rock

and confirmed in this work it is established that the applied stress has a great effect on the creep behaviour of any rock. The value of the applied stress necessary to cause an appreciable amount of creep to occur in a reasonable time from an experimental point of view, apart from other factors depends on the ultimate strength of the tested rock under the loading conditions of the experiments. It was therefore decided to apply different axial stresses as a percentage of the ultimate strength at every confining pressure. At the same time it was decided to apply similar axial stresses in both dry and saturated conditions and at the various confining pressures in all the possible cases. This was done to ensure accurate comparisons in the determination of the effects of saturation and confining pressure on the creep under closely controlled conditions. The following percentages of ultimate stresses with the shown ranges were used for the required testing stresses; $(33 \pm 7)\%$, $(50 \pm 7)\%$, $(65 \pm 6)\%$ and $(85 \pm 5)\%$. Various confining pressure levels were chosen for this study, namely; 0 (uniaxial), 10, 20 and 30 N/mm^2. Axial and lateral creep were measured. The axial creep results and factors affecting it will be discussed in this Chapter.

The average results of three or four specimens tested at similar applied stresses, confining pressures and under similar environmental conditions will be given as results of the creep tests. In order to give an idea of the reliability of the results, one set of the creep results of three specimens in dry condition tested under 63 N/mm^2 axial stress ($61.3\% \sigma_u$) at 30 N/mm^2 confining pressure is plotted in Fig. (6.26) and the average results are plotted on the same graph. It can be seen that there are noticeable differences in the results of the different specimens deformed under similar stress conditions. These differences are the results of the effect of slight variation of temperature and humidity from

test to test, small differences in mechanical properties of specimen, possible experimental errors, etc.

6.2.1 Creep behaviour.

The creep behaviour of gypsum was studied under uniaxial and triaxial compression in dry and water saturated conditions. The creep curves obtained for the two environmental conditions under various axial and confining stresses obey the following relationships reasonably well:

1) Logarithmic law; $\varepsilon = A + B \log t$ ..... (6.22)

and/or 2) Power law ; $\varepsilon = C\, t^{n}$ ..... (6.23)

where ε is the creep strain at any time in microstrain, t is the loading time in hours and A, B, C and n are constants which depend on the material, test condition and environmental conditions.

a. Dry condition.

The results of the creep tests in dry condition are given in the form of tables and figures, Tables (6.8) to (6.11) and figures Fig.(6.14) to (6.25). In each table the axial stresses at a given confining pressure are given as a percentage of the ultimate strength of the rock (σ_u) and in N/mm^2. The instantaneous strain in each case is also given.

The creep curves followed the logarithmic law, Eq. (6.22) for the low applied stresses, power law, Eq. (6.23) or power and logarithmic laws for medium applied stresses and power laws only for high applied stresses.

1) For uniaxial compression the following relationships were obtained, see Table (6.8) and Figs. (6.14), (6.15) and (6.16):

at $\sigma_1 = 15\ N/mm^2 = 36\%\ \sigma_u$

$\varepsilon = 39 + 30 \log t$ ..... (6.24)

at $\sigma_1 = 21\ N/mm^2 = 50.3\%\ \sigma_u$

$\varepsilon = 48t^{0.425}$ $t < 4.5$ hrs. ..... (6.25)

Table (6.8) Axial creep of dry gypsum in uniaxial compression.

Time hours	Axial stress, N/mm^2			
	15 36% σ_u	21 50.3% σ_u	27 65% σ_u	34 81.8% σ_u
	Instantaneous strain, Microstrain			
	380	560	780	930
	Creep strain, Microstrain			
0.1	11.2	16.5	21.3	39.5
0.3	18.4	27.3	35.1	47.5
0.5	27.5	35.7	44.6	56.9
1.0	35.1	49.1	60.5	69.0
2.0	42.2 ± 4%	66.4 ± 5%	78.8 ± 4%	80.9 ± 1%
3.0	48.3	77.0	82.7	90.4
4.0	52.0	89.1	102.0	100.4
5.0	56.0	100.4	108.5	109.5
6.0	58.3	108.5	113.8	116.8
12.0	73.1	123.5	127.5	138.8
24.0	81.2 ± 5%	138.9 ± 4%	145.1 ± 5%	163.5 ± 1%
48.0	86.8	152.7	164.6	184.9
72.0	93.2	167.0	176.8	206.7
96.0	101.4	179.5	188.8	224.4
120.0	107.2	187.9	199.2	244.3
144.0	112.0	192.4	209.6	255.9
168.0	119.4	197.4	221.3	266.0
192.0	124.7	205.9	230.3	277.9
216.0	125.2	208.5	239.1	290.1
240.0	125.7	211.2	247.3	305.1 ± 5%
264.0	126.1	214.9	255.0	314.6
288.0	126.1 ± 6%	218.9 ± 4%	262.4 ± 5%	323.5
312.0		224.3	268.8	333.6
336.0		230.5	275.2	342.5
360.0		233.9	283.6	355.4
384.0		239.9	289.8	361.8
408.0		243.1	284.8	367.1
432.0		245.6	298.9	372.5
456.0		247.2	303.1	376.4
480.0		248.6	306.0	381.8
504.0		249.9	308.0	385.6
528.0		250.6	310.6	390.1
552.0		250.6 ± 3%	313.0	394.4
576.0			314.9	398.9
600.0			316.2	404.4
624.0			318.3	407.9
648.0			319.1	412.9
672.0			320.1	415.0
696.0			320.7	416.8
720.0			321.0 ± 6%	418.6 ± 5%

Table (6.9) Axial creep of dry gypsum in triaxial at 10 N/mm^2 confining pressure.

Time hours	Axial stress, N/mm^2			
	21 33.7% σ_u	27 43.3% σ_u	41 65.7% σ_u	50 80.2% σ_u
	Instantaneous strain, Microstrain			
	460	640	1020	1330
	Creep strain, Microstrain			
0.1	6.3	12.1	58.5	48.2
0.3	12.1	19.1	78.6	68.2
0.5	17.1	25.1	100.1	102.2
1.0	22.7	30.2	120.7	132.2
2.0	29.1 ± 4%	39.5 ± 5%	154.6 ± 3%	163.1 ± 6%
3.0	33.6	44.7	174.4	188.5
4.0	35.6	50.1	193.9	204.0
5.0	40.1	55.2	208.4	219.4
6.0	44.2	59.5	222.6	232.9
12.0	52.3	69.6	277.2	301.0
24.0	59.4 ± 5%	84.3 ± 5%	337.3 ± 4%	383.1 ± 6%
48.0	65.8	101.5	428.6	464.2
72.0	72.8	115.2	501.9	564.3
96.0	76.6	132.0	528.9	645.2
120.0	81.3	146.2	555.6	703.8
144.0	89.0	155.8	569.1	760.3
168.0	93.4	170.3	582.0	801.5
192.0	98.2	182.6	593.5	831.7
216.0	105.1	201.1	603.4	866.9
240.0	108.8	214.6 ± 4%	616.6 ± 4%	899.8 ± 5%
264.0	112.1	230.5	624.9	932.2
288.0	114.1	237.2	632.4	954.6
312.0	114.9	252.1	642.4	981.7
336.0	115.5	260.8	654.5	1005.3
360.0	116.1	270.7	663.4	1022.0
384.0	116.1 ± 6%	278.2	671.4	1038.5
408.0	116.1	287.8	680.5	1054.0
432.0	116.1	295.5	685.8	1064.0
456.0	116.1	302.4	694.1	1076.1
480.0		307.5	700.1	1084.2
504.0		311.1	705.0	1092.6
528.0		314.4	711.5	1100.5
552.0		315.2	717.3	1107.0
576.0		317.5	721.9	1111.7
600.0		318.7	724.9	1115.6
624.0		319.5	728.2	1120.3
648.0		320.0	730.2	1123.3
672.0		320.0 ± 4%	732.2 ± 6%	1125.5
696.0			734.8	1128.2
720.0			736.2	1130.0 ± 5%

Table (6.10) Axial creep of dry gypsum in triaxial at 20 N/mm^2 confining pressure.

Time hours	Axial stress, N/mm^2			
	27 34.5% σ_u	41 52.4% σ_u	50 64% σ_u	63 80.6% σ_u
	Instantaneous strain, Microstrain			
	650	950	1200	1560
	Creep strain, Microstrain			
0.1	11.1	23.3	24.6	25.2
0.3	16.4	37.8	44.5	54.5
0.5	23.4	57.7	65.8	72.2
1.0	28.2	65.9	74.9	93.7
2.0	32.9 ± 6%	71.1 ± 5%	86.2 ± 4%	126.3 ± 8%
3.0	36.5	77.2	97.2	148.0
4.0	38.8	82.2	107.4	167.5
5.0	41.2	85.3	115.1	179.5
6.0	43.5	93.9	122.7	194.5
12.0	51.6	101.5	141.7	236.0
24.0	62.8 ± 4%	121.7 ± 5%	159.5 ± 6%	289.9 ± 8%
48.0	93.6	155.7	196.5	340.1
72.0	106.1	181.9	234.2	391.3
96.0	114.4	198.9	263.1	426.4
120.0	124.6	216.9	289.1	461.9
144.0	134.9	238.2	314.2	490.1
168.0	140.9	253.1	341.2	517.6
192.0	148.2	274.4	362.3	533.7
216.0	153.1	296.1	385.7	554.4
240.0	157.9 ± 4%	308.8 ± 4%	403.9 ± 7%	570.5 ± 6%
264.0	162.7	322.8	420.6	584.8
288.0	166.4	341.3	441.9	599.6
312.0	172.4	358.5	451.7	610.2
336.0	177.7	376.6	465.2	625.1
360.0	181.8	389.9	477.3	636.7
384.0	185.4	403.3	491.8	647.8
408.0	188.9	410.8	498.9	657.5
432.0	191.2	419.1	509.3	666.7
456.0	193.3	425.5	518.9	675.4
480.0	194.6	433.6	527.9	682.5
504.0	195.8	439.7	535.8	689.4
528.0	196.6	444.5	543.4	695.4
552.0	195.8 ± 3%	449.9 ± 4%	550.9	703.1
576.0	196.8	454.5	558.9	709.2
600.0	196.8	458.7	565.5	714.4
624.0		461.2	570.4	720.2
648.0		463.3	579.1	725.5
672.0		465.9	585.6	731.3
696.0		468.0	590.9	736.6
720.0		470.4	595.6 ± 7%	740.9 ± 4%

Table (6.11) Axial creep of dry gypsum in triaxial at 30 N/mm^2 confining pressure.

Time hours	Axial stress, N/mm^2			
	27 26.3% σ_u	41 39.8% σ_u	50 48.7 σ_u	63 61.3% σ_u
	Instantaneous strain, Microstrain			
	540	860	1080	1400
	Creep strain, Microstrain			
0.1	6.8	10.6	17.7	24.5
0.3	10.0	15.6	32.4	49.5
0.5	14.0	19.8	45.3	65.8
1.0	21.1	25.5	54.7	88.2
2.0	24.9 ± 3%	32.7 ± 4%	62.8 ± 5%	106.1 ± 4%
3.0	28.9	38.5	68.0	125.5
4.0	32.5	43.6	73.5	140.1
5.0	35.6	48.1	79.0	149.4
6.0	38.5	52.1	84.7	159.0
12.0	45.0	65.0	103.4	191.1
24.0	54.3 ± 3%	78.1 ± 2%	125.4 ± 6%	248.8 ± 4%
48.0	74.1	104.2	156.3	286.5
72.0	87.1	131.8	175.9	307.8
96.0	79.9	145.2	193.1	331.4
120.0	108.7	158.0	209.2	353.5
144.0	117.3	174.0	224.8	372.0
168.0	124.8	185.1	237.4	388.8
192.0	131.4	193.7	249.5	404.6
216.0	136.7	206.2	260.8	417.4
240.0	141.9 ± 4%	215.2 ± 2%	272.0 ± 6%	429.2 ± 5%
264.0	146.9	223.0	283.0	442.8
288.0	151.3	230.8	294.1	452.8
312.0	155.2	237.3	304.4	462.5
336.0	158.0	243.7	314.6	472.0
360.0	160.3	249.6	324.6	481.0
384.0	162.5	254.7	334.9	489.4
408.0	164.1	249.5	342.9	500.8
432.0	165.5	263.1	362.4	505.8
456.0	166.2	267.1	371.8	513.8
480.0	166.4 ± 5%	271.2	379.6	520.4
504.0		274.0	387.1	528.1
528.0		275.2	393.8	534.1
552.0		278.1	401.0	541.1
576.0		279.6	407.8	548.0
600.0		279.6 ± 2%	414.1	552.4
624.0			420.3	558.8
648.0			425.4	364.8
672.0			431.7	570.9
696.0			435.5	577.0
720.0			441.4 ± 6%	582.4 ± 4%

$$\varepsilon = 68\ t^{0.215} \qquad t \geq 4.5 \text{ hrs.} \quad \ldots\ldots \quad (6.26)$$

at $\sigma_1 = 27\ N/mm^2 = 65\%\ \sigma_u$

$$\varepsilon = 56\ t^{0.358} \qquad t < 6.2 \text{ hrs.} \quad \ldots\ldots \quad (6.27)$$

$$\varepsilon = 72\ t^{0.235} \qquad t \geq 6.2 \text{ hrs.} \quad \ldots\ldots \quad (6.28)$$

at $\sigma_1 = 34\ N/mm^2 = 81.8\%\ \sigma_u$

$$\varepsilon = 70\ t^{0.278} \qquad t < 6.5 \text{ hrs.} \quad \ldots\ldots \quad (6.29)$$

$$\varepsilon = 74\ t^{0.268} \qquad t \geq 6.5 \text{ hrs.} \quad \ldots\ldots \quad (6.30)$$

The values of the creep strain given in Table (6.8) were plotted against time on semi-log and log-log graphs as shown in Fig. (6.15) and (6.16) respectively. A linear relationship was plotted for 15 N/mm^2 stress on semi-log and for 21, 27 and 34 N/mm^2 on log-log graphs. This indicated that the logarithmic law fits the data well at 15 N/mm^2 and power laws the data of 21, 27 and 34 N/mm^2. The first term in the logarithmic equation A in Eq. (6.22) represents the value of the creep strain at time t = 1 hour and the number proceeding log t, B in Eq. (6.22) represents the slope of the straight line drawn of the creep strain versus time on semi-log graph, see Fig. (6.15), which can be calculated by $B = \frac{\varepsilon_2 - \varepsilon_1}{\log t_2 - \log t_1}$. As well as this graphical method, the least square method was used to calculate the values of A and B. This method will be discussed in the appendix (B). For the power law, of the constants C and n in Eq. (6.23), n represents the slope of the straight line on log-log graph, see Fig. (6.16) and can be calculated by $n = \frac{\log \varepsilon_2 - \log \varepsilon_1}{\log_2 - \log_1}$. Both C and n values were also calculated by least square method. In cases where the straight line changgs its slope but still fits the creep data in power law form as shown in Fig. (6.16), the power law requires different values of the constants C and n to represent these data within the time range after the gradient change. The value of the new n represents the new slope of

the straight line and the value of the new C is found by extending the new straight line to the time of t = 1 hour.

2) For triaxial compression at 10 N/mm^2 confining pressure the following relationships were obtained for the dry gypsum, see Table (6.9) and Figs. (6.17), (6.18) and (6.19):

at σ_1 = 21 N/mm^2 = 33.7% σ_u

ε = 30 + 26 log t ..... (6.31)

at σ_1 = 27 N/mm^2 = 43.3% σ_u

ε = 44 + 29 log t t < 72 hrs. ..... (6.32)

ε = 43 $t^{0.301}$ t ≥ 72 hrs. ..... (6.33)

at σ_1 = 41 N/mm^2 = 65.7% σ_u

ε = 122 $t^{0.315}$ ..... (6.34)

at σ_1 = 50 N/mm^2 = 80.2% σ_u

ε = 129 $t^{0.350}$ ..... (6.35)

The creep behaviour at this confining pressure level followed the power law, Eq. (6.23) for all the axial stresses except under the low stress 21 N/mm^2 and in the earlier stages of the test for 27 N/mm^2 at t < 72 hrs. where they followed the logarithmic relationship, Eq. (6.22).

3) For the triaxial compression at 20 N/mm^2 confining pressure, the following relationships were obtained, Table (6.10) and Figs. (6.20), (6.21) and (6.22):

at σ_1 = 27 N/mm^2 = 34.5% σ_u

ε = 30 + 20 log t t < 24 hrs. ..... (6.36)

ε = 32 $t^{0.260}$ t ≥ 24 hrs. ..... (6.37)

at σ_1 = 41 N/mm^2 = 52.4% σ_u

ε = 57 $t^{0.275}$ ..... (6.38)

at σ_1 = 50 N/mm^2 = 64% σ_u

$$\varepsilon = 70\ t^{0.301} \quad \ldots\ldots \quad (6.39)$$

at σ_1 = 63 N/mm^2 = 80.6% σ_u

$$\varepsilon = 94\ t^{0.409} \quad t < 4 \text{ hrs.} \quad \ldots\ldots \quad (6.40)$$

$$\varepsilon = 108\ t^{0.315} \quad t \geq 4 \text{ hrs.} \quad \ldots\ldots \quad (6.41)$$

At this level of the confining pressure, the creep data followed the power law, Eq. (6.23), except at σ_1 = 27 N/mm^2 where they followed the logarithmic law, Eq. (6.22) at t < 24 hrs. then a departure from this law to power law was obtained.

4) For triaaxial compression at 30 N/mm^2 confining pressure, the following relationships were obtained, Table (6.11) and Figs. (6.23), (6.24) and (6.25):

at σ_1 = 27 N/mm^2 = 26.3% σ_u

$$\varepsilon = 21 + 23 \log t \quad t < 24 \text{ hrs.} \quad \ldots\ldots \quad (6.42)$$

$$\varepsilon = 32\ t^{0.23} \quad t \geq 24 \text{ hrs.} \quad \ldots\ldots \quad (6.43)$$

at σ_1 = 41 N/mm^2 = 39.8% σ_u

$$\varepsilon = 32 + 30 \log t \quad t < 30 \text{ hrs.} \quad \ldots\ldots \quad (6.44)$$

$$\varepsilon = 48\ t^{0.235} \quad t \geq 30 \text{ hrs.} \quad \ldots\ldots \quad (6.45)$$

at σ_1 = 50 N/mm^2 = 48.7% σ_u

$$\varepsilon = 56\ t^{0.24} \quad \ldots\ldots \quad (6.46)$$

at σ_1 = 63 N/mm^2 = 61.3% σ_u

$$\varepsilon = 82\ t^{0.344} \quad t < 20 \text{ hrs.} \quad \ldots\ldots \quad (6.47)$$

$$\varepsilon = 113\ t^{0.241} \quad t \geq 20 \text{ hrs.} \quad \ldots\ldots \quad (6.48)$$

The creep behaviour at this level of the confining pressure followed the power law, Eq. (6.23), except under 27 N/mm^2 and 41 N/mm^2 where they followed logarithmic law, Eq. (6.22) for the first 24 hrs and 30 hrs respectively, then the data departed from this law to power law.

In the previous equations, from (6.24) to (6.48), all the constants A, B, C and n were found by using the graphical method and checked by using the least square method. All the results were in close agreement. An example is given in appendix (C) to illustrate the use of the least square method. By calculating the correlation coefficient (R) the degree of correlation showed the equations to be a satisfactory representation of the data.

b. Saturated condition:

The results of the creep tests for the water saturated gypsum are given in Tables (6.12) to (6.15) and figures Fig. (6.27) to Fig.(6.38). Axial stresses, confining pressures, instantaneous strains and the creep strains are given in the tables for each test case. The creep data followed the power law or power and logarithmic law for the low applied stresses, whereas for the medium and high applied stress, the creep behaviour followed the power law.

1) For uniaxial compression the following relationships were obtained, see Table (6.12) and Figs. (6.27), (6.28) and (6.29)

at $\sigma_1 = 8\ N/mm^2 = 37\%\ \sigma_u$

$$\varepsilon = 51\ t^{0.250} \quad \text{.....} \quad (6.49)$$

at $\sigma_1 = 11\ N/mm^2 = 52\%\ \sigma_u$

$$\varepsilon = 124\ t^{0.430} \quad t < 2\ hrs. \quad \text{.....} \quad (6.50)$$

$$\varepsilon = 147\ t^{0.256} \quad t \geq 2\ hrs. \quad \text{.....} \quad (6.51)$$

at $\sigma_1 = 15\ N/mm^2 = 70.9\%\ \sigma_u$

$$\varepsilon = 205\ t^{0.5} \quad t < 1\ hr. \quad \text{.....} \quad (6.52)$$

$$\varepsilon = 205\ t^{0.263} \quad t \geq 1\ hr. \quad \text{.....} \quad (6.53)$$

at $\sigma_1 = 17\ N/mm^2 = 80.4\%\ \sigma_u$

$$\varepsilon = 260\ t^{0.525} \quad t < 1\ hr. \quad \text{.....} \quad (6.54)$$

$$\varepsilon = 260\ t^{0.269} \quad t \geq 1\ hr. \quad \text{.....} \quad (6.55)$$

Table (6.12) Axial creep of saturated gypsum in uniaxial compression.

Time hours	Axial stress, N/mm^2			
	8 37% σ_u	11 52% σ_u	15 70.9% σ_u	17 80.4% σ_u
	Instantaneous strain, Microstrain			
	290	410	560	660
	Creep strain, Microstrain			
0.1	19.9	45.2	75.0	88.6
0.3	33.8	68.5	96.6	138.8
0.5	40.7	93.8	154.1	200.1
1.0	49.5	122.2	205.1	274.6
2.0	57.1 ± 4%	149.9 ± 3%	240.9 ± 5%	316.5 ± 4%
3.0	68.2	177.7	294.1	345.5
4.0	77.3	200.2	310.9	374.0
5.0	84.5	215.1	333.9	393.5
6.0	90.1	228.1	352.9	410.5
12.0	105.9	262.1	399.3	475.5
24.0	125.7 ± 6%	305.6 ± 4%	445.2 ± 5%	529.3 ± 4%
48.0	162.9	373.3	507.3	607.8
72.0	193.7	422.8	553.2	663.6
96.0	218.9	469.0	586.9	730.2
120.0	245.4	501.1	628.9	797.8
144.0	269.7	525.5	673.5	857.3
168.0	295.4	541.9	705.4	920.6
192.0	318.4	557.9	734.8	955.9
216.0	337.2	568.2	749.3	980.6
240.0	355.0 ± 7%	590.5 ± 4%	767.2 ± 8%	987.7 ± 9%
264.0	369.3	612.3	780.0	1011.8
288.0	385.0	632.1	794.9	1027.9
312.0	398.6	649.0	812.5	1041.3
336.0	412.9	658.6	827.9	1052.1
360.0	423.8	677.7	839.9	1062.8
384.0	435.5	695.6	850.9	1072.2
408.0	442.4	708.6	860.7	1079.3
432.0	450.5	719.5	871.5	1087.3
456.0	459.1	731.5	881.4	1094.2
480.0	466.6	744.1	891.1	1100.5
504.0	474.8	751.4	899.7	1108.5
528.0	479.5	757.9	907.2	1117.0
552.0	485.0	764.0	916.0	1122.6
576.0	489.7	770.3	924.7	1129.5
600.0	495.1	775.5	930.2	1134.2
624.0	498.6	780.0	938.3	1139.2
648.0	501.6	783.9	945.1	1144.6
672.0	503.6	785.6	952.9	1149.2
696.0	505.9	790.2	957.3	1152.6
720.0	507.3 ± 7%	793.2 ± 5%	962.3 ± 2%	1157.0 ± 6%

Table (6.13) Axial creep of saturated gypsum in triaxial at 10 N/mm^2 confining pressure.

Time hours	Axial stress, N/mm^2			
	15 33% σ_u	21 46.3% σ_u	27 59.5% σ_u	41 90.3% σ_u
	Instantaneous strain, Microstrain			
	410	640	840	1270
	Creep strain, Microstrain			
0.1	29.1	36.2	35.6	88.3
0.3	39.9	45.4	59.0	144.9
0.5	51.3	60.6	78.0	184.9
1.0	67.9	83.8	95.0	241.5
2.0	80.7 ± 6%	94.5 ± 4%	117.0 ± 5%	330.5 ± 8%
3.0	88.9	105.9	135.0	379.0
4.0	97.4	115.3	152.2	424.1
5.0	104.0	125.3	159.6	467.3
6.0	111.9	134.6	193.0	502.1
12.0	126.0	165.3	239.8	664.3
24.0	143.1 ± 5%	221.6 ± 6%	307.6 ± 6%	1024.4 ± 10%
48.0	187.2	258.9	401.8	1235.8
72.0	229.2	293.5	461.6	1382.6
96.0	262.4	324.0	535.0	1501.5
120.0	294.1	354.1	630.4	1599.6
144.0	330.7	379.0	684.4	1656.8
168.0	360.5	420.4	717.0	1672.8
192.0	395.9	445.1	739.8	1722.5
216.0	414.6	462.8	748.8	1764.3
240.0	434.6 ± 5%	478.3 ± 7%	823.2 ± 8%	1797.6 ± 9%
264.0	452.9	492.3	833.7	1838.1
288.0	473.7	514.1	844.6	1879.8
312.0	492.9	527.2	848.6	1913.9
336.0	507.1	541.2	866.2	1935.0
360.0	515.8	568.2	899.9	1949.7
384.0	534.2	577.1	927.2	1959.9
408.0	546.9	580.3	952.9	1978.3
432.0	559.6	598.4	980.0	1992.0
456.0	570.2	611.3	999.3	2013.3
480.0	579.4	623.2	1032.2	2018.3
504.0	588.0	637.2	1039.9	2023.1
528.0	599.5	646.8	1054.5	2028.7
552.0	607.4	658.3	1071.4	2032.9
576.0	613.6	667.3	1084.3	2036.8
600.0	619.9	676.8	1093.6	2040.7
624.0	628.8	683.9	1102.8	2042.6
648.0	636.3	692.8	1112.1	2046.3
672.0	642.3	701.7	1119.1	2049.5
696.0	646.6	706.6	1122.7	2051.4
720.0	649.5 ± 4%	711.1 ± 8%	1125.4 ± 8%	2054.0 ± 5%

Table (6.14) Axial creep of saturated gypsum in triaxial at 20 N/mm^2 confining pressure.

Time hours	Axial stress, N/mm^2			
	27 37.7% σ_u	41 57.2% σ_u	50 69.7% σ_u	63 87.9% σ_u
	Instantaneous strain, Microstrain			
	800	1300	1640	2080
	Creep strain, Microstrain			
0.1	15.5	103.3	162.1	266.0
0.3	28.7	168.4	270.7	462.6
0.5	37.4	195.5	370.4	546.9
1.0	45.3	237.3	491.4	644.6
2.0	53.6 ± 7%	285.4 ± 4%	721.3 ± 5%	737.9 ± 8%
3.0	60.2	325.8	790.1	807.7
4.0	67.1	362.5	840.0	868.8
5.0	73.3	388.3	903.2	952.5
6.0	78.7	413.9	948.7	997.8
12.0	112.1	509.3	1131.5	1176.6
24.0	157.3 ± 6%	608.0 ± 4%	1267.1 ± 6%	1441.7 ± 8%
48.0	208.3	738.6	1440.5	1545.6
72.0	254.8	854.8	1586.7	1662.0
96.0	293.9	970.1	1680.0	1752.7
120.0	334.7	1042.1	1752.0	1817.8
144.0	361.7	1082.7	1788.7	1897.5
168.0	386.4	1115.8	1831.4	1960.9
192.0	412.6	1147.8	1866.5	2022.6
216.0	433.7	1169.9	1892.9	2068.6
240.0	448.1 ± 5%	1192.8 ± 2%	1922.5 ± 8%	2108.5 ± 6%
264.0	460.7	1217.6	1945.6	2150.7
288.0	474.3	1239.3	1971.0	2187.0
312.0	486.9	1259.2	1989.8	2224.7
336.0	500.3	1275.8	2008.0	2259.4
360.0	510.5	1288.9	2022.9	2289.9
384.0	519.2	1302.2	2037.6	2319.2
408.0	527.2	1310.8	2050.8	2343.3
432.0	535.8	1323.7	2067.0	2354.5
456.0	544.7	1333.9	2076.0	2380.7
480.0	554.3	1344.6	2085.5	2398.3
504.0	561.8	1353.4	2099.0	2415.7
528.0	568.8	1362.0	2112.9	2433.1
552.0	575.1	1371.9	2124.6	2445.6
576.0	581.3	1380.2	2135.5	2463.0
600.0	587.5	1388.9	2145.9	2477.8
624.0	593.3	1397.5	2155.3	2491.6
648.0	598.8	1404.5	2164.9	2505.8
672.0	604.6	1412.6	2174.9	2517.6
696.0	609.1	1419.4	2184.5	2532.5
720.0	614.5 ± 4%	1425.9 ± 3%	2193.5 ± 8%	2543.8 ± 6%

Table (6.15) Axial creep of saturated gypsum in triaxial at 30 N/mm^2 confining pressure.

Time hours	Axial stress, N/mm^2			
	27 29.3% σ_u	41 44.5% σ_u	50 54.3% σ_u	63 68.3% σ_u
	Instantaneous strain, Microstrain			
	700	1100	1350	1780
	Creep strain, Microstrain			
0.1	12.5	81.5	142.2	196.7
0.3	23.5	132.7	180.3	347.9
0.5	31.7	155.0	213.6	436.1
1.0	40.0	182.2	246.1	531.7
2.0	48.4 ± 6%	204.2 ± 3%	250.0 ± 2%	581.3 ± 6%
3.0	56.7	220.0	277.3	625.6
4.0	61.0	234.9	292.7	670.3
5.0	65.3	244.9	310.5	708.9
6.0	70.2	254.1	323.0	745.2
12.0	92.3	296.5	432.6	869.4
24.0	110.2 ± 4%	353.1 ± 4%	570.3 ± 3%	999.5 ± 6%
48.0	147.1	390.8	612.2	1054.2
72.0	172.5	412.0	645.2	1105.3
96.0	195.4	442.8	670.2	1144.8
120.0	216.7	465.9	688.9	1183.8
144.0	232.9	485.4	705.2	1207.8
168.0	248.2	505.1	722.2	1237.4
192.0	261.7	520.9	736.4	1260.8
216.0	275.2	534.4	750.6	1286.9
240.0	287.3 ± 4%	547.7 ± 4%	765.2 ± 3%	1313.0 ± 4%
264.0	297.1	559.2	777.7	1332.9
288.0	303.3	570.8	794.8	1352.3
312.0	316.7	582.0	805.4	1372.1
336.0	325.8	591.2	816.5	1385.1
360.0	334.1	600.3	840.9	1400.4
384.0	341.4	609.5	851.0	1414.9
408.0	348.7	618.0	860.4	1426.9
432.0	355.7	627.3	871.0	1439.0
456.0	362.9	635.7	881.8	1449.8
480.0	369.5	645.0	890.9	1461.3
504.0	375.6	651.8	900.2	1474.1
528.0	381.4	660.1	908.6	1485.5
552.0	388.2	667.7	917.2	1495.1
576.0	391.0	673.5	924.9	1504.8
600.0	398.6	680.9	933.9	1515.0
624.0	404.5	688.0	942.2	1525.0
648.0	409.9	693.8	952.0	1536.1
672.0	415.0	699.6	961.6	1545.6
696.0	419.0	705.9	969.8	1553.0
720.0	423.6 ± 3%	711.6 ± 5%	979.4 ± 3%	1561.7 ± 3%

Thus the creep behaviour universally followed the power law at zero confining pressure level ($\sigma_3 = 0$) for all the applied axial stress levels. In the case of the stresses, 11, 15 and 17 N/mm^2 the creep constants C and n in Eq. (6.23) changed within the first 1 or 2 hours of the tests which results in a change in the slope of the straight lines on the log-log graphs at these times, see Figs. (6.28) and (6.29).

2) For triaxial compression at 10 N/mm^2 confining pressure, the following relationships were obtained, see Table (6.13) and Figs. (6.30), (6.31) and (6.32),:

at $\sigma_1 = 15\ N/mm^2 = 33\%\ \sigma_u$

$$\varepsilon = 60 + 40 \log t \qquad t < 50 \text{ hrs.} \quad ..... \quad (6.56)$$

$$\varepsilon = 65\ t^{0.322} \qquad t \geq 50 \text{ hrs.} \quad ..... \quad (6.57)$$

at $\sigma_1 = 21\ N/mm^2 = 46.3\%\ \sigma_u$

$$\varepsilon = 74\ t^{0.338} \quad ..... \quad (6.58)$$

at $\sigma_1 = 27\ N/mm^2 = 59.5\%\ \sigma_u$

$$\varepsilon = 92\ t^{0.386} \quad ..... \quad (6.59)$$

at $\sigma_1 = 41\ N/mm^2 = 90.3\%\ \sigma_u$

$$\varepsilon = 250\ t^{0.390} \qquad t < 72 \text{ hrs.} \quad ..... \quad (6.60)$$

$$\varepsilon = 555\ t^{0.214} \qquad t \geq 72 \text{ hrs.} \quad ..... \quad (6.61)$$

The creep data at this confining pressure generally followed the power law, Eq. (6.23) except at low stress, 15 N/mm^2 where it followed logarithmic law, Eq. (6.22), for the first 50 hrs then a departure from this to a power law was obtained.

3) For triaxial compression at 20 N/mm^2 confining pressure, the following relationships were obtained, see Table (6.14) and Figs. (6.33), (6.34) and (6.35):

at $\sigma_1 = 27\ N/mm^2 = 37.7\%\ \sigma_u$

$$\varepsilon = 50 + 40 \log t \qquad t < 17 \text{ hrs.} \quad \ldots\ldots \quad (6.62)$$

$$\varepsilon = 82\ t^{0.267} \qquad t \geq 17 \text{ hrs.} \quad \ldots\ldots \quad (6.63)$$

at $\sigma_1 = 41\ N/mm^2 = 57.2\%\ \sigma_u$

$$\varepsilon = 240\ t^{0.290} \quad \ldots\ldots \quad (6.64)$$

at $\sigma_1 = 50\ N/mm^2 = 69.7\%\ \sigma_u$

$$\varepsilon = 503\ t^{0.220} \qquad t < 90 \text{ hrs.} \quad \ldots\ldots \quad (6.65)$$

$$\varepsilon = 360\ t^{0.312} \qquad t \geq 90 \text{ hrs.} \quad \ldots\ldots \quad (6.66)$$

at $\sigma_1 = 63\ N/mm^2 = 87.9\%\ \sigma_u$

$$\varepsilon = 680\ t^{0.210} \qquad t < 150 \text{ hrs.} \quad \ldots\ldots \quad (6.47)$$

$$\varepsilon = 410\ t^{0.328} \qquad t \geq 150 \text{ hrs.} \quad \ldots\ldots \quad (6.68)$$

At this confining pressure level, the creep data again followed the power law, Eq. (6.23), except at low axial stress, 27 N/mm^2 where a logarithmic law was followed for the first 17 hrs. after which the creep followed the power law.

4) For triaxial compression at 30 N/mm^2 confining pressure, the following relationships were obtained; see Table (6.15) and Figs. (6.36), (6.37) and (6.38):

at $\sigma_1 = 27\ N/mm^2 = 29.3\%\ \sigma_u$

$$\varepsilon = 45 + 38 \log t \qquad t < 40 \text{ hrs.} \quad \ldots\ldots \quad (6.69)$$

$$\varepsilon = 109\ t^{0.0178} \qquad t \geq 40 \text{ hrs.} \quad \ldots\ldots \quad (6.70)$$

at $\sigma_1 = 41\ N/mm^2 = 44.5\%\ \sigma_u$

$$\varepsilon = 178\ t^{0.202} \quad \ldots\ldots \quad (6.71)$$

at $\sigma_1 = 50\ N/mm^2 = 54.3\%\ \sigma_u$

$$\varepsilon = 225\ t^{0.246} \quad \ldots\ldots \quad (6.72)$$

at $\sigma_1 = 63\ N/mm^2 = 68.3\%\ \sigma_u$

$$\varepsilon = 452\ t^{0.259} \quad \ldots\ldots \quad (6.73)$$

The creep data of this confining pressure level once again followed the power law, Eq. (6.23) except at low stress, 27 N/mm^2, where the data followed the logarithmic law at the first 40 hrs. after which departure from this to a power law was obtained.

6.2.2 Effect of varying axial stress.

The effect of axial stress on the creep of dry and saturated gypsum was studied under uniaxial and triaxial compression. It can be seen from the tables (6.8) to (6.15) and the Figs. (6.14) to (6.38) that creep strain occurred at every axial stress and both the instantaneous and creep strains are increased with the axial stress. The instantaneous strains were used to find the Modulus of Elasticity for the two environmental conditions at various confining pressures. This was done by plotting the axial stress (as percentage of the ultimate stress, σ_u) versus the corresponding instantaneous strain, Fig. (6.39). It can be seen that the instantaneous strain increases with the given axial stress linearly at a particular confining pressure and under both dry and saturated conditions. Elizzi[15] reported the same behaviour for dry gypsum and anhydrite. Table (6.16) gives the Modulus of Elasticity calculated by this way for the two environmental conditions and under uniaxial and triaxial compression.

Table (6.16) Modulus of Elasticity from instantaneous strain.

Mod of tests	Modulus of Elasticity (E), N/mm^2	
	Dry	Saturated
Uniaxial $\sigma_3 = 0$	3.65×10^4	2.58×10^4
Triaxial		
$\sigma_3 = 10\ N/mm^2$	3.90×10^4	3.01×10^4
$\sigma_3 = 20\ N/mm^2$	4.07×10^4	3.15×10^4
$\sigma_3 = 30\ N/mm^2$	4.59×10^4	3.56×10^4

For dry conditions:-

In uniaxial and triaxial tests at 0, 10, 20 and 30 N/mm^2 confining pressure, the creep curves followed the logarithmic law, Eq. (6.22), at low stresses and for a short duration in the beginning of some of the creep tests at medium stresses. These cases are; at uniaxial under 15 N/mm^2 (36% σ_u) stress Eq. (6.24), at 10 N/mm^2 confining pressure under 21 N/mm^2 (33.7% σ_u) axial stress Eq. (6.31) and for the first 72 hrs. under 27 N/mm^2 (43.3% σ_u) axial stress Eq. (6.32), at 20 N/mm^2 confining pressure under 27 N/mm^2 (34.5% σ_u) axial stress for the first 24 hrs. Eq. (6.36), and at 30 N/mm^2 confining pressure under 27 N/mm^2 (26.3% σ_u) axial stress for the first 24 hrs. Eq. (6.42) and under 41 N/mm^2 (39.8% σ_u) axial stress for the first 30 hrs. Eq. (6.44). The same creep behaviour was reported by many other investigators; Griggs[70,71], Pomeroy[72], Misra[79], Williams and Elizzi[15,100]. Hofer and Knoll[90] stated that the creep processes take place according to the logarithmic law, Eq. (6.22) under low stresses and temperature.

It can be seen from the relationships obtained of the logarithmic form that the constants A & B are increased with increasing the axial stress for the given confining pressure. This is shown in Eqs. (6.31) and (6.32) for 21 and 27 N/mm^2 axial stresses respectively at 10 N/mm^2 confining pressure and in Eqs. (6.42) and (6.44) for 27 and 41 N/mm^2 respectively at 30 N/mm^2 confining pressure. The values of A and B are given in Table (6.17). These results are in agreement with the results obtained by Griggs[70], Misra[79], Williams and Elizzi[15,100] and others.

The creep behaviour followed the power law, Eq. (6.23) in uniaxial and triaxial tests at high and medium axial stresses except for a short duration at some of the medium stresses. The following investigators reported a similar behaviour of the creep; Comte[83] on artificial rock

salt, King[93] on potash, Singh[97] on Sicilian marble, Williams and Elizzi[100] on gypsum and anhydrite. Hofer and Knoll[90] stated that at medium and high applied stresses the creep processes take place according to the power law.

For saturated conditions:-

In the case of the saturated specimens in uniaxial and triaxial tests at 0, 10, 20 and 30 N/mm^2 confining pressures, the creep behaviour followed the power law, Eq. (6.23), except for a short duration at the beginning of the tests of some of the low axial stresses, namely; 15 N/mm^2 (33% σ_u) at 10 N/mm^2 confining pressure, 27 N/mm^2 (37.7% σ_u) at 20 N/mm^2 confining pressure and 27 N/mm^2 (29.3% σ_u) at 30 N/mm^2 confining pressure. See Eqs. (6.56), (6.62) and (6.69).

Griggs[71] suggested that the creep of alabaster immersed in water follows a power law at applied stresses. Wawersik[96] reported that the creep behaviour of the water saturated westerly granite and Navajo sandstone followed the power law. Afrouz and Harvey[95] expressed their results of the water saturated soft rocks as a power law relationship. The effect of the saturation on the creep will be discussed in this chapter later.

The power "n" in the power law relationship of both dry and saturated conditions was found to be $0 < n < 1$. Tables (6.17) and (6.18) give the creep equations, the constants A and B of the logarithmic equations, ($\varepsilon = A + B \log t$), the constants C and n of the power equations, ($\varepsilon = Ct^n$), and the creep rate at various times after loading for gypsum deformed under uniaxial and triaxial stresses and for dry and saturated conditions respectively. The values of the constants C and n are plotted against the axial stresses at various confining pressures and for both environmental conditions, Fig. (6.41) and Fig. (6.42). It can be seen from these results that both C and n values increase with increasing axial stresses

Table (6.17) Creep equation constants and creep rate of dry gypsum in uniaxial and triaxial compression creep tests.

σ_3	$\frac{\sigma_1}{\sigma_u} \times 100$ / σ_1	Creep equation	Constants A or C	Constants B or n	Creep rate, microstrain/hr. at t = 1 hr.	12 hr.	24 hr.	48 hr.	96 hr.	120 hr.	240 hr.	360 hr.	480 hr.	720 hr.
0 Uni-axial	36% / 15	$\varepsilon = 39 + 30 \log t$	39	30	30	2.5	1.25	0.63	0.32	0.25	0.13	0.08	-	-
	50.3%	$\varepsilon = 48\ t^{0.425}$, $t \leq 4.5$	48	0.425	20.4	-	-	-	-	-	-	-	-	-
	21	$\varepsilon = 68\ t^{0.215}$, $t \geq 4.5$	68	0.215	-	2.27	1.21	0.7	0.4	0.35	0.20	0.14	0.12	0.08
	65%	$\varepsilon = 56\ t^{0.358}$, $t \leq 6.2$	56	0.358	20.1	-	-	-	-	-	-	-	-	-
	27	$\varepsilon = 72\ t^{0.235}$, $t \leq 6.2$	72	0.235	-	2.53	1.49	0.88	0.52	0.44	0.26	0.19	0.15	0.11
	81.8%	$\varepsilon = 70\ t^{0.278}$, $t \leq 6.5$	70	0.278	19.5	-	-	-	-	-	-	-	-	-
	34	$\varepsilon = 74\ t^{0.268}$, $t \geq 6.5$	74	0.268	-	3.2	1.94	1.17	0.7	0.60	0.36	0.27	0.21	0.16
10	33.7% / 21	$\varepsilon = 30 + 26 \log t$	30	26	26	2.16	1.08	0.54	0.27	0.21	0.11	0.07	0.05	-
	43.3%	$\varepsilon = 44 + 29 \log t$, $t \leq 72$	44	29	29	2.41	1.2	0.6	-	-	-	-	-	-
	27	$\varepsilon = 40\ t^{0.301}$, $t \geq 72$	40	0.301	-	-	-	-	0.48	0.42	0.25	0.18	0.14	0.10
	65.7% / 41	$\varepsilon = 122\ t^{0.315}$	122	0.315	38.4	7.0	4.36	2.71	1.69	1.44	0.99	0.68	0.56	0.42
	80.2% / 50	$\varepsilon = 129\ t^{0.35}$	129	0.35	45.2	8.98	5.72	3.65	2.32	2.0	1.28	0.98	0.82	0.62
20	34.5%	$\varepsilon = 30 + 20 \log t$, $t \leq 24$	30	20	20	1.67	0.83	-	-	-	-	-	-	-
	27	$\varepsilon = 32\ t^{0.26}$, $t \geq 24$	34	0.26	-	-	-	0.47	0.28	0.24	0.14	0.11	0.08	0.06
	52.4% / 41	$\varepsilon = 57\ t^{0.275}$	57	0.275	15.68	2.59	1.57	0.95	0.57	0.49	0.29	0.22	0.18	0.13
	64% / 50	$\varepsilon = 70\ t^{0.301}$	70	0.301	21.1	3.71	2.29	1.4	0.87	0.74	0.46	0.34	0.28	0.21
	80.6%	$\varepsilon = 94\ t^{0.409}$, $t \leq 721$	94	0.409	38.45	8.85	3.83	-	-	-	-	-	-	-
	63	$\varepsilon = 108\ t^{0.315}$, $t \geq 721$	108	0.315	-	-	-	-	1.49	1.28	0.8	0.6	0.5	0.38
30	26.3%	$\varepsilon = 21 + 23 \log t$, $t \leq 17$	21	23	23	1.9	-	-	-	-	-	-	-	-
	27	$\varepsilon = 32\ t^{0.23}$, $t \geq 17$	32	0.23	-	-	0.63	0.37	0.22	0.18	0.11	0.08	0.06	0.04
	39.8%	$\varepsilon = 32 + 30 \log t$, $t \leq 30$	32	30	30	2.5	1.25	-	-	-	-	-	-	-
	41	$\varepsilon = 48\ t^{0.235}$, $t \geq 30$	48	0.235	-	-	-	0.58	0.34	0.29	0.17	0.12	0.1	0.07
	48.7% / 50	$\varepsilon = 56\ t^{0.240}$	56	0.344	13.44	2.03	1.29	0.71	0.42	0.35	0.21	0.15	0.12	0.09
	61.3%	$\varepsilon = 82\ t^{0.344}$, $t \leq 20$	82	0.344	28.2	5.53	-	-	-	-	-	-	-	-
	63	$\varepsilon = 113\ t^{0.251}$, $t \geq 20$	113	0.251	-	-	2.6	1.56	0.93	0.79	0.47	0.35	0.28	0.20

Table (6.18) Creep equation constants and creep rate of saturated gypsum in uniaxial and triaxial compression tests.

σ_3	$\frac{\sigma_1}{\sigma_u} \times 100$	Creep equation	Constants C or A	Constants n or B	Creep rate, microstrain/hr at t = 1 hr.	12 hr.	24 hr.	48 hr.	96 hr.	120 hr.	240 hr.	360 hr.	480 hr.	720 hr.
0 Uniaxial	37% 8	$\varepsilon = 51\ t^{0.25}$	51	0.25	12.75	1.98	1.18	0.70	0.42	0.35	0.21	0.15	0.12	0.09
	52%	$\varepsilon = 124\ t^{0.42}$ $t \leq 2$	124	0.42	52.1	-	-	-	-	-	-	-	-	-
	11	$\varepsilon = 147\ t^{0.257}$ $t \geq 2$	147	0.257	-	5.96	3.56	2.12	1.27	1.01	0.64	0.48	0.38	0.28
	70.9%	$\varepsilon = 205\ t^{0.5}$ $t \leq 1$	205	0.5	102.5	-	-	-	-	-	-	-	-	-
	15	$\varepsilon = 205\ t^{0.263}$ $t \geq 1$	205	0.263	-	8.63	5.18	3.11	1.87	1.56	0.95	0.70	0.57	0.42
	80.4%	$\varepsilon = 260\ t^{0.525}$ $t \leq 1$	260	0.525	136.5	-	-	-	-	-	-	-	-	-
	17	$\varepsilon = 260\ t^{0.269}$ $t \geq 1$	260	0.269	-	11.37	6.85	4.12	2.49	2.11	1.27	0.95	0.77	0.57
10	33%	$\varepsilon = 60 + 40 \log t$ $t \leq 50$	60	40	40	3.33	1.66	0.84	-	-	-	-	-	-
	15	$\varepsilon = 65\ t^{0.322}$ $t \geq 50$	65	0.322	-	-	-	-	0.95	0.82	0.51	0.39	0.32	0.24
	46% 21	$\varepsilon = 74\ t^{0.338}$	74	0.338	25.0	4.83	3.05	1.93	1.22	1.05	0.66	0.51	0.42	0.32
	59.5% 27	$\varepsilon = 92\ t^{0.386}$	92	0.386	35.51	7.72	5.05	3.29	2.15	1.88	1.23	0.96	0.8	0.63
	90.3% 41	$\varepsilon = 250\ t^{0.395}$	250	0.395	98.75	21.96	14.43	9.49	6.24	5.45	3.59	2.81	2.35	1.84
20	37.7%	$\varepsilon = 50 + 40 \log t$ $t \leq 17$	50	40	40	3.33	-	-	-	-	-	-	-	-
	27	$\varepsilon = 82\ t^{0.267}$ $t \geq 17$	82	0.267	-	-	2.13	1.28	0.77	0.66	0.39	0.29	0.24	0.18
	57.2% 41	$\varepsilon = 240\ t^{0.29}$	240	0.29	54.96	11.9	7.29	4.46	2.72	2.32	1.42	1.07	0.87	0.65
	69.7%	$\varepsilon = 503\ t^{0.22}$ $t \leq 3.6$	503	0.22	110.66	-	-	-	-	-	-	-	-	-
	50	$\varepsilon = 360\ t^{0.312}$ $t \geq 3.2$	360	0.312	-	20.32	12.61	7.83	4.86	4.17	2.59	1.96	1.61	1.22
	87.8%	$\varepsilon = 680\ t^{0.21}$ $t \leq 12$	680	0.21	14.28	-	-	-	-	-	-	-	-	-
	63	$\varepsilon = 410\ t^{0.328}$ $t \geq 12$	410	0.328	-	25.32	15.89	9.97	6.26	5.38	3.38	2.57	2.12	1.61
30	29.3%	$\varepsilon = 45 + 38 \log t$ $t \leq 35$	45	38	38	3.16	1.58	-	-	-	-	-	-	-
	27	$\varepsilon = 109\ t^{0.178}$ $t \geq 40$	109	0.178	-	-	-	0.81	0.46	0.38	0.21	0.15	0.12	0.09
	44.5% 41	$\varepsilon = 178\ t^{0.202}$	178	0.202	36	4.95	2.82	1.64	0.94	0.79	0.45	0.33	0.26	0.19
	54.3% 50	$\varepsilon = 225\ t^{0.246}$	225	0.246	55.35	8.76	5.24	3.13	1.87	1.59	0.95	0.70	0.57	0.42
	68.4% 63	$\varepsilon = 452\ t^{0.258}$	452	0.258	116.6	18	10.69	6.2	3.77	3.19	1.89	1.39	1.12	0.83

at any given confining pressure in both dry and saturated conditions. The same behaviour has been reported by Williams and Elizzi[15,100].

The creep rate increases with increasing axial stresses at constant confining pressure for a given loading time as shown in Tables (6.17) and (6.18) for both dry and saturated conditions respectively and as shown in Fig. (6.43). When the creep rates were plotted against the axial stress (σ_1) on log-log graph for a various constant loading time, straight lines were obtained indicating that the relationship between the creep rate ($\dot{\varepsilon}$) and the axial stress (σ_1) followed the power law of the form; $\dot{\varepsilon} = R\ \sigma_1^K$ where R and K are constants; R represents the creep rate value at σ_1 = 1 N/mm^2 and K represents the slope of the straight line on the log-log graph. Fig. (6.44) shows four sets of these lines at 0 (uniaxial) and 10 N/mm^2 confining pressure under dry and saturated condition at various loading times (t). It can be noted from this figure that at each level of σ_3 the set of the relationships consists of several straight lines parallel or nearly parallel to each other, in other words, they have one slope or the same K value.

Misra[79] found the same relationship in uniaxial creep tests on several rocks in dry condition. Afronz and Harvey[95] found that the average secondary creep rate of soft to medium strength rocks in both dry and water saturated conditions followed in general the relationship $\dot{\varepsilon} = m\ \sigma_1^n$ where m and n are constants. Elizzi[15] reported the same relationship between the creep rate and the applied stress in dry uniaxial and triaxial creep tests.

At constant differential stresses ($\sigma_1 - \sigma_3$), the creep rate increases with increasing axial stress in both dry and water saturated conditions. Figs. (6.45) and (6.46) show the relationships between the creep rate and the axial stress at $(\sigma_1 - \sigma_3)$= 10 N/mm^2 at various loading time for dry and saturated conditions respectively. It can be seen that all the relationships

are linear, the straight lines emanating from one point on the σ_1-axis (negative value). Therefore, for every $(\sigma_1 - \sigma_3)$ value there will be a set of these straight lines expressed in the general equation;

$\dot{\varepsilon} = (g + \sigma_1) K$; where $\dot{\varepsilon}$ is the creep rate, g is the absolute value of σ_1 at $\dot{\varepsilon} = 0$ and K is the slope of the straight line. From Figs. (6.45) and (6.46) the following equations at $\sigma_1 - \sigma_3 = 10$ N/mm^2 are obtained:

For dry condition (g = 11);

$$\dot{\varepsilon} = (11 + \sigma_1) K \quad \ldots\ldots \quad (6.74)$$

For saturated condition (g = 26);

$$\dot{\varepsilon} = (26 + \sigma_1) K \quad \ldots\ldots \quad (6.75)$$

The values of K at this particular $(\sigma_1 - \sigma_3)$ for different values of t in both dry and saturated gypsum are given in Table (6.19).

Table(6.19) Values of K for various t at $(\sigma_1 - \sigma_3) = 10$ N/mm^2.

Time (hours)	K x 10^{-3}	
	Dry	Saturated
24	23.6	69.3
120	7.3	19.2
360	2.7	10.2
720	1.8	6.4

6.2.3 Effect of Confining pressure.

The Moduli of Elasticity calculated by using the instantaneous strains,were explained in the previous section and shown in Fig. (6.39), these Moduli of Elasticity are plotted versus confining pressure in Fig. (6.40). This figure shows an increase of the Modulus of Elasticity in a linear relationship with the confining pressure in both environmental conditions dry and saturated. These results are in agreement with

Murrell's[116] results for the behaviour of Darley Dale sandstone under triaxial compression and Elizzi's[15] results on dry gypsum and anhydrite.

The creep strain decreases with the confining pressure at a constant axial stress. Figs. (6.47) and (6.48) show the creep strain - time relationships at various confining pressures namely; 10, 20 and 30 N/mm^2 under a constant axial stress of 27 N/mm^2, these figures are for dry and saturated conditions respectively. It can be seen that the effect of increasing the confining pressure of equal increments is larger at low values of σ_3 than higher. At constant differential stresses $(\sigma_1 - \sigma_3)$, the effect of varying confining pressure on the creep strain is shown in Figs. (6.49) and (6.50) for dry and saturated gypsum respectively. As the confining pressure increases the creep strain increases at a constant differential stress $(\sigma_1 - \sigma_3)$ in dry and saturated conditions.

"Increasing the confining pressure on any rock changes some of its mechanical properties, it makes the rock more ductile than its nature at atmospheric pressure, it makes the rock deform under suitable axial load, plastically rather than in a brittle manner" Murrell[116]. The creep property is one of the rock's mechanical characteristics that is also affected by the change of confining pressure even under constant differential stresses. Williams and Elizzi[100] reported the same behaviour of the dry rock subjected to triaxial creep.

Values of the creep equation constants C and n, Eq. (6.23), were plotted against the confining pressure at a constant axial stress. Figs. (6.51) and (6.52) show the effect of σ_3 on the values at $\sigma_1 = 41$ N/mm^2 and $\sigma_1 = 35$ N/mm^2 respectively. It can be observed that the increase in confinement decreases the values of the constants C and n in both dry and saturated conditions, this effect is non-linear. In other words, the effect of increasing confining pressure at constant axial stress is to decrease the

creep rate. The creep rate was plotted versus confining pressure at constant σ_1 = 41 N/mm^2 in dry and saturated conditions for various values of t (time) in Fig. (6.53). A rapid decrease in the creep rate can be seen as the confining pressure increases, and the effect of equal variation of σ_3 is larger at low values of σ_3 than higher. This could be explained as the confining pressure may decrease the size, number and propagation of fracture during creep. Comte[83], Robertson[78], Williams and Elizzi[100] and others reported the same behaviour in different rocks subjected to triaxial creep.

Figs. (6.54) and (6.55) for dry and saturated conditions respectively show that at constant differential stresses $(\sigma_1 - \sigma_3)$ = 10, the creep rate increases slightly with the confining pressure, the variation of the confining pressure has the largest effect at the earlier stage of the creep and is greater in dry than in saturated conditions. The relationship between the creep rates and the confining pressure were constructed for various constant values of differential stresses $(\sigma_1 - \sigma_3)$, in Figs. (6.56) and (6.57) for dry and saturated specimens respectively at given time t = 24 hours. In dry condition, curves indicated linear relationships between the creep rate and the confining pressure for the values of $(\sigma_1 - \sigma_3)$ up to 25 N/mm^2. In saturated condition similar behaviour was obtained, with linear relationship up to $(\sigma_1 - \sigma_3)$ = 15 N/mm^2, then the relationships become non-linear thereafter.

In most cases of the dry condition the creep rate increases with the confining pressure. For values of $(\sigma_1 - \sigma_3)$ more than 25 ... takes place in this relationship in that a minimum ... a particular value of confining pressure, when both ... decrease in confinement results in increasing creep rate.

In saturated condition the creep rate decreases with the confining pressure for $(\sigma_1 - \sigma_3)$ values more than 15 N/mm^2. The effect of the

saturation will be discussed later in this chapter. Similar behaviour has been reported by Williams and Elizzi[100] on dry rocks.

It can be seen from Figs. (6.56) and (6.57) that the creep rate in both dry and saturated conditions increases with increasing the differential stresses at any given confining pressure, this is very clearly shown in Figs. (6.59) and (6.60) for dry and saturated conditions. This is in agreement with the results obtained by the investigators Comte[83] on dry rock salt and Wawersik[96] on saturated westerly granite.

6.2.4 Water role in uniaxial and triaxial creep.

As mentioned before, specimens in dry and water saturated conditions at similar levels of confining pressures were subjected to the similar axial stresses within the range set by the values of the ultimate stress which could be carried by the saturated sample. This was done to ensure the best comparison, and to determine the effect of the water saturation.

Table (6.20) gives the instantaneous strains for dry and saturated conditions. It can be seen that the instantaneous strain for the saturated condition is more than that of the dry under the similar condition of σ_1 and σ_3. The increase in the strain ranging from 23% to 39% of the dry value with about 30% as an average value in triaxial tests, in uniaxial the increase is about 47%. The Moduli of Elasticity which are calculated by using the instantaneous strains as described in Sec.(6.2.2) for both environmental conditions, were given in Table (6.16) and shown in Fig. (6.40). The saturation decreased the Modulus by about 29% in the uniaxial condition of loading and 23% in triaxial at all the confining pressure levels. These results are in agreement with various investigators; Afronz and Harvey[95] reported an appreciable increase in instantaneous strain of the soft to medium strength rocks in uniaxial due to water saturation. Mann and Fatt[53] reported a decrease in

Table (6.20) Effect of saturation on the Instantaneous strain (ε_o) in uniaxial and triaxial creep.

σ_3 N/mm^2	σ_1 N/mm^2	Dry		Saturated		Increase in ε_o due to saturation %
		% σ_u	Inst. strain (ε_o) μ s.	% σ_u	Inst. strain (ε_o) μ s.	
0 Uniaxial	15	36	380	70.9	560	47
10	21	33.7	460	46.3	640	39
	27	43.3	640	59.5	840	31
	41	65.7	1020	90.3	1310	29
20	27	34.5	650	37.7	800	23
	41	52.4	950	57.2	1300	37
	50	64	1200	69.7	1640	37
	63	80.6	1560	87.9	2080	33
30	27	26.3	540	29.3	700	30
	41	39.8	860	44.5	1100	28
	50	48.7	1080	54.3	1350	25
	63	61.3	1400	68.3	1780	27

Modulus of Elasticity of three sandstones by 8-20%. Mogilevskaya[57] reported a decrease in Modulus of Elasticity of limestone by 5-20%, and in A.S.T.M. publication, in 1976, Chamberlain et al.[124] reported that the Modulus of Elasticity of three shales decreased by 10%, 59% and 61% under 100% humidity.

The effect of water saturation was found to increase the creep strain by remarkable amounts. Figs. (6.14) to (6.38) show the creep strain/time relationships of dry and saturated conditions under uniaxial and triaxial loading at different stress levels. Tables (6.8) to (6.15) give the detailed results of all these cases. To give a clear idea about the effect of saturation, creep curves for dry and saturated conditions for specimens subjected to similar stress conditions were plotted in Fig. (6.58). These cases are σ_1 = 50 N/mm^2 at σ_3 = 20 N/mm^2 and σ_1 = 41 N/mm^2 at σ_3 = 30 N/mm^2. It can be seen from this particular example that the effect of the presence of water was to increase the creep strain by about 3 to 7 times with 4 fold increase as an average in the first case and about 2.5 to 6 times with 3 fold increase as an average in the second case.

The creep strain in dry condition subjected to uniaxial and triaxial compression followed the logarithmic law, Eq. (6.22), at low axial stresses and at a short duration in the beginning of some of the medium stresses and follow the power law, Eq. (6.23), for the rest of the medium stresses and for the high stresses. Whereas in saturated conditions the creep strain followed the logarithmic law, Eq. (6.22) at a short duration of most of the low stresses and followed the power law, Eq. (6.23) at the rest of the low stresses and at medium and high stresses. This means that the water changes the creep behaviour from logarithmic relationships to power law. Since the water decreases the rock strength, it seems likely that the weaker the rock the lower the stress at which the

creep law changes to power law. Comte[83] found that the creep curves of the rock salt followed the power law from the very beginning of the tests. His work confirms the above conclusion because generally, rock salt is weaker than gypsum. Elizzi[15] reported that the creep curves of gypsum changed from logarithmic law to power law at lower stress than that of the anhydrite (stress given as % σ_u). His work confirms the above conclusion as well because generally the gypsum is weaker than anhydrite. Griggs[71] found that the creep curves of alabaster in water followed the power law, Eq. (6.23) at low stresses. Wawersik[96] reported a power law relationship for the saturated westerly granite subjected to triaxial compression.

The creep equation constants C and n of the power law were found to be increased by the influence of water. Figs. (6.41) and (6.42) show the effect of water on the values of these constants at various confining pressures. It can be seen that value of C increases sometimes by 400% and the value of n by 25%. In other words, the effect of the water saturation is to increase the creep rate. Fig. (6.43) shows the comparisons between the creep rate of the dry and saturated gypsum at various σ_3 for a given time t = 240 hours. Fig. (6.53) shows the creep rate/confining pressure relations for dry and saturated conditions at various times under constant σ_1 = 41 N/mm^2. All the results indicated that the creep rate increases by appreciable amount when the samples were saturated with water (see tables (6.17) and (6.18)). This increase reached up to 10 fold with 5 fold as an average value. The creep rate in both dry and saturated conditions followed the form $\dot{\epsilon} = R\ \sigma_1^K$, as discussed previously in Sec. (6.2.2). The constants R and K are increased with water saturation indicating that the effect of the axial stress (σ_1) on

the creep rate in saturated condition is more than that on the dry. The creep rate of gypsum at constant $(\sigma_1 - \sigma_3)$ was found to be more in saturated than that in dry conditions at any given time and confining pressure, see Figs. (6.54) and (6.55). The same behaviour was found when the rock was subjected to constant $(\sigma_1 - \sigma_3)$ and the creep rate taken at particular time and axial stress, see Figs. (6.45) and (6.46). Figs. (6.56) and (6.57) for dry and saturated conditions respectively show that the increasing creep rate of saturated gypsum with $(\sigma_1 - \sigma_3)$ at constant values of σ_3 and time is more than in the case of dry material under the same stress conditions, this is clearly shown in Figs. (6.59) and (6.60).

Griggs[70] (1939) reported increase in creep rate of alabaster immersed in water more than 25 times that when it was dry under a constant load of 100 Kg/cm^2. Griggs[71] (1940) reported also,that the creep rate under a constant differential stress greatly accelerated and exhibited an entirely different behaviour when saturated with water and this increase became higher when the saturated specimens were subjected to higher differential stresses. Misra[79] reported that water saturation increases the creep rate of many rocks by appreciable amounts.

Afronz and Harvey[95] reported an increase in creep rate of the saturated coal of 3 fold and in saturated shales of 8 fold. Wawersik[96] found that the creep rate of saturated westerly granite and sandstone increased by at least two times. Wu and Thomson[98] reported an appreciable increase in axial creep rate of Westerly granite by water saturation.

The creep rates were plotted versus the differential stresses $(\sigma_1 - \sigma_3)$ at various confining pressures in Figs. (6.59) and (6.60) for dry and saturated conditions respectively. A linear relationship was obtained for each σ_3. It can be seen that the behaviour of these relationships was completely changed by the water saturation. The creep rate in dry

conditions increases with the $(\sigma_1 - \sigma_3)$ at constant σ_3 and with σ_3 at constant $(\sigma_1 - \sigma_3)$ and the straight lines are nearly parallel to each other. Whereas in saturated conditions the creep rate increases with the σ_3 at constant $(\sigma_1 - \sigma_3)$ up to the $\sigma_1 - \sigma_3 = 15$ N/mm^2 then the creep rate starts to decrease with the σ_3 for $(\sigma_1 - \sigma_3)$ higher than 15 N/mm^2. This may be explained in conjunction with the solubility of the gypsum. Due to relatively high solubility of the gypsum in water, the solubility of the gypsum (alabaster) and the mobility of the solute increase with the pressure up to same pressure value[125]. It might be expected that the effect of increased confining pressure by forcing liquie into and through the pores of the solid, will increase the effective surface area and so results in a higher initial creep rate until those open spaces become filled with deposited material.

Griggs[71] stated that the effect under differential stresses would be to dissolve material at the points of stress concentration and thus relieve the localized stress inevitable in any crystalline aggregate. This would have the effect of rendering the stress distribution more homogeneous throughout the specimen. In other words a decreased stress-concentration effect means a decrease of the creep rate at higher differential stress with the confining pressure. Wawersik[96] reported the same behaviour in the creep rate of the saturated westerly granite under differential stresses.

Figs. (6.59) and (6.60) indicate that the creep mechanism of saturated rock is different from that of the dry rock. Observing the effect of σ_3 at constant $(\sigma_1 - \sigma_3)$ on the saturated gypsum, we see an increase in the creep rate with increasing σ_3 up to a certain value of $(\sigma_1 - \sigma_3)$. Above this value the creep rate starts to decrease for higher values of $(\sigma_1 - \sigma_3)$ and the reversal of the effect of σ_3 occurs. This shows that more complex creep processes may be taking place in the case of

the saturated gypsum, possibly solution, recrystallization, etc. becoming dominant.

In evaluating the effect of water on the creep and creep rate of the gypsum, the following investigators suggested the following; Griggs[70] (1939) suggested that when the gypsum (alabaster) is immersed in water dissolution would occur at the most highly stressed regions and deposition at the free regions, the creep would thus take place by recrystallization. Griggs[71] (1940), however, found that the creep rate of the alabaster specimens increased when the soaking solution was subjected to pressure. He suggested that the creep rate of alabaster is not due to simple recrystallization but may be a function of ionic mobility of gypsum in the solvent (Ca^{++} SO_4^{--}). Misra[79] reported that the effect of water on the creep of the partially soluble rocks, anhydrite and beerstone, is mainly due to solution in it. Varo and Passaris[102] (1977) reported that the creep of the halite in saturated brine is due to recrystallization and in water the effect is one of solution.

The behaviour of the creep was changed in most of the cases from logarithmic law, Eq. (6.22) to power law, Eq. (6.23), under the same stress conditions by the water saturation in this study. This effect was explained by Griggs[70] as being due to recrystallization. On the other hand, the gypsum is relatively highly soluble in water. In the author's view it seems difficult to adequately separate the effects of solution, recrystallization and ionic mobility. Clearly the more soluble the rock the more the effects of solution. Recrystallization must be affected by solubility and by ionic mobility. It thus seems most likely that all these factors influence the creep behaviour of saturated gypsum.

6.2.5 Empirical Equation.

The creep data of dry and saturated gypsum in an axial direction, were regressed using a least squares curve fitting computer program (multiple regression) for the combination of the variables. The creep strain was considered as the dependent variable and the independent variables were loading time and axial stress. This program considered a combination of ten curve types, including exponential functions, power law functions and logarithmic functions. For each confining pressure a power law function gave the best fit for times greater than 24 hours and within the given experimental loading times. This function was of the form:

$$\varepsilon = a\ \sigma_1^{\ b}\ t^{c} \qquad \ldots\ldots \qquad (6.76)$$

Where ε is the creep in microstrain, σ_1 is the axial stress in N/mm^2, t is the loading time in hours and a, b and c are constants depending on the environmental conditions and confining pressure.

The values of the constants a, b and c are given in Table (6.21) for the specified conditions. A plot showing the variation of the values of a, b and c with confining pressure (σ_3) is given in Figs. (6.61) and (6.62) for dry and saturated conditions respectively.

Hansen[131] (1977) reported that the axial creep of dry salt could be represented by a similar empirical equation in which the differential stresses ($\sigma_1 - \sigma_3$) are used in the place of axial stress (σ_1).

The predicted creep strain using the above equation, was compared with the actual values. It was found that the variation for most of the values (not less than 90% of the total) did not exceed 12% in each case. To give a clear idea about the general variations in the results of the actual and predicted, "Standard Error of Estimate, SEE" and the combined "Correlation coefficients, COR. COF" were calculated for each case.

Table (6.21) Constants of the Empirical equations at dry and saturated gypsum for various confining pressures. ($\epsilon = a\ \sigma_1^{\ b}\ t^c$).

Constant / σ_3 N/mm^2	Dry Condition a	b	c	SEE*	COR.** COF.
0 (uniaxial)	1.46413	1.19285	0.22041	20	0.968
10	0.01036	2.48775	0.30364	48	0.990
20	0.14127	1.51930	0.36438	36	0.987
30	0.20246	1.38385	0.33990	19	0.987
Saturated Condition					
0 (uniaxial)	5.60454	1.22733	0.29695	60	0.977
10	1.12259	1.43017	0.34792	104	0.963
20	0.25839	1.90908	0.22277	233	0.947
30	0.58702	1.74686	0.23135	53	0.986

*SEE - Standard Error of Estimate (See Appendix (C) for Computation).
**COR.COF. - Correlation Coefficient.

These values are given in Table (6.21). It can be seen that the correlation coefficient is not less than 0.947 in any of the cases, which indicates a good significant degree of correctness.

σ_t = 4 N/mm²

ε = A + B log t ---- For curves (a),(b),(c) and (d)

Beams of 240mm long x 40mm wide

(d) — 15mm thick

(c) — 20mm thick

(b) — 25mm thick

(a) — 28mm thick

Creep strain, microstrain

Time, hours

0 24 48 120 240 360 480 600 720

0 10 20 30 40 50 60 70 80 90 100 110

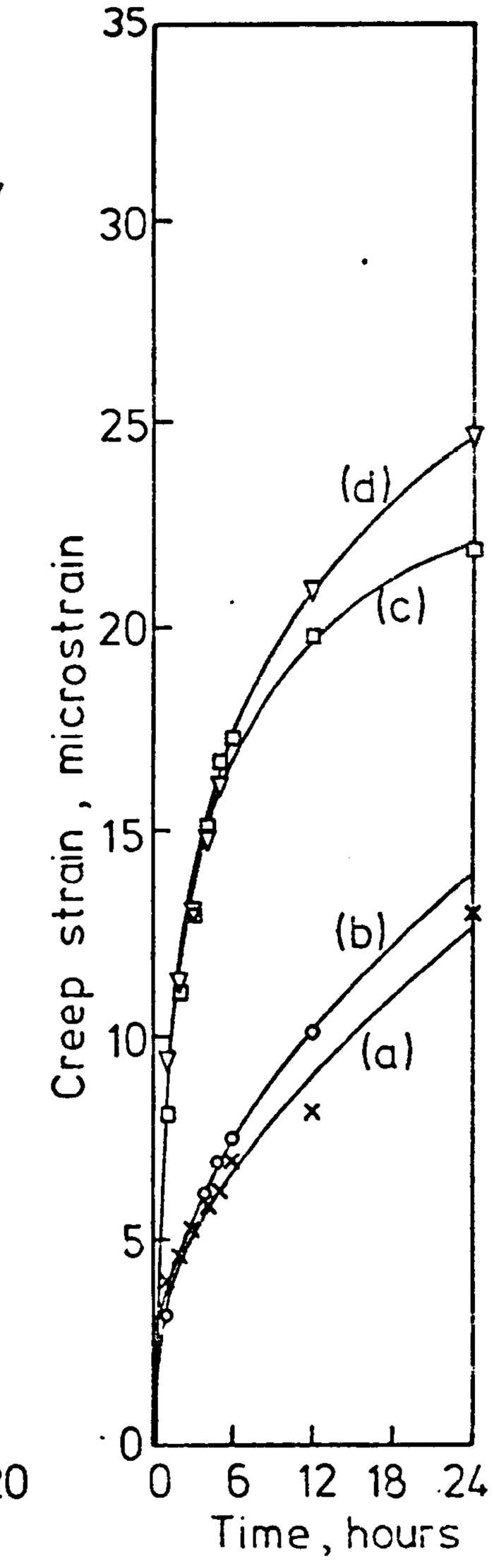

FIG. (6-1) CREEP IN BENDING FOR VARIOUS BEAM THICKNESSES IN DRY CONDITION

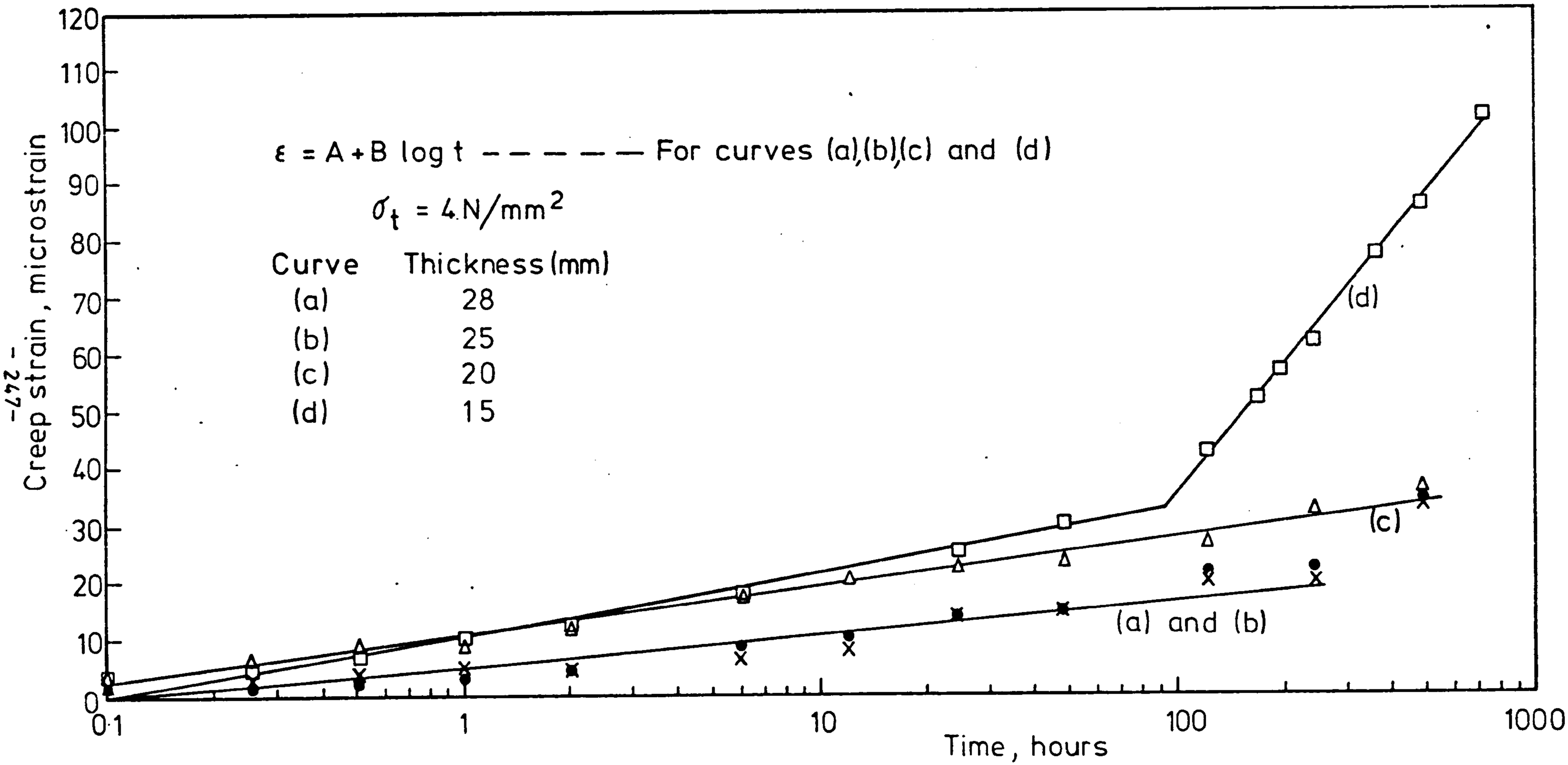

FIG. (6-2) CREEP OF DRY GYPSUM IN BENDING FOR VARIOUS BEAM THICKNESSES (SEMI-LOG GRAPH)

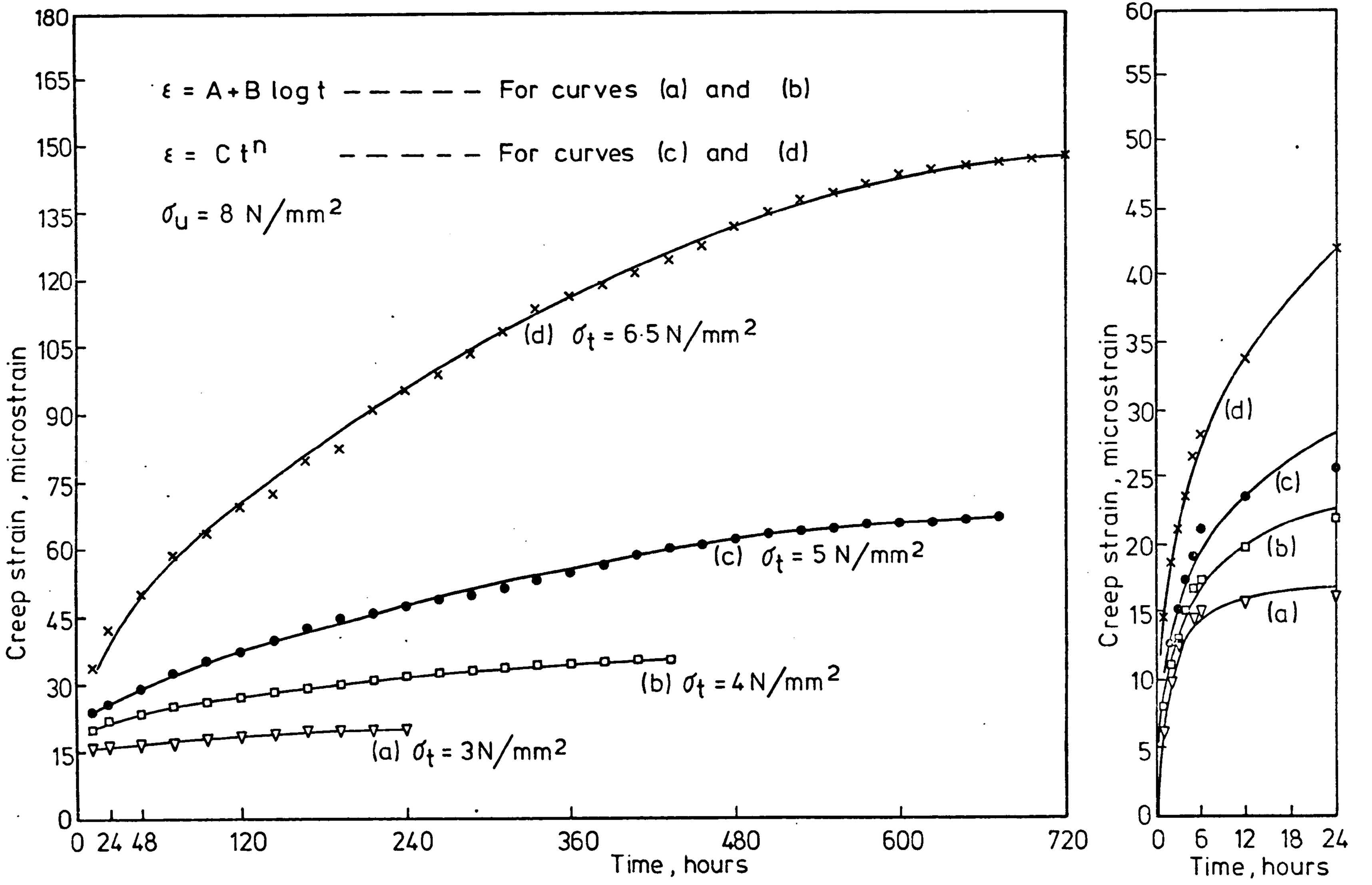

FIG. (6-3) CREEP OF DRY GYPSUM IN BENDING

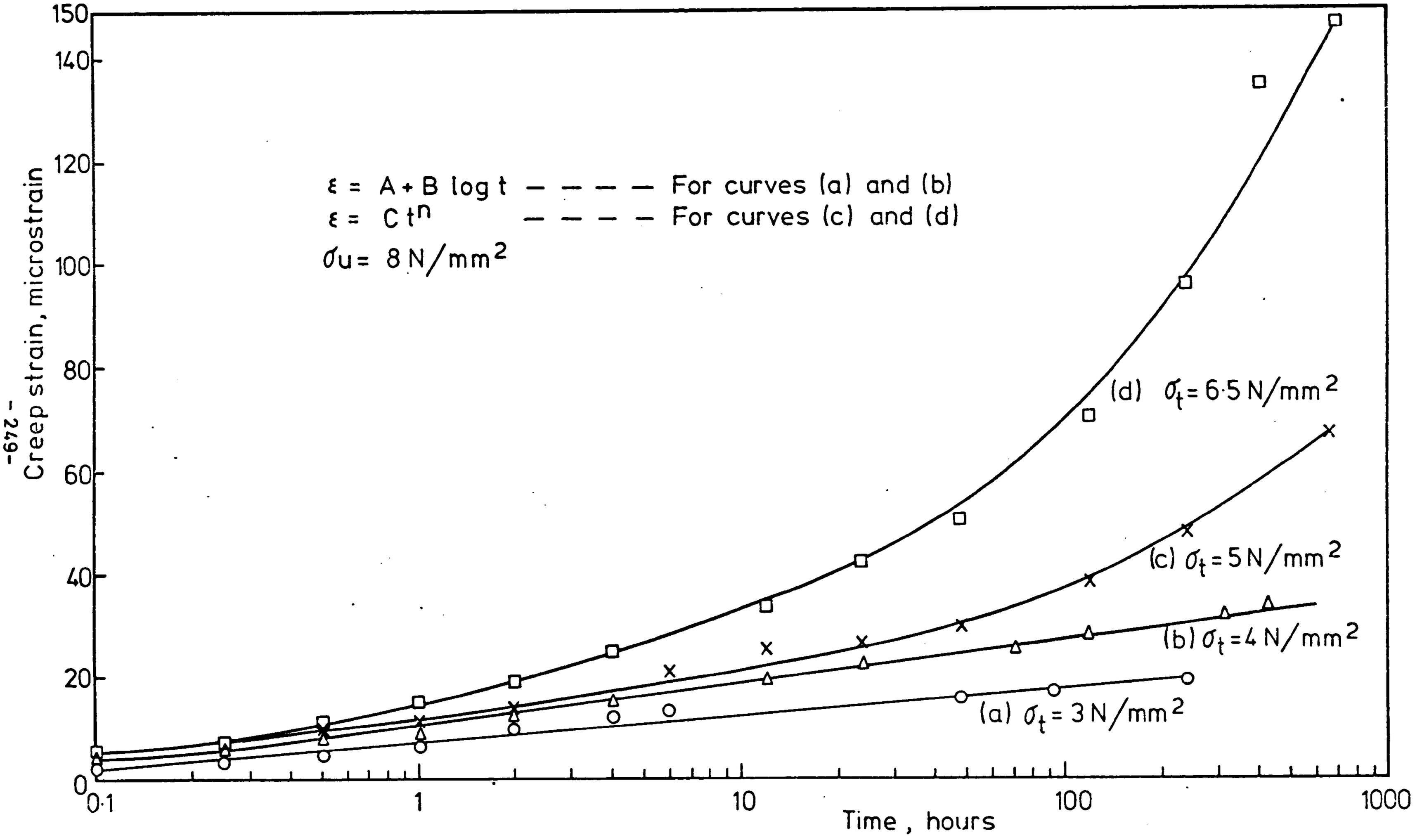

FIG. (6-4) CREEP OF DRY GYPSUM IN BENDING (SEMI-LOG GRAPH)

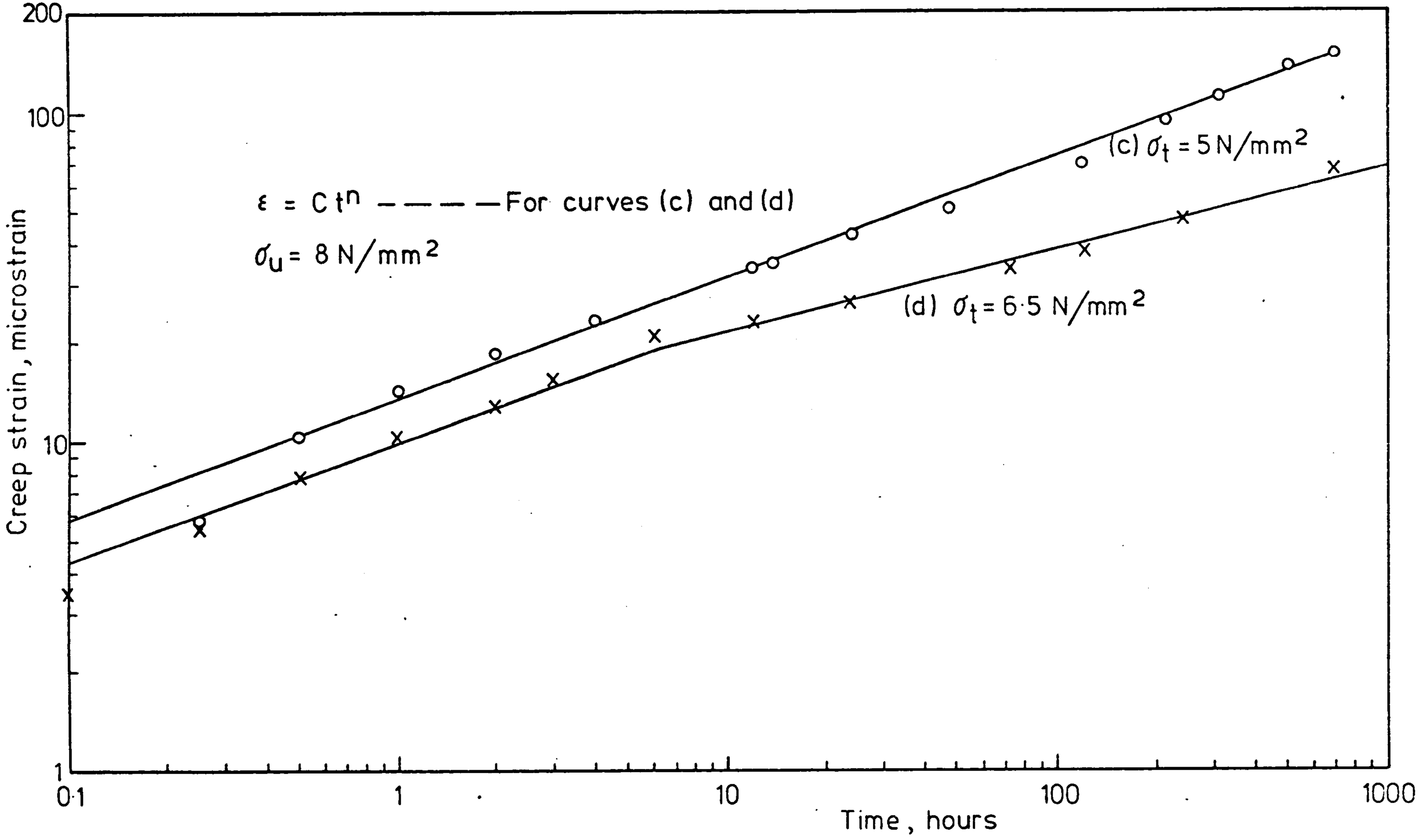

FIG. (6-5) CREEP OF DRY GYPSUM IN BENDING (LOG-LOG GRAPH)

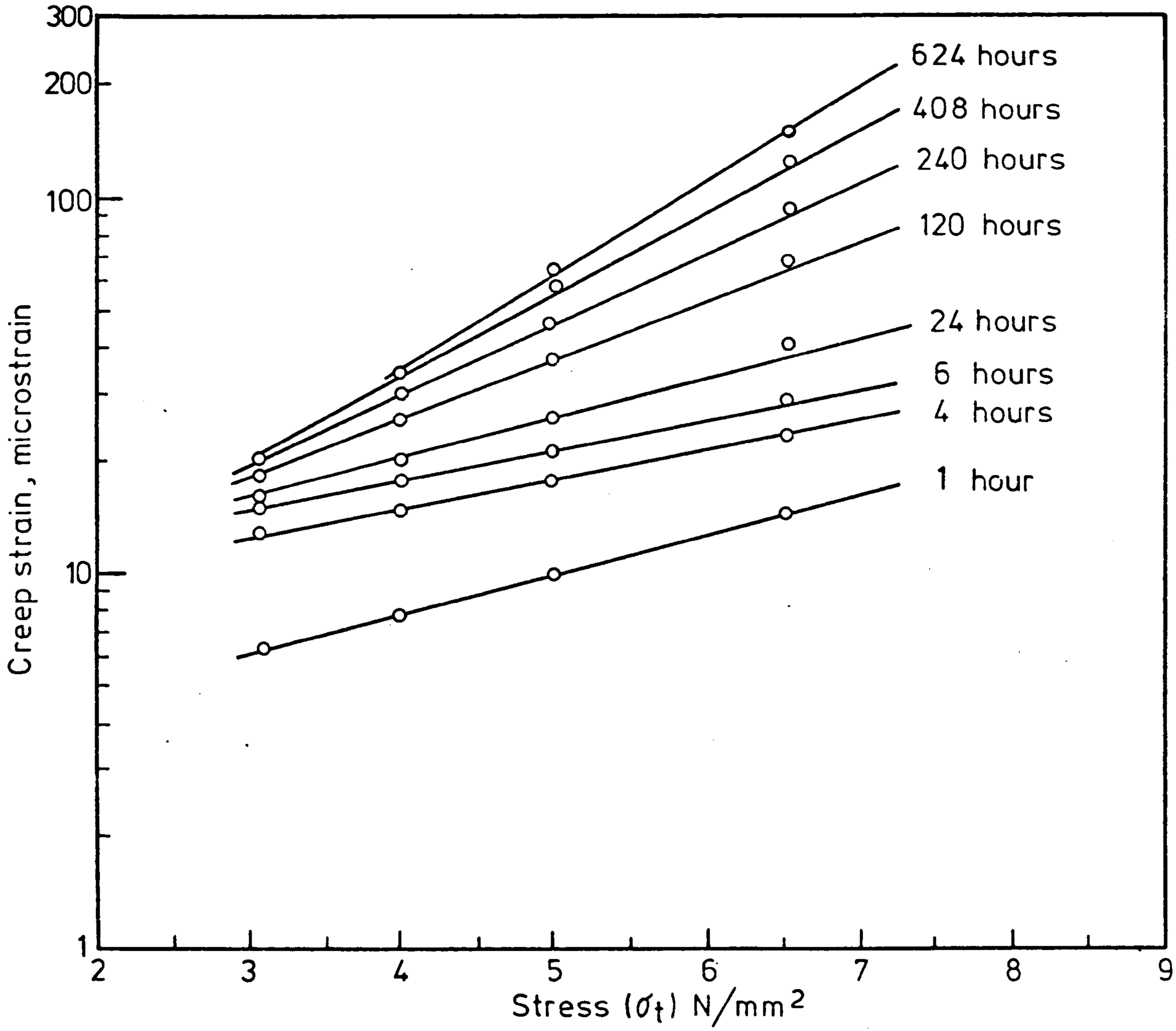

FIG.(6-6) CREEP STRAIN Vs. STRESS IN BENDING UNDER DRY CONDITIONS (SEMI - LOG GRAPH)

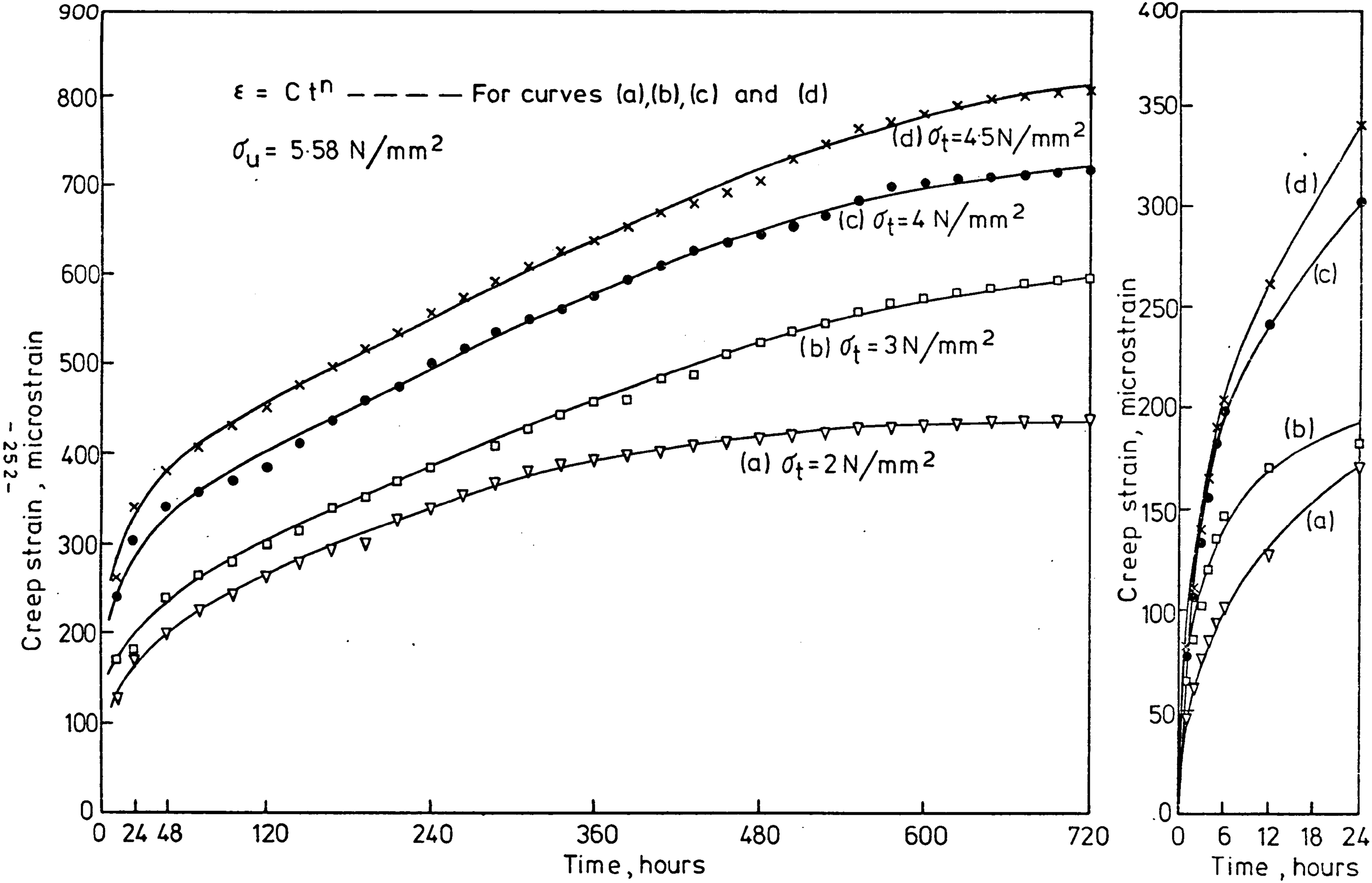

FIG. (6-7) CREEP OF SATURATED GYPSUM IN BENDING

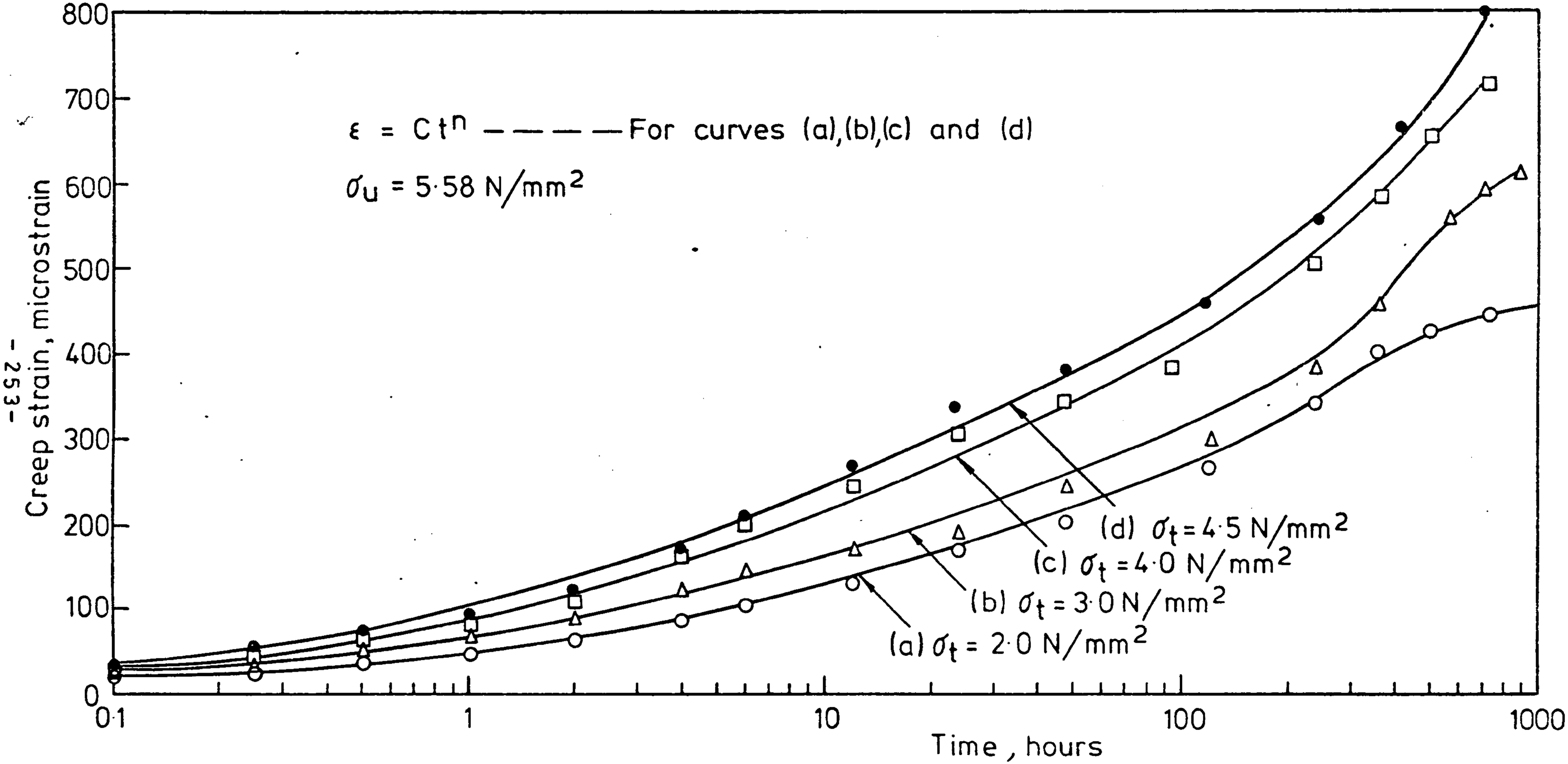

FIG. (6-8) CREEP OF SATURATED GYPSUM IN BENDING (SEMI-LOG GRAPH)

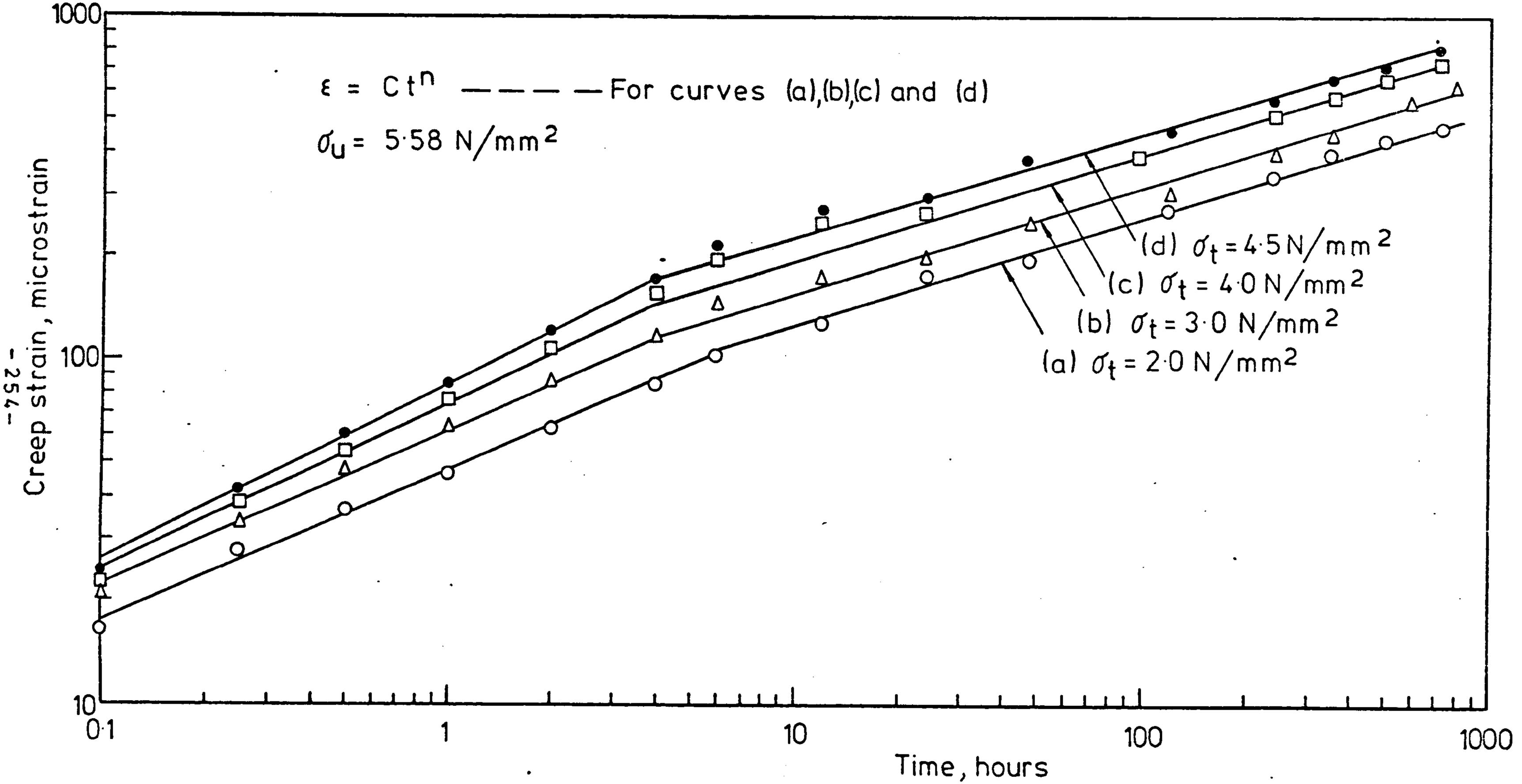

FIG. (6-9) CREEP OF SATURATED GYPSUM IN BENDING (LOG-LOG GRAPH)

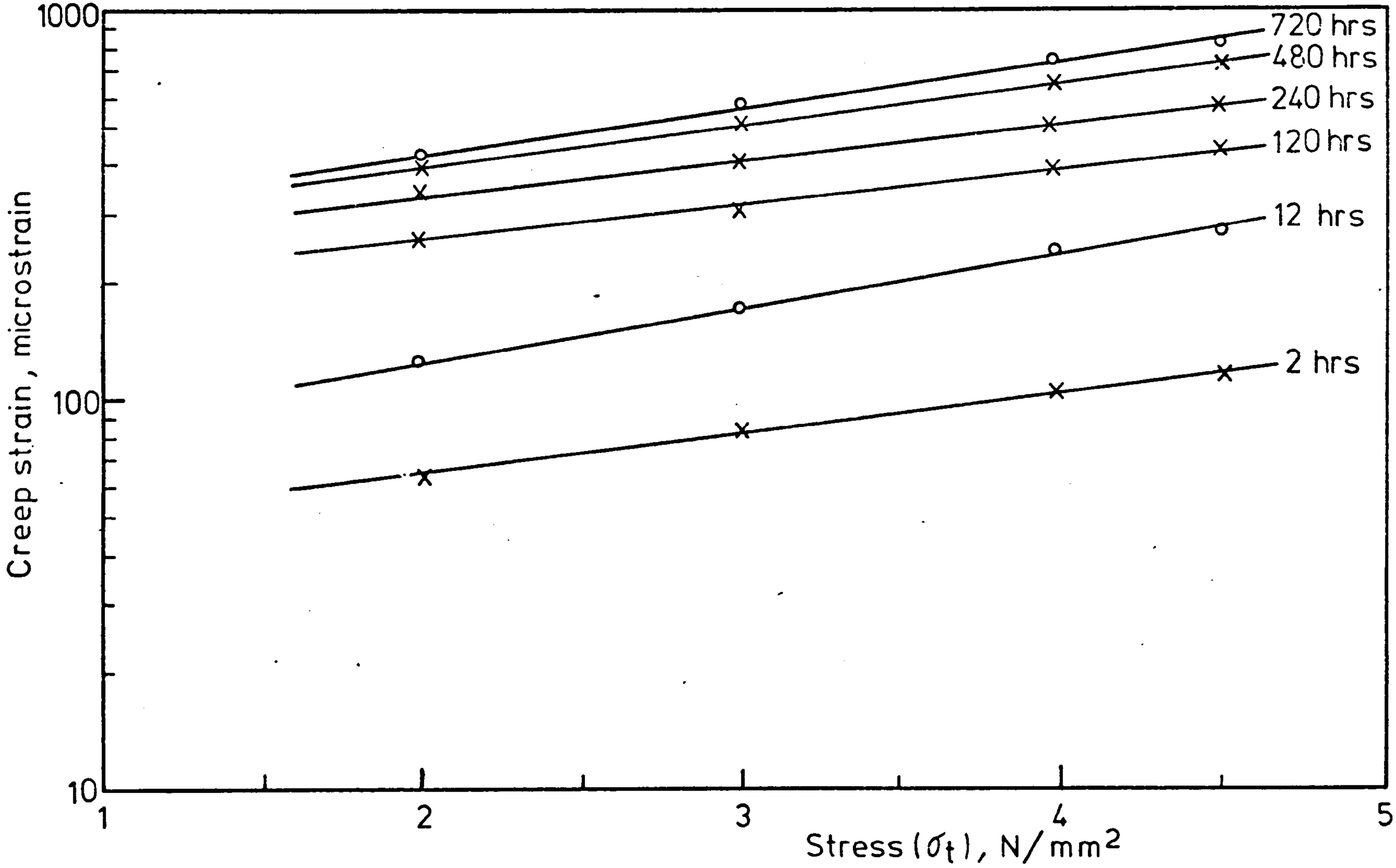

FIG. (6-10) CREEP STRAIN Vs STRESS IN BENDING UNDER SATURATED CONDITION (SEMI-LOG GRAPH)

$E_{dry} = 4 \cdot 49 \times 10^4 \ N/mm^2$

$E_{sat.} = 2 \cdot 5 \times 10^4 \ N/mm^2$

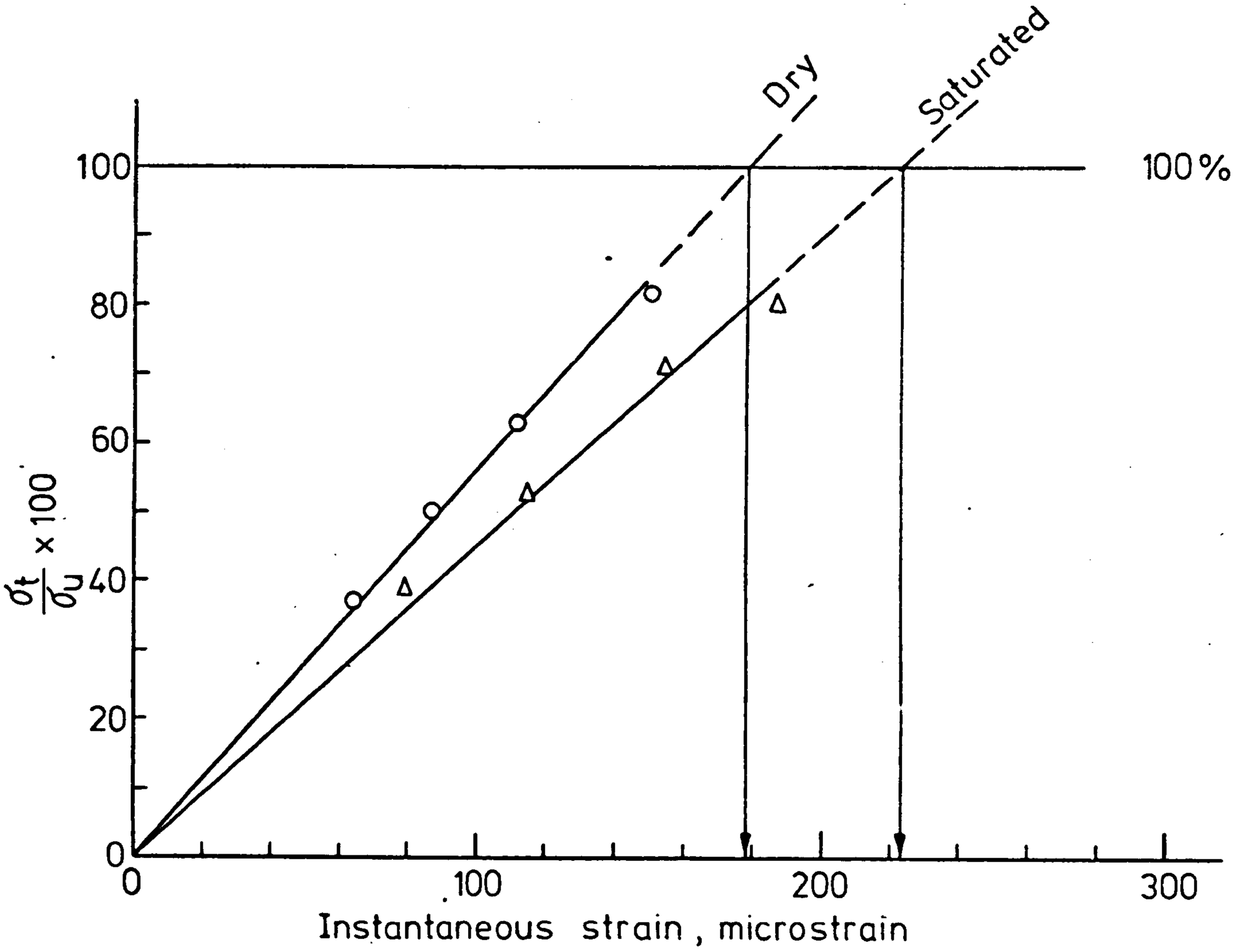

FIG.(6-11) DETERMINATION OF E OF DRY AND SATURATED GYPSUM IN BENDING

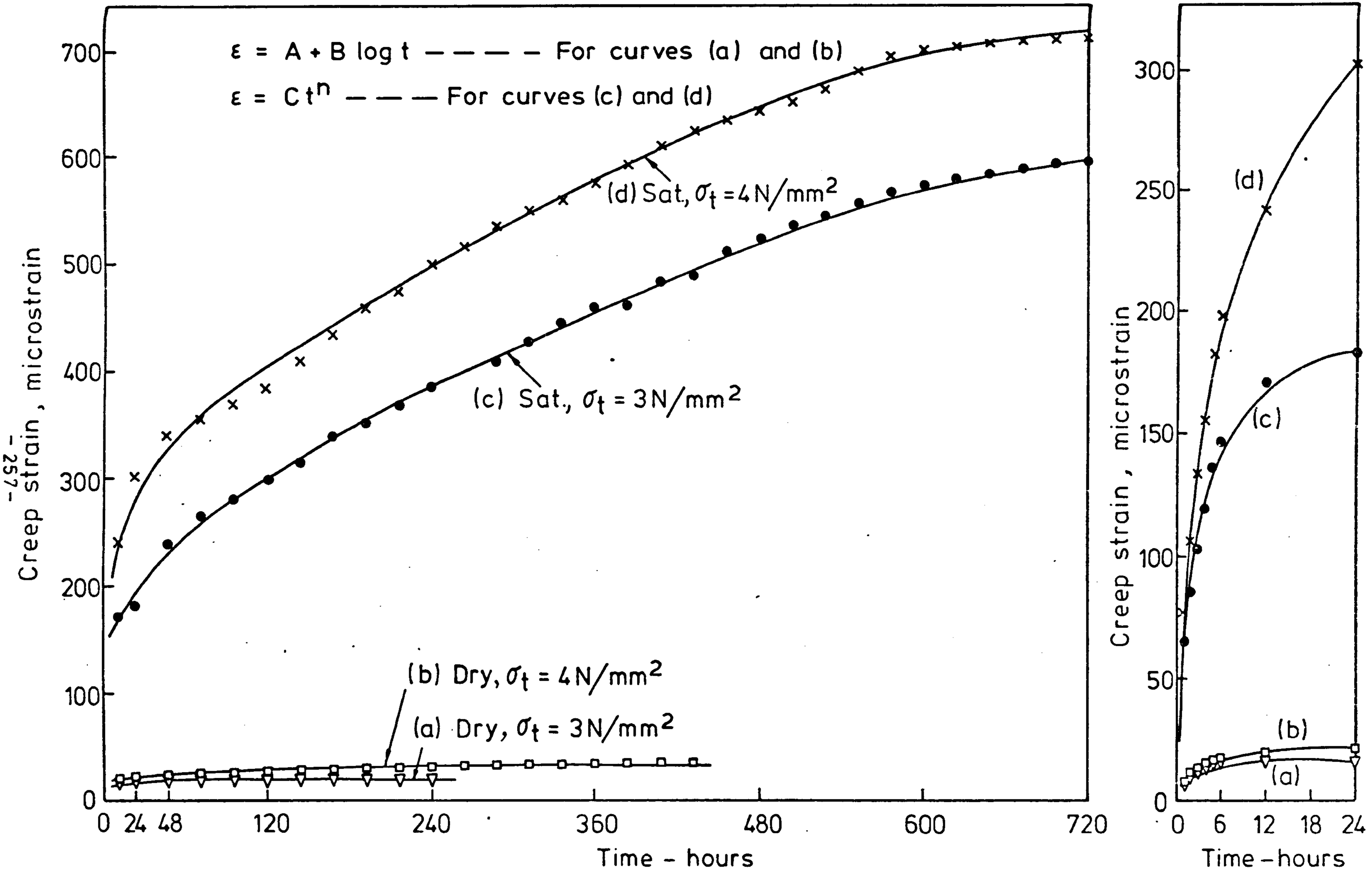

FIG. (6–12) CREEP IN BENDING FOR DRY AND SATURATED CONDITIONS

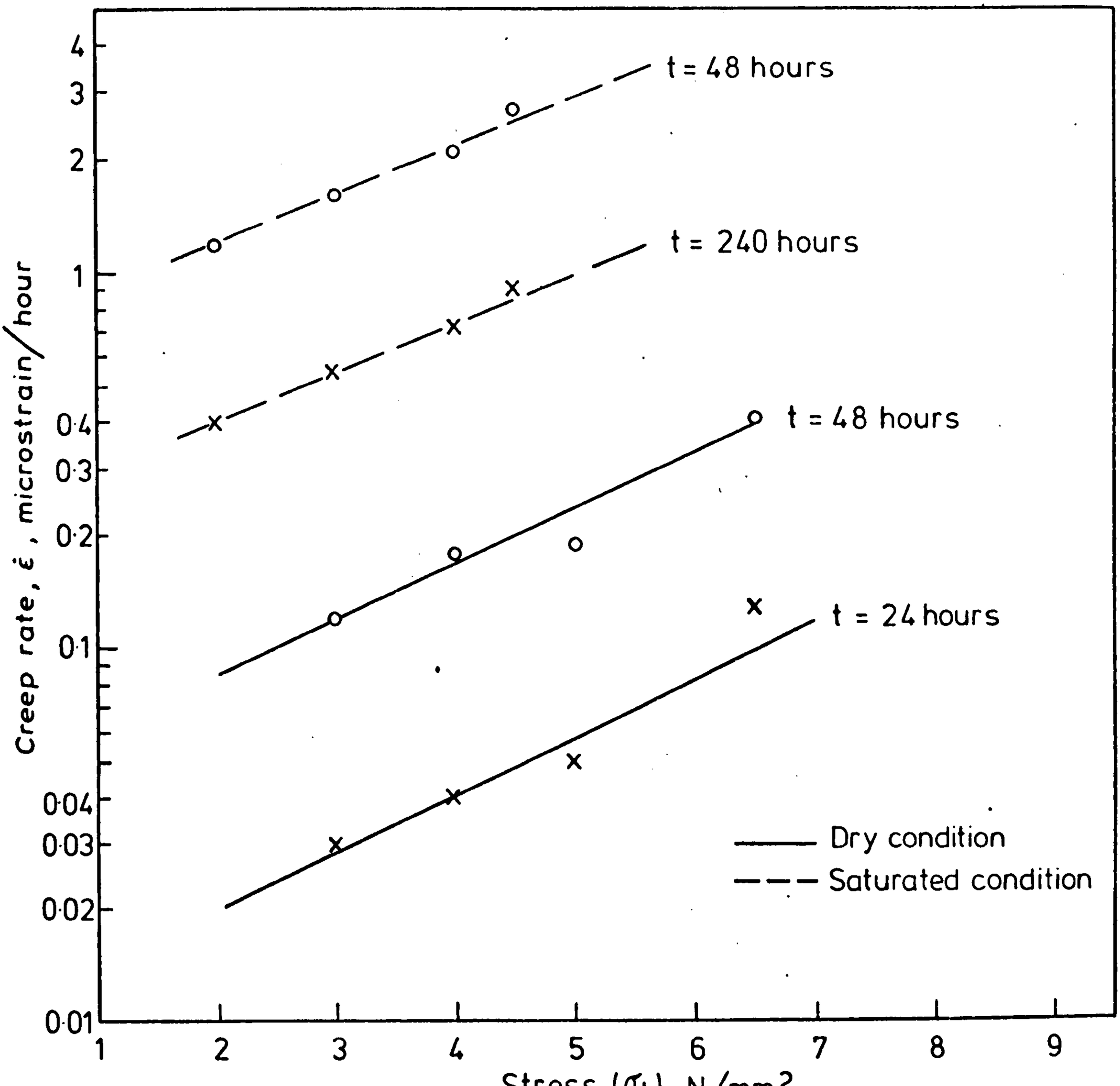

FIG.(6–13) EFFECT OF SATURATION ON THE CREEP RATE IN BENDING (SEMI-LOG GRAPH)

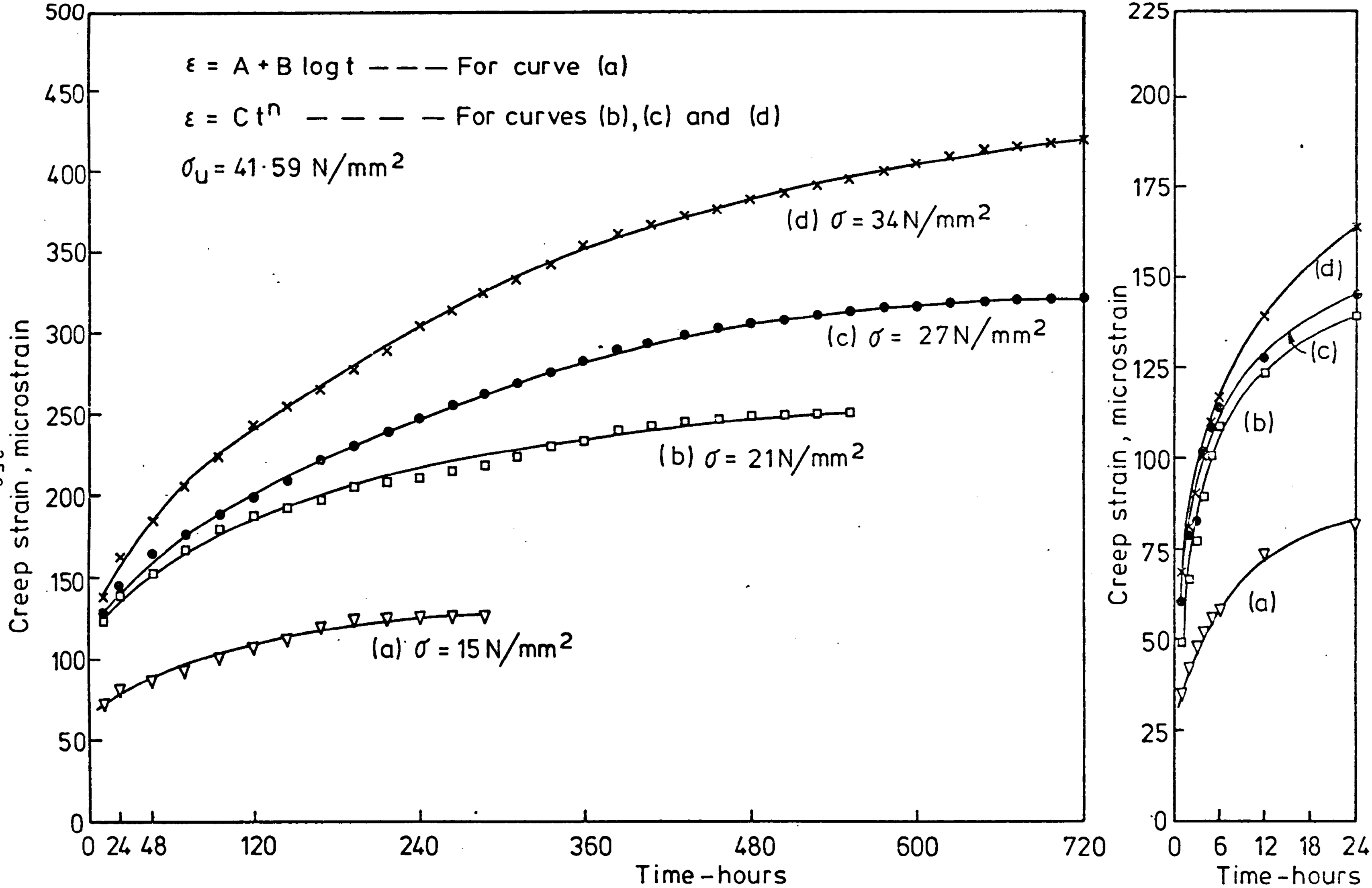

FIG. (6-14) AXIAL CREEP OF DRY GYPSUM IN UNIAXIAL COMPRESSION

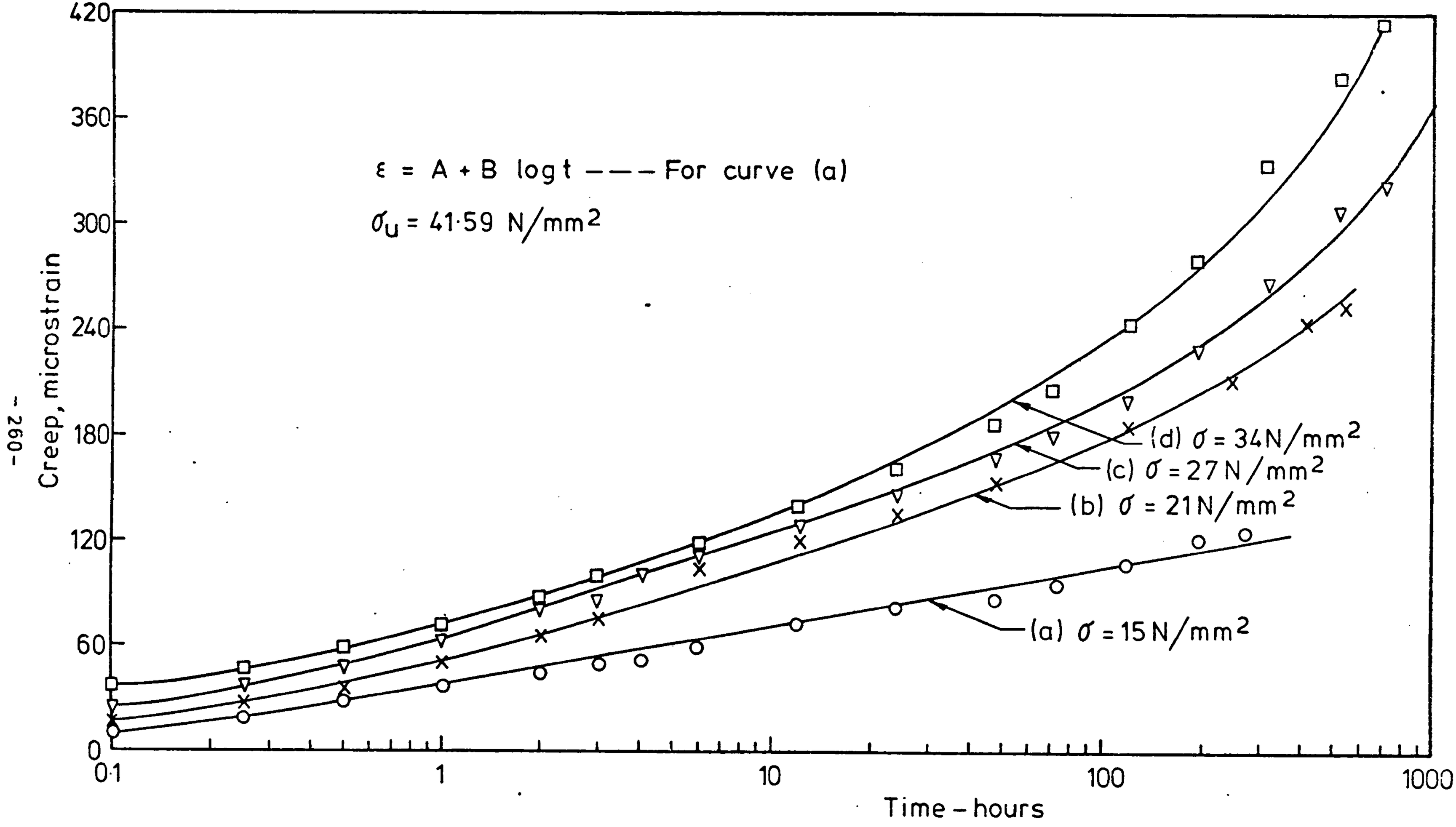

FIG. (6-15) AXIAL CREEP OF DRY GYPSUM IN UNIAXIAL COMPRESSION (SEMI-LOG GRAPH)

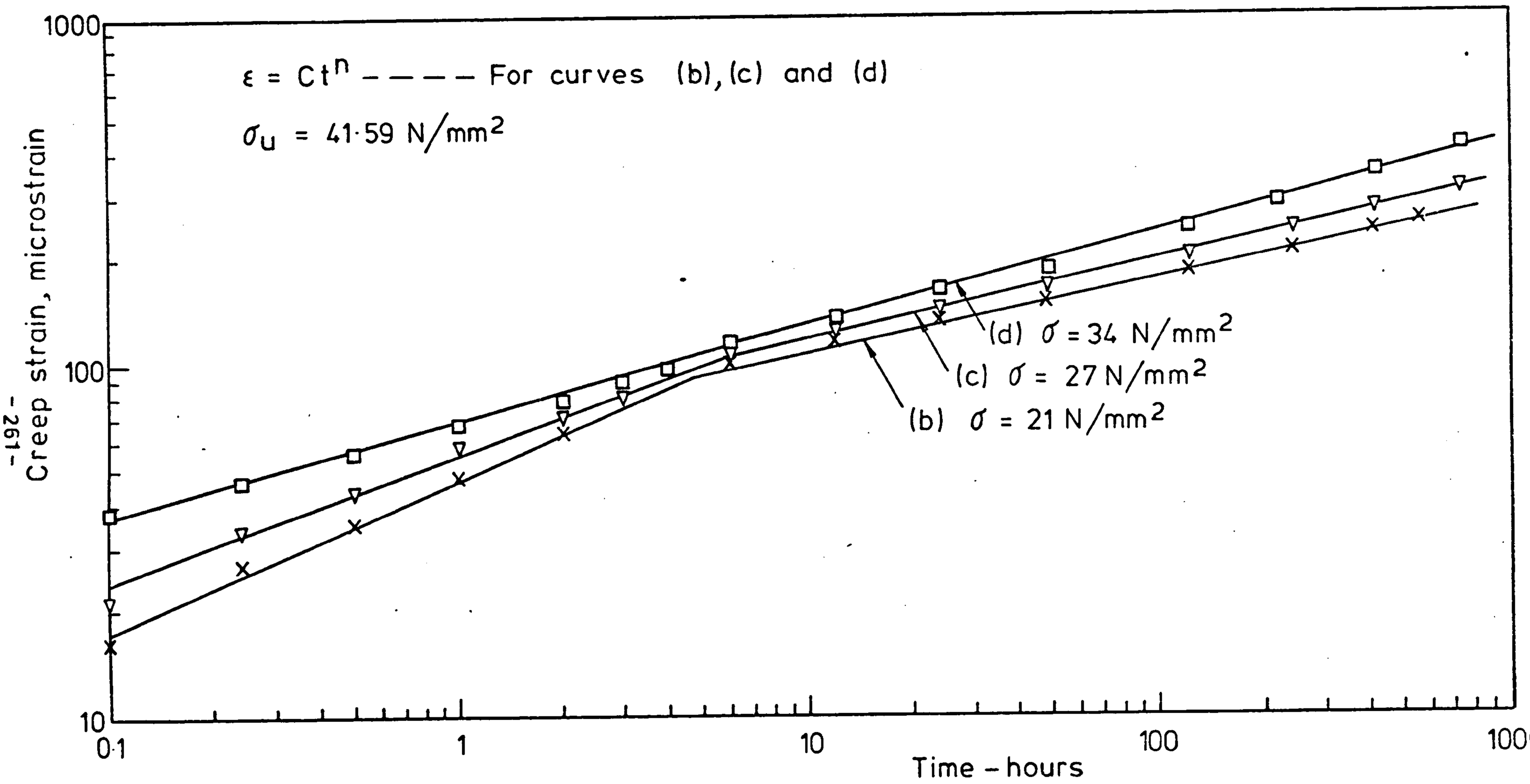

FIG. (6–16) AXIAL CREEP OF DRY GYPSUM IN UNIAXIAL COMPRESSION (LOG-LOG GRAPH)

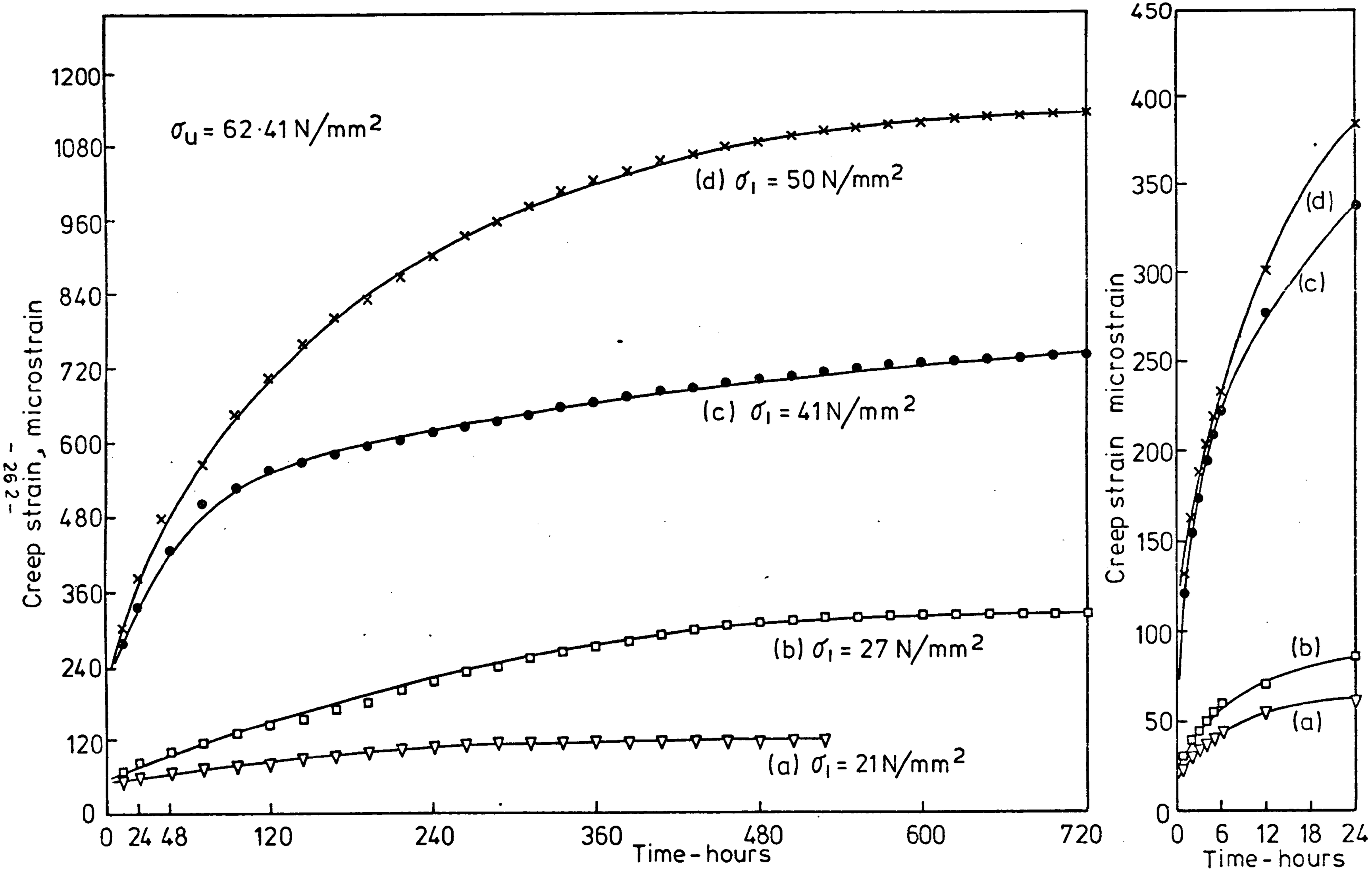

FIG. (6-17) AXIAL CREEP OF DRY GYPSUM IN TRIAXIAL COMPRESSION AT 10 N/mm² CONFINING PRESSURE

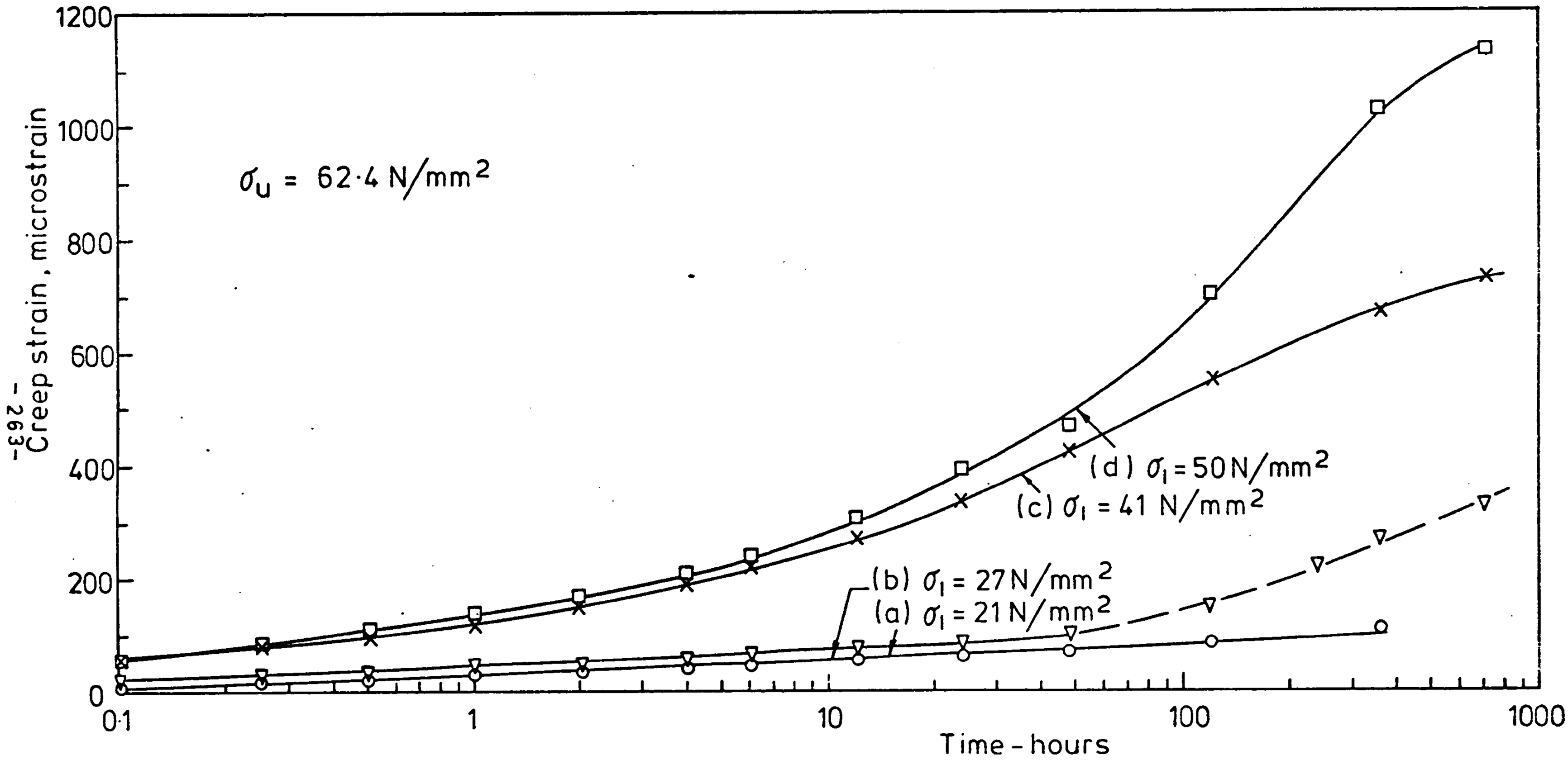

FIG. (6–18) AXIAL CREEP OF DRY GYPSUM IN TRIAXIAL COMPRESSION AT 10N/mm² CONFINING PRESSURE (SEMI-LOG GRAPH)

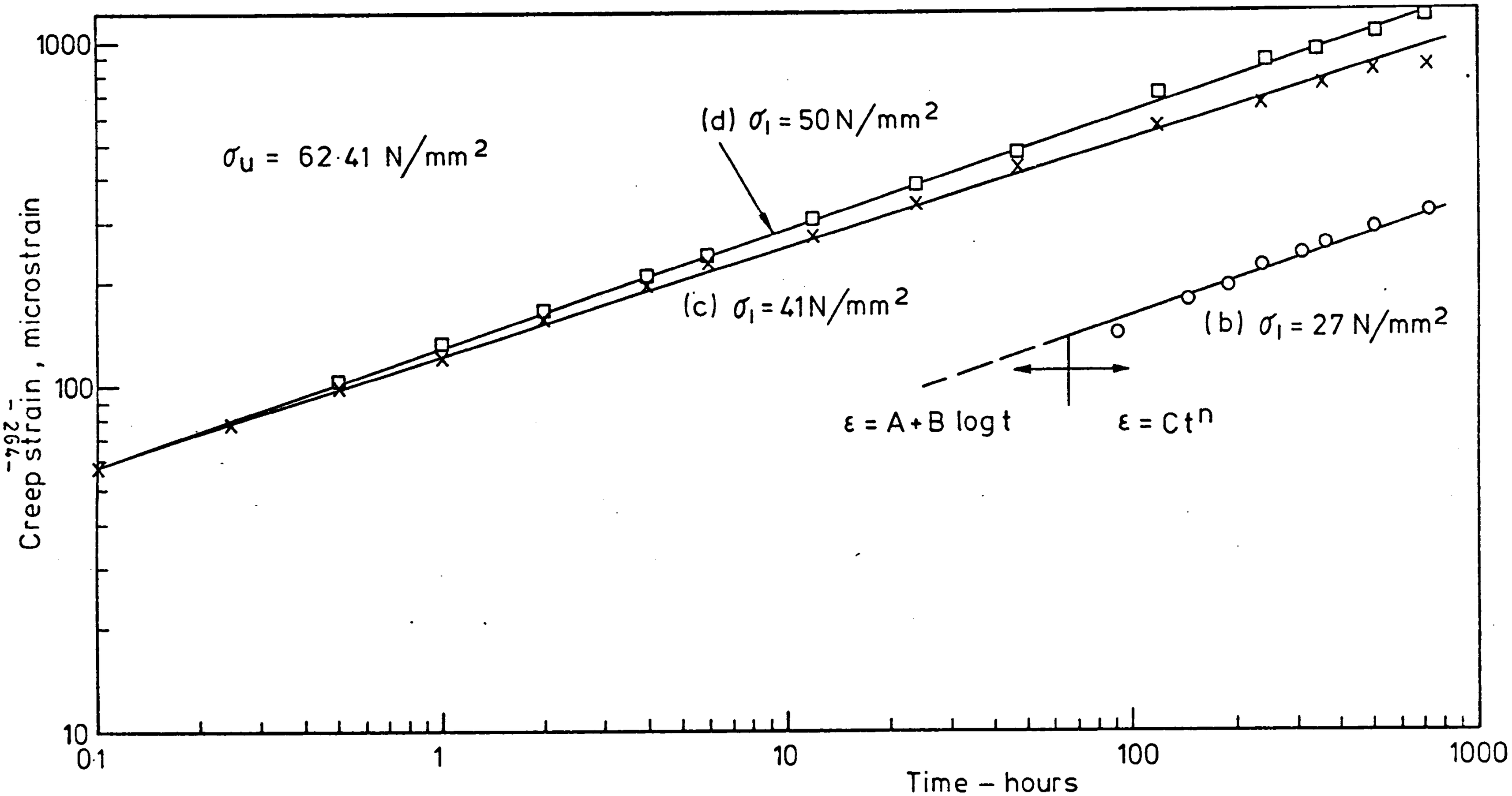

FIG.(6–19) AXIAL CREEP OF DRY GYPSUM IN TRIAXIAL COMPRESSION AT 10 N/mm² CONFINING PRESSURE (LOG–LOG GRAPH)

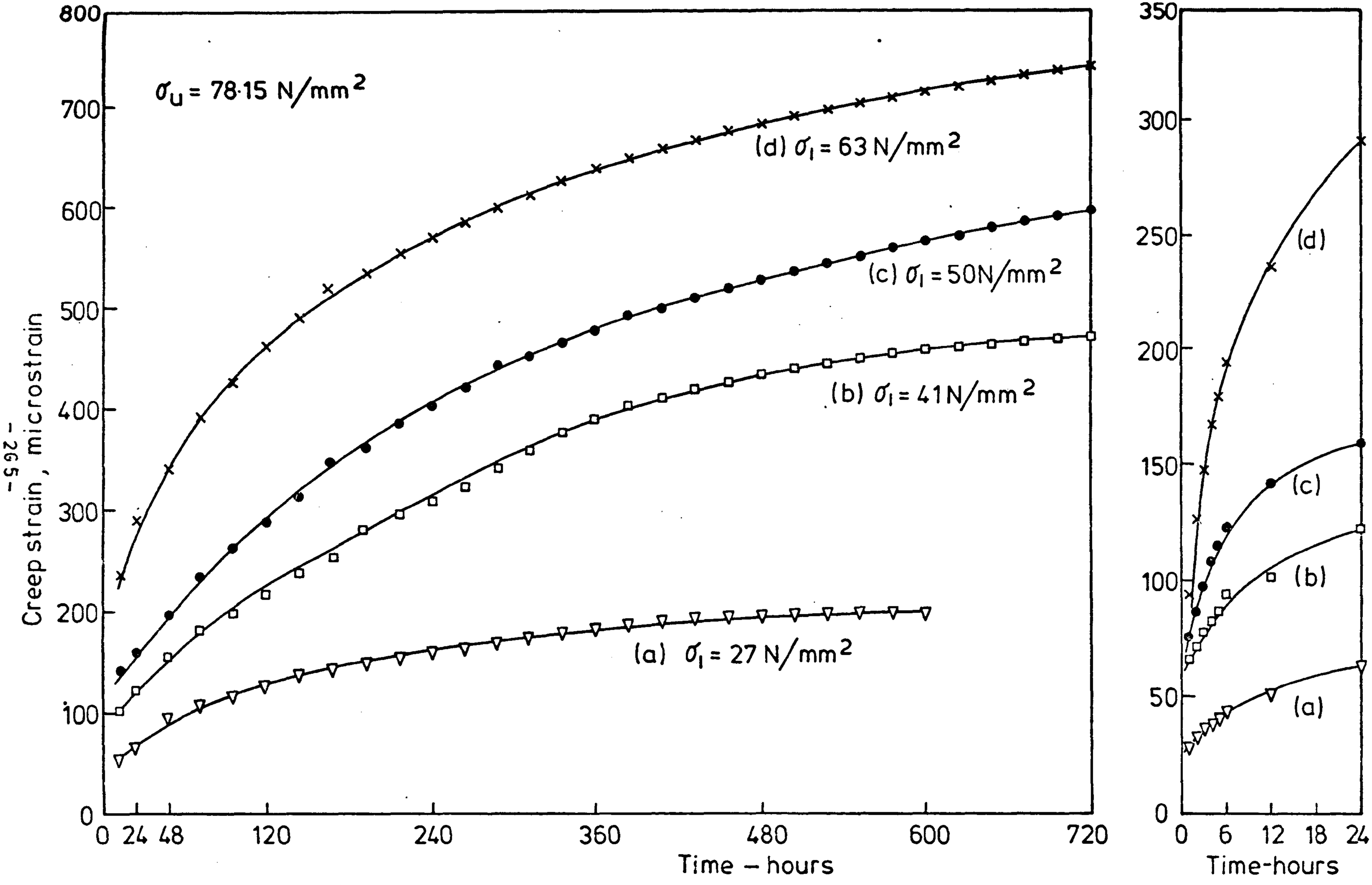

FIG. (6-20) AXIAL CREEP OF DRY GYPSUM IN TRIAXIAL COMPRESSION AT 20N/mm² CONFINING PRESSURE

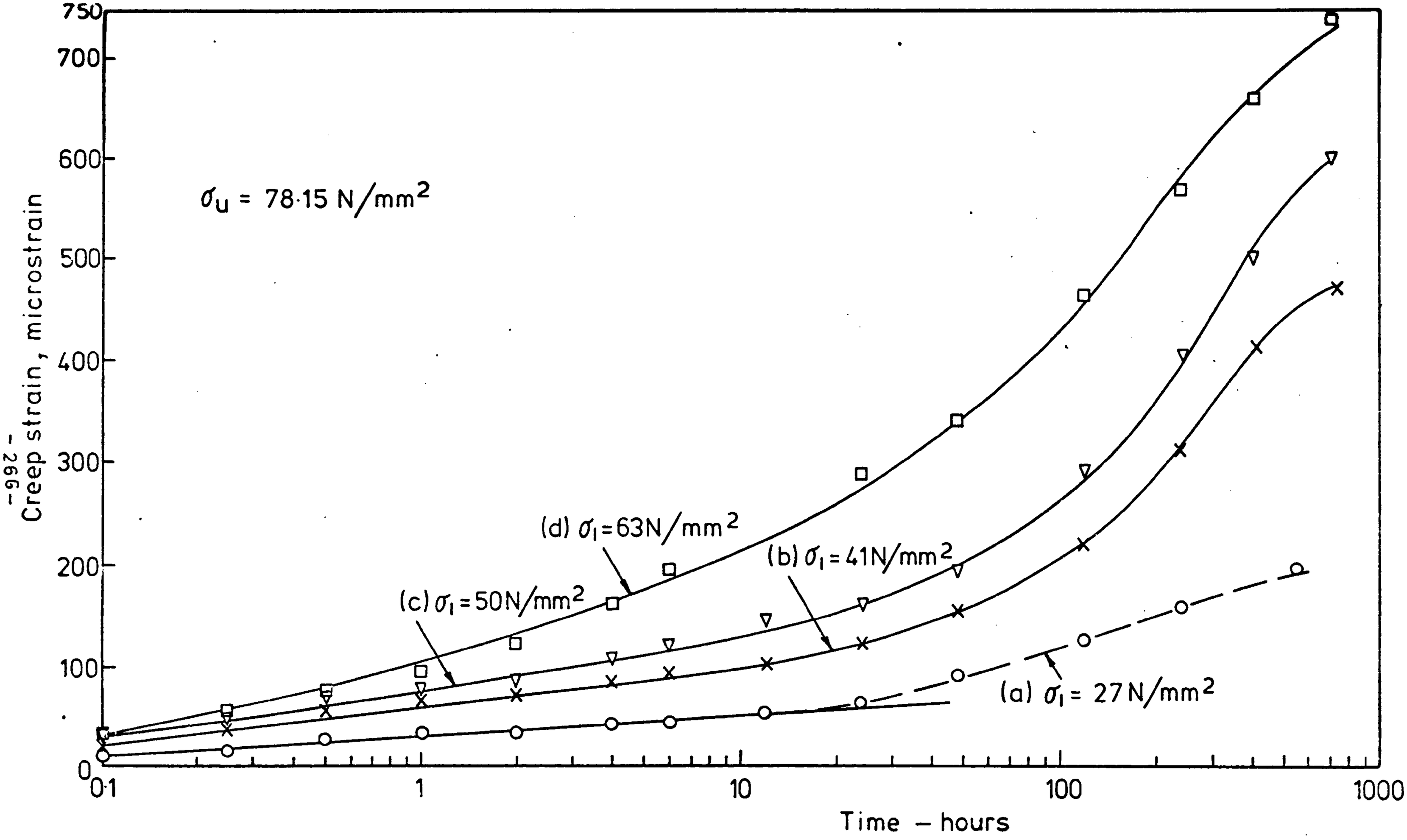

FIG. (6-21) AXIAL CREEP OF DRY GYPSUM IN TRIAXIAL COMPRESSION AT 20N/mm² CONFINING PRESSURE (SEMI-LOG GRAPH)

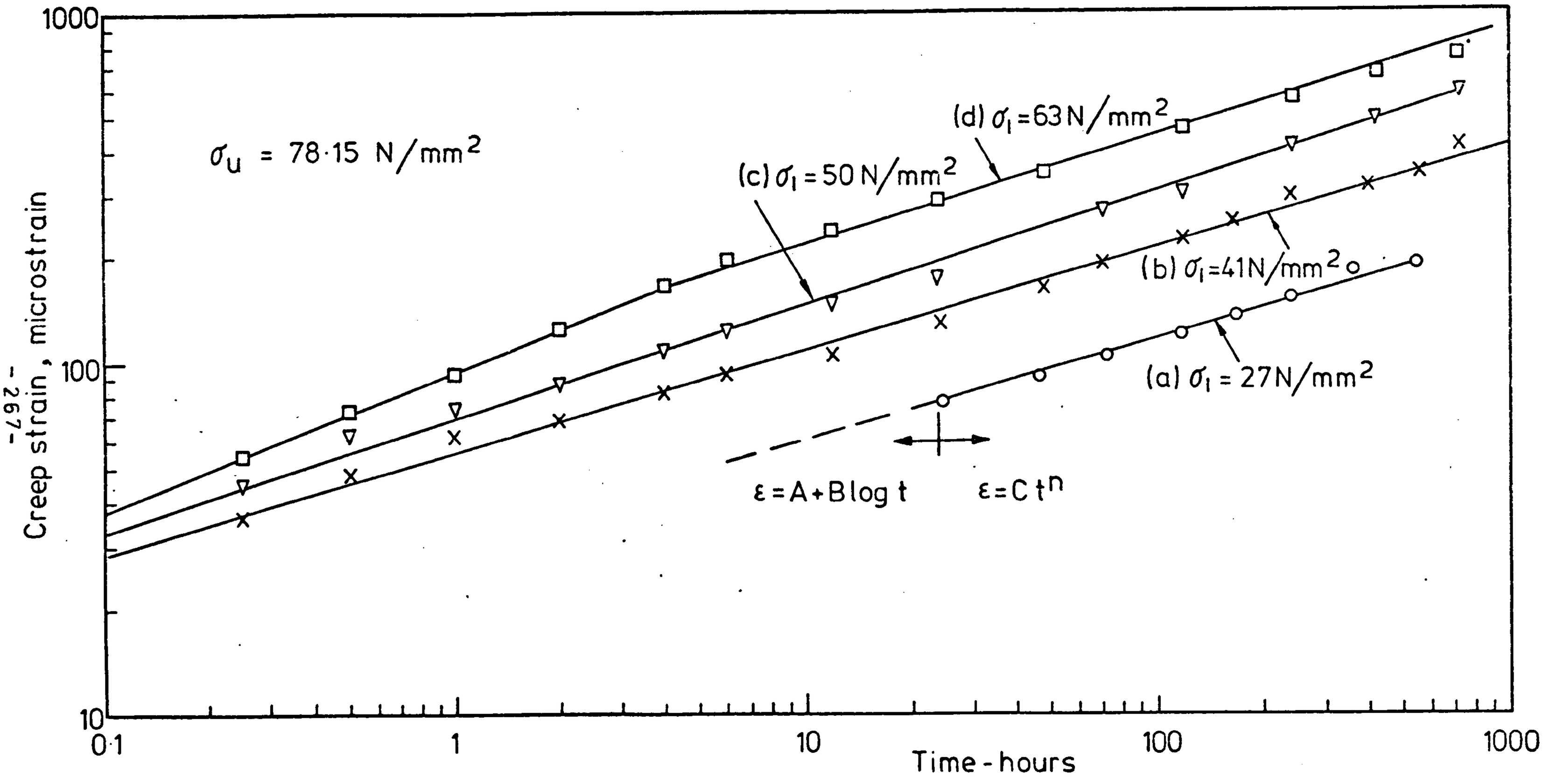

FIG.(6-22) AXIAL CREEP OF DRY GYPSUM IN TRIAXIAL COMPRESSION AT 20N/mm² CONFINING PRESSURE (LOG-LOG GRAPH)

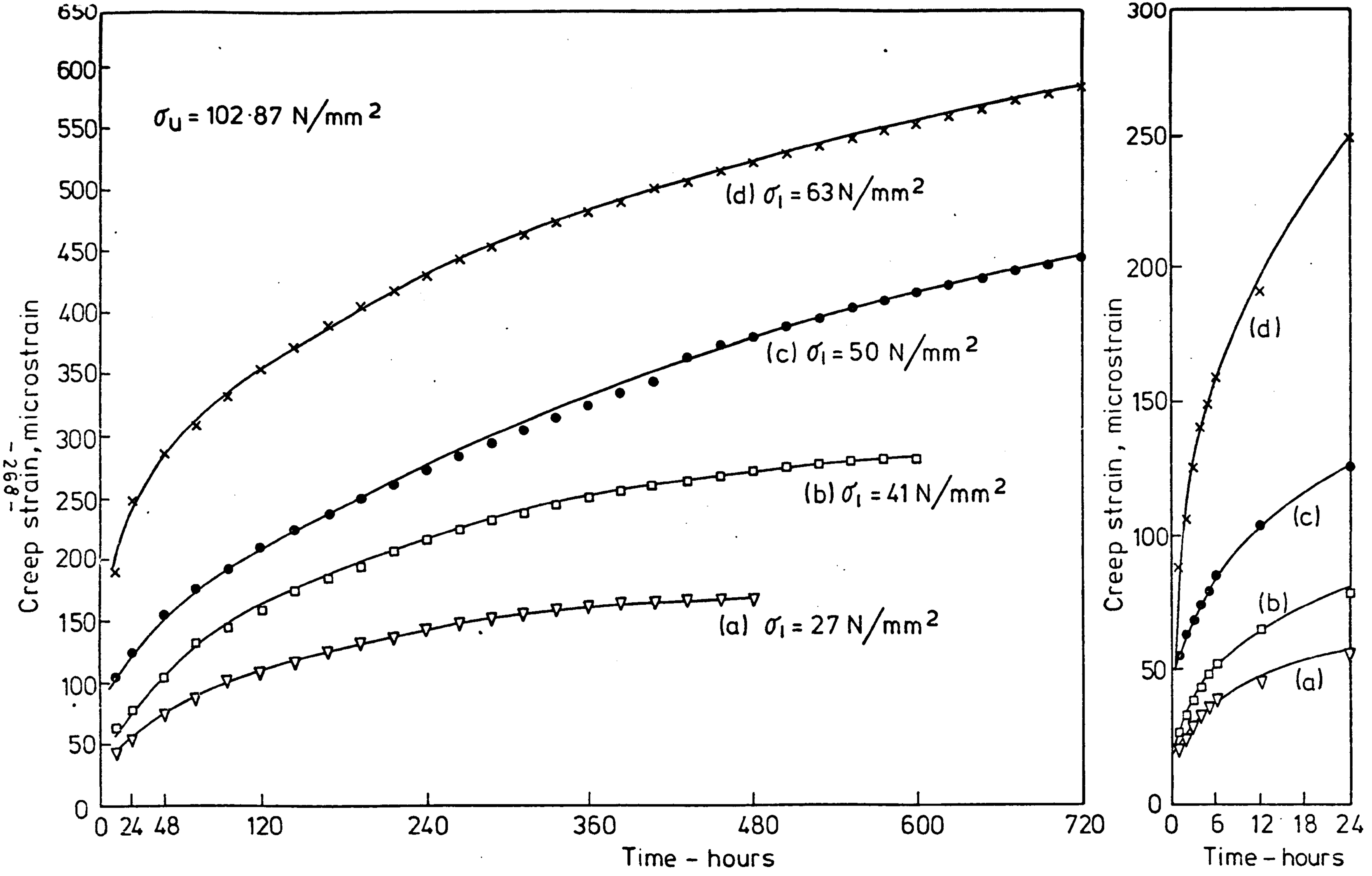

FIG. (6-23) AXIAL CREEP OF DRY GYPSUM IN TRIAXIAL COMPRESSION AT 30 N/mm² CONFINING PRESSURE

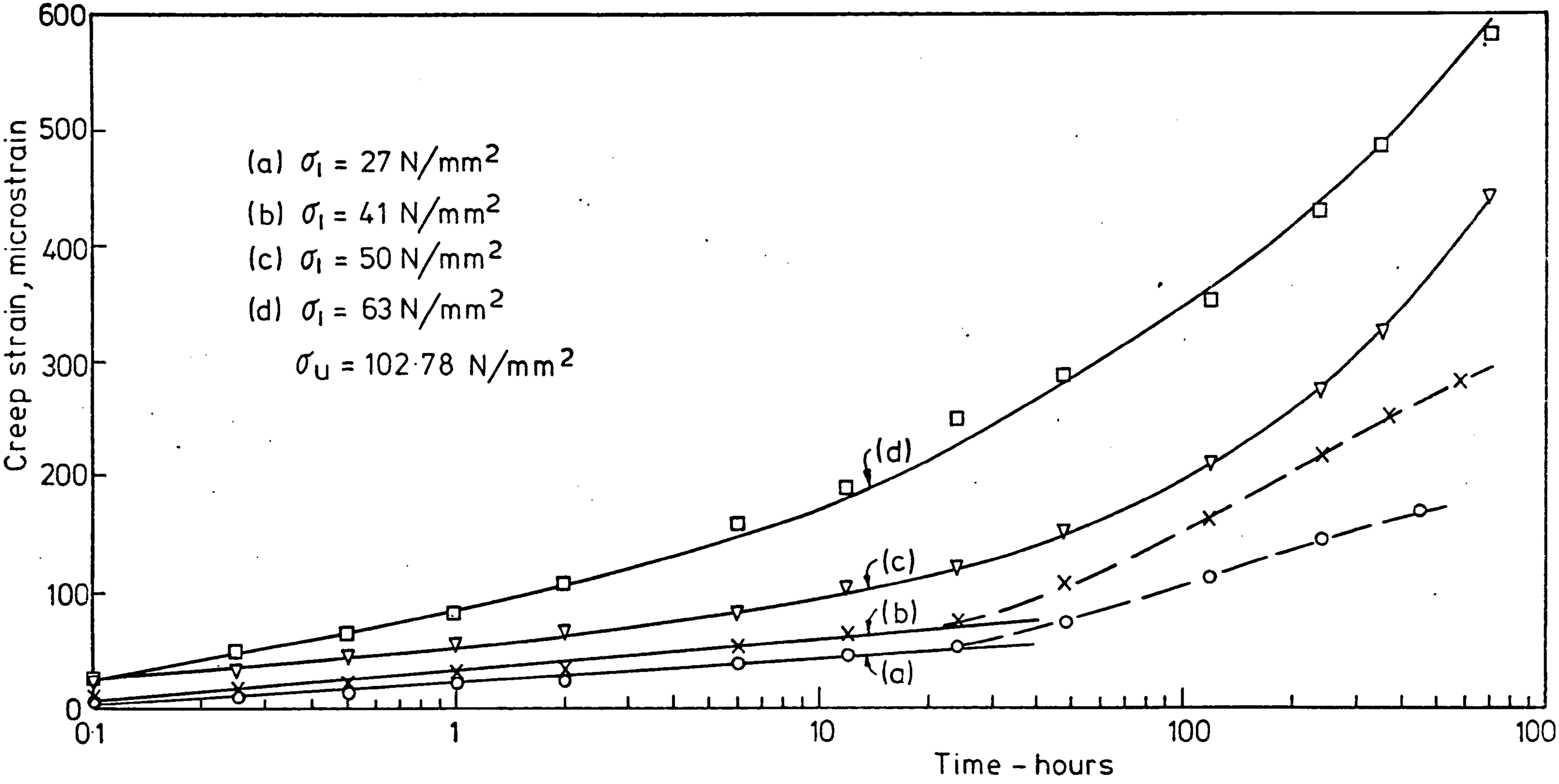

FIG. (6-24) AXIAL CREEP OF DRY GYPSUM IN TRIAXIAL COMPRESSION AT 30N/mm² CONFINING PRESSURE (SEMI-LOG GRAPH)

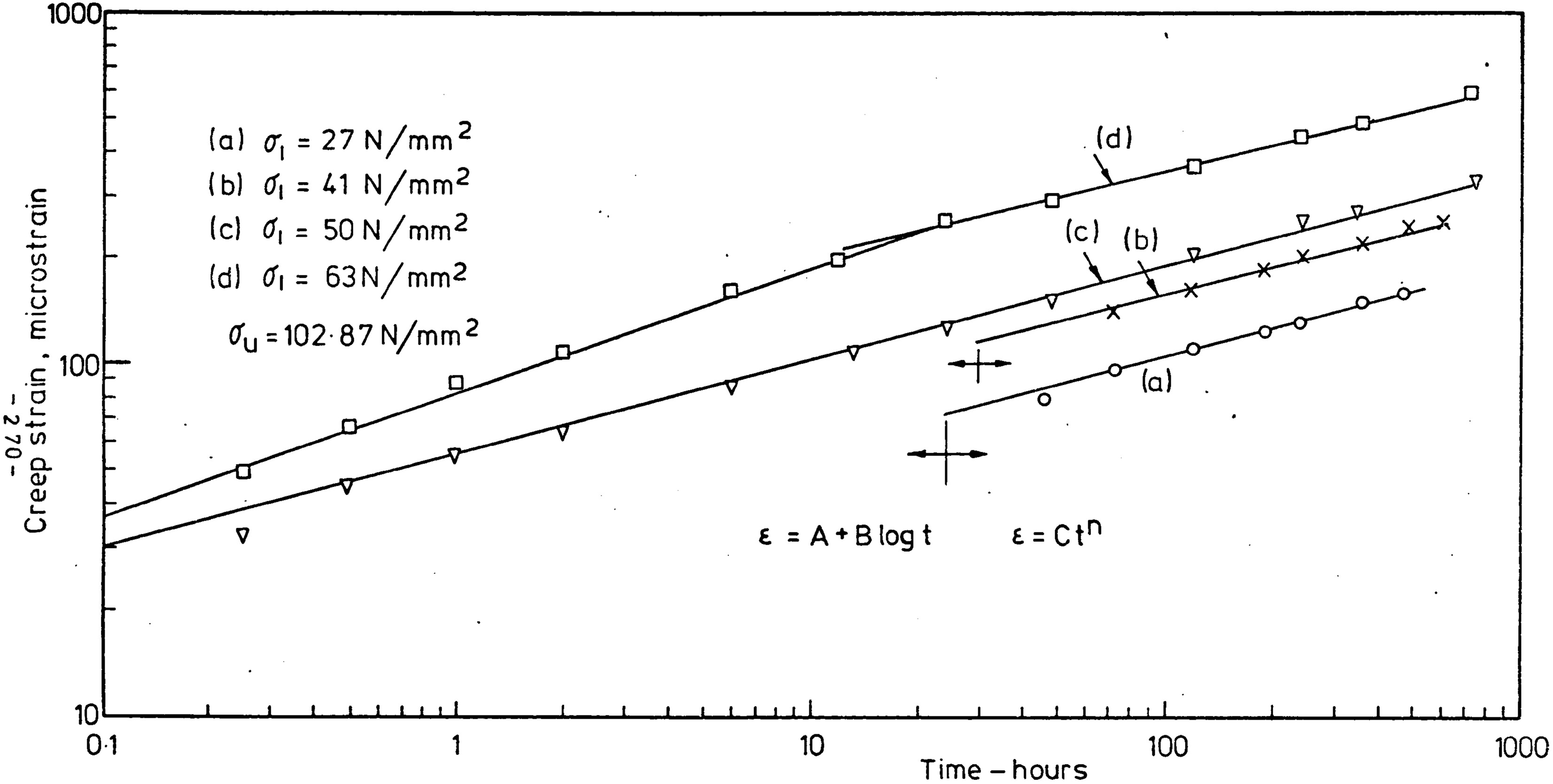

FIG. (6–25) AXIAL CREEP OF DRY GYPSUM IN TRIAXIAL COMPRESSION AT 30N/mm² CONFINING PRESSURE (LOG - LOG GRAPH)

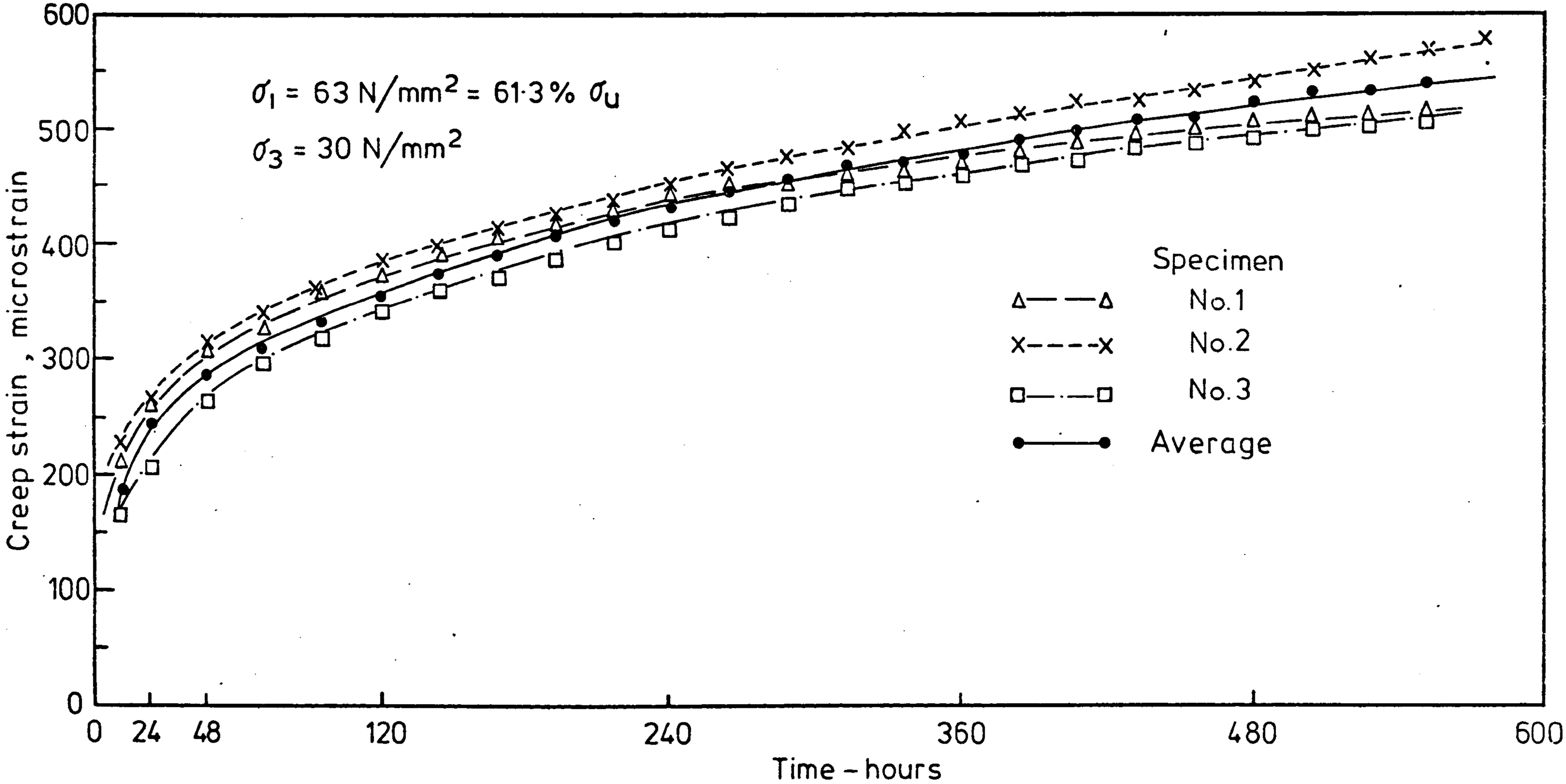

FIG. (6-26) CREEP CURVE OF DRY GYPSUM IN TRIAXIAL COMPRESSION TAKEN AS AN AVERAGE OF THREE TESTS

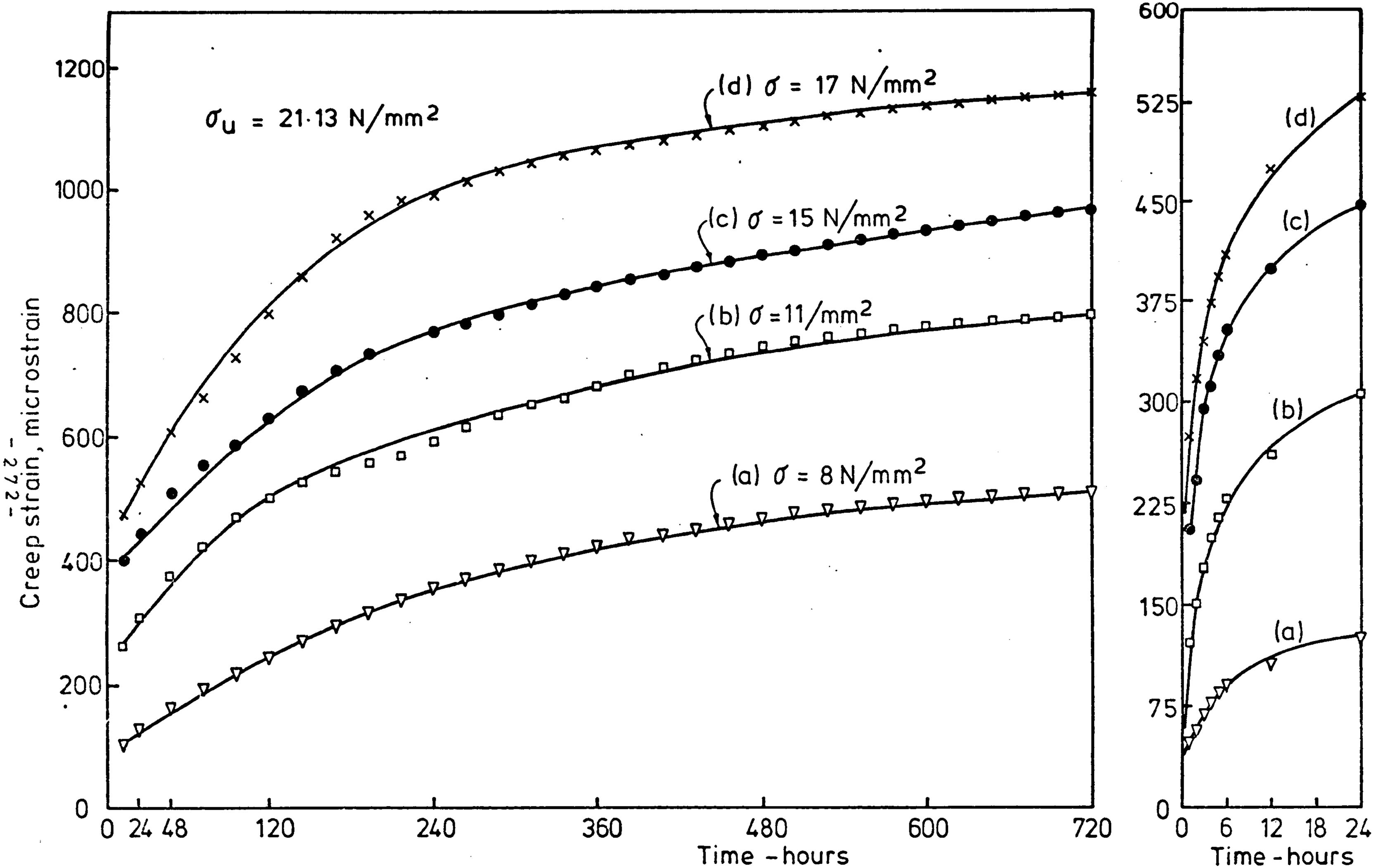

FIG. (6-27) AXIAL CREEP OF SATURATED GYPSUM IN UNIAXIAL COMPRESSION

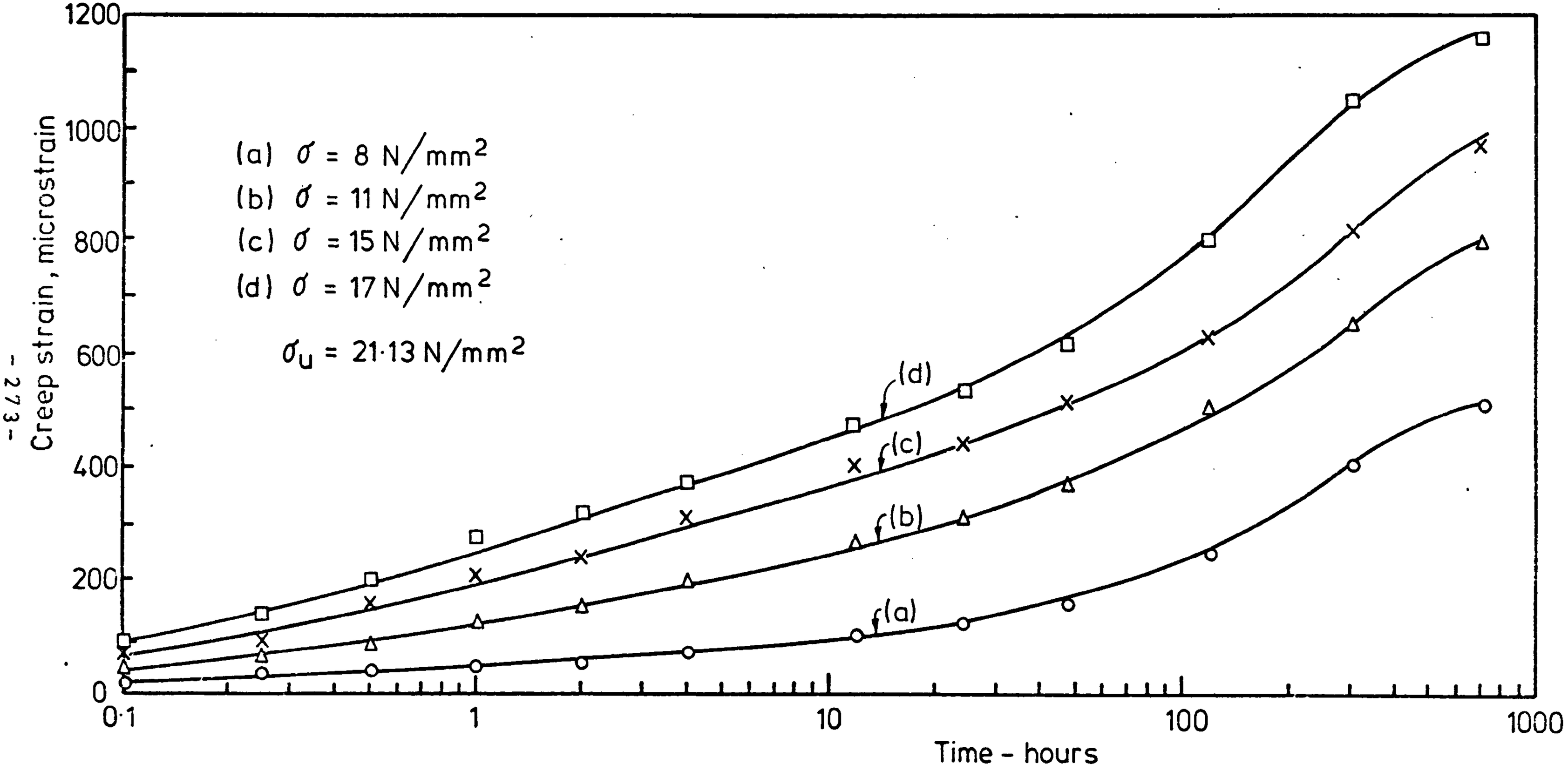

FIG. (6-28) AXIAL CREEP OF SATURATED GYPSUM IN UNIAXIAL COMPRESSION (SEMI-LOG GRAPH)

(SEMI-LOG GRAPH)

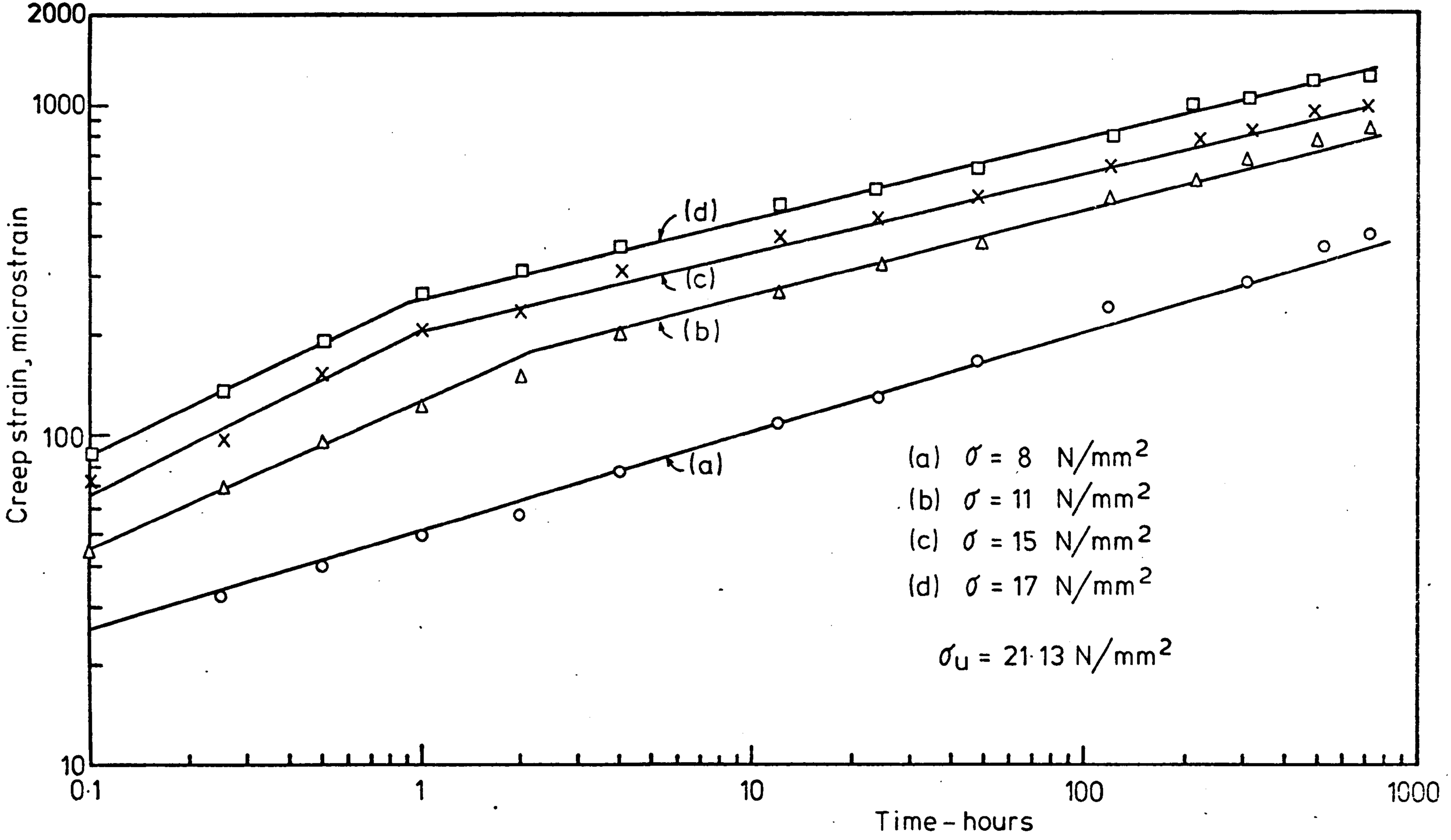

FIG. (6-29) AXIAL CREEP OF SATURATED GYPSUM IN UNIAXIAL COMPRESSION (LOG-LOG GRAPH)

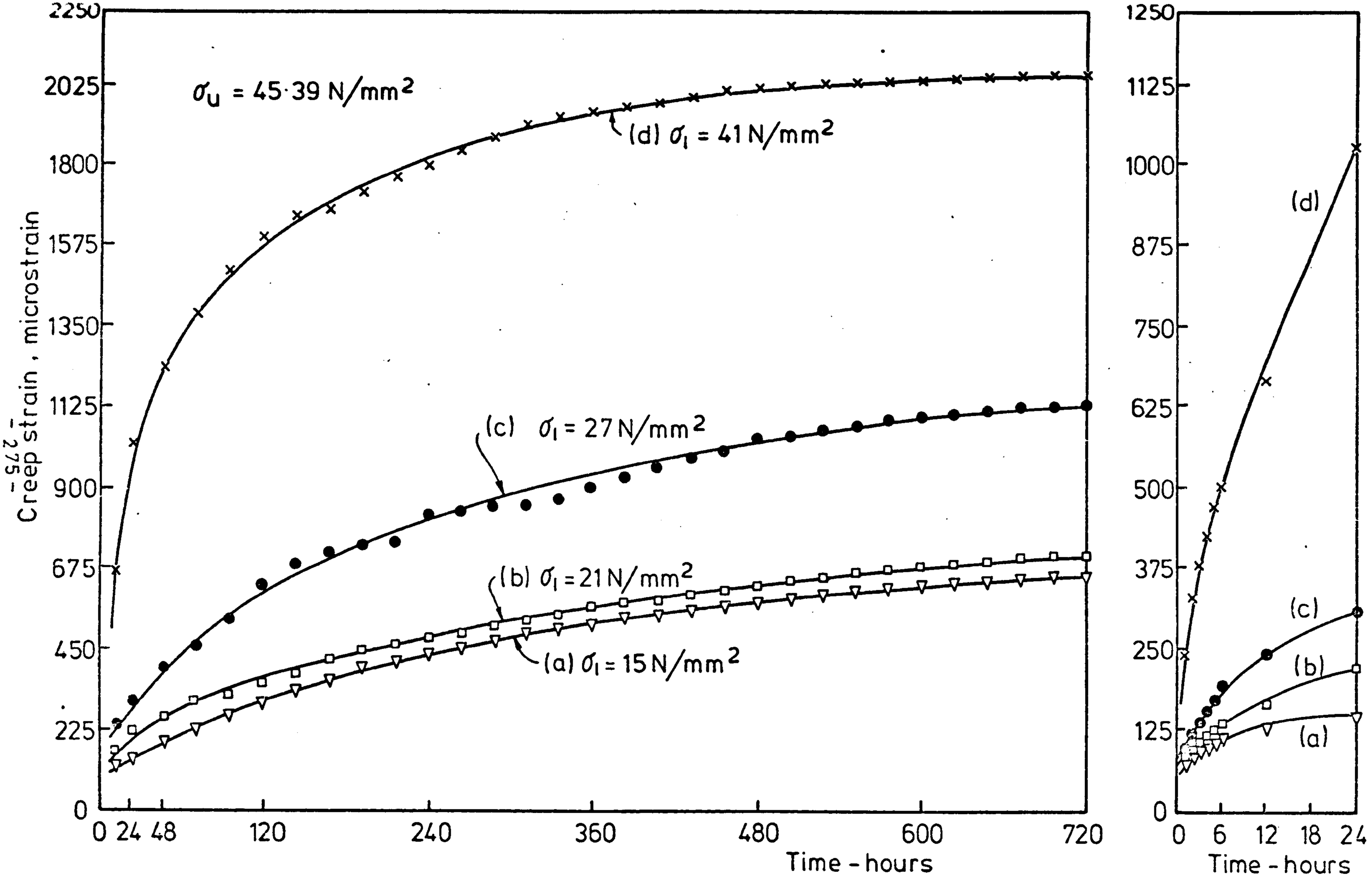

FIG. (6-30) AXIAL CREEP OF SATURATED GYPSUM IN TRIAXIAL COMPRESSION AT 10N/mm² CONFINING PRESSURE

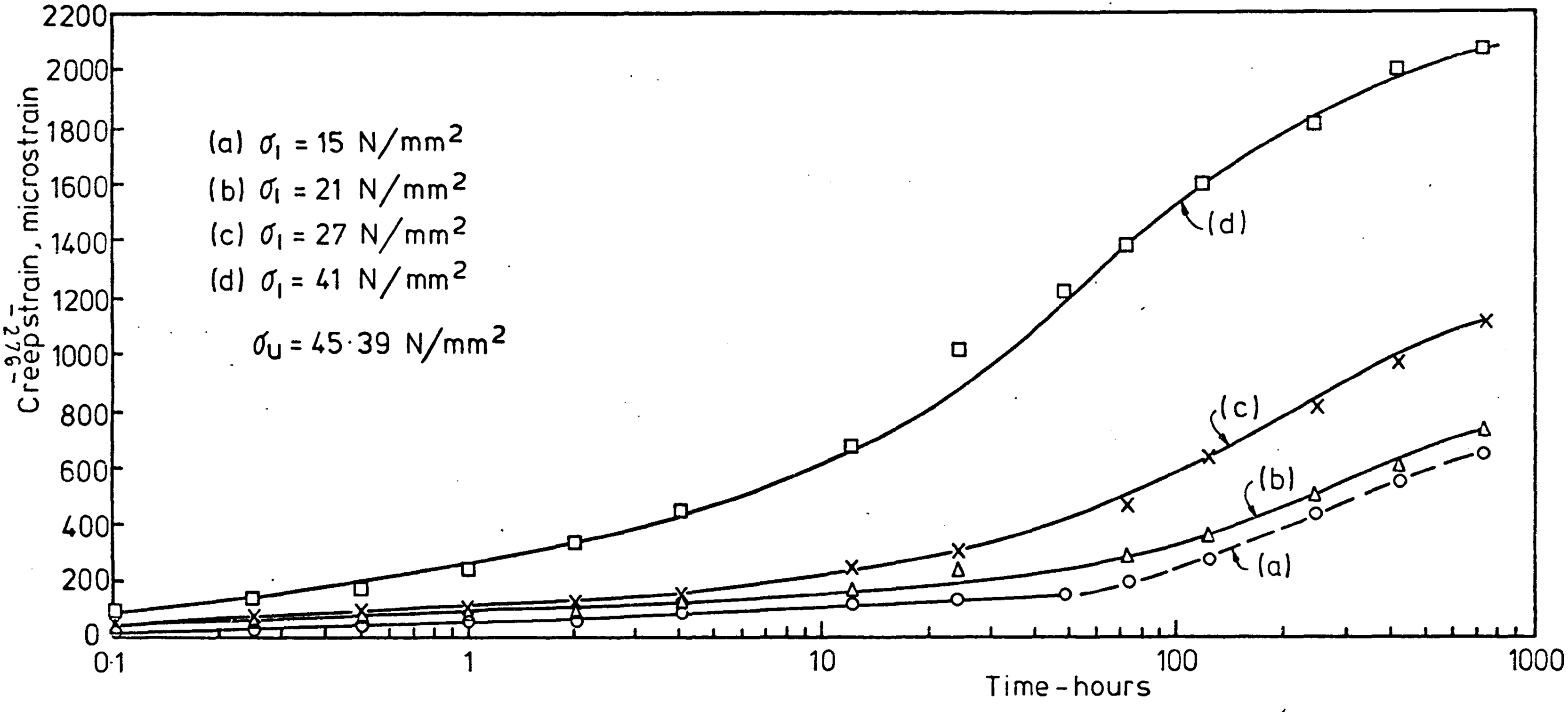

FIG. (6-31) AXIAL CREEP OF SATURATED GYPSUM IN TRIAXIAL COMPRESSION AT 10 N/mm² CONFINING PRESSURE (SEMI-LOG GRAPH)

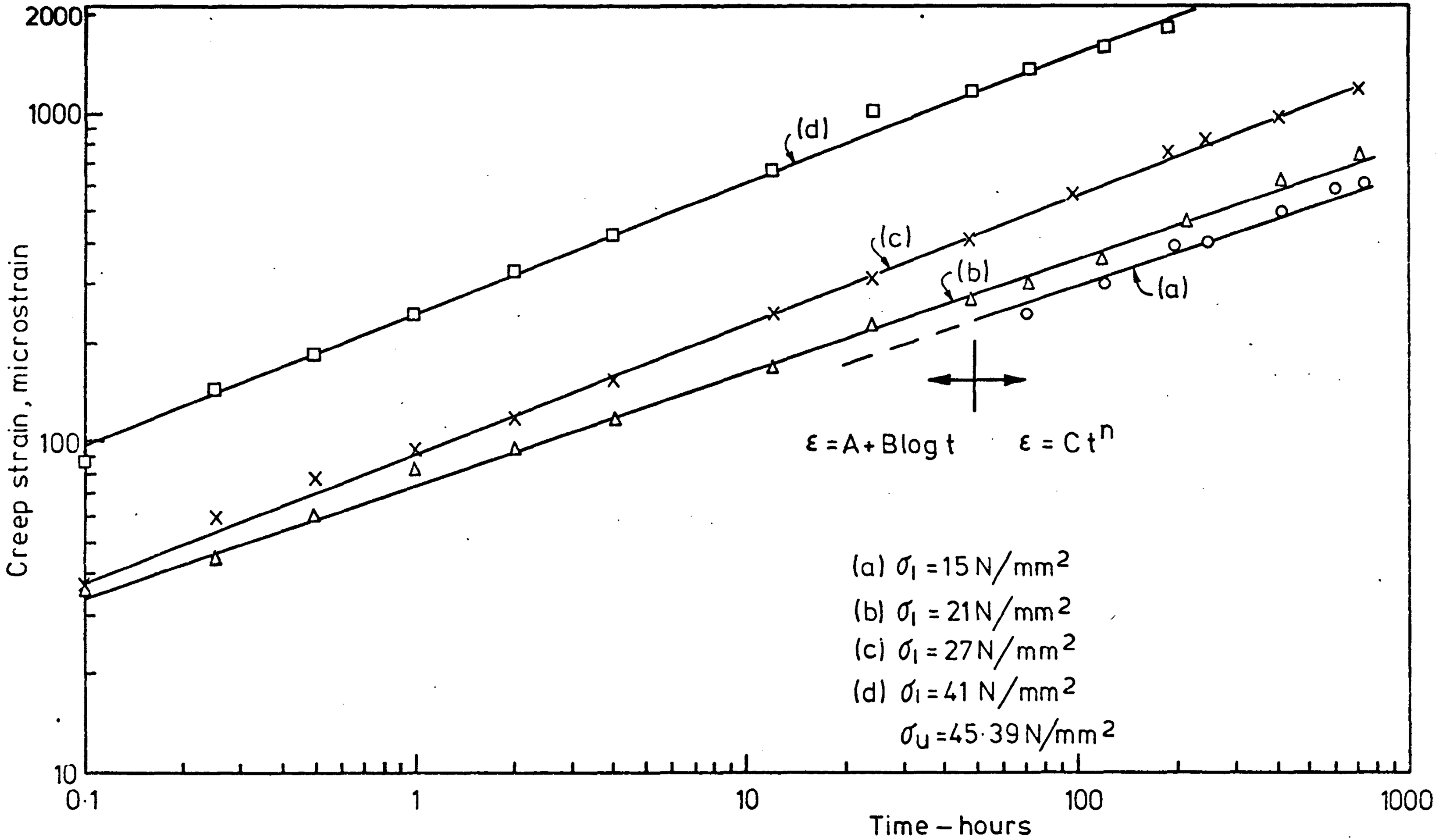

FIG. (6-32) AXIAL CREEP OF SATURATED GYPSUM IN TRIAXIAL COMPRESSION AT 10 N/mm² CONFINING PRESSURE (LOG-LOG GRAPH)

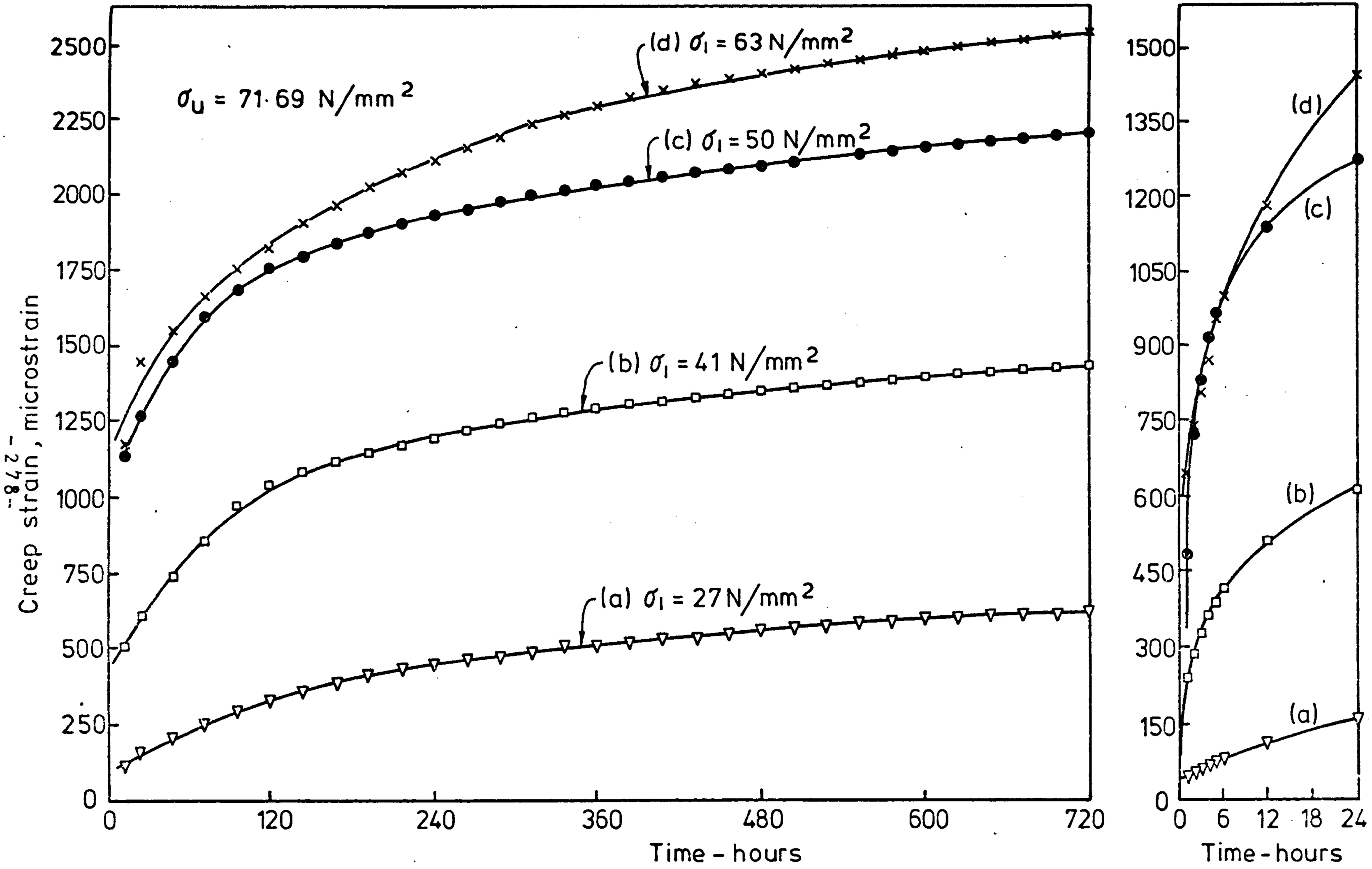

FIG.(6-33) AXIAL CREEP OF SATURATED GYPSUM IN TRIAXIAL COMPRESSION AT 20N/mm² CONFINING PRESSURE

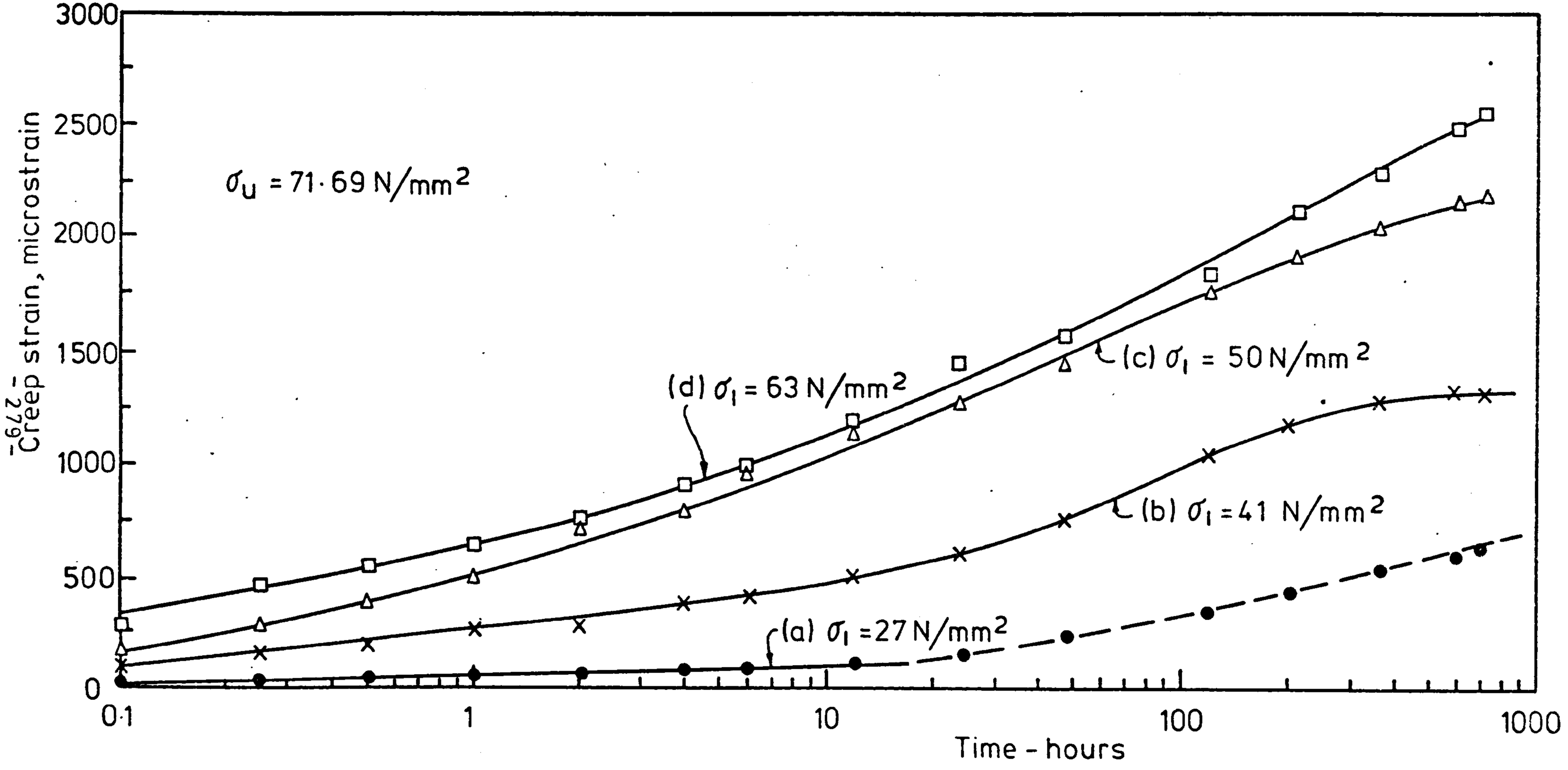

FIG. (6–34) AXIAL CREEP OF SATURATED GYPSUM IN TRIAXIAL COMPRESSION AT 20N/mm² CONFINING PRESSURE (SEMI-LOG GRAPH)

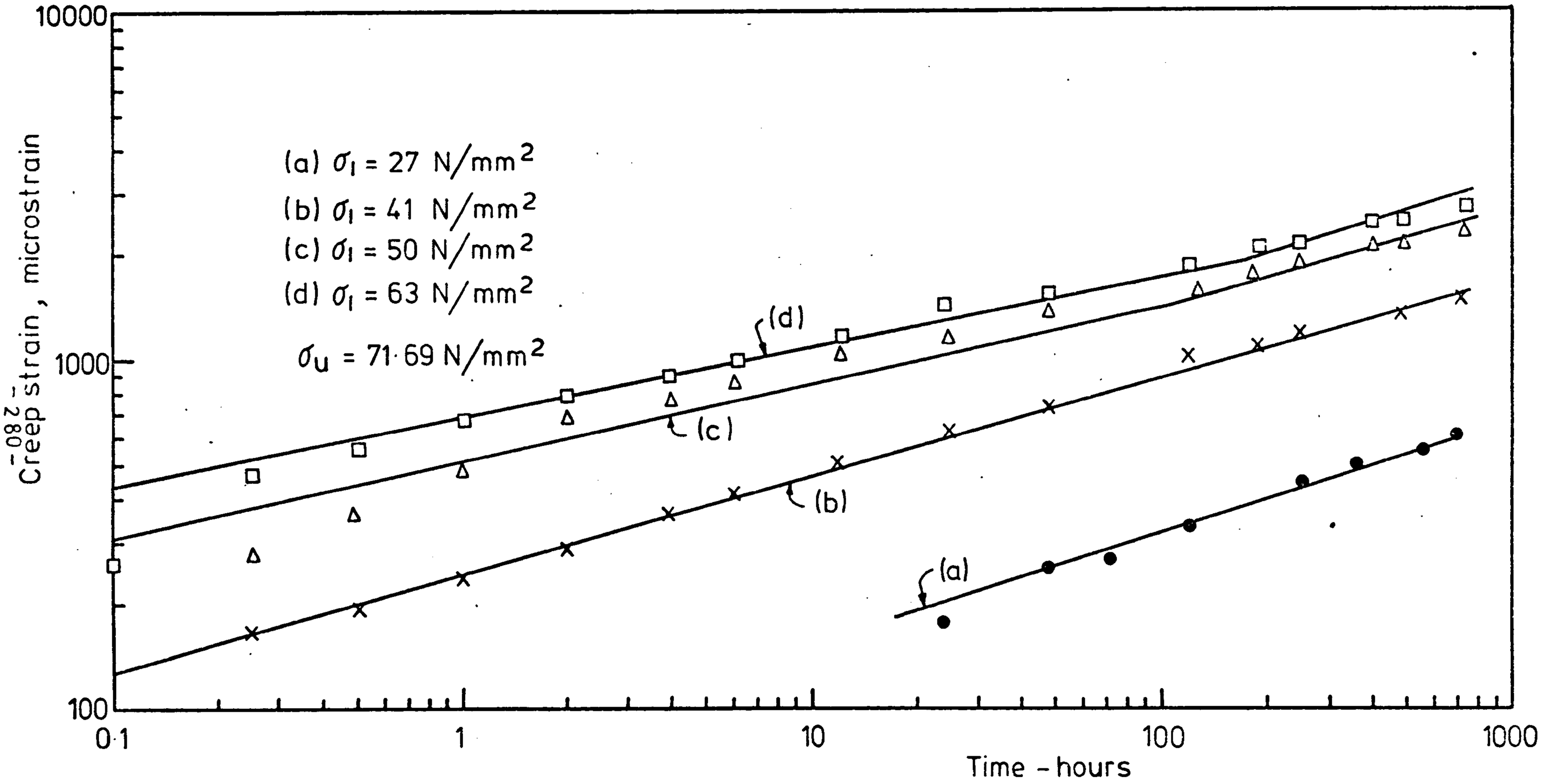

FIG.(6-35) AXIAL CREEP OF SATURATED GYPSUM IN TRIAXIAL COMPRESSION AT 20 N/mm^2 CONFINING PRESSURE (LOG-LOG GRAPH)

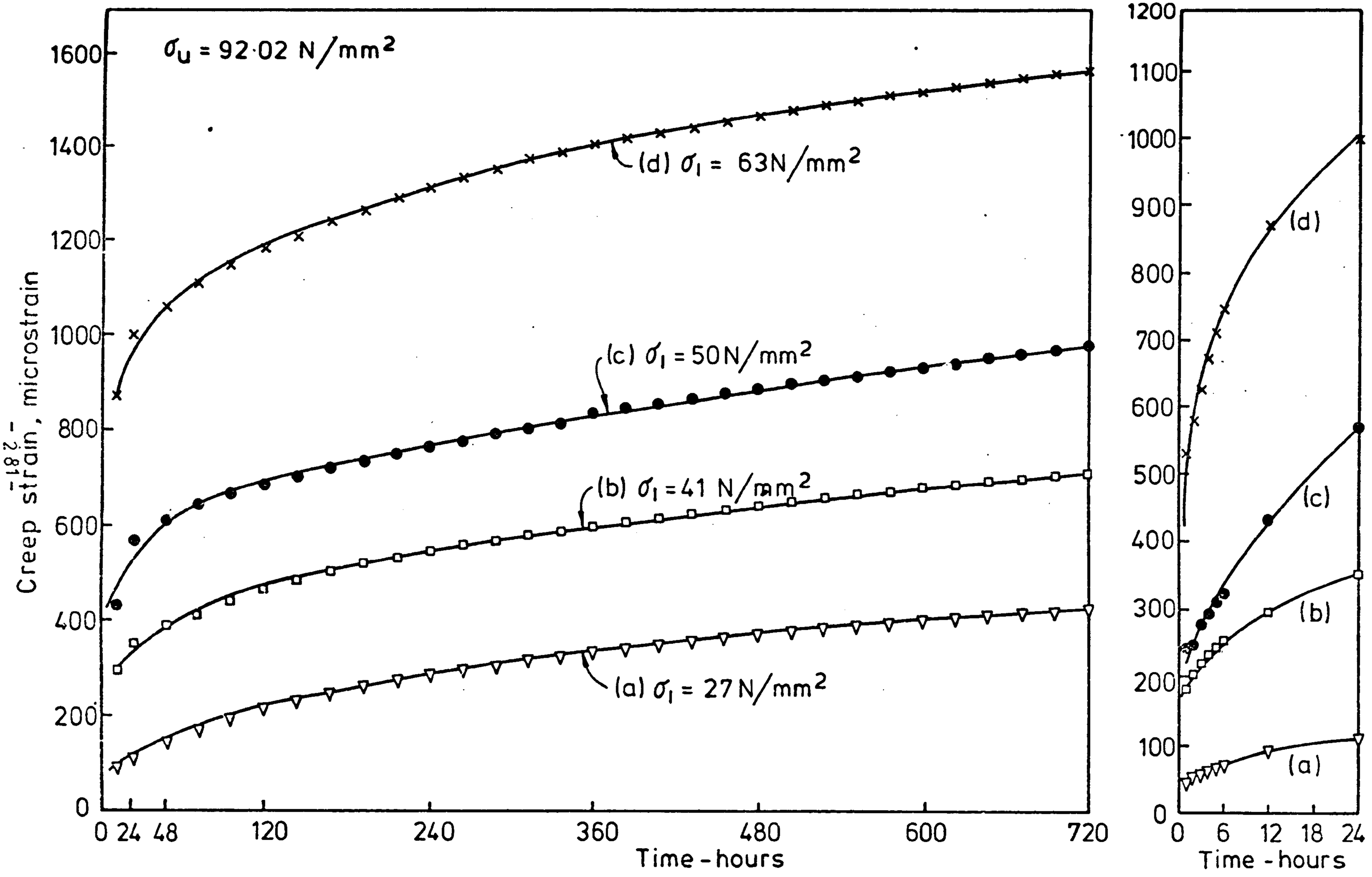

FIG. (6-36) AXIAL CREEP OF SATURATED GYPSUM IN TRIAXIAL COMPRESSION AT 30 N/mm² CONFINING PRESSURE

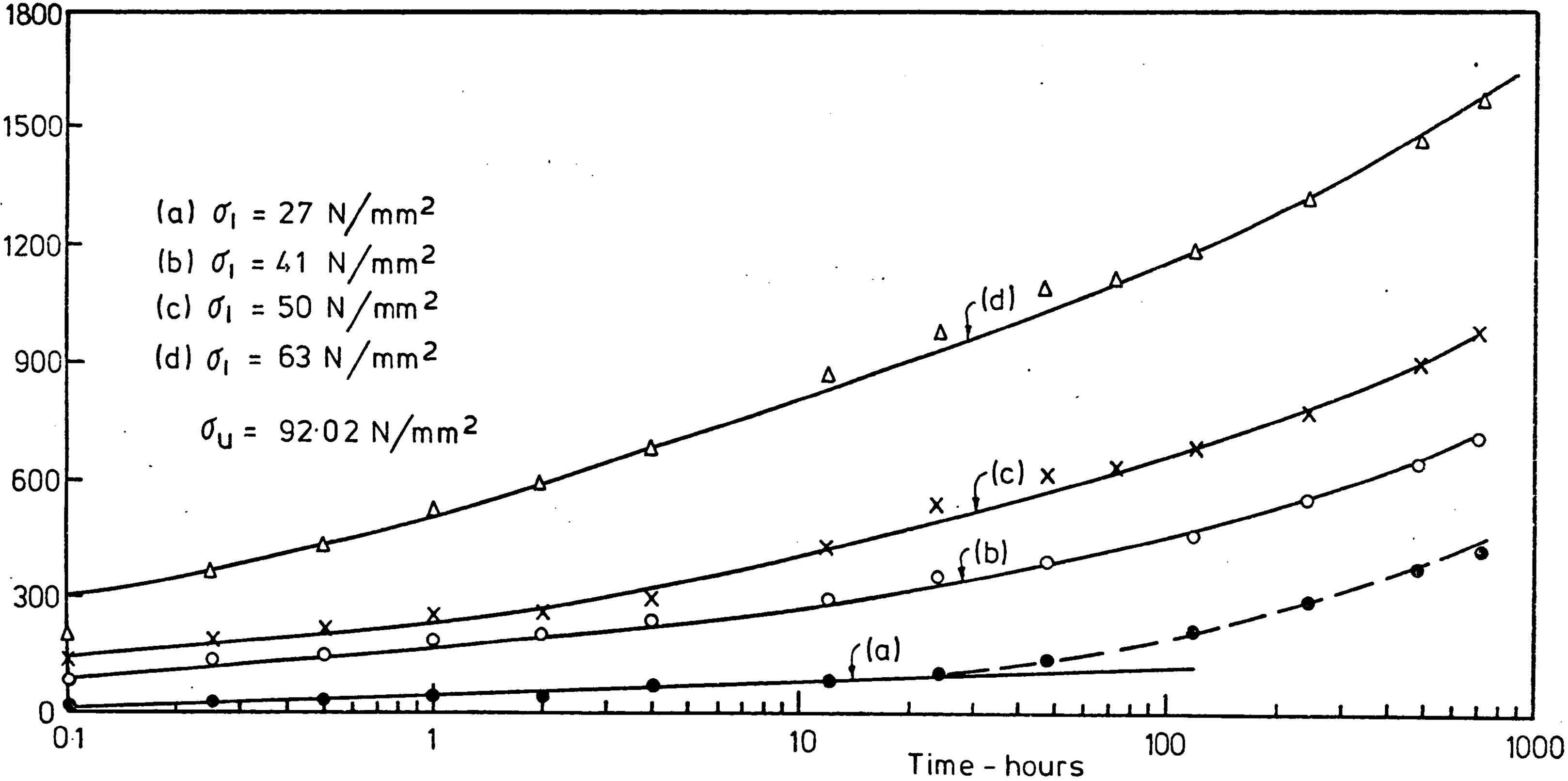

FIG. (6-37) AXIAL CREEP OF SATURATED GYPSUM IN TRIAXIAL COMPRESSION AT 30 N/mm² CONFINING PRESSURE (SEMI-LOG GRAPH)

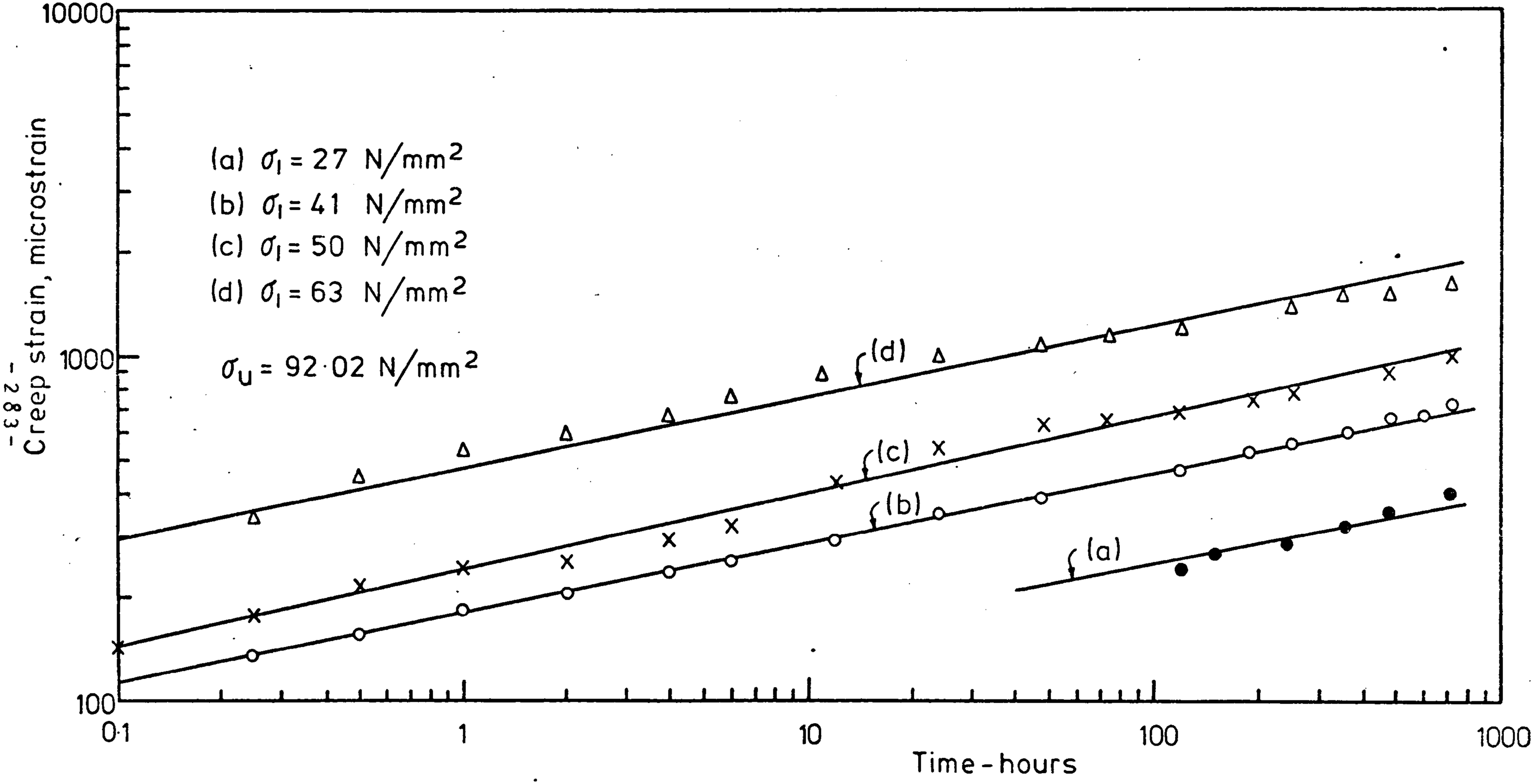

FIG.(6-38) AXIAL CREEP OF SATURATED GYPSUM IN TRIAXIAL COMPRESSION AT 30 N/mm² CONFINING PRESSURE (LOG-LOG GRAPH)

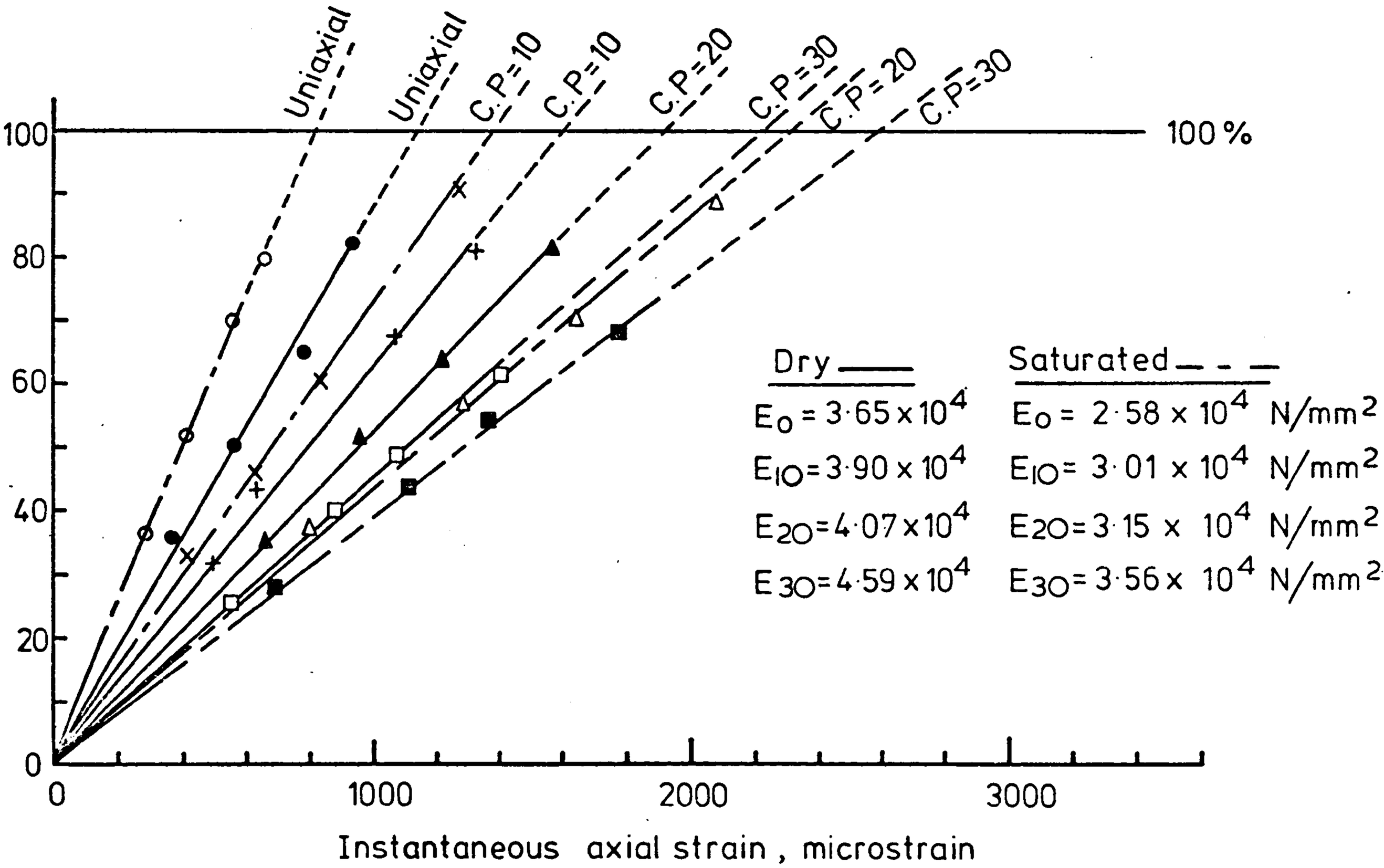

FIG. (6-39) DETERMINATION OF MODULUS OF ELASTICITY OF GYPSUM AT VARIOUS σ_3

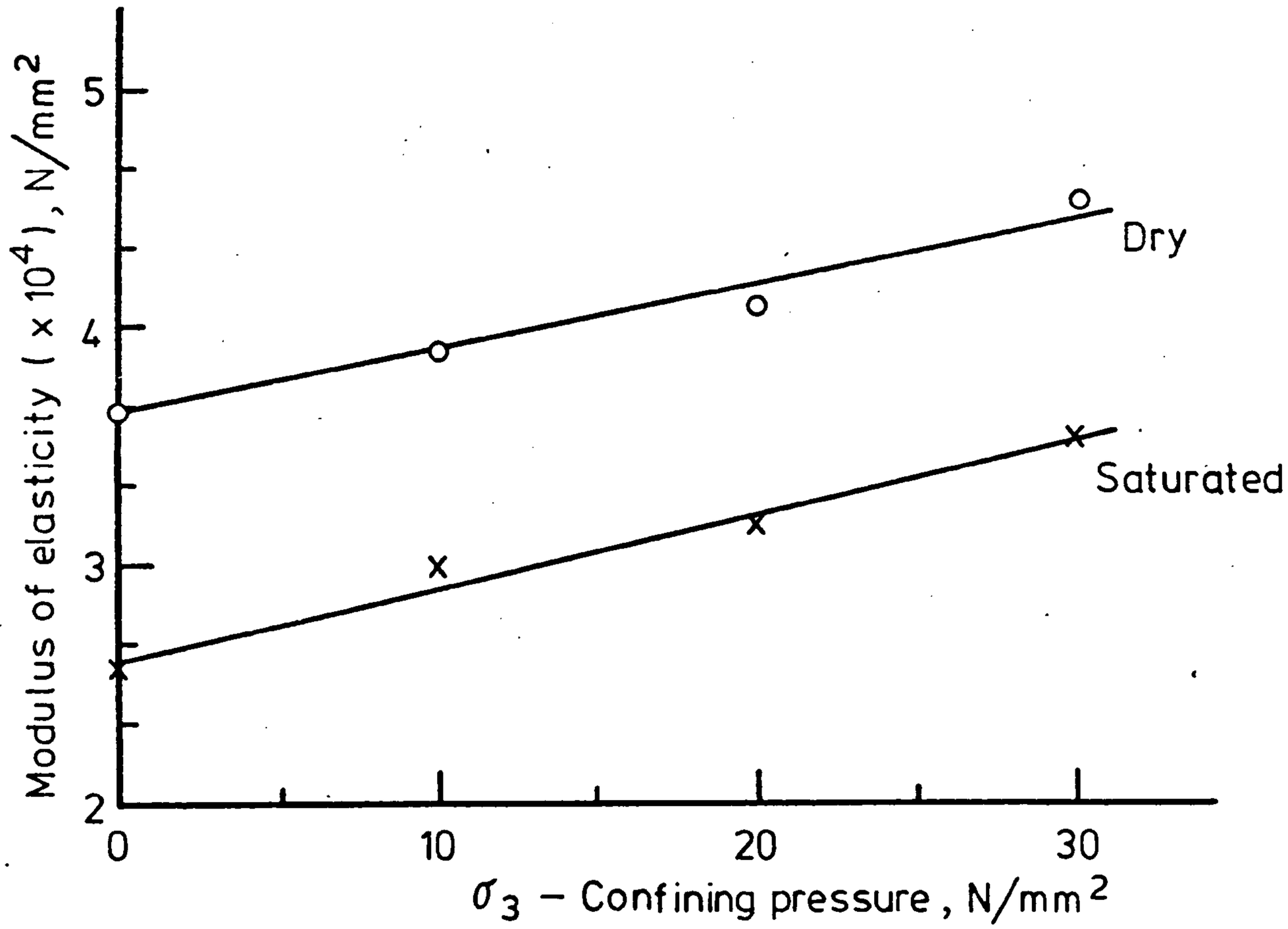

FIG. (6-40) MODULUS OF ELASTICITY IN DRY AND SATURATED CONDITIONS AT VARIOUS CONFINING PRESSURES

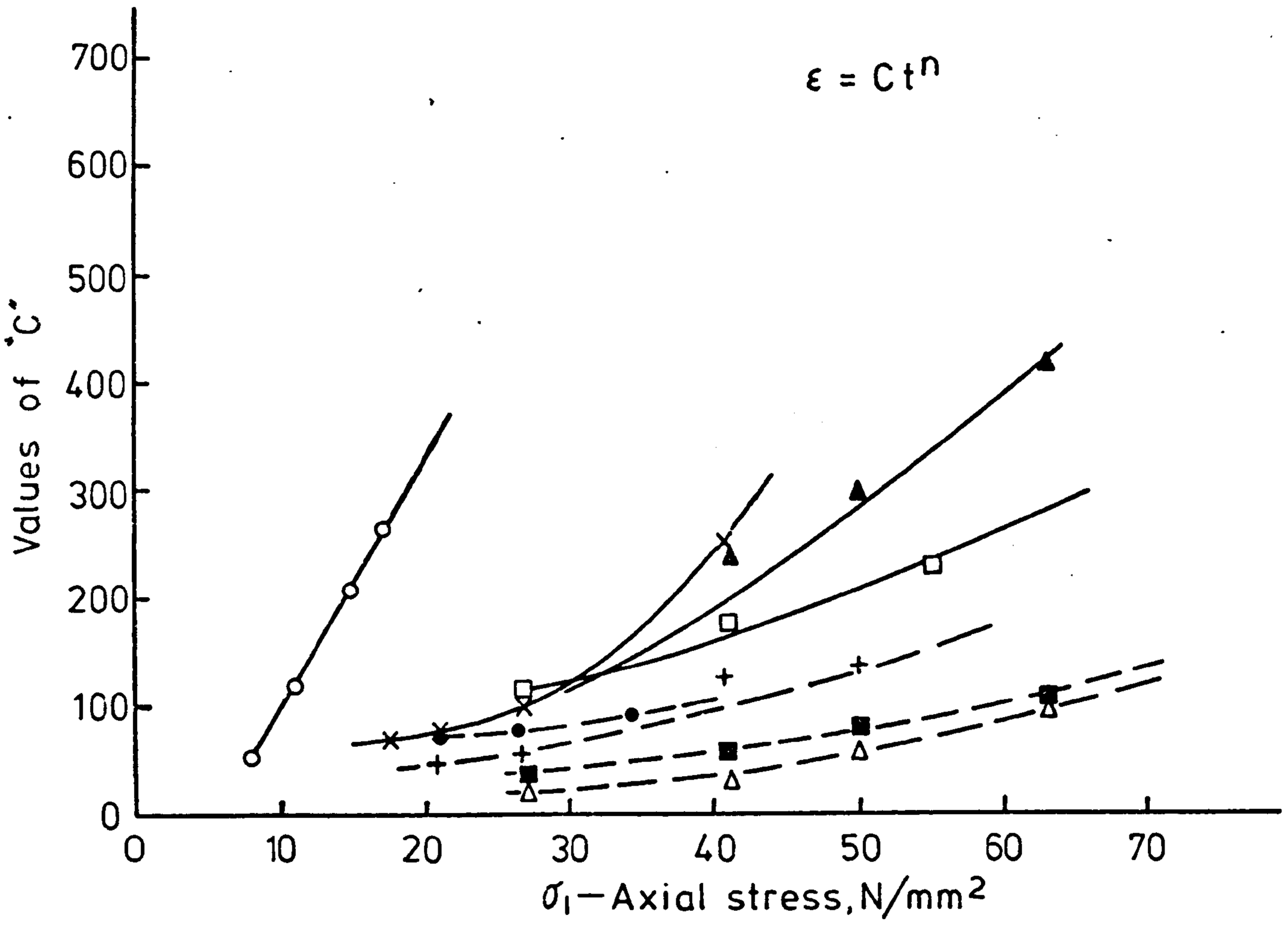

FIG. (6-41) VALUES OF "C" Vs. σ_1 AT CONSTANT CONFINING PRESSURE IN AXIAL CREEP

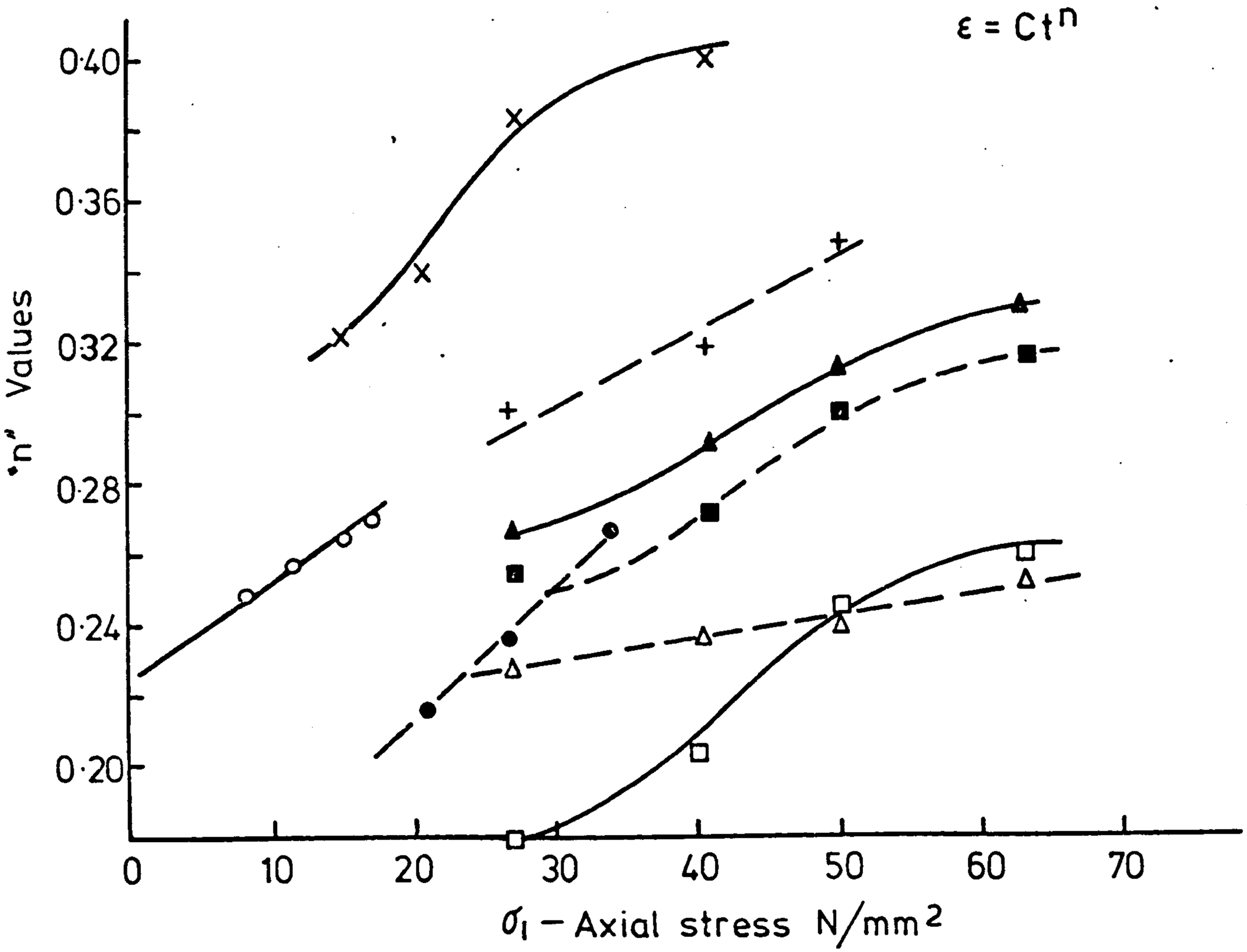

FIG. (6-42) VALUES OF "n" Vs. σ_1 AT CONSTANT CONFINING PRESSURE IN AXIAL CREEP

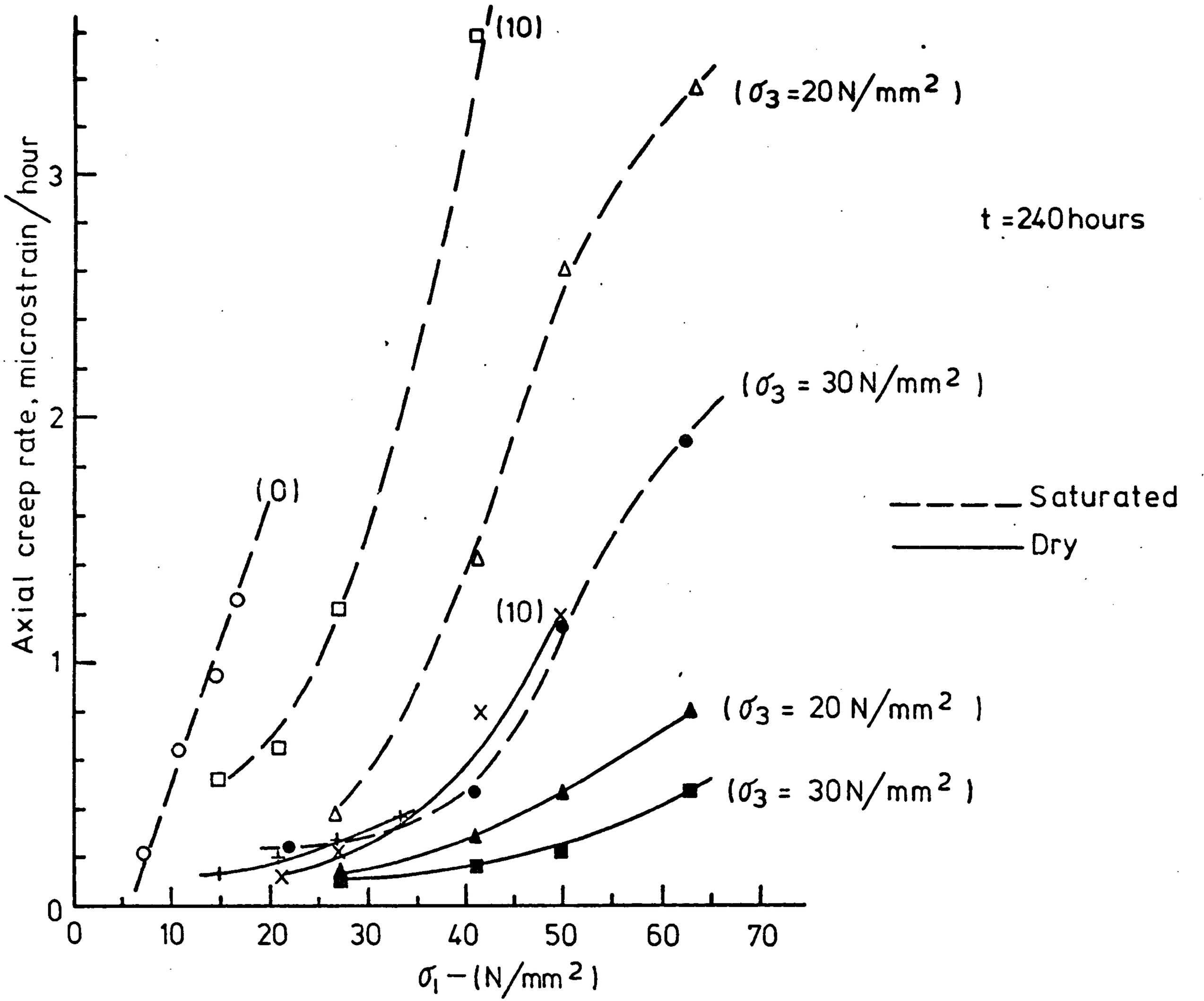

FIG. (6-43) AXIAL CREEP RATE Vs. σ_1 AT CONSTANT σ_3 IN BOTH DRY AND SATURATED CONDITIONS

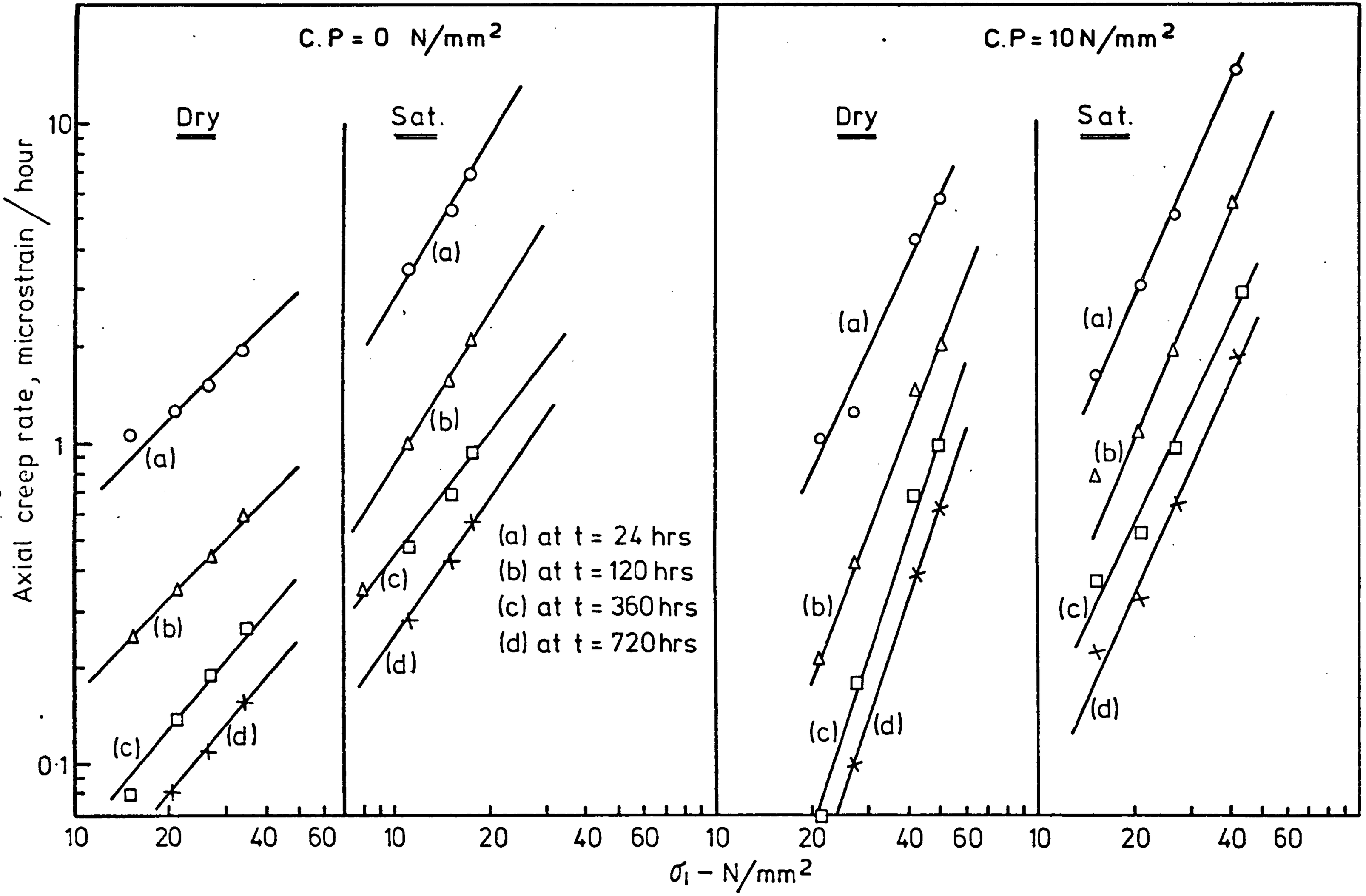

FIG. (6-44) AXIAL CREEP RATE Vs σ_1 AT VARIOUS σ_3 (LOG-LOG GRAPH)

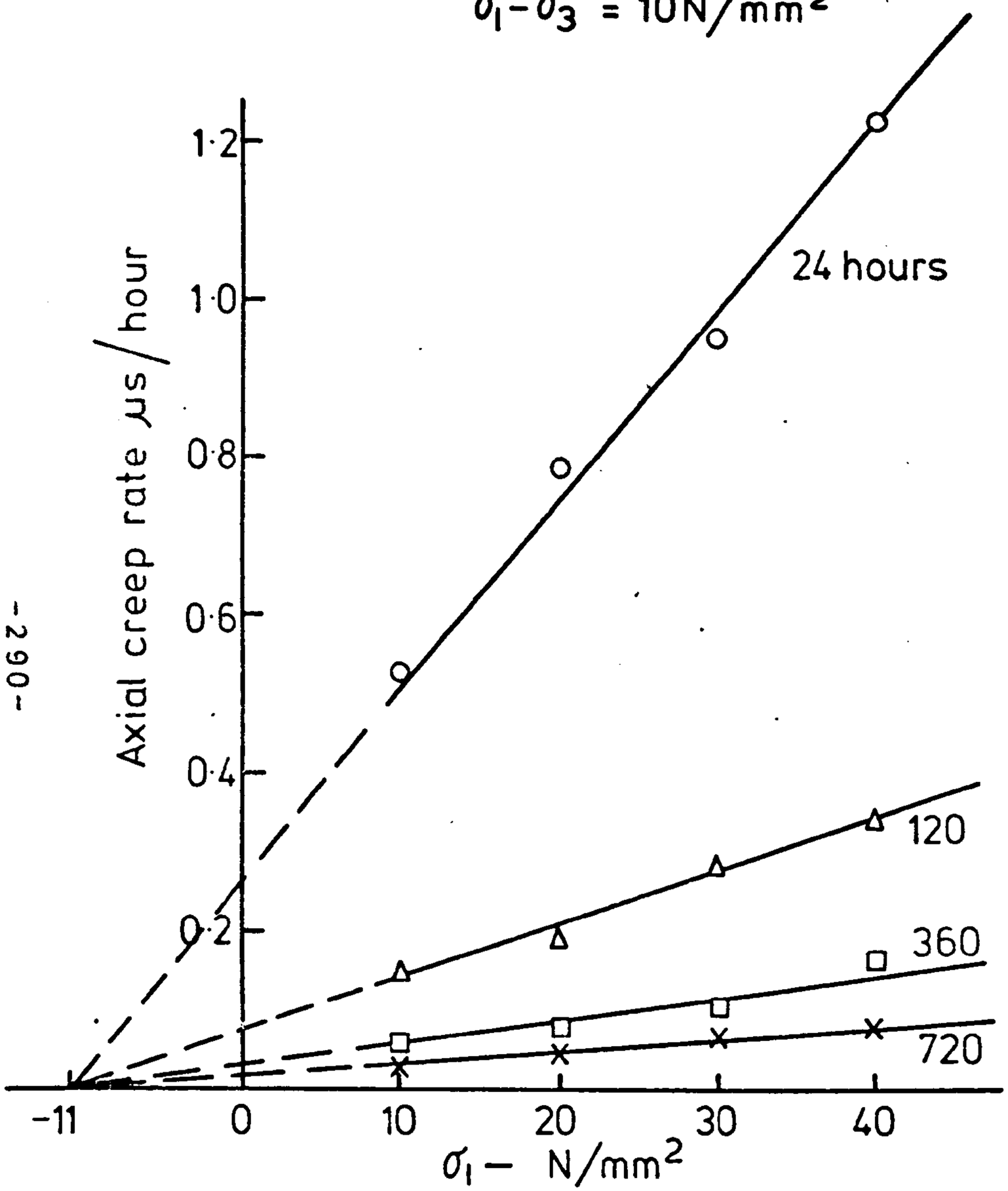

FIG. (6-45) AXIAL CREEP RATE Vs. σ_1 AT CONSTANT $(\sigma_1 - \sigma_3) = 10\,N/mm^2$ IN DRY CONDITION

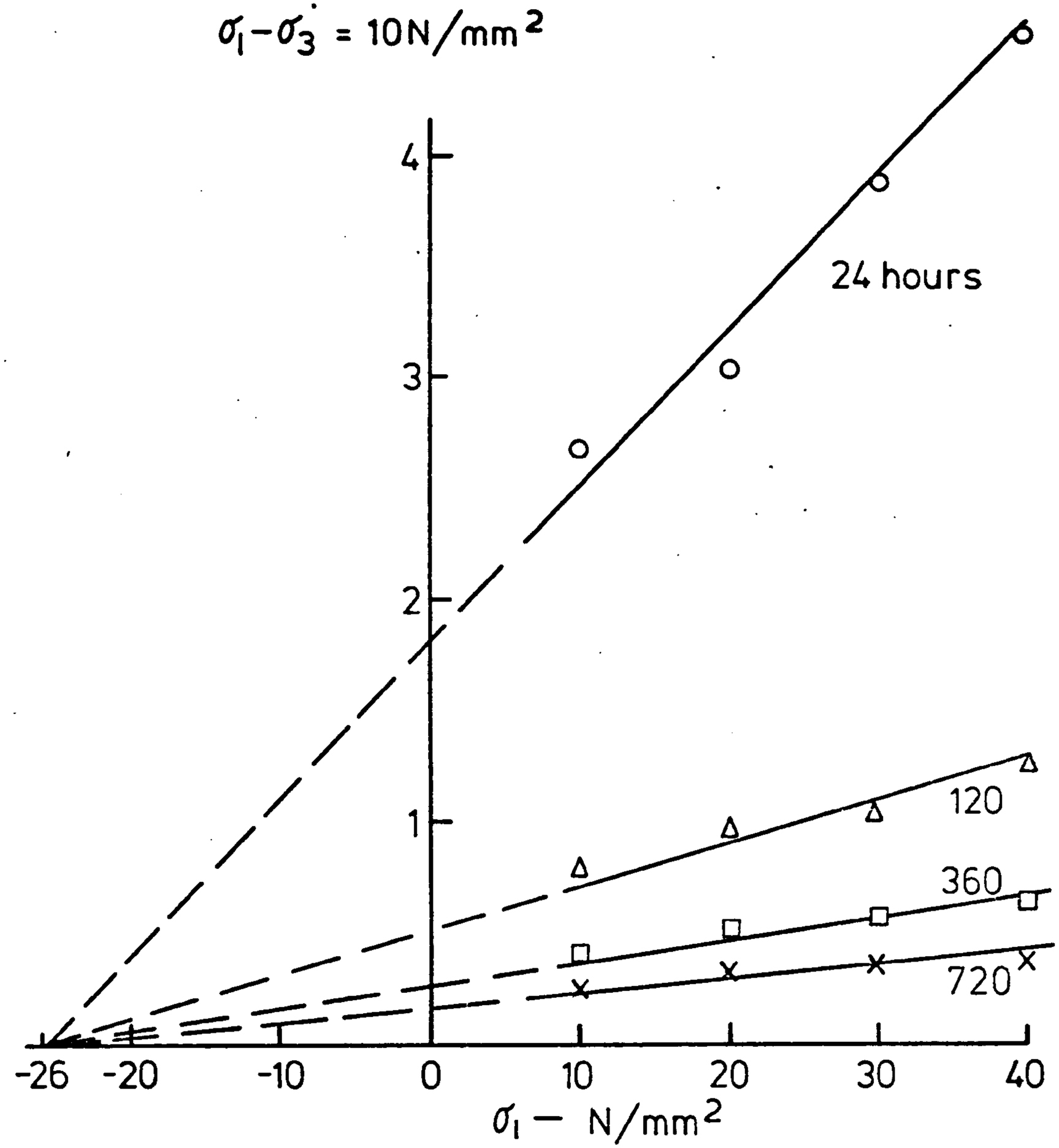

FIG. (6-46) AXIAL CREEP RATE Vs. σ_1 AT CONSTANT $(\sigma_1 - \sigma_3) = 10N/mm^2$ IN SATURATED CONDITION

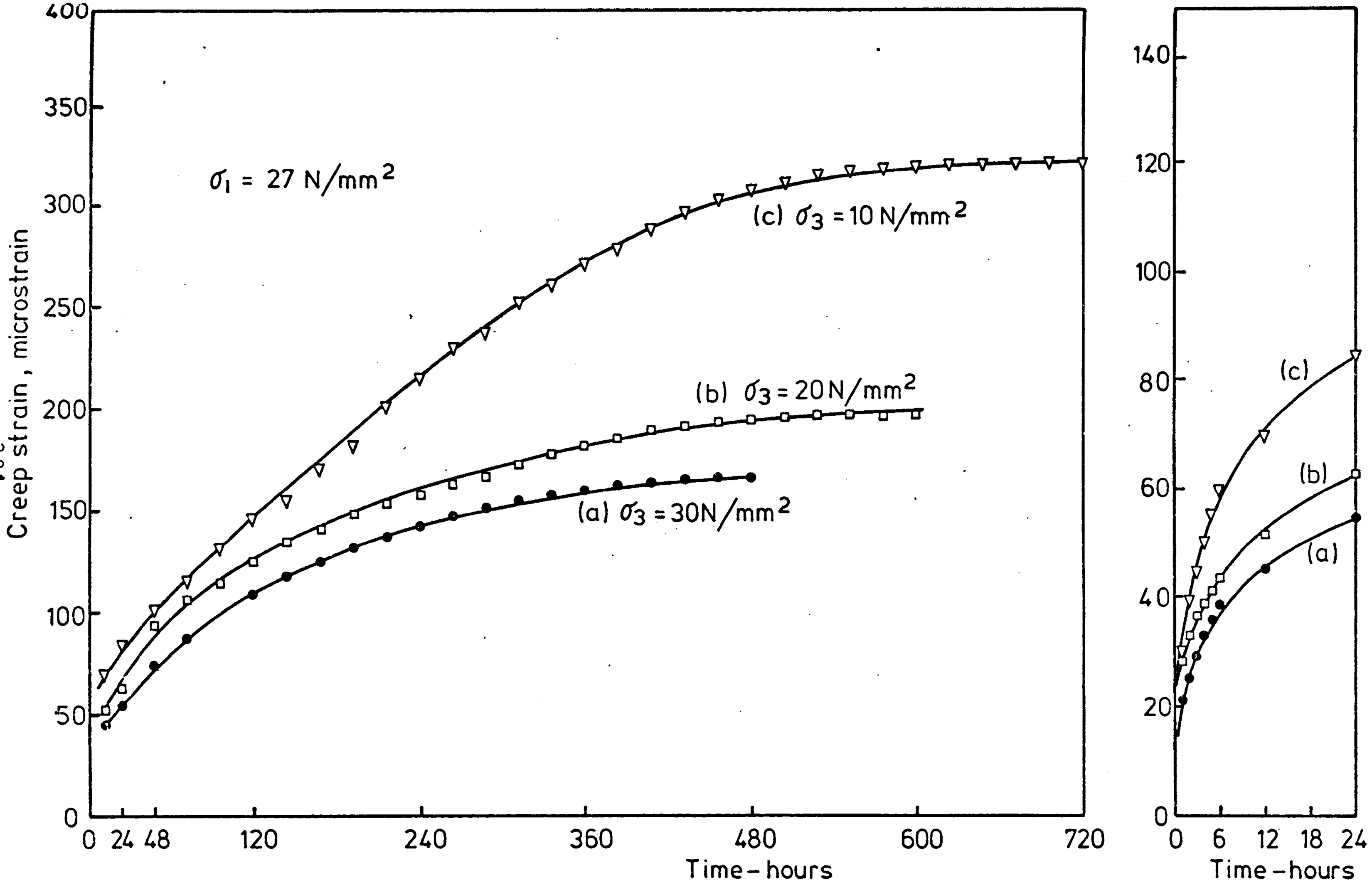

FIG. (6-47) AXIAL CREEP OF DRY GYPSUM UNDER 27 N/mm^2 AXIAL STRESS AT VARIOUS σ_3

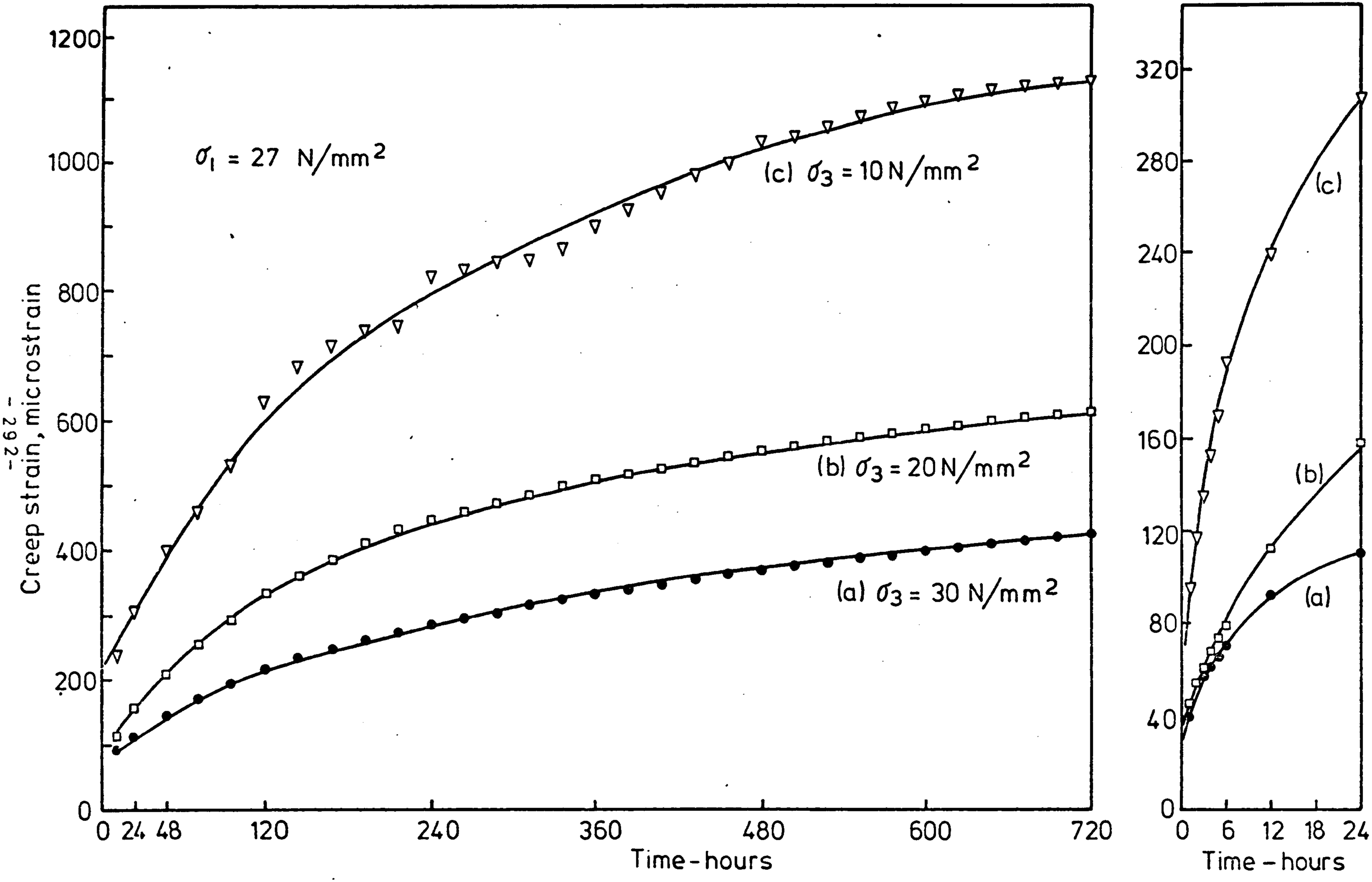

FIG. (6-48) AXIAL CREEP OF SATURATED GYPSUM UNDER 27 N/mm² AT VARIOUS σ_3

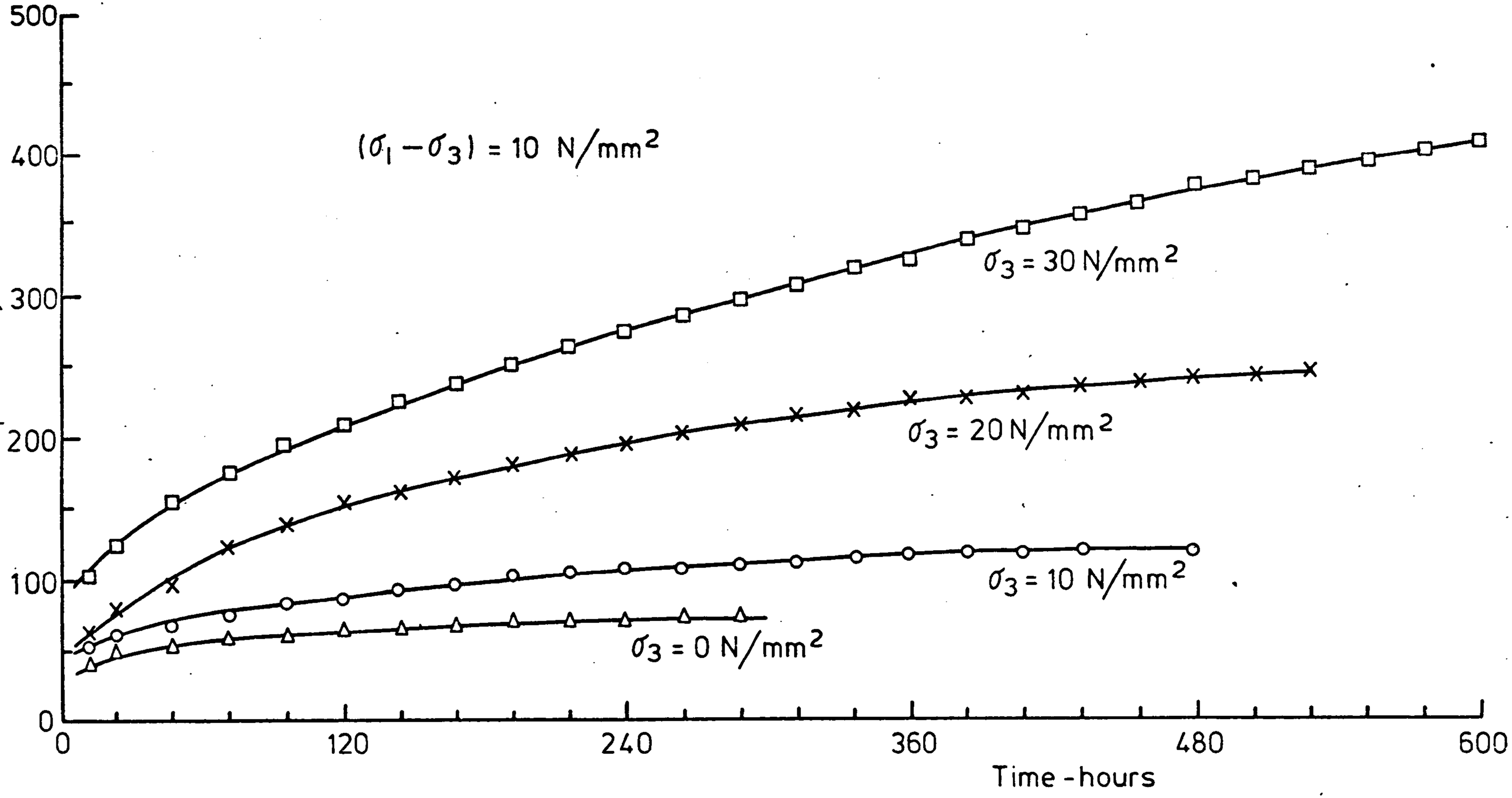

FIG. (6-49) AXIAL CREEP OF DRY GYPSUM AT CONSTANT $(\sigma_1 - \sigma_3) = 10$ N/mm^2

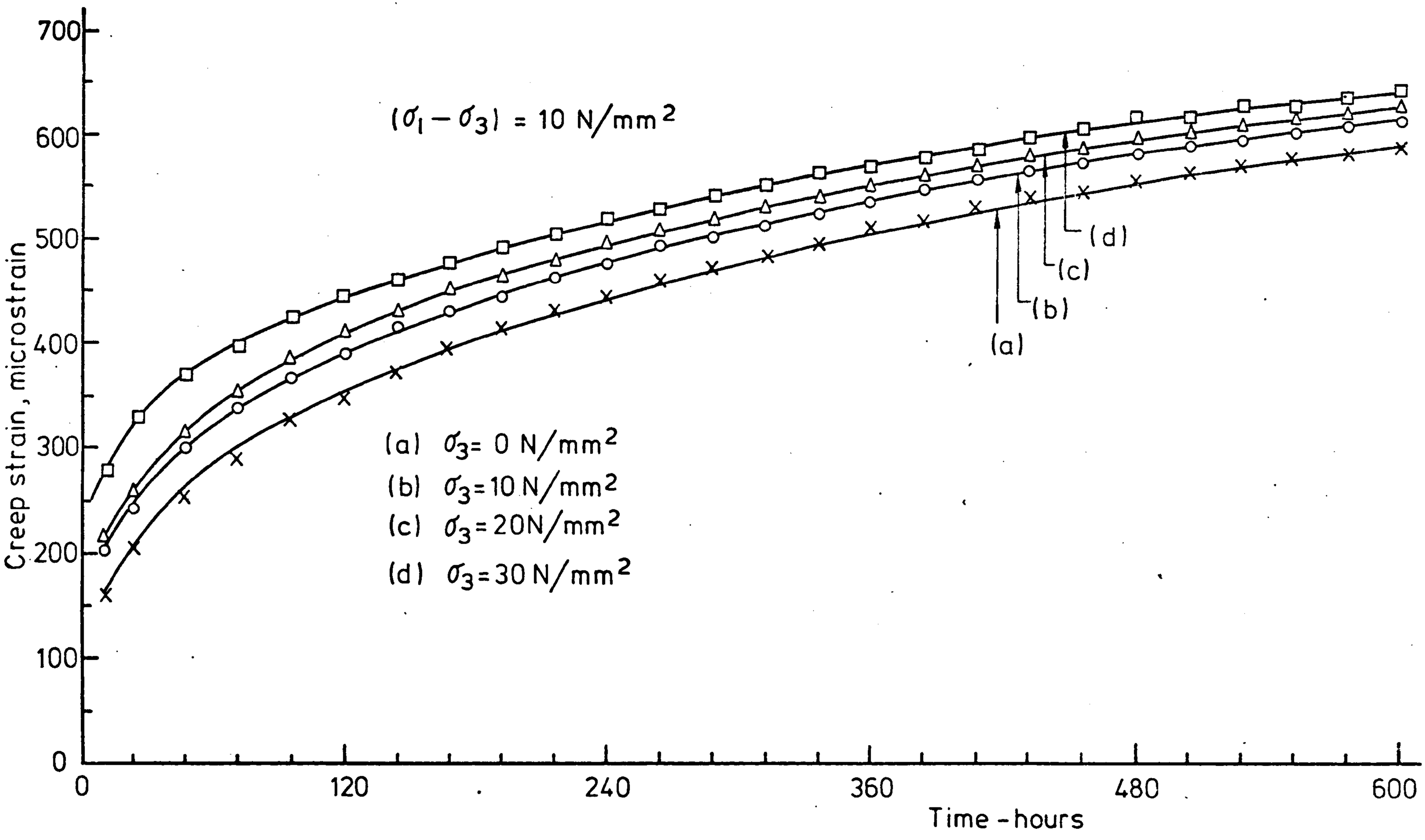

FIG. (6-50) AXIAL CREEP OF SATURATED GYPSUM AT CONSTANT $(\sigma_1 - \sigma_3)$ = 10 N/mm²

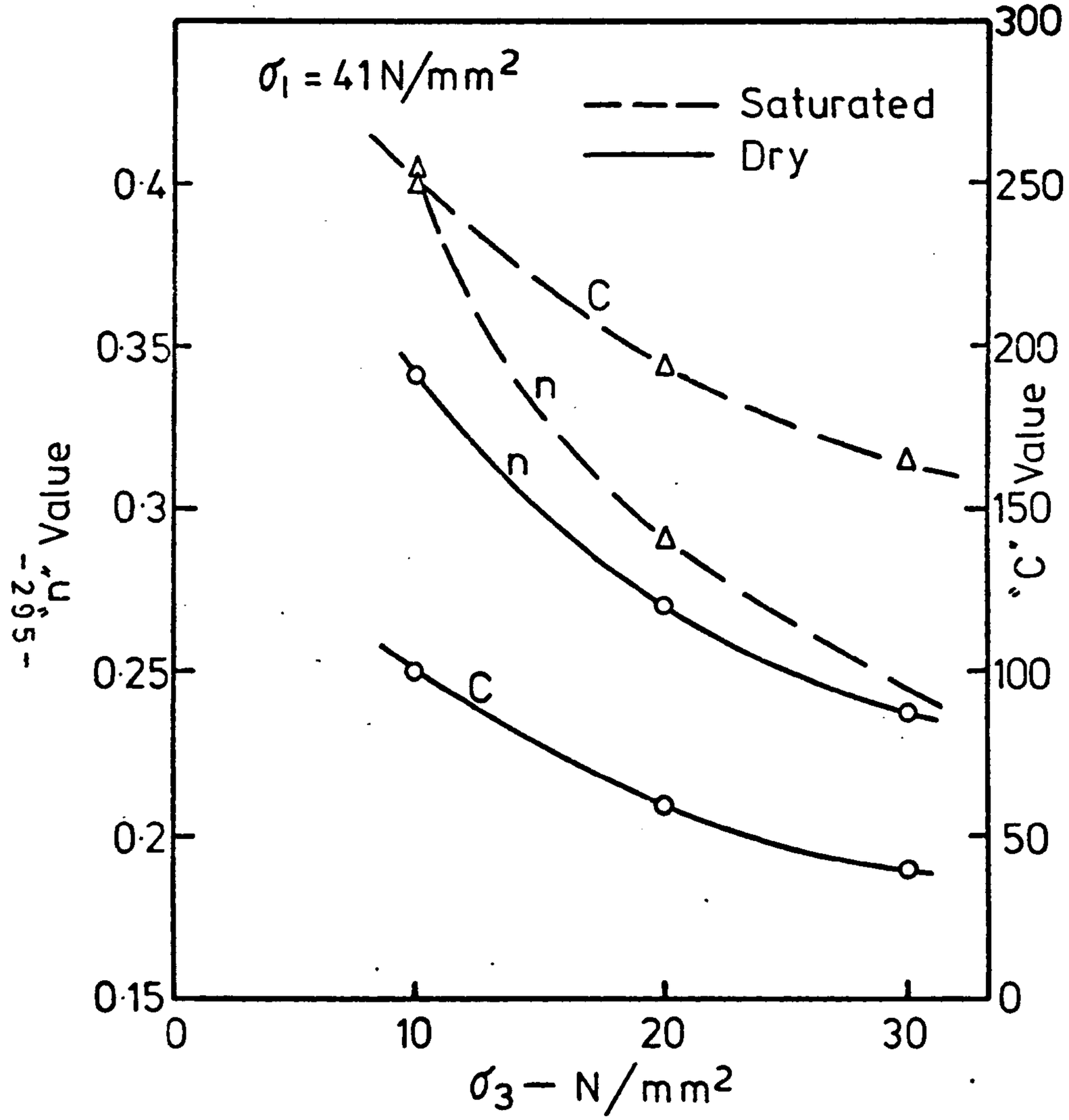

FIG.(6-51) EFFECT OF CONFINING PRESSURE ON "C" AND "n" VALUES AT CONSTANT $\sigma_1 = 41 N/mm^2$

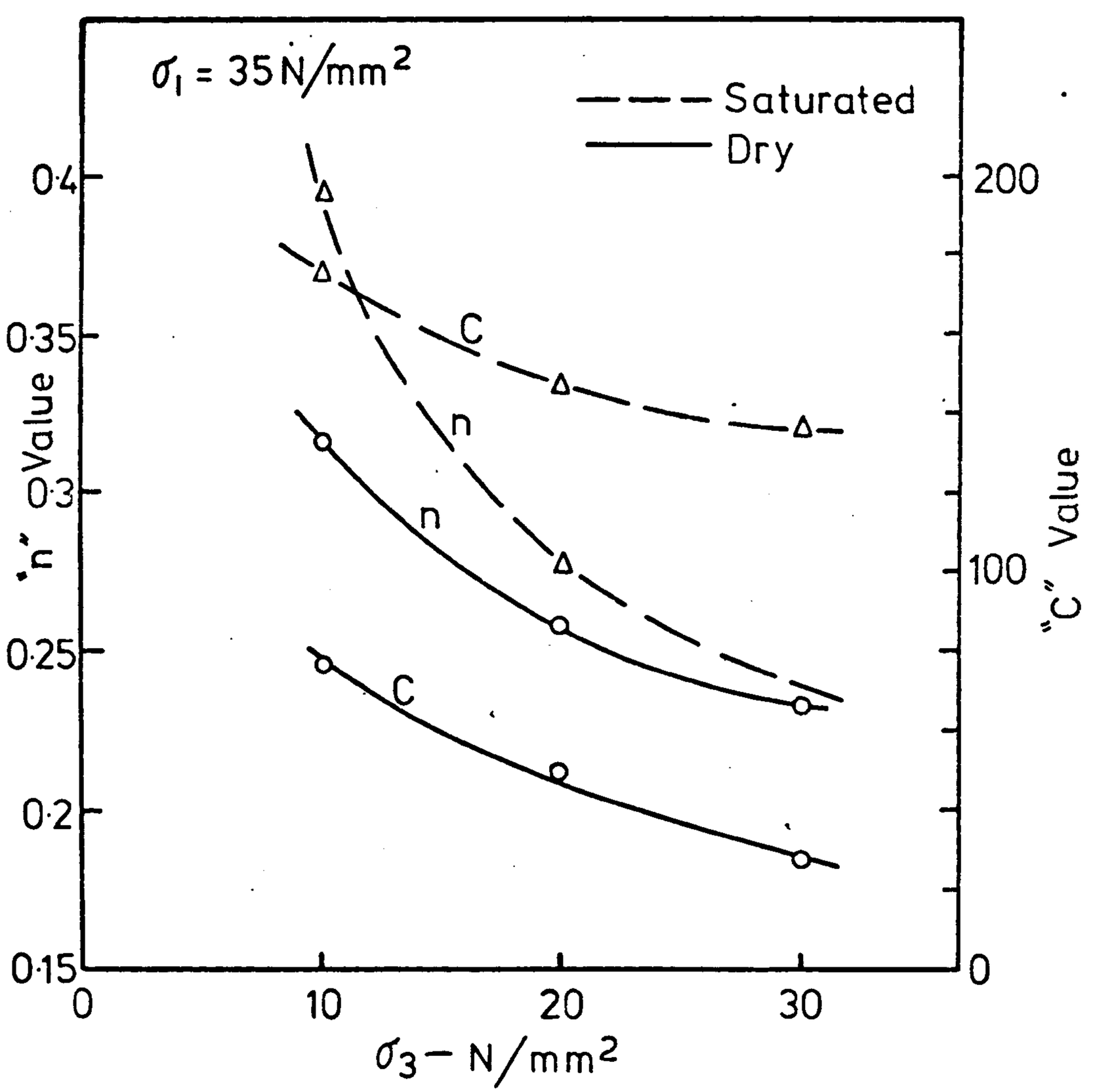

FIG.(6-52) EFFECT OF CONFINING PRESSURE ON "C" AND "n" VALUES AT CONSTANT $\sigma_1 = 35 N/mm^2$

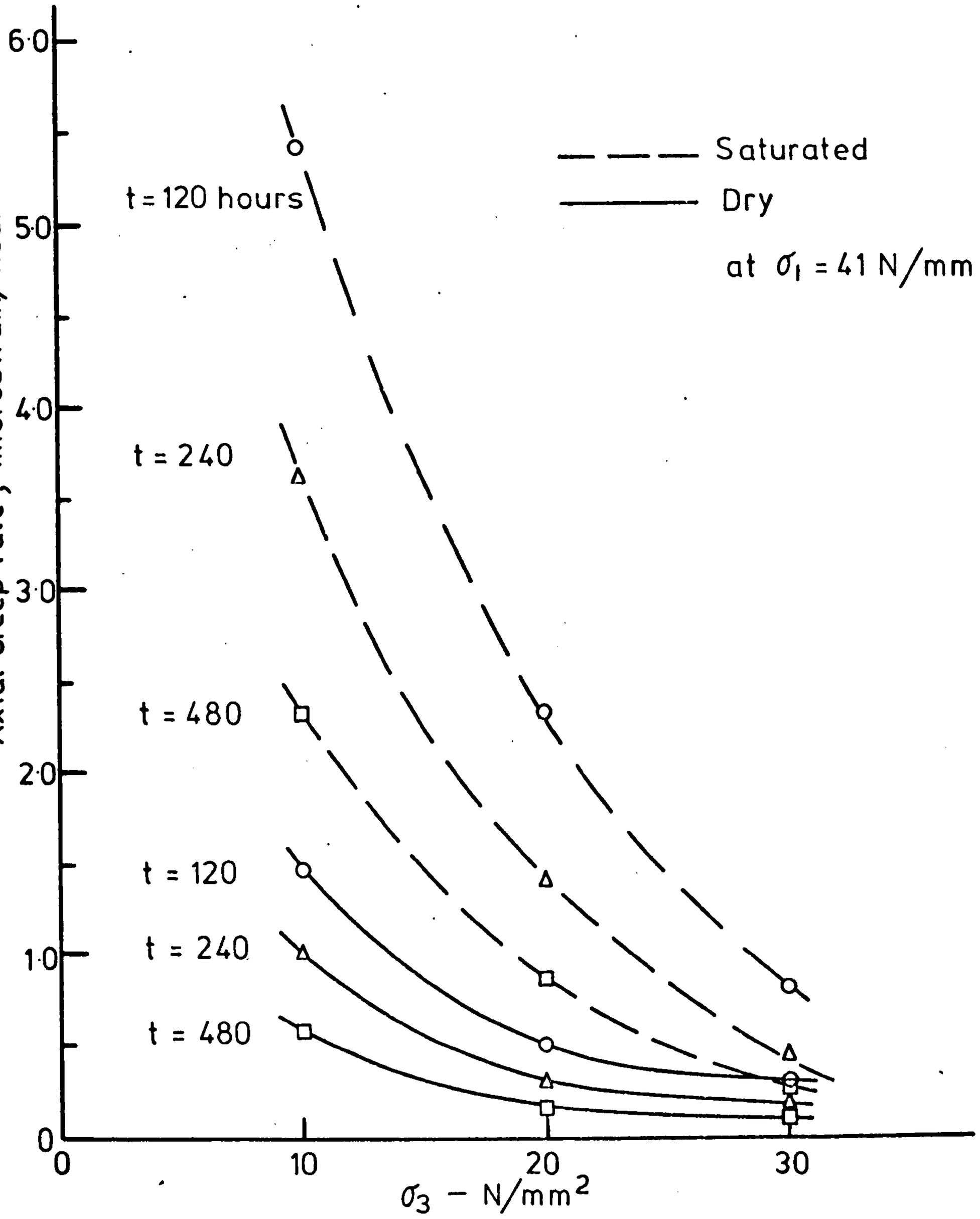

FIG. (6-53) AXIAL CREEP RATE Vs. CONFINING PRESSURE AT CONSTANT $\sigma_1 = 41\ N/mm^2$

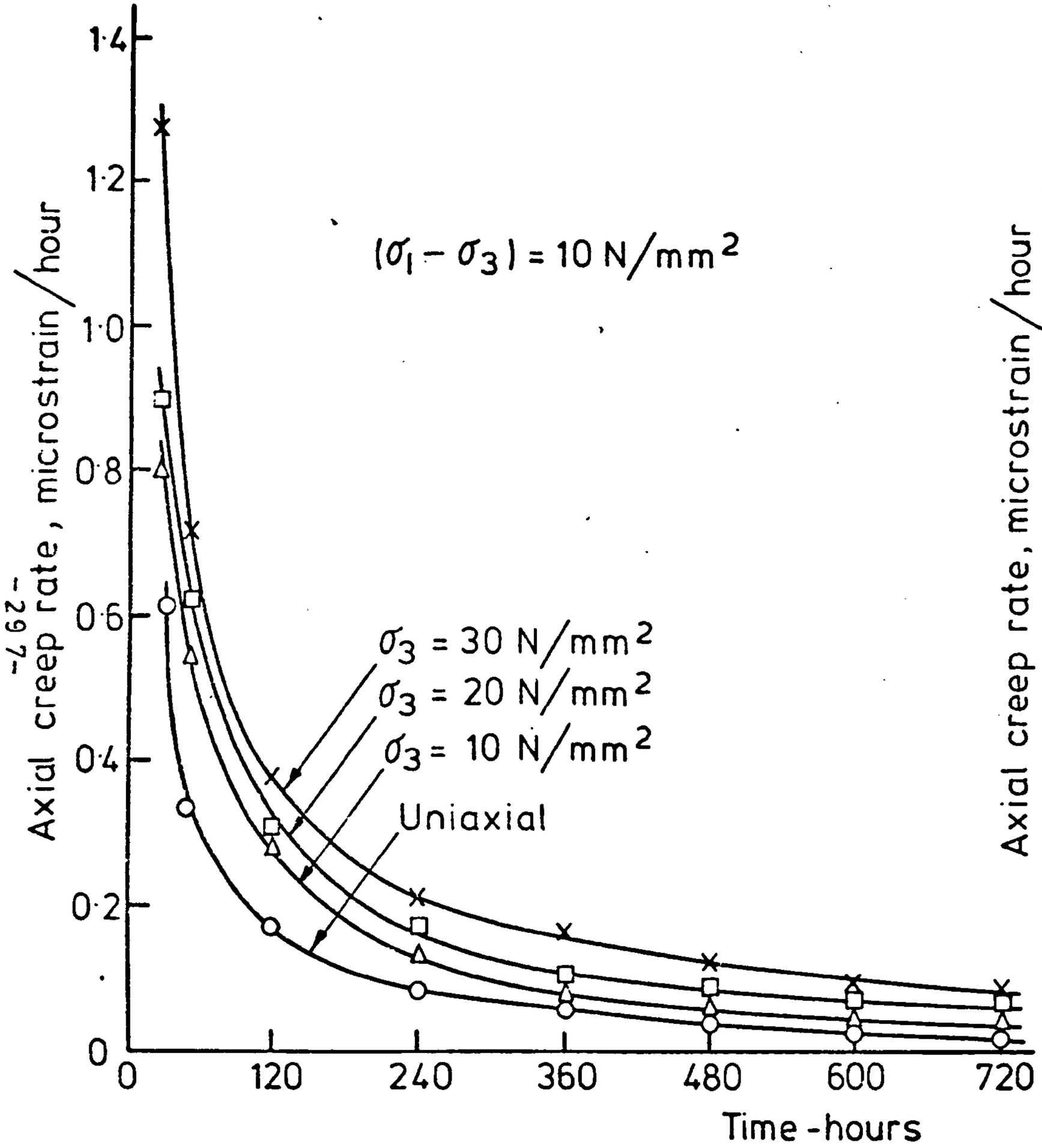

FIG.(6-54) AXIAL CREEP RATE OF DRY GYPSUM AT CONSTANT $(\sigma_1-\sigma_3)$

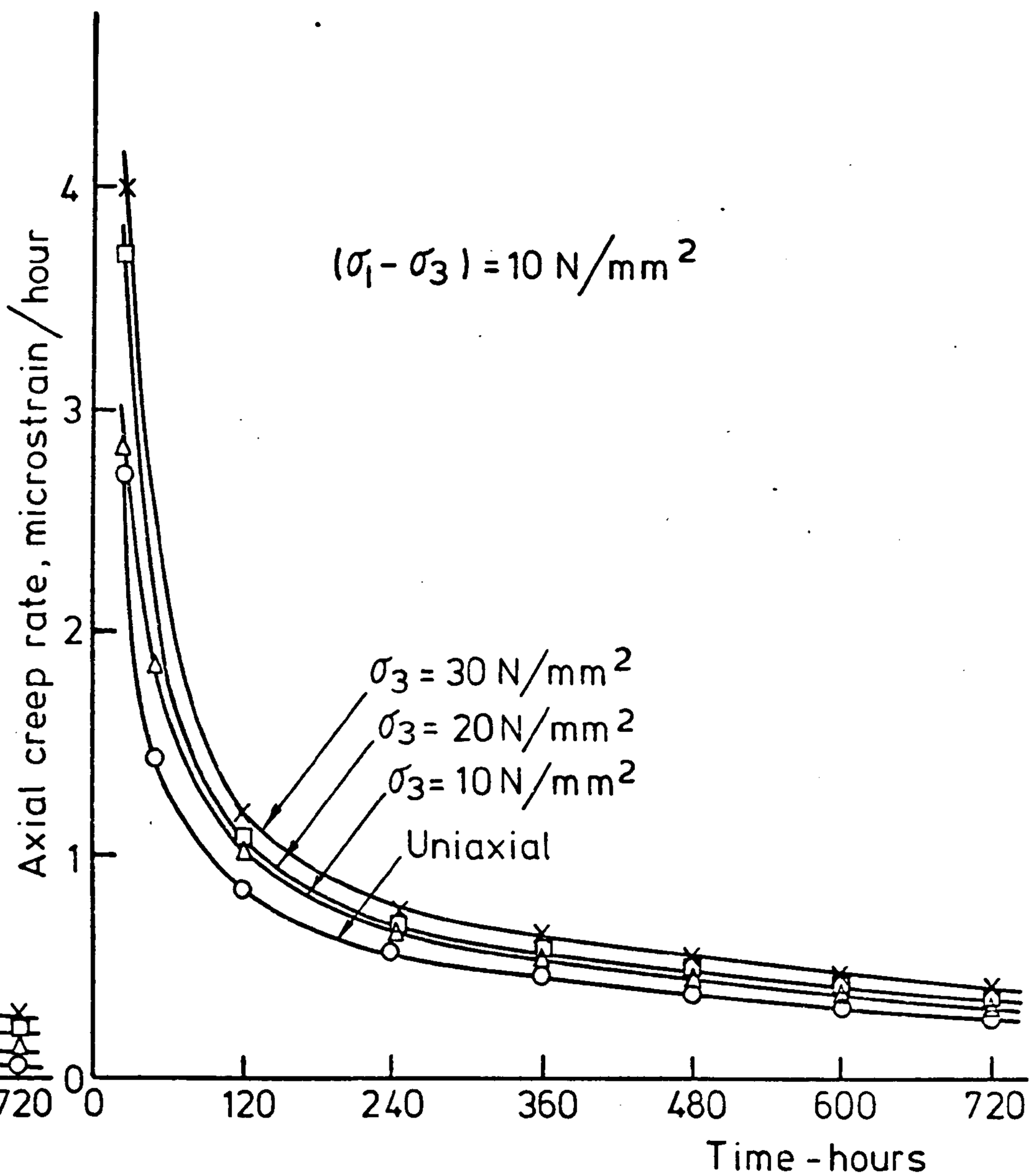

FIG.(6-55) AXIAL CREEP RATE OF SATURATED GYPSUM AT CONSTANT $(\sigma_1-\sigma_3)$

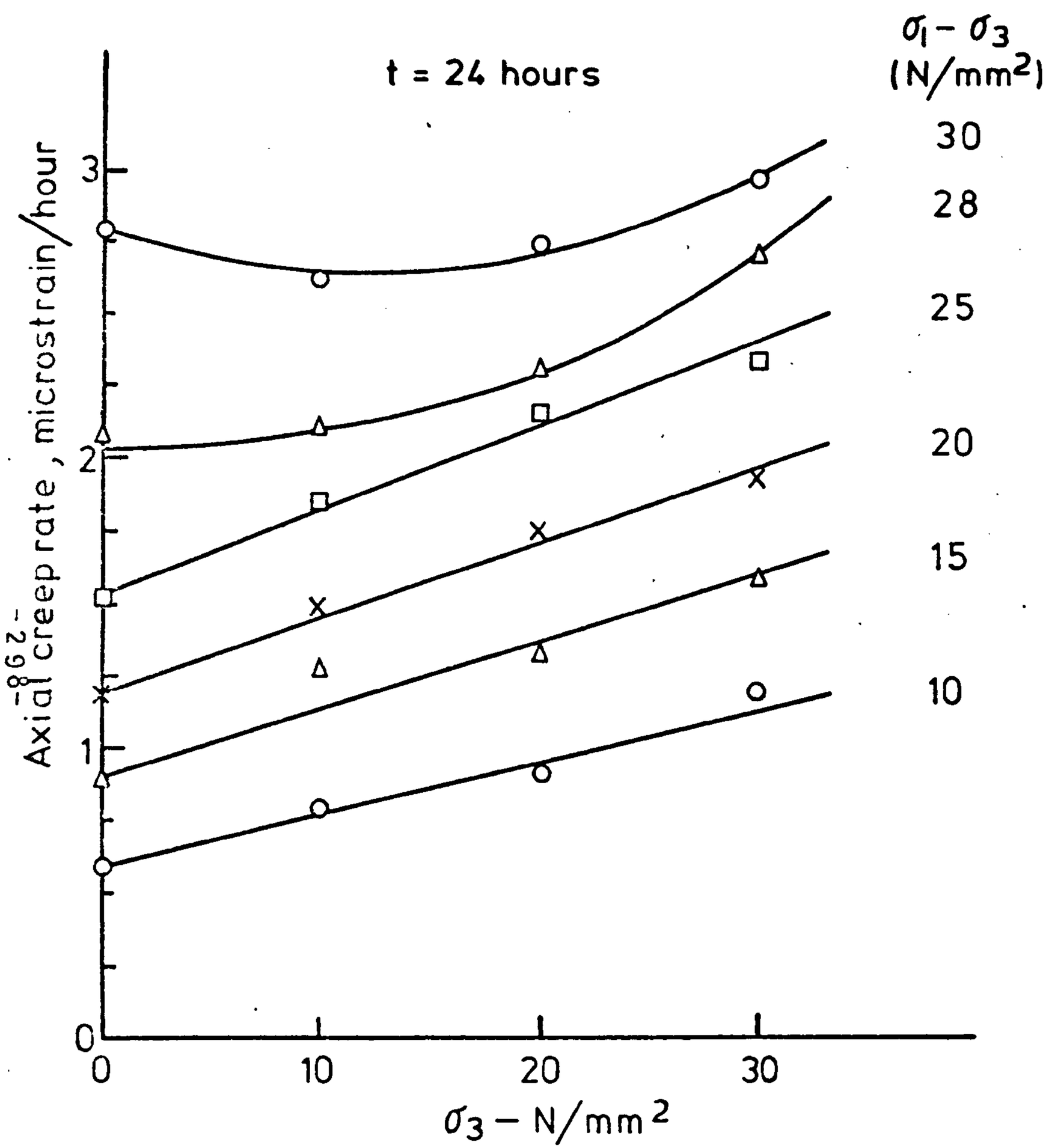

FIG. (6-56) EFFECT OF CONFINING PRESSURE ON THE AXIAL CREEP RATE OF DRY GYPSUM AT CONSTANT $(\sigma_1 - \sigma_3)$

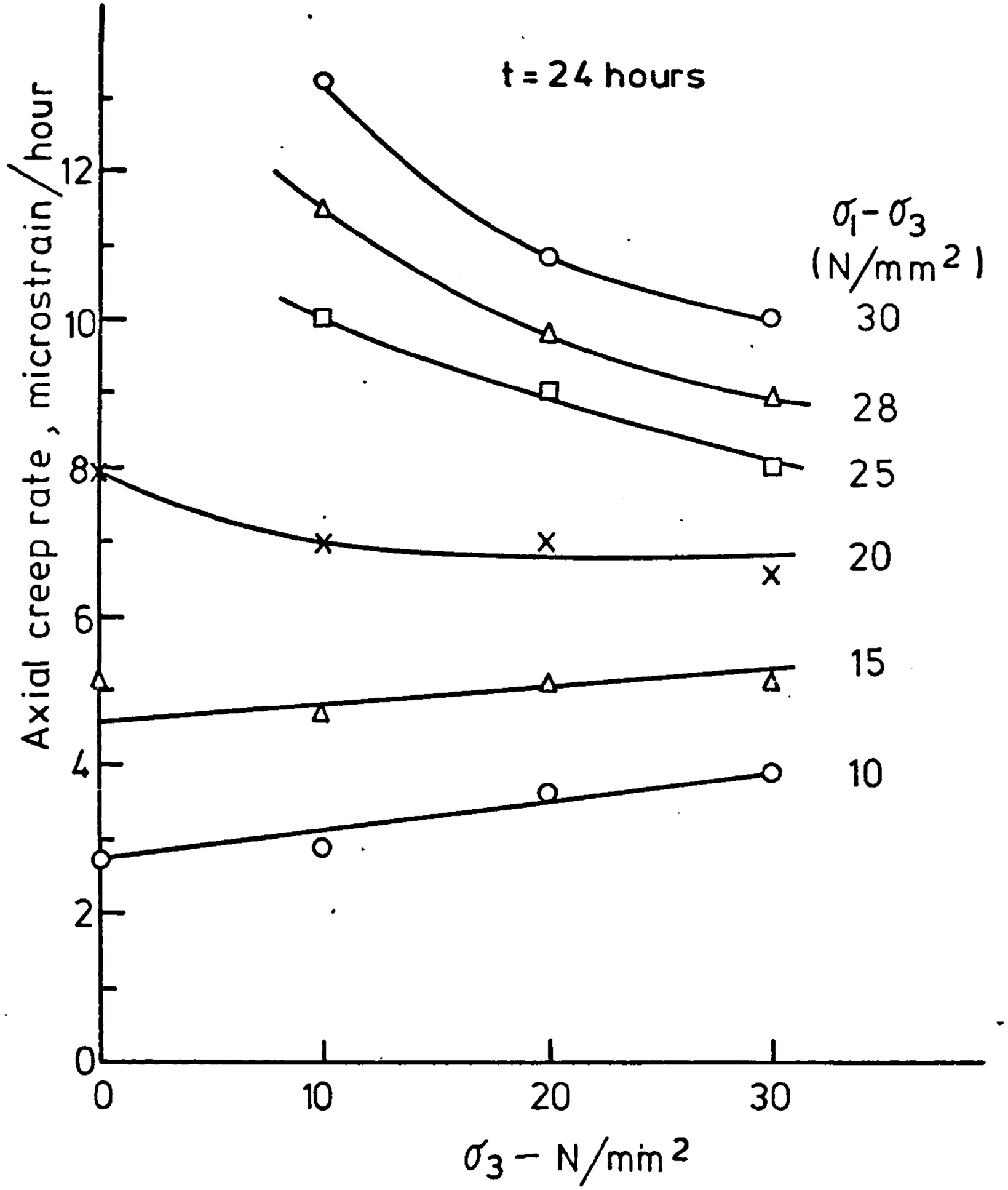

FIG. (6-57) EFFECT OF CONFINING PRESSURE ON THE AXIAL CREEP RATE OF SATURATED GYPSUM AT CONSTANT $(\sigma_1 - \sigma_3)$

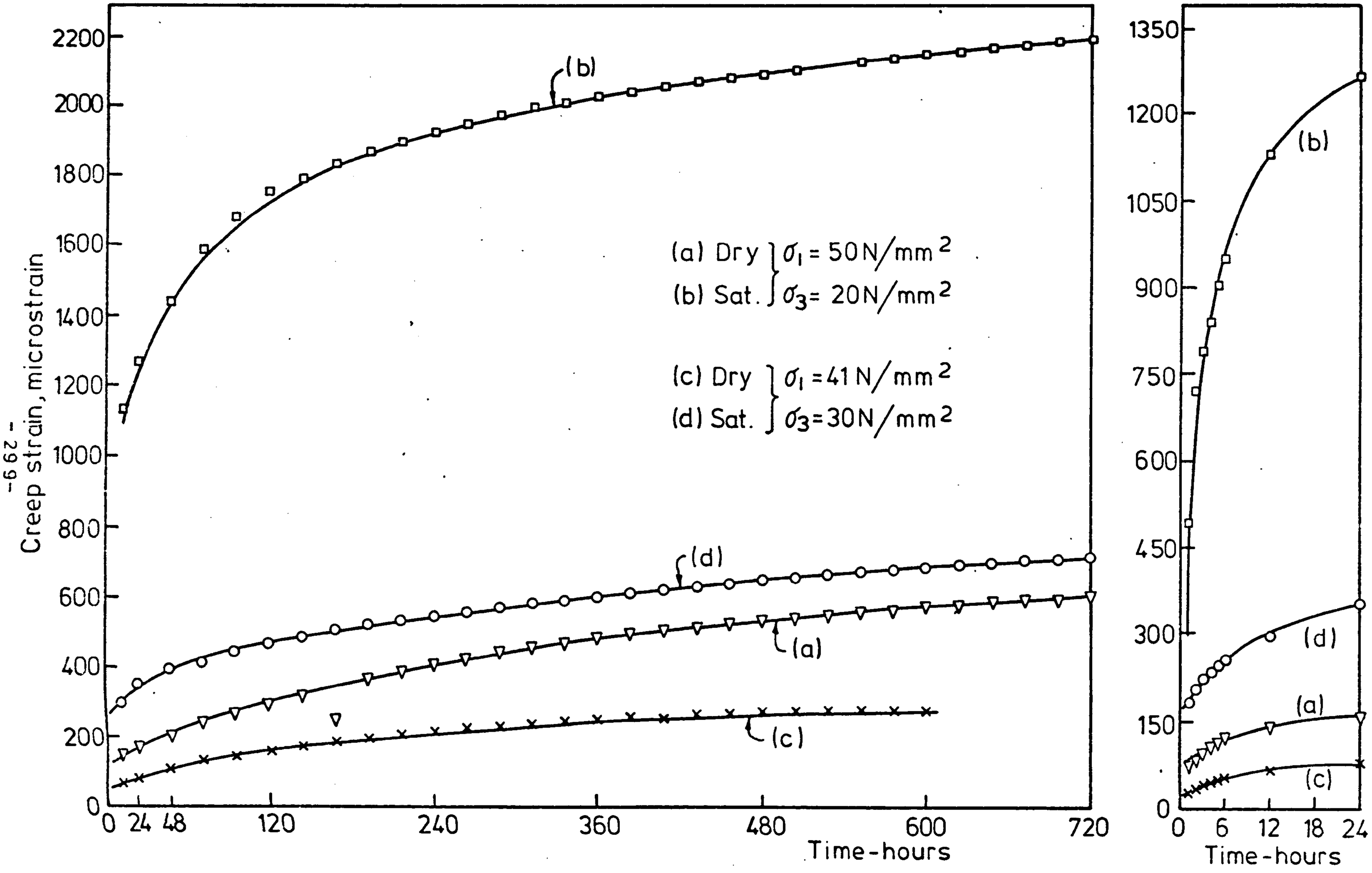

FIG.(6-58) EFFECT OF SATURATION ON THE AXIAL CREEP STRAIN AT VARIOUS STRESS CONDITIONS

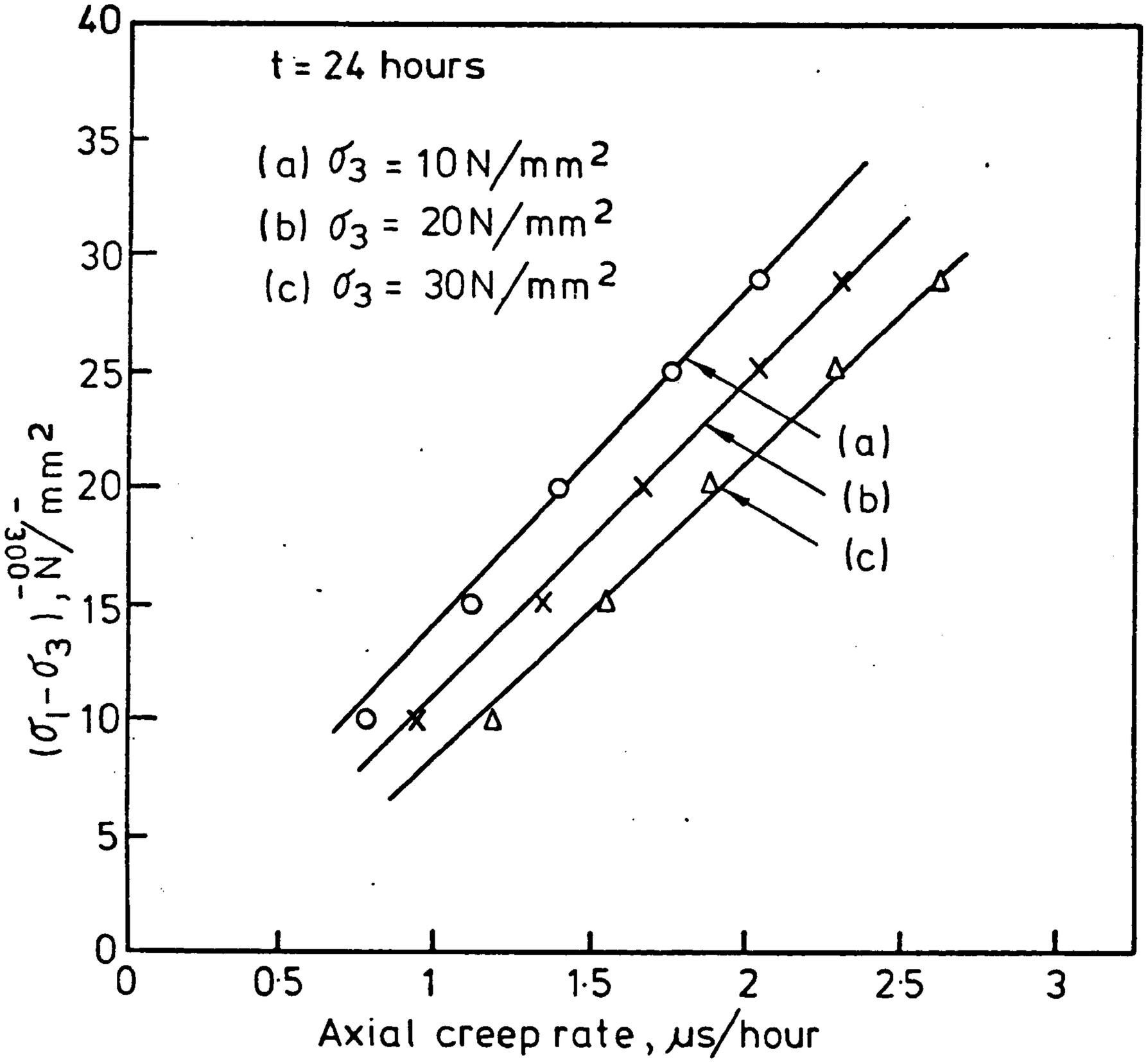

FIG.(6-59) AXIAL CREEP RATE OF DRY GYPSUM Vs. $(\sigma_1-\sigma_3)$ AT CONSTANT σ_3

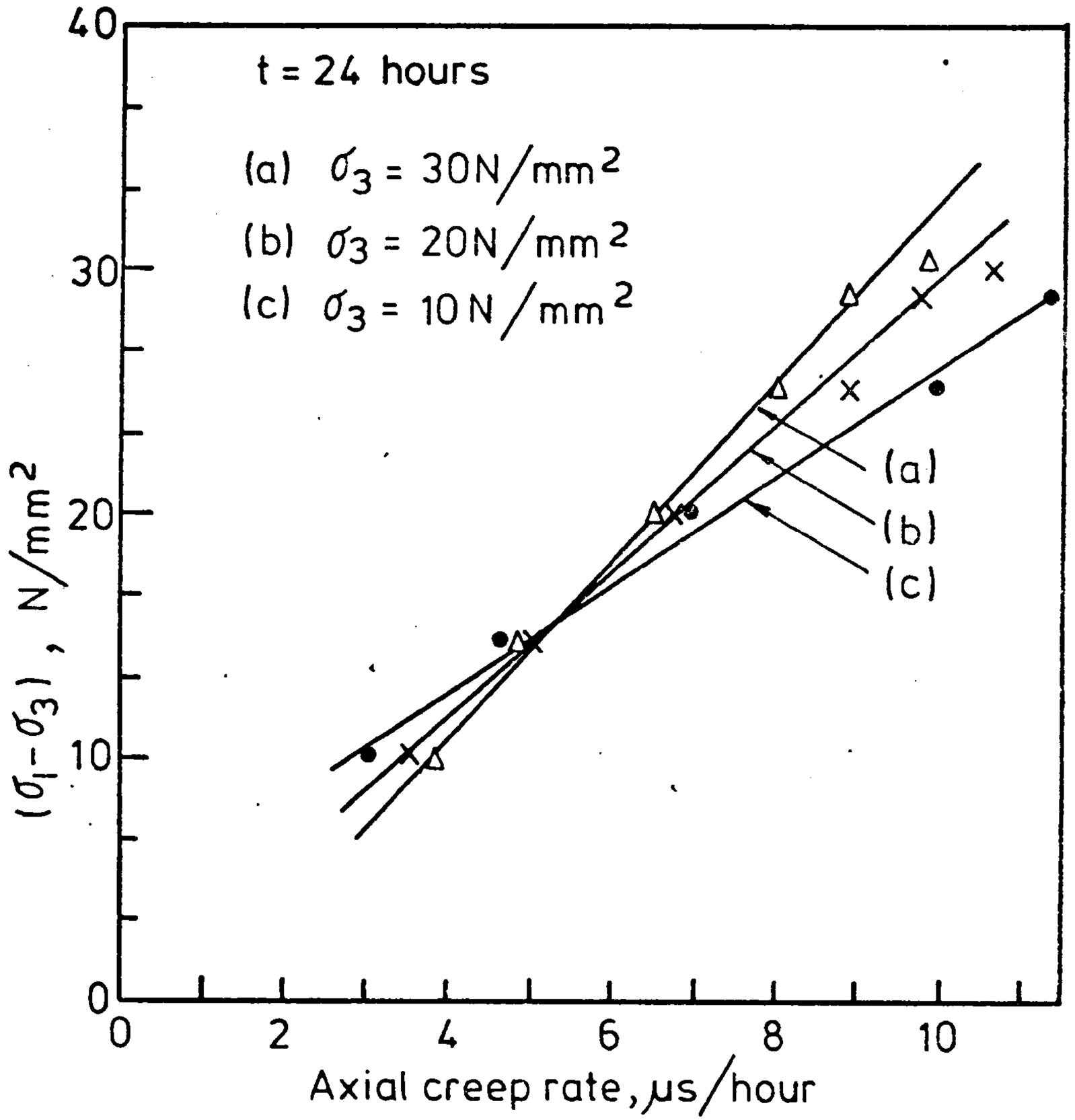

FIG.(6-60) AXIAL CREEP RATE OF SATURATED GYPSUM Vs. $(\sigma_1-\sigma_3)$ AT CONSTANT σ_3

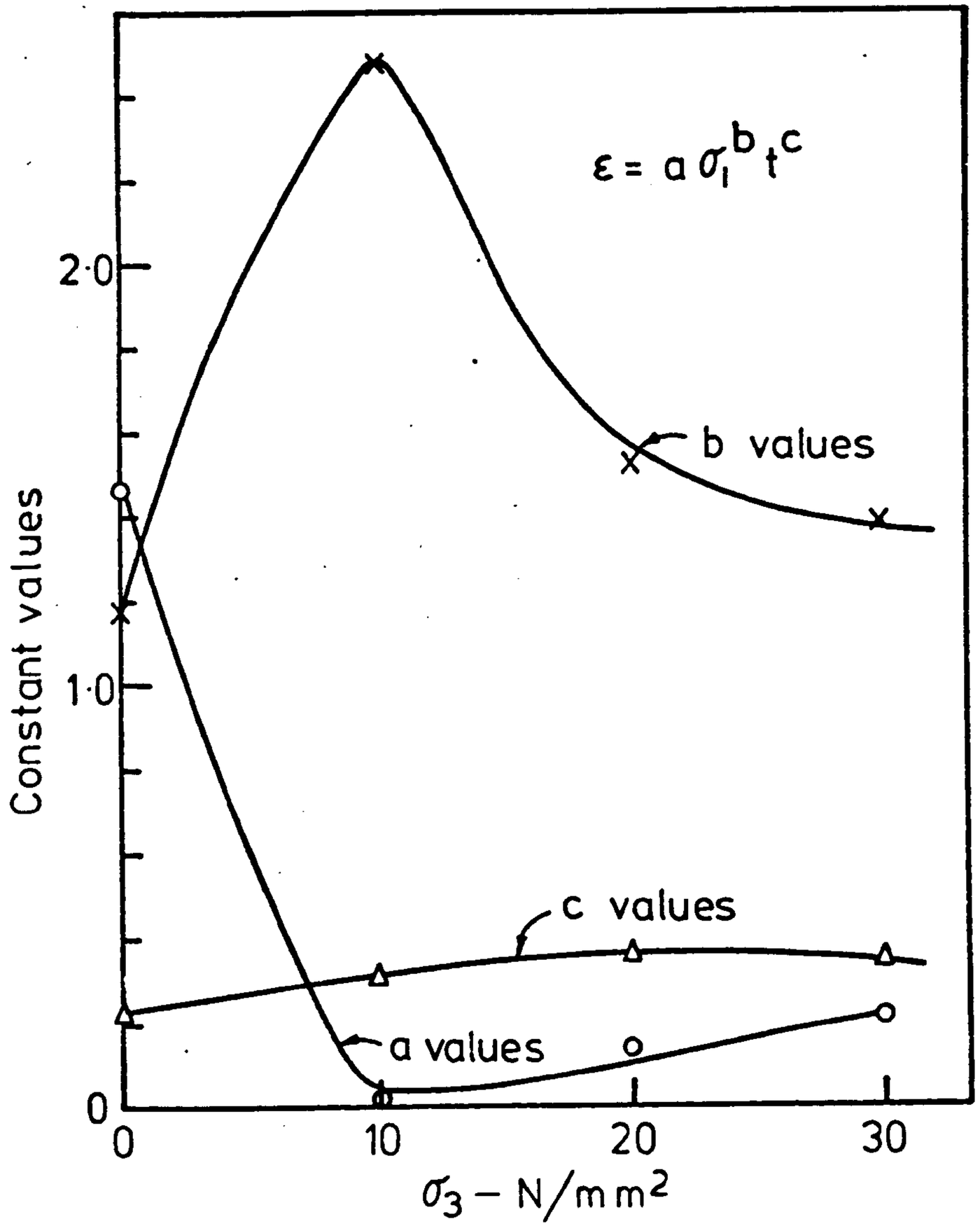

FIG.(6-61) VALUES OF a, b & c Vs. σ_3 IN AXIAL CREEP OF DRY CONDITIONS

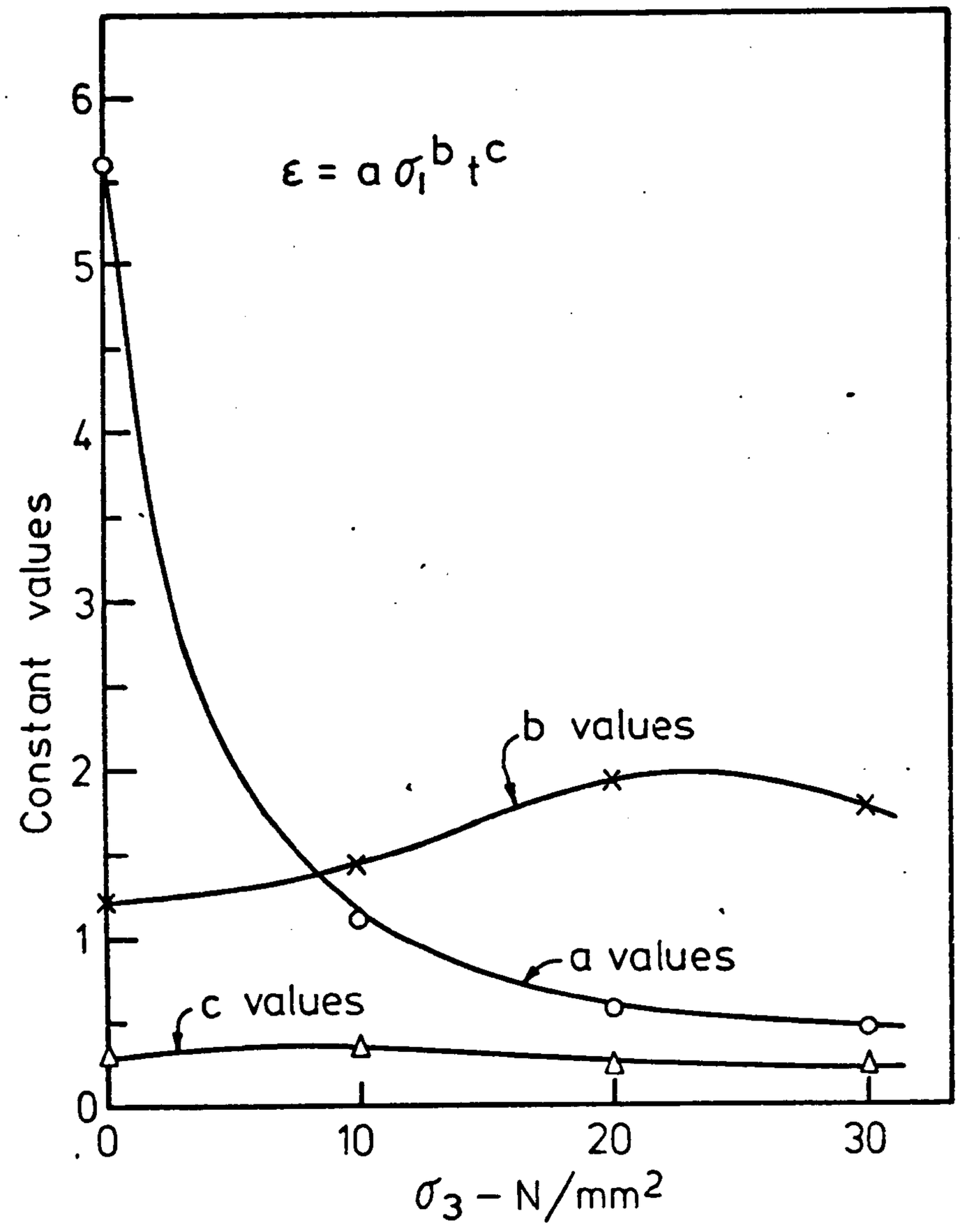

FIG.(6-62) VALUES OF a, b & c Vs. σ_3 IN AXIAL CREEP OF SATURATED CONDITIONS

Chapter 7.

LATERAL AND VOLUMETRIC CREEP IN COMPRESSION.

Lateral creep was measured under uniaxial and triaxial compression at room temperature, the tests being performed in both dry and saturated conditions. The axial stresses and confining pressures were the same as those used for the axial creep (axial and lateral creep strains were measured from the same specimen under any condition), the axial stresses used were; $(33 \pm 7)\%$; $(50 \pm 7)\%$ $(65 \pm 6)\%$ and $(85 \pm 5)\%$ of the failure stresses. The confining pressure levels were 0, 10, 20 and 30 N/mm^2. Volumetric creep strains were calculated by using the axial and lateral creep strains under the same conditions. Lateral and volumetric creep behaviours and some factors affecting them will be discussed in this chapter.

7.1 General Consideration of the Lateral Creep Measurements.

The creep strains were measured at five different points on the specimen surface by attaching 10 strain gauges in five pairs along the specimen at equal intervals, the two strain gauges of each pair were mounted on the opposite sides of the specimen, see (Section 5.2.2.1.6) and Fig. (5.20). The results obtained indicated that the lateral creep strains are approximately symmetrical about the middle of the specimen, i.e. the creep strain at L/6 from the top end of the specimen is nearly equal to that at L/6 from the bottom end as indeed might be expected. The lateral creep strain at L/6 was for the purposes of the tests considered equal to that at 5L/6 while that at 2L/6 was assumed to equal that at 4L/6, where L is the specimen length, and averages were taken of these pairs of positions to give the lateral strain values. The results indicated that the lateral creep strain within the middle third of the specimen is nearly uniform over the whole test period. This behaviour was observed in both dry and saturated

conditions and at various confining pressures. Tables (7.1) and (7.2) give the average value of the creep strain at different positions along the specimen for dry and saturated conditions respectively under 27 N/mm^2 axial stress at 30 N/mm^2 confining pressure. Figs. (7.1) and (7.2) show the distribution of the lateral creep strain along the specimen for dry and saturated conditions respectively at various axial stresses under 30 N/mm^2 confining pressure. It can be seen from the tables and the figures that the lateral creep strain within the middle third of the specimen rarely exceeds 5%. In this study the author considered the average lateral creep within the middle third of the specimen as the lateral creep strain under any given stress condition. Peng[31] measured the lateral strains at 8 points along the granite specimens of size 63.5 mm long by 31.8 mm diameter by using strain gauges, he reported a uniform strain in the middle third of the specimen subjected to uniaxial and triaxial stresses and under similar end conditions to those used in this study (direct contact with steel platens with a spherical seat at the end.

7.2 Lateral Creep Behaviour in Dry and Saturated Conditions.

The behaviour of the lateral creep under uniaxial and triaxial stresses in both environmental conditions obeyed reasonably well either the power law, Eq. (6.23), which is $\varepsilon = Ct^n$, or power law and logarithmic law, Eq. (6.22) which is $\varepsilon = A + B \log t$. The graphical presentation of these relationships are given in detail in chapter 6.

Figs. (7.11) and (7.12) show the creep strain-time relationships on semi-log and log-log graph respectively for dry condition under triaxial loading at 10 N/mm^2 confining pressure with the creep equations. Figs. (7.13) and (7.14) show also the creep strain-time relationship on semi-log and log-log graphs respectively for saturated conditions under uniaxial stress with creep equations.

Table (7.1) Axial, Lateral and Volumetric creep at σ_1 = 27 N/mm^2, σ_3 = 30 N/mm^2 in dry condition.

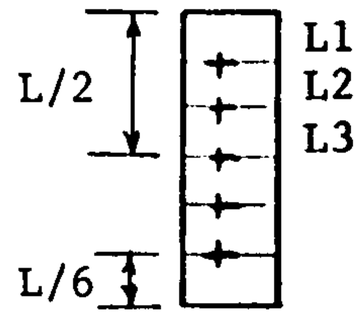

Time, hours	Axial	Lateral			Volumetric	Average Lateral
		L_1	L_2	L_3		
	Instantaneous strain, Microstrain					
	540	72	106	114	320	-110
	Creep strain, Microstrain					
0.1	6.8	2.0	2.7	4.0	0.1	-3.4
0.3	10.0	4.0	5.4	6.1	-1.5	-5.7
0.5	14.0	6.4	7.8	8.8	-2.6	-8.3
1.0	21.1	9.1	11.4	11.8	-2.1	-11.6
2.0	24.9	11.8	13.4	15.2	-3.7	-14.3
3.0	28.9	14.1	17.5	18.5	-7.1	-18.0
4.0	32.6	16.2	19.9	21.9	-9.2	-20.9
5.0	35.6	17.9	22.5	24.5	-11.4	-23.5
6.0	38.5	19.2	24.5	26.9	-12.9	-25.7
12.0	45.0	24.2	31.3	34.0	-20.3	-32.6
24.0	54.3	29.0	39.4	41.7	-26.8	-40.6
48.0	74.1	35.4	47.5	51.5	-24.9	-49.5
72.0	87.1	41.1	55.9	58.7	-27.5	-57.3
96.0	79.9	45.8	62.9	67.7	-50.7	-65.3
120.0	108.0	49.8	69.7	74.4	-35.4	-72.1
144.0	117.3	54.3	76.5	80.5	-39.7	-78.5
168.0	124.8	58.3	81.8	85.6	-42.6	-83.7
192.0	131.4	61.9	86.2	90.9	-45.7	-88.6
216.0	136.7	65.4	88.3	97.0	-48.6	-92.7
240.0	141.9	68.0	96.9	103.7	-58.7	-100.3
264.0	146.9	70.7	101.7	108.3	-63.1	-105.0
288.0	151.3	72.4	106.8	113.4	-68.9	-110.1
312.0	155.2	74.4	111.1	118.5	-74.4	-114.8
336.0	158.0	75.8	114.4	120.1	-76.5	-117.3
360.0	160.3	77.4	116.9	121.5	-78.1	-119.2
384.0	162.5	78.1	117.4	122.9	-77.8	-120.2
408.0	164.1	78.8	118.2	123.5	-77.5	-120.9
432.0	165.5	79.5	118.9	123.9	-77.3	-121.4
456.0	166.2	79.5	118.9	123.9	-76.6	-121.4
480.0	166.4	79.5	118.9	123.9	-76.4	-121.4

Table (7.2) Axial, Lateral and Volumetric Creep at σ_1 = 27 N/mm^2, σ_3 = 30 N/mm^2 in saturated condition.

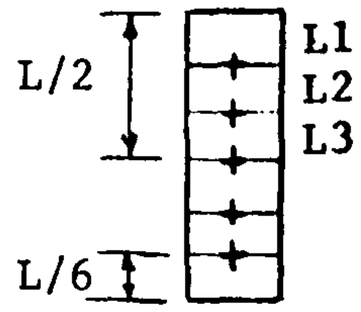

Time, hours	Axial	Lateral			Volumetric	Average Lateral
		L_1	L_2	L_3		
	Instantaneous strain, Microstrain					
	700	104	169	183	348	-176
	Creep strain, Microstrain					
0.1	12.5	6.4	10.8	13.1	-11.4	-12.0
0.3	23.5	12.4	18.5	21.3	-16.3	-19.9
0.5	31.7	19.5	26.0	30.0	-24.3	-28.0
1.0	40.0	25.6	39.7	45.5	-45.2	-42.6
2.0	84.4	31.0	47.2	53.5	-16.3	-50.4
3.0	56.7	38.4	56.9	62.3	-62.5	-59.6
4.0	61.0	43.4	63.6	68.4	-71.0	-66.0
5.0	65.3	49.2	69.0	75.4	-79.1	-72.2
6.0	70.2	53.5	74.0	80.8	-84.6	-77.4
12.0	92.3	62.9	92.9	97.0	-97.6	-95.0
24.0	110.2	72.7	114.1	123.5	-127.4	-118.8
48.0	147.1	81.1	137.7	144.4	-135.0	-141.1
72.0	172.5	88.2	157.3	162.9	-147.7	-160.1
96.0	195.4	96.7	172.7	179.1	-156.4	-175.9
120.0	216.7	104.0	185.1	195.6	-164.0	-190.3
144.0	232.9	113.1	198.3	208.4	-173.8	-203.4
168.0	248.2	120.9	211.4	222.5	-185.7	-217.0
192.0	261.7	126.5	221.4	234.3	-194.0	-227.9
216.0	275.2	133.0	232.5	245.1	-202.4	-238.8
240.0	287.3	140.1	242.4	255.5	-210.6	-249.0
264.0	297.1	146.5	250.5	267.7	-221.1	-259.1
288.0	303.3	151.8	258.6	276.6	-231.9	-267.6
312.0	316.7	157.3	267.2	285.1	-235.6	-276.2
336.0	325.8	161.9	277.8	293.6	-245.6	-285.7
360.0	334.1	165.3	288.3	302.0	-256.2	-295.2
384.0	341.4	167.4	292.6	310.1	-261.3	-301.4
408.0	348.7	171.0	299.3	316.8	-267.4	-308.1
432.0	355.7	175.0	306.0	323.8	-274.1	-314.9
456.0	362.9	178.5	309.8	330.3	-277.2	-320.1
480.0	369.5	183.1	318.2	335.6	-284.3	-326.9
504.0	375.6	187.1	326.9	340.7	-292.0	-333.8
528.0	381.4	189.9	333.0	345.4	-297.0	-339.2
552.0	388.2	192.6	339.1	351.5	-302.4	-345.3
576.0	391.0	197.7	345.1	357.5	-311.6	-351.3
600.0	398.6	200.7	351.2	361.3	-313.9	-356.3
624.0	404.5	201.3	356.2	365.3	-317.0	-360.7
648.0	409.9	206.7	359.6	369.7	-319.4	-364.7
672.0	415.0	209.4	363.6	371.7	-320.3	-367.7
696.0	419.0	211.4	365.9	374.7	-321.6	-370.3
720.0	423.6	213.4	368.7	377.4	-322.5	-373.1

The relationships obtained in dry and saturated conditions are as follows:

a. Dry Condition.

The results of the lateral creep are in the form of tables and figures and are given in tables from (7.3) to (7.6) and figures from Fig. (7.3) to Fig. (7.6).

1) For uniaxial compression, see Table (7.3) and Fig. (7.3), the creep behaviour followed the following relationships according to the applied stresses:

at $\sigma_1 = 15\ N/mm^2 = 36\%\ \sigma_u$

$$\varepsilon = 32.5\ t^{0.355} \qquad t \leq 2 \text{ hrs.} \quad ..... \quad (7.1)$$

$$\varepsilon = 34\ t^{0.254} \qquad t > 2 \text{ hrs.} \quad ..... \quad (7.2)$$

at $\sigma_1 = 21\ N/mm^2 = 50.3\%\ \sigma_u$

$$\varepsilon = 32.5\ t^{0.355} \qquad t < 12 \text{ hrs.} \quad ..... \quad (7.3)$$

$$\varepsilon = 36.5\ t^{0.296} \qquad t \geq 12 \text{ hrs.} \quad ..... \quad (7.4)$$

at $\sigma_1 = 27\ N/mm^2 = 65\%\ \sigma_u$

$$\varepsilon = 32.5\ t^{0.355} \qquad t < 25 \text{ hrs.} \quad ..... \quad (7.5)$$

$$\varepsilon = 37.5\ t^{0.318} \qquad t \geq 25 \text{ hrs.} \quad ..... \quad (7.6)$$

at $\sigma_1 = 34\ N/mm^2 = 81.8\%\ \sigma_u$

$$\varepsilon = 37.5\ t^{0.355} \qquad t < 54 \text{ hrs.} \quad ..... \quad (7.7)$$

$$\varepsilon = 45\ t^{0.34} \qquad t \geq 54 \text{ hrs.} \quad ..... \quad (7.8)$$

It is clear from the above equations that the lateral creep in uniaxial loading followed the power law for all the applied stresses. The values of the constants C and n, Eq. (6.23), are changed within a short time from the beginning of the tests indicated by a change in the slope of the straight lines on the log-log graphs.

Table (7.3) Lateral Creep of dry gypsum in Uniaxial Compression.

Time	Axial stress, N/mm^2			
	15 36% σ_u	21 50.3% σ_u	27 65% σ_u	34 81.8% σ_u
	Instantaneous strain, Microstrain			
	100	152	198	261
	Creep strain, Microstrain			
0.1	14.1	14.2	14.2	15.8
0.3	21.5	22.1	22.9	22.3
0.5	27.0	27.5	27.4	29.5
1.0	33.2	33.0	32.7	36.3
2.0	39.7 ± 6%	40.1 ± 5%	39.5 ± 6%	45.0 ± 3%
3.0	46.1	47.4	48.0	55.8
4.0	51.1	54.5	54.3	64.5
5.0	53.6	58.2	59.4	72.9
6.0	56.2	62.8	63.8	69.3
12.0	69.1	76.2	81.0	97.8
24.0	79.6 ± 6%	93.7 ± 6%	94.8 ± 8%	119.2 ± 4%
48.0	89.5	107.3	109.3	143.3
72.0	97.2	119.1	122.2	163.4
96.0	107.0	133.5	137.4	178.5
120.0	116.9	142.9	148.4	197.5
144.0	124.4	151.2	155.7	212.3
168.0	131.7	160.3	165.4	226.2
192.0	138.8	170.4	175.7	244.5
216.0	141.7	178.9	186.5	258.2
240.0	143.6	187.5 ± 7%	197.8 ± 5%	268.5 ± 5%
264.0	146.2	194.6	207.8	278.5
288.0	146.3 ± 7%	203.2	217.3	285.6
312.0		209.8	226.6	297.7
336.0		217.0	234.5	311.5
360.0		223.9	242.5	320.1
384.0		228.6	250.8	327.2
408.0		231.5	259.9	334.7
432.0		234.2	266.6	345.0
456.0		236.9	273.3	353.8
480.0		239.5	279.4	361.8
504.0		241.6	285.3	368.3
528.0		243.0	289.6	373.7
552.0		244.6 ± 7%	293.7	378.6
576.0			296.9	383.0
600.0			299.7	385.9
624.0			302.2	388.4
648.0			303.9	390.2
672.0			305.3	391.9
696.0			306.2	392.7
720.0			307.1 ± 5%	393.9 ± 5%

Table (7.4) Lateral Creep of dry gypsum in triaxial at 10 N/mm^2 confining pressure.

Time, hours	Axial stress, N/mm^2			
	21 33.7% σ_u	27 43.3% σ_u	41 65.7% σ_u	50 80.2% σ_u
	Instantaneous strain, Microstrain			
	110	143	250	308
	Creep strain, Microstrain			
0.1	5.4	5.7	56.6	66.7
0.3	8.6	10.0	75.9	84.9
0.5	12.6	17.1	90.8	102.5
1.0	17.7	21.0	106.1	121.7
2.0	23.7 ± 8%	27.1 ± 6%	124.2 ± 5%	140.7 ± 10%
3.0	28.1	31.7	137.6	157.9
4.0	30.3	35.6	150.9	167.7
5.0	33.7	39.0	163.7	178.4
6.0	36.5	42.3	177.0	191.7
12.0	45.4	53.7	195.7	228.8
24.0	64.7 ± 7%	68.7 ± 7%	219.7 ± 5%	270.7 ± 11%
48.0	85.5	87.5	253.5	326.8
72.0	101.3	104.5	286.7	365.0
96.0	113.1	123.4	312.2	395.5
120.0	124.6	138.8	333.2	419.7
144.0	135.1	152.2	353.5	442.7
168.0	144.8	162.9	368.5	460.7
192.0	157.9	174.1	380.7	480.6
216.0	167.5	184.2	390.4	496.6
240.0	177.1 ± 7%	194.4 ± 7%	398.9 ± 4%	515.0 ± 10%
264.0	185.0	204.3	407.0	533.1
288.0	193.9	213.0	413.2	543.4
312.0	201.7	221.6	418.0	555.1
336.0	207.8	229.4	424.0	569.1
360.0	213.1	236.2	429.0	577.8
384.0	216.7	243.8	234.0	587.8
408.0	220.1	249.3	437.0	599.1
432.0	222.8	255.8	441.5	607.0
456.0	225.1	261.4	444.0	615.3
480.0	226.2	265.9	449.0	622.2
504.0	227.2	269.6	452.2	626.7
528.0	227.2 ± 6%	275.5	455.2	631.6
552.0		278.9	458.0	634.9
576.0		283.6	460.5	638.2
600.0		287.7	463.3	641.7
624.0		290.8	466.0	644.2
648.0		293.6	467.9	647.0
672.0		295.4	469.3	650.0
696.0		297.3	470.5	652.3
720.0		298.9 ± 8%	471.0 ± 4%	654.2 ± 8%

Table (7.5) Lateral Creep of dry gypsum in triaxial at 20 N/mm^2 confining pressure.

Time, hours	Axial stress, N/mm^2			
	27 34.5% σ_u	41 52.4% σ_u	50 64% σ_u	63 80.6% σ_u
	Instantaneous strain, Microstrain			
	129	200	280	356
	Creep strain, Microstrain			
0.1	3.6	9.1	14.4	25.9
0.3	7.2	16.0	18.9	40.3
0.5	11.3	20.5	24.2	57.5
1.0	15.1	26.1	29.4	76.2
2.0	19.6 ± 5%	29.7 ± 8%	34.3 ± 8%	120.0 ± 6%
3.0	24.7	33.1	39.2	140.5
4.0	29.4	36.0	44.1	153.1
5.0	32.8	39.2	48.1	162.2
6.0	35.7	43.1	52.6	169.2
12.0	43.8	65.0	94.6	196.9
24.0	53.4 ± 4%	98.0 ± 8%	134.6 ± 8%	219.4 ± 8%
48.0	63.2	141.0	157.6	280.5
72.0	73.0	182.8	174.6	311.7
96.0	80.7	201.6	194.2	339.2
120.0	88.4	215.2	210.8	361.3
144.0	94.4	226.4	226.3	373.3
168.0	99.2	236.4	240.2	386.7
192.0	104.4	243.9	252.5	402.2
216.0	109.0	251.1	262.7	417.3
240.0	114.9 ± 4%	257.7 ± 8%	273.1 ± 7%	433.5 ± 7%
264.0	119.7	264.7	283.4	443.1
288.0	123.8	270.3	290.8	457.1
312.0	127.7	276.6	299.0	468.9
336.0	131.3	281.4	307.3	480.3
360.0	134.9	285.0	314.8	491.9
384.0	138.1	290.1	322.2	501.8
408.0	141.5	295.2	328.8	512.1
432.0	144.9	300.2	335.1	520.9
456.0	149.7	304.4	341.6	529.2
480.0	150.6	307.6	347.7	537.7
504.0	154.0	310.6	353.8	544.8
528.0	156.6	313.5	360.7	552.0
552.0	158.2	316.1	364.7	560.5
576.0	159.5	318.1	370.1	567.8
600.0	160.7 ± 3%	319.6	375.1	572.8
624.0		320.8	379.5	581.8
648.0		321.7	384.0	588.4
672.0		322.8	388.6	593.5
696.0		323.2	392.4	597.9
720.0		323.6 ± 9%	395.9 ± 4%	601.7 ± 5%

Table (7.6) Lateral Creep of dry gypsum in triaxial at 30 N/mm^2 confining pressure.

Time, hours	Axial stress, N/mm^2			
	27 26.3% σ_u	41 39.8% σ_u	50 48.7% σ_u	63 61.3% σ_u
	Instantaneous strain, Microstrain			
	110	162	201	257
	Creep strain, Microstrain			
0.1	3.4	6.1	7.3	12.3
0.3	5.7	9.4	13.5	26.0
0.5	8.3	12.4	19.0	37.5
1.0	11.5	16.9	23.9	47.2
2.0	14.3 ± 4%	22.9 ± 3%	32.4 ± 4%	62.0 ± 6%
3.0	18.0	29.3	39.3	73.0
4.0	20.9	34.7	44.6	83.4
5.0	23.5	39.4	49.4	93.0
6.0	25.7	43.5	51.9	101.9
12.0	32.6	56.6	61.1	144.3
24.0	40.6 ± 6%	72.4 ± 3%	73.2 ± 6%	182.2 ± 6%
48.0	49.5	87.4	96.8	224.3
72.0	57.3	100.2	119.8	255.2
96.0	65.3	111.8	140.2	284.0
120.0	72.1	122.8	155.8	305.7
144.0	78.5	131.3	170.3	320.9
168.0	83.7	140.4	180.0	338.8
192.0	88.6	147.5	189.7	354.0
216.0	92.7	156.4	197.3	368.4
240.0	100.3 ± 7%	163.2 ± 4%	205.3 ± 6%	381.5 ± 7%
264.0	105.0	169.5	211.8	392.4
288.0	110.1	174.6	220.0	404.0
312.0	114.8	179.5	225.2	413.5
336.0	117.3	184.2	232.3	422.7
360.0	119.2	187.2	237.2	431.7
384.0	120.2	190.9	245.0	439.4
408.0	120.9	193.7	250.5	446.7
432.0	121.4 ± 8%	196.0	256.4	454.0
456.0	121.4	197.2	261.3	461.0
480.0	121.4	197.9	265.7	467.7
504.0		198.2 ± 6%	269.4	473.7
528.0		198.2	272.2	479.7
552.0		198.2	275.2	485.9
576.0			277.4	491.5
600.0			278.9	495.5
624.0			280.0 ± 7%	501.5
648.0			280.0	506.4
672.0			280.0	510.9
696.0				514.7
720.0				517.6 ± 8%

2) For triaxial compression at 10 N/mm^2 confining pressure, the following relationships were obtained, see Table (7.4) and Fig.(7.4):

at σ_1 = 21 N/mm^2 = 33.7% σ_u

ε = 17 + 47 log t $t \leq 16$ hrs. ..... (7.9)

ε = 40 $t^{0.222}$ $t > 16$ hrs. ..... (7.10)

at σ_1 = 27 N/mm^2 = 43.3% $_u$

ε = 26 + 71 log t $t \leq 16$ hrs. ..... (7.11)

ε = 44 $t^{0.23}$ $t > 16$ hrs. ..... (7.12)

at σ_1 = 41 N/mm^2 = 65.7% σ_u

ε = 104 $t^{0.267}$ ..... (7.13)

at σ_1 = 50 N/mm^2 = 80.2% σ_u

ε = 118 $t^{0.267}$ ..... (7.14)

The lateral creep behaviour at this confining pressure level followed the power law, Eq. (6.23), except at the low and medium stresses for a short duration from the beginning of the tests where the logarithmic law was followed, Eq. (6.22), after which the results deviated to follow the power law. Namely at σ_1 = 21 N/mm^2 (33.7% σ_u) for the first 16 hours and at σ_1 = 27 N/mm^2 (43.3% σ_u) for the first 16 hours also.

3) For triaxial compression at 20 N/mm^2 confining pressure, the following relationships were obtained, see Table (7.5) and Fig. (7.5):

at σ_1 = 27 N/mm^2 = 34.5% σ_u

ε = 17 + 19 log t $t \leq 30$ hrs. ..... (7.15)

ε = 24.5 $t^{0.22}$ $t > 30$ hrs. ..... (7.16)

at σ_1 = 41 N/mm^2 = 52.4% σ_u

ε = 25 $t^{0.338}$ $t \leq 20$ hrs. ..... (7.17)

ε = 64 $t^{0.230}$ $t > 20$ hrs. ..... (7.18)

at σ_1 = 50 N/mm^2 = 64% σ_u

ε = 32.5 $t^{0.387}$ $t < 160$ hrs. ..... (7.19)

ε = 69 $t^{0.242}$ $t \geq 160$ hrs. ..... (7.20)

at σ_1 = 63 N/mm^2 = 80.6% σ_u

ε = 80 $t^{0.49}$ $t \leq 2$ hrs. ..... (7.21)

ε = 97 $t^{0.271}$ $t > 2$ hrs. ..... (7.22)

At this level of confining pressure, the creep behaviour followed a power law, Eq. (6.23), except for the low axial stress σ_1 = 27 N/mm^2 when for the first 17 hours a logarithmic law was followed after which a change to a power law occurred.

4) For triaxial compression at 30 N/mm^2 confining pressure, the following relationships were obtained, see Table (7.6) and Fig. (7.6):

at σ_1 = 27 N/mm^2 = 26.3% σ_u

ε = 12 + 15 log t $t \leq 14$ hrs. ..... (7.23)

ε = 24 $t^{0.189}$ $t > 14$ hrs. ..... (7.24)

at σ_1 = 41 N/mm^2 = 39.8% σ_u

ε = 18 $t^{0.39}$ $t < 160$ hrs. ..... (7.25)

ε = 48 $t^{0.20}$ $t \geq 160$ hrs. ..... (7.26)

at σ_1 = 50 N/mm^2 = 48.7% σ_u

ε = 24.3 $t^{0.4}$ $t < 190$ hrs. ..... (7.27)

ε = 78 $t^{0.21}$ $t \geq 190$ hrs. ..... (7.28)

at σ_1 = 63 N/mm^2 = 61.3% σ_u

ε = 46 $t^{0.41}$ $t < 190$ hrs. ..... (7.29)

ε = 137 $t^{0.225}$ $t \geq 190$ hrs. ..... (7.30)

It is clear from the above equations that the lateral creep behaviour followed the power law, Eq. (6.23), except under low axial stress σ_1 = 27 N/mm^2

(26.3% σ_u) when results followed a logarithmic law before deviating after 14 hours to follow the power law thereafter.

b. Saturated Condition.

The lateral creep results of the saturated gypsum subjected to the uniaxial and triaxial stresses are given in tables from (7.7) to (7.10) and shown in figures from (7.7) to (7.10).

1) For uniaxial compression, the following relationships were obtained according to the applied stresses, see Table (7.7) and Fig. (7.7):

at $\sigma_1 = 8\ N/mm^2 = 37\%\ \sigma_u$

$$\varepsilon = 62\ t^{0.271} \quad \ldots\ldots \quad (7.31)$$

at $\sigma_1 = 11\ n/mm^2 = 52\%\ \sigma_u$

$$\varepsilon = 160\ t^{0.28} \quad \ldots\ldots \quad (7.32)$$

at $\sigma_1 = 15\ N/mm^2 = 70.9\%\ \sigma_u$

$$\varepsilon = 230\ t^{0.285} \quad \ldots\ldots \quad (7.33)$$

at $\sigma_1 = 17\ N/mm^2 = 80.4\%\ \sigma_u$

$$\varepsilon = 283\ t^{0.29} \quad \ldots\ldots \quad (7.34)$$

The lateral creep behaviour in uniaxial stresses in saturated conditions followed the power law for all applied stresses.

2) For triaxial loading at 10 N/mm^2 confining pressure, the following relationships were obtained, see Table (7.8) and Fig. (7.8):

at $\sigma_1 = 15\ N/mm^2 = 33\%\ \sigma_u$

$$\varepsilon = 45 + 30 \log t \qquad t \leq 24 \text{ hrs.} \quad \ldots\ldots \quad (7.35)$$

$$\varepsilon = 76\ t^{0.206} \qquad t > 24 \text{ hrs.} \quad \ldots\ldots \quad (7.36)$$

at $\sigma_1 = 21\ N/mm^2 = 46.3\%\ \sigma_u$

$$\varepsilon = 140 + 75 \log t \qquad t \leq 12 \text{ hrs.} \quad \ldots\ldots \quad (7.37)$$

$$\varepsilon = 158\ t^{0.229} \qquad t > 12 \text{ hrs.} \quad \ldots\ldots \quad (7.38)$$

Table (7.7) Lateral Creep of saturated gypsum in uniaxial compression.

Time, hours	Axial stress, N/mm^2			
	8 37% σ_u	11 52% σ_u	15 70.9% σ_u	17 80.4% σ_u
	Instantaneous strain, Microstrain			
	110	162	250	282
	Creep strain, Microstrain			
0.1	33.2	84.0	119.3	145.1
0.3	42.6	108.5	154.9	189.3
0.5	51.4	131.8	188.8	231.5
1.0	62.0	160.0	230.0	283.0
2.0	74.8 ± 6%	194.3 ± 8%	280.2 ± 6%	346.0 ± 5%
3.0	83.5	217.6	314.6	389.2
4.0	90.3	235.9	341.4	423.0
5.0	95.9	251.1	363.9	451.3
6.0	100.8	264.2	383.3	475.8
12.0	121.6	320.8	467.0	581.8
24.0	146.7 ± 5%	389.6 ± 8%	569.0 ± 6%	711.3 ± 4%
48.0	177.0	473.0	693.2	869.7
72.0	197.6	529.9	778.2	978.2
96.0	213.6	574.3	844.6	1063.3
120.0	226.9	611.4	900.1	1134.4
144.0	238.4	643.4	948.1	1195.9
168.0	248.6	671.7	990.7	1250.6
192.0	257.7	697.3	1029.1	1300.0
216.0	266.1	720.7	1064.3	1345.2
240.0	273.8 ± 5%	742.3 ± 7%	1096.7 ± 4%	1386.9 ± 3%
264.0	281.0	762.4	1126.9	1425.8
288.0	287.7	781.2	1155.2	1462.2
312.0	294.0	798.9	1181.8	1496.6
336.0	299.9	815.6	1207.1	1529.1
360.0	305.6	831.5	1231.0	1560.0
384.0	311.0	846.7	1253.9	1589.4
408.0	316.1	861.2	1275.8	1617.6
432.0	321.1	875.1	1296.7	1644.7
456.0	325.8	888.4	1316.8	1670.7
480.0	330.4	901.3	1336.2	1695.7
504.0	334.8	913.7	1354.9	1719.9
528.0	339.0	925.7	1373.0	1743.2
552.0	343.1	937.3	1390.5	1765.8
576.0	347.1	948.5	1407.5	1787.8
600.0	351.0	959.4	1424.0	1809.0
624.0	354.7	970.0	1440.0	1829.7
648.0	358.4	980.3	1455.5	1849.9
672.0	361.9	990.3	1470.7	1869.5
696.0	365.4	1000.1	1485.5	1888.6
720.0	368.7 ± 5%	1009.7 ± 7%	1499.9 ± 5%	1907.3 ± 4%

Table (7.8) Lateral Creep of saturated gypsum in triaxial at 10 N/mm^2 confining pressure.

Time, hours	Axial stress, N/mm^2			
	15 33% σ_u	21 46.3% σ_u	27 59.5% σ_u	41 90.3% σ_u
	Instantaneous strain, Microstrain			
	140	220	282	467
	Creep strain, Microstrain			
0.1	22.8	66.2	109.2	135.8
0.3	29.6	97.4	154.5	186.7
0.5	34.7	118.0	196.0	222.8
1.0	41.7	142.7	233.5	257.4
2.0	48.6 ± 4%	166.7 ± 6%	272.3 ± 4%	308.4 ± 8%
3.0	55.1	186.7	295.6	348.3
4.0	60.4	197.3	334.5	371.2
5.0	64.7	203.8	360.5	399.7
6.0	68.7	206.8	390.7	434.2
12.0	83.3	225.4	554.1	609.8
24.0	103.3 ± 5%	268.7 ± 5%	817.3 ± 6%	994.5 ± 8%
48.0	133.0	350.1	854.9	1371.8
72.0	149.5	396.3	883.8	1637.0
96.0	172.4	434.6	904.4	1895.2
120.0	193.0	475.8	940.8	2074.9
144.0	206.2	497.5	963.6	2127.0
168.0	219.5	519.1	1004.3	2175.2
192.0	232.0	534.7	1023.1	2232.9
216.0	244.1	547.1	1039.3	2278.8
240.0	255.6 ± 5%	557.9 ± 4%	1058.9 ± 6%	2329.0 ± 8%
264.0	265.0	569.4	1080.9	2380.4
288.0	274.7	580.8	1101.1	2426.2
312.0	285.0	589.8	1120.7	2473.5
336.0	295.5	600.8	1139.2	2513.2
360.0	303.4	615.8	1154.1	2546.2
384.0	313.2	628.1	1166.0	2578.1
408.0	324.4	644.0	1178.2	2606.4
432.0	328.6	649.7	1193.2	2625.5
456.0	337.8	657.2	1205.7	2660.7
480.0	345.7	666.7	1219.6	2665.1
504.0	352.4	675.4	1234.0	2681.7
528.0	358.2	684.9	1250.4	2691.4
552.0	362.9	695.3	1273.1	2705.5
576.0	366.8	703.2	1281.7	2714.1
600.0	370.7	709.8	1295.7	2720.8
624.0	376.9	714.6	1308.7	2727.0
648.0	379.8	719.3	1315.4	2732.1
672.0	383.0	722.1	1323.0	2736.7
696.0	385.2	725.2	1329.5	2739.3
720.0	386.5 ± 6%	727.1 ± 4%	1333.3 ± 7%	2742.9 ± 6%

Table (7.9) Lateral Creep of saturated gypsum in triaxial at 20 N/mm^2 confining pressure.

Time, hours	Axial stress, N/mm^2			
	27 37.7% σ_u	41 57.2% σ_u	50 69.7% σ_u	63 87.9% σ_u
	Instantaneous strain, Microstrain			
	212	348	435	548
	Creep strain, Microstrain			
0.1	22.6	30.6	43.5	452.8
0.3	32.2	44.2	71.7	671.2
0.5	46.6	58.6	96.5	761.8
1.0	57.4	73.9	140.6	848.3
2.0	67.0 ± 4%	84.8 ± 5%	207.0 ± 4%	912.9 ± 5%
3.0	77.5	93.9	265.5	907.8
4.0	86.8	105.0	318.0	993.5
5.0	94.5	114.1	362.0	1024.4
6.0	103.0	123.4	403.2	1057.8
12.0	122.0	148.3	558.5	1133.2
24.0	148.6 ± 3%	173.6 ± 5%	722.5 ± 4%	1184.7 ± 5%
48.0	171.0	205.4	790.5	1262.0
72.0	188.9	230.8	848.2	1356.2
96.0	209.2	257.8	893.7	1427.6
120.0	227.6	276.6	932.6	1498.0
144.0	246.0	295.8	961.1	1545.8
168.0	262.4	313.6	985.9	1572.2
192.0	275.1	327.2	1004.5	1597.3
216.0	288.4	340.9	1028.9	1598.5
240.0	301.5 ± 3%	357.1 ± 3%	1045.7 ± 5%	1631.7 ± 3%
264.0	315.3	368.3	1057.7	1648.5
288.0	328.4	383.2	1073.6	1668.5
312.0	340.9	392.9	1081.2	1685.2
336.0	352.9	405.2	1093.0	1702.4
360.0	368.5	417.1	1102.8	1715.8
384.0	380.4	428.4	1111.6	1731.1
408.0	391.4	437.9	1121.2	1742.8
432.0	402.8	449.8	1128.2	1753.2
456.0	414.5	460.7	1139.0	1768.4
480.0	425.2	469.4	1147.7	1781.3
504.0	437.0	477.4	1157.1	1792.7
528.0	447.9	486.7	1164.9	1800.8
552.0	458.1	493.4	1173.2	1816.5
576.0	468.2	502.5	1180.2	1825.1
600.0	478.7	510.6	1189.5	1832.8
624.0	488.9	518.3	1198.0	1844.1
648.0	499.0	526.3	1206.0	1853.7
672.0	508.7	532.4	1212.9	1862.9
696.0	518.9	539.0	1220.3	1872.9
720.0	519.1 ± 2%	544.8 ± 3%	1226.2 ± 6%	1881.3 ± 3%

Table (7.10) Lateral Creep of saturated gypsum in triaxial at 30 N/mm^2 confining pressure.

Time, hours	Axial stress, N/mm^2			
	27 29.3% σ_u	41 44.5% σ_u	50 54.3% σ_u	63 68.3% σ_u
	Instantaneous strain, Microstrain			
	127	241	357	454
	Creep strain, Microstrain			
0.1	12.0	19.2	32.6	102.5
0.3	19.9	36.7	55.6	142.7
0.5	28.0	47.6	83.0	190.7
1.0	42.6	64.7	123.6	238.7
2.0	50.4 ± 5%	74.8 ± 2%	154.8 ± 3%	312.1 ± 4%
3.0	59.6	85.0	184.3	379.3
4.0	66.0	91.9	213.8	438.2
5.0	72.2	99.0	269.7	465.6
6.0	77.4	104.2	259.9	501.1
12.0	95.0	123.7	335.9	682.4
24.0	118.8 ± 4%	154.6 ± 2%	461.2 ± 3%	792.3 ± 4%
48.0	141.1	175.4	521.0	931.1
72.0	160.1	198.1	551.5	982.1
96.0	175.9	210.4	580.5	1021.1
120.0	190.3	224.6	608.2	1043.6
144.0	203.4	236.7	630.8	1069.7
168.0	217.0	247.1	652.3	1093.9
192.0	227.9	257.4	671.5	1126.9
216.0	238.8	265.9	691.7	1160.5
240.0	249.0 ± 4%	276.9 ± 4%	709.0 ± 5%	1191.3 ± 3%
264.0	259.1	286.7	726.1	1213.6
288.0	267.6	296.3	741.4	1231.2
312.0	276.2	305.8	754.6	1253.5
336.0	285.7	315.1	770.1	1275.2
360.0	295.2	324.6	782.9	1290.3
384.0	301.4	349.4	794.5	1305.1
408.0	308.1	342.7	804.8	1319.6
432.0	314.9	350.4	816.5	1333.0
456.0	320.1	356.4	825.4	1350.2
480.0	326.9	363.9	835.6	1357.9
504.0	333.8	370.9	846.6	1368.4
528.0	339.2	378.6	857.5	1378.4
552.0	345.3	386.0	866.0	1390.4
576.0	351.3	392.3	874.1	1398.8
600.0	356.3	403.7	883.5	1409.6
624.0	360.7	409.2	891.5	1415.8
648.0	364.7	414.8	899.9	1427.0
672.0	367.7	418.3	906.1	1433.8
696.0	370.3	422.2	911.6	1440.5
720.0	373.1 ± 3%	425.2 ± 4%	916.3 ± 5%	1446.6 ± 2%

at σ_1 = 27 N/mm^2 = 59.5% σ_u

ε = 238 $t^{0.30}$ $t \leq$ 24 hrs. ..... (7.39)

ε = 270 $t^{0.238}$ $t >$ 24 hrs. ..... (7.40)

at σ_1 = 41 N/mm^2 = 90.3% σ_u

ε = 265 $t^{0.297}$ $t \leq$ 1 hr. ..... (7.41)

ε = 265 $t^{0.40}$ $t >$ 1 hr. ..... (7.42)

It can be seen from the above equations that the lateral creep at this level of confining pressure followed the power law, except for low axial stresses within a short duration of the beginning of the tests. Where the logarithmic law was followed, see Eqs. (7.35) and (7.37).

3) For triaxial compression at 20 N/mm^2 confining pressure, the following relationships were obtained, see Table (7.9) and Fig. (7.9):

at σ_1 = 27 N/mm^2 = 37.7% σ_u

ε = 75 + 37 log t $t <$ 60 hrs. ..... (7.43)

ε = 77 $t^{0.238}$ $t \geq$ 60 hrs. ..... (7.44)

at σ_1 = 41 N/mm^2 = 57.2% σ_u

ε = 96 + 54 log t $t <$ 60 hrs. ..... (7.45)

ε = 93 $t^{0.251}$ $t \geq$ 60 hrs. ..... (7.46)

at σ_1 = 50 N/mm^2 = 69.7% σ_u

ε = 170 + 120 log t $t \leq$ 4 hrs. ..... (7.47)

ε = 339 $t^{0.258}$ $t >$ 4 hrs. ..... (7.48)

at σ_1 = 53 N/mm^2 = 87.9% σ_u

ε = 825 + 245 log t $t <$ 35 hrs. ..... (7.49)

ε = 472 $t^{0.282}$ $t \geq$ 35 hrs. ..... (7.50)

At this level of the confining pressure, the lateral creep behaviour followed

the logarithmic law for a short time at the beginning of the tests (less than 60 hours), then followed the power law thereafter.

4) For triaxial compression at 30 N/mm^2 confining pressure, the following relationships were obtained, see Table (7.10) and Fig. (7.10):

at σ_1 = 27 N/mm^2 = 29.3% σ_u

$$\varepsilon = 45 + 42 \log t \qquad t \leq 1.5 \text{ hrs.} \quad \ldots\ldots \qquad (7.51)$$

$$\varepsilon = 66\ t^{0.215} \qquad t > 1.5 \text{ hrs.} \quad \ldots\ldots \qquad (7.52)$$

σ_1 = 41 N/mm^2 = 44.5% σ_u

$$\varepsilon = 70 + 75 \log t \qquad t \leq 3 \text{ hrs.} \quad \ldots\ldots \qquad (7.53)$$

$$\varepsilon = 75\ t^{0.223} \qquad t > 3 \text{ hrs.} \quad \ldots\ldots \qquad (7.54)$$

σ_1 = 50 N/mm^2 = 54.5% σ_u

$$\varepsilon = 123 + 89 \log t \qquad t < 35 \text{ hrs.} \quad \ldots\ldots \qquad (7.55)$$

$$\varepsilon = 239\ t^{0.232} \qquad t \geq 35 \text{ hrs.} \quad \ldots\ldots \qquad (7.56)$$

σ_1 = 63 N/mm^2 = 68.4% σ_u

$$\varepsilon = 240 + 145 \log t \qquad t < 40 \text{ hrs.} \quad \ldots\ldots \qquad (7.57)$$

$$\varepsilon = 358\ t^{0.267} \qquad t \geq 40 \text{ hrs.} \quad \ldots\ldots \qquad (7.58)$$

The lateral creep behaviour at this confining pressure followed the logarithmic law in a similar way of that at 20 N/mm^2 confining pressure, for a short duration at the beginning of the tests (less than 40 hrs) then departed to follow the power law thereafter.

In the previous equations, from (7.1) to (7.58) the constants A, B, C and n, in Eqs. (6.22) and (6.23), were found by using the graphical method and checked by using the least square method. All the results were in a good and reasonable agreement.

7.3 Effect of the Axial Stress on the lateral Creep.

The effect of varying the axial stress on the lateral creep was studied in uniaxial and triaxial compression and in dry and saturated conditions.

It can be seen from the tables (7.3) to (7.10) and the figures (7.3) to (7.10) that the lateral creep strain occurred at every stress and both the instantaneous and the creep strains are increased with increasing the axial stress. The instantaneous lateral strain was plotted against the axial stresses at various confining pressures, see Fig. (7.15). It can be noted that the relationship is nearly linear for the given axial stresses as a percentage of σ_u (which is not more than 90% σ_u) with a small scatter at high stresses. The instantaneous axial and lateral strains were used together to find the Poisson's ratio, see Fig. (6.39) and (7.15), in which:

$$\text{Poisson's ratio } (\mathcal{f}) = \frac{\text{lateral instantaneous strain}}{\text{axial instantaneous strain}}$$

Table (7.11) gives the values of the Poisson's ratio calculated by this method for various confining pressures in the two environmental conditions.

Table (7.11) Poisson's ratio calculated by using instantaneous strain.

Confining Pressure, N/mm^2	Poisson's ratio	
	Dry	Saturated
Zero (Uniaxial)	0.27	0.41
10	0.23	0.35
20	0.21	0.26
30	0.20	0.25

The Poisson's ratio calculated from the short term tests with their non-linear axial and lateral stress strain curves, Table (4.15) is found to be more than that calculated from the instantaneous axial and lateral strains, Table (7.11), under similar confining pressure levels. Since the stress-instantaneous strain curves in both axial and lateral results

are straight lines which may be considered as elastic behaviour, it represents the initial tangent or the elastic portion of the non-linear stress-strain curves. In other words, the observed increase in the Poisson's ratio of high stresses is due to the fact that the material deforms in an elastic manner up to certain axial stress which is less than the ultimate, following which strains become affected by plastic deformation. The increase in the Poisson's ratio with increasing stress in some rocks has been associated with the plastic deformation in the specimen[126].

The effect of the axial stress on the lateral creep behaviour in both dry and saturated conditions is as follows:

a. <u>For dry Condition:</u>

The creep behaviour of gypsum uniaxial and triaxial stress conditions generally followed the power law, Eq. (6.23), at all confining pressures under all the axial stresses, except within a short time (less than 30 hrs.) of the beginning of tests with specimens subjected to low axial stresses (27-35% σ_u), at 10, 20 and 30 N/mm^2 confining pressure where the behaviour followed the logarithmic law, Eq. (6.22), see Eqs. (7.9), (7.15) and (7.23).

b. <u>For Saturated Condition:</u>

The lateral creep behaviour under the saturated condition followed the power law also, Eq. (6.23), except in the following cases where it followed the logarithmic law, Eq. (6.22); within a short time (less than 60 hrs. of beginning of tests) under low and medium axial stress (not more than 47% σ_u) at 10 N/mm^2 confining pressure, see Eqs. (7.35) and (7.37), and at 20 and 30 N/mm^2 confining pressure within a short time (less than 60 hrs.) of the beginning of the tests.

Sangha and Chir[127] reported that the lateral creep strain of sandstone increases with increasing the axial stresses at constant confining pressure and at any particular time.

Hofer and Knoll[90] reported that at low stress the creep behaviour of the carnallitite was represented by a logarithmic law and at medium and high stresses the creep was represented by a power law. Singh[97] found that the lateral creep of dry Sicilian marble in uniaxial compression followed the power law, Eq. (6.23). Barron and Toews[128] found that the radial creep data around a mine shaft in salt can be fitted by a logarithmic relationship of the form, $\varepsilon = A \log (1 + Bt)$ where A and B are constants.

It can be seen from the relationships obtained that an increase in the axial stress increases the values of the constants A and B of the logarithmic law at a constant confining pressure, these values are given in tables (7.12) and (7.13) for dry and saturated conditions respectively. It can be seen also that the values of the constants C and n of the power law are increased with the axial stress, the values of the power law n was found to be $0 < n < 1$, see tables (7.12) and (7.13). The values of the constants C and n are plotted against the axial stress for various confining pressures in Fig. (7.16) and (7.17) for C and n respectively, and under both environmental conditions. These figures show non-linear relationships under the triaxial stresses while nearly linear under the uniaxial stresses as was also the case with the axial creep, Figs. (6.41) and (6.42). An increase in the creep equation constants A, B, C and n with increasing axial stress means in other words, increasing the creep rate with increasing the axial stress.

The values of the creep rate at various axial stresses, loading times and confining pressure levels are given in tables (7.12) and (7.13) for dry and saturated conditions respectively. The creep rate plotted against the axial stress for various confining pressure at given time, t = 240 hrs. is shown in Fig. (7.18) for both environmental conditions. It can be seen that the creep rate increases in a non-linear manner in the case of the

Table (7.12) Lateral creep equation constants and creep rate of dry gypsum in uniaxial and triaxial compression creep tests.

σ_1 kg/mm²	$\frac{\sigma_1}{\sigma_u} \times 100$ / σ_1	Creep equation	Constants C or A	Constants n or B	Creep Rate, microstrain/hr. at t = 1 hr.	12 jr.	24 hr.	48 hr.	96 hr.	120 hr.	240 hr.	360 hr.	480 hr.	720 hr.
0 Uniaxial	36%	$\varepsilon = 32.5t^{0.355}$ $t \leq 2$	32.5	0.355	11.54	-	-	-	-	-	-	-	-	-
	15	$\varepsilon = 34\ t^{0.257}$ $t \geq 2$	34	0.257	-	4.0	0.83	0.49	0.29	0.25	0.15	0.11	0.09	0.07
	50.3%	$\varepsilon = 32.5\ t^{0.355}$ $t \leq 12$	32.5	0.355	11.54	2.32	-	-	-	-	-	-	-	
	21	$\varepsilon = 36.5\ t^{0.296}$ $t \geq 12$	36.5	0.296	-	-	1.15	0.71	0.44	0.37	0.23	0.17	0.14	0.11
	65%	$\varepsilon = 32.5\ t^{0.355}$ $t \leq 25$	32.5	0.355	11.54	2.32	1.49	-	-	-	-	-	-	-
	27	$\varepsilon = 37.5\ t^{0.318}$ $t \geq 25$	37.5	0.318	-	-	-	0.85	0.53	0.46	0.28	0.22	0.18	0.14
	81.8%	$\varepsilon = 37.5\ t^{0.355}$ $t \leq 54$	37.5	0.355	13.3	2.7	1.7	0.95	-	-	-	-	-	-
	34	$\varepsilon = 45\ t^{0.34}$ $t \geq 54$	45	0.34	-	-	-	-	0.75	0.65	0.41	0.31	0.26	0.2
10	33.7%	$\varepsilon = 17+47 \log t$ $t \leq 10$	17	47	47	-	-	-	-	-	-	-	-	-
	21	$\varepsilon = 40\ t^{0.222}$ $t \geq 10$	40	0.222	-	1.28	0.75	0.44	0.25	0.21	0.13	0.09	0.07	0.05
	43.3%	$\varepsilon = 26+71 \log t$ $t \leq 10$	26	71	71	-	-	-	-	-	-	-	-	-
	27	$\varepsilon = 44\ t^{0.23}$ $t \geq 10$	44	0.23	-	1.5	0.88	0.51	0.30	0.25	0.15	0.11	0.09	0.06
	65.7% 41	$\varepsilon = 104\ t^{0.242}$	104	0.242	25.17	3.83	2.26	1.33	0.79	0.67	0.40	0.29	0.23	0.17
	80.2% 50	$\varepsilon = 118\ t^{0.267}$	118	0.267	31.5	5.1	3.07	1.85	1.11	0.94	0.57	0.42	0.34	0.25
20	34.5%	$\varepsilon = 17+19 \log t$ $t \leq 30$	17	19	19	1.58	1.25	-	-	-	-	-	-	-
	27	$\varepsilon = 24.5\ t^{0.22}$ $t \geq 30$	24.5	0.22	-	-	-	0.26	0.15	0.13	0.08	0.05	0.04	0.03
	52.4%	$\varepsilon = 25\ t^{0.338}$ $t \leq 100$	25	0.338	8.45	1.63	1.03	0.65	0.43	-	-	-	-	-
	41	$\varepsilon = 64\ t^{0.23}$ $t \geq 100$	64	0.23	-	-	-	-	-	0.37	0.22	0.16	0.13	0.09
	64%	$\varepsilon = 32.5\ t^{0.387}$ $t \leq 160$	32.5	0.387	12.57	2.74	1.79	1.17	0.77	0.66	-	-	-	-
	50	$\varepsilon = 69\ t^{0.242}$ $t \leq 160$	69	0.242	-	-	-	-	-	-	0.26	0.2	0.15	0.11
	80.6%	$\varepsilon = 80\ t^{0.49}$ $t \leq 2$	80	0.49	39.2	-	-	-	-	-	-	-	-	-
	63	$\varepsilon = 97\ t^{0.271}$ $t \geq 2$	97	0.271	-	4.36	2.59	1.56	0.94	0.80	0.48	0.36	0.29	0.21
30	26.3%	$\varepsilon = 12+15 \log t$ $t \leq 14$	12	15	15	0.8	-	-	-	-	-	-	-	-
	27	$\varepsilon = 24\ t^{0.189}$ $t \geq 14$	24	0.189	-	-	0.35	0.2	0.11	0.09	0.05	0.04	0.03	0.02
	39.8%	$\varepsilon = 18\ t^{0.39}$ $t \leq 160$	18	0.39	7.02	1.55	1.0	0.67	0.43	0.38	-	-	-	-
	41	$\varepsilon = 48\ t^{0.20}$ $t \geq 160$	48	0.2	-	-	-	-	-	-	0.12	0.09	0.07	0.05
	48.7%	$\varepsilon = 24.3\ t^{0.4}$ $t \leq 190$	24.3	0.4	9.72	2.18	1.44	0.95	0.63	0.55	-	-	-	-
	50	$\varepsilon = 78\ t^{0.210}$ $t \geq 190$	78	0.21	-	-	-	-	-	-	0.22	0.16	0.12	0.09
	61.3%	$\varepsilon = 46\ t^{0.41}$ $t \leq 190$	46	0.41	18.86	4.34	2.89	1.92	1.28	1.11	-	-	-	-
	63	$\varepsilon = 137\ t^{0.225}$ $t \geq 190$	137	0.225	-	-	-	-	-	-	0.44	0.35	0.26	0.19

Table (7.13) Lateral creep equation constants and creep rate of saturated gypsum in uniaxial and triaxial compression creep tests.

σ_1 kg/cm^2	$\frac{\sigma_1}{\sigma_u} \times 100$ / σ_1	Creep equation	Constants C or A	Constants n or B	Creep Rate, microstrain/hr. at t = 1 hr.	12 hr.	24 hr.	48 hr.	96 hr.	120 hr.	240 hr.	360 hr.	480 hr.	720 hr.
0 Uniaxial	37% 8	$\varepsilon = 62\ t^{0.271}$	62	0.271	16.8	2.75	1.71	1.03	0.62	0.53	0.32	0.24	0.19	0.14
	52% 11	$\varepsilon = 160\ t^{0.28}$	160	0.28	44.8	7.87	4.54	2.76	1.68	1.43	0.87	0.65	0.53	0.39
	70.9% 15	$\varepsilon = 230\ t^{0.285}$	230	0.285	65.6	11.1	6.76	4.12	2.51	2.13	1.30	0.98	0.79	[illegible]
	80.4% 17	$\varepsilon = 283\ t^{0.29}$	283	0.29	82.1	14.1	8.59	5.24	3.21	2.74	1.68	1.26	1.02	0.77
10	33%	$\varepsilon = 45 + 30 \log t$ $t \leq 24$	45	30	30	2.5	1.25	-	-	-	-	-	-	-
	15	$\varepsilon = 76\ t^{0.206}$ $t \geq 24$	76	0.206	-	-	-	0.73	0.42	0.35	0.20	0.16	0.12	0.08
	46.3%	$\varepsilon = 140 + 75 \log t$ $t \leq 12$	140	75	75	6.25	-	-	-	-	-	-	-	
	21	$\varepsilon = 158\ t^{0.229}$ $t > 12$	158	0.229	-	-	3.12	1.83	1.07	0.90	0.53	0.39	0.31	0.23
	59.5%	$\varepsilon = 238\ t^{0.30}$ $t \leq 24$	238	0.3	71.4	12.54	7.7	-	-	-	-	-	-	-
	27	$\varepsilon = 270\ t^{0.238}$ $t \geq 24$	270	0.238	-	-	-	3.36	1.98	1.67	0.98	0.72	0.58	0.42
	90.3%	$\varepsilon = 265\ t^{0.297}$ $t \leq 1$	265	0.297	77.9	-	-	-	-	-	-	-	-	-
	41	$\varepsilon = 265\ t^{0.4}$ $t > 1$	265	0.4	-	2.38	1.57	10.4	7.5	6.0	4.0	3.1	2.6	2.0
20	37.7%	$\varepsilon = 75 + 37 \log t$ $t \leq 60$	75	37	37	3.08	1.54	0.77	-	-	-	-	-	-
	27	$\varepsilon = 77\ t^{0.238}$ $t \geq 60$	77	0.238	-	-	-	-	0.57	0.48	0.28	0.21	0.17	0.12
	57.2%	$\varepsilon = 96 + 54 \log t$ $t \leq 60$	96	54	54	4.5	2.25	1.12	-	-	-	-	-	-
	41	$\varepsilon = 93\ t^{0.251}$ $t \geq 60$	93	0.251	-	-	-	-	0.76	0.65	0.38	0.28	0.23	[illegible]
	69.7%	$\varepsilon = 170 + 120 \log t$ $t \leq 4$	170	120	120	-	-	-	-	-	-	-		
	50	$\varepsilon = 339\ t^{0.258}$ $t \geq 4$	339	0.258	-	13.83	8.27	4.95	2.96	2.51	1.5	[illegible]	[illegible]	0.46
	87.9%	$\varepsilon = 825 + 245 \log t$ $t \leq 35$	825	245	245	20.41	10.2	-	-	-	-	-	-	-
	63	$\varepsilon = 472\ t^{0.282}$ $t \geq 35$	472	0.282	-	-	-	8.26	5.02	4.28	2.60	1.94	1.58	1.18
10	29.3%	$\varepsilon = 45+42 \log t$ $t \leq 1.5$	45	42	42	-	-	-	-	-	-	-	-	-
	27	$\varepsilon = 66\ t^{0.215}$ $t \geq 1.5$	66	0.215	-	2.02	1.17	0.68	0.39	0.33	0.19	0.14	0.11	0.08
	44.5%	$\varepsilon = 70+75 \log t$ $t \leq 3$	70	75	75	-	-	-	-	-	-	-	-	
	41	$\varepsilon = 75\ t^{0.223}$ $t \geq 3$	75	0.223	-	2.43	1.41	0.83	0.48	0.41	0.24	0.17	0.14	[illegible]
	54.3%	$\varepsilon = 123+89 \log t$ $t \leq 35$	123	89	89	7.42	3.71	-	-	-	-	-	-	-
	50	$\varepsilon = 239\ t^{0.232}$ $t \leq 35$	239	0.232	-	-	-	2.84	1.67	1.40	[illegible]	[illegible]	[illegible]	[illegible]
	68.4%	$\varepsilon = 240+145 \log t$ $t \leq 40$	240	145	145	12.1	6.1	-	-	-	-	-	-	-
	63	$\varepsilon = 358\ t^{0.267}$ $t \geq 40$	358	0.267	-	-	-	5.60	3.37	2.86	1.72	1.28	1.04	0.77

triaxial stresses whereas a nearly linear relationship exists in the case of the uniaxial stresses. Fig. (7.19) shows the creep rate versus the axial stress on log-log graph. A linear relationship was obtained for every time under each given confining pressure. The figure shows four sets of straight lines in two pairs, one for uniaxial and the other for triaxial at 10 N/mm^2 confining pressure, each pair consists of dry and saturated sets. The linear relationship on the log-log graph indicated that the creep rate follows a power law of the form; $\dot{\varepsilon} = R\,\sigma_1^{K}$ where $\dot{\varepsilon}$ is the creep rate in microstrain per hour, σ_1 is the axial stress in N/mm^2 and R and K are constants with R representing the creep rate at $\sigma_1 = 1\ N/mm^2$ and K representing the slope of the straight line on the log-log graph. Since the straight lines of each σ_3 level are parallel or nearly parallel to each other, they have the same slope or K value. The following equations fit the data at 10 N/mm^2 confining pressure:

For dry condition

$$\dot{\varepsilon} = R\,\sigma_1^{1.766} \quad \text{.....} \quad (7.59)$$

For saturated condition

$$\dot{\varepsilon} = R\,\sigma_1^{2.625} \quad \text{.....} \quad (7.60)$$

This lateral creep rate behaviour is essentially similar to that in the axial creep studies of the same specimens (Chapter 6).

Hebblewhite et al.[103] measured the radial creep rate at a deep point in a shaft excavation of potash mine, he found that the radial creep rate was represented by a power law of a form $\dot{\varepsilon} = At^{B}$ where A and B are constants. Singh[97] reported that the axial stress increases both the axial and lateral creep rates.

At constant differential stresses $(\sigma_1 - \sigma_3)$, it was found that the lateral creep rate decreases with increasing the axial stresses; this behaviour being the opposite of that observed with axial creep. The

relationship between the axial stress and the creep rate at $(\sigma_1 - \sigma_3)$ = 10 N/mm^2 is plotted in Figs. (7.20) and (7.21) for dry and saturated conditions respectively. It can be seen that the creep rate decreases slightly in a non-linear pattern with increasing the axial stress. It appears from this result that an increase in confining pressure results in a decrease of ductility of the material although to a similar extent than the increase in that property observed when considering axial strains. The effect of confining pressure will be discussed in more detail in the next section.

7.4 Lateral Creep Under Various Confining Pressures.

The values of the Poisson's ratio calculated by using the instantaneous axial and lateral strains are plotted against the confining pressure in Fig. (7.22) for both dry and saturated conditions. It can be noted that the Poisson's ratio (which represents the initial tangent Poisson's ratio) decreases with increasing the confining pressure. This indicated that the resistance to the lateral deformation with increasing confinement is greater than the corresponding resistance to the axial deformation. These results are in agreement with the results obtained by Dhir and Sangha[33,34]. It is also clear from the Fig. (7.22) that the effect of the confining pressure on the Poisson's ratio of the saturated rock is more than the dry rock. Lama and Vutukuri[126] reported that the confining pressure lowers the values of the initial tangent Poisson's ratio for weaker rocks, but for stronger rocks it may not have any influence. The above conclusion confirms this result because, generally the saturated gypsum is weaker than the dry.

The lateral creep strain was found to decrease with increasing the confining pressure at a constant axial stress. Figs. (7.23) and (7.24) for dry and saturated conditions respectively show the lateral creep curves under

a constant axial stress of 27 N/mm^2 at various confining pressure levels, namely; 10, 20, and 30 N/mm^2. It can be seen that the effect of the confining pressure of equal increments is larger at low values of σ_3 than higher. As in the case of the instantaneous lateral strain, the effect of equal variation of σ_3 is larger on the lateral creep strain of the saturated specimen than on the dry specimens.

At constant $(\sigma_1 - \sigma_3)$, the effect of the confining pressure on the lateral creep strain is shown in Figs. (7.25) and (7.26) for dry and saturated conditions respectively. It is clear from these figures that the lateral creep strain decreases with increasing confining pressure at constant differential stress, and the effect of equal increments of σ_3 on the creep strain at constant $(\sigma_1 - \sigma_3)$ is higher at the low values of σ_3 than the higher as observed in the case of instantaneous strain and creep strain with the confining pressure. Increasing σ_3 at constant $(\sigma_1 - \sigma_3)$ means increasing σ_1 by the same amount to keep the difference constant. Since the results showed a decrease in the creep strain, this indicated that the effect of the confining pressure on the lateral strain is more than the effect of the axial stress. Sangha and Dhir[33,34] also found that the confining pressure decreases the lateral deformation of the sandstone at constant $(\sigma_1 - \sigma_3)$.

Fig. (7.27) shows the effect of σ_3 on the values of the creep equation constants C and n, Eq. (6.23). It can be seen that at constant axial stress, increasing the confining pressure decreases the values of these constants in both environmental conditions dry and saturated. The decrease in the constants C and n corresponds with a decrease in the lateral creep rate with increasing the confinement at a constant axial stress as observed earlier (Fig. 7.18). Fig. (7.28) shows the influence of the confining pressure on the lateral creep rate under a constant $\sigma_1 = 41$ N/mm^2 at various loading times and in both dry and saturated conditions. It is clear that increasing

the confining pressure decreases the lateral creep rate in a non-linear manner. The effect of variation of σ_3 is observed to be greater at low values of σ_3 than at higher for both dry and saturated conditions especially in the latter, and the curves plotted at various loading times are approximately parallel to each other. A possible explanation for this is that the confining pressure causes a decrease in the size, number and propagation of the cracks during the creep process, and particularly the cracks which are parallel to the axial stress direction or at small angle to it.

Murrell[24] considered that the confining pressure causes a closing or change of the shape of some of the cracks and other defects in rock. Figs. (7.29) and (7.30) show the effect of the confining pressure on the lateral creep rate at constant $(\sigma_1 - \sigma_3) = 10$ N/mm^2 for dry and saturated conditions respectively. It can be seen that increasing confining pressure results in a decrease in the creep rate at constant $(\sigma_1 - \sigma_3)$ at a particular loading time. The figures show also a decrease in the creep rate with the time at a given σ_3, and this effect is more marked at the earlier stages of the creep than the later. The lateral creep rate at 24 hrs. is plotted against confining pressure for various $(\sigma_1 - \sigma_3)$ values in Figs. (7.31) and (7.32) for dry and saturated conditions respectively. The effect of confinement is shown to be greater in the saturated conditions than the dry. In saturated conditions the effect of σ_3 on the lateral creep rate increases with increasing $(\sigma_1 - \sigma_3)$. Figs. (7.33) and (7.34) show also the effect of the differential stresses on the lateral creep rate at constant confining pressures. Since increasing σ_3 at constant $(\sigma_1 - \sigma_3)$ means increasing σ_1 by the same magnitude, this indicates that the effect of the confining pressure on the lateral creep rate is more than the effect of the axial stress when both σ_1 and σ_3 varied by the same increments, as observed in the case of lateral creep strain.

Wawersik[96] reported a decrease of the lateral creep rate of the saturated westerly granite with increasing the confining pressure at constant $(\sigma_1 - \sigma_3)$.

It can be seen from Figs. (7.33) and (7.34) that the lateral creep rate in both environmental conditions are increased with increasing $(\sigma_1 - \sigma_3)$ at a constant σ_3. The relationship between the lateral creep rate and the differential stresses is found to be linear or nearly linear for a constant σ_3 in dry and saturated conditions. The straight lines for the various σ_3 values are parallel to each other in the case of the dry conditions whereas in saturated conditions the slope of the straight lines increases with the confining pressure indicating that the effect of the confining pressure at high values of $(\sigma_1 - \sigma_3)$ is more than at lower. This means that in dry conditions the value of $(\sigma_1 - \sigma_3)$ alone has the largest influence on the lateral creep strain and confinement only a minor one. This is not true in the case of saturated rock where variation in σ_3 and of $(\sigma_1 - \sigma_3)$ both influence creep rate to a large extent.

Wawersik[96] reported similar behaviour for the lateral creep rate of the saturated westerly granite with $(\sigma_1 - \sigma_3)$ at constant σ_3. Murrell[116] reported that at low differential stresses the dimeteral strain at constant σ_3 is comparatively small, but as the pores are closed up the amount of strain per unit of stress increases. Then as the stress increases, the opening of the cracks causes the dimetral strain to increase at more rapid rate with the stress.

7.5 Influence of Water Saturation on the Lateral Creep.

The effect of saturation on lateral creep was studied in the same way as in the axial creep. In most of the cases an effect similar to that on the axial creep was obtained. A brief discussion will be given here for the lateral creep behaviour in the water saturated conditions. Table (7.14)

gives the instantaneous lateral strain in dry and saturated condition under similar stress levels. It can be seen that the water saturation increases these strains by appreciable amounts, the increase ranging from 50 to 150% with 80% as an average value. The initial tangent Poissons ratio which was calculated by using the instantaneous strains is increased by 25-52% due to water saturation, see Table (7.11). Man and Fatt[53] reported an increase in the lateral strain of three sandstones by about 100% for Bandera sandstone and 35% for the other two. He reported also an increase in the Poisson's ratio by about 100% for the Bandera sandstone and a small amount for the other two.

The water saturation was found to increase the lateral creep strain by remarkable amounts. Figs. (7.3) to (7.10) gives the creep curves of dry and saturated conditions, the details are given in Tables (7.3) to (7.10) for the uniaxial and triaxial stress conditions. The lateral creep strain/time relationships are plotted for dry and saturated conditions under the same stress level of σ_1 and σ_3 in Fig. (7.35). It can be seen from this particular example that the presence of water increased the strain by a ratio of about 2 to 5 with 4 as an approximate average value, in the case of $\sigma_1 = 41$ N/mm^2 and $\sigma_3 = 10$ N/mm^2, and increased the strain by about 2 to 4 times with 2.7 as an average in the case of $\sigma_1 = 63$ N/mm^2 and $\sigma_3 = 30$ N/mm^2. Figs. (7.25) and (7.26) show the increase in the creep strain under a constant $(\sigma_1 - \sigma_3)$ due to water saturation.

The creep data in most of the cases followed the same behaviour in both dry and saturated conditions either the logarithmic law, Eq. (6.22), or the power law, Eq. (6.23), except in a few cases where the behaviour changed from the logarithmic law in dry condition to power law in saturated condition or from power law in dry to logarithmic in saturated under high confining pressure for a short duration from the beginning of the tests, see Tables (7.12) and (7.13).

Table (7.14) Effect of Saturation on the lateral instantaneous strain (ε_o) in unixial and triaxial creep.

σ_3 N/mm^2	σ_1 N/mm^2	Dry		Saturated		Increase in ε_o due to saturation %
		% σ_u	Inst. Strain (ε_o) μs	% σ_u	Inst. Strain (ε_o) μs	
0 Uniaxial	15	36	100	70.9	250	150
10	21	33.7	110	46.3	220	100
	27	43.3	143	59.5	280	97
	41	65.7	250	90.3	467	87
20	27	34.5	129	37.7	212	65
	41	52.4	200	57.2	348	74
	50	64	280	69.7	435	56
	63	80.6	356	87.9	548	54
30	27	26.3	110	29.3	176	60
	41	39.8	162	44.5	241	49
	50	48.7	201	54.3	357	78
	63	61.3	257	68.3	454	77

The values of the creep equation constants C and n was found to be increased by water saturation. Figs. (7.16) and (7.17) show the effect of the saturation on the values of C and n respectively. The water increases the value of C by up to about 400% sometimes and increases the n values by about 25%. Increasing the constants C and n in the presence of water means an increase of the creep rate. Figs. (7.18) and (7.28) show the effect of the saturation on the lateral creep rate at various axial stresses,confining pressures and loading times. It can be seen from these figures and from the tables (7.12) and (7.13) that water saturation increases the lateral creep rate by appreciable amounts. The effect of the saturation on the lateral creep rate was found to be an increase with increasing σ_1 and a decrease when increasing σ_3. The lateral creep rate was increased by the water saturation by about 1 to 10 with 6 fold as an average value. As discussed in Sec. (7.3) the lateral creep rate increases in both environmental conditions with the axial stress and followed the relationship $\dot{\epsilon} = R\ \sigma_1^K$, the constants R and K are found to increase with the saturation, i.e. the value of R is increased by about 50-90% with 60% as an average. This means that the effect of the saturation increases the effect of the axial stress on the lateral creep rate.

At constant $(\sigma_1 - \sigma_3)$, Figs. (7.20), (7.21), (7.29) and (7.30) show that the water saturation increases the lateral creep rate under any similar condition of varying σ_1, σ_3 or the loading time. As mentioned previously, in both dry and saturated conditions lateral creep rate increases with increasing $(\sigma_1 - \sigma_3)$ at constant σ_3 values, see Figs. (7.31), (7.32), (7.33) and (7.34). These figures show that the effect of increasing the lateral creep rate in saturated condition with $(\sigma_1 - \sigma_3)$ is greater than this effect in dry condition, on the other hand, the decrease of the lateral creep rate with increasing σ_3 at constant $(\sigma_1 - \sigma_3)$ seems to be uniform in dry conditions

whereas in saturated conditions the decrease becomes more with increasing σ_3 especially at the low values of σ_3.

The creep behaviour of dry and saturated rocks, as shown in Figs. (7.33) and (7.34) indicates that in dry condition the differential stresses $(\sigma_1 - \sigma_3)$ has the largest influence on the lateral creep rate and the confinement (σ_3) only a minor one. Whereas in saturated gypsum the variation of both σ_3 and $(\sigma_1 - \sigma_3)$ influences the creep rate to a large extent. This result shows that the mechanism of the lateral creep in dry and water saturated conditions are different. In the dry condition the flow processes related to shear stresses, in this case $(\sigma_1 - \sigma_3)$ gave equal gradients of the linear relationships with creep rate for various σ_3 values and this shear stress appears to largely control deformation in the lateral direction. In saturated rock, the increase of the gradient of the linear relationships, $(\sigma_1 - \sigma_3)$ vs. $\dot{\varepsilon}$, with increasing σ_3 and the change of the σ_3 effect on the creep rate at constant $(\sigma_1 - \sigma_3)$, i.e. suggesting that at low values of $(\sigma_1 - \sigma_3)$ the effect of σ_3 on creep rate may be reversed indicate more complex creep processes in the saturated conditions, (possibly solution, recrystallization, etc.) as was observed in consideration of axial creep.

The first stage of the creep process probably represents a period of closing the cracks which are perpendicular or diagonal to the axial stress direction and opening the cracks parallel to the direction, after which cracks may propagate, the presence of water shortens the time of propagation, in other words, increases the rate of propagation, the cracks then coalescing and forming weakened zones[98].

In a constant-stress creep test, cracks will tend to grow until the local stress decreases to a value insufficient to let further growth continue. They will not propagate further unless the crack tip stress is increased or crack tip strength is decreased. The crack tip strength can be decreased by

moisture in which case the crack growth can be continued more readily[104].

Vutukuri et al.[120] stated that liquids attack the crack tips, dissolving the material and increasing the stresses at the apex, thereby helping in their propagation.

Increasing the crack propagation (especially the cracks parallel to the axial stress direction) in presence of water, means increasing the rate of the lateral creep strain (expansion) with the time.

The effect of the saturation on the lateral creep was found to be similar in most cases to that of the axial creep. It is suggested that the effect of the water on lateral creep is either due to the recrystallization, as explained by Griggs[70] on the gypsum (alabaster), or due to the solution, as explained by Misra[79] on anhydrite and Varo & Passanis[102] on halite, or due to partly by both. The effect of water on the creep rate may also be explained as a function of ionic mobility of gypsum in water as described by Griggs[71] or due to the increase of the propagation of the cracks which are parallel to the axial stress direction by increasing the crack tip stress as described by other investigators[104,120].

7.6 Comparisons Between Axial and Lateral Creep.

As mentioned before, both creep strains axial and lateral were recorded under similar uniaxial and triaxial stresses, these measurements being performed in dry and water saturated conditions. The axial creep strain results are given in tables (6.8) to (6.15) and shown in Figs. (6.14) to (6.38). The lateral creep strain results are given in tables (7.3) to (7.10) and shown in Figs. (7.3) to (7.10). It can be seen from these results that in most cases the lateral creep strain under uniaxial stress is greater than the axial creep strain at a given loading time in both dry and saturated conditions. Fig. (7.36) shows a comparison between the axial and lateral creep strains in dry and saturated conditions subjected to a uniaxial stress

of 15 N/mm^2. It is clear that the lateral creep strain is more than the axial at any given time, and both followed the same pattern. These results are in agreement with the results of several investigators such as Wu and Thomson[98] on a Westerly granite and Singh[97] on Sicilian marble.

The axial and lateral creep curves under triaxial stresses at a constant σ_1 and for various σ_3 are shown in Figs. (7.37) and (7.38) for dry and saturated conditions respectively. In triaxial loading the lateral creep strain decreases with increasing confinement and in most cases the lateral creep strain is less than the axial in any conditions, except under low confining pressure in saturated condition when the lateral creep strain is more than the axial. The difference between the axial and lateral creep strains increase with increasing the confinement. In other words, the effect of the confining pressure in decreasing the strain is found to be more on the lateral creep strain than on the axial. Sangha and Dhir[33,34] reported that increasing the confining pressure resulted in greater increase in the resistance to the lateral deformation than axial deformation. Wawersik[96] found that the lateral creep strain of saturated Westerly granite is greater than the axial under low confining pressure. The lateral creep strain curves in triaxial loading condition was found to follow the same general trend as the axial creep curves as observed in the case of uniaxial stresses, see Figs. (7.36), (7.37) and (7.38). The investigators Singh[97], Wu and Thomsen[98] and Kranz[104] reported that both axial and lateral creep curves follow the same pattern as far as different stages of creep are concerned.

It can be seen from the Figs. (6.49) and (6.50) for axial creep and Figs. (7.25) and (7.26) for the lateral creep, that at a constant $(\sigma_1 - \sigma_3)$ the axial creep strain increases with increasing σ_3 whereas the lateral creep strain decreases with increasing σ_3 for the two environmental

conditions. Since increasing σ_3 means increasing σ_1 by the same amount in order to keep $(\sigma_1 - \sigma_3)$ constant, this indicates that increasing σ_1 and σ_3 by equal increments means that σ_1 dominates the situation for the axial creep strain behaviour and σ_3 similarly dominates the situation for the lateral creep . This behaviour was observed for the given confining pressure levels (0, 10, 20 and 30 N/mm^2). The effect of confining pressure variation on the lateral creep becomes less at high values of σ_3.

In uniaxial compression, it was found that the lateral creep rate is more than the axial at a given loading time, see Tables (6.17) and (7.18) for the axial creep rate and Tables (7.12) and (7.13) for the lateral creep rate. The axial and lateral creep rates are plotted versus axial stress for various confining pressures at a constant time t = 480 hrs. in Figs. (7.39) and (7.40) for dry and saturated conditions respectively. It can be noted from these figures that the lateral creep rate in both environmental conditions is more than the axial creep rate in the uniaxial stress conditions.

"Under a constant load the crack width may have increased with the time and the average length of the cracks increases in time, as does the total stress-induced cracked space at a rate which parallels strain measured on the rock surface." (Kranz[104], 1979).

Kranz[104] reported also that the creep rate in lateral direction is always more than the axial direction in uniaxial tests. He explained it as, crack width increases very rapidly or that crack coalescence, at small angles to the axial stress direction, contributes more to lateral strain. The following investigators reported that the lateral creep rate is more than the axial under uniaxial stresses; Evans and Wood[69] on granite, marble and shale, Singh[97] on Sicilian marble and Kranz[104] on Barre granite.

In triaxial tests it was found that in most cases the lateral creep rate is less than the axial creep rate, see Tables (6.17), (6.18) for the axial and (7.12) and (7.13) for the lateral. As mentioned before both axial and lateral creep rates increase with the axial stress at constant σ_3. This increase becomes more rapid in the lateral direction than in the axial at high axial stresses, and this effect is found to be more marked at lower or medium confining pressure levels, see Figs. (7.39) and (7.40). At high axial stresses sufficient to produce new cracks which may be associated with the old cracks or the grain boundaries, then provided these cracks are parallel or nearly so with the sample axis, large lateral strain must occur, and low confining pressures will not have a tendency to inhibit this action. The effect of the confining pressure on the axial and lateral creep rate at constant axial stress is shown in Figs. (7.41) and (7.42) for dry and saturated conditions respectively. It can be seen from these figures, previous figures (7.39) and (7.40) and from the tables (6.17), (6.18), (7.12) and (7.13), that increasing confining pressure decreases both the axial and lateral creep rates. This effect was found to be somewhat greater on the lateral creep rate than on the axial, and the effect of equal variation of σ_3 results in larger differences between the axial and lateral creep rates at low values of σ_3 than higher; this behaviour was observed in both dry and saturated conditions.

At constant $(\sigma_1 - \sigma_3)$, as the axial stress increases the axial creep rate increases and the lateral creep rate decreases, see Figs. (6.45) and (6.46) for the axial rate and (7.20) and (7.21) for the lateral creep rate. The same behaviour was found at constant $(\sigma_1 - \sigma_3)$ when the confining pressure increases, see Figs. (6.54), (6.55), (6.56) and (6.57) for axial creep rate and Figs. (7.29),(7.30),(7.31) and (7.32) for

lateral creep rate. Since increasing σ_1 or σ_3 at constant $(\sigma_1 - \sigma_3)$ means an increase in both σ_1 and σ_3 with the same levels. This indicates the same effect observed on the creep strain, that for equal increments of σ_1 and σ_3, σ_1 dominates the axial creep rate and σ_3 dominates the lateral creep rate.

7.7 Empirical Equation.

The lateral creep results in uniaxial and triaxial loading of the dry and saturated conditions were regressed using the least squares curve fitting computer program (multiple regression) for the combination of factors affecting the creep strain. The creep strain was considered as dependent variable and both axial stress and loading time as independent variables. The method of analysis was similar to that used in axial creep. A best fit in every case for times greater than 24 hours within the given experimental maximum times was found to be a power law function of the following form:

$$\varepsilon = d\ \sigma_1^{e}\ t^{f} \qquad \ldots\ldots \qquad (7.61)$$

where ε is the lateral creep strain in microstrain, σ_1 is the axial stress in N/mm^2, t is the loading time in hours and d, e and f are constants depending on the environmental conditions and confining pressures. Values of the constants are given in Table (7.15) for dry and saturated conditions at various confining pressure, and as plotted against σ_3 in Figs. (7.56) and (7.57) for dry and saturated conditions respectively.

The predicted values of the creep strain using the above equation were compared with the actual values. There are a few values (not more than 10% of the total) in each case where the variation was greater than 12%. The "Standard Error of Estimate, SEE" and the "Correlation Coefficient, COR. COF" were calculated for each case to give a clear idea about the variation between the actual and predicted values as in the case of axial creep.

Table (7.15) Constants of the Emperical Equation at the specified conditions.

$(\varepsilon = d\ \sigma_1^{e}\ t^{f})$

Constants σ_3 N/mm^2	Dry Condition d	e	f	SEE*	COR.COF.**
0 (Uniaxial)	1.89274	0.92945	0.31095	27	0.949
10	0.49249	1.28551	0.34146	35	0.946
20	0.13809	1.51025	0.32468	21	0.989
30	0.07659	1.56459	0.34254	20	0.977
Saturated Condition					
0 (Uniaxial)	0.87209	2.07960	0.28141	98	0.981
10	0.25209	2.08174	0.25710	116	0.962

*SEE - Standard Error of Estimate, see Appendix (C) for computation.

**COR.COF. - Correlation Coefficient.

The values of SEE and COR.COF. are given in Table (7.15). It can be seen that in any case the correlation coefficient is not less than 0.946, which indicates a good significant degree of correctness.

Equations for saturated conditions at σ_3 = 20 and 30 N/mm^2 are not given because of their low correlation.

7.8 Volumetric Creep and the Effects of Axial Stress and Confining Pressure.

Volumetric creep strain was measured by using the axial and lateral creep strain, i.e. $\varepsilon_V = \varepsilon_A - 2\ \varepsilon_L$ where ε_V is the volumetric creep strain, ε_A is the axial creep strain and ε_L is the lateral creep strain. The behaviour of the volumetric creep was studied in dry and saturated conditions, and the effects of axial stress and confining pressure will be discussed. A positive value of ε_V means a decrease in specimen volume.

In this study this will be called a decrease in volumetric strain. Conversely negative values of ε_v means increasing specimen volume referred to as an increase in volumetric strain.

To give a general idea about the volumetric creep curve in comparison with the axial and lateral creep curves from which it is calculated these relationships are plotted in Figs. (7.43) and (7.44) for dry and saturated conditions respectively under various stress conditions. It can be seen that the volumetric creep strain increases with the time under a constant stress although it was found in many cases that initially the volumetric creep strain decreases, (+ ve) (or decrease in volume), sharply then the volumetric creep increases after a short time to become negative (increase in specimen volume) and follows the trend of the lateral creep curve, see Figs. (7.43 D) and (7.44 C) for dry and saturated conditions respectively. This may be explained as; initially the pre-existing cracks and pores are closed, especially the cracks perpendicular to the axial stress or at a large angle to it, in other words, the material is consolidated giving a decrease in specimen volume. After a short time, new cracks are produced probably associated with the old cracks or the grain boundaries. Since the cracks tend to grow in a direction more or less parallel to maximum applied stress[104], there will be more strain in the lateral direction with the time under the load. This increase in the lateral strain is indicated by specimen expansion (increase in volumetric creep). Kranz[104] stated that under constant load the crack width and the average length increases in time.

The time-dependent deformation of brittle rocks is a result of micro-fracturing, the creep therefore is a process of time-dependent dilatancy[129]. Similar behaviour of volumetric creep has been reported for different rocks by the investigators; Wu and Thomsen[98] and Scholz[129] on Westerly granite

and Cogan[99] on saturated Dolomite and hard shale. If a specimen of a particulate material is stressed axially under a triaxial confinement, the degree of compression of dilation will depend partly on the initial density of the material and partly on the confining pressure (Price and Farmer[50], 1979).

The effect of the axial stress and the confining pressure on the volumetric creep strain of gypsum will be discussed here. The influence of the axial stress at a constant confining pressure in dry conditions is shown in Figs. (7.45), (7.46) and (7.47) for confining pressure zero, 20 and 30 N/mm^2 respectively, and in saturated condition in Figs. (7.48), (7.49), and (7.50) for confining pressure, zero, 10, and 30 N/mm^2 respectively. It can be seen that the volumetric creep takes place at all the stress levels, and increases with increasing axial stress at constant confining pressure.

Rong et al.[130] reported that the average length and density of the cracks increases with increasing the axial stress at constant σ_3, and the volume dilatancy increases as a result of that. Scholz[129] stated that the creep deformation in compression is produced by microfracturing, this microfracturing consequently is a time as well as stress dependent process. Cogan[99] found an increase in the volumetric creep strain of Dolomite with increasing the axial stress at constant confining pressure.

The volumetric creep rate was found to increase with increasing the axial stress under uniaxial condition for both dry and saturated gypsum, see Figs. (7.45)and (7.48). This is influenced by the fact that the axial stress increases the lateral creep rate more than the axial creep rate under uniaxial stresses, see Sec. (7.6). Under triaxial stresses, at constant confining pressure the volumetric creep rate increases with increasing the axial stress at higher values of σ_1, under both dry and

saturated conditions, see Figs. (7.46) and (7.47) for dry and Figs. (7.49) and (7.50) for saturated. This must result from an increase of the lateral creep rate with increasing σ_1 at higher values of σ_1 which is greater than the increase of the axial creep rate, see Section (7.6) and Figs. (7.39) and (7.40).

The average length of the cracks and their density increases with the uniaxial stress, the rate of increase becomes rapid at σ_1 values greater than 60% σ_u, whereas in triaxial stresses when $(\sigma_1 - \sigma_3)$ increases (in other words increasing σ_1 at constant σ_3) to about 90% σ_u the number and length of the cracks increases with extreme rapidity[130].

Wawersik[96] found that the secondary volumetric creep rate of water saturated westerly granite increases with increasing $(\sigma_1 - \sigma_3)$ or increasing σ_1 at constant σ_3. Cogan[99] also reported an increase of the volumetric creep rate of Dolomite and hard shale by increasing σ_1 at constant σ_3.

As observed and mentioned before, the creep behaviour in some cases changed from logarithmic law to power low, and in many cases the behaviour in the power law changed its gradient (on log-log graph) to a smaller value after a certain loading time. It can be seen from the tables (6.17), (6.18), (7.12) and (7.13) that the time of change of creep behaviour in dry condition in both axial and lateral directions increases in general with increasing the applied axial stress at a constant σ_3. The time of change varied from 4.5 to 72 hours from the beginning of the test in the axial direction while in the lateral direction it varied from 2 to 190 hours.

In saturated gypsum it is observed that there is no unique trend for the axial stress effect on the time of change in creep behaviour. This may be due to the possibility of the difference in the creep processes in dry and saturated gypsum, in which the saturated rock suggested to be as a result of solution, recrystallization, etc. It can be seen from the

above mentioned tables, that this change in the creep behaviour causes the decrease of the creep rate with the time to be more effective. Since the effect of the lateral creep on the volumetric creep is greater than the axial, i.e. the behaviour change takes place in lateral creep and does not occur in axial at the corresponding stress conditions (which happened in most of the cases) the lateral creep change is dominant. This means that the volumetric creep rate should in general decrease with time but in most cases this changed the direction of the volumetric creep curve. These cases are shown in dry conditions at σ_3 = 20 N/mm^2 under σ_1 = 41 and 50 N/mm^2 and at σ_3 = 30 N/mm^2 under σ_1 = 41, 50 and 63 N/mm^2, see Figs. (7.46) and (7.47) for 20 and 30 N/mm^2 confining pressure respectively. In saturated rock the cases are shown at σ_3 = 10 N/mm^2 under σ_1 = 27 N/mm^2 and at σ_3 = 30 N/mm^2 under σ_1 = 63 N/mm^2, see Figs. (7.49) and (7.50) for 10 and 30 N/mm^2 confining pressure respectively.

The volumetric creep strain is plotted against the time for various confining pressures at constant axial stress in Figs. (7.51) and (7.52) for dry and saturated conditions respectively. It can be noted that the effect of increasing confining pressure at a constant axial stress is to decrease the volumetric creep strain, and the effect of equal variation of σ_3 is more at low values of σ_3 than higher. In this respect it should be noted that the effect of increasing the confining pressure in decreasing the lateral creep strain is more than its effect on the axial creep strain and this effect is more pronounced at low values of σ_3 than higher, see Sec. (7.6).

Among Cogan's[90] results,it is clear that the effect of increasing σ_3 from 50 to 500 psi at constant σ_1, decreases the volumetric creep strain of a hard shale by an appreciable amount. Rong et al.[130] reported among

their results, that the volume dilatancy of Gabbro under uniaxial stress (zero confining pressure) is seven times that at 1.3 Kb confining pressure at a constant σ_1 of about 1.5 Kb. It can be seen, observing the gradient of the curves in Fig. (7.51) and (7.52), that the volumetric creep rate decreases with increasing the confining pressure at a constant axial stress. This is due to the effect of σ_3 on the lateral creep rate which as in the case of strain is more than its effect on the axial creep rate at a constant σ_1, see Sec. (7.6). Cogan[99] reported a similar behaviour of the volumetric creep rate of the saturated dolomite.

At constant $(\sigma_1 - \sigma_3)$ the volumetric creep rate at 48 hours was plotted versus confining pressure in dry and saturated conditions in Figs. (7.53) and (7.54) respectively. It can be seen that in dry conditions the volumetric creep rate decreases with increasing confining pressure for the low values of σ_3 up to a certain value, then starts to increase with increasing σ_3 for higher values of σ_3. In saturated conditions the volumetric creep rate decreases with increasing the confining pressure throughout, this effect is much more pronounced at the lower values of σ_3 and becomes slight at higher values of σ_3. As discussed previously, increasing confining pressure at constant $(\sigma_1 - \sigma_3)$ increased the axial creep rate slightly in dry conditions and decreased it in a saturated condition, see Figs. (6.56) and (6.57). Whereas in the case of lateral creep for dry rock the increase of σ_3 at constant $(\sigma_1 - \sigma_3)$ caused the creep rate to decrease to a certain value then started to increase for higher values of σ_3, while in saturated condition the creep rate decreased with increasing σ_3, see Figs. (7.31) and (7.32). It has been noted that the effect of lateral creep rate on the volumetric creep rate is more than the effect of the axial creep rate. The result of this is that the effect of confining pressure on the volumetric creep at constant $(\sigma_1 - \sigma_3)$ is found to be similar to its

effect on the lateral creep rate in both environmental conditions. These results are similar to the behaviour of the volumetric creep rate of saturated Westerly granite which is reported by Wawersik[96] at constant $(\sigma_1 - \sigma_3)$, and of saturated dolomite and shale which is tabulated by Cogan[99].

Volumetric creep strain is plotted versus the time in dry and saturated conditions under similar stresses in Fig. (7.55). This figure shows the effect of saturation on the volumetric creep strain and the volumetric creep rate under uniaxial and triaxial stresses. It can be seen that the water saturation increases the volumetric creep strain and volumetric creep rate by appreciable amounts. The creep rate of the saturated rock increases very rapidly relative to the dry value. At constants $(\sigma_1 - \sigma_3)$ the volumetric creep rate is greater in saturated condition than the dry under similar stresses, see Figs. (7.53) and (7.54). These figures show that the effect of increasing the volumetric creep rate with $(\sigma_1 - \sigma_3)$ is greater than this effect in dry condition.

Kranz[104] reported that in constant stress creep tests, the cracks will tend to grow, the presence of water increases the ability of the growth by decreasing the crack tip strength and makes further propagation, in other words, increase the rate of the specimen dilation.

In general it should be remembered that crack growth is a function of stress at the tip and the surface energy of the rock. Increasing stress will increase crack growth, while the presence of water on the surfaces will decrease surface energy and result in increased crack growth without the necessity to increase the stress levels, i.e. its presence weakens the rock.

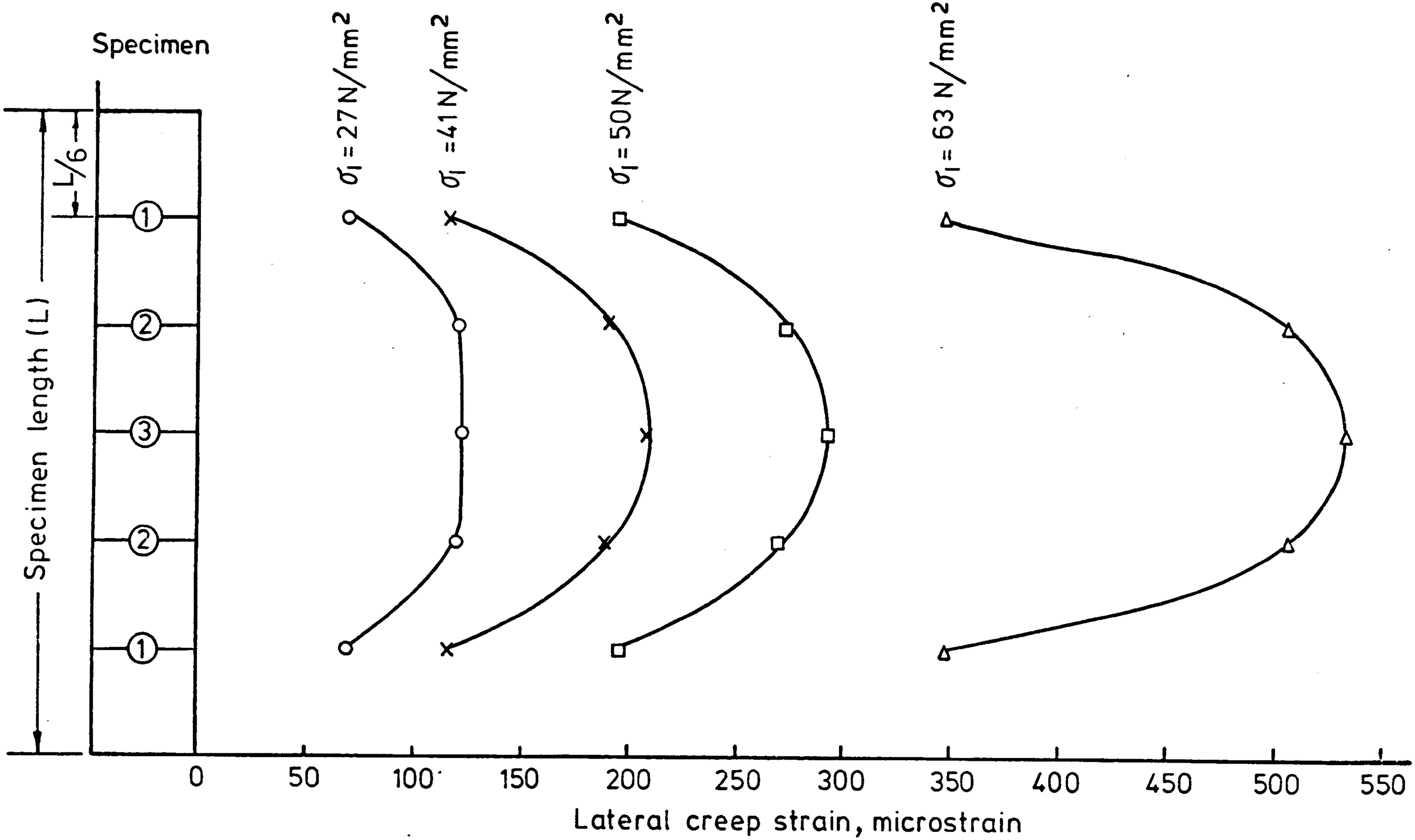

FIG.(7-1) LATERAL CREEP STRAIN ALONG THE SPECIMEN AT $\sigma_3 = 30\,N/mm^2$ IN DRY CONDITIONS AT VARIOUS σ_1

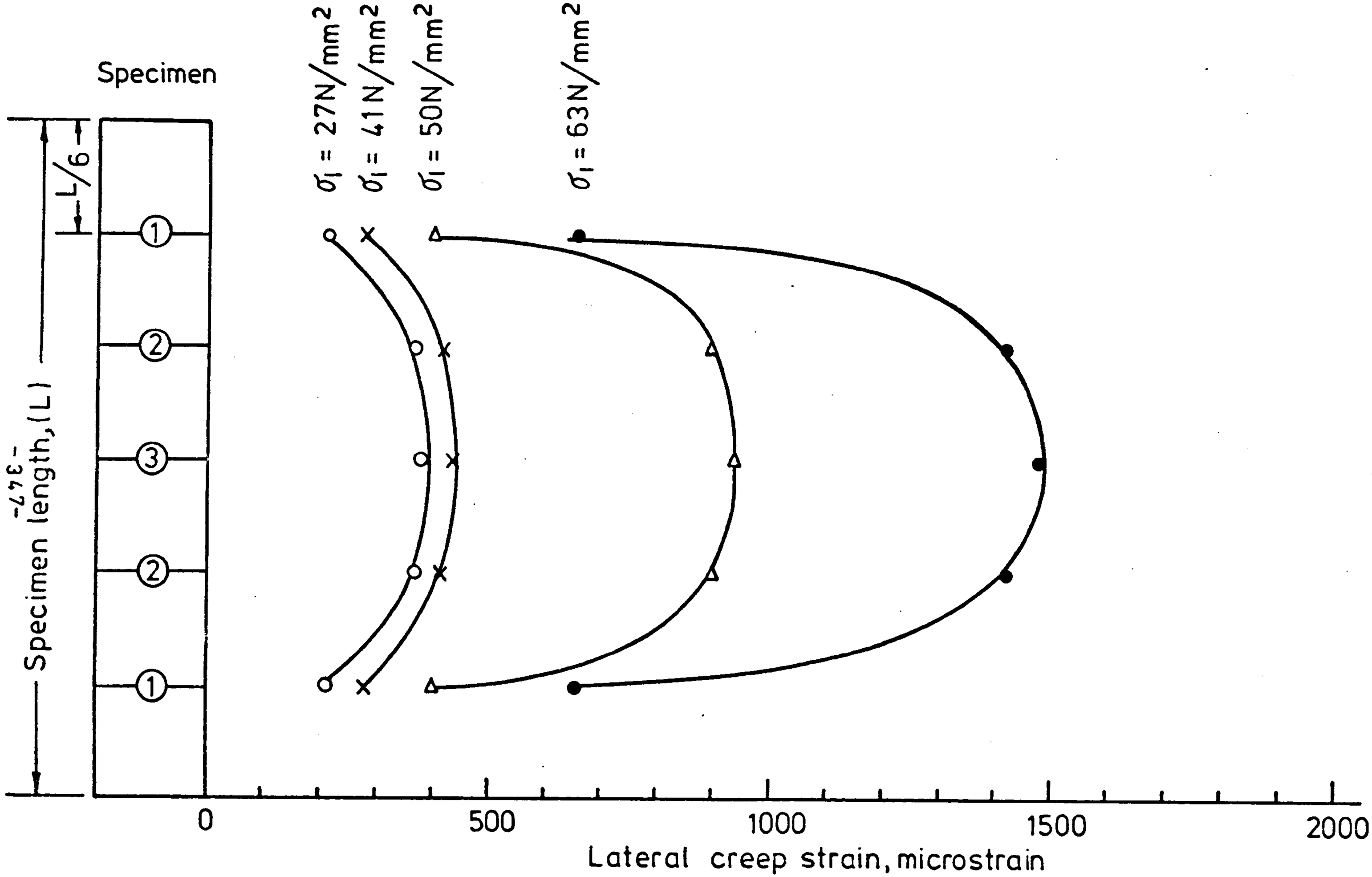

FIG(7-2) LATERAL CREEP STRAIN ALONG THE SPECIMEN AT $\sigma_3 = 30\ N/mm^2$ IN SATURATED CONDITIONS AT VARIOUS σ_1

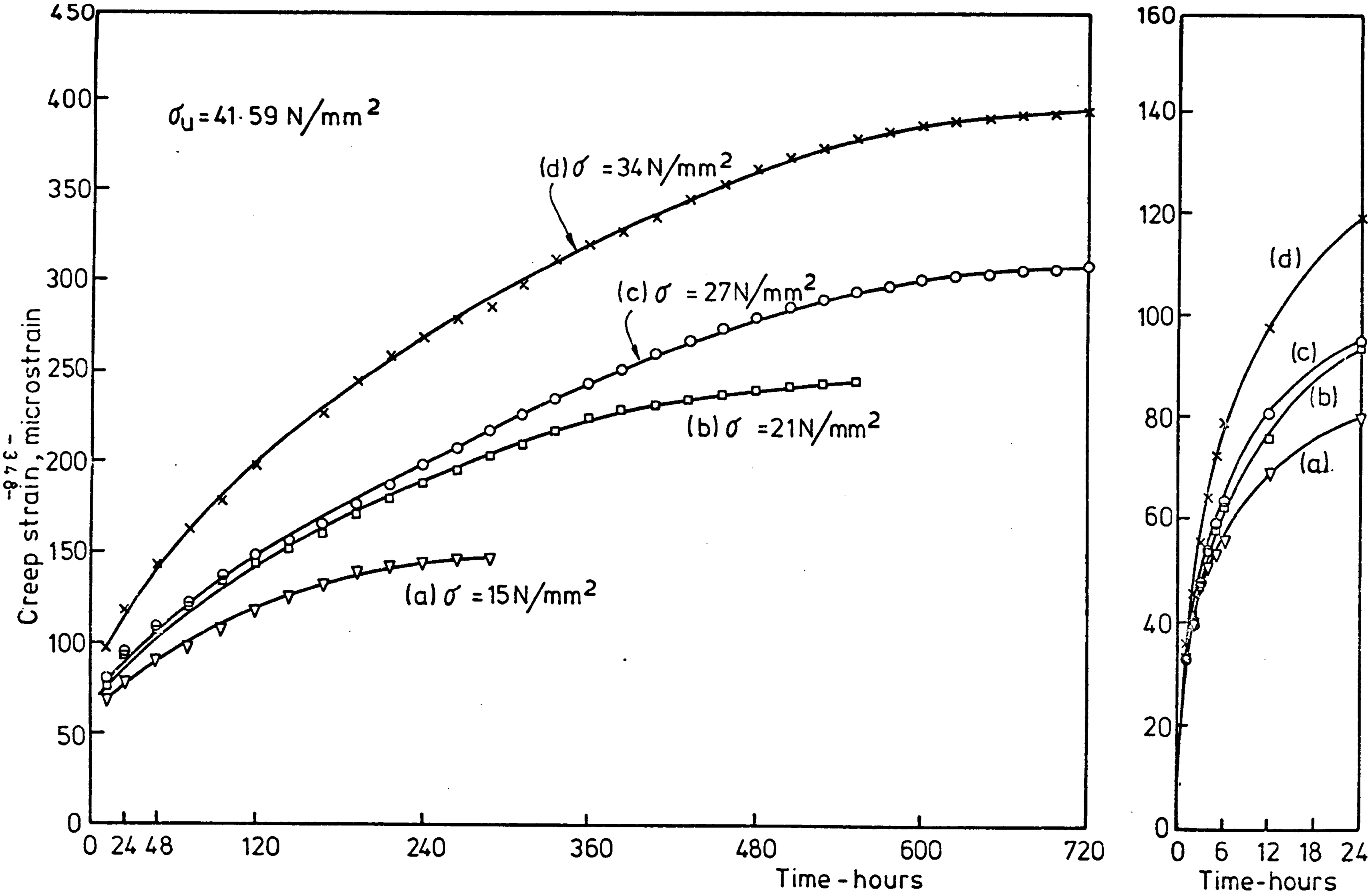

FIG.(7-3) LATERAL CREEP STRAIN OF DRY GYPSUM IN UNIAXIAL COMPRESSION

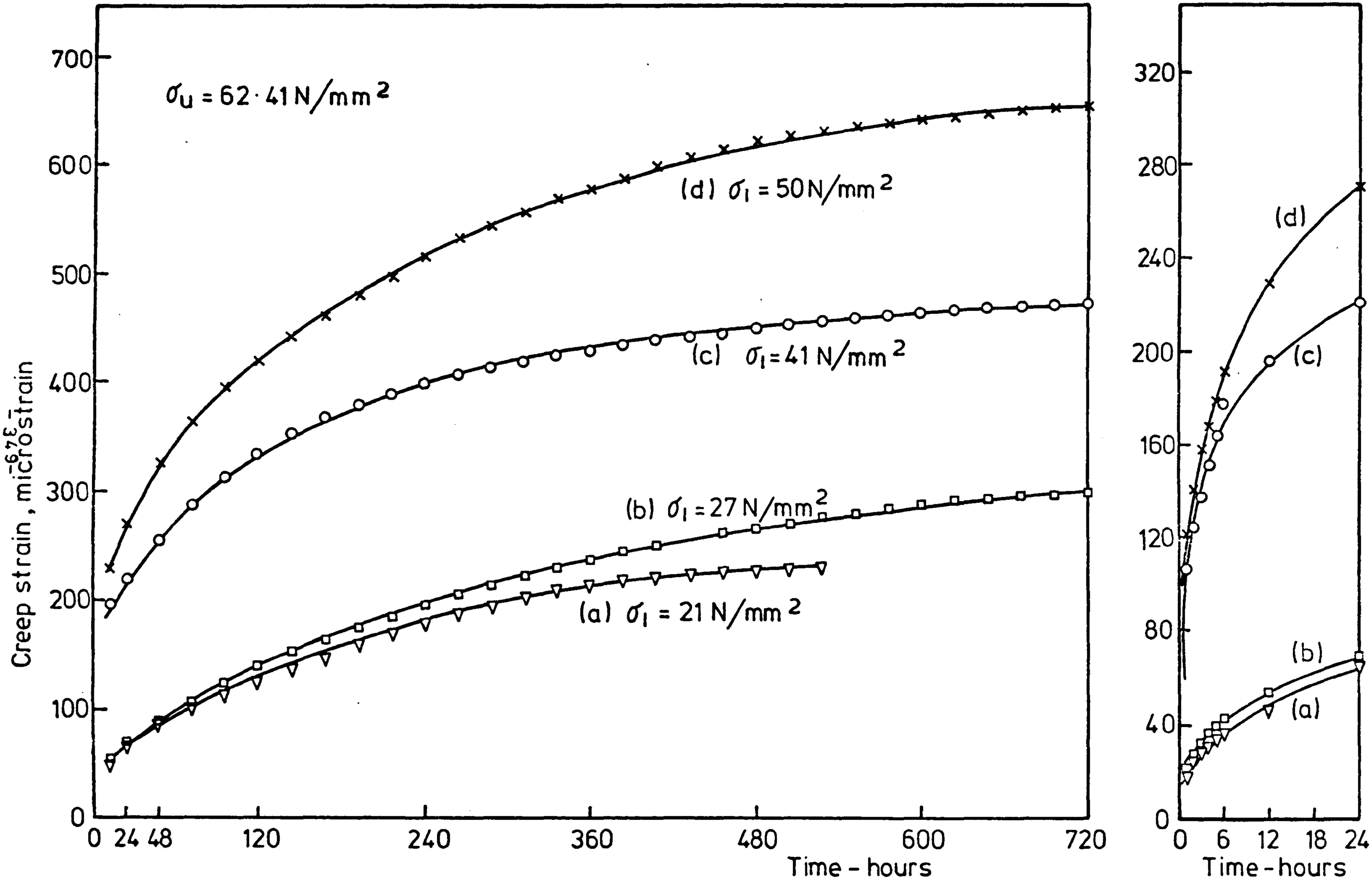

FIG. (7-4) LATERAL CREEP STRAIN OF DRY GYPSUM IN TRIAXIAL COMPRESSION AT ION/mm² CONFINING PRESSURE

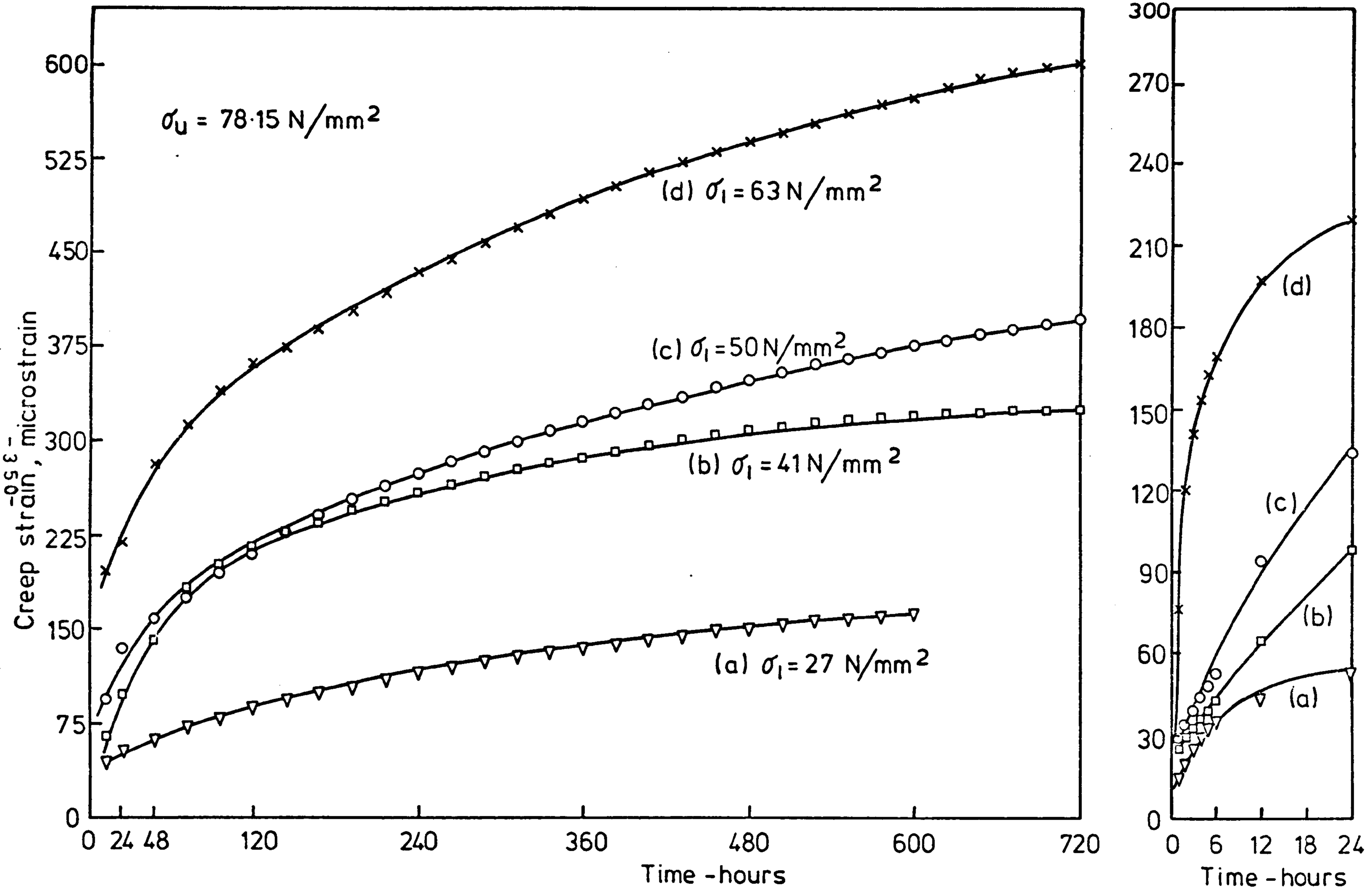

FIG. (7-5) LATERAL CREEP OF DRY GYPSUM IN TRIAXIAL COMPRESSION AT 20N/mm² CONFINING PRESSURE

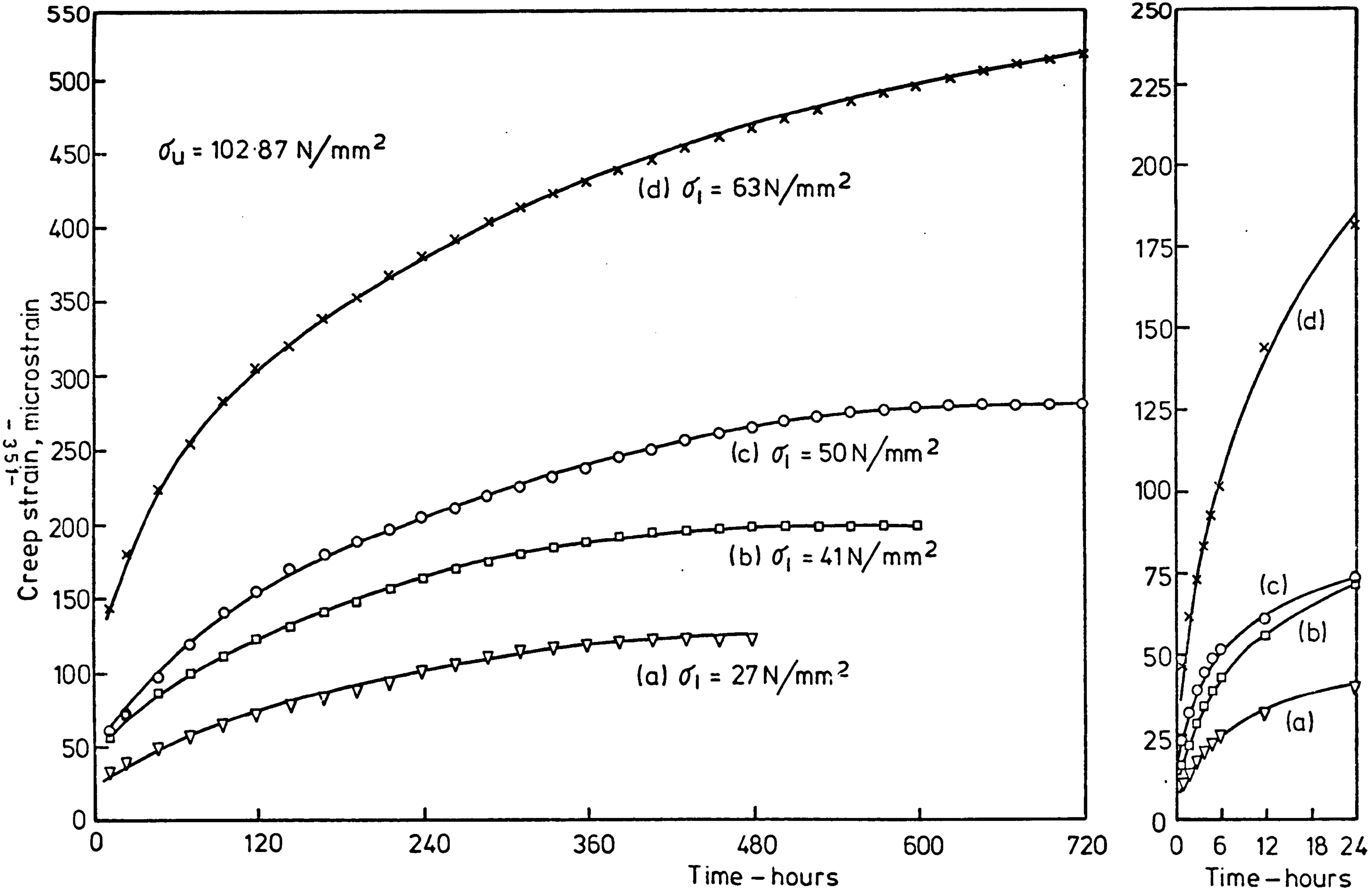

FIG. (7-6) LATERAL CREEP OF DRY GYPSUM IN TRIAXIAL COMPRESSION AT 30N/mm² CONFINING PRESSURE

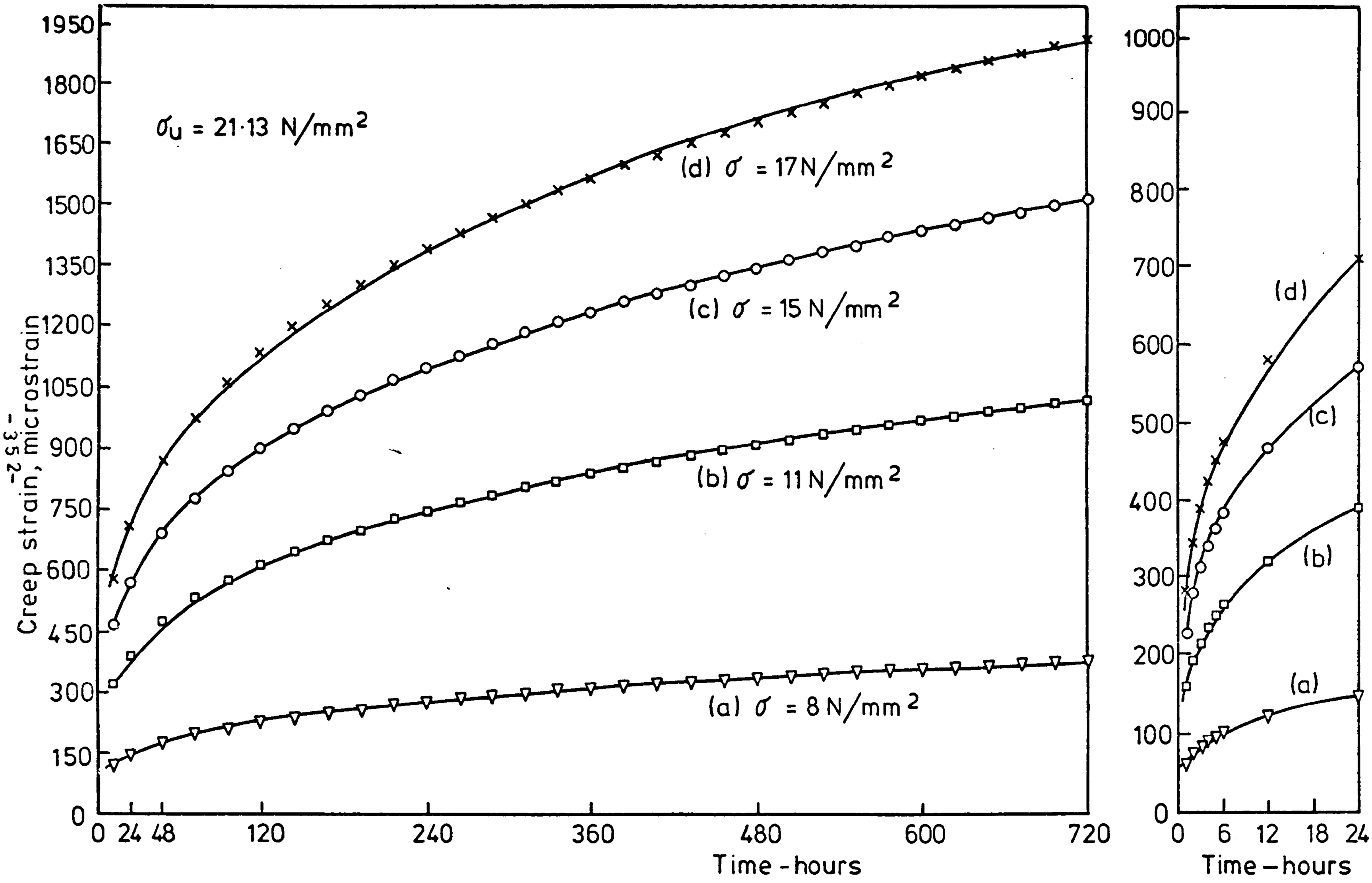

FIG. (7-7) LATERAL CREEP OF SATURATED GYPSUM IN UNIAXIAL COMPRESSION

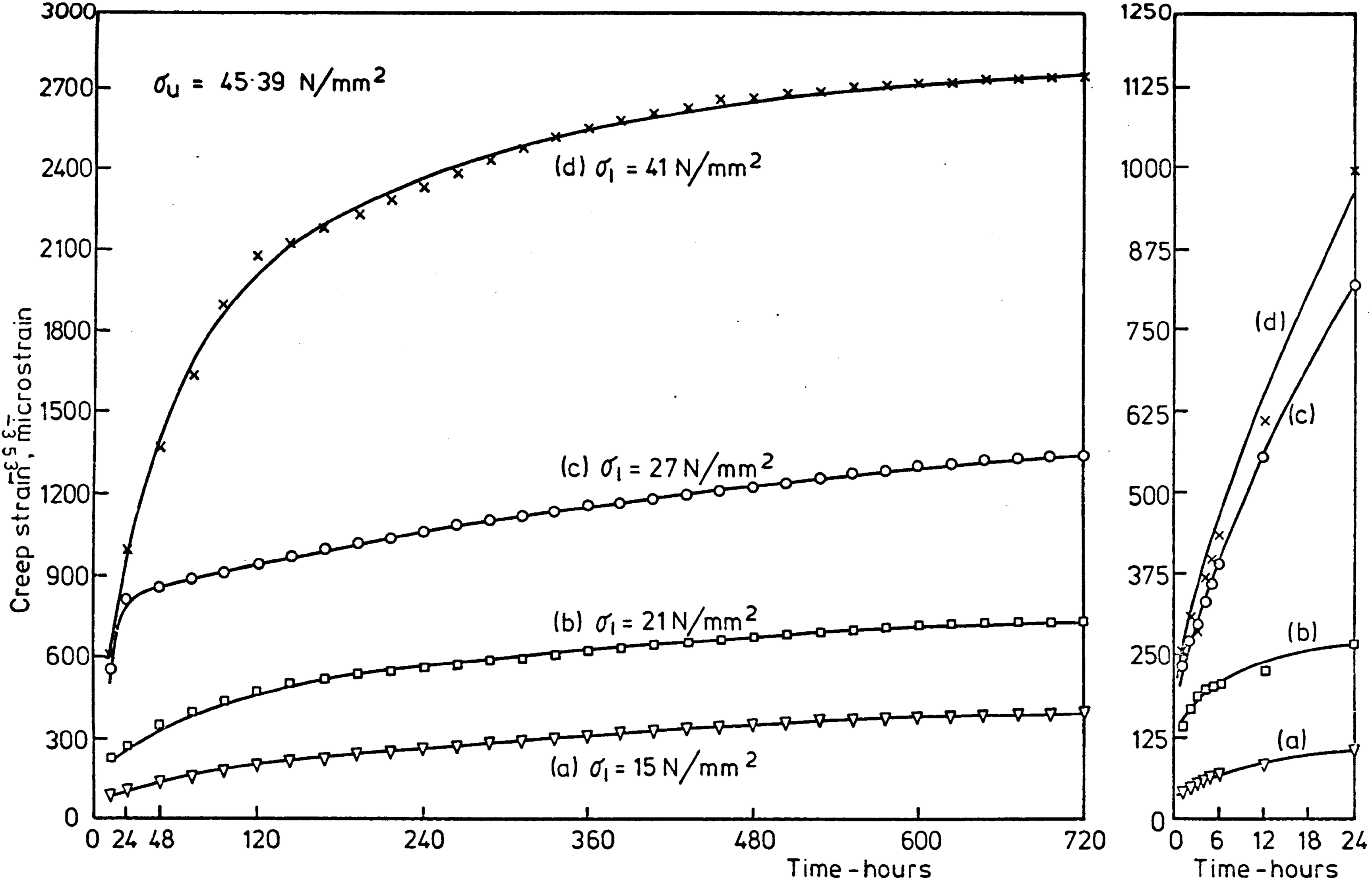

FIG. (7-8) LATERAL CREEP OF SATURATED GYPSUM IN TRIAXIAL COMPRESSION AT 10N/mm² CONFINING PRESSURE

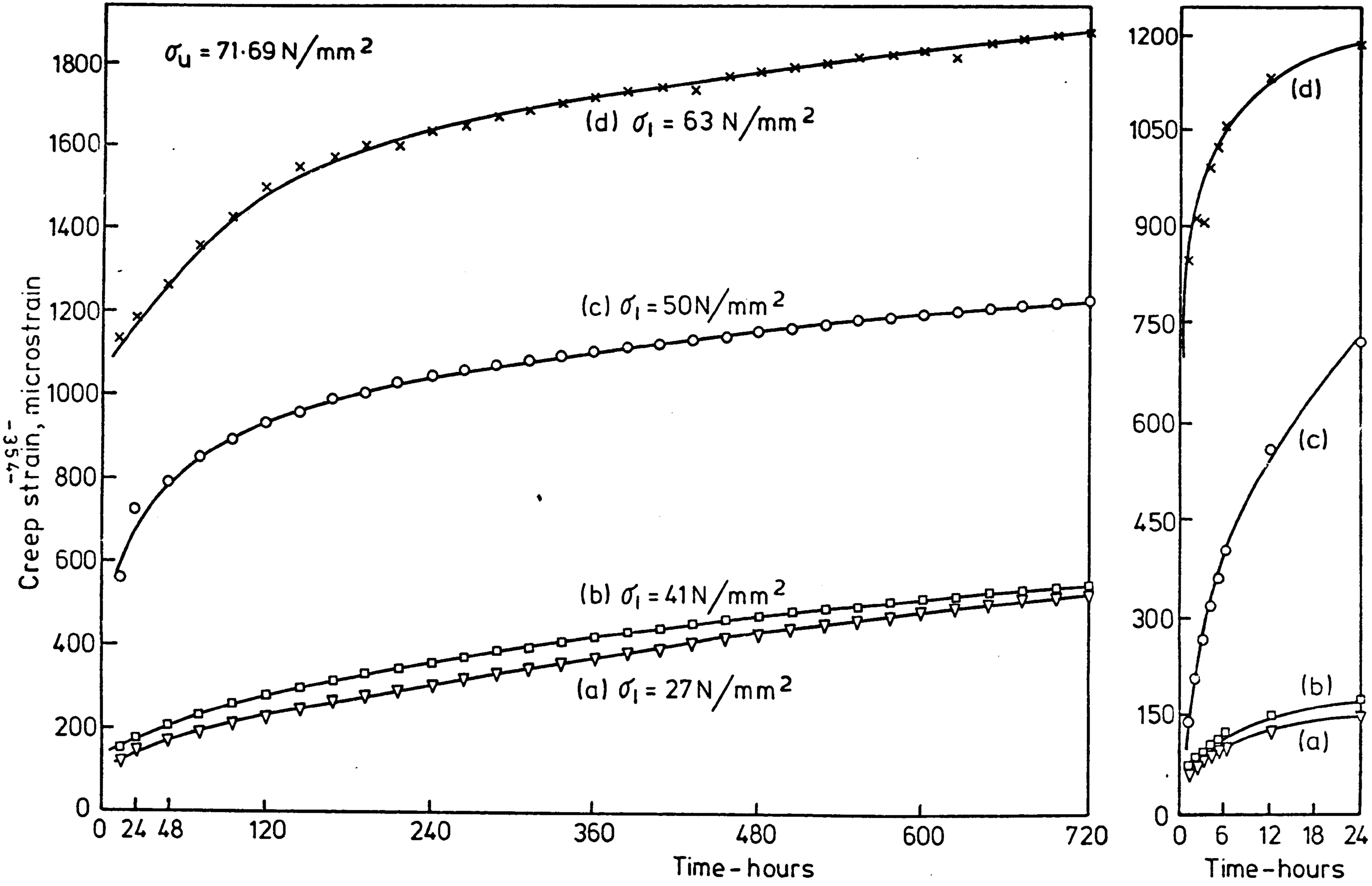

FIG.(7-9) LATERAL CREEP OF SATURATED GYPSUM IN TRIAXIAL COMPRESSION AT 20N/mm² CONFINING PRESSURE

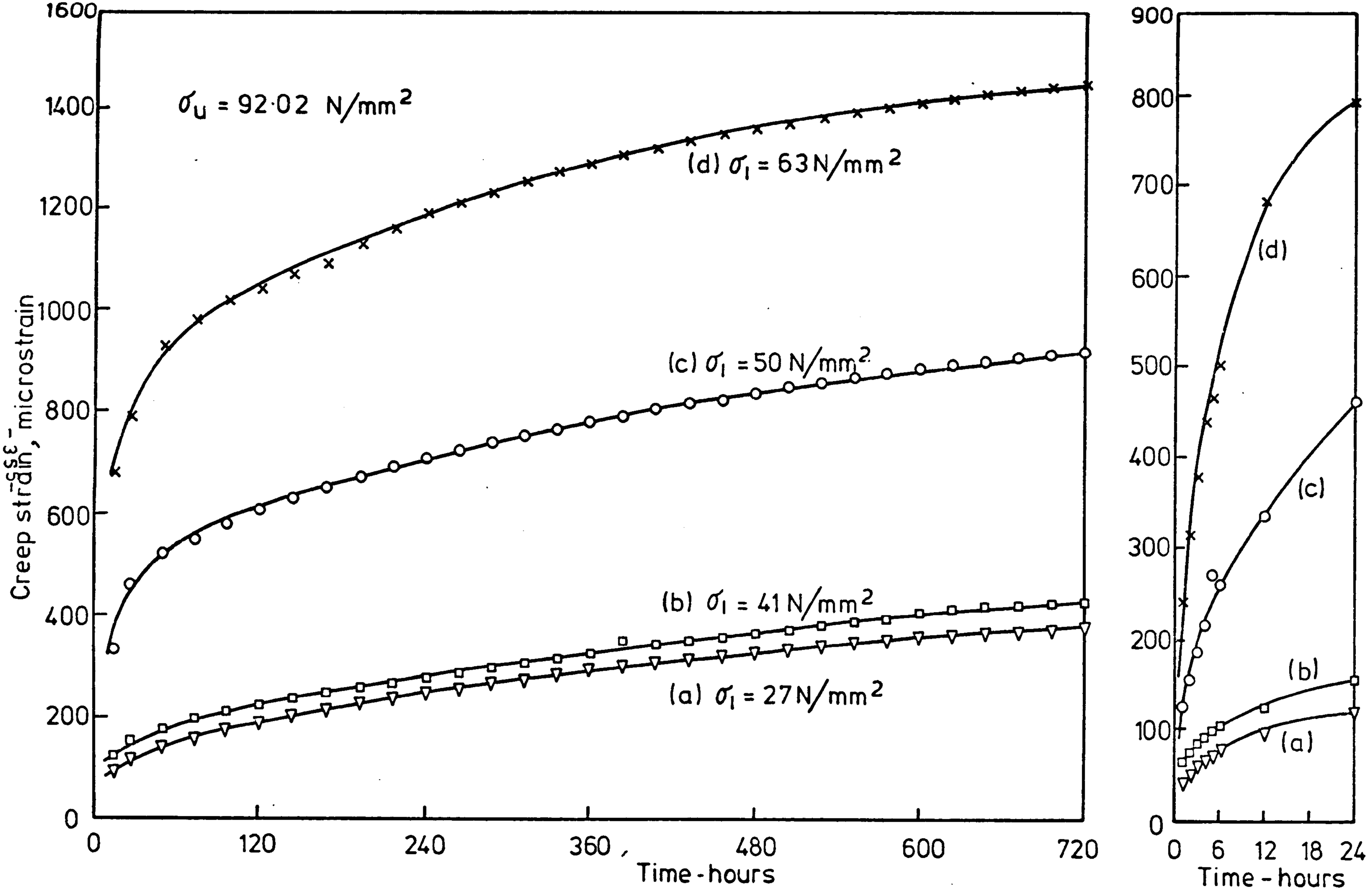

FIG. (7-10) LATERAL CREEP OF SATURATED GYPSUM IN TRIAXIAL COMPRESSION AT 30N/mm² CONFINING PRESSURE

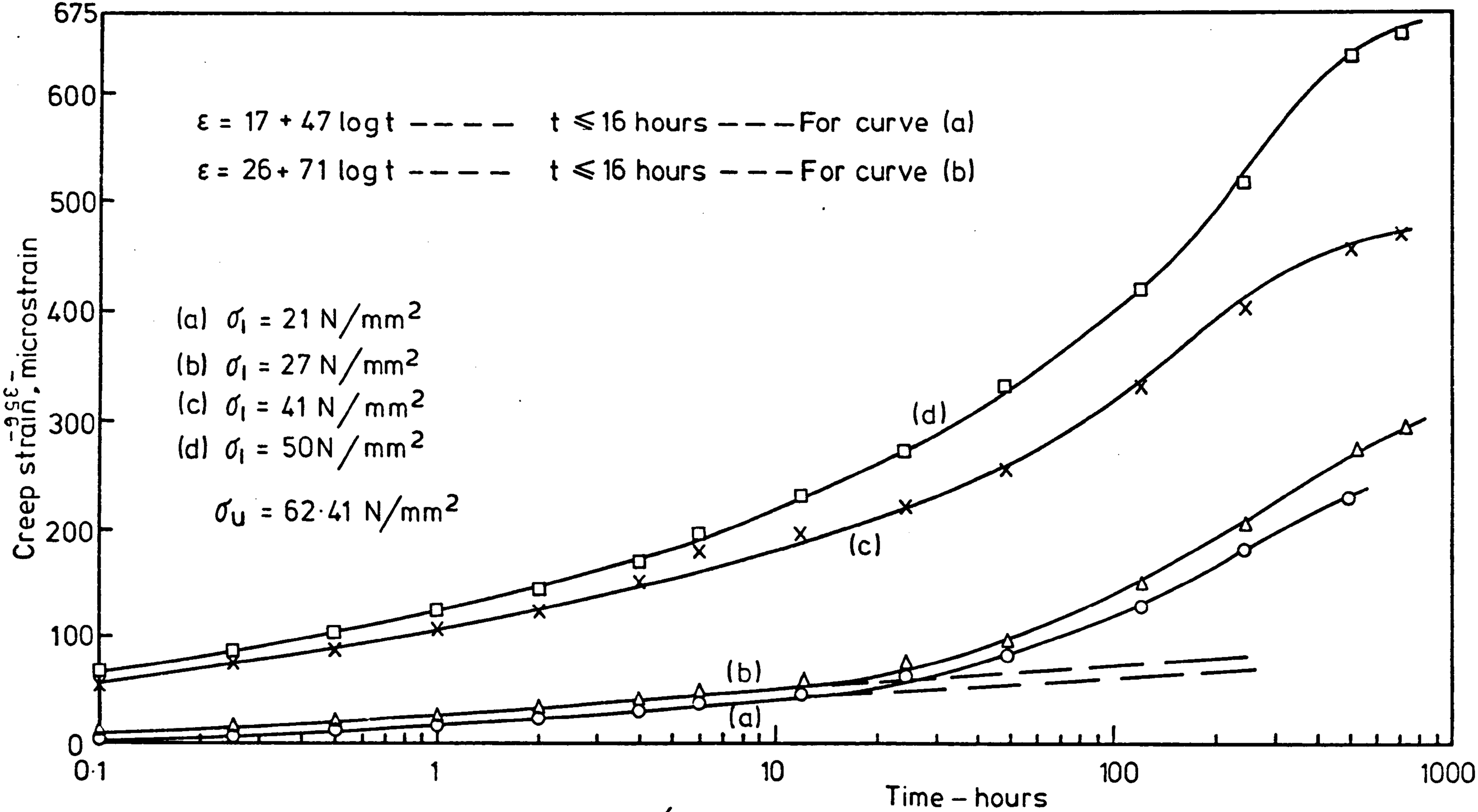

FIG. (7–11) LATERAL CREEP OF DRY GYPSUM IN TRIAXIAL COMPRESSION AT $10 N/mm^2$ CONFINING PRESSURE (SEMI – LOG GRAPH)

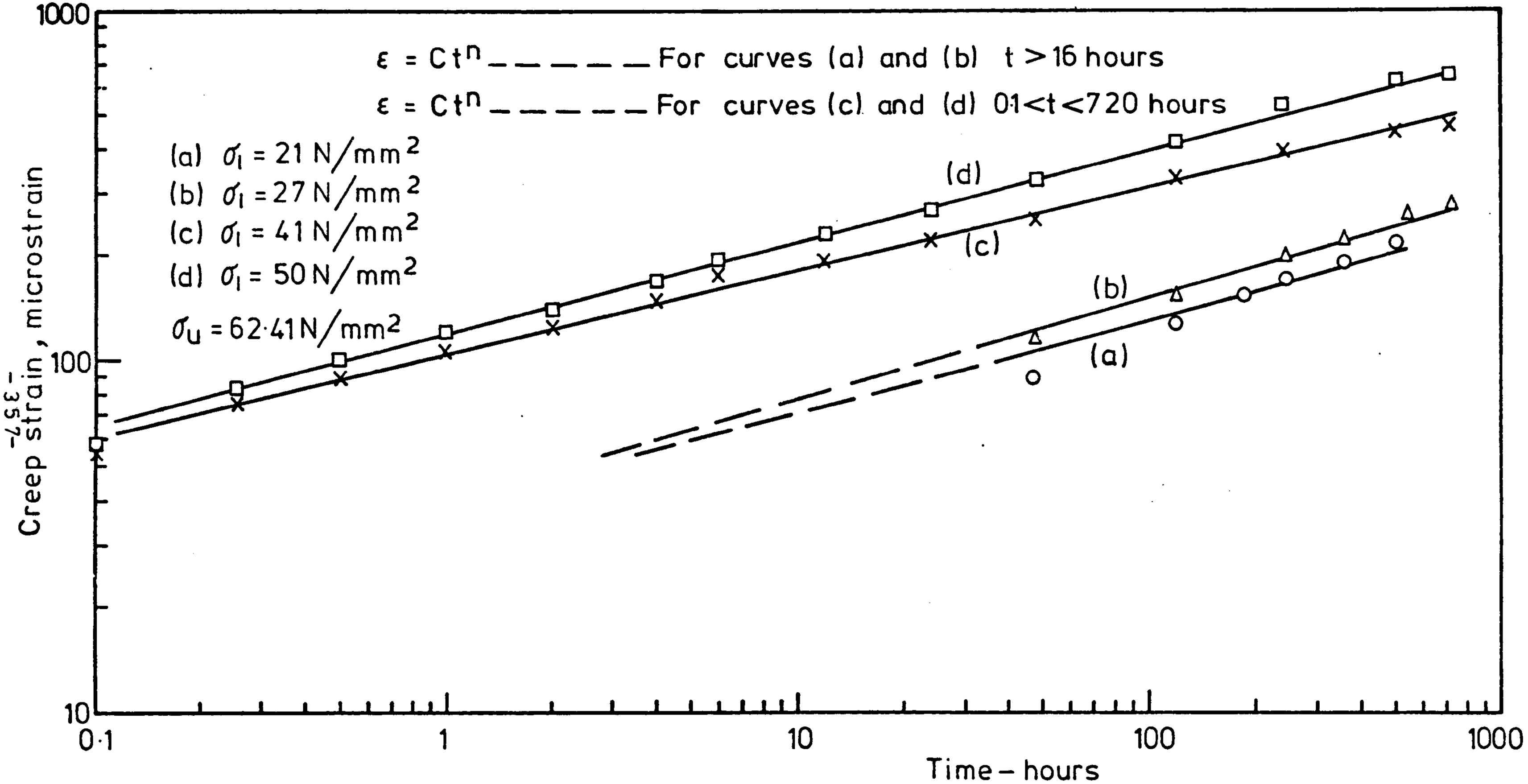

FIG. (7–12) LATERAL CREEP OF DRY GYPSUM IN TRIAXIAL COMPRESSION AT 10N/mm² CONFINING PRESSURE (LOG – LOG GRAPH)

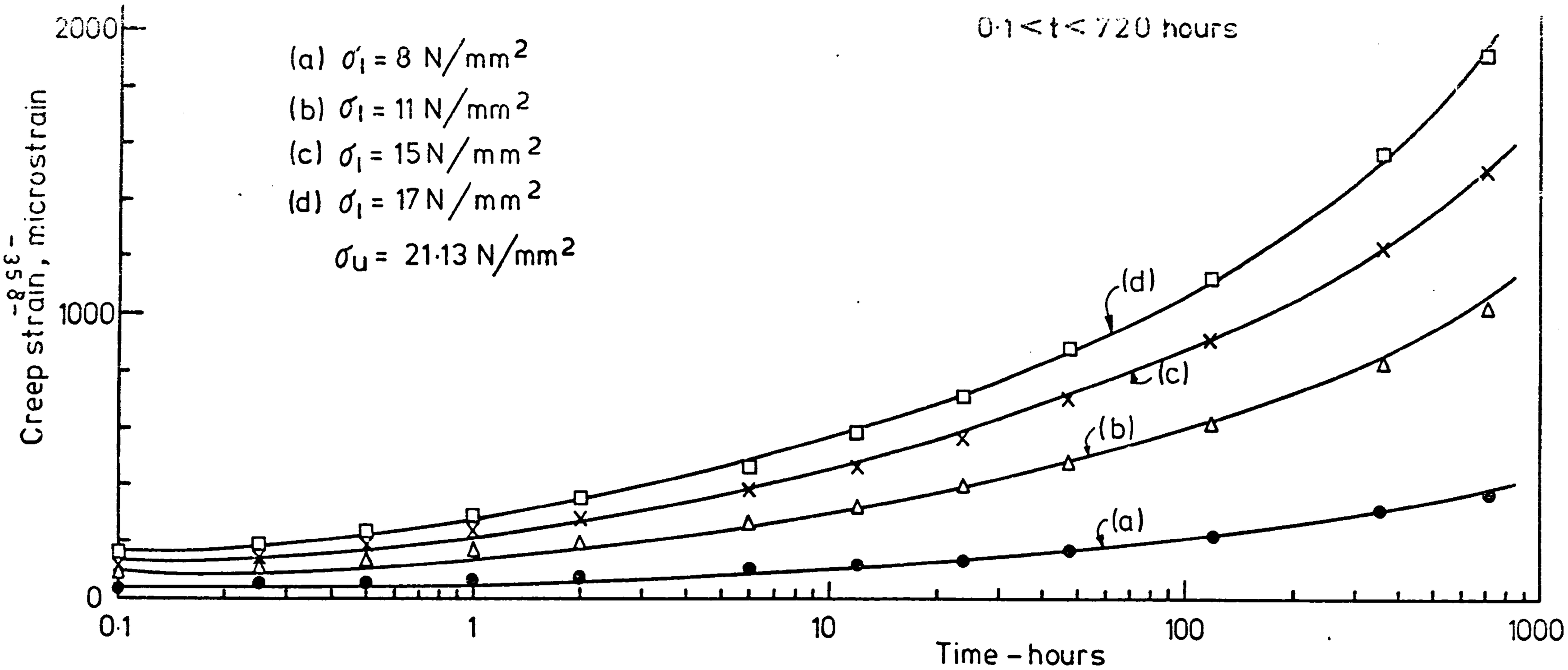

FIG. (7-13) LATERAL CREEP OF SATURATED GYPSUM IN UNIAXIAL COMPRESSION (SEMI-LOG GRAPH)

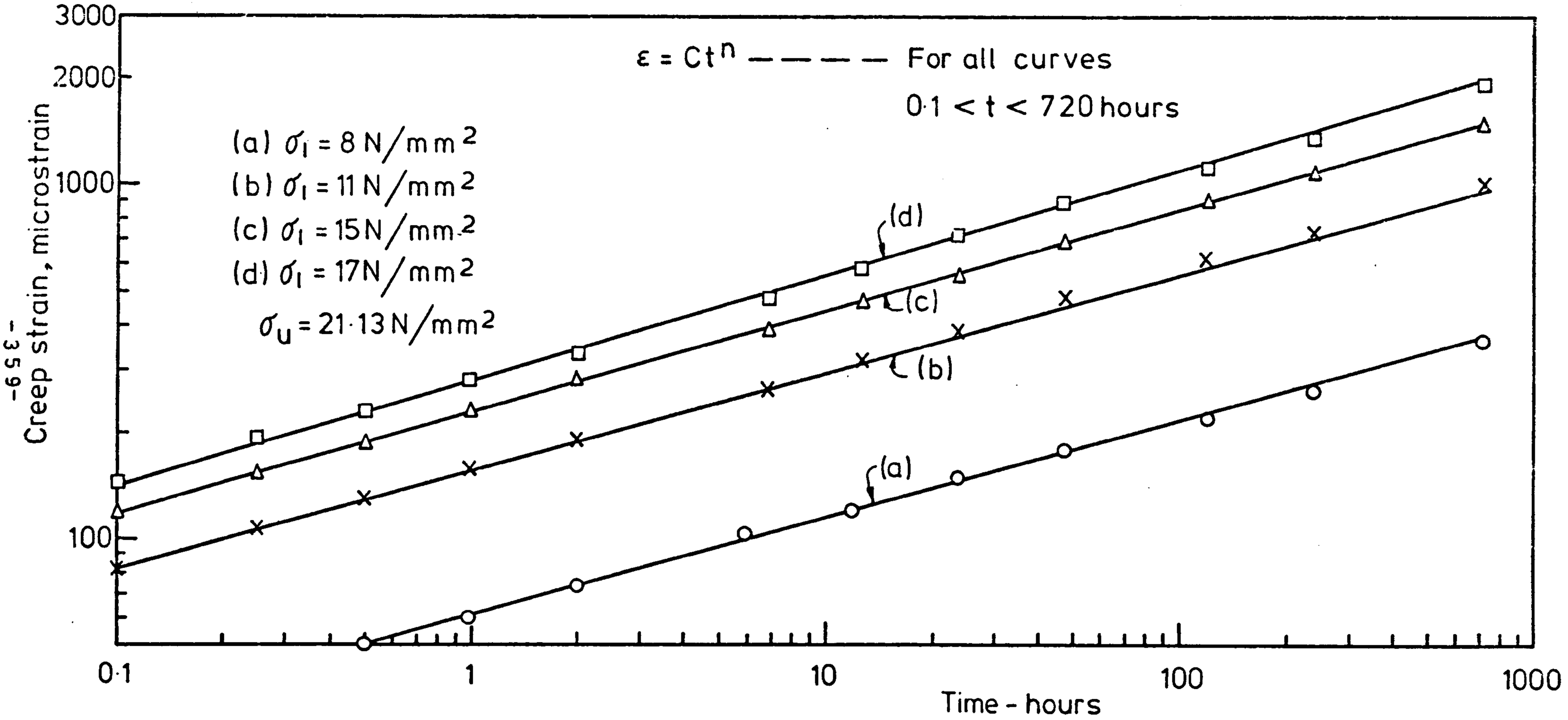

FIG. (7-14) LATERAL CREEP OF SATURATED GYPSUM IN UNIAXIAL COMPRESSION (LOG-LOG GRAPH)

DAMAGED TEXT IN ORIGINAL

Poisson's Ratio

Dry	Saturated
$f_o = 0.27$	$f_o = 0.41$

—— Dry

- - - - Saturated

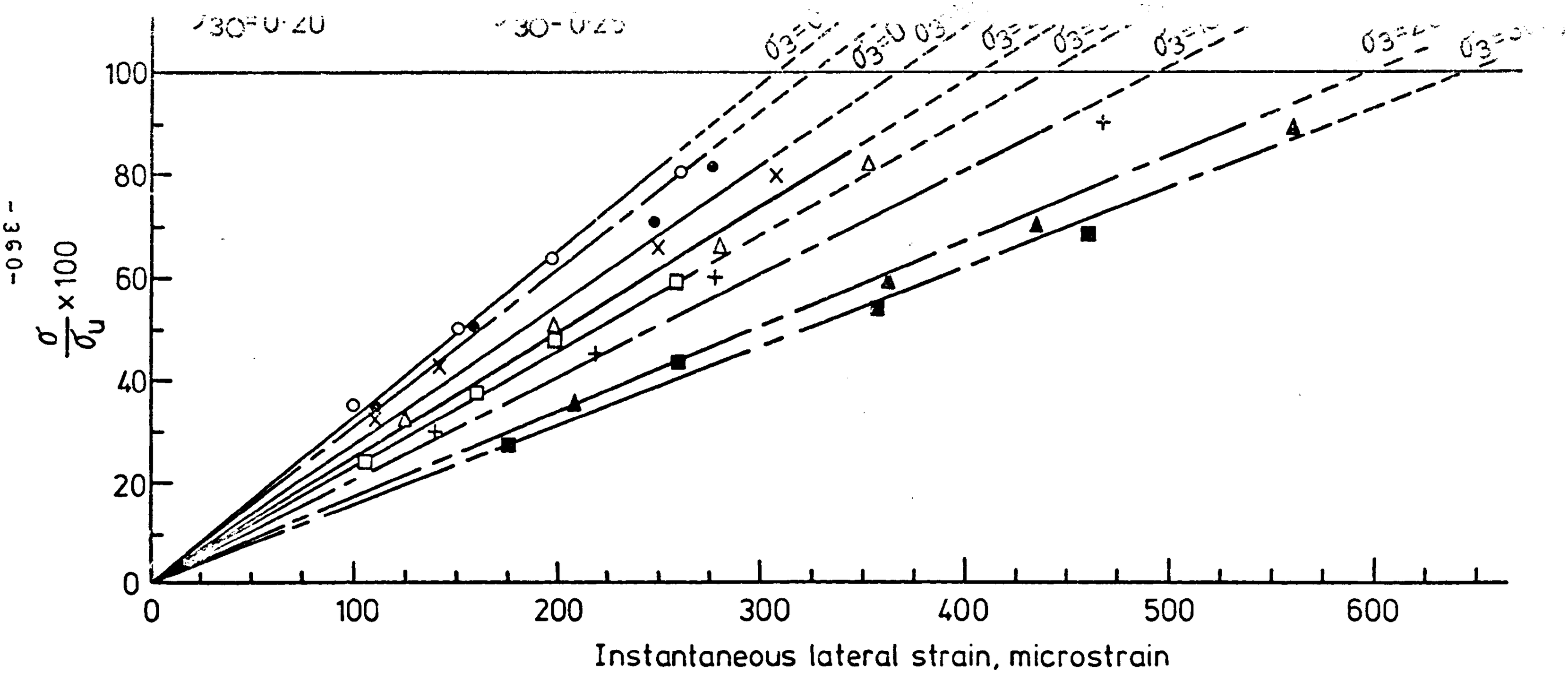

FIG. (7-15) DETERMINATION OF POISSON'S RATIO AT VARIOUS CONFINING PRESSURES

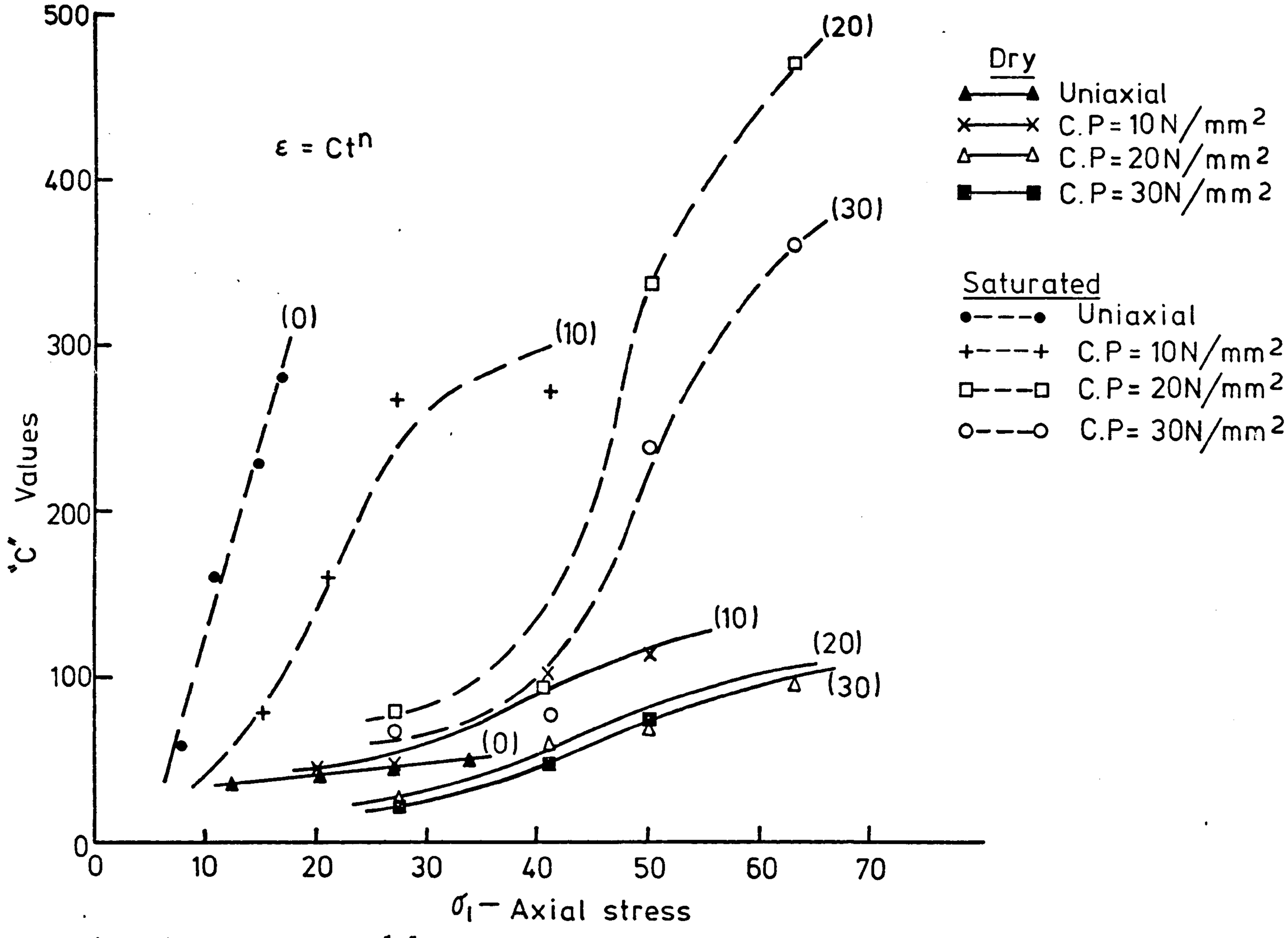

FIG. (7-16) VALUES OF 'C' Vs. σ_1 AT CONSTANT CONFINING PRESSURE IN LATERAL CREEP

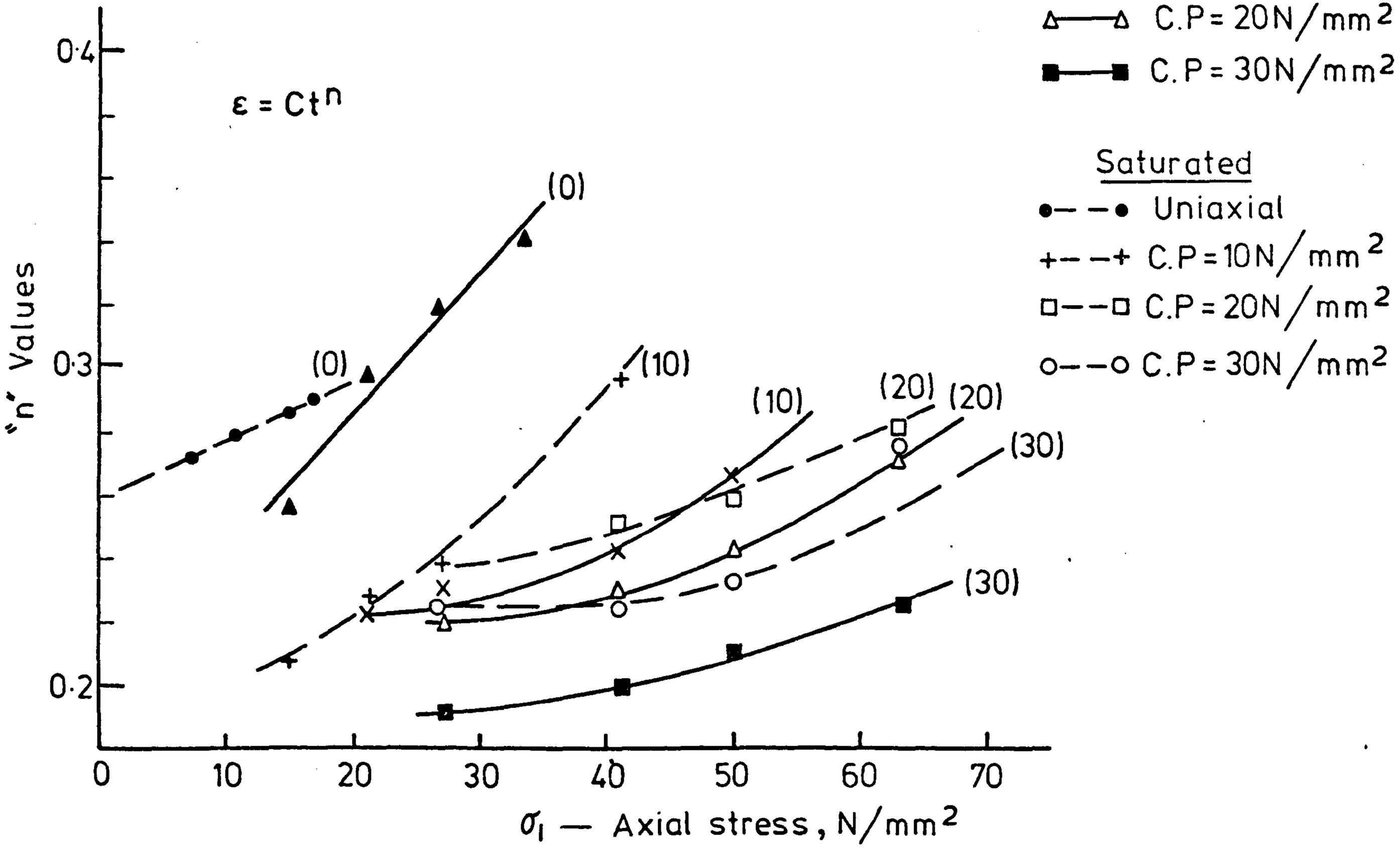

FIG. (7-17) VALUES OF "n" Vs. σ_1 AT CONSTANT CONFINING PRESSURE IN LATERAL CREEP

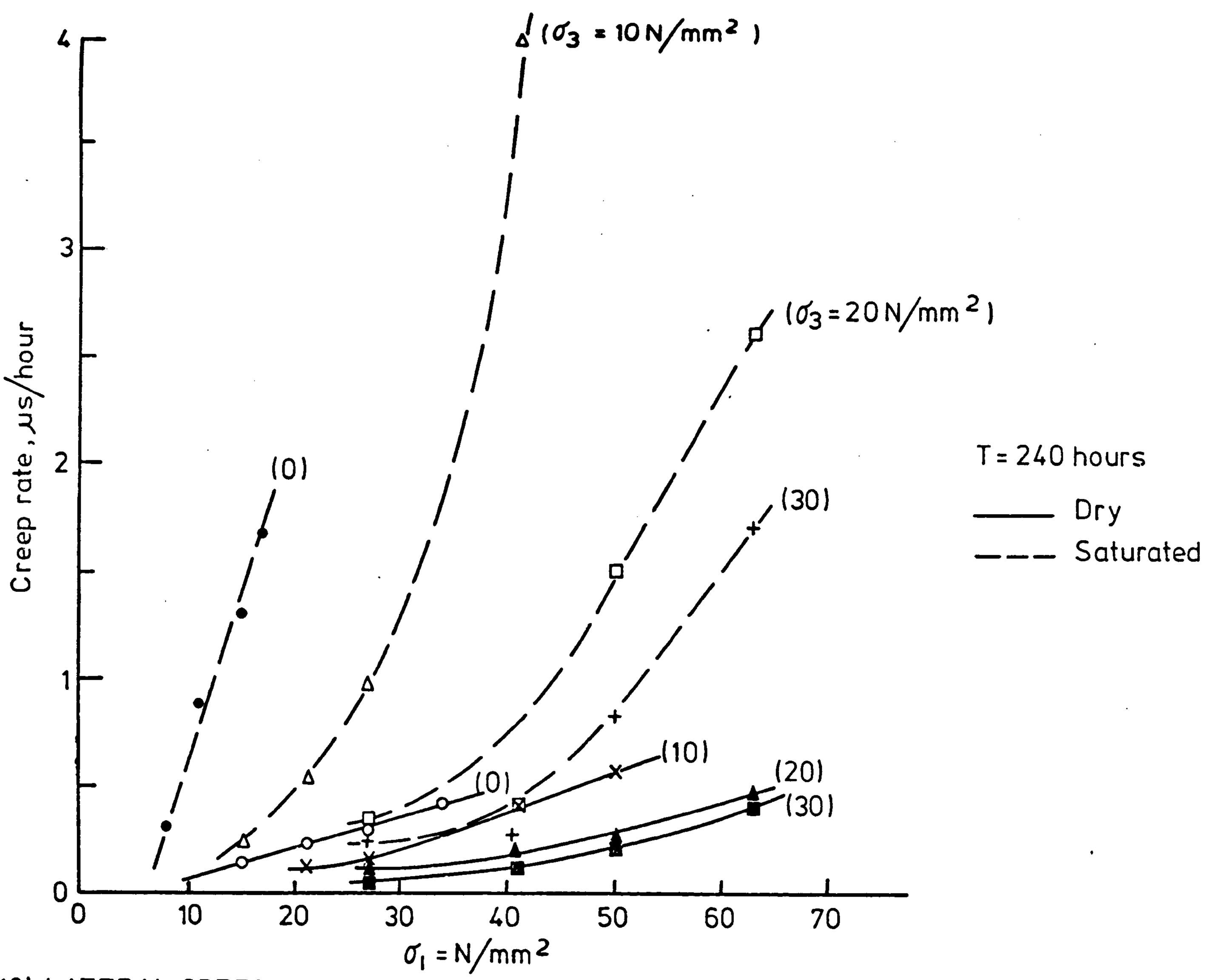

FIG.(7-18) LATERAL CREEP RATE Vs. σ_1 AT CONSTANT σ_3 FOR DRY AND SATURATED CONDITIONS

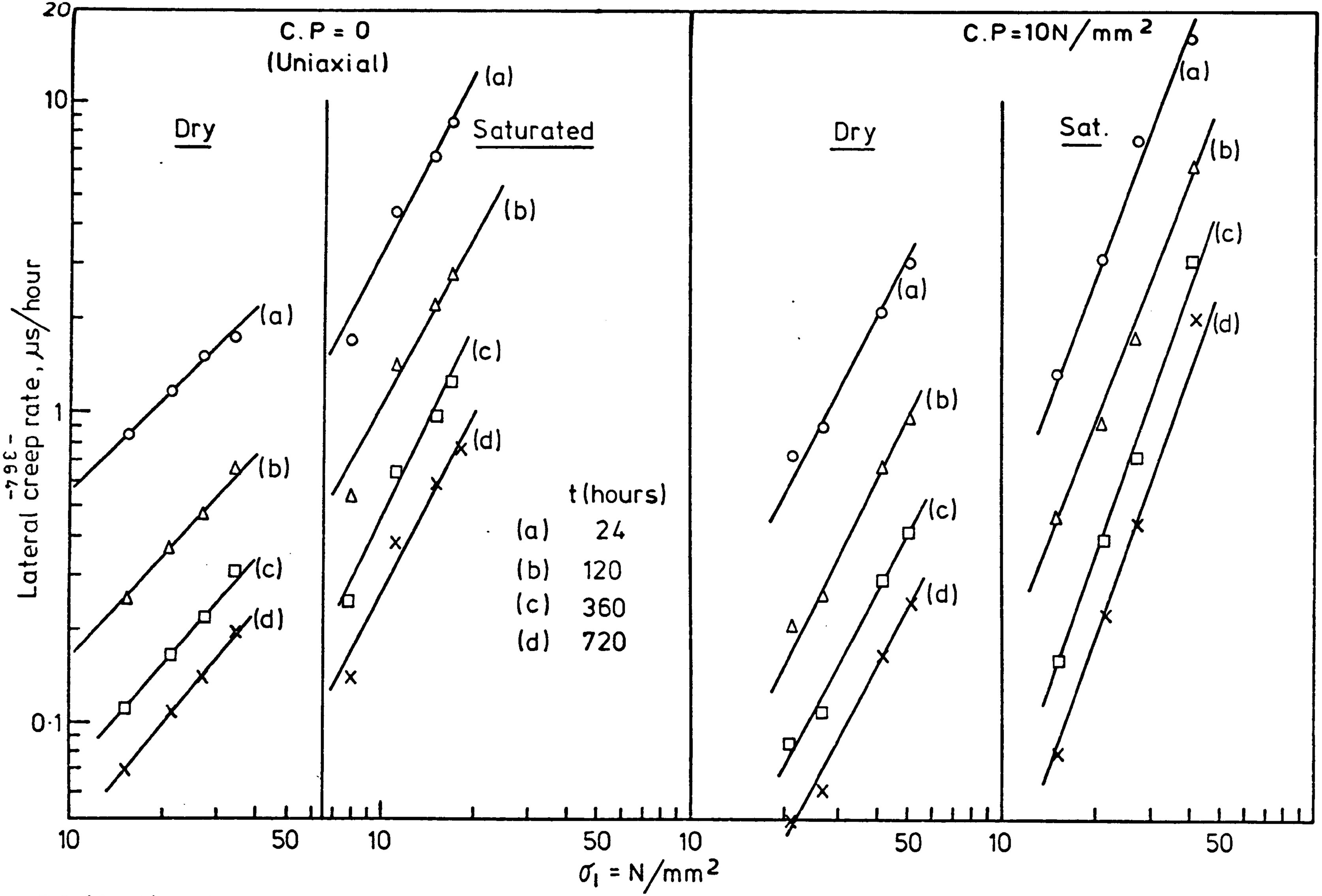

FIG. (7-19) LATERAL CREEP RATE Vs. σ_1 AT VARIOUS σ_3 (LOG-LOG GRAPH)

$(\sigma_1 - \sigma_3) = 10\ N/mm^2$

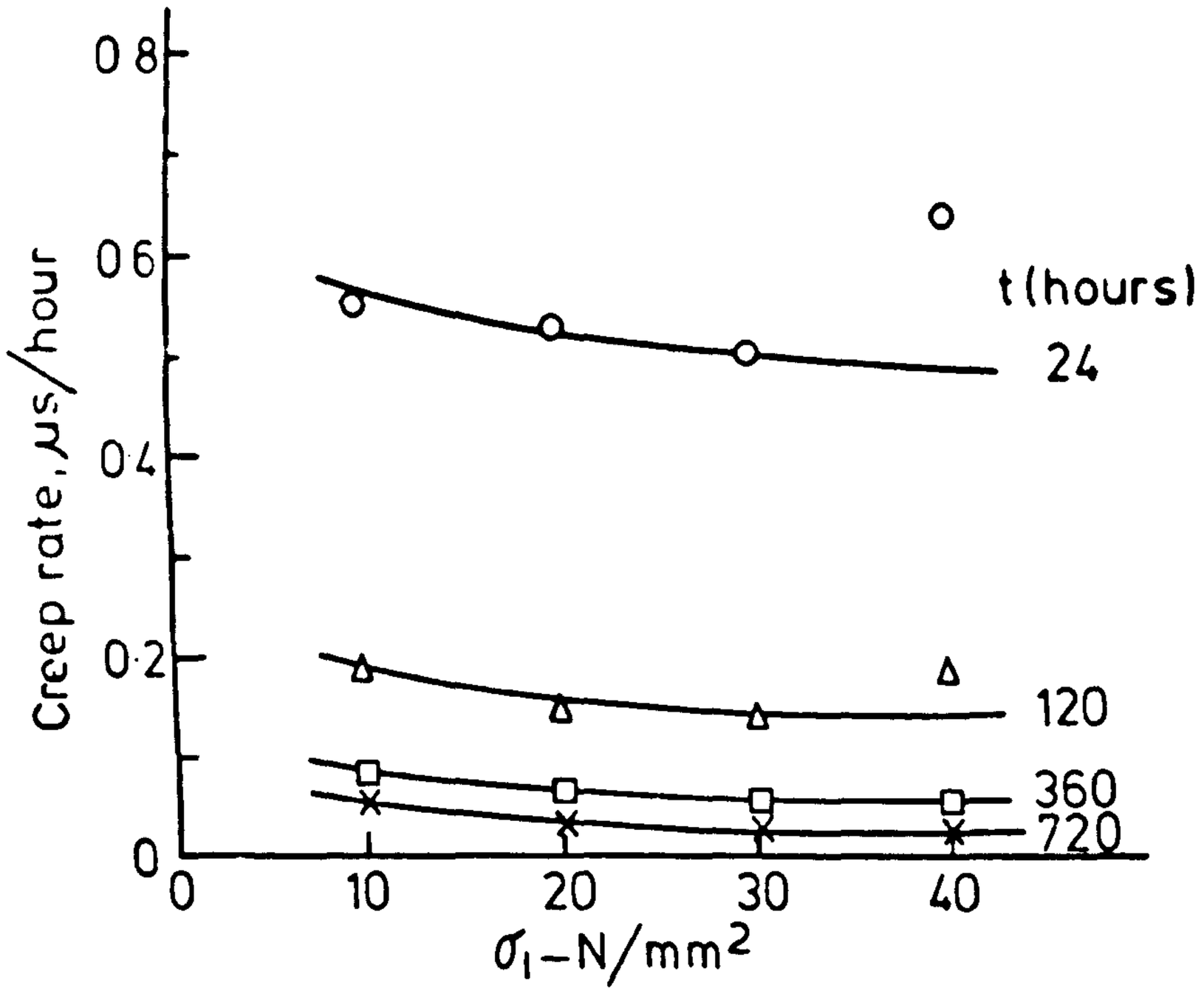

FIG.(7-20) LATERAL CREEP RATE Vs. σ_1 AT CONSTANT $(\sigma_1-\sigma_3)$ IN DRY CONDITIONS

$(\sigma_1 - \sigma_3) = 10\ N/mm^2$

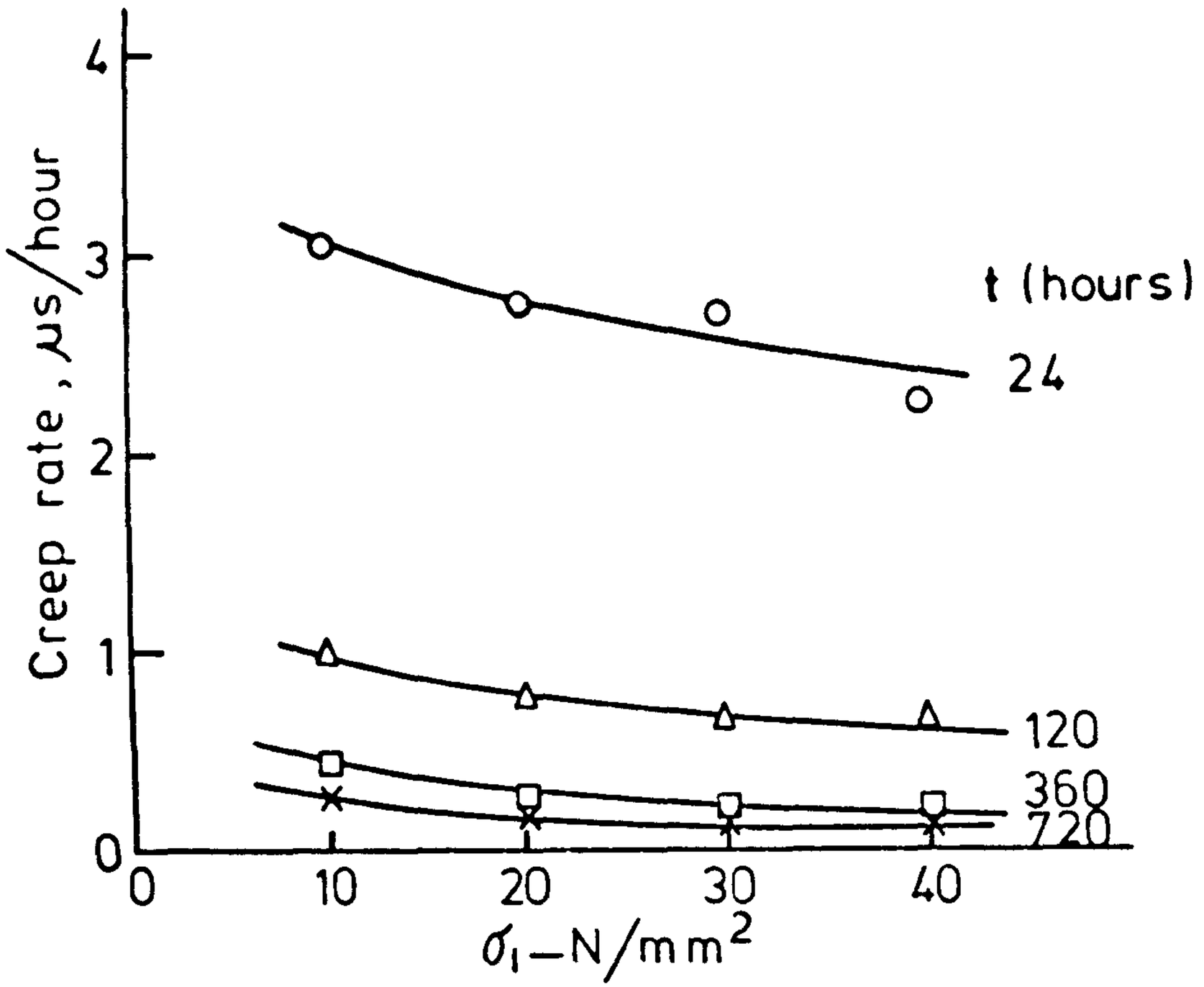

FIG.(7-21) LATERAL CREEP RATE Vs. σ_1 AT CONSTANT $(\sigma_1-\sigma_3)$ IN SATURATED CONDITIONS

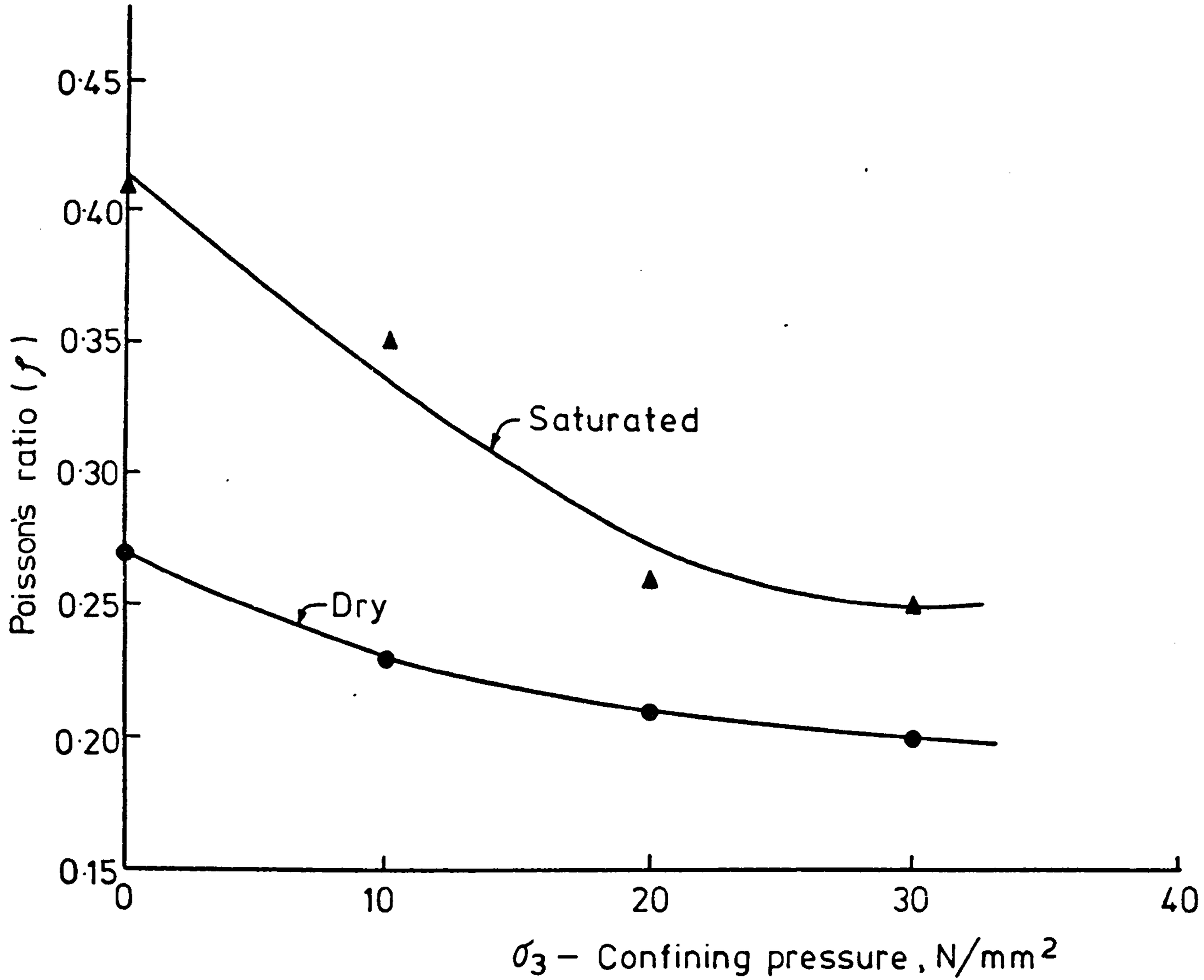

FIG.(7-22) EFFECT OF CONFINING PRESSURE ON THE POISSON'S RATIO IN DRY AND SATURATED CONDITIONS

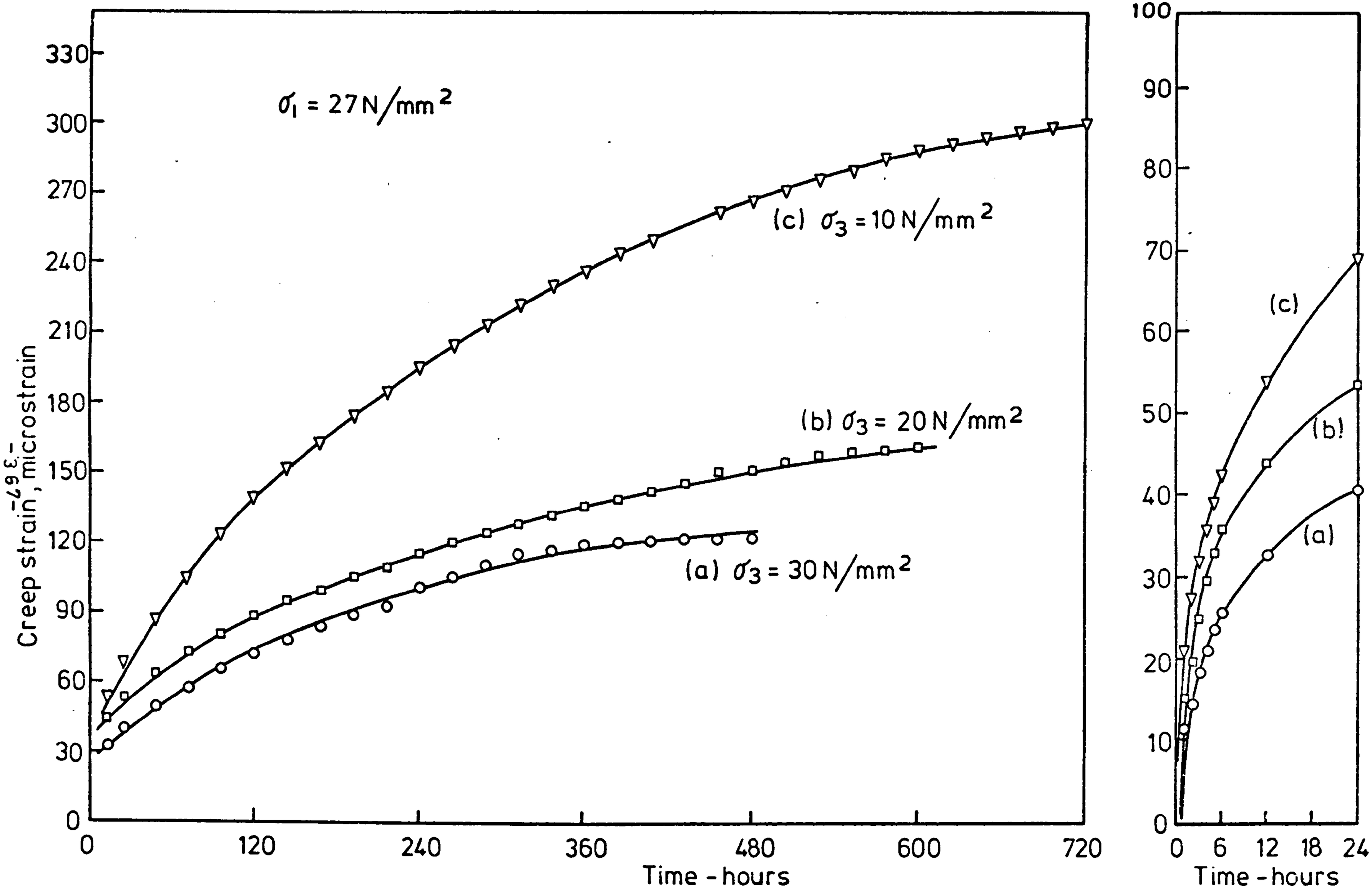

FIG. (7-23) EFFECT OF CONFINING PRESSURE ON THE LATERAL CREEP STRAIN AT σ_1 = 27 N/mm^2 IN DRY CONDITIONS

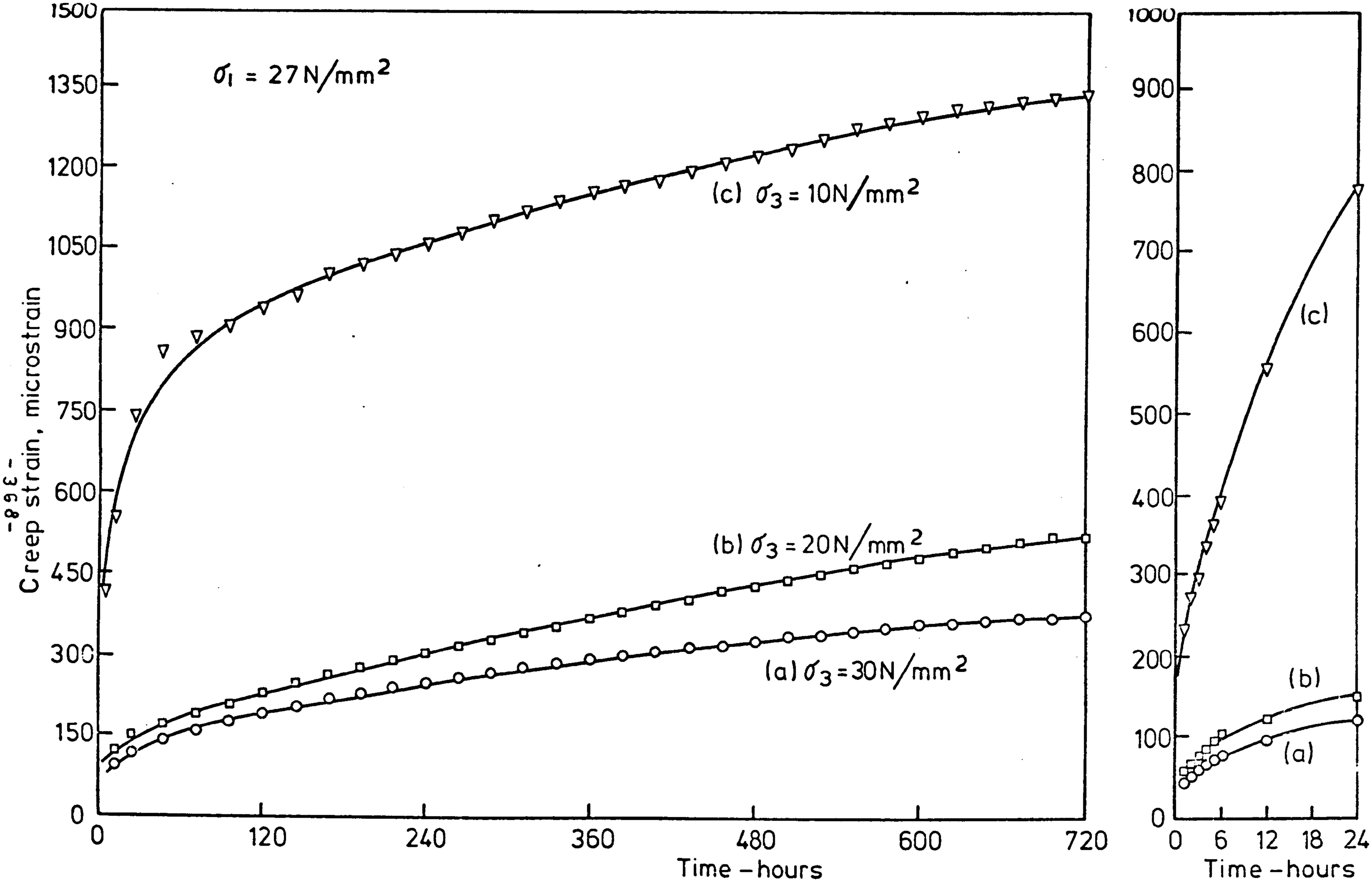

FIG.(7-24) EFFECT OF CONFINING PRESSURE ON THE LATERAL CREEP STRAIN AT CONSTANT σ_1 = 27N/mm² IN SATURATED CONDITIONS

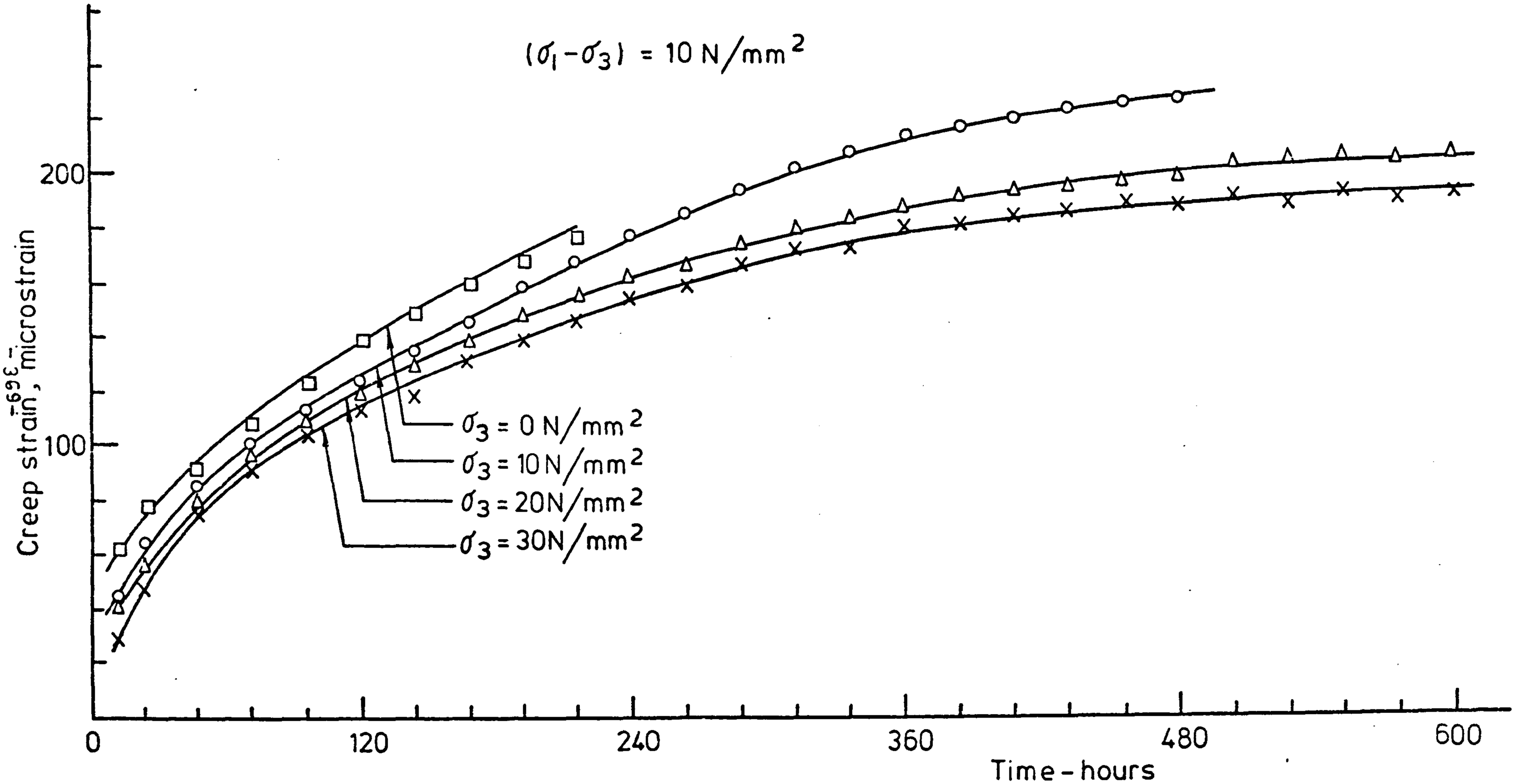

FIG. (7-25) LATERAL CREEP OF DRY GYPSUM AT CONSTANT $(\sigma_1-\sigma_3)$

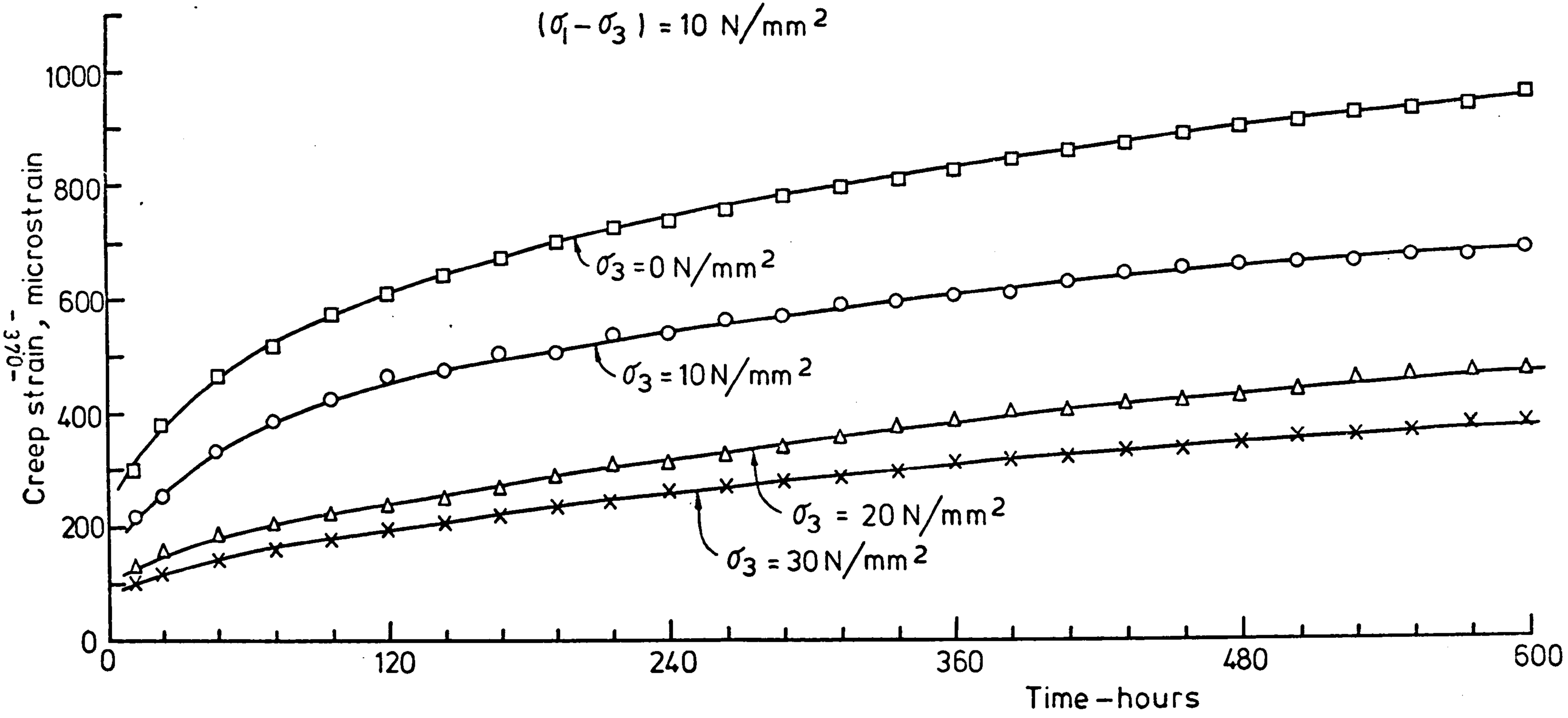

FIG. (7-26) LATERAL CREEP OF SATURATED GYPSUM AT CONSTANT $(\sigma_1 - \sigma_3)$

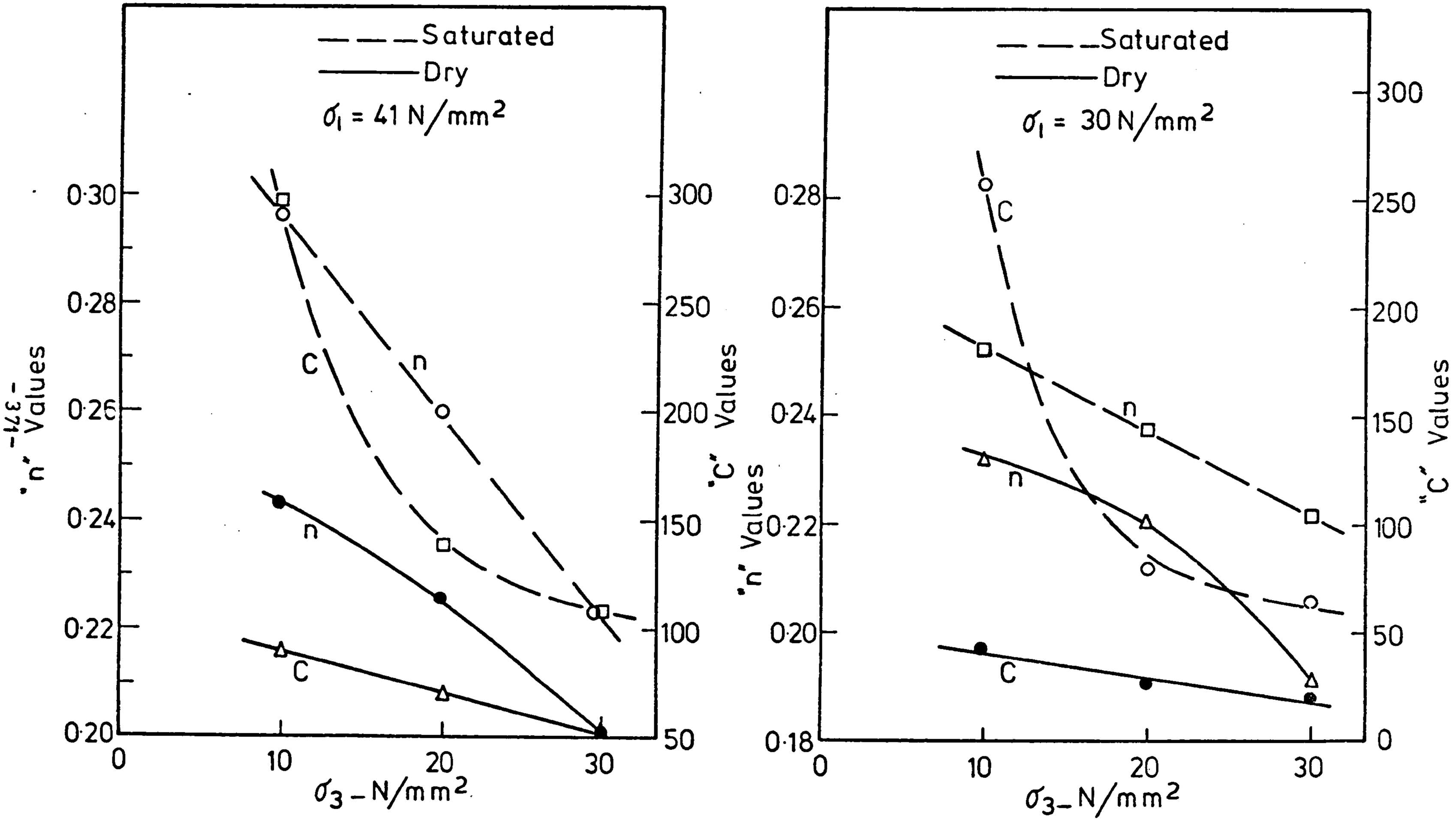

FIG.(7-27) EFFECT OF CONFINING PRESSURE ON "C" AND "n" VALUES AT CONSTANT σ_1 IN LATERAL CREEP

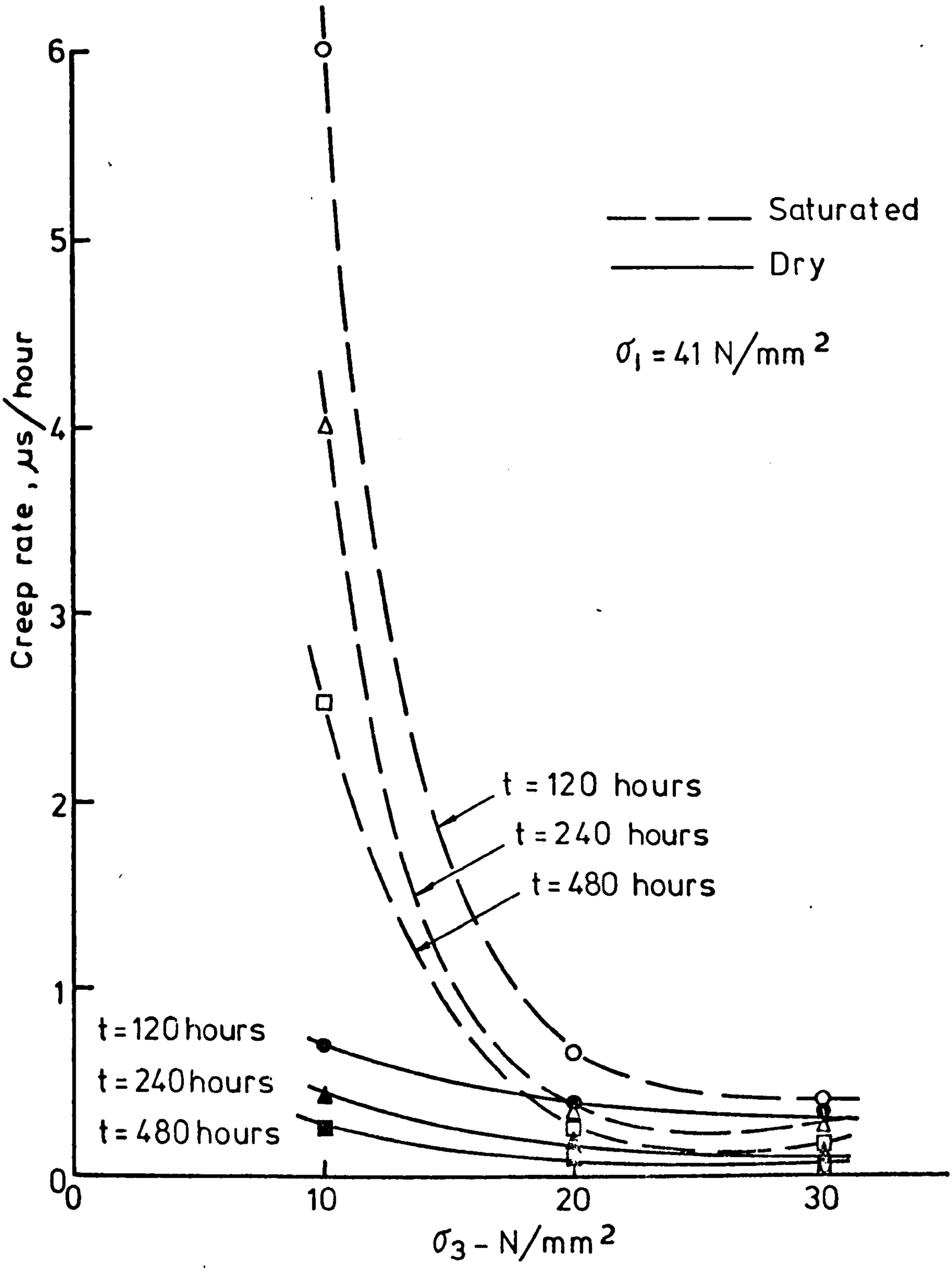

(7-28) LATERAL CREEP RATE Vs. CONFINING PRESSURE AT CONSTANT σ_1 IN DRY AND SATURATED CONDITIONS

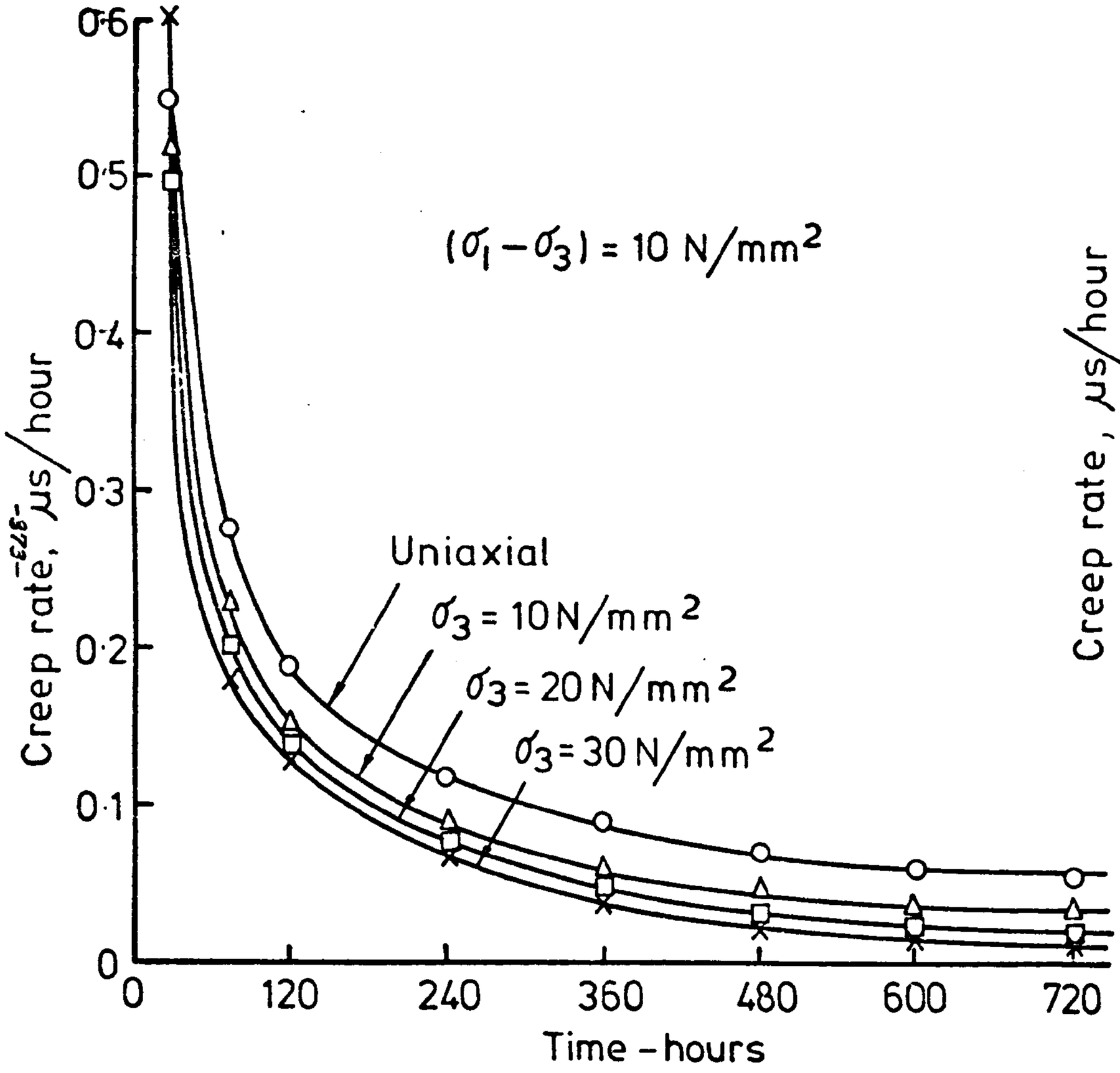

FIG.(7-29) LATERAL CREEP RATE OF DRY GYPSUM AT CONSTANT $(\sigma_1-\sigma_3)$

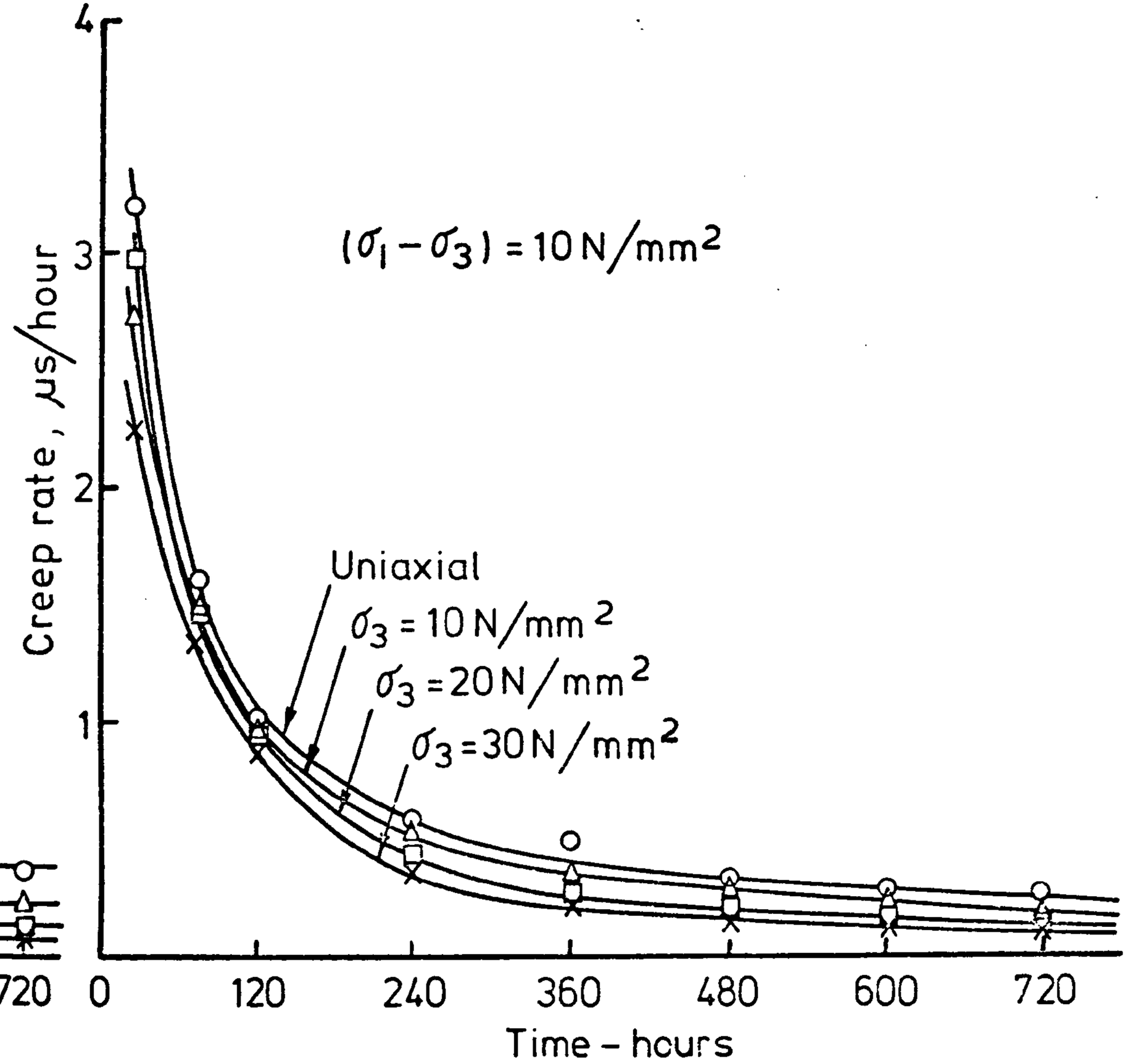

FIG.(7-30) LATERAL CREEP RATE OF SATURATED GYPSUM AT CONSTANT $(\sigma_1-\sigma_3)$

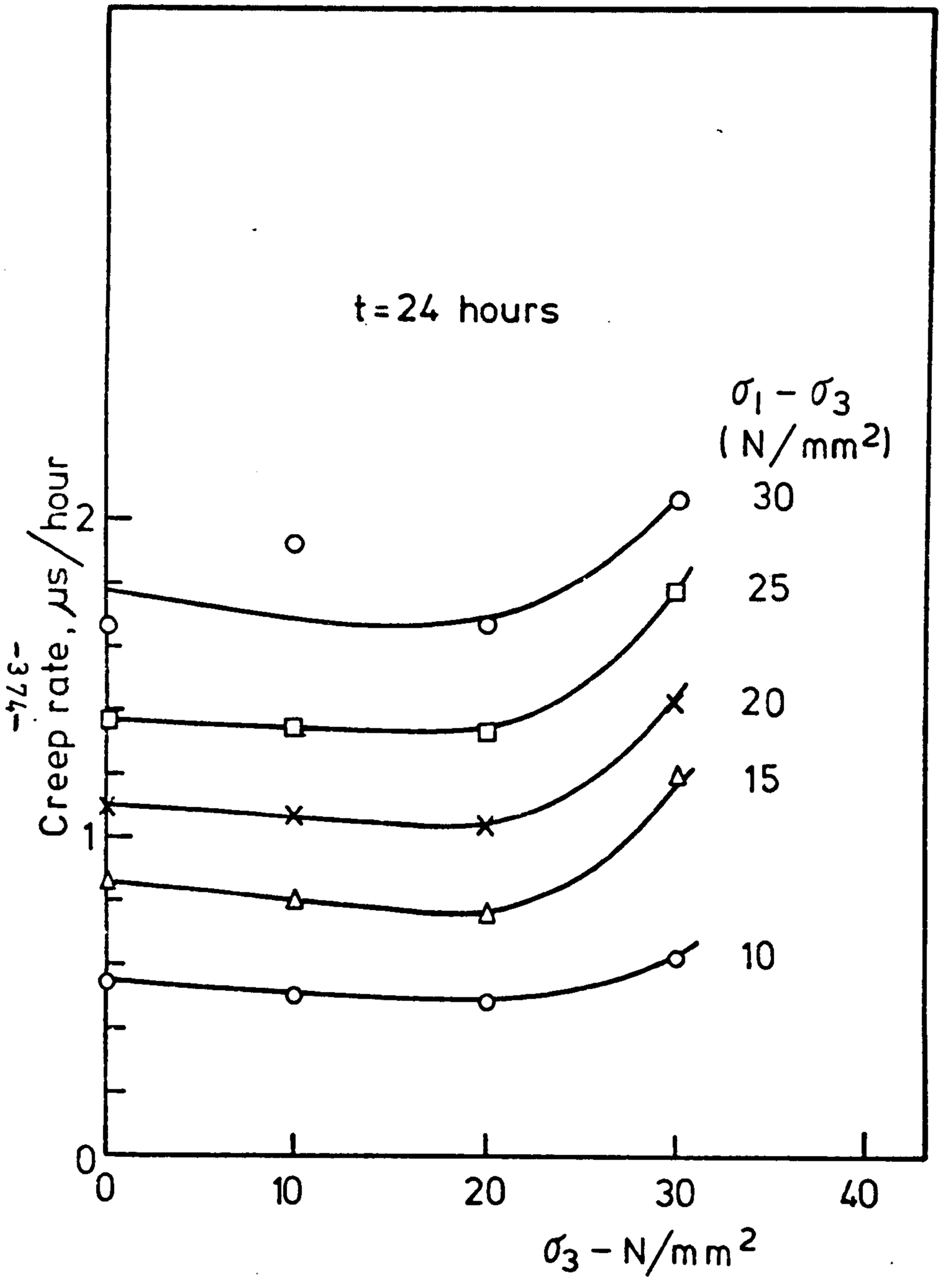

FIG.(7-31) EFFECT OF σ_3 ON THE LATERAL CREEP RATE AT CONSTANT $(\sigma_1 - \sigma_3)$ IN DRY CONDITIONS

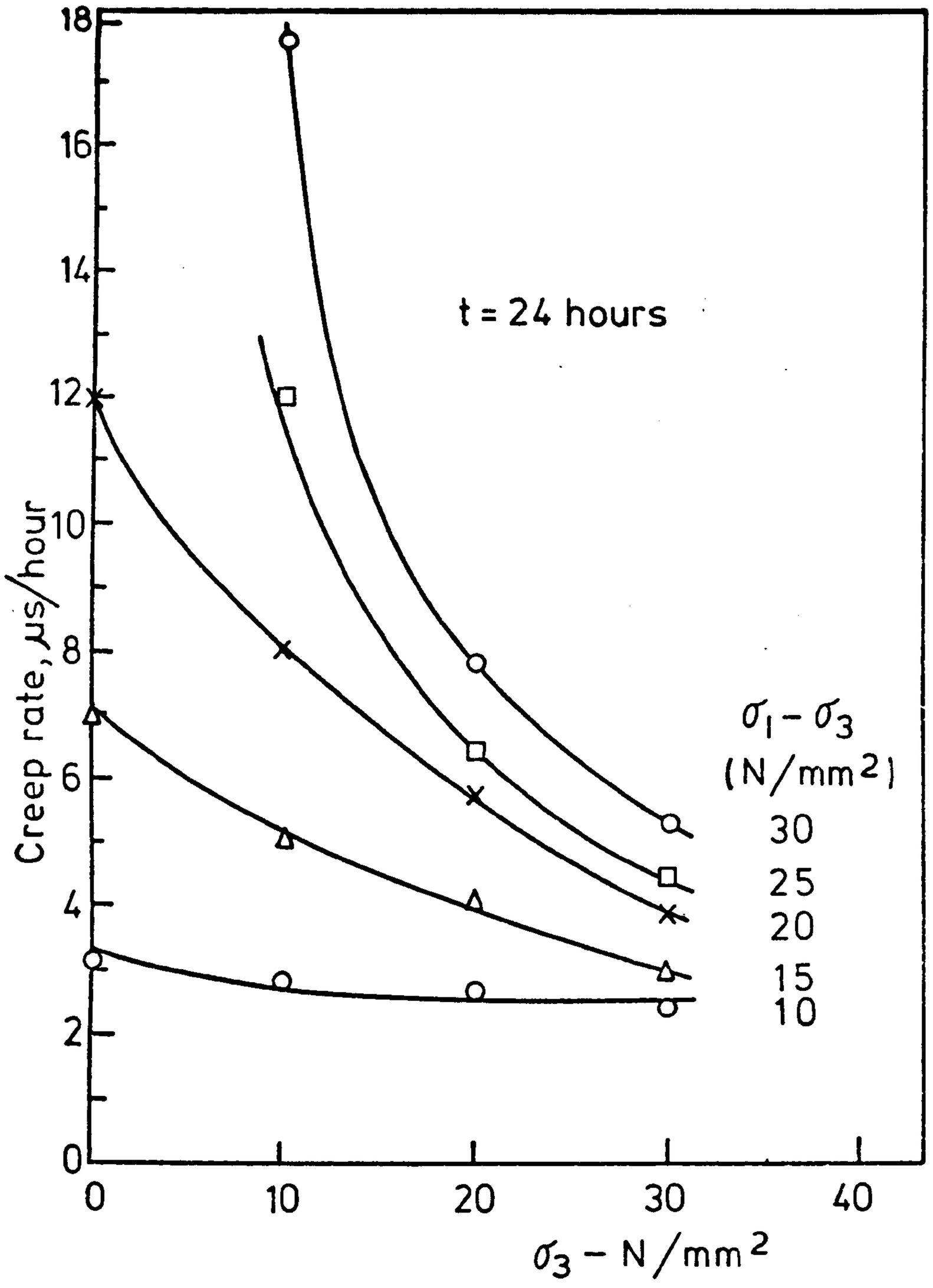

FIG.(7-32) EFFECT OF σ_3 ON THE LATERAL CREEP RATE AT CONSTANT $(\sigma_1 - \sigma_3)$ IN SATURATED CONDITIONS

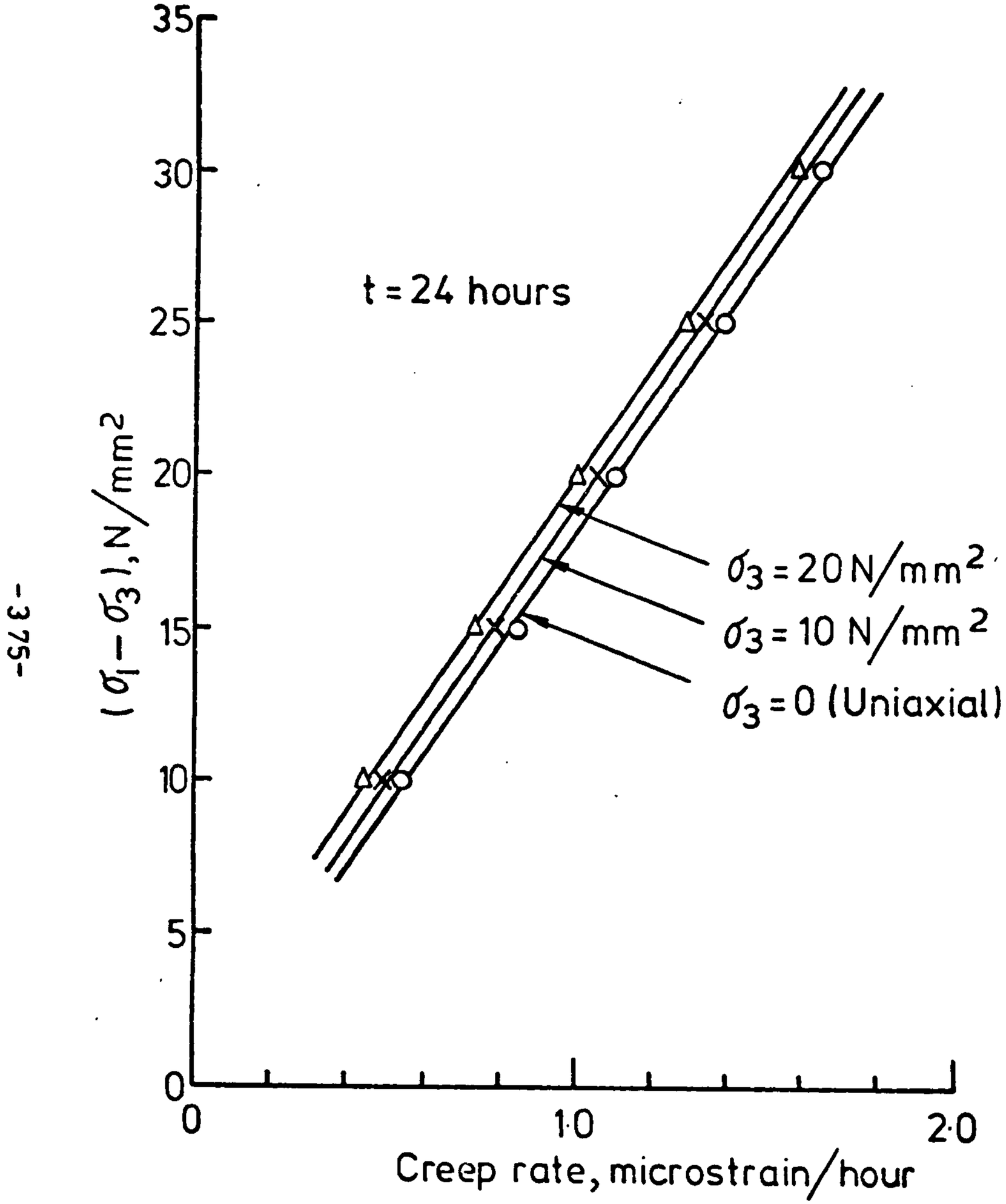

FIG.(7-33) LATERAL CREEP RATE Vs. $(\sigma_1 - \sigma_3)$ AT CONSTANT σ_3 IN DRY CONDITIONS

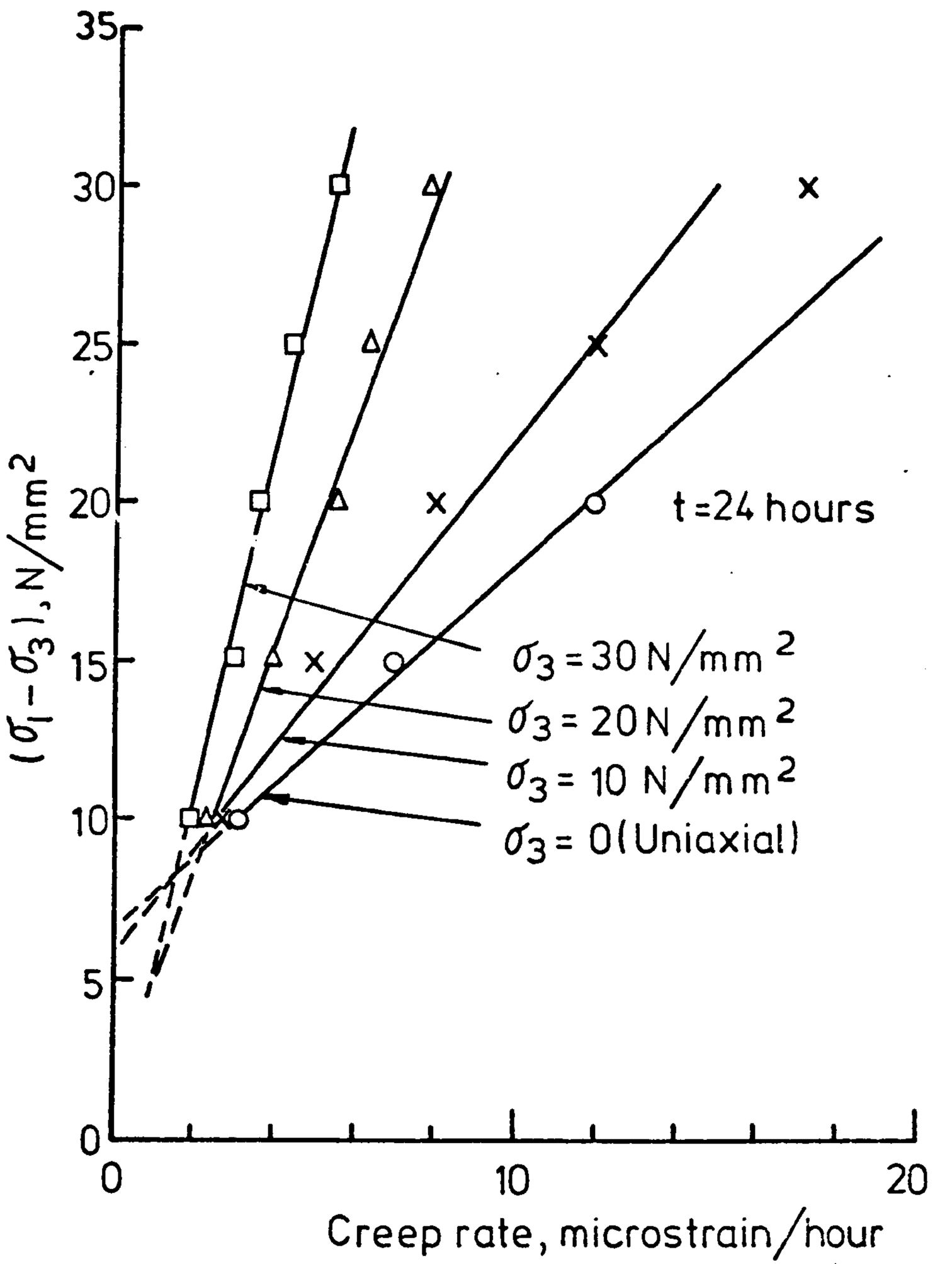

FIG.(7-34) LATERAL CREEP RATE Vs. $(\sigma_1 - \sigma_3)$ AT CONSTANT σ_3 IN SATURATED CONDITIONS

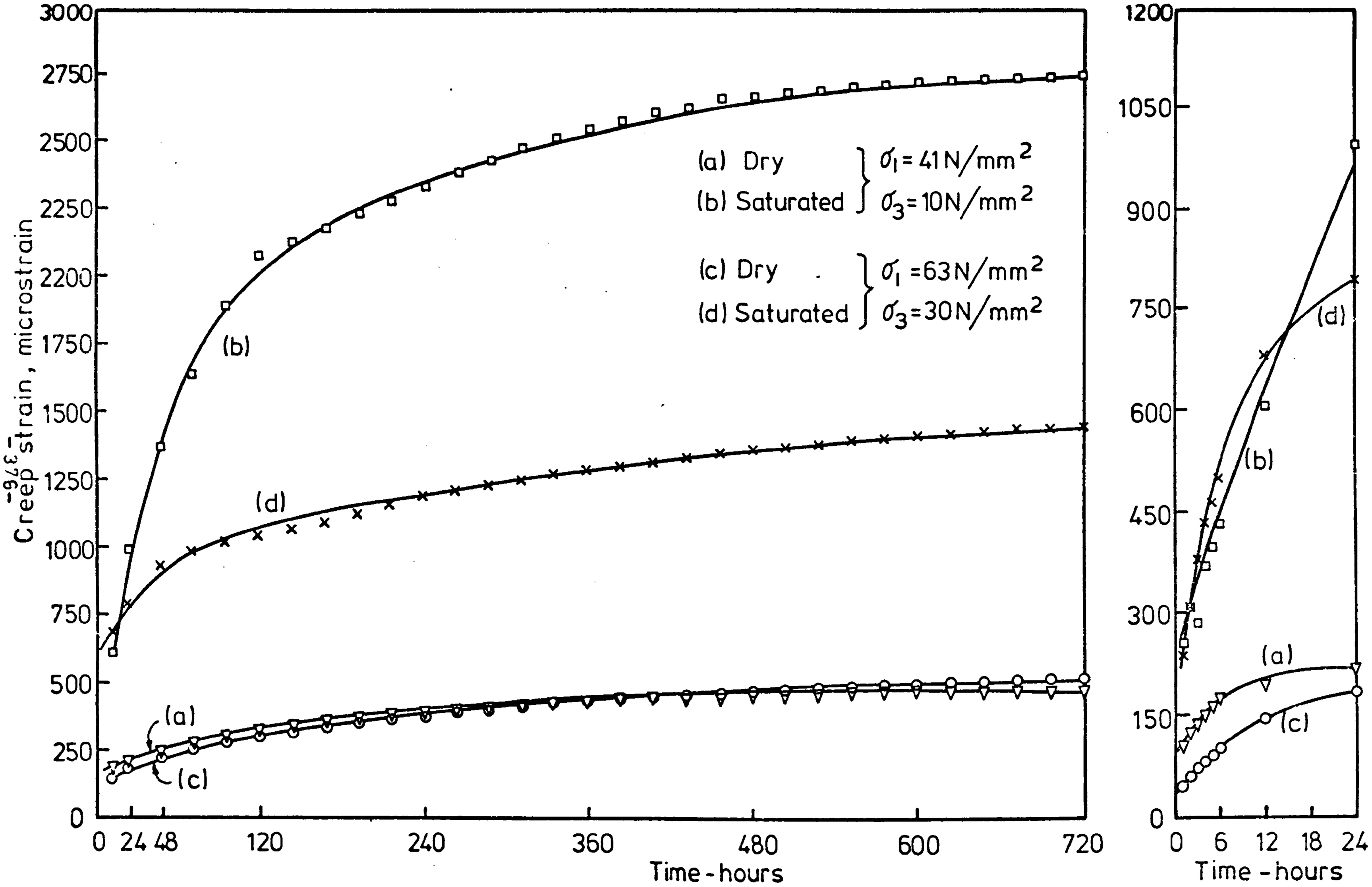

FIG.(7-35) EFFECT OF SATURATION ON THE LATERAL CREEP STRAIN AT VARIOUS STRESS CONDITIONS

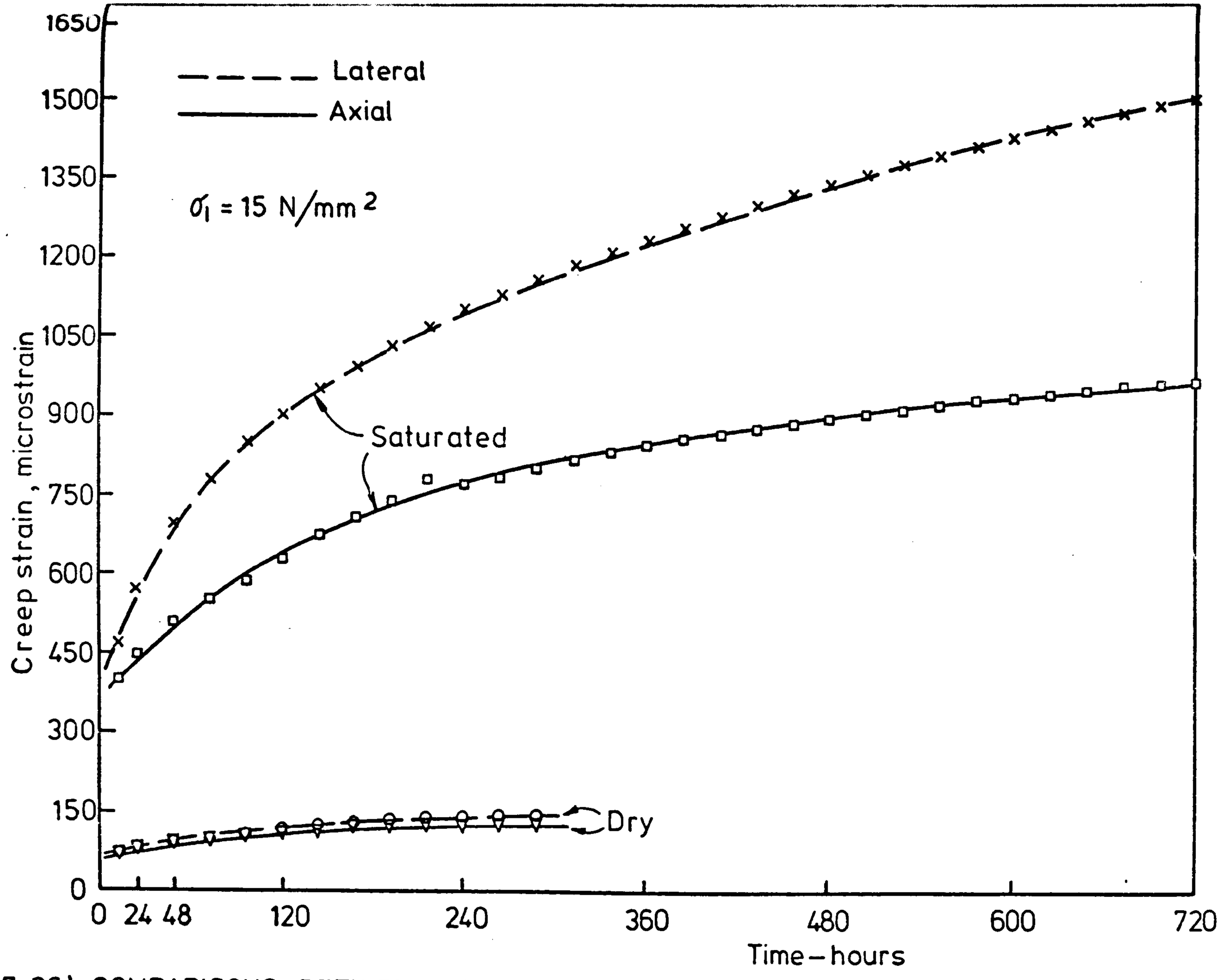

FIG.(7-36) COMPARISONS BETWEEN AXIAL AND LATERAL CREEP IN UNIAXIAL COMPRESSION IN DRY AND SATURATED CONDITIONS

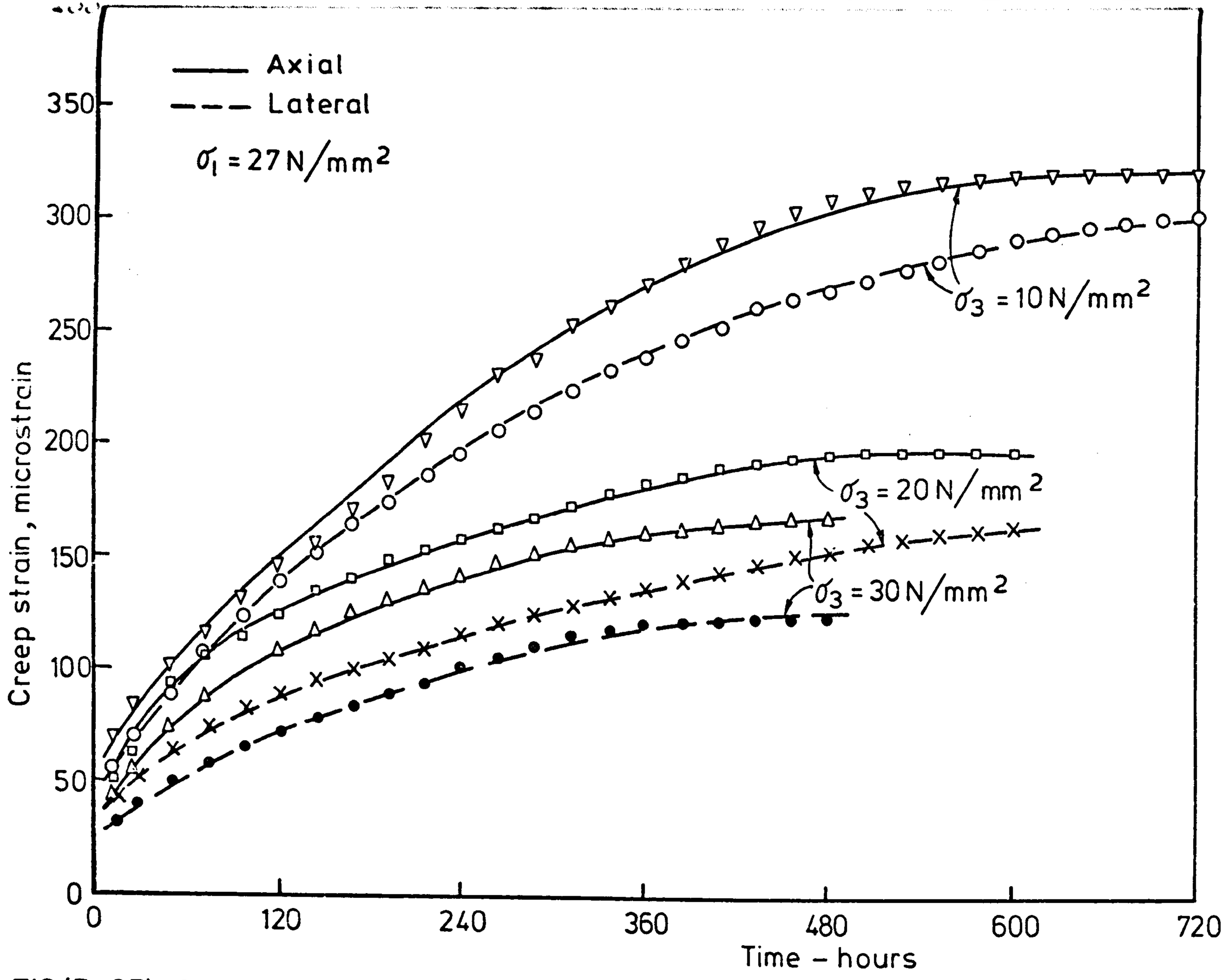

FIG.(7-37) COMPARISON BETWEEN AXIAL AND LATERAL CREEP STRAINS IN TRIAXIAL COMPRESSION AT VARIOUS VALUES OF σ_3 IN DRY CONDITIONS

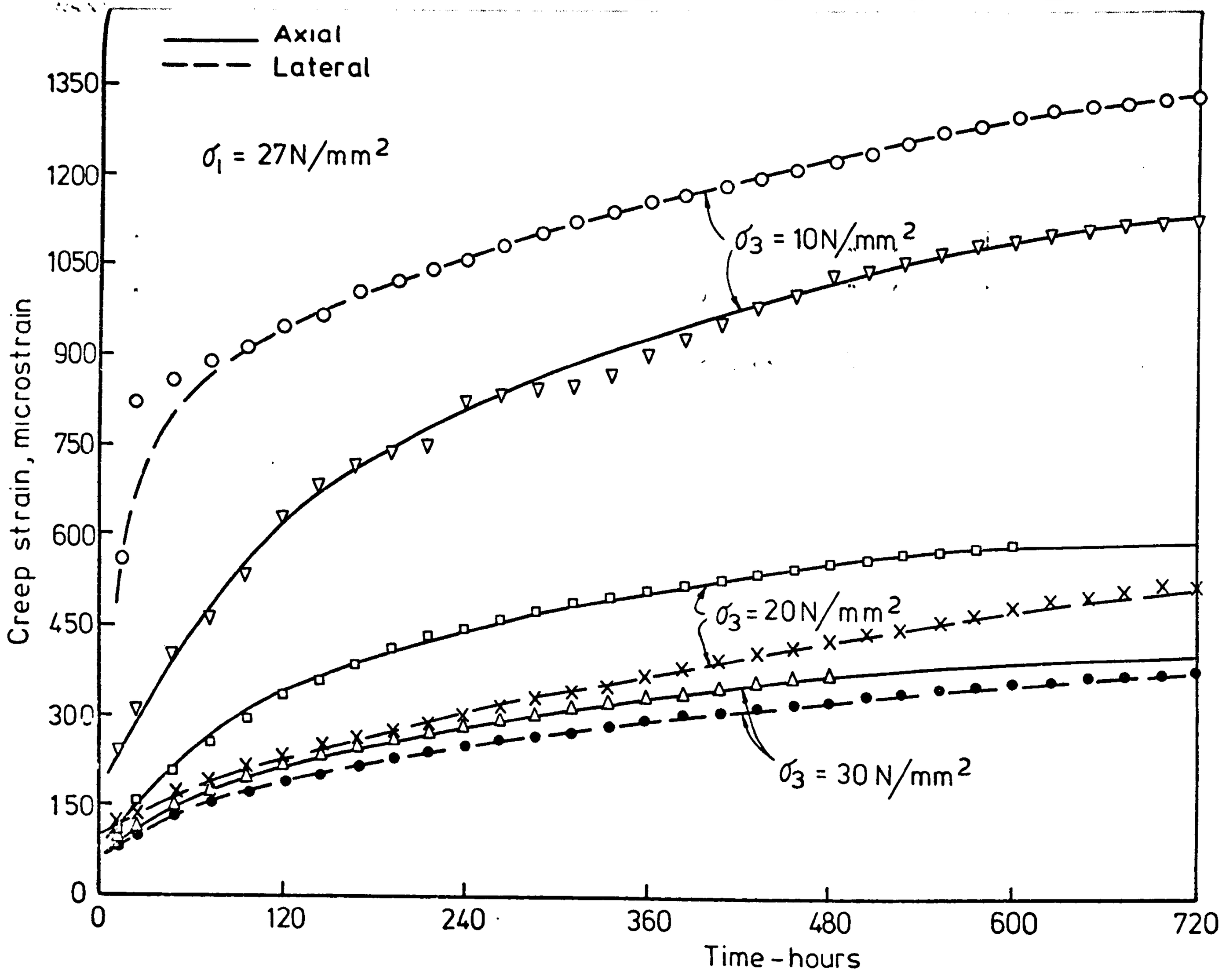

FIG. (7-38) COMPARISON BETWEEN AXIAL AND LATERAL CREEP STRAINS IN TRIAXIAL COMPRESSION AT VARIOUS VALUES OF σ_3 IN SATURATED CONDITIONS

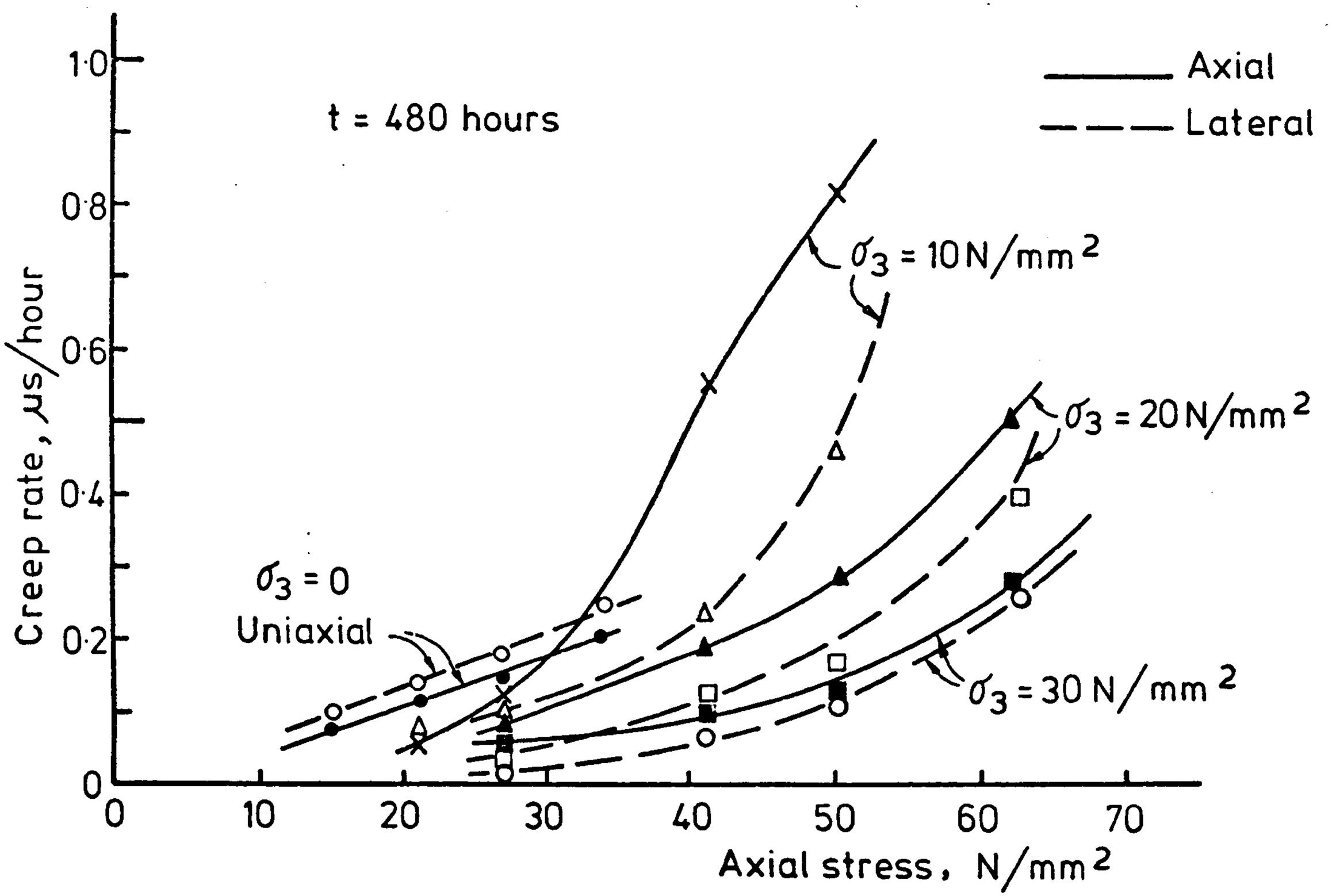

FIG.(7-39) AXIAL AND LATERAL CREEP RATE Vs. AXIAL STRESS AT CONSTANT σ_3 IN DRY CONDITION

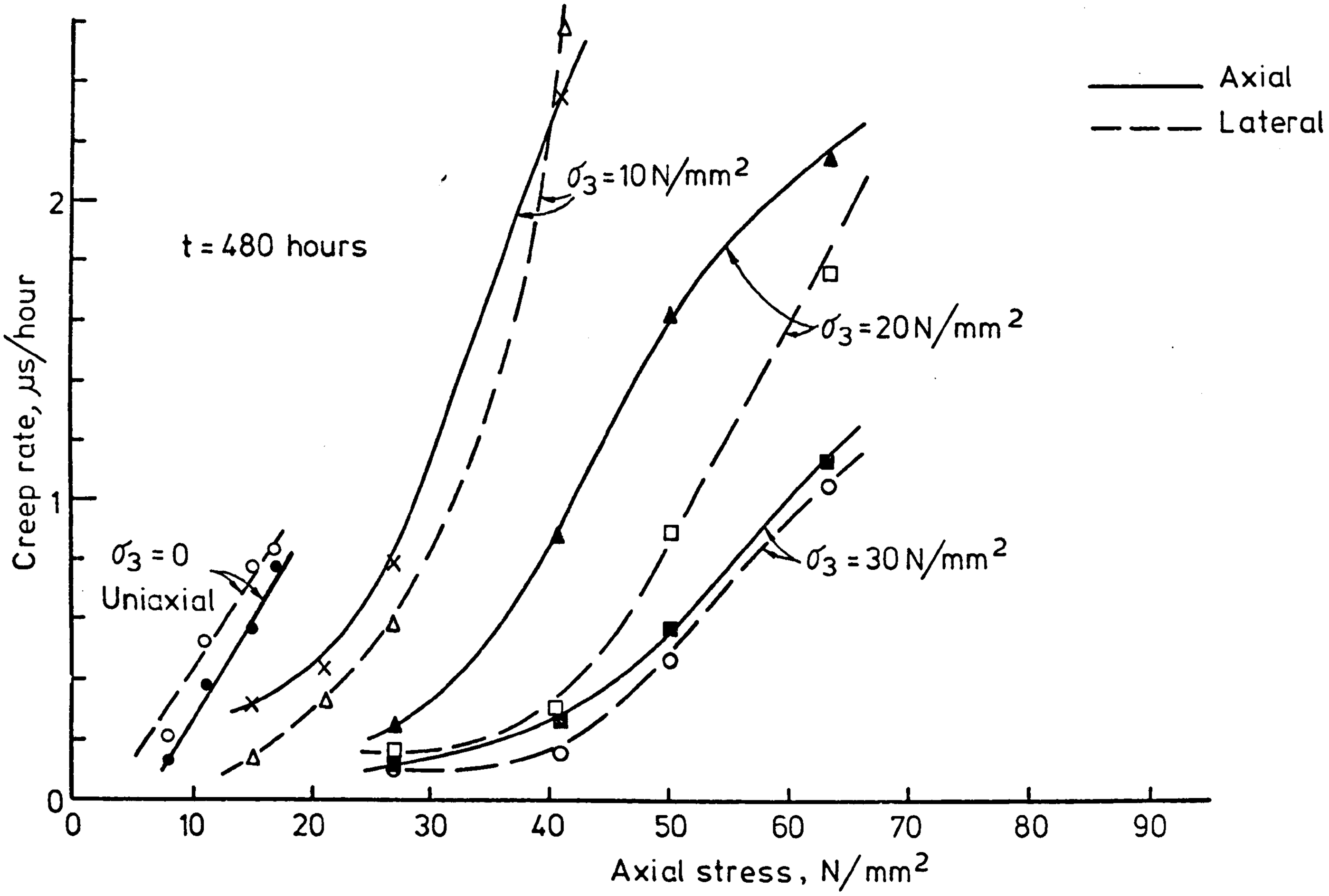

FIG. (7-40) AXIAL AND LATERAL CREEP RATE Vs. AXIAL STRESS AT CONSTANT σ_3 IN SATURATED CONDITION

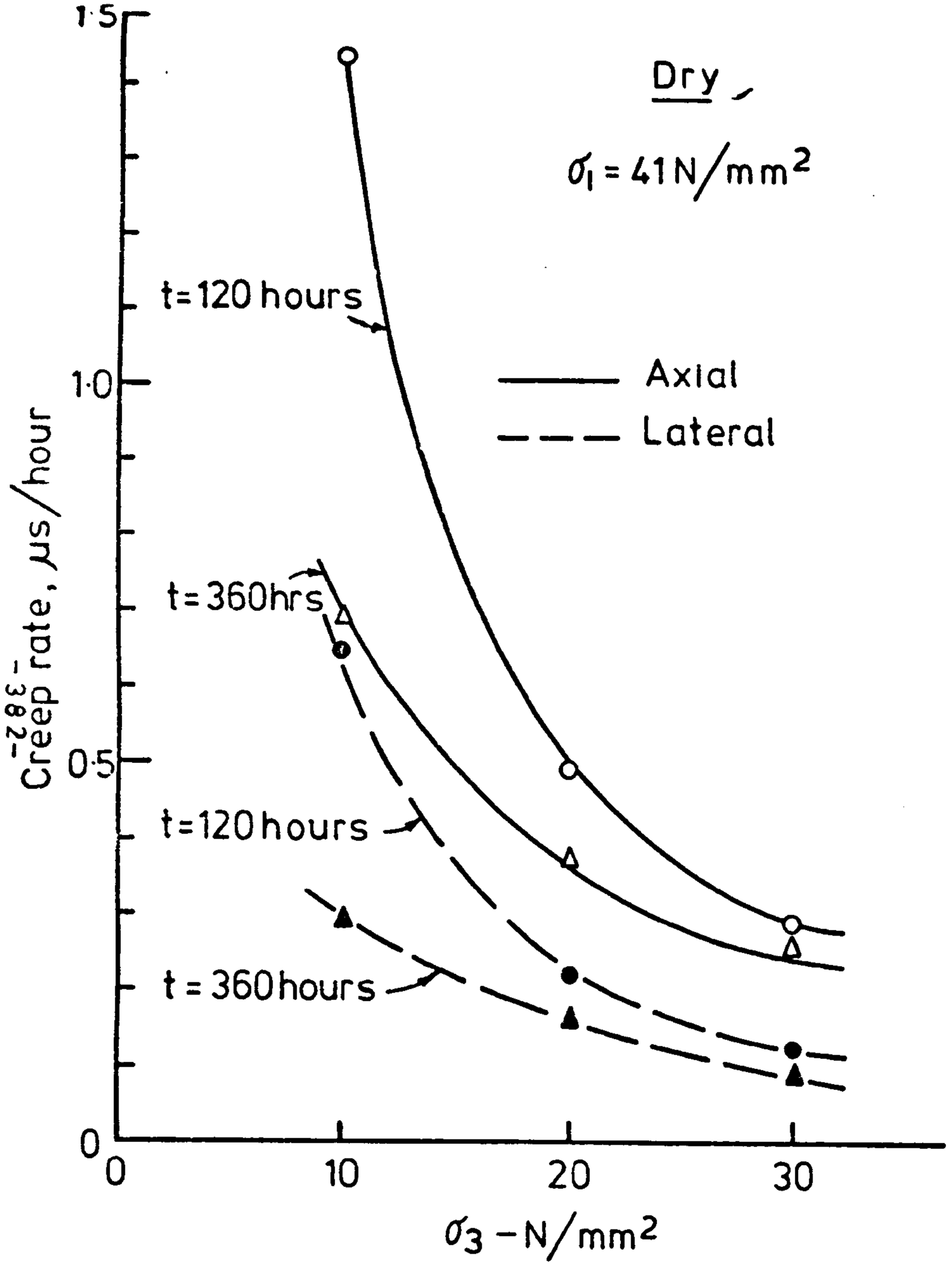

FIG. (7-41) EFFECT OF σ_3 ON AXIAL AND LATERAL CREEP RATES AT CONSTANT σ_1 IN DRY CONDITION

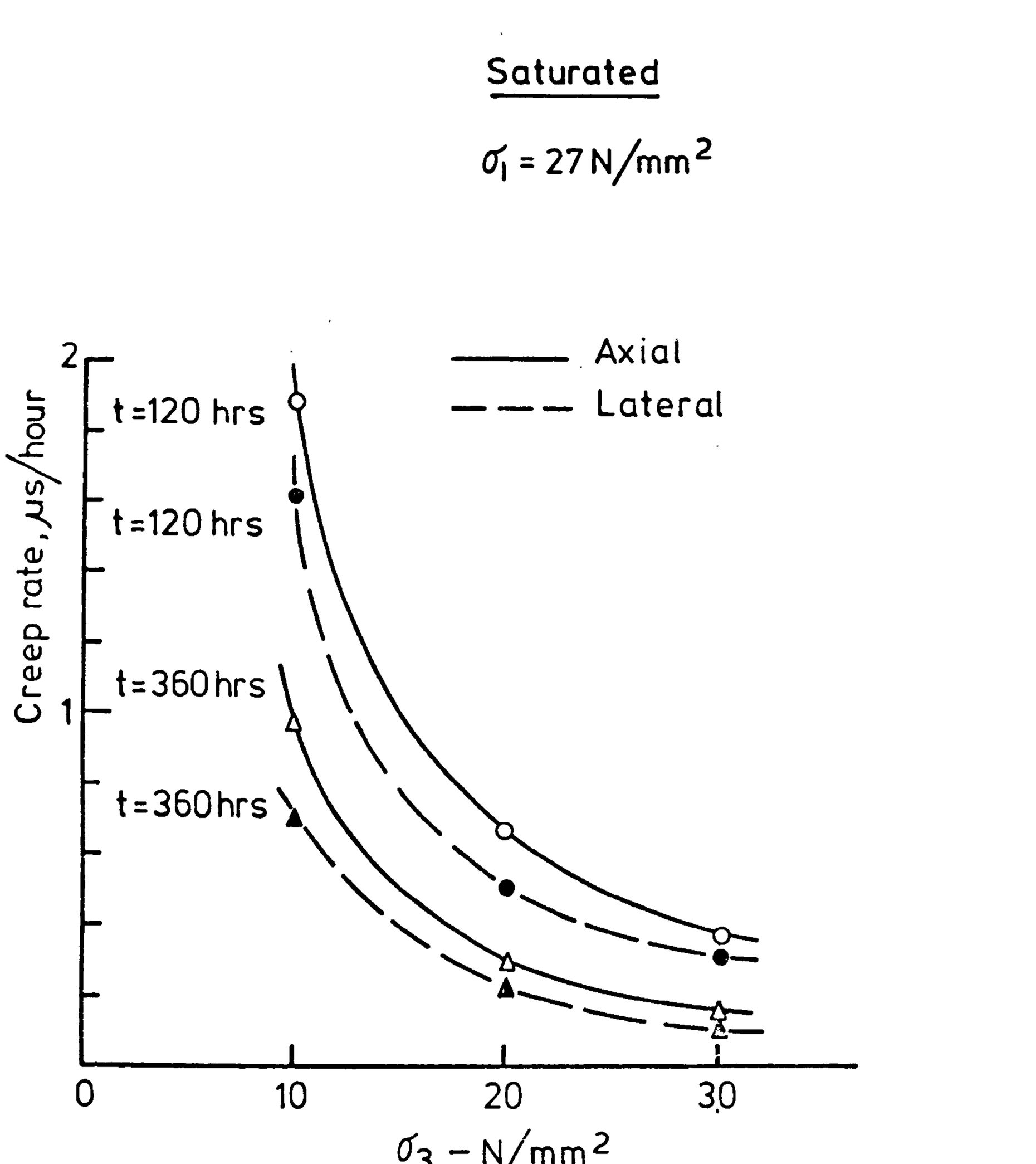

FIG.(7-42) EFFECT OF σ_3 ON AXIAL AND LATERAL CREEP RATES AT CONSTANT σ_1 IN SATURATED CONDITION

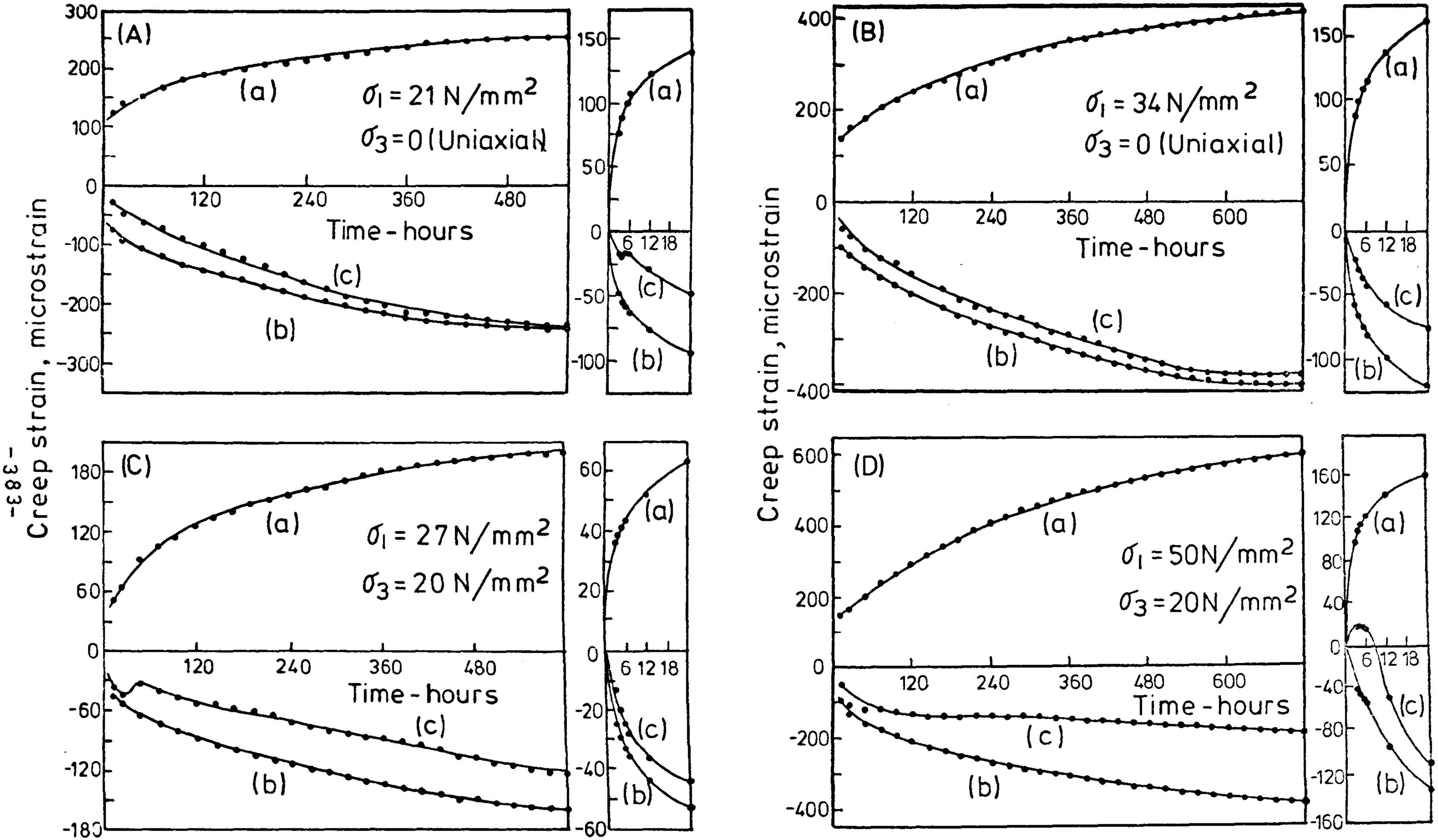

Curve (a) Axial creep strain, (b) Lateral creep strain, (c) Volumetric creep strain, (−ve) increase, (+ve) decrease

FIG.(7-43) AXIAL, LATERAL AND VOLUMETRIC CREEP STRAIN OF DRY GYPSUM UNDER VARIOUS STRESS CONDITIONS

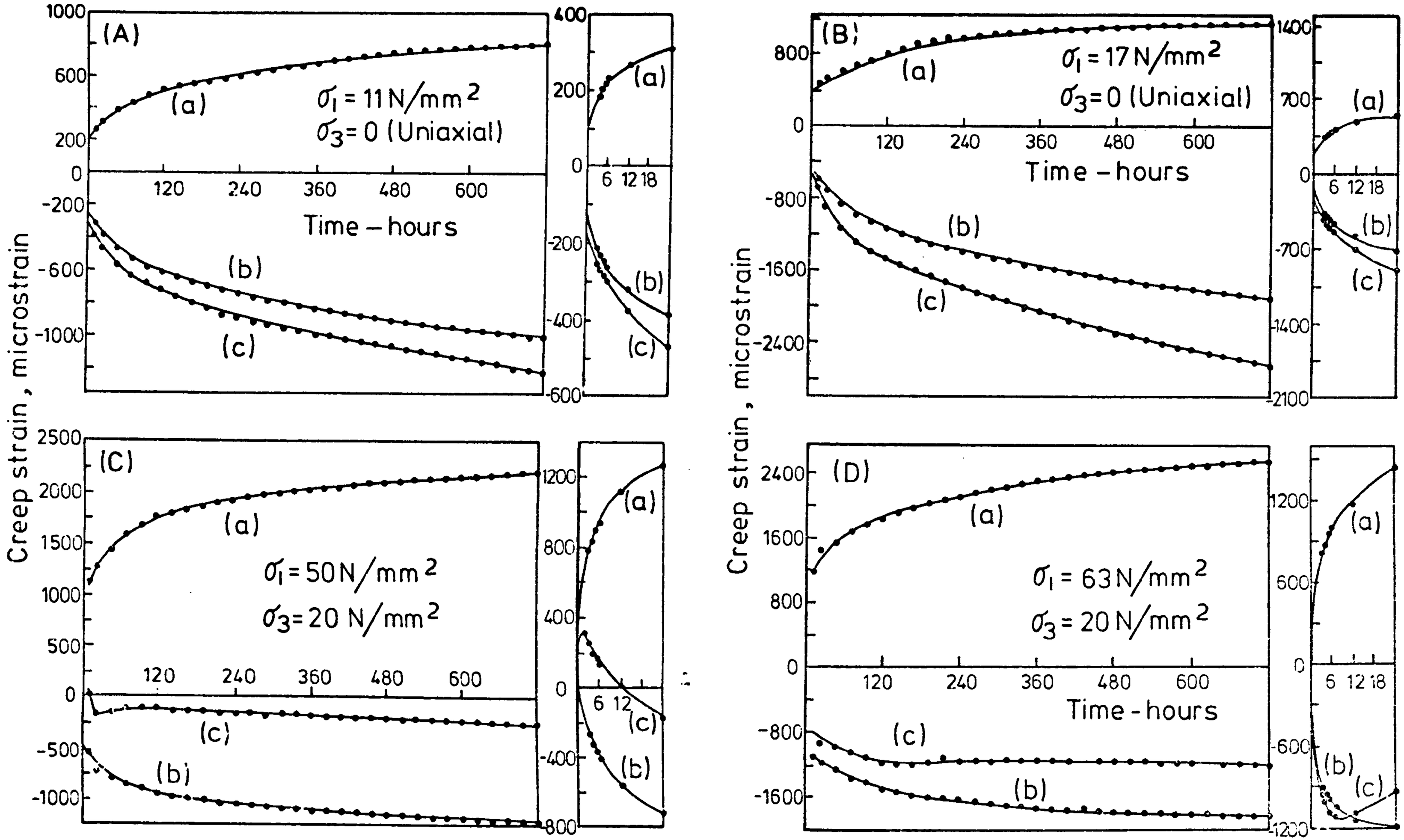

Curve (a) Axial creep strain, (b) Lateral creep strain, (c) Volumetric creep strain, (-ve) increase, (+ve) decrease

FIG.(7-44) AXIAL, LATERAL AND VOLUMETRIC CREEP STRAIN OF SATURATED GYPSUM UNDER VARIOUS STRESS CONDITIONS

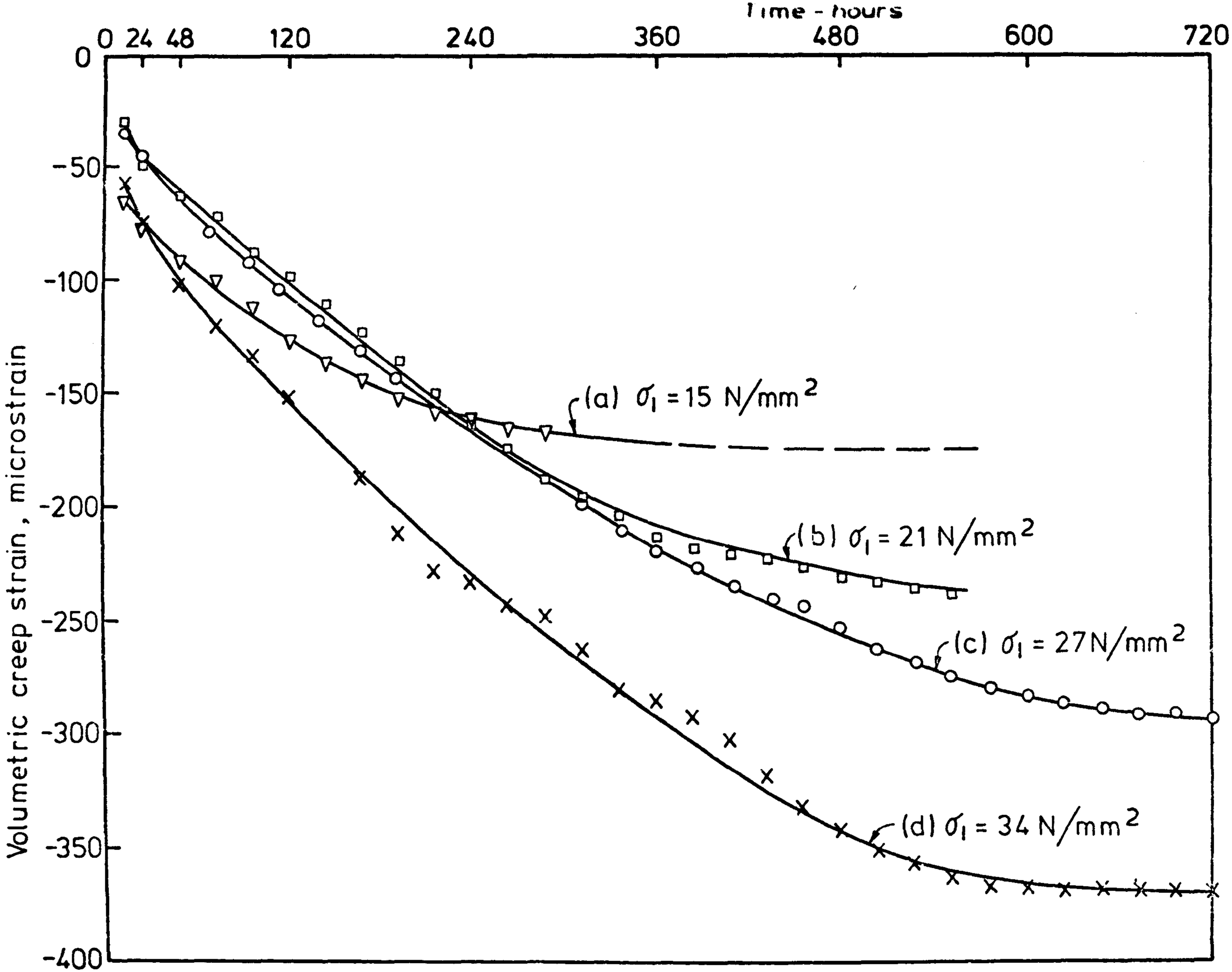

FIG. (7-45) VOLUMETRIC CREEP OF DRY GYPSUM IN UNIAXIAL COMPRESSION

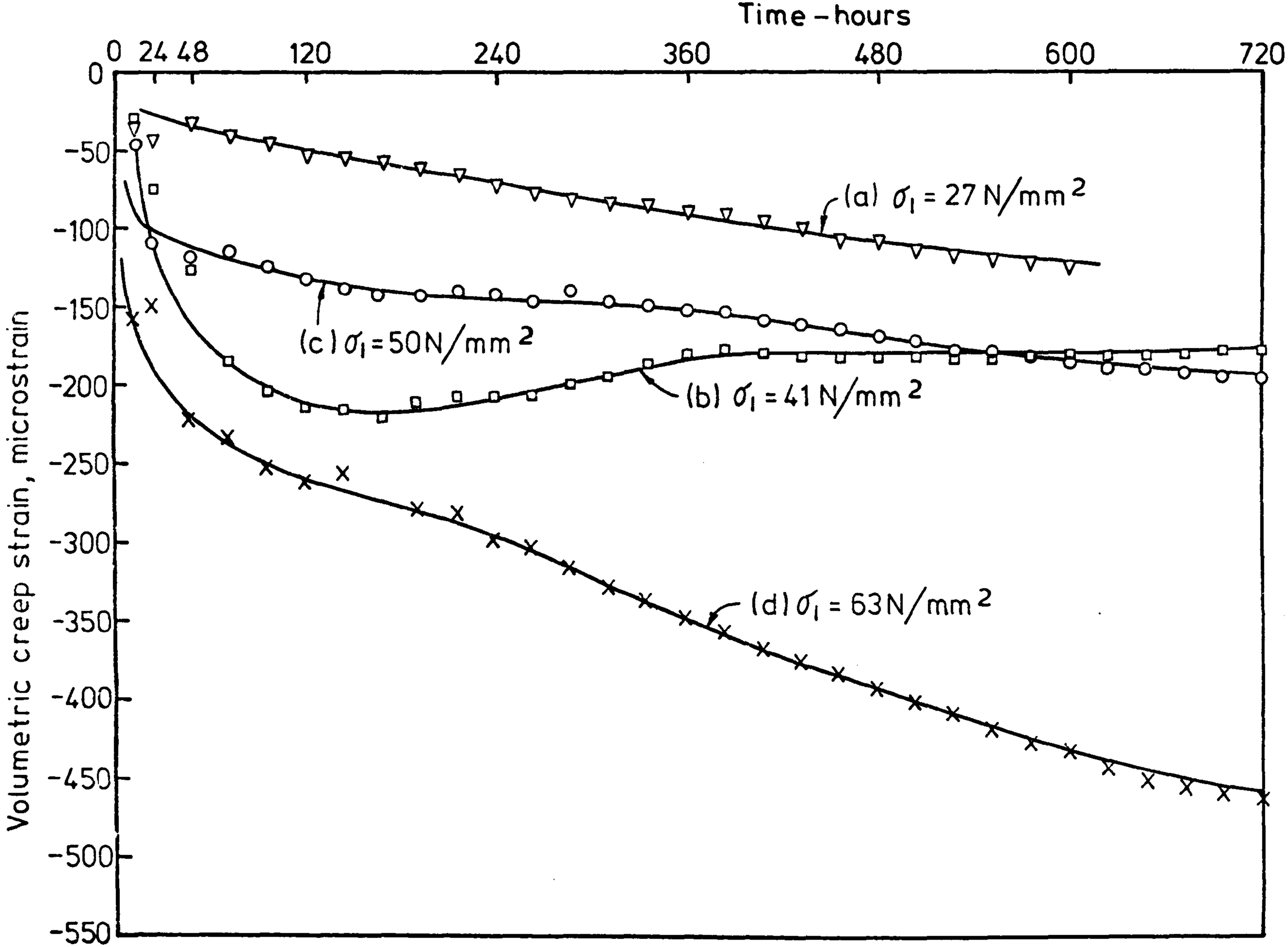

FIG.(7-46) VOLUMETRIC CREEP OF DRY GYPSUM IN TRIAXIAL COMPRESSION AT 20N/mm^2 CONFINING PRESSURE

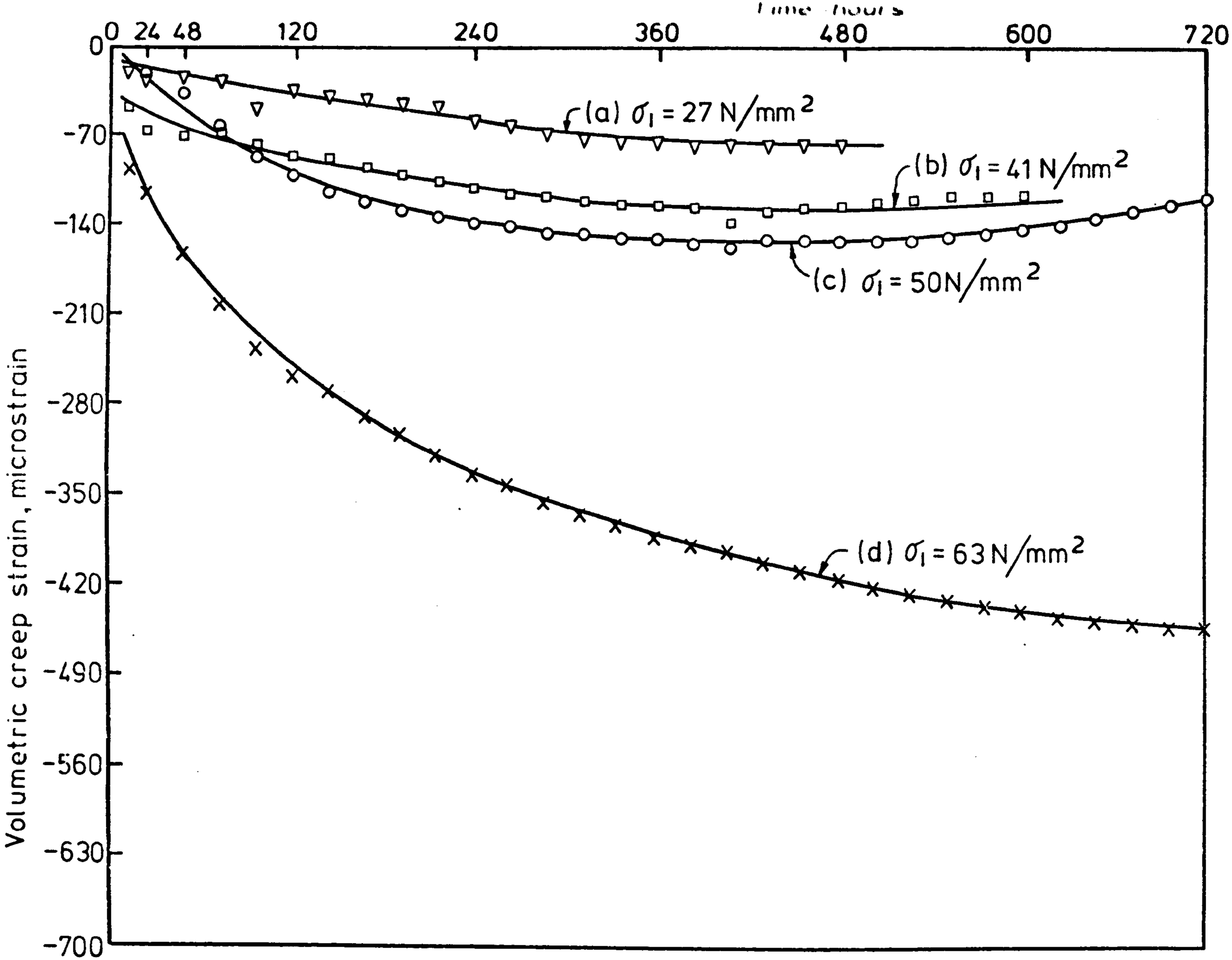

FIG.(7-47) VOLUMETRIC CREEP OF DRY GYPSUM IN TRIAXIAL COMPRESSION AT 30N/mm CONFINING PRESSURE

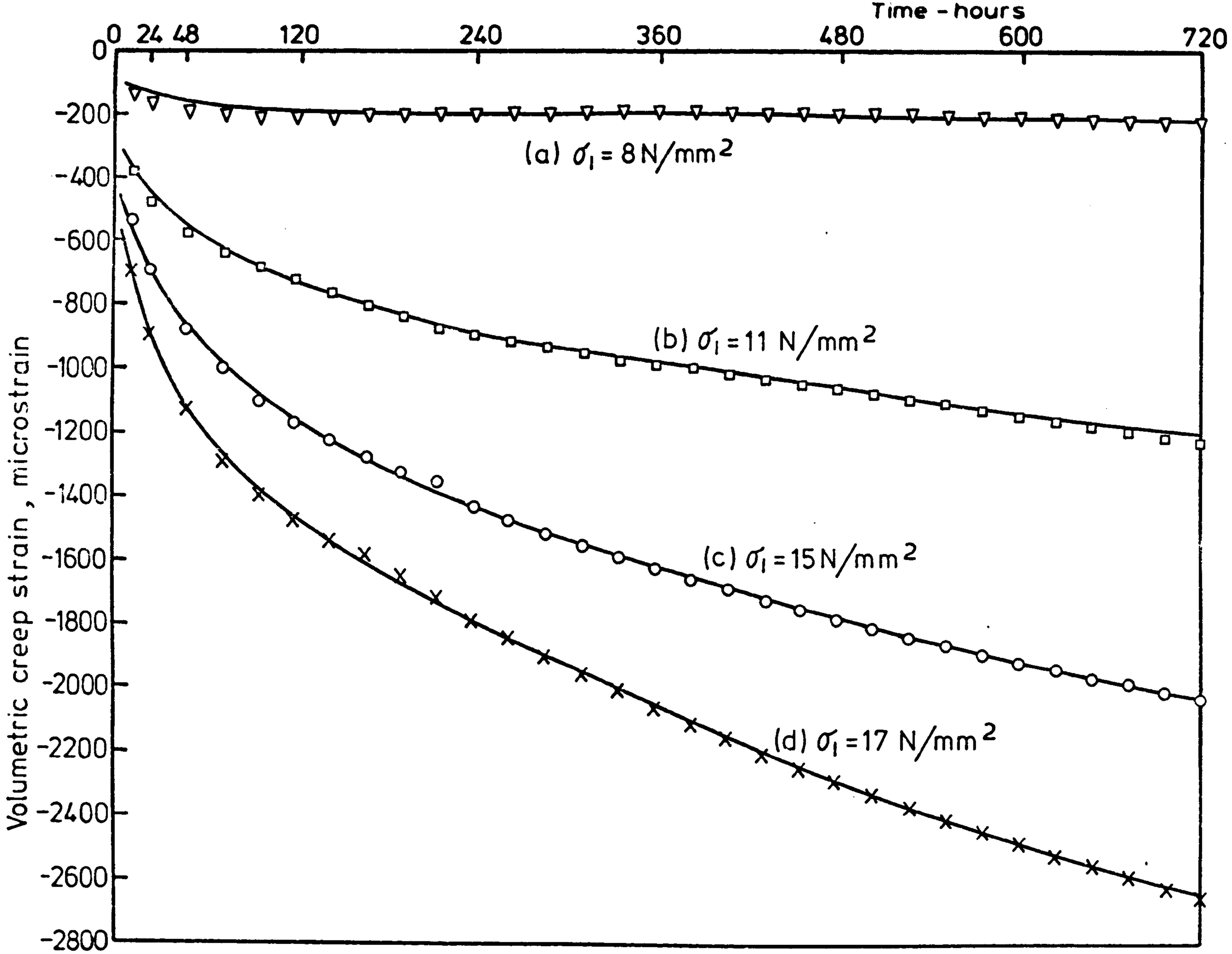

FIG. (7-48) VOLUMETRIC CREEP STRAIN OF SATURATED GYPSUM IN UNIAXIAL COMPRESSION

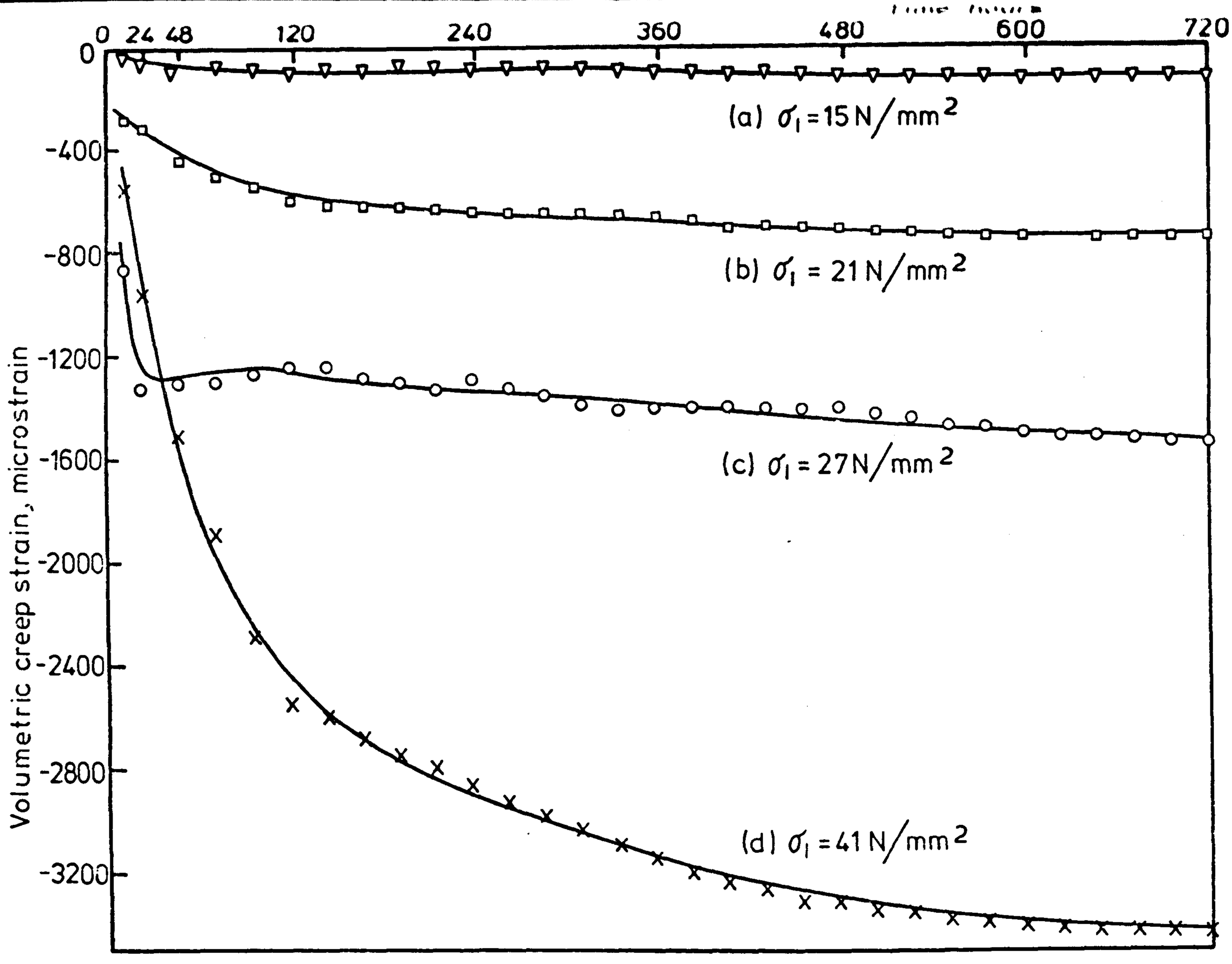

FIG.(7-49) VOLUMETRIC CREEP STRAIN OF SATURATED GYPSUM IN TRIAXIAL COMPRESSION AT $10\ N/mm^2$ CONFINING PRESSURE

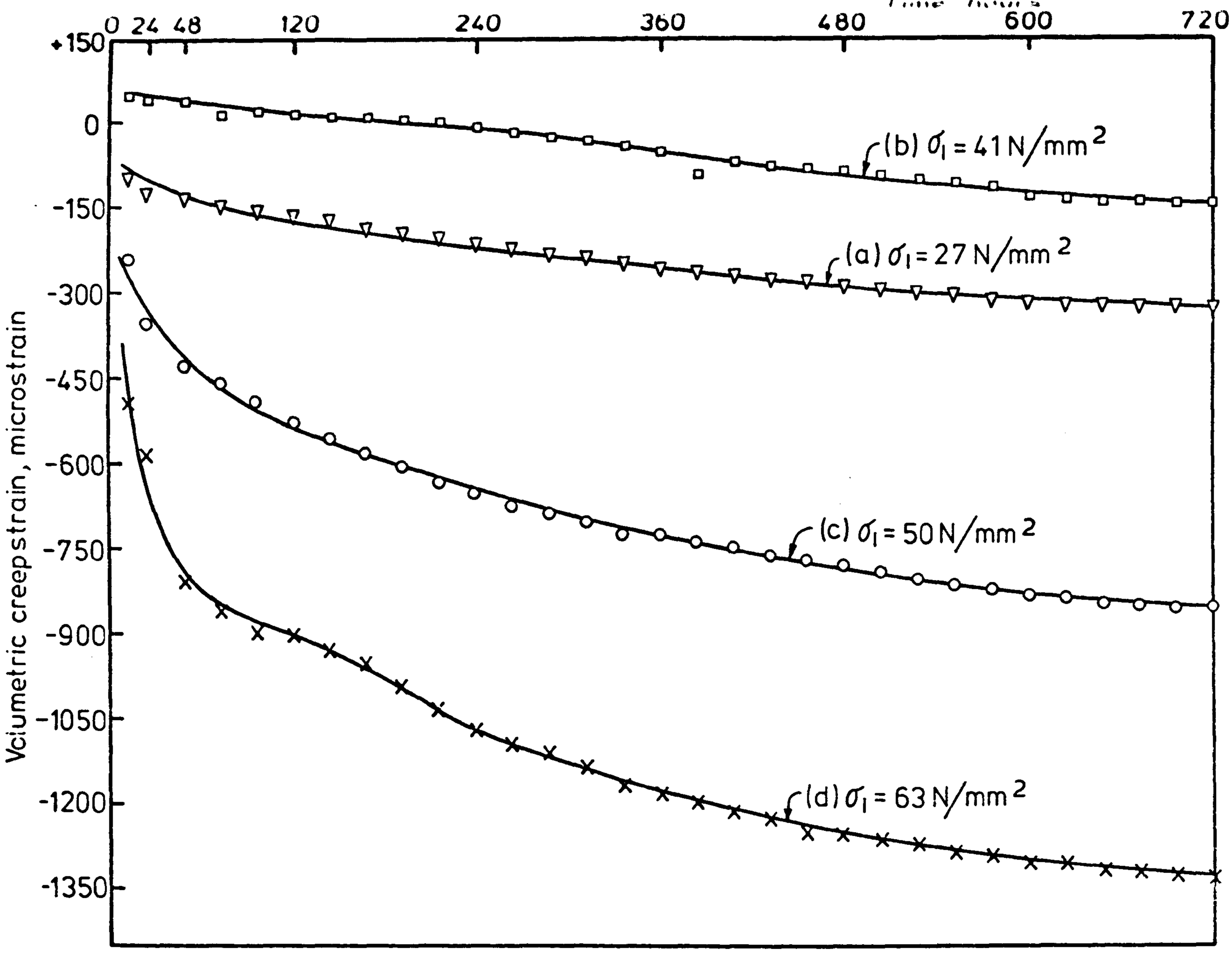

FIG. (7-50) VOLUMETRIC CREEP STRAIN OF SATURATED GYPSUM IN TRIAXIAL COMPRESSION AT $30\ N/mm^2$ CONFINING PRESSURE

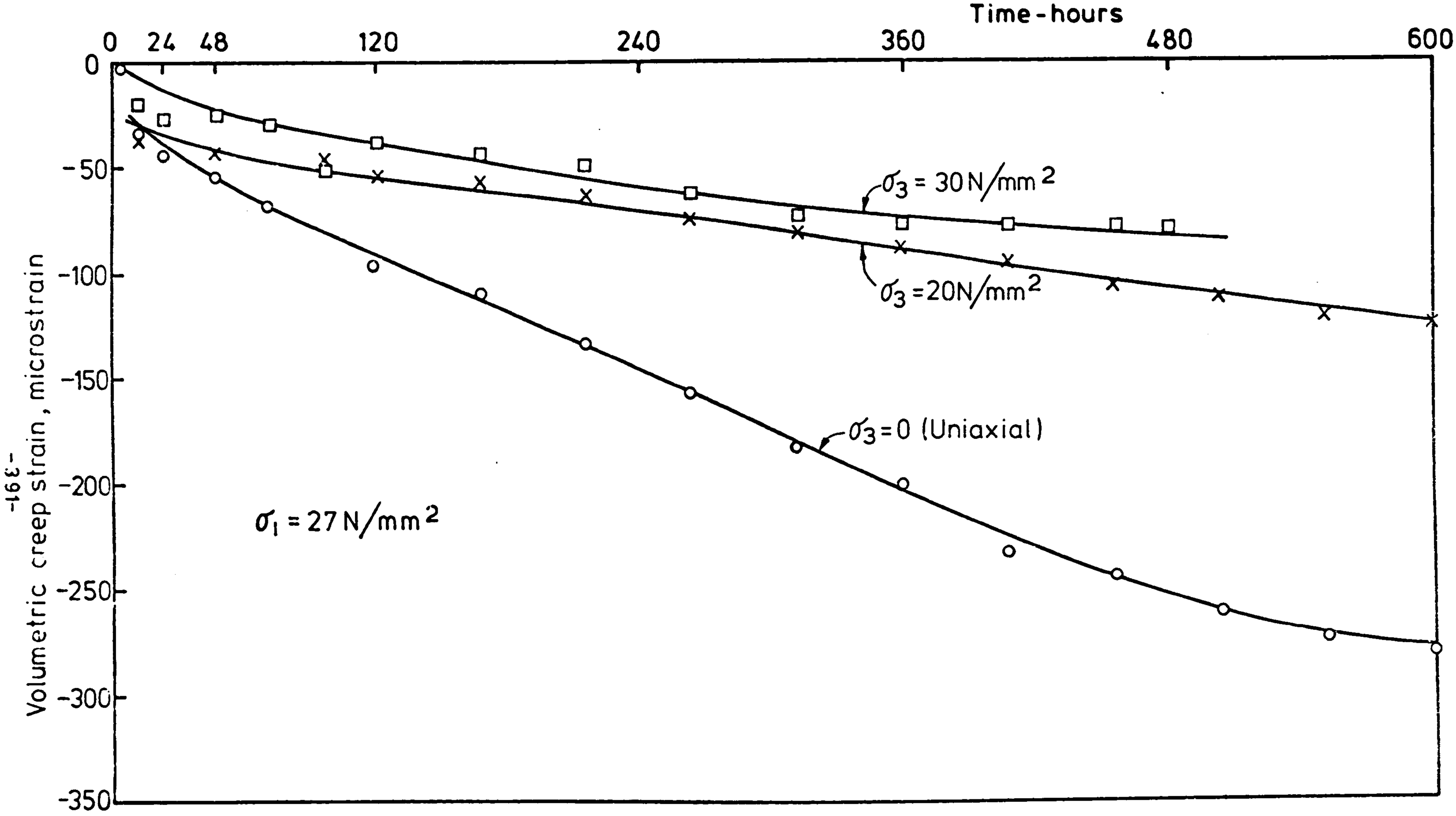

FIG.(7-51) EFFECT OF CONFINING PRESSURE ON THE VOLUMETRIC CREEP STRAIN IN DRY CONDITION AT CONSTANT $\sigma_1 = 27\ N/mm^2$

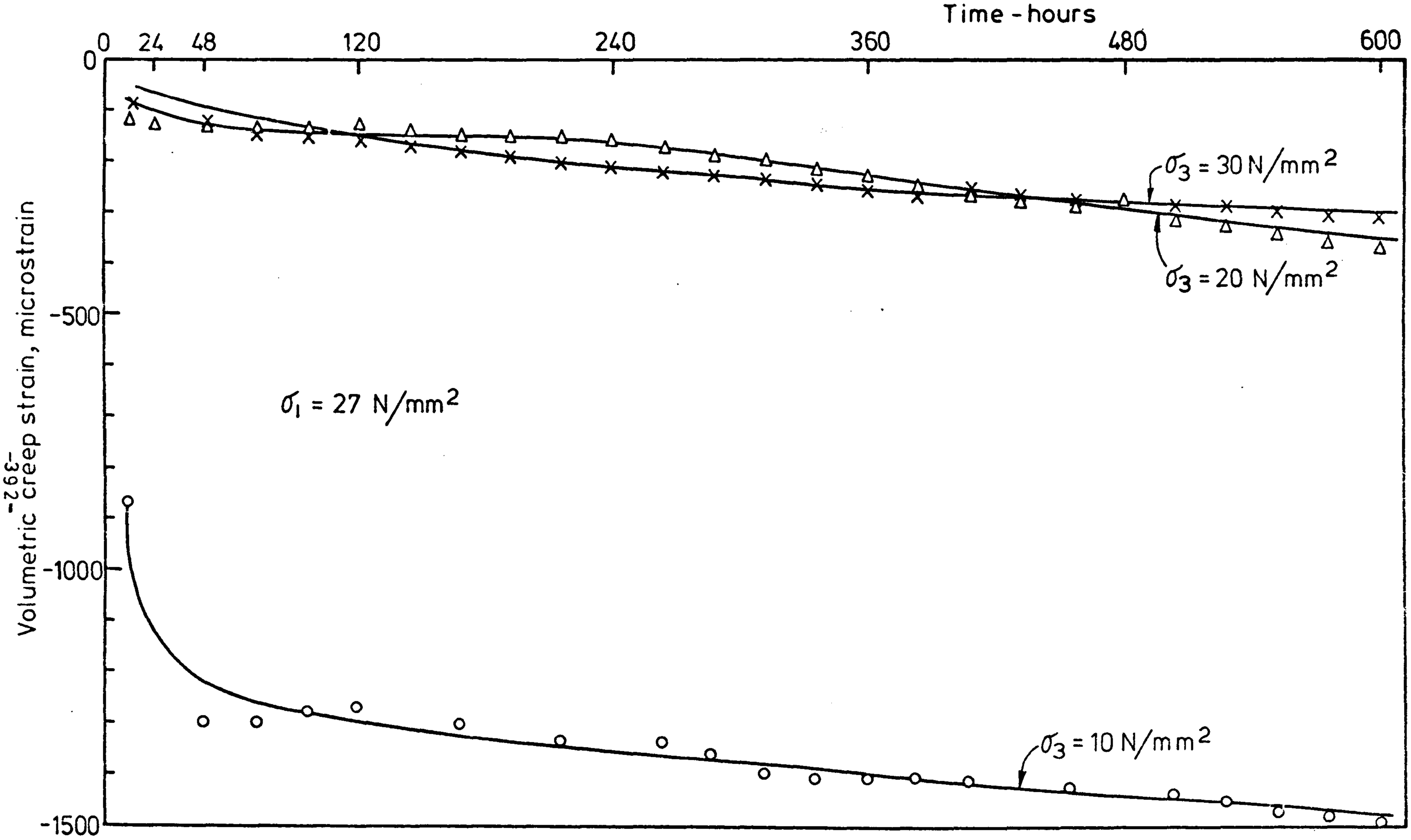

FIG.(7-52) EFFECT OF CONFINING PRESSURE ON THE VOLUMETRIC CREEP STRAIN IN SATURATED CONDITION AT CONSTANT σ_1 = 27 N/mm^2

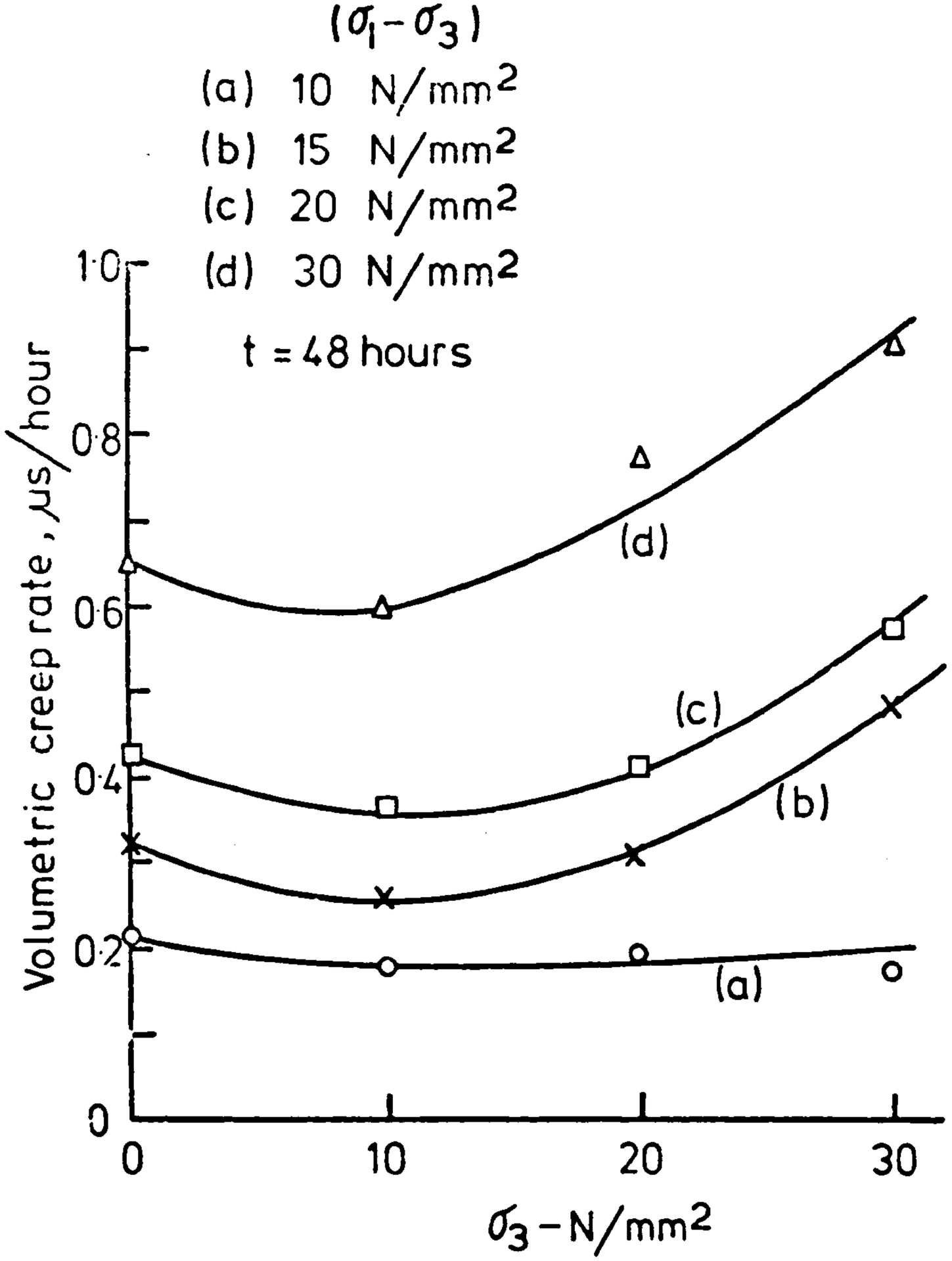

FIG.(7-53) EFFECT OF σ_3 ON THE VOLUMETRIC CREEP RATE AT CONSTANT $(\sigma_1-\sigma_3)$ IN DRY CONDITION

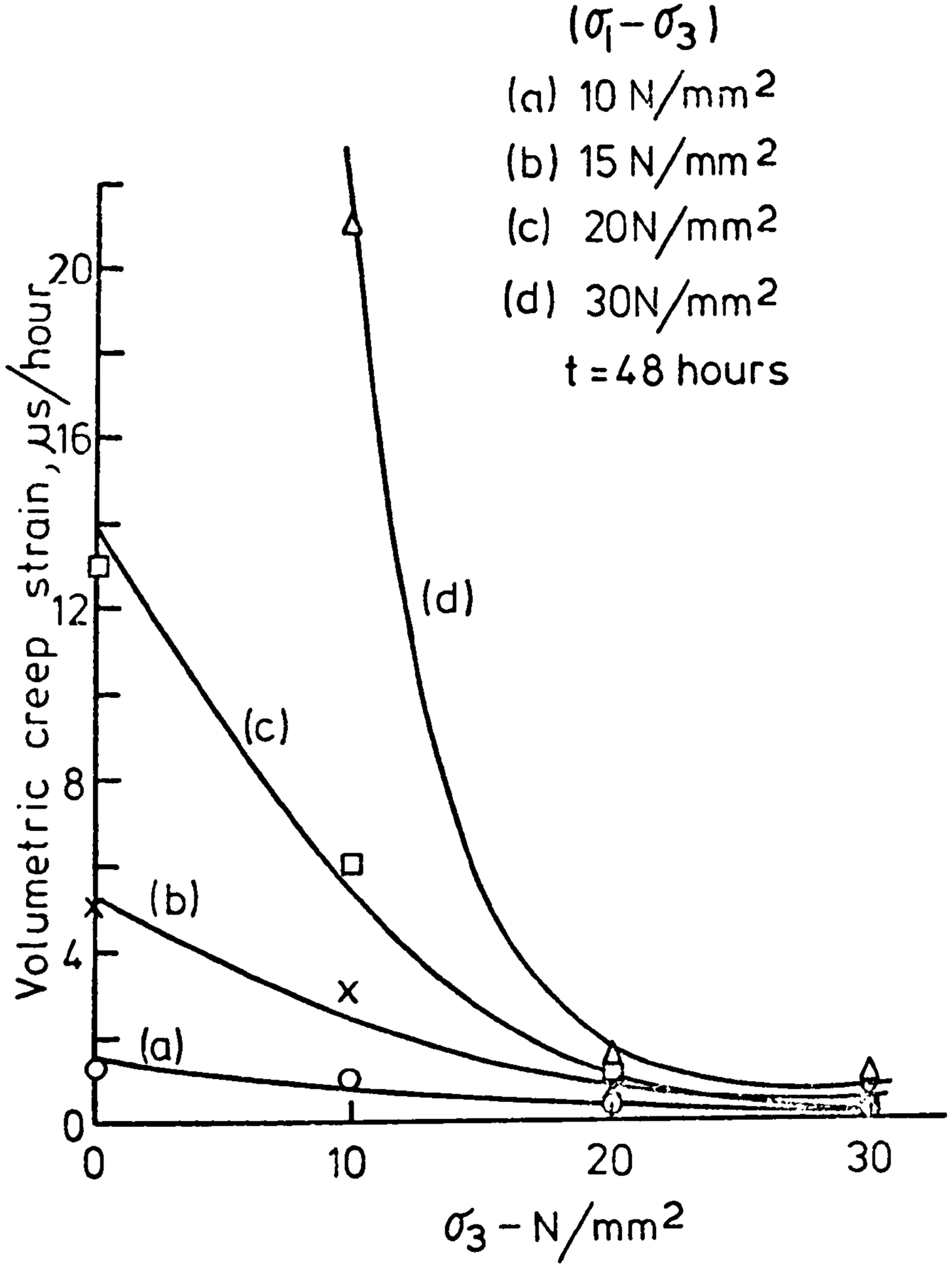

FIG.(7-54) EFFECT OF σ_3 ON THE VOLUMETRIC CREEP RATE AT CONSTANT $(\sigma_1-\sigma_3)$ IN SATURATED CONDITION

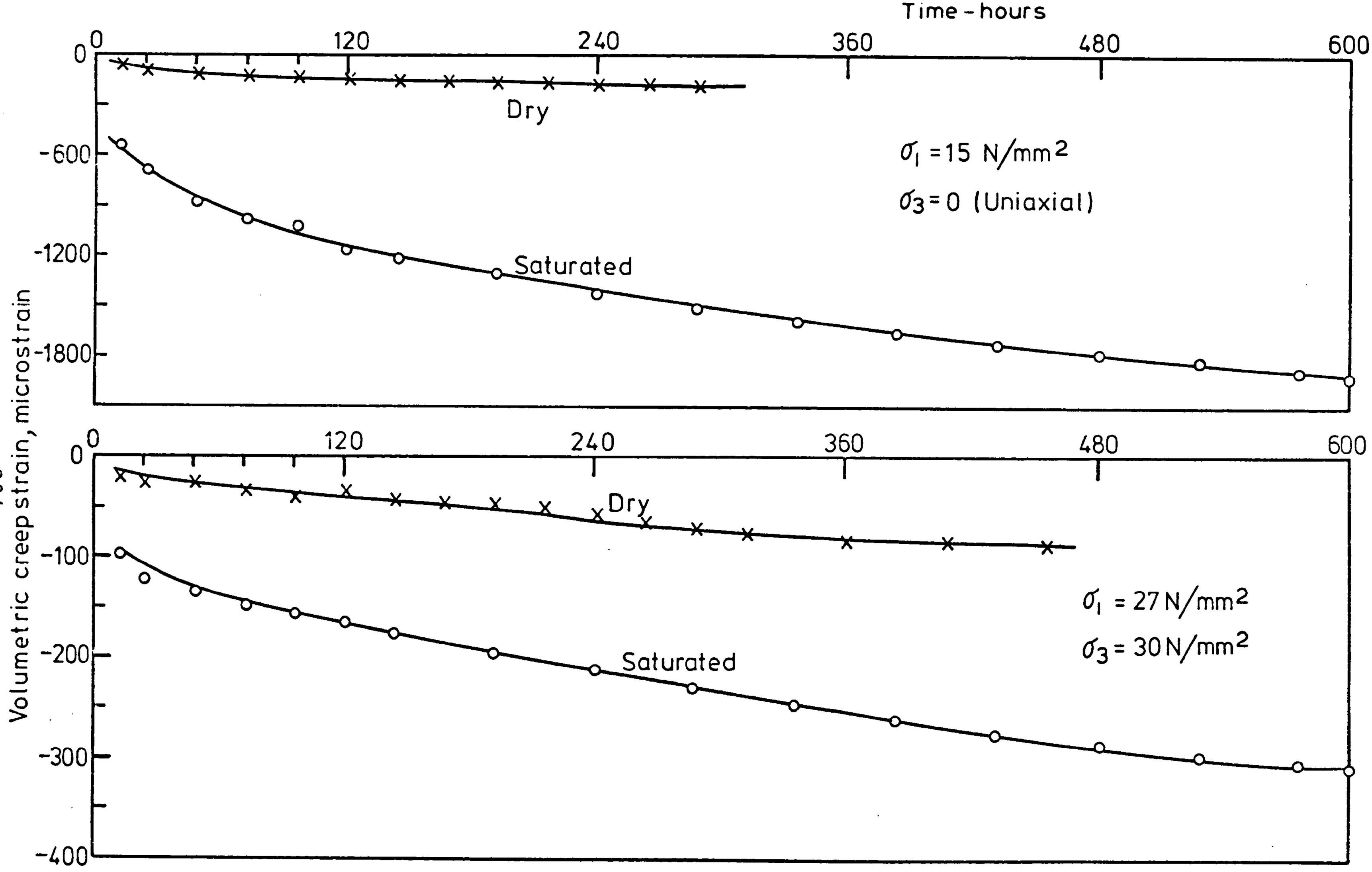

FIG. (7-55) EFFECT OF SATURATION ON VOLUMETRIC CREEP STRAIN AT VARIOUS STRESS CONDITIONS

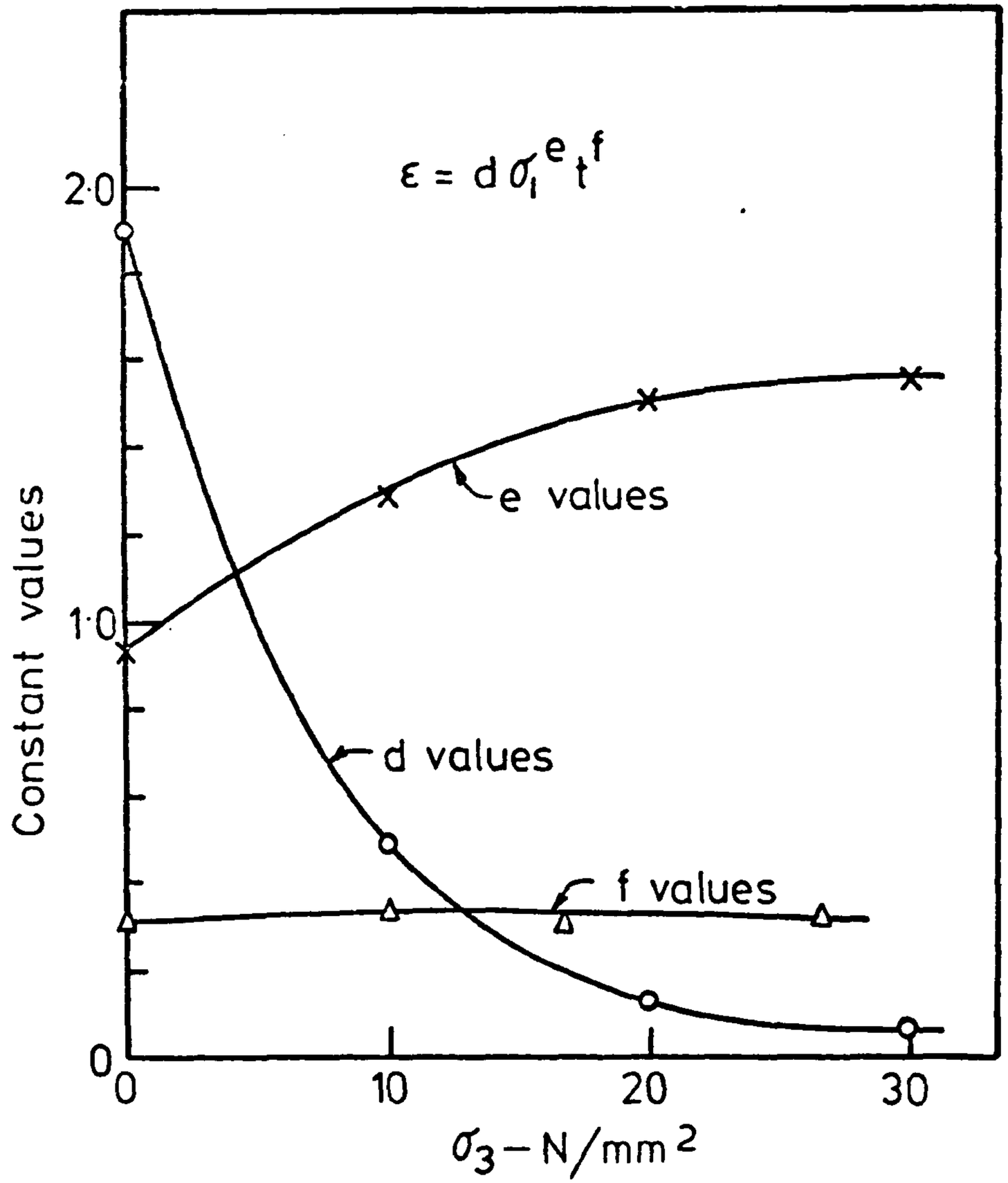

FIG.(7-56) VALUES OF d, e & f Vs. σ_3 IN LATERAL CREEP OF DRY CONDITIONS

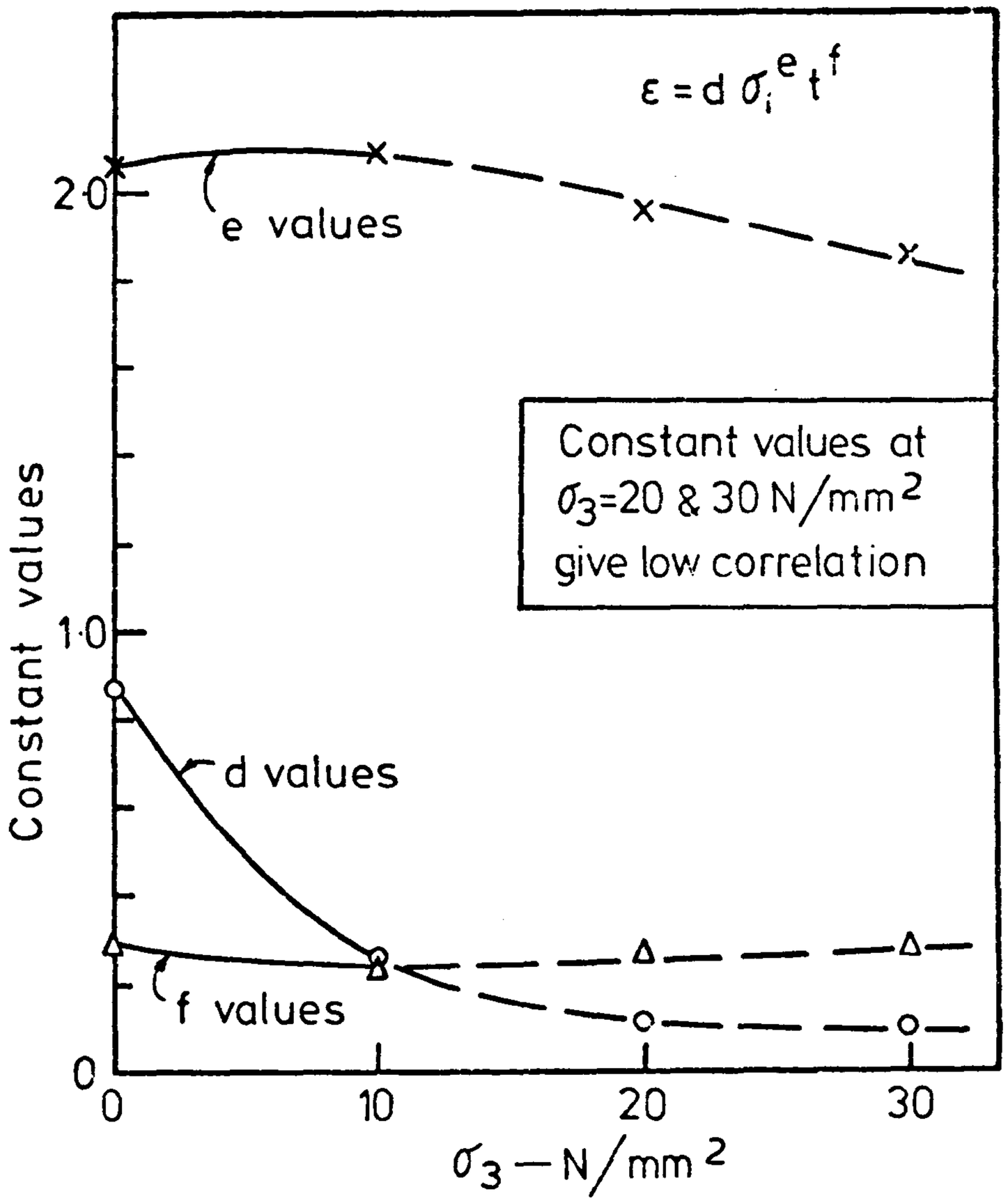

FIG.(7-57) VALUES OF d, e & f Vs. σ_3 IN LATERAL CREEP OF SATURATED CONDITIONS

Chapter 8.

CONCLUSIONS AND SUGGESTIONS FOR FUTURE WORK.

The main aim of this work was to investigate the three dimensional creep behaviour of gypsum in dry and saturated conditions under uniaxial and triaxial compression and bending modes of loading. A further aim was to determine the effects of the specimen size and water saturation on the bending, uniaxial tensile, uniaxial compressive, and triaxial compressive short term strengths.

Within the limits of the experiments performed, the under-mentioned conclusions are drawn on the basis of the results presented and discussion made thereupon in the previous chapters.

8.1 Short Term Tests.

(1) Bending, uniaxial tensile, uniaxial compressive, and triaxial compressive strengths were found to decrease with increasing specimen size in dry and saturated conditions.

(2) Uniaxial tensile and compressive strength values fitted the Weibull theory in both environmental conditions.

(3) Water saturation decreased the rock strength in bending, uniaxial tensile, uniaxial and triaxial compression tests.

(4) The saturation increases the strain in bending, axial and lateral directions when compared with the equivalent situation with dry sample.

(5) It was found that the tensile strength from bending is greater than the uniaxial tensile strength measured by direct pull in both dry and saturated conditions.

(6) Water saturation decreases the Modulus of Elasticity and increased the Poisson's ratio of the gypsum.

(7) The axial stress (as percentage of maximum stress) required to develop the onset of the unstable fracture is decreased by saturation and increases with increasing confining pressure.

(8) The strength and ductility increase in a non-linear relationship with increasing confining pressure.

(9) The confining pressure decreases the values of the Poisson's ratio in both dry and saturated gypsum.

(10) As the confining pressure increases the volumetric strain decreases in both environmental conditions (decrease in volume) at all stress levels.

8.2 Long Term Tests.

(1) In bending creep strain, instantaneous strain and creep rate increase with increasing the applied stress.

(2) Water saturation increases the bending creep strain, instantaneous strain and creep rate at a given applied stress.

(3) The creep in bending was found to follow the logarithmic equation $\varepsilon = A + B \log t$ at low stresses and power law equation $\varepsilon = C\ t^n$ at high applied stresses in dry conditions. Whereas in saturated conditions the creep follows the power law equation at all applied stresses.

(4) An empirical equation was predicted for the creep in bending for both dry and saturated conditions. The equation is in the form:

$\varepsilon = D\ 10^{E\sigma_t}\ t^F$, where D, E and F are constants. The values of these constants are increased with water saturation.

(5) Axial and lateral creep take place at all stress levels and are affected by confining pressure and saturation.

(6) Axial creep in dry condition followed the power law equation, $\varepsilon = C\ t^n$, except at low stresses and in the early stage of the tests of medium stresses where it followed the logarithmic equation, $\varepsilon = A + B \log t$. In saturated conditions the creep followed the power law at all times except for a short duration of the beginning of the low stress tests where the logarithmic law applied. This applies at all confining pressures.

(7) Lateral creep in dry and saturated conditions followed the power law $\varepsilon = C\ t^n$, except at the earlier stage of the low or low and medium stresses where the logarithmic law, $\varepsilon = A + B \log t$ was followed.

(8) The instantaneous axial and lateral strains increased with increasing axial stress in both environmental conditions. The Moduli of Elasticity and Poisson's ratio were evaluated making use of the instantaneous strains.

(9) Axial and lateral creep strains increased with increasing axial stress in both dry and saturated conditions at constant confining pressure.

(10) The power equation constants C and n in axial and lateral creep behaviour increase with increasing axial stress at constant confining pressure. On the contrary they decrease as the confining pressure increases at constant axial stress in both environmental conditions.

(11) The water saturation increases the creep strain in axial and lateral direction and also the volumetric creep strain.

(12) Saturation increases the creep equation constants A, B, C and n (items 6 and 7).

(13) The creep strain in both axial and lateral directions decreases with increasing confining pressure at constant axial stress in both dry and saturated conditions. This effect was found to be greater on the lateral creep strain than the axial.

(14) In uniaxial loading the lateral creep strain is greater than the axial in both environmental conditions, whereas in triaxial loading the lateral creep strain becomes less than the axial and this effect increases with increasing confining pressure.

(15) By analysing the axial and lateral creep results obtained an empirical equation of a power law function was presented for the determination of the creep strain at each confining pressure level and in dry and saturated conditions. This equation gives an acceptable accuracy in each case and

it is in the form: $\varepsilon = a\,\sigma_1^{\,b}\,t^{c}$, where a, b and c are constants, depending on the environmental and test conditions.

(16) The axial stress and confining pressure have a great effect on the creep rate. It was found for the two environmental conditions, that the creep rate in both axial and lateral directions increased with increasing axial stress at constant confining pressure, and, decreased with increasing confining pressure at constant axial stress.

(17) The effect of decreasing the creep rate with increasing confining pressure was found to be greater on the lateral direction than the axial.

(18) The lateral creep rate is greater than the axial under uniaxial loading, whereas under triaxial loading the lateral creep rate is less than axial in dry and saturated conditions.

(19) The relationship between creep rate and axial stress, in both environmental conditions for axial and lateral direction, was found to follow the power equation $\dot{\varepsilon} = R\,\sigma_1^{\,K}$ where $K > 1$. R and K are constants which depend on the environmental and test conditions. K was found to be a constant at any time in the creep period at a given confining pressure.

(20) The axial, lateral and then volumetric creep rates were found to increase by appreciable amounts when the samples were saturated with water under any particular stress condition.

(21) In both dry and saturated conditions the creep rate in axial and lateral directions increases with increasing differential stresses $(\sigma_1 - \sigma_3)$.

(22) In dry conditions the axial creep rate increases with increasing confining pressure at constant $(\sigma_1 - \sigma_3)$, while in saturated condition increases up to $(\sigma_1 - \sigma_3) = 15\ N/mm^2$ then starts to decrease with increasing σ_3 for $(\sigma_1 - \sigma_3) > 15\ N/mm^2$.

(23) Lateral creep strain decreases with increasing σ_3 at constant $(\sigma_1 - \sigma_3)$ while axial strain increases.

(24) The lateral creep rate in dry and saturated conditions decreases with increasing σ_1 or σ_3 at constant $(\sigma_1 - \sigma_3)$. The effect of σ_3 was found to be greater in the case of saturated conditions than in dry.

(25) It is suggested that the creep behaviour of the water saturated gypsum is influenced by solution, ionic mobility and recrystallization.

(26) The volumetric creep strain was found to increase with time, and in most of the cases, initially decreased (decrease in volume), sharply then increased after a short time (increase in volume) and followed the trend of the lateral creep curve.

(27) In both dry and saturated condition, it was found that the volumetric creep strain increases with increasing σ_1 at constant σ_3 and decreases with increasing σ_3 at constant σ_1.

(28) In both environmental conditions, the volumetric creep rate increases with increasing σ_1 under uniaxial loading, and at higher values of σ_1 in triaxial loading at constant σ_3.

(29) Volumetric creep rate decreases with increasing σ_3 at constant σ_1.

(30) At constant $(\sigma_1 - \sigma_3)$ the volumetric creep rate in dry condition was found to decrease with increasing σ_3 up to a certain value of σ_3, then starts to increase for higher values of σ_3, whereas in saturated conditions the volumetric creep rate decreased with increasing σ_3 throughout.

8.3 Suggestions for Future Work.

The author endeavoured within the limited time and opportunity available to make an assessment of the following: (a) Effect of beam size on the bending creep behaviour of the rock in different environmental conditions and under significantly reasonable applied stress levels.

(b) The influence of higher confining pressure in dry and saturated gypsum to throw more light on its behaviour under these conditions.

Admittedly, it has not been possible to include several specimen beam sizes under several stress levels, and, to carry on tests at higher confining pressure levels in dry and saturated conditions within the field of experimental investigation. These could be taken as future projects for research.

The author suggests that it would be of interest to carry on similar creep tests on other evaporite rocks such as, anhydrite, rock salt, potash, etc., to obtain a wider knowledge of the behaviour of evaporite rock before making any generalization.

It is suggested that it would be of advantage to construct more powerful apparatus for applying both confining and axial stresses, and to design a lateral strain measuring device to measure lateral creep strains within the pressure cell itself in order to compare the results with the data obtained in this study using strain gauges in the pressure cell mounted on the specimen. This will enable an extension of triaxial creep studies into the testing of rock at higher stresses or into harder rock materials outside the range of evaporite rocks. A further extension of the work on triaxial creep should also include the operation of apparatus enabling the testing of larger rock specimens. This will allow size effects in triaxial conditions to be tested, and also tests on specimens of rock having large crystals in their structure.

A large number of testing cell units with data logging facilities would allow a more rapid collection of creep data.

REFERENCES

1. Phillips, D.W., 1948. "Tectonics of Mining" Colliery Eng., Vol.25, pp.199-202; 278-282.

2. Pomeroy, C.D. and Morgans, W.T.A., 1956. "The Tensile Strength of Coal" Brit. J.App. Phys., Vol.7, pp.243-246.

3. Berenbaum, R. and Brodie, I., 1959. "Measurements of Tensile Strength of Brittle Materials" Brit.J.App.Phys., Vol.10, pp.281-287.

4. Evans, I., 1961. "The Tensile Strength of Coal" Colliery Eng., Vol.38, pp.428-434.

5. Hobbs, D.W., 1964. "The Tensile Strength of Rocks" Int. J. Rock Mech. Min. Sci., Vol.1, pp.385-396.

6. Hobbs, D.W., 1965. "An Assessment of a Technique for Determining the Tensile Strength of Rock" Brit.J.App. Phys., Vol.16, pp.259-268.

7. Jaeger, J.C. and Hoskins, E.R., 1966. "Stress and Failure in Rings of Rocks Loaded in Diametral Tension or Compression" Brit. J.App.Phys., Vol.17, pp.685-692.

8. Lundborg, N., 1967. "The Strength-Size Relation of Granite" Int. J. Rock Mech. Min. Sci., Vol.4, pp.269-272.

9. Hobbs, D.W., 1967. "Rock Tensile Strength and its Relation to a Number of Alternative Measures of Rock Strength" Int.J. Rock Mech. Min. Sci., Vol.4, pp.115-127.

10. Hardy, H.R. and Jayaraman, N.I., 1970. "An Investigation of methods for Determination of the Tensile Strength of Rock." Proc. 2nd Cong. Int. Soc. Rock Mech., Beograd, Vol.3, Paper 5-12, pp.85-92.

11. Hawkes, I. and Mellor, M., 1970. "Uniaxial Testing in Rock Mechanics Laboratory." Eng. Geol., Vol.4, No. 3, pp. 177-285.

12. Datta, R.N., 1969. "Stress-Strain Characteristics in Bending and Determination of the Tensile Strength of Rocks." Ph.D. Thesis, Univ. of Sheffield.

13. Hardy, M.P., Hudson, J.A. and Fairhurst, C., 1973. "The Failure of Rock Beams - Part I Theoretical Studies." Int. J. Rock Mech. Min. Sci., Vol.10, pp.53-67.

14. Hudson, J., Hardy, M.P. and Fairhurst, C. 1973. "The Failure of the Rock Beams - Part II Experimental Studies." Int. J. Rock Mech. Min. Sci., Vol.10, pp.69-82.

15. Elizzi, M.A., 1976. "The Time-Dependent Behaviour of Some Evaporite Rocks." Ph.D. Thesis, Univ. of Sheffield.

16. Williams, F.T. and Elizzi, M.A., 1976. "Bending Creep Tests in Gypsum." J.Iraq Engs. Soc., No. 1, Ser. 58, pp.3-14.

17. Adams, F.D. and Nicholson, J.T., 1901. "An Experimental Investigation into the Flow of Marble." Philosp. Trans. of the Royal Soc. of London, Vol.195, pp.363-401.

18. Schwartz, A.E., 1964. "Failure of Rock in the Triaxial Shear Test." Proc. 6th Symp. Rock Mech. Univ. of Missouriat Rolla, pp.109-151.

19. Von Karman, T., 1911. "Festigkeitsuersuche Unter Allseitigem Druck." Zeits. Ver. Deutsch. Ingenieure, Vol.55, pp.1749-1757. Cited by A.E. Schwartz(18).

20. Griggs, D.T., 1936. "Deformation of Rocks Under High Confining Pressures." J. Geol., Vol.44, pp.541-577.

21. Robertson, E.C., 1955. "Experimental Study of the Strength of Rocks." Geol. Soc. Amer. Bull., Vol.88, pp.1275-1314.

22. Handin, J.W. and Hager, R.V., 1957. "Experimental Deformation of Sedimentary Rocks Under Confining Pressure: Tests at Room Temperature on Dry Samples." Am. Ass. Petr. Geol. Bull., Vol.41, No. 1A, pp.1-50.

23. Price, N.J., 1958. "A study of Rock Properties in Condition of Triaxial Stresses." Proc. Conf. on Mechanical Properties of Non-Metallic Brittle Materials, Butterworth Publications, London, pp.106-122.

24. Murrell, S.A.F., 1958. "The Strength of Coal Under Triaxial Compression." Proc. Conf. on Mechanical Properties of Non-Metallic Brittle Materials, Butterworth Scientific Publications, London, pp.123-142.

25. Hobbs, D.W., 1964. "The Strength and Stress-Strain Characteristics of Coal in Triaxial Compression." J. Geol., Vol. 72, pp.214-231.

26. Shih, T.M., 1963. "Investigation of the Physical Properties of Gaspe Skarn." Proc. Rock Mech. Symp., Queen's Univ., Pub. Dept. Min. Tech. Surveys, Ottawa.

27. Hofer, K.H. and Thoma , K., 1968. "Triaxial Tests on Salt Rocks." Int. J. Rock Mech. Min. Sci., Vol.5, pp.195-203.

28. Bieniawski, Z.T., Denkhaus, H.G. and Vogler, V.W., 1969. "Failure of Fractured Rock." Int. J. Rock Mech. Min. Sci., Vol.6, pp.323-341.

29. Bodonyi, J., 1970. "Laboratory Test of Certain Rocks Under Axially Symmetrical Loading Conditions." Proc. 2nd Cong. Int. Soc. Rock Mech., Vol.1, Paper 2-17, Geograd.

30. Wawersik, W.R. and Fairhurst, C., 1970. "A study of Brittle Rock Fracture in Laboratory Compression Experiments." Int. J. Rock Mech. Min. Sci., Vol.7, pp.561-575.

31. Peng, S.D., 1971. "Stresses Within Elastic Circular Cylinders Loaded Uniaxially and Triaxially." Int. J. Rock Mech. Min. Sci., Vol.8, pp.399-432.

32. Brady, B.T., 1971. "The Effect of Confining Pressure on the Elastic Stress Distribution in a Radially End-Constrained Circular Cylinder." Int. J. Rock Mech. Min. Sci., Vol.8, pp.153-164.

33. Dhir, R.K. and Sangh, C.M., 1974. "Strength and Deformation Properties of Rock like Materials tested in Triaxial Compression." First Aust. Conf. Eng. Mater., Univ. New South Wales.

34. Sangha, C.M. and Dhir, R.K., 1975. "Strength and Deformation of Rock Subjected to Multiaxial Compressive Stresses." Int. J. Rock Mech. Min. Sci., Vol.12, pp.277-282.

35. Janach, W., 1977. "Failure of Granite Under Compression."Int. J. Rock Mech. Min. Sci., Vol.14, pp.209-215.

36. Gaddy, F.L., 1956 "A study of Ultimate Strength of Coal as Related to the Absolute Size of the Cubical Specimens Tested." Bull. Virginia Polytechnic Inst., Vol.49, No. 10, pp.1-27.

37. Evans, I. and Pomeroy, C.D., 1958. "The Strength of Cubes of Coal in Uniaxial Compression." Proc. Conf. on Mechanical Properties of Non-Metallic and Brittle Materials, Butterworth, London, pp.5-28.

38. Evans, I., Pomeroy, C.D. and Berenbaum, R., 1961. "The Compressive Strength of Coal." Colliery Eng., Vol.38, pp.75-80, 123-127 and 172-178.

39. Skinner, W.J., 1959. "Experiments on the Compressive Strength of Anhydrate." The Engineer, Vol.207, pp.255-259 and 288-292.

40. Mogi, K., 1962. "The Influence of the Dimensions of Specimen on the Fracture Strength of Rocks." Bull. Earthquake Res. Inst. Tokyo Univ., Vol.40, pp.175-185.

41. Jaeger, J.C., 1967. "Brittle Failure of Rocks." Proc. 8th Sym. Rock Mech. (Failure and Breakage of Rocks), Univ. Minnesota, pp.25-28.

42. Bieniawski, Z.T., 1968. "The Effect of Specimen Size on Compressive Strength of Coal." Int. J. Rock Mech. Min. Sci., Vol.5, pp.325-335.

43. Pratt, H.R., Black, A.D., Brown, W.S. and Brace, W.F., 1972. "The Effect of Specimen Size on the Mechanical Properties of Unjointed Diorite." Int. J. Rock Mech. Min. Sci., Vol.9, pp.513-529.

44. Mead, W.J., 1925. "The Geologic Role of Dilatancy." J. Geol., Vol.33, pp.685-698.

45. Bridgman, P.W., 1949. "Volume Changes in the plastic Stages of Simple Compression." J. Appl. Phys., Vol.20, pp.1241-1251.

46. Pellegrino, A., 1970. "Mechanical Behaviour of Soft Rocks Under High Stresses.' Proc. 2nd Cong. Int. Soc. Rock Mech., Vol.2, Paper 3-251, Beograd.

47. Cook, N.G.W., 1970. "An Experiment Proving that Dilatancy is a Pervasive Volumetric Property of Brittle Rock Loaded to Failure." Rock Mech., Vol.2, pp.181-188.

48. Crouch, S.L., 1970. "Experimental Determination of Volumetric Strains in Failed Rock." Int. J. Rock Mech. Min. Sci., Vol.7, pp.589-603.

49. Crouch, S.L., 1972. "The Post Failure Behaviour of Norite in Triaxial Compression." Eng. Geol., Vol.6, pp.19-30.

50. Price, A.M. and Farmer, I.W., 1979. "Application of Yield Modulus to Rock." Int. J. Rock Mech. Min. Sci., Vol.16, pp.157-159.

51. Rehbinder, P. and Lightman, V., 1957. "Effect of Surface Active Media on Strains and Rupture in Solids." Proc. 2nd Int. Cong. Surface Activity, Vol.3, pp.563-580.

52. Price, N.J., 1960. "The Compressive Strength of Coal Measure Rocks." Colliery Eng., Vol.37, pp.283-292.

53. Mann, R.L. and Fatt, A., 1960. "Effects of Pore Fluids on the Elastic Properties of Sandstone." Geophysics, Vol.25, No. 2, pp.433-444.

54. Boozer, G.D., Hiller, K.H. and Serdengeceti, S., 1962. "Effects of Pore Fluids on the Deformation Behaviour of Rocks Subjected to Triaxial Compression." Proc. 5th Sym. Rock Mech., Univ. Minnesota, pp.579-625.

55. Cloback, P.S.B. and Wiid, B.L., 1965. "The Influence of Moisture Content on the Compressive Strength of Rocks." Proc. 3rd Canad. Rock Mech. Symp. Toronto, pp.65-83.

56. Wiid, B.L., 1970. "Influence of Moisture on Pre-Rupture Fracturing of Two Rock Types." Proc. 2nd Cong. Int. Soc. Rock Mech., Vol.2, Paper 3-35, Beograd, pp.239-245.

57. Mogilevskaya, S.E., 1970. "Effect of Composition, Fractures of Structure Fabric and Water Saturation on Rock Deformability." Proc. 2nd Cong. Int. Soc. Rock Mech., Vol.1, Paper 2-10, Beograd, pp.333-339.

58. Rutter, E.H., 1972. "The Effect of Strain-Rate Changes on the Strength and Ductility of Solenhofen Limestone at Low Temperature and Confining Pressure" Int. J. Rock Mech. Min. Sci., Vol.9, pp.183-189.

59. Broch, E. and Franklin, J.A., 1972. "The Point Load Strength Test." Int. J. Rock Mech. Min. Sci., Vol.9, pp.669-697.

60. Farmer, I.W. and Attewell, P.B., 1973. "The Effect of Particle Strength on the Compression of Crushed Aggregate." Rock Mech., Vol.5, pp.237-248.

61. Parate, N.S., 1973. "Influence of Water on the Strength of Limestone." Trans. Soc. Min. Eng. AIME, Vol.254, No. 2, pp.237-248.

62. Broch, E., 1974. "The Influence of Water on Some Rock Properties." Proc. 3rd Cong. Intr. Soc. Rock Mech., Denver, pp.33-38.

63. Vutukuri, V.S., 1974. "The Effect of Liquids on the Tensile Strength of Limestone." Int. J. Rock Mech. Min. Sci., Vol. 11, pp.27-29.

64. Van Eeckhout, E.M., 1976. "The Mechanisms of Strength Reduction Due to Moisture in Coal Mine Shales." Int. J. Rock Mech. Min. Sci., Vol.13, pp.61-67.

65. Ballivy, G., Ladanyi, B. and Gill, D.E., 1976. "Effect of Water Saturation History on the Strength of Low-Porosity Rocks." ASTM Specif. Tech. Pub. No. STP 599, pp.4-20.

66. Michelson, A.A., 1917. "The Law of Elastico-Viscous Flow." J.Geol., Vol. 25, pp.405-410.

1920. "The Law of Elastico-Viscous Flow" J. Geol., Vol. 28, pp.166-168.

67. Phillips, D.W., 1932. "Physical Properties of Coal Measure Rock, and Experimental Work on the Development of Fracture." Trans. Inst. Mining Eng.,Vol.82, pp.432-450.

68. Evan, R.H., 1936. "The Elasticity and Plasticity of Natural Stones." Proc. Leeds phil. lit. Soc.,Vol.3, No. 3, pp.145-158.

69. Evan, R.H. and Wood, R.H., 1937. "Transverse Elasticity of Natural Stones." Proc. Leeds phil. lit. Soc., Vol.3, No. 5, pp.340-352.

70. Griggs, D.T., 1939. "Creep of Rocks." J. Geol., Vol.74, pp.225-251.

71. Griggs, D.T., 1940. "Experimental Flow of Rocks Under Conditions Favouring Recrystallization." Geol. Soc. Am. Bull., Vol.51, pp.1001-1022.

72. Pomeroy, C.D., 1956. "Creep in Coal at Room Temperature". Nature, Vol.178, pp.278-280.

73. Lomnitz, C., 1956. "Creep Measurements in Igneous Rocks." J. Geol., Vol.64, pp.473-504.

74. Terry, N.B. and Morgans, B.A., 1958. "Studies of the Rheological Behaviour of Coal". Proc. Conf. on Mechanical Properties of Non-Metallic Brittle Materials, Butterworth Publications, London, pp.239-256.

75. Kendall, H.A., 1958. "An Investigation of Creep Phenomenon Exhibited by Solenhofen Limestone, Halite and Cement Under Confining Pressure." M.Sc. Thesis, Agr. and Mech. College of Texas.

76. Matsushima, S., 1960. "On the Flow and Fracture of Igneous Rocks." Kyoto Univ. Disaster Prevent. Res. Inst. Bull., Vol.10, No. 36, pp.2-9 cited by: Lama, R.C. and Vutukuri, V.S.(77).

77. Lama, R.D. and Vutukuri, V.S., 1978. "Handbook on Mechanical Properties of Rocks." Vol.3, Trans. Tech. Publications, Germany.

78. Robertson, E.C., 1960. "Creep of Solenhofen Limestone Under Moderate Hydrostatic Pressure?" Mem. Geol. Soc. Amer., Vol.79, pp.227-244.

79. Misra, A.K., 1962. "An Investigation of Time-Dependent Deformation or - Creep - in Rocks." Ph.D. Thesis, Univ. of Sheffield.

80. Price, N.J., 1964. "A study of Time Strain Behaviour of Coal Measure Rocks." Int. J. Rock Mech. Min. Sci., Vol.1, pp.277-303.

81. MaClain, W.C., 1964. "Time-Dependent Behaviour of Pillars in Alsace Potash Mine." Proc. 6th Sym. Rock Mech., Univ. Missouri,Rolla, pp.489-500.

82. Bradshaw, R.L., Boegly, W.J. and Empson, F.M., 1964. "Correlation of Convergence Measurements in Salt Mines with Laboratory Creep Test Data." Proc. 6th Sym. Rock Mech., Univ. Missouri, Rolla, pp.501-513.

83. Comte, P.L., 1965. "Creep in Rock Salt." J. Geol., Vol.73, pp.469-485.

84. Hendron, A.J., 1968. "Mechanical Properties of Rocks." in Rock Mech. in Engineering Practice (K.C. Stagg and O.C. Zienkiewicz, Eds.) Wiley, New York, pp.21-53.

85. Farmer, I.W., 1968. "Engineering Properties of Rocks." E. & F.N. Spon Ltd., London.

86. Myrvang, A., 1970. "Some Experience on the Determination of Creep Properties of Rocks." Proc. 2nd Cong. Int. Soc. Rock Mech., Vol.1, Paper 2-41, Beograd, pp.577-579.

87. Hobbs, D.W., 1970. "Stress-Strain Time Behaviour of Number of Coal Measure Rocks." Int. J. Rock Mech. Min. Sci., Vol.7, pp.149-170.

88. Kanagawer, T. and Nakaari, K., 1970. "Restraint of Swelling Creep and Effect of Absorption of Water on Triaxial Strength and Deformability of Rocks." Rock Mech. in Japan, Vol.1, pp.74-76(77).

89. Cruden, D.M., 1971. "The Form of the Creep Law For rock Under Uniaxial Compression." Int. J. Rock Mech. Min. Sci., Vol.8, pp.105-126.

90. Hofer, K.H. and Knoll, P., 1971. "Investigation into the Mechanism of Creep Deformation in Carnallitite, and Practical Applications." Int. J. Rock Mech. Min. Sci., Vol. 8, pp.61-73.

91. Winkel, B.V., Gerstle, K.H. and Ko, H.W., 1972. "Analysis of Time-Dependent Deformation of Opening in Salt Media." Int. J. Rock Mech. Min. Sci., Vol.9, pp.249-260.

92. Peng, S.S., 1973. "Time-Dependent Aspects of Rock Behaviour as Measured by a Servocontrolled Hydraulic Testing Machine." Int. J. Rock Mech. Min. Sci., Vol.10, pp.235-246.

93. King, M.S., 1973. "Creep in Model Pillars of Saskatchewan Potash." Int. J. Rock Mech. Min. Sci., Vol.10, pp.263-271.

94. Matveyev, B.V., and Kartashov, J.M., 1974. "A study of Rock Creep Under Laboratory Conditions." Proc. 3rd Cong. Int. Soc. Rock Mech., Denver, pp.342-347.

95. Afronz, A. and Harvey, J.M., 1974. "Rheology of Rocks Within the Soft to Medium Strength Range." Int. J. Rock Mech. Min. Sci., Vol.11, pp.281-290.

96. Wawersik, W.R., 1974. "Time-Dependent Behaviour of Rock in Compression." Proc. 3rd Cong. Int. Soc. Rock Mech., Denver, pp.357-363.

97. Singh, D.P., 1975. "A study of Creep of Rocks." Int. J. Rock Mech. Min. Sci., Vol.12, pp.271-275.

98. Wu, F.T. and Thomson, L., 1975. "Microfracturing and Deformation of Westerly Granite Under Creep Conditions." Int. J. Rock Mech. Min. Sci., Vol.12, pp.167-173.

99. Cogan, J., 1976. "Triaxial Creep Tests of Opohonga Limestone and Ophir Shale." Int. J. Rock Mech. Min. Sci., Vol.13, pp.1-10.

100. Williams, F.T. and Elizzi, M.A., 1977. "Creep Properties of Sherburn gypsum Under Triaxial Loading." Proc. Conf. Rock Eng. British Geol. Soc., Univ. of Newcastle Upon Tyne, Vol. 1, pp.71-83.

101. Williams, F.T. and Elizzi, M.A., 1976. "An Apparatus for the Determination of Time-Dependent Behaviour of Rocks Under Triaxial Loading." Int. J. Rock Mech. Min. Sci., Vol.13, pp.245-248.

102. Varo, L. and Passaris, E.K.S., 1977. "The Role of Water in the Creep Properties of Halite." Proc. Conf. Rock Eng. British Geol.Soc., Univ. of Newcastle Upon Tyne, Vol. 1, pp.85-100.

103. Hebblewhite, B.K., Miller, H.D.S. and Potts, E.L.J., 1979. "A method for Predicting Time-Dependent Deformation in Evaporites Around a Vertical Shaft." Proc. Conf. Rock Eng. British Geol. Soc., Univ. of Newcastle Upon Tyne, Vol.1, pp.529-539.

104. Kranz, R.L., 1979. "Crack Growth and Development During Creep of Barre Granite." Int. J. Rock Mech. Min. Sci., Vol.16, pp.23-35.

105. Newman, K. and Lachance, L., 1964. "The Testing of Brittle Material Under Uniform Uniaxial Compressive Stresses." Proc. Amer. Soc. Test. Mat., 64, pp.1044-1067.

106. Obert, L. and Duvall, W.I., 1967. "Rock Mechanics and the Design of Structure in Rock." John Wiley and Sons, New York.

107. Dhir, R.K., 1966. "A study of the photoelastic Stressmeter." Ph.D. Thesis, Univ. of Sheffield.

108. Fairhurst, C., 1961. "Laboratory Measurement of Some Physical Properties of Rock." 4th Symp. Rock Mech., Penn. State Univ.

109. Bates,R.L., 1960. "Geology of Industrial Rocks and Materials." Hopper & Brothers, New York.

110. Posnjak, E., 1938. "The System $CaSO_4$-H_2O." Amer. J. of Science, Ser. 5, Vol.35A, pp.247-272.

111. Macdonald, G.J.F., 1953. "Anhydrite-Gypsum Equilibrium Relations." Amer. J. of Science, Vol.251, pp.884-898.

112. Palache, C., Berman, H. and Frondel, C., 1951. "The System of Mineralogy." 7th Ed., John Wiley and Sons, New York.

113. Jaeger, J.C. and Cook, N.G.W., 1976. "Fundamentals of Rock Mechanics." 2nd Ed., Chapman and Hall, London.

114. Duckworth, W.H., 1951. "Precise Tensile Properties of Ceramics body." J. Amer. Cer. Soc., Vol.34, No. 1, pp.1-9.

115. Obert, L., Winders, S.L. and Duval, W.I., 1946. "Standard Test for Determining the Physical Properties of Mine Rock." Bureau of Mines Rept. of Investigation, No. 3891, p.67.

116. Murrell, S.A.F., 1962. "The Effect of the Triaxial Stress System on Strength of Brittle Materials with Particular Reference to Rock." Ph.D. Thesis, Univ. of Sheffield.

117. Wijk, G., Rehbinder, G. and Lögdström, G., 1978. "The Relation Between the Uniaxial Tensile Strength and the Sample Size for Bohus Granites." Rock Mech., Vol.10, pp.201-209.

118. Jahn, H., 1966. "Messung der Gebirgsfestigkeit In situ Bei Wachsendem Mass-Stabsverhältnis." Proc. 1st Cong. Int. Soc. Rock Mech., Lisbone, (8).

119. Shyang Yu, Y., 1963. "Investigation of the Physical Properties of Sigma Mine Prophyry.P Proc. Rock Mech. Symp., Queen's Univ., Pub. Dept. Tech. Surveys, Ottawa, pp.80-88.

120. Vutukuri, V.S., Lama, R.D. and Salluja, S.S., 1974. "Handbook on Mechanical Properties of Rocks." Vol.1, Trans. Tech. Publication.

121. A.S.T.M. STP-402 "Testing Techniques for Rock Mechanics." pp.84 and p.79.

122. Bordia, S.K., 1972. "Complete Stress-Volumetric strain Equation for Brittle Rock up to Strength Failure." Int. J. Rock Mech. Min. Sci. Vol.9, pp.17-24.

123. Hoek, E. and Franklin, J.A., 1968. "A Simple Triaxial Cell for Field and Laboratory Testing of Rock." Trans. Inst. Mining and Metal., Vol.77, pp.A22-A26.

124. Chamberlain, P.G., Van Eeckhout, E.M., and Podnieks, E.R., 1976. "Four Factors Influencing Observed Rock Properties". A.S.T.M. Specif. Tech. Pub., No. STP-599, pp.21-36.

125. Goranson, R.W., 1940. "Flow in Stressed Solids: An Interpretation." Geol. Soc. Amer. Bull., Vol.51, pp.1023-1034.

126. Lama, R.D. and Vutukuri, V.S., 1978. "Handbook on Mechanical Properties of Rocks." Vol. 2, Trans. Tech. Publication, Germany.

127. Sangha, C.M. and Dhir, R.K., 1972. "Influence of Time on the Strength, Deformation and Fracture Properties of a Lower Devonian Sandstone." Int. J. Rock Mech. Min. Sci., Vol.9, pp.343-354.

128. Barron, K. and Toews, N.A., 1963. "Deformation around a mine Shaft in Salt." Proc. Rock Mech. Symp., Queen's Univ., Pub. Dept. Tech. Survey, Ottawa, pp.115-134.

129. Scholz, O., 1970 "The Role of Microfracturing in Rock Deformation." Proc. 2nd Cong. Int. Soc. Rock Mech., Vol.1, Paper 2-8, Beograd, pp.323-327.

130. Rong, C., Xlao-Xin, Y. and Hung-Sen, X., 1979. "Studies of the Fracture of Gabbro.", Int. J. Rock Mech. Min. Sci., Vol.16, pp.187-193.

131. Hansen, F.D., 1977. "Evaluation of an inelastic law for salt creep." Proc. 18th Symp. of A.S.C.E. Rock Mech., Keyston, Colorado, PP4B5-1:4B5-5.

APPENDIX A.

Petrological and Mineralogical Description of Gypsum.

Gypsum is one of the rocks within the evaporite class. These rocks are non-clastic sedimentary rocks resulting from the evaporation of saline water. Most evaporites are derived from bodies of sea water.

Gypsum occurs in several forms, each characterised by its own textural identity. The massive, fine-grained, translucent variety is called alabaster; well-formed, crystalline, clear varieties are named sclenite, whilst the white, earthy opaque, more massive types are called Gypsum rock. Gypsum is one of the least soluble of salts in sea water and is therefore, one of the first to be deposited as the salt concentration rises. All varieties have been deposited from saline waters and their characteristic occurrance is controlled by varying physico-chemical environments. All are precipitated in temperature conditions in saturated water below 25^{o} C, above this temperature the anhydrous form, anhydrite is deposited. It is also formed by the decomposition of pyrite ($Fe\ S_2$) in the prasence of calcium carbonate. Gypsum is frequently formed by the hydration of anhydrite in the presence of water under low external pressure (at the maximum average depth of 100-150 m). The majority of the huge gypsum deposits in the world have been formed in this way.

Gypsum is a chemical compound of 46.5% SO_3, 32.6% Ca O and 20.9% H_2O. It is known as a hydrous calcium sulphate and represented by the chemical formula $Ca\ SO_4 . 2\ H_2O$. Gypsum is the most common natural sulphate, it has considerable variation in colour, but pinks, reds, yellows and whites are most common. The tints and colours sometimes found in gypsum are due to the presence of iron, and the presence of organic matter or disseminated clay gives rise to a pale grey colour.

Gypsum is a soft rock of Mohs hardness equal to 1.5-2 (can be scratched by the finger nail) and specific gravity of 2.32. It has a monoclinic crystal form.

Commercially gypsum is used for the production of plaster of paris, uncalcined (natural) gypsum is used as a retarder in Portland cement. It is sometimes used instead of bricks, in the construction of walls and partitions in the building industry.

The gypsum which was used in this research is from the British Gypsum Co. mine at Sherburn in Elmet, North Yorkshire, U.K. Its average composition was (91.5%) gypsum, (5.5%) anhydrite, (2.7%) carbonate and (0.3%) clay. The workings of the mine lie at a depth of about (50) meters below ground surface. Generally it has a fine crystal structure and is pink in colour. Its method of formation has been the hydration of anhydrite mass, and mining to greater depths results in the gradual appearance of anhydrite bands in the gypsum rock deposit.

Table (B4-1) Experimental data and mean values of triaxial tests of dry specimens (LxD = 76.2 x 25.4 mm).

σ_3 N/mm^2	Specimen No.	Test results			Mean values		
		σ_1 N/mm^2	Z N/mm^2	θ deg.	σ_1 N/mm^2	Z N/mm^2	θ deg.
0	See table (4.6)				41.59	0	63.8
5	5D-S1	47.82	29.10	60.0	50.21	30.13	62.1
	5D-S2	52.63	31.08	61.5			
	5D-S3	48.36	30.09	64.5			
	5D-S4	47.75	29.10	62.0			
	5D-S5	54.49	31.28	62.5			
10	10D-S1	60.19	38.76	60.5	62.41	38.03	60.8
	10D-S2	61.57	37.20	59.5			
	10D-S3	69.67	40.73	61.5			
	10D-S4	58.22	35.41	61.5			
15	15D-S1	70.15	63.05	59.3	67.30	59.70	59.1
	15D-S2	64.43	57.33	59.0			
	15D-S3	65.26	55.36	59.2			
	15D-S4	69.37	63.06	58.8			
20	20D-S1	80.91	76.38	61.5	78.15	73.96	58.3
	20D-S2	82.94	75.78	57.0			
	20D-S3	78.55	74.79	57.4			
	20D-S4	70.65	68.87	57.0			
25	25D-S1	87.92	83.57	58.3	86.84	80.12	56.5
	25D-S2	82.00	73.90	57.5			
	25D-S3	85.16	78.05	56.0			
	25D-S4	92.26	84.96	54.0			
30	30D-S1	95.32	91.57	51.0	102.87	99.71	51.0
	30D-S2	113.08	107.16	51.5			
	30D-S3	105.0	103.80	50.5			
	30D-S4	98.08	96.31	51.5			
35	35D-S1	120.09	113.52	51.6	109.23	103.17	53.3
	35D-S2	95.22	83.38	53.0			
	35D-S3	103.90	98.78	52.5			
	35D-S4	117.72	112.98	56.0			

Table (B4-2) Experimental data and mean values of triaxial tests of saturated specimens (LxD = 76.2 x 25.4 mm).

σ_3 N/mm^2	Specimen No.	Test results			Mean values		
		σ_1 N/mm^2	Z N/mm^2	θ deg.	σ_1 N/mm^2	Z N/mm^2	θ deg.
0	See table (4.7)				21.13	0	62.8
5	5S-S1 5S-S2 5S-S3 5S-S4	36.13 36.53 35.34 32.97	19.24 15.29 19.24 18.25	60.5 61.5 64.0 62.0	35.24	18.01	62.0
10	10S-S1 10S-S2 10S-S3 10S-S4	44.0 44.60 49.93 43.03	38.22 31.12 35.26 30.92	60.5 58.0 63.5 58.8	45.39	33.90	60.2
15	15S-S1 15S-S2 15S-S3 15S-S4	59.40 55.65 58.90 58.51	55.16 50.03 55.55 52.00	57.5 60.0 59.5 55.0	58.12	53.19	58.0
20	20S-S1 20S-S2 20S-S3 20S-S4	73.80 66.90 75.19 70.85	69.86 61.00 70.06 66.90	58.0 56.5 55.5 57.2	71.69	66.97	56.8
25	25S-S1 25S-S2 25S-S3 25S-S4	81.80 78.80 80.42 81.40	77.26 76.86 77.06 77.85	56.0 57.0 55.5 54.5	80.61	77.26	55.8
30	30S-S1 30S-S2 30S-S3 30S-S4	76.0 97.69 97.69 96.70	68.09 89.80 91.77 94.73	54 56 55.5 54.5	92.02	86.10	55

Table (B4-3) Experimental data and mean values of triaxial tests of dry specimens (LxD = 95.25x31.75 mm).

σ_3 N/mm^2	Specimen No.	Test results			Mean values		
		σ_1 N/mm^2	Z N/mm^2	θ deg.	σ_1 N/mm^2	Z N/mm^2	θ deg.
0	See table (4.6)				32.82	0	65.5
5	5D-R1	56.06	34.95	66.0	53.80	31.15	64.3
	5D-R2	50.10	33.77	65.5			
	5D-R3	60.20	30.03	62.5			
	5D-R4	48.90	25.84	63.2			
10	10D-R1	64.31	47.55	60.5	64.1	44.19	58.7
	10D-R2	57.23	44.65	56.0			
	10D-R3	66.92	41.77	61.0			
	10D-R4	67.97	42.80	57.3			
15	15D-R1	74.75	61.14	53.0	73.31	61.32	54.5
	15D-R2	69.60	58.74	51.5			
	15D-R3	78.51	63.15	57.5			
	15D-R4	70.38	62.25	56.0			
20	20D-R1	79.58	70.92	54.5	76.62	72.93	53.5
	20D-R2	74.07	68.09	56.0			
	20D-R3	77.75	74.13	55.0			
	20D-R4	75.09	78.58	48.5			
25	25D-R1	78.42	87.41	50.5	85.83	81.14	52.0
	25D-R2	90.07	82.48	48.0			
	25D-R3	90.75	79.13	56.5			
	25D-R4	84.09	75.55	53.0			
30	30D-R1	93.35	85.84	52.0	96.45	93.34	51.0
	30D-R2	98.37	94.33	50.5			
	30D-R3	100.12	97.14	50.0			
	30D-R4	93.96	96.06	51.5			
35	35D-R1	102.35	98.51	50.0	103.12	99.58	50.5
	35D-R2	100.84	100.32	48.5			
	35D-R3	105.76	96.41	49.5			
	35D-R4	103.53	103.08	54.0			

Table (B4-4) Experimental data and mean values of triaxial tests of saturated specimens (LxD = 95.25 x 31.75 mm).

σ_3 N/mm^2	Specimen No.	Test results			Mean values		
		σ_1 N/mm^2	Z N/mm^2	θ deg.	σ_1 N/mm^2	Z N/mm^2	θ deg.
0	See table (4.7)				17.29	0	67
5	5S-R1 5S-R2 5S-R3 5S-R4	36.46 39.62 32.29 34.71	19.68 22.46 19.05 19.33	63.0 61.5 60.0 55.5	35.77	20.13	60
10	10S-R1 10S-R2 10S-R3 10S-R4	46.47 47.86 48.74 48.24	30.77 32.16 30.91 35.44	58 56.5 55.0 58.5	47.83	32.32	57
15	15S-R1 15S-R2 15S-R3 15S-R4	49.56 52.68 55.84 53.82	43.13 45.28 48.44 44.95	54.5 53.0 51.5 55.0	53.0	45.45	53.5
20	20S-R1 20S-R2 20S-R3 20S-R4	62.69 61.68 58.14 62.18	60.54 58.39 55.90 55.90	52.0 50.0 51.0 49.0	61.17	57.68	50.5
25	25S-R1 25S-R2 25S-R3 25S-R4	68.0 64.58 69.38 66.10	65.59 61.17 63.44 62.88	50.5 46.5 49.0 50.0	67.02	63.27	49.0
30	30S-R1 30S-R2 30S-R3 30S-R4	78.14 76.25 70.34 74.12	78.13 75.75 70.12 67.24	50.5 46.5 48.5 46.5	74.71	72.81	48.0
35	35S-R1 35S-R2 35S-R3 35S-R4	80.16 82.25 77.18 75.73	74.24 76.31 79.90 77.80	46.5 49.0 47.5 49.0	78.83	77.06	48.0

Appendix C.

Statistical Consideration of the Regression.

C.1 Linear Regressions.

The creep relationship in most of the cases in uniaxial and triaxial compression and in bending in both dry and saturated conditions followed a power law equation in the form

$$\varepsilon = C\, t^{n} \qquad \ldots\ldots \qquad (C.1)$$

In order to ensure that the creep data will fit the above equation well, the data was plotted on a log-log graph, when a straight line is normally obtained. n in the equation represents the slope of this line and C is the creep strain at time t = 1 hour. Both graphical and least squares methods were used to find the values of n and C. The least squares method was applied in the following way:

Equation (C.1) can be rewritten in the form

$$\log \varepsilon = \log C + n \log t \qquad \ldots\ldots \qquad (C.2)$$

let $\log \varepsilon = Y$

$\log t = X$

and $\log C = Z$

Equation (C.2) can be rewritten in the form

$$Y = Z + nX \qquad \ldots\ldots \qquad (C.3)$$

The slope (n) and the intercept (Z) of the straight line which represents equation (C.3) can be calculated by

$$n = \frac{\Sigma XY - \frac{(\Sigma X)\ (\Sigma Y)}{N}}{\Sigma X^2 - \frac{(\Sigma X)^2}{N}} \qquad \ldots\ldots \qquad (C.4)$$

$$Z = \bar{Y} - n\bar{X} \qquad \ldots\ldots \qquad (C.5)$$

where N is the number of the readings, $\bar{Y}$ is the mean of the Y- values and $\bar{X}$ is the mean of X-values.

A sample solution for X, Y, ΣXY, ΣX, ΣY and ΣX^2 is given in Table (C.1). The values of creep strain (ε) and corresponding times (t) are taken from Table (6.15) of Chapter 6.

Solving for n and K using the data given in Table (C.1)

$$n = \frac{209.496 - \frac{75.859 \times 105.568}{40}}{189.914 - \frac{(75.859)^2}{40}}$$

$\therefore$ $n = 0.202$

$Z = \bar{Y} - n\bar{X}$

$Z = 2.639 - 0.202 \times 1.896$

$\therefore$ $Z = 2.256$

Substitute the value of Z in Z = log C to find C = 178. Substitute the values of n and C in equation (C.1), the following power equation of the axial creep in saturated condition at σ_1 = 41 N/mm^2 and σ_3 = 30 N/mm^2 was obtained

$$\varepsilon = 178\ t^{0.202} \quad \ldots\ldots \quad (C.6)$$

In order to find the degree of correctness of the assumption that the plotted data on the log-log graphs represents a straight line, the correlation coefficient (R) was found for each case. The results obtained were extremely satisfactory. A sample of this calculation is given here for the axial creep in saturated condition at σ_1 = 41 N/mm^2 and σ_3 = 30 N/mm^2.

$$R = \frac{\Sigma(X-\bar{X})(Y-\bar{Y})}{(N-1)\ (DX.DY)} \quad \ldots\ldots \quad (C.7)$$

where R is the correlation factor, X, $\bar{X}$, Y, $\bar{Y}$ and N as given in Table (C.1) and equation (C.4); DX and DY are the standard deviations of X and Y values respectively, where:

$$DX = \sqrt{\frac{\Sigma(X-\bar{X})^2}{N-1}} \qquad \ldots\ldots \qquad (C.8)$$

$$DY = \sqrt{\frac{\Sigma(Y-\bar{Y})^2}{N-1}} \qquad \ldots\ldots \qquad (C.9)$$

Substituting the values of X, $\bar{X}$, N, Y and $\bar{Y}$ in the above equations:

$$DX = 1.088$$

$$DY = 0.239$$

$$R = \frac{10.096}{39 \times 1.088 \times 0.239}$$

$\therefore$ R = 0.995 which indicates a good degree of correctness.

C.2 Standard Error of Estimate.

Empirical equations were found for the determination of the creep strain in axial and lateral directions in the form:

$$\varepsilon = a\,\sigma_1^{\,b}\,t^{c} \qquad \ldots\ldots \qquad (C.10)$$

In order to show that the actual creep strain fits the above equation, the combined correlation of coefficient (COR.COF.) and the Standard Error of Estimate (SEE) were calculated. Standard Error of Estimate gives the reliability of the predicted values. The following method was used for computing SEE.

$$SEE = \sqrt{\frac{\Sigma(Y-Y')^2}{N-K-1}}$$

where: SEE is the standard error of estimate, Y is the actual creep strain, Y' is the predicted creep strain, N is the number of reading and K is the number of the independent variables (time and axial stress).

For a sample solution, values of Y, Y' $(Y - Y')$ and $Y - Y')^2$ are given in Table (C.2). These values are taken from the lateral creep in dry conditions at σ_1 = 27, 41, 50 and 63 N/mm^2 and at σ_3 = 30 N/mm^2.

N = 120 K = 2 SEE = $\sqrt{\frac{46987.38}{120 - 2 - 1}}$

$\therefore$ SEE = 20.04

Table (C.1) Axial creep of saturated gypsum at σ_1 = 41 N/mm^2 and σ_3 = 30 N/mm^2

Time (t)	Creep Strain (ε)	log t = X	log ε = Y	X.Y	X^2	$X-\bar{X}$	$Y-\bar{Y}$	$(X-\bar{X})^2$	$(Y-\bar{Y})^2$	$(X-\bar{X})\cdot(Y-\bar{Y})$
0.1	81.5	-1.000	1.911	-1.911	1.000	-2.896	-0.728	8.387	0.530	2.108
0.3	132.7	-0.602	2.123	-1.278	0.232	-2.498	-0.516	6.240	0.266	1.288
0.5	155.0	-0.301	2.190	-0.659	0.091	-2.197	-0.449	4.827	0.202	0.986
1	182.2	0	2.261	0	0	-1.896	-0.378	3.595	0.143	0.717
2	204.2	0.301	2.310	0.695	0.091	-1.595	-0.329	2.544	0.108	0.525
3	220	0.477	2.343	1.118	0.228	-1.419	-0.296	2.014	0.088	0.420
4	234.9	0.602	2.371	1.427	0.362	-1.294	-0.268	1.674	0.072	0.347
5	244.9	0.699	2.389	1.670	0.489	-1.197	-0.250	1.433	0.063	0.299
6	254.1	0.778	2.405	1.871	0.606	-1.118	-0.234	1.250	0.055	0.262
12	296.5	1.079	2.472	2.667	1.165	-0.817	-0.167	0.667	0.028	0.136
24	353.1	1.380	2.548	3.516	1.905	-0.516	-0.091	0.266	0.008	0.047
48	390.8	1.681	2.592	4.357	2.827	-0.215	-0.047	0.046	0.002	0.010
72	412.0	1.857	2.615	4.943	3.450	-0.039	-0.024	0.002	0.001	0.001
96	442.8	1.982	2.646	5.244	3.929	0.086	0.007	0.007	0.000	0.001
120	465.9	2.079	2.668	5.547	4.323	0.183	0.029	0.034	0.001	0.005
144	485.4	2.185	2.686	5.796	4.659	0.262	0.047	0.069	0.002	0.012
168	505.1	2.225	2.703	6.014	4.952	0.329	0.064	0.108	0.004	0.021
192	520.9	2.283	2.717	6.203	5.213	0.387	0.078	0.150	0.006	0.030
216	534.4	2.334	2.728	6.367	5.450	0.438	0.089	0.192	0.008	0.039
240	547.7	2.380	2.739	6.519	5.665	0.484	0.100	0.234	0.010	0.048
264	559.2	2.422	2.748	6.656	5.864	0.526	0.109	0.277	0.011	0.057

Table (C.1) Continued.

Time (t)	Creep Strain (ε)	log t = X	log ε = Y	X.Y	X^2	$X-\bar{X}$	$Y-\bar{Y}$	$(X-\bar{X})^2$	$(Y-\bar{Y})^2$	$(X-\bar{X})\cdot(Y-\bar{Y})$
288	570.8	2.459	2.756	6.777	6.049	0.563	0.117	0.317	0.014	0.066
312	582.0	2.494	2.765	6.896	6.221	0.598	0.126	0.358	0.016	0.075
336	591.2	2.526	2.772	7.002	6.382	0.630	0.133	0.397	0.018	0.084
360	600.3	2.556	2.778	7.101	6.535	0.660	0.139	0.436	0.019	0.092
384	609.5	2.584	2.785	7.196	6.679	0.688	0.146	0.473	0.021	0.101
408	618	2.611	2.791	7.287	6.816	0.715	0.152	0.511	0.023	0.109
432	627.3	2.635	2.798	7.372	6.943	0.739	0.159	0.546	0.025	0.118
456	635.7	2.659	2.803	7.453	7.070	0.763	0.164	0.582	0.027	0.125
480	645.0	2.681	2.810	7.534	7.188	0.785	0.171	0.616	0.029	0.134
504	651.8	2.702	2.814	7.603	7.300	0.806	0.175	0.650	0.031	0.141
528	660.1	2.723	2.820	7.679	7.415	0.827	0.181	0.684	0.033	0.150
552	667.7	2.742	2.825	7.746	7.519	0.847	0.186	0.716	0.035	0.157
576	673.5	2.761	2.828	7.808	7.623	0.865	0.189	0.748	0.036	0.164
600	680.9	2.778	2.833	7.870	7.717	0.882	0.194	0.778	0.038	0.172
624	688.0	2.795	2.838	7.932	7.812	0.899	0.199	0.808	0.040	0.179
648	693.8	2.812	2.841	7.989	7.907	0.916	0.202	0.839	0.041	0.185
672	699.6	2.827	2.845	8.043	7.992	0.931	0.206	0.867	0.043	0.192
696	705.9	2.843	2.849	8.099	8.083	0.947	0.210	0.897	0.044	0.199
720	711.6	2.857	2.852	8.148	8.162	0.961	0.213	0.924	0.045	0.205
		ΣX = 75.859 $\bar{X}$ =1.896	ΣY = 105.568 $\bar{Y}$ =2.639	ΣXY = 209.496	ΣX^2 = 189.914			$\Sigma(X-\bar{X})^2$ = 46.163	$\Sigma(Y-\bar{Y})^2$ = 2.226	$\Sigma(X-\bar{X})\cdot(Y-\bar{Y})$ = 10.096

Table (C.2) Lateral creep strain in dry conditions at σ_1 = 27, 41 50 and 63 N/mm^2 and at σ_3 = 30 N/mm^2.

Time hours	σ_1 N/mm^2	Actual creep Y	Predicted Y'	Y - Y'	(Y - Y')^2
48	27	49.50	50.068	-0.568	0.3226
72	27	57.30	57.528	-0.228	0.0519
96	27	65.30	63.486	1.814	1.814
120	27	72.05	68.529	3.521	12.397
144	27	78.50	72.945	5.555	30.858
168	27	83.700	76.900	6.800	46.240
192	27	88.550	80.499	8.051	64.819
216	27	92.65	83.813	8.837	78.093
240	27	100.30	86.893	13.407	179.748
---	--	------	------	------	--------
---	---	------	------	------	--------
---	---	------	------	------	--------
---	---	------	------	------	--------
---	---	------	------	------	--------
552	63	485.85	435.137	50.713	2571.81
576	63	491.50	441.527	49.973	2497.30
600	63	495.650	447.744	47.906	2294.98
624	63	501.50	453.800	47.700	2275.29
648	63	506.35	459.705	46.645	2175.76
672	63	510.85	465.468	45.382	2059.53
696	63	514.70	471.096	43.604	1901.31
720	63	517.65	476.599	41.051	1685.18
Total number of cases is 120, sample of calculation is presented.					$\Sigma(Y-Y')^2$ = 46987.38